Intrusive history and volatile evolution of the Endeavour porphyry Cu-Au deposits, Goonumbla district, NSW, Australia

Vanessa Lickfold, BSc (Hons), MSc

UNIVERSITY OF TASMANIA

Submitted in fulfilment of the requirements for the degree of Doctor of Philosophy

March 2002

CODES SRC

Centre for Ore Deposit Research

Declaration

This thesis contains no material that has been accepted for a degree or diploma by the University or any other institution, except by way of background information and duly acknowledged in the thesis, and to the best of the candidate's knowledge and belief, contains no material previously published or written by another person, except where due acknowledgement is made in the text of the thesis.

Vanessa Lickfold

Date: 31/10/02

This thesis is not to be made available for loan or copying for two years following the date this statement was signed. Following that time the thesis may be made available for loan and limited copying in accordance with the *Copyright Act* 1968.

Vanessa Lickfold

Date: 31/10/02

Abstract

The Goonumbla Volcanic Complex (GVC) of central-west New South Wales, Australia, is part of the Ordovician Macquarie Island Arc. The upper unit of the GVC, the Wombin Volcanics, comprises submarine shoshonitic lavas and associated volcaniclastic rocks, and hosts four economic porphyry Cu-Au deposits, Endeavour 22 (E22), E26, E27 and E48. Together these deposits have a combined ore reserve of 63.6Mt @ 1.1% Cu and 0.5g/t Au. Mineralisation is centred on thin, pipe-like quartz monzonite porphyry (QMP) complexes that intruded the Wombin Volcanics in an extensional regime towards the end of the Late Ordovician.

Despite being some of the smallest economic porphyry deposits in the world in terms of tonnage and cross-sectional area, detailed pit mapping and drillcore logging has led to the recognition of eight intrusive phases within the QMP complexes of the Endeavour deposits. The oldest intrusive phase is a coarse-grained, equigranular monzodiorite intrusion that is restricted to the deeper parts of E26. This intrusion has a sheared contact with the next oldest phase, equigranular to weakly porphyritic biotite quartz monzonite (BQM) intrusions, which are recognised at all four deposits. A series of three variably felsic QMP phases emplaced over a short period of time after the BQM comprise the central QMP complexes; 1) volumetrically minor early- and late-mineral biotite phyric QMP (B-QMP) dykes and dykelets, 2) volumetrically dominant syn-mineral K-feldspar phyric QMP intrusions (K-QMP) and 3) less abundant syn-to late-mineral augite-biotite K-feldspar phyric QMP (KA-QMP) intrusions, which intruded the cores of the K-QMP bodies. Basaltic trachyandesite dykes and augite phyric monzonite porphyry ("zero" porphyry) dykes at E26 represent post-mineral phases of intrusive activity associated with the Endeavour deposits. Mafic dykes of uncertain age also intrude the Endeavour deposits.

Four main stages of hydrothermal activity have been recognised at each deposit. The Early Stage, associated with the intrusion of the BQM and comprising biotite-magnetite alteration of the host volcanic rocks and K-feldspar alteration of the BQM, overprinted pre-mineral albite-sericite alteration assemblages in the BQM and host volcanic rocks at each deposit. Transitional Stage vein dykes, brain rock and other related anisotropic textures formed during the transition from magmatic to hydrothermal activity. Main Stage sulphide mineralisation at all four deposits is spatially and temporally associated with the K-QMP, and to a lesser extent, KA-QMP intrusions and their associated orthoclase alteration assemblages, which are characterised by multiple generations of quartz, K-feldspar and sulphide veins. Late Stage phyllic alteration is magmatic – hydrothermal in origin and comprises sericite-quartz-Cu-sulphide-carbonate-haematite assemblages. Part of the distal carbonate-quartz-sericite-base-metal sulphide propylitic assemblages may be associated with the proximal phyllic assemblage. A second generation of phyllic alteration is related to minor late stage faulting. Weak to moderate post-mineral propylitic alteration assemblages associated with the thermal collapse of the Endeavour systems are the last alteration event related to the QMP intrusive complexes.

Fluid inclusions in quartz from early, transitional, main and late stage veins have been analysed from all four deposits. Microthermometric results indicate that the Endeavour deposits were emplaced to depths between 1000 and 1700m below the palaeo surface. Early, metal-rich magmatic – hydrothermal fluids, were typically hot (>550°C) and had salinities of ~60 wt% NaCl ± KCl eq., whereas those associated with transitional "magmatic" quartz were slightly cooler (550 – 500°C), though still as saline. Fluids that produced the transitional "hydrothermal" quartz had average calculated salinities of ~55wt% NaCl + KCl eq. and circulated at temperatures of ~500°C; they were more metal-rich than the equally saline, cooler (~460°C) fluids associated with the main mineralising event. These relationships are interpreted to imply that transitional hydrothermal fluids represent the ore-carrying fluids, which cooled and thus precipitated metal sulphides during the main mineralising event of the Endeavour deposits. Late stage fluids were the coolest (350 – 400°C) and least saline (~40 wt% NaCl eq.) and had elevated K and Ca contents compared to other fluids; features consistent with wallrock buffering of cooling magmatic – hydrothermal fluids.

$\delta^{34}S$ values for the Endeavour sulphides range from -19.7 to +0.7‰ (mean -5.1‰; standard deviation 2.7‰); those for sulphates range from +4.4 to +21.8‰ (mean +9.2‰; standard deviation 4.2‰). The isotopic compositions of sulphate – sulphide pairs and temperature estimates from the fluid inclusion study were used to establish that the initial $\delta^{34}S_{\Sigma S}$ of the magmatic – hydrothermal fluid was ~+1.5‰. A broad temporal and lateral zonation towards heavier isotopic compositions in sulphides with time and distance from the cores of the Endeavour deposits is interpreted to reflect wallrock buffering as the systems cooled. The extremely negative $\delta^{34}S$ values may reflect local sulphide precipitation from hyper-oxidised ore fluids with H_2S:SO_2 ratios much less than the original magmatic – hydrothermal fluid.

Biotite halogen contents indicate that the magmas that produced the BQM and QMP intrusions were depleted in Cl and enriched in F relative to the magmatic – hydrothermal fluids that produced Cl-rich secondary biotite. These magmatic – hydrothermal fluids also caused Cl-enrichment in many of the primary biotite phenocrysts in the K-QMP intrusions. Apatites in regional intrusions are relatively Cl-poor and Fe-rich compared to the F- and Fe-depleted apatites in the BQM and QMP intrusions associated with the Endeavour deposits. The higher F contents of biotites and apatites, and lower Fe contents of apatites in ore-related intrusions are consistent with higher degrees of fractionation in these intrusions compared to regional intrusions.

Geochemical characteristics of the regional volcanic and intrusive rocks define a systematic trend consistent with high-temperature magmatic fractionation of basaltic trachyandesite through trachyte, with increasing K_2O and decreasing TiO_2, Al_2O_3, Fe_2O_3, CaO and MgO contents with increasing SiO_2 contents. These trends continue through to the QMP intrusions associated with the Endeavour deposits. However, while there is progressive fractionation through the sequence of ore-related QMP intrusions, a direct progression by fractionation from the BQM intrusions to the QMP intrusions is not indicated. Contrary to previous models that invoke the BQM as the parent stock from which the QMP phases emanated, this study shows that the Ba, Sr, Rb, Y, Nb and Zr contents of the BQM preclude it from generating the trace element compositions characteristic of the QMP complexes solely by crystal fractionation. The REE patterns of QMP phases are also not explainable by crystal fractionation effects alone. Instead, the QMP complexes and associated alteration and mineralisation assemblages at E22, E26, E27 and E48 are interpreted to have formed in response to the emplacement of a series of mafic shoshonitic melts into the base of a crystallising, zoned, monzodiorite to monzonite magma chamber. Episodic movement along deep-seated, mantle-tapping (?) structure(s), possibly the Lachlan Transverse Zone, could have triggered the emplacement of these mafic shoshonitic melts. Related movements on shallow-crustal fault systems above the magma chamber probably caused instantaneous depressurisation and the repeated simultaneous egress of melt (QMP) and exsolved aqueous fluid into dilatant zones. Localised fracturing and additional volatile exsolution from the QMP melt is thought to have led to the formation of the narrow QMP complexes and associated Cu-Au-bearing stockwork veins and related orthoclase alteration. The volatile-rich aqueous fluid partitioned LREE preferentially to MREE, preferentially to HREE, resulting in the development of distinctive "u-shaped" REE patterns of the ore-related intrusions.

Acknowledgements

My sincerest thanks and appreciation are extended to my principal supervisor, Dr David Cooke, not only for initiating this research project in collaboration with *Northparkes Mines* , but for supervising me on my Endeavour experience. Your support, patience, guidance and help throughout my time here in Hobart have been invaluable. To my second supervisor, Prof. Tony Crawford, thank you too for your encouragement and assistance, especially in the last few months with all that geochem!

Northparkes Mines is thanked for the financial support of this project. To Stuart Smith, the late Michael House, Craig Stewart, Justin Paul, Murray Spratt and the rest of the geology team at *Northparkes*, thanks for going that little bit further to get me what needed for this project. A special note of thanks to Stuart for his guidance, ability to invoke geological discussion, and assistance in making my trips to Parkes as comfortable and as trouble-free as they were.

I would like to extend my gratitude to everyone at CODES and the School of Earth Sciences; Simon, Peter, Di, June, Lynne, Lyn, Loreto, Phil, Nilar, Katie and Alistair, for all the assistance over the last three and a half years. Dr Dave Steele at the CSL is thanked sincerely for his invaluable help in sorting out how to analyse apatite effectively on the microprobe. I would also like to thank Dima for his insights into melt inclusions and magmatic processes while I was analysing my fluid inclusions. Garry Davidson and Mike Solomon are thanked for reviewing early versions of the S isotope and fluid inclusion chapters respectively. Sincere thanks to Carol Simpson and Phil Blevin for allowing me to look at some of their Goonumbla samples.

An especially heartfelt thank you to Steve, Catherine, Chris, James and Rohan for all your help in the last few days (and weeks) of getting this thesis together. To my office mates, James, Sarah, Darryl and Wallace, thanks for your company for the last few years, it's been a great office to work in – you can now have the blind on my side open again and enjoy getting inspiration from the view! And to my fellow students, past and present; Briony, Sarah, Darryl, Catherine, Cathryn, Mike, James, Ben, Rohan, Mike, Rob, Glen, Peter, Karin, Andrew, Andrew and Andrew, Kirstie, Ali, Steve, Neil, Zorah, Alan and Meng, your friendship and encouragement will not be forgotten.

I would like to end by deeply thanking my family, Dad, Mum, Sue, Jani and Scott, for always encouraging me and having faith in me. Also to my parents for instilling in me the courage to pursue my dreams, for without that, I would not have embarked on this venture. To my friends, both here and in South Africa, thanks for always being there for me.

Table of Contents

APPENDICES

List of Figures

List of Tables

CHAPTER 1
Introduction

1.1 Preamble

Understanding the complex interplay of magmatic and hydrothermal phenomena in shallow crustal magmatic systems is critical for the study of porphyry Cu-Au and related hydrothermal ore deposits. Evidence from volcanic systems indicates that magmatic gases and brines commonly exsolve as separate phases in the apices of many shallow crustal magma chambers (e.g. Johnson *et al.*, 1994; Lowenstern, 1995). These processes can lead to the development of distinctive vein and hydrothermal alteration mineral assemblages within magmatic – hydrothermal ore deposits (e.g. Burnham, 1979; Hedenquist and Lowenstern, 1994). However, although workers have presented models to explore the movement of magmatic volatiles through crystallising intrusions (e.g. Candela, 1994; Shinohara and Kazahaya, 1995), the igneous rock compositions and textures that form during progressive degassing of a mineralised intrusive complex have received comparatively little attention.

Kirkham and Sinclair (1988) and Lowenstern and Sinclair (1996) described crenulate or comb quartz textures, which they attributed to the magmatic – hydrothermal transition at the Henderson Mo and Logtung W-Mo (Yukon Territory, Canada) porphyry deposits, respectively. Candela and Blevin (1995) described textural features of some high-level granite plutons from the New England orogenic belt in eastern Australia, which they interpreted to represent pathways along which magmatic fluid phases migrated. Similar crenulate quartz textures occur in parts of the quartz monzonite porphyry complexes central to the four Endeavour porphyry Cu-Au deposits. By studying the nature of these and other related textures, this thesis aims to document the transition from magmatic to hydrothermal conditions in these systems.

A feature common to porphyry-style deposits is their association with multi-phase intrusions (Sillitoe and Gappe, 1984). Examples include the eleven intrusive phases recognised in the Henderson Mo porphyry deposit in Colorado, U.S.A. (Carten *et al.*,

1988) and the four intrusive phases recognised in the porphyry Cu deposit at El Salvador, Chile (Gustafson and Hunt, 1975). Ore formation is typically related to one or two of the intrusive phases, while the remaining phases dilute or truncate grade. Careful study of the intrusive relationships, in conjunction with the grade distribution, can help determine which intrusive phases are related to ore formation.

This thesis focuses on the intrusive history of the quartz monzonite porphyry (QMP) complexes central to each of the four mineralised porphyry Cu-Au deposits in the Goonumbla district of New South Wales, Australia (hereinafter referred to as the Endeavour deposits). These four deposits are among the smallest economic porphyry Cu-Au deposits in the world in terms of both tonnage and cross-sectional area (~300 x 200m^2) and they are well exposed to depths of 1500m below surface due to extensive diamond drilling and underground block caving at the Endeavour 26 deposit. These features provide an ideal opportunity for investigating the sequence of intrusive activity and the nature of volatile evolution in the roof zones of the Endeavour porphyry Cu-Au systems.

Previous studies of the Endeavour systems have focused on single deposits and investigations have generally been restricted to the QMP intrusive complexes central to each deposit. There have been no comparisons with intrusions that occur elsewhere in the region within the Goonumbla Volcanic Complex (GVC). Consequently, most previous studies have not investigated the differences between mineralised and unmineralised intrusions in the Goonumbla region. In light of this, key aims of this thesis include the careful geologic documentation of the sequence of intrusive events within in the QMP complexes associated with the Endeavour deposits, and the establishment of textural criteria that will enable the distinction between mineralised and unmineralised intrusions, not only within the ore-related QMP, but also within the surrounding mineral district. By studying the geochemical characteristics of the mineralised and unmineralised rocks of the GVC, it may be possible to speculate on the tectonic environment and petrogenesis of emplacement of the porphyry deposits, and to determine whether certain geochemical characteristics are unique to the mineralised intrusions.

Many workers believe that ore metals in porphyry systems are derived from the related crystallising magma and transported into the upper portions of the magma chamber and adjacent areas in magmatic – hydrothermal fluids (Henley and McNabb, 1978; Burnham, 1979; Candela, 1989a and b; Beane and Bodnar, 1995). Fluid inclusions in the four

Endeavour Cu-Au porphyry deposits can be used to determine P-T-X conditions for the mineralising systems. Sulphur isotopic compositions of sulphides and sulphates can be used in conjunction with fluid inclusion studies to provide information on the chemical conditions at the time of ore formation, the temperature and mechanisms of sulphide precipitation and the source/s of sulphur in the Endeavour porphyry systems.

1.2 This study

1.2.1 Objectives

This collaborative study between *CODES* and *North Limited* (now *Rio Tinto*) was initiated with several aims:

- to unravel the intrusive history of the QMP complexes at E22, E26, E27 and E48;
- to document any textures that are likely to provide evidence for magmatic – hydrothermal transition within specific intrusive phases within the QMP complexes;
- to establish an appropriate paragenetic framework suitable for studying the alteration/mineralisation assemblages and fluid evolution in these deposits;
- to determine when volatiles exsolved from the magmas and to establish the prevailing P-T-X conditions;
- to establish the typical magmatic sulphur isotopic composition of the Endeavour systems and determine how these changed with the evolution of a volatile phase and the passage of this phase through the ore-forming environment;
- to investigate the petrologic relationships between the various intrusions associated with mineralisation, and with the regional intrusive and volcanic units of the GVC;
- to establish textural and geochemical criteria that allow discrimination between mineralised and unmineralised intrusions in the greater GVC;
- to propose a revised genetic model for the Endeavour porphyry deposits that is constrained by the tectonic and structural setting, intrusive history, alteration/ mineralisation paragenesis, volatile evolution and fluid chemistry as well as the geochemistry of the magmatic – hydrothermal systems and their host rocks.

1.2.2 Methods

These aims were achieved by conducting the following investigations:

- detailed (1:500) logging and sampling of diamond drillcore, pit wall mapping (E27) and regional sampling of the *Northparkes* deposits and the Goonumbla district over three fields seasons (6 months) to document textural features, mineralogy and timing relationships of the various intrusive phases;

- petrographic and textural studies of intrusive rocks from the GVC (mine-related and regional) using polished thin sections to supplement drillcore logging and hand specimen descriptions;
- fluid inclusion studies of quartz from veins and dykes using doubly polished thick (~150μm) sections. The samples were selected to represent both the spatial and temporal distribution of ore formation and related hydrothermal alteration assemblages, and the data are used to determine the P-T-X conditions of the ore-forming fluids;
- electron microprobe and proton-induced X-ray emission (PIXE) probe analyses of fluid inclusions to determine the metal, cation and anion concentrations in the ore-forming fluids;
- sulphur isotope studies on sulphides and sulphates from all paragenetic stages to investigate whether a change in sulphur isotopic composition occurred with respect to time and/or distance from the centres of the Endeavour deposits;
- electron microprobe analyses of biotite and apatite to determine whether spatial or temporal variations in halogen concentrations occurred;
- whole rock XRF major element, XRD trace element and solution ICP-MS rare earth element analyses of the least altered regional and ore-related rocks in order to investigate the differences between mineralised and unmineralised intrusive rocks within the Endeavour deposits as well as in the GVC as a whole; and
- $^{39}Ar/^{40}Ar$ dating of biotite and U-Pb (SHRIMP) dating of zircon grains to constrain timing relationships of intrusive phases in the GVC.

1.3 Background

1.3.1 Location and environment

The Goonumbla district is situated 20 – 30km northwest of the rural town of Parkes in central-west New South Wales, Australia, approximately 300km west of Sydney (Figure 1.1). The first porphyry-related Cu-Au mineral occurrence was discovered in 1976 and subsequent exploration led to the discovery of several mineralised centres in the area, including the Endeavour 22 (E22), Endeavour 26 (E26), Endeavour 27 (E27) and Endeavour 48 (E48) deposits. Cu-Au ore at each of these deposits is Ordovician in age and

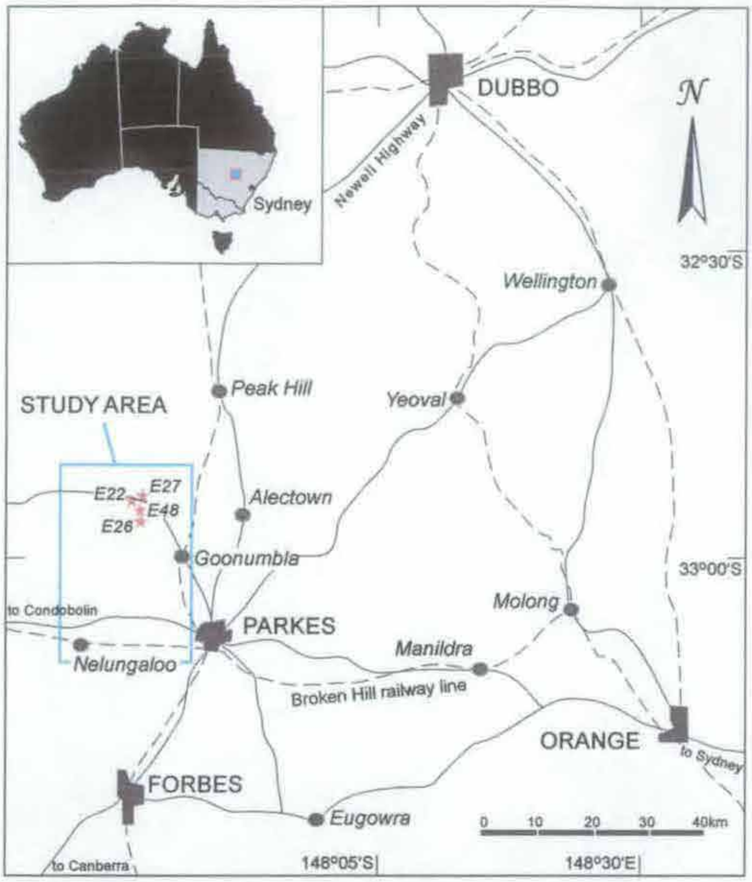

Figure 1.1 Location of the Endeavour porphyry Cu-Au deposits, New South Wales, Australia (modified after Heithersay *et al.*, 1990).

Figure 1.2 A photograph of the E27 open pit northern wall showing the complex geometry of the multi-phase quartz monzonite porphyry intrusion and the commonly stark contrast in appearance to the host volcanic sequence.

is contained in a quartz – sulphide stockwork or sheeted vein network that is centred on a pipe-like, multi-phase quartz monzonite porphyry (QMP) intrusive complex (Figure 1.2).

Parkes and the surrounding region is flat to gently undulating, with elevations between ~260 to 300m above sea level. Despite the semi-arid climate, the region is predominantly agricultural and produces wheat, canola and wool (Jones, 1985). Vehicular access to the Endeavour deposits northwest of Parkes is via well-maintained sealed roads. Railway lines to Sydney, Broken Hill, Dubbo and many other centres pass through Parkes (Figure 1.1). The Parkes shire has a population of ~15 000 and is the base for most mine-associated personnel.

1.3.2 Exploration and mining history

Copper mineral occurrences from the Parkes district have been reported since the late eighteenth century (Carne, 1908). Most of these early-reported occurrences were small oxide outcrops in the Ordovician volcanic rocks and did not record any substantial production (Jones, 1985).

In the mid 1960's, *Anaconda Company* conducted an exploration programme looking for volcanic-hosted massive sulphide deposits. During this exploration programme, *Anaconda Company* evaluated the Peak Hill Gold Mine, a high sulphidation epithermal Au deposit ~25km northeast of the Endeavour porphyry deposits that was being mined at the turn of the century. *Geopeko Limited* targeted the area for further porphyry exploration in 1971 following an appraisal of the mineral potential of the Lachlan Fold Belt in New South Wales (Jones, 1985). Their first mineral discovery was by geological mapping in 1974; a Pb-Zn skarn deposit (E7) ~15km southwest of the Endeavour porphyry Cu-Au deposits. This discovery encouraged more widespread geological and geophysical surveys of the Parkes district, which included the delineation of the regional geology beneath the extensive soil cover, by reverse air-blast (RAB) scout drilling. One of these drillholes intersected disseminated copper ore associated with weak potassic alteration in (trachy)andesites in 1976. Subsequent work on this first showing of porphyry-style mineralisation led to the delineation of the E22 bed-rock Cu-Au anomaly. The discovery diamond drillhole through this anomaly was drilled in 1977 and intersected disseminated Cu-Au ore over its entire 319m length (Jones, 1985). Subsequent drilling by *Geopeko Limited* led to the discovery of the E26 and E27 deposits and a number of sub-economic mineral occurrences, e.g. E28, E31 and E37. The E48 deposit was discovered in September 1992 by percussion drilling centred on a combined aeromagnetic/RAB drillchip geochemical anomaly (Hooper and Stoltz, 1994).

In November 1992, the *North Broken Hill Peko Limited* board approved the development of the Northparkes project to mine and process Cu-Au ore from the E22, E26 and E27 deposits; a mine life of at least 20 years is expected for the project (House, 1994). The Northparkes project commenced with open pit operations and processing oxide ores at E22 and E27, and continued onto mining and processing of sulphide ores from these two deposits before commencing underground operations at E26 in the mid 1990's. The processing plant at Northparkes heralded its first gold pour in May 1994 (House, 1994). A pre-feasibility study on the mining of E48 is currently underway. *Northparkes Mines Limited*, a company now wholly owned by *Rio Tinto*, currently mines the E22 and E27 deposits as open pits and the E26 deposit as an underground block cave mine (Figure 1.3).

Figure 1.3 An aerial view, looking north, of the operations at *Northparkes Mines* taken in December 1997, showing the E22 and E27 open pits and the pit overlying the E26 block cave mine. Also shown are the processing plant and tailings dams. Photograph courtesy of *Northparkes Mines Limited.*

1.3.3 Nomenclature

Northparkes Mines Limited and its predecessors, *North Limited* and *Geopeko Limited*, defined several Cu and Cu-Au porphyry-related mineral occurrences throughout central western New South Wales from the 1970's to the 1990's. Each occurrence is referred to as an "Endeavour" deposit or prospect, and has an accompanying number that was designated by its order in the discovery sequence, e.g. Endeavour 31 was discovered after Endeavour 28, etc. Because of this, Endeavour deposits/prospects are not restricted to the Parkes district. In this thesis, reference to the "Endeavour deposits" applies specifically to the four economic porphyry Cu-Au deposits currently being mined by (E22, E26 and E27), or at pre-feasibility stage with (E48) *Northparkes Mines Limited* unless otherwise stated. Note also that E26 was formerly known as E26 north, or E26N (House, 1994).

1.3.4 Ore reserves

A statement of identified mineral resources and ore reserves as at 30 June 1995 is presented in Table 1.1 as a summary of *Northparkes Mines* pre-production resources. Oxide Au and Cu-Au ore from the open pit operations at E22 and E27 were the first ores to be processed through the plant, although some oxide ore remains as stockpile material. The initial reserves at the E22 and E27 open pits have been mined out, however new resources have been added so that mining of the two pits is still underway. Most of the current production is from the E26 underground operations. Current (December 2001) resource and reserves figures are presented in Table 1.2.

Tonnages and grades of the E28, E31 and E37 prospects are summarised in Table 1.3 (taken from Jones, 1985).

Table 1.1 Pre-production mineral resources and ore reserves for *Northparkes Mines Limited* economic porphyry Cu-Au deposits in the Goonumbla region. eCu grade is an "equivalent Cu" grade derived from the Cu and Au grades using a commercially sensitive formula that includes forecast prices, recoveries, etc. * denotes a 0.8% eCu grade for E26 above 9800mRL and a 1.2% eCu grade for E26 below 9800mRL.

Identified Mineral Resources, June 1995					
Measured Resources					
Ore type	*Deposit*	*Cut-off grade*	*Mt*	*% Cu*	*g/t Au*
Oxide Au	E22	0.8 g/t Au	0.052	-	1.4
	E27	0.8 g/t Au	0.053	-	1.3
	Total measured		**0.105**	-	**1.4**
Oxide Cu-Au	E22	1.5% eCu	0.376	1.1	1.0
	E27	1.5% eCu	0.662	1.0	1.3
	Total measured		**1.038**		**1.2**
Indicated Resources					
Sulphide Cu-Au	E22	0.6% eCu	18.153	0.7	0.6
	E27	0.6% eCu	13.696	0.7	0.7
	E26 (above 9400mRL)	0.8% eCu	61.170	1.4	0.4
	E48 (above 9600mRL)	0.8% eCu	28.400	1.1	0.6
	Total indicated		**121.419**	**1.1**	**0.5**
Inferred Resources					
Sulphide Cu-Au	E26 (below 9700RL)	0.8% eCu	4.166	1.0	0.2
	E48 (9400 - 9600RL)	0.8% eCu	5.000	0.7	0.5
	Total inferred		**9.166**	**0.8**	**0.4**

Ore Reserves, June1995					
Proved Reserves					
Ore type	*Deposit*	*Cut-off grade*	*Mt*	*% Cu*	*g/t Au*
Oxide Au	E22 open pit	0.8 g/t Au	0.042	-	1.5
	E27 open pit	0.8 g/t Au	0.039	-	1.4
	ROM stockpile	0.8 g/t Au	0.077	-	1.4
	Total proved		**0.158**	-	**1.4**
Oxide Cu-Au	E22 open pit	1.5% eCu	0.312	1.1	1.0
	E27 open pit	1.5% eCu	0.559	1.0	1.3
	ROM stockpile	1.5% eCu	0.811	1.4	1.0
	Total proved		**1.682**	**1.2**	**1.1**
Probable Reserves					
Sulphide Cu-Au	E22 open pit	0.6% eCu	11.160	0.7	0.6
	E27 open pit	0.6% eCu	10.648	0.7	0.8
	E26 underground	0.8 / 1.2% eCu *	43.960	1.5	0.5
	E48 underground	0.8% eCu	21.500	1.1	0.5
	Total probable		**87.268**	**1.2**	**0.5**

Table 1.2 Mineral resources and ore reserves as at December 2001. eCu and * – as described for Table 1.1 above; # E26 probable reserve derived from E26 measured resource.

Identified Mineral Resources, December 2001						
Ore type	*Deposit*	*Status*	*Cut-off grade*	*Mt*	*% Cu*	*g/t Au*
Sulphide Cu-Au	E22	measured	0.5% eCu	14.1	0.6	0.5
	E27	measured	0.5% eCu	6.4	0.6	0.6
	E26	measured	0.8/0.9% eCu*	12.4	1.0	0.1
	E48	indicated	0.9% eCu	2.3	1.2	0.6
	Total resources			**35.2**	**0.8**	**0.4**

Ore Reserves, December 2001						
Ore type	*Deposit*	*Status*	*Cut-off grade*	*Mt*	*% Cu*	*g/t Au*
Sulphide Cu-Au	Oxide stockpiles	proved	0.7% eCu	2.7	1.0	0.8
	Sulphide stockpiles	proved	variable	4.7	0.6	0.4
Sulphide Cu-Au	E22 open pit	proved	0.5% eCu	1.0	0.8	0.7
	E27 open pit	proved	0.5% eCu	2.6	0.6	0.6
	E26 underground	probable#	0.8/0.9% eCu*	30.0	1.2	0.4
	E48 underground	probable	0.9% eCu	22.6	1.2	0.5
	Total reserves			**63.6**	**1.1**	**0.5**

Table 1.3 Tonnages and grades of selected Endeavour prospects (from Jones, 1985). eCu and * – as described for Table 1.1 above.

Deposit	*Cut-off grade*	*Mt*	*% Cu*	*g/t Au*
E28	0.3	8.1	0.35	0.04
E31	0.3	6.6	0.35	0.39
E37	0.3 eCu*	6.8	0.66	0.02

1.4 Previous work

Jones (1985) described the geology of many of the Endeavour mineral occurrences in the Goonumbla district, including E22, E26 and E27. Heithersay *et al.* (1990), House (1994), Heithersay and Walshe (1995) and Harris (1997) documented the general geology, the multiple intrusive phases within the QMP complex and the associated alteration – mineralisation assemblages of the E26 deposit. Multi-phase QMP complexes and associated alteration – mineralisation assemblages at E48 and E27 have been described by Wolfe (1994) and Hooper *et al.* (1996), and by Squires (1992) respectively. The magmatic origin of the sericite alteration assemblages at E48 and E26 has been described by Wolfe *et al.* (1996) and Harris and Golding (2001) respectively. Other work conducted in the Goonumbla district northwest of Parkes includes geologic descriptions of the Cu-Au mineral occurrences at E31 (Arundell, 1998) and E37 (Gordon, 1990) and a study of the fluid evolution at E48 (Howland-Rose, 1996). Studies of the E28 Cu-Au prospect and carbonate – base-metal veins associated with the E26 and E48 porphyry deposits (Kolkert, 1998) and of the E44 Pb-Zn skarn prospect west-southwest of *Northparkes Mines* operations (Jones, 1991) have also been conducted.

Regional studies include an overview of the geologic setting of the Narromine area including the Goonumbla Volcanic Complex (Bowman *et al.*, 1982). The regional geology of the Parkes district was also described by the New South Wales Department of Minerals and Energy (Clarke, 1990; Krynen *et al.*, 1990a). The Parkes Special map sheet (Krynen *et al.*, 1990b) was also produced at this time. An account of the stratigraphy and paleovolcanology of the Goonumbla Volcanics (Hall, 1993) within the GVC, a discussion on the association of the Endeavour porphyry Cu-Au deposits with shoshonitic magmatism (Müller *et al.*, 1994) and a description of the regional-scale alteration of the Goonumbla district (Radclyffe, 1995). The regional geology of the Narromine and Forbes areas has been updated by Sherwin (1996) and Duggan *et al.* (1999) respectively. U-Pb (SHRIMP) dating of a number of regional intrusions has also been completed (Butera *et al.*, 2001) and the volcanology of the GVC is currently being described (Simpson *et al.*, 2002).

Several confidential reports that include the Endeavour porphyry deposits have also been compiled in the last few years. The deposits were part of the *AMIRA* (Australian Mineral Industries Research Association) P425 project on the magmatic and hydrothermal evolution of major intrusive related gold deposits of eastern Australia, which was conducted between 1994 and 1997 (Blevin and Morrison, 1997). In 1999, *North Limited* undertook a detailed structural analysis of the Goonumbla region to provide a better understanding of the regional structural history and to identify the structural controls on Cu-Au mineral occurrences in the area (North, 1999). The most recent study that included the Endeavour deposits was the *CODES – DMR – SPIRT* New South Wales Ordovician Project (*CODES*, Centre for Ore Deposit Research, University of Tasmania; *DMR*, Department of Mineral Resources, New South Wales; and *SPIRT*, Strategic Partnerships with Industry, Research and Training scheme). The main objective of this project was to develop a new tectonic interpretation for the Ordovician mafic volcanic belts that outcrop in eastern Australia (Crawford *et al.*, 2001). The current study has had access to several of these confidential reports and any information used from them is cited accordingly.

1.5 Thesis organisation

Chapter 2 reviews the regional geological setting of the GVC hosting the Endeavour deposits and summarises these rocks in the context of the Ordovician mafic volcanic – intrusive belts of the Lachlan Fold Belt of eastern Australia. Detailed descriptions of the intrusive phases at E22, E26, E27 and E48 are presented together with an interpretation of the sequence of intrusive emplacement for each deposit in Chapter 3. Chapter 4 provides a broad paragenetic framework for the alteration and mineralisation assemblages recognised at *Northparkes* that is applicable to all four deposits. This framework is the basis for describing the temporal evolution of volatiles and the chemistry of the fluids within the systems, which are the subjects of Chapters 5 (fluid inclusions) and 6 (S isotopes). Chapter 7 focuses on the geochemistry of apatite and biotite, minerals that occur as primary accessory minerals in many of the volcanic and intrusive rocks of the GVC as well as in the hydrothermal alteration assemblages associated with mineralisation. Whole rock geochemistry is discussed in Chapter 8. The geological evolution of the Endeavour porphyry Cu-Au deposits and a genetic model for their formation are presented in Chapter 9.

CHAPTER 2

Geological Setting

2.1 Introduction

The Endeavour deposits are hosted within the Ordovician Goonumbla Volcanic Complex. The complex forms part of the Ordovician to Early Silurian Junee-Narromine Volcanic Belt, which occurs in the eastern Lachlan Fold Belt (LFB) of New South Wales, Australia (Figure 2.1). The Junee-Narromine is one of four such volcanic belts in the region, the others being the Molong and the Rockley-Gulgong Volcanic Belts to the east and the Kiandra Volcanic Belt to the southeast (Figure 2.1). In addition to the Ordovician volcanic belts, the LFB in New South Wales comprises Cambrian greenstones, Ordovician to Early Silurian quartz turbidites and Silurian to Early Devonian volcanic and sedimentary rocks (Suppel *et al.*, 1998). Silurian to Early Devonian granitoids also occur throughout the LFB. Locally some of the I-type granites are associated with Mo and Cu mineralisation, and several S-type intrusions have produced Sn and minor W mineralisation (Blevin and Chappell, 1995).

This chapter outlines the tectonic evolution of the LFB in NSW and includes a brief account of relevant mineral occurrences. A description of the geology of the Goonumbla region is also presented.

2.2 Tectonic setting

Various tectonic settings have been proposed for the Ordovician volcanic belts of NSW. These range from intraoceanic island arc (e.g. Pemberton and Offler, 1985; Blevin and Morrison, 1997), hotspot mantle plume (e.g. Fergusson and Coney, 1992), to oceanic intraplate volcanism (e.g. Wyborn, 1992). Notwithstanding the different tectonic settings proposed for the volcanic belts, most workers now agree that these volcanic belts are remnants of the Early Ordovician to Early Silurian Macquarie Island Arc (Glen and Walshe, 1999).

The LFB is interpreted to have formed by complex accretionary processes from Cambrian to Carboniferous times related to the closure of a back-arc basin (the Wagga Marginal Basin; Figure 2.1; Scheibner and Basden, 1998) and associated collision of an oceanic arc (the Macquarie Arc; Figure 2.1; Glen *et al.*, 1998) with the proto Pacific margin of Gondwanaland (Gray and Foster, 1997; Glen *et al.*, 1998; Foster *et al.*, 1999; Crawford, 2001a). The Macquarie Arc is believed to have been accreted onto the margin during the Early Silurian as a single arc (Glen *et al.*, 1998) and its current geometry is attributed to post-accretion disruption and dislocation by extension or sinistral strike-slip faulting (Glen, 1992; Wyborn, 1992).

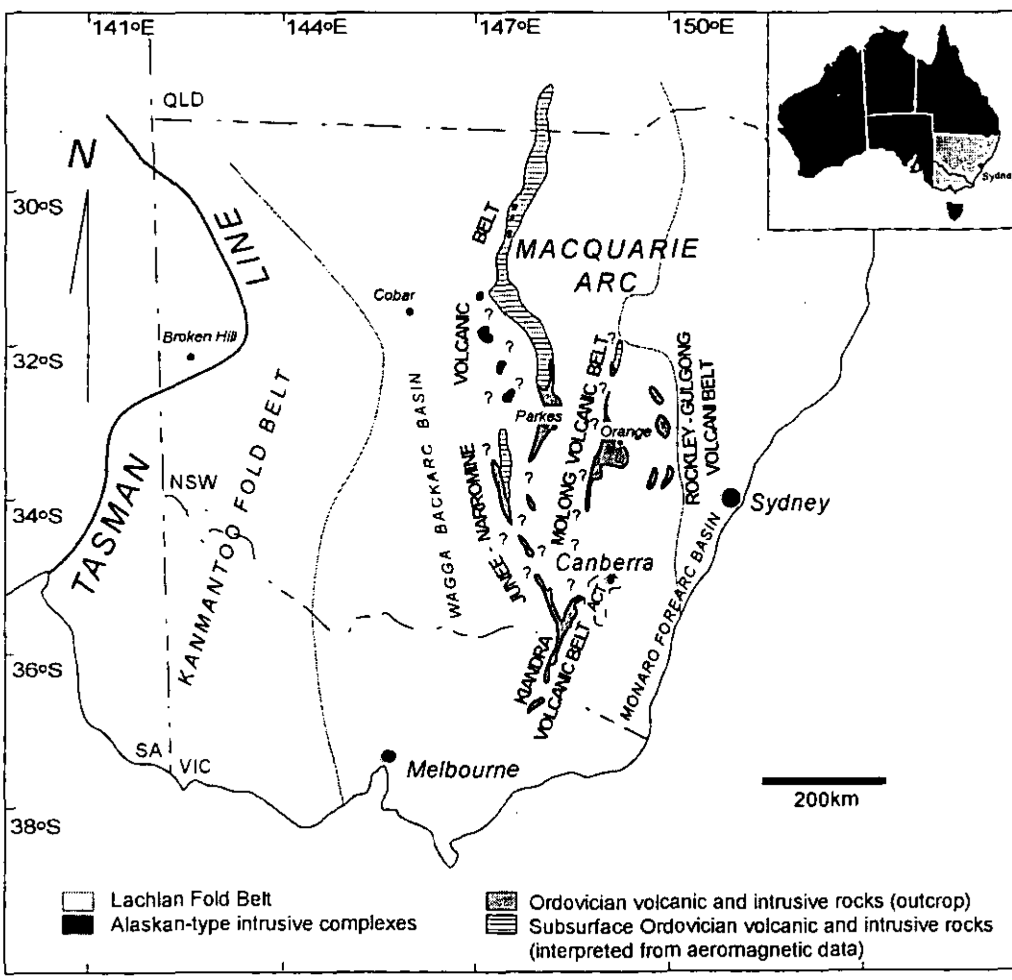

Figure 2.1 Ordovician to Early Silurian volcanic (and intrusive) rocks in the eastern Lachlan Fold Belt of New South Wales (modified from Scheibner and Basden, 1998).

2.2.1 Precambrian to pre-Ordovician Volcanic Belts

Archaean and Lower to Middle Proterozoic cratonic rocks are unknown east of the Tasman Line (Figure 2.1). The oldest rocks preserved in the eastern LFB are the widespread Early Ordovician to Early Silurian successions of quartz-rich turbidites and broadly contemporaneous mafic volcanic rocks, cherts and limestones (Wyborn, 1992). Because of this, the nature of the basement in central and eastern NSW is not well understood. Crawford and Direen (1998) have interpreted the Late Proterozoic tectonic history of the eastern passive margin of Gondwanaland based on geophysical data, and a synthesis of their findings is presented here as an introduction to the current hypothesis regarding the tectonic setting, and thus possible nature of the basement in the eastern LFB.

Precambrian evolution of the passive margin along eastern Gondwanaland started ~600Ma ago, with mixed carbonate-clastic sedimentation into an extensive marginal basin that led to a ribbon-like continental slice being rifted from cratonic Australia. Evolving rift magmatism, represented by alkalic to tholeiitic volcanism, led to the formation of a volcanic passive margin by 600 – 580Ma (Figure 2.2a; Crawford and Berry, 1992).

An active plate margin with east-directed subduction developed along eastern Gondwanaland at ~525 – 520Ma, when part of the passive volcanic margin began rifting away from the craton to form the Kanmantoo Trough marginal sea (Figure 2.2b; Crawford and Direen, 1998). Further outboard a proto-arc was established, while inboard, sedimentation into the Kanmantoo Trough was initiated (Figure 2.2b).

Sedimentation continued for ~10 million years before the onset of the tectonothermal deformation of the Delamarian Orogeny (~515Ma), indicating a rapid transition from tensional to compressional tectonics (Figure 2.2c) along the eastern Gondwanaland margin (Crawford and Direen, 1998). The Delamarian Orogeny probably reflects initial collision of the intra-oceanic arc with a continental ribbon (leading to emplacement of bonninitic ophiolites), and subsequent ongoing deformation, exhumation of underthrust crust and syn- to post-collisional magmatism (Crawford and Berry, 1992).

There has been considerable speculation as to what happened between the end of the Delamarian Orogeny in the Late Cambrian and the onset of the Benambran Orogeny in the Late Ordovician to Early Silurian, specifically with regards the tectonic environment in which the volcanic and turbiditic sequences developed. Chappell *et al.* (1988) used granitoid chemistry to distinguish nine distinct basement terranes in the LFB. They interpreted these basement terranes to represent fragments of the Late Proterozoic or Early Palaeozoic continental crust (see also Rutland, 1976). Suppel and Scheibner (1990)

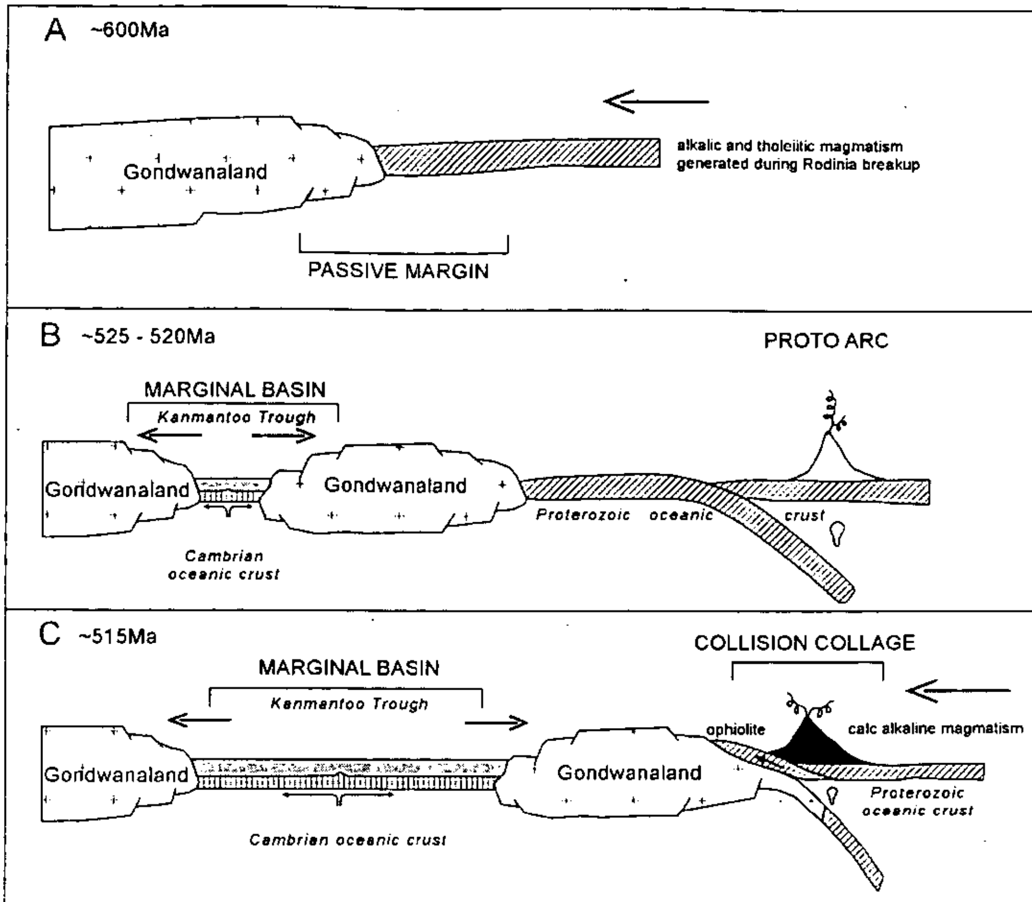

Figure 2.2 Schematic sketches showing the proposed tectonic evolution of the eastern coast of Australia during Precambrian to pre Ordovician volcanic belt times (modified after Crawford and Berry, 1992 and Crawford and Direen, 1998).

and Heithersay (1991) suggested that Cambro-Ordovician sediments of the Girilambone Group and Jindalee Group form the basement to the Ordovician volcanic rocks in the eastern LFB near Parkes. Crawford and Direen (1998) and Direen (1999) postulated that following this collision by Late Cambrian times, the subduction zone "jumped" eastwards during the Early Ordovician to begin a new island arc, the Macquarie Arc. Depending on the polarity of the new subduction zone, the basement onto which the Macquarie Arc was constructed could have been Latest Neoproterozoic crust generated during the 600 – ~525Ma rifting event (see also Crook, 1980), Kanmantoo Trough turbidites (see also Heithersay *et al.*, 1990), or a sliver of rifted-off cratonic Australian continental crust (see also Scheibner, 1973).

Determining the nature of the basement to the Ordovician volcanic belts was a major focus of the NSW SPIRT Project, which was conducted between 1998 and 2000. This project reviewed, built-upon and expanded previous hypotheses concerning the nature of the basement and the tectonic setting and included new research to develop the most recent and robust framework of the tectonic evolution of the Ordovician volcanic belts in NSW to date. The evolution of the Early Ordovician to Early Silurian volcanic belts in the LFB of NSW presented below is based on this research (Crawford, 2001a).

2.2.2 *Early Ordovician to Early Silurian*

The collective work assembled during the SPIRT project led Crawford (2001a) to suggest that west-directed subduction and the initiation of the Macquarie Arc commenced at ~485Ma beneath the arc-continent collisional collage that formed during the Delamarian Orogeny (Figures 2.2c and 2.3a). This collage, the basement to the Macquarie Arc, included allochthonous sheets of Middle Cambrian fore-arc derived ophiolites of the earlier subduction system (greenstones) that had been thrust onto an east-facing passive margin around ~510Ma. Crawford (2001a) postulated that the subducting oceanic crust at this time was that which formed during the rifting of a microcontinental block from eastern Gondwana at ~600Ma (cf. Figure 2.2a).

A sharp decrease in magmatism in the Macquarie Arc from ~475Ma to ~465Ma, and the accumulation of sediments in a continuously deepening basin were interpreted to reflect arc subsidence in response to rollback of the trench that accompanied oceanward fallback of the subducting slab. This rollback is thought to have initiated the opening of a backarc basin (the Wagga backarc basin) at ~475Ma (Figure 2.3b), with associated regional subsidence, postulated to have been caused by the Macquarie Arc splitting so that the Junee-Narromine Volcanic Belt became the eastern, oceanward part of the arc at this time.

With continued rifting and subsidence of the backarc basin, Crawford (2001a) proposed that renewed magmatism in the Middle Ordovician (~465 – 450Ma) saw the building of a new arc atop the rifted Early Ordovician arc and its underlying collisional collage some distance to the east of the spreading centre (Figure 2.3c). Magmas erupted at this stage were high-K calc alkaline to shoshonitic in composition.

Crawford (2001a) suggested that widespread limestones record shoaling of the growing Macquarie Arc at ~450Ma. It is thought that the west-directed subduction was disturbed at this time by the arrival of a seamount (Glen *et al.*, 1998) or possibly a microcontinental block (Crawford, 2001a), which effectively blocked the subduction zone (Figure 2.3d). In response to the continued convergence, which was taken up by a brief episode of east-directed subduction of the young hot Wagga backarc crust, the Macquarie Arc was uplifted.

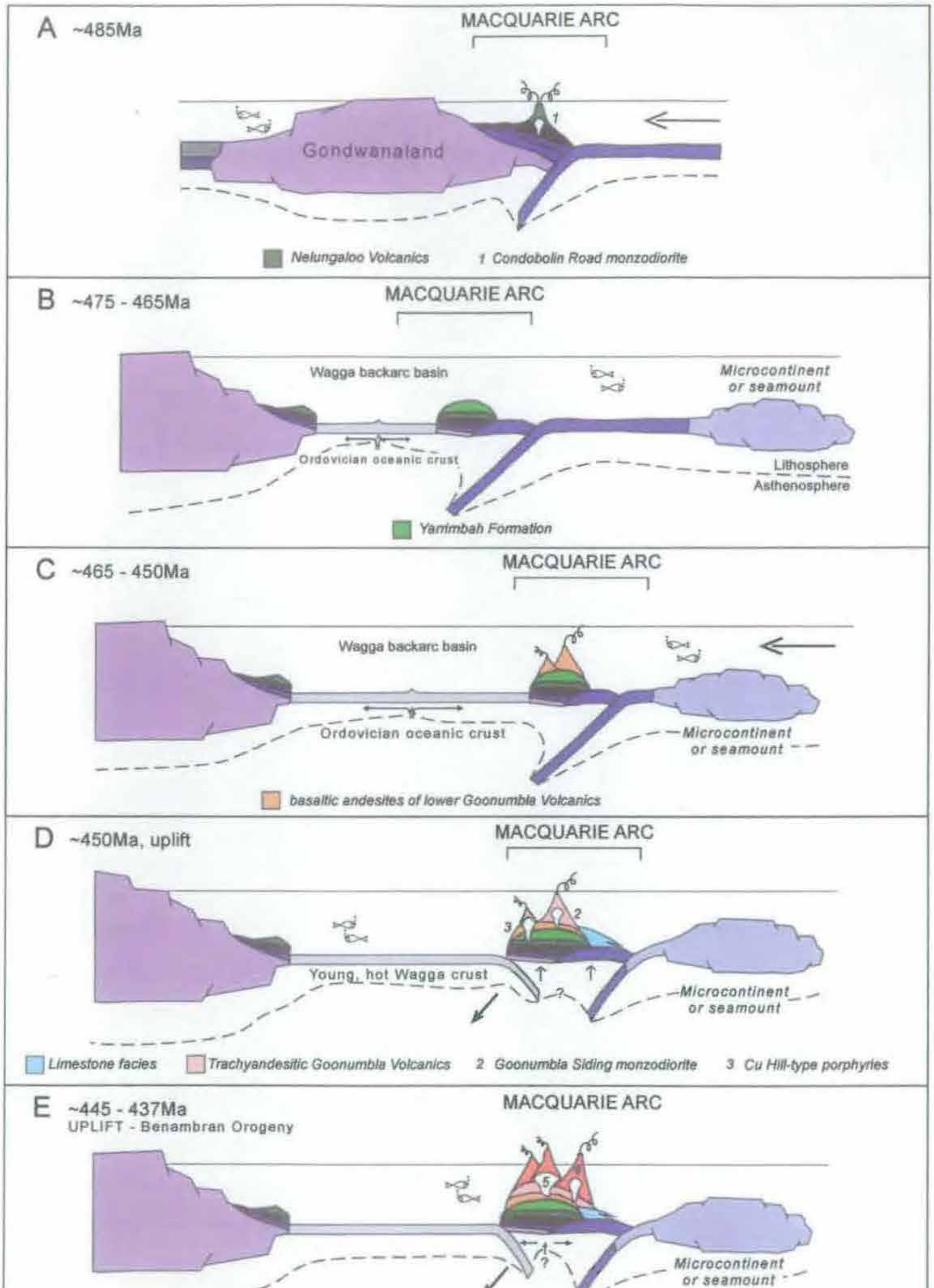

Figure 2.3 Schematic evolution of the Macquarie Arc (modified from Crawford, 2001a). Note that the sketches are not drawn to scale and are vertically exaggerated for detail.

This uplift and shoaling of the arc is reflected in the accumulation of widespread limestones at ~450Ma, and emplacement of a short-lived but distinctive suite of low- to medium-K dacitic porphyries with many characteristics of melts derived from subducted basaltic oceanic crust.

By ~445Ma, magmatism had reverted to its pre-disturbance, evolving shoshonitic character. However, by this time, volcanic and intrusive rocks were more felsic and evolved than previously, perhaps due to crustal thickening accompanying the microcontinent collision. This magmatism may have been triggered by regional extension of arc lithosphere (Figure 2.3e), analogous to the eruption of Late Miocene shoshonites in Fiji following the rotation of arc lithosphere away from active subduction (Crawford, 2001a). The extensional event is inferred to have been short-lived (~445 – 437Ma), and ceased with the abrupt onset of the Benambran Orogeny. Mantle-derived shoshonitic magmas were probably no longer able to reach the upper crust during the compressional tectonic setting of the Benambran Orogeny and thus cooled deep in the crust. During extension in the Late Silurian, these shoshonitic rocks were partially melted to produce the widespread S-type granites in the area west of the main Macquarie Arc (Sun and Wyborn, 1994).

The economic Cu-Au porphyry and related mineral occurrences in the Macquarie Arc rocks are associated with syn-uplift monzonitic and quartz monzonite intrusions that are Latest Ordovician in age (Walshe *et al.*, 1995; Wyborn, 1996; Holliday *et al.*, 2002). Although these intrusions occur throughout the Macquarie Arc, few are associated with notable mineralisation. Significantly, those that are, occur where there are major piles of felsic lavas, which have been interpreted as volcanic centres that appear to have been loci for magmatic – hydrothermal activity associated with the porphyry deposits of the Macquarie Arc. Two examples of such volcanic centres are the Wombin Volcanics of the Junee-Narromine Volcanic Belt, which host the Endeavour deposits (Crawford, 2001a) and the Forest Reefs Volcanics in the Molong Volcanic Belt, which host the Cadia deposits (Holliday *et al.*, 2002).

2.2.3 Post-Ordovician history of the Lachlan Fold Belt

After the Late Ordovician – Early Silurian Benambran Orogeny, the LFB was affected by three major deformation events: 1) the Early Devonian (~410Ma) Bowning-Bindi deformation; 2) the Devonian (~400 – 395Ma) Tabberabbaran Orogeny and 3) the Early

Carboniferous (~350Ma) Kanimblan Orogeny (Suppel and Scheibner, 1990; Scheibner, 1993; Gray and Foster, 1997).

Subsequent to the Benambran Orogeny, an Early to Middle Silurian extension event affected mainly the eastern portion of the LFB. This led to marked crustal thickening across the fold belt and caused a change from open-ocean, deep-marine conditions along the Gondwanaland continental margin in the Late Ordovician, to a mixed continental, shallow-deep marine basin with parts emergent in the Late Silurian (Gray and Foster, 1997). East-west folding and metamorphism affected these rocks during the next tectonic event, the Bowning-Bindi Orogeny (Gray and Foster, 1997; Scheibner and Basden, 1998). Renewed extension and the formation of epicontinental basins with associated quartz sandstone and conglomerate sedimentation, and the intrusion of widespread S- and I-type granite plutons throughout the LFB followed this orogeny during the Devonian Tabberabbaran Orogeny (Gray and Foster, 1997). While this Devonian deformation caused thrusting in the east, it caused extension in the western LFB (Scheibner, 1993) and a "pre-craton" stage in the evolution of the eastern LFB was abruptly terminated with the onset of the widespread thrusting that characterises the Tabberabberan Orogeny. Following the Tabberabberan Orogeny, the diachronous onset of a transitional tectonic setting, the Kanimblan Orogeny, resulted in the conversion of the LFB into a neocraton (Scheibner, 1993). Late Carboniferous to Holocene platformal sediments accumulated on the neocraton created by the Kanimblan Orogeny to end the formation of the LFB (Scheibner, 1993). Much of the pre-Carboniferous LFB is buried beneath these later sediments.

Of these tectonic events, the eastern LFB hosting the Macquarie Arc was most strongly affected by the Early Carboniferous Kanimblan Orogeny, which produced tight, north-south trending folds in the Silurian to Devonian sequences and both east- and west-dipping thrusts in the Ordovician turbidites and volcanic rocks (Gray and Foster, 1997). Glen (1992) noted that some of the north-south trending structures must also have been active during the earlier tectonic events in the eastern LFB and that Early Silurian east-trending folds and thrusts occur throughout the eastern LFB. Despite the multiplicity of deformation events to affect the LFB after the Late Ordovician, the Ordovician volcanic belts remain largely undeformed. It appears that they acted as buttresses during the deformation events, around which the Ordovician to Devonian flysh were strongly deformed (Scheibner, 1993).

Several major west-northwest trending transverse structures have been recognised in the LFB, the most significant being the Lachlan Transverse Zone (LTZ: Figure 2.4; Glen and Wyborn, 1997; Glen and Walshe, 1999). Glen and Walshe (1999) proposed that the LTZ represents the continuation of a fundamental cratonic structural weakness that propagated into the Neoproterozoic to Palaeozoic oceanic crust of the LFB. The intersection of the Ordovician volcanic belts in the eastern LFB with these transverse zones appears to have provided a locus for the emplacement of shoshonitic magmas and related porphyry Cu-Au deposits in the Macquarie Arc.

2.3 Other Macquarie Arc-related mineral occurrences

In addition to the four economic Endeavour deposits near Parkes, the Junee-Narromine Volcanic Belt hosts sub-economic porphyry Cu-Au mineral occurrences at E20, E28, E31 and E37 in the Parkes district (Figures 2.4 and 2.5) and at Lake Cowal (E39) and Marsden (Downes and Burton, 1999; Figure 2.4). Pb-Zn skarn mineralisation occurs at E6, E7 and E44 (Jones, 1991) in the Parkes area (Figure 2.4) and high sulphidation epithermal Au mineralisation occurs at Peak Hill north of Parkes (Degeling *et al.*, 1995), Lake Cowal (E35; Downes and Burton, 1999) and Gidginbung (Lindhorst and Cook, 1990), north of Temora, are also hosted in Junee-Narromine Volcanic Belt rocks (Figure 2.4). In addition to high sulphidation epithermal and skarn related mineralisation, Lake Cowal hosts E42, a mesothermal Au deposit that shows a mineralisation style intermediate between porphyry- and epithermal-styles (McInnes *et al.*, 1998).

The Ordovician Molong Volcanic Belt, east of the Junee-Narromine Volcanic Belt hosts the Cadia group of Cu-Au porphyry-skarn mineral deposits (Figure 2.4), the largest cluster of known deposits in terms of contained metal in all of the Macquarie Arc related rocks (Holliday *et al.*, 2002). The Molong Volcanic Belt also hosts the Junction Reefs Fe-Au skarn deposit (Gray *et al.*, 1995) and the Cargo (Richardson, 1976) and Copper Hill (Scott, 1978) porphyry mineral occurrences (Figure 2.4).

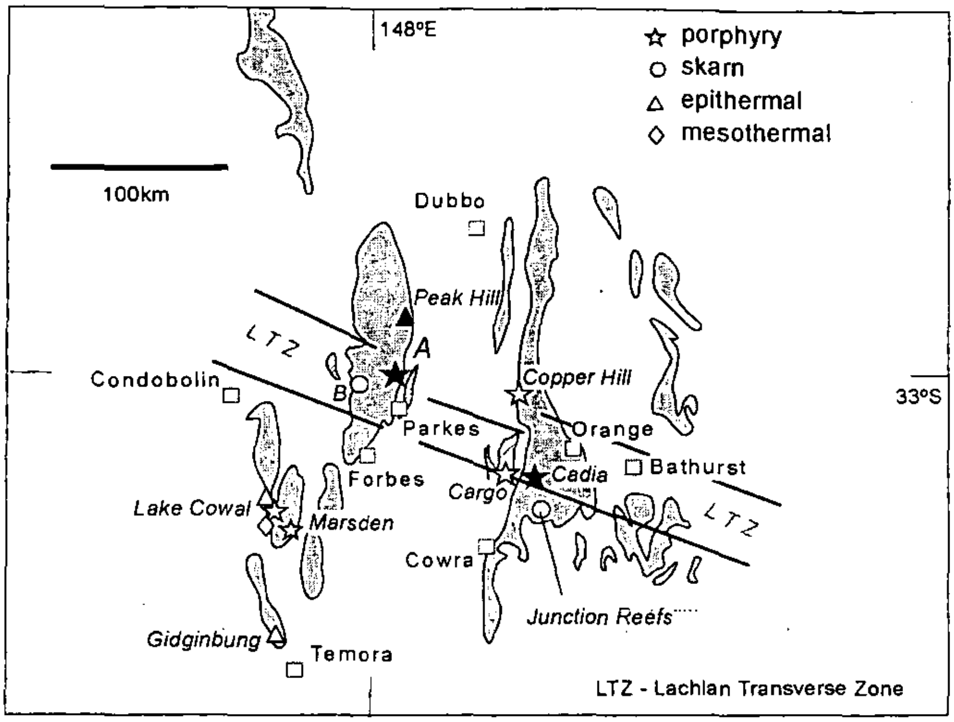

Figure 2.4 Cu-Au mineral occurrences in the Macquarie Arc related rocks of the eastern LFB. Open symbols represent sub-economic occurrences; A – E22, E26, E27, E48 economic and E20, E28, E31 and E37 sub-economic porphyry Cu-Au deposits; B – E6, E7 and E44 skarn deposits. The Lachlan Transverse Zone (LTZ) is a transverse crustal lineament that appears to have controlled the distribution of the Late Ordovician porphyry Cu-Au deposits (Glen and Walshe, 1999).

2.4 Local geology

2.4.1 The Goonumbla Volcanic Complex

2.4.1.1 Nelungaloo Volcanics

The oldest rocks exposed in the Goonumbla region of the Junee-Narromine Volcanic Belt are the Nelungaloo Volcanics (Figure 2.3a), the basal units of the Early Ordovician to Early Silurian Goonumbla Volcanic Complex (Sherwin, 1999). The Nelungaloo Volcanics crop out in the core of the Forbes Anticline (Figure 2.5) and, assuming no structural repetition, have a thickness of at least 650m (Krynen *et al.*, 1990a). They comprise a sequence of mainly plagioclase + clinopyroxene + olivine + Fe-Ti oxide-phyric coherent andesites that are overlain by volcanic conglomerate, coarse-grained volcanic sandstone and the sediments of the Yarrimbah Formation (Figure 2.3b: Krynen *et al.*, 1990a; Heithersay and Walshe, 1995; Duggan *et al.*, 1999). Monzodiorite intrusions in the Nelungaloo Volcanics crop out in two areas. The first, referred to as the "Condobolin Road monzodiorite", crops out on the Condobolin Road ~10km west of Parkes and the second is a series of outcrops northeast and southwest of Nelungaloo (Figure 2.5). These monzodiorites are dark green/grey, coarse-grained and equigranular in their interiors, but weakly to strongly porphyritic at their margins. They contain abundant (up to 80%), euhedral plagioclase, augite (~15%) and interstitial alkali feldspar (5 – 10%). Early Ordovician fossil ages from the Yarrimbah Formation (Krynen *et al.*, 1990a; Glen *et al.*, 2001) and a U-Pb (SHRIMP) age of 484.3 ± 2.9Ma from the Condobolin Road monzodiorite that has intruded the base of the unit (Butera *et al.*, 2001), constrain the age of the Nelungaloo Volcanics as Early Ordovician.

2.4.1.2 Goonumbla Volcanics

Separated from the underlying Nelungaloo Volcanics by a low-angle unconformity, the middle unit of the GVC, the Goonumbla Volcanics, is exposed on the western limb of the Forbes Anticline and in the core of the Milpose Syncline (Figure 2.5; Krynen *et al.*, 1990a). A narrow strip of Goonumbla Volcanics equivalent rocks on the eastern limb of the Forbes Anticline abuts the Parkes Thrust east of "Goonumbla" (Figure 2.5). The Goonumbla Volcanics are a 2.5 – 4km thick sequence of mainly basaltic andesitic to trachyandesitic coherent and less abundant volcaniclastic rocks. The basal unit of the Goonumbla Volcanics, an apatite-free, olivine-bearing basaltic andesite lava (Figure 2.3c), is volumetrically minor when compared to the trachyandesitic lavas and associated volcaniclastic conglomerates that comprise the bulk of the Goonumbla Volcanics. The trachyandesitic lavas overlying the basal unit (Figure 2.3d) are a sequence of massive to autobrecciated trachyandesitic lavas that contain ubiquitous plagioclase + augite + Fe-Ti oxides + apatite phenocrysts in a variably glassy matrix (Crawford, 2001b). Many of the massive examples may actually be shallow, conformable sills based on the local occurrence of pepperitic margins (Simpson and Cas, 1999; Kolkert, 1998). Intrusive rocks into the Goonumbla Volcanics are mainly monzodioritic in composition (Krynen *et al.*, 1990a; b), and occur at three main localities – Cardiff, Goonumbla Hill and Goonumbla Siding (Figure 2.5). These monzodiorite intrusions are fine- to medium-grained and massive to weakly porphyritic in texture. They are petrographically similar to the monzodiorite bodies that intruded the Nelungaloo Volcanics; however, they generally contain a higher proportion of interstitial alkali feldspar (Crawford, 2001b). A monzodiorite intrusion at the base of the Goonumbla Volcanics near the Goonumbla Siding (Figure 2.5) has been dated, using U-Pb (SHRIMP), at 450.8 ± 4.2Ma (Butera *et al.*, 2001), constraining a Mid to Late Ordovician age for the lower Goonumbla Volcanics. Fossils from the Goonumbla Volcanics as a whole yield Darriwilian to Early Bolindian ages (Krynen *et al.*, 1990a; Percival, 1998), indicating that the upper Goonumbla Volcanics are probably Late Ordovician in age.

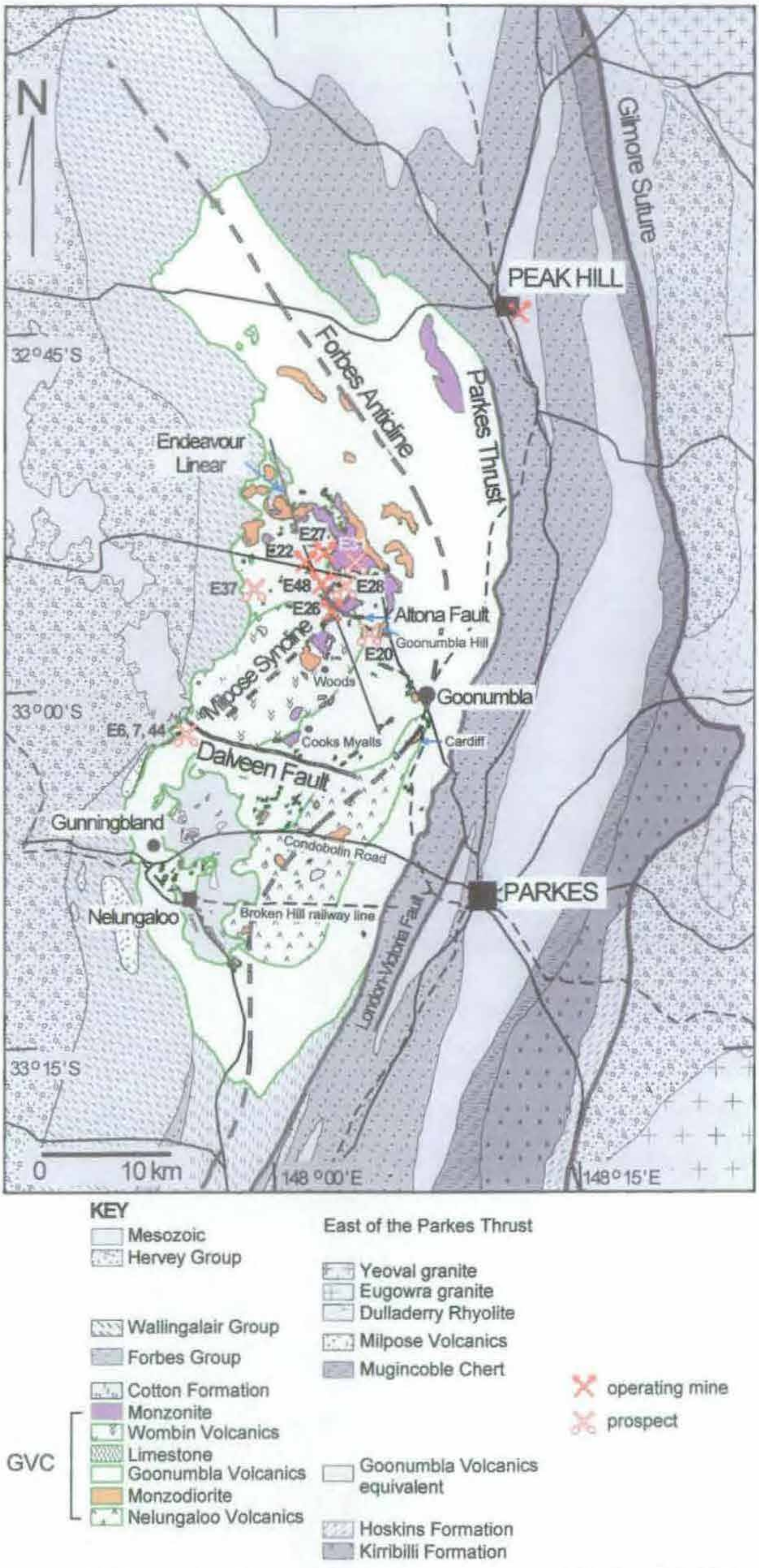

Figure 2.5 Local geology of the Goonumbla region (modified from Heithersay *et al.*, 1990 and Heithersay and Walshe, 1995).

2.4.1.3 Wombin Volcanics

Conformably overlying the Goonumbla Volcanics are the intermediate to felsic Wombin Volcanics (Krynen *et al.*, 1990a), which crop out on both limbs of the Forbes Anticline and in the southwestern part of the Milpose Syncline (Figure 2.5). They comprise a 700 – 1000m thick sequence of typically dark red ignimbrites, polymictic volcanic breccia and other volcanic sediments with less abundant porphyritic trachyandesitic and flow-banded trachytic lavas (Bowman *et al.*, 1982; Simpson *et al.*, 2000; Simpson *et al.*, 2002). The colour of the Wombin Volcanics is thought to be due to the presence of pervasive microcrystalline haematite distributed through the feldspar phenocrysts and groundmass components. These dark red units are typically glassier than other volcanic rocks in both the Goonumbla and Nelungaloo Volcanics. Simpson *et al.* (2000) interpreted the Goonumbla and Wombin Volcanics as a thick (several km), subaqueous volcaniclastic apron that formed on the flanks of shallow marine to possibly subaerial stratovolcano during the Mid to Late Ordovician. The presence of ignimbrites and trachyte lava has been interpreted by Simpson *et al.* (2000) to indicate voluminous explosive eruptions and sector collapse on possibly subaerial part of the volcano hosting the subaqueous volcaniclastic apron.

Numerous monzonite and quartz monzonite bodies have intruded the Wombin Volcanics. These intrusions contain mainly plagioclase + augite phenocrysts with subordinate alkali feldspar and interstitial biotite, apatite, alkali feldspar and Fe-Ti oxides (and quartz in the more felsic examples). They include the quartz monzonite porphyry (QMP) pipes associated with the Endeavour deposits. The groundmass of these intrusions typically comprises microcrystalline to aphanitic dark red alkali feldspar and quartz. The age of the Wombin Volcanics is not well constrained, however, samples described as "andesite" and "gabbro" in Krynen *et al.* (1990a) yielded Latest Ordovician to Earliest Silurian K-Ar ages. In addition, zircon grains from two monzonite intrusions, the "Woods" monzonite and a monzonite dyke ~3km east of Cooks Myalls (Figure 2.5), have yielded U-Pb (SHRIMP) ages of 439.1 ± 4.5Ma and 438.9 ± 4.7Ma respectively (Butera *et al.*, 2001). An $^{40}Ar/^{39}Ar$ isotopic age of 439.2 ± 1.2Ma from white mica alteration associated with mineralisation at E26 was used by Perkins *et al.* (1990) to propose that quartz monzonite porphyry intrusion and mineralisation/ alteration were coeval. The two U-Pb (SHRIMP) ages of Butera *et al.* (2001) corroborate this hypothesis.

2.4.2 Volcanic rocks east of the Parkes thrust

The deep marine volcaniclastic and extrusive/shallow intrusive shoshonitic rocks of the Nash Hill, Mingelo, Parkes, Back Yamma and Daroobalgie Volcanics (Krynen *et al.*, 1990a; Sherwin, 1996; Crawford, 2001b) east of the Parkes Thrust (Figure 2.5) are generally considered as equivalents of the Goonumbla Volcanics. Similarities in stratigraphic position, geochemical characteristics and Late Ordovician to Early Silurian ages of these units with the Goonumbla Volcanics support this interpretation (Crawford, 2001b). These volcanic units are not discussed further in this thesis.

2.4.3 Cover sequence

Sedimentary rocks of the Late Ordovician to Early Silurian Cotton Formation conformably overlie the GVC (Figure 2.5) southwest of Parkes (Krynen *et al.*, 1990a). Late Silurian deep-water sediments of the Forbes Group, Early Devonian terrestrial sediments and volcanic rocks of the Wallingalair Group and Milpose Volcanics and Devonian quartz-rich sediments of the Hervey Group (Krynen *et al.*, 1990a) also crop out in the Goonumbla district (Figure 2.5); the latter define the low ridges and hills that flank the city of Parkes.

2.4.4 Structure and metamorphism

Most of the GVC has been metamorphosed to prehnite – pumpellyite or lower greenschist facies, with rare occurrences of zeolite facies rocks (Heithersay *et al.*, 1990; Gray and Foster, 1997). The vertical attitude and undeformed nature of the Late Ordovician QMP intrusions associated with mineralisation at the Endeavour deposits, and the shallow dip of the host sedimentary rocks imply that post-mineralisation deformation events had only a minor effect on the GVC in the vicinity of the Endeavour deposits (Jones, 1985; Arundell, 1997). These minor effects of post-Ordovician deformation in the Goonumbla region are described below.

2.4.4.1 Local faulting and folding

Northeast-trending folds that have no associated axial planar cleavage are some of the oldest preserved structures in the Goonumbla region. One of these folds is the Forbes Anticline (Figure 2.5; North, 1999). The fact that the vertically attenuated, mineralised QMP intrusions have intruded shallowly-dipping volcanic strata implies that the folding occurred prior to intrusion in the Late Ordovician. Conjugate east-southeast-trending dextral and north-trending sinistral ductile shear zones are associated with this northeast-trending folding. The Dalveen Fault (Figure 2.5), which has a dextral offset of <2km (Simpson and Cas, 1999), is an example of such a dextral shear zone.

An episode of fracturing, QMP emplacement and vein formation followed the folding and faulting. Jones (1985) suggested that the preferred orientation of intrusive activity in the Endeavour deposits possibly indicates that a deep-seated crustal weakness was active at the time of QMP emplacement. In addition, it has been established that the Goonumbla region was probably under E-W extensional stresses at the time of ore formation and the QMP pipe-like intrusions were probably emplaced at the intersection of major northwest- and northeast-trending fracture zones (Harris, 1997; North, 1999; Crawford, 2001a).

Early Devonian east-west shortening, with associated broad open folding and jointing, had little effect on the GVC. However, the north-northeast-trending Parkes Thrust east of the GVC is interpreted as major crustal suture active since the Late Ordovician and reactivated during the Bowning-Bindi Orogeny (Krynen *et al.*, 1990a; Scott, 1999). Most of the deformation associated with this latter episode of tectonism affected the area east of the Parkes Thrust within a zone of high-strain that was undergoing dextral transpression. Rocks east of the Parkes Thrust were tightly folded and faulted and are interpreted to have been uplifted relative to the units west of the structure (Sherwin, 1996; Scott, 1999). West of the Parkes Thrust, the deformation resulted in the formation of broad regional open north-trending folds, forming basin and dome interference structures where they were superimposed on the Late Ordovician folding (Scott, 1999). The Milpose Syncline, as defined by Jones (1985), is an example of one of these basin structures (Figure 2.5).

In the late Early Devonian, deformation only affected the northern portion of the GVC resulting in the formation of a dextral north-trending set and an east-trending sinistral set of strike-slip faults (Glen, 1992; Stuart-Smith *et al.*, 1992; North, 1999). Close to Peak Hill, open northwest-trending folds with well-developed axial planar crenulation cleavage are attributed to this late Early Devonian deformational event (Sherwin, 1996).

Early Carboniferous deformation in the GVC resulted in the formation of new conjugate strike-slip faults and reverse reactivation of the Parkes Thrust during the Kanimblan Orogeny (Fergusson and Coney, 1992b; North, 1999). Conjugate faults are observed throughout the Goonumbla region, with displacements commonly in the order of a few 100's of metres and more rarely up to 2km. These strike-slip faults are concentrated around the edges of the GVC, implying that the GVC acted as a buttress that partitioned strain to the northeast and southwest (Scheibner, 1993; North, 1999). Other east-southeast-trending faults are interpreted to be part of this tectonic episode. East-southeast-trending sinistral faults on the northern wall of the E27 pit and the Altona Fault that truncated mineralisation at E28 and E48 (Figure 2.5) are interpreted as Early Carboniferous faults (North, 1999).

2.4.4.2 Lineaments

A number of prominent lineaments are obvious on aeromagnetic data from the Parkes district. Many of these lineaments parallel the major fault sets described above; however, a few occur as "corridors" that include most of the mineral deposits, e.g. the Endeavour Linear (Figure 2.5: Jones, 1985; Heithersay *et al.*, 1990). The fact that most of the ore-related intrusions lie along these aeromagnetically-defined lineaments indicates a structural control on the emplacement of quartz monzonite porphyries associated with Cu-Au mineralisation (House, 1994). This hypothesis is supported by the presence of strong phyllic alteration assemblages in the rocks that mark both the northern and southern extensions of the Endeavour Linear (Heithersay *et al.*, 1990).

2.5 Summary

The key elements of the Ordovician Macquarie Arc with respect to high grade Cu-Au porphyry deposit formation in the Goonumbla and Cadia districts are Late Ordovician shoshonitic magmatism in areas where transverse structures (e.g. the Lachlan Transverse Zone) have cut the Macquarie Arc. Major piles of felsic lavas accumulated in what have been interpreted as shallow marine to possibly emergent volcanic centres where these transverse intersected the arc. Porphyry-style mineralisation in the Ordovician volcanic belts of NSW is associated with subvolcanic intrusions within these volcanic centres.

Although several major tectonic events have affected the LFB, the largely undeformed nature of the Ordovician volcanic belts implies that they acted as buttresses during subsequent ductile deformational events. Syn QMP-intrusion brittle structures were important in the GVC in terms of localising intrusive activity (e.g. the Endeavour Linear and northwest- and northeast-trending fractures). In addition, brittle movement on post QMP-intrusion structures caused disruption and dislocation of some of the minerals deposits (e.g. the low angle Altona Thrust truncating mineralisation at E28 and E48).

CHAPTER 3

Intrusive History

3.1 Introduction

The QMP complexes central to the Endeavour deposits are vertically attenuated, pipe-like intrusive bodies. They are associated with mineralisation and alteration assemblages that have been interpreted to have formed by the late-stage release of magma and volatiles on the margins of a larger, zoned pluton inferred to occur beneath current drilling depths (Heithersay, 1994; Heithersay and Walshe, 1995; Blevin and Morrison, 1997). Multiple intrusive phases have been recognised within these QMP complexes previously (e.g. Heithersay *et al.*, 1990; Wolfe, 1994 and Harris, 1997), however, these studies have generally focused on single deposits and have not compared the intrusive phases of one deposit with those of the others. Since there are many similarities between the QMP complexes central to each of the Endeavour deposits (Jones, 1985; House, 1994), a detailed study of the intrusive relationships, in conjunction with the grade distribution patterns has been undertaken to determine which of the intrusive phases were related to ore formation and which were not.

This chapter initially gives brief geological descriptions of the deposits in terms of host rock characteristics and structural features. Thereafter it focuses on describing, in detail, the eight intrusive phases recognized at E22, E26, E27 and E48 in the interpreted order of emplacement. A discussion of the correlations between metal grades and individual intrusions concludes the chapter.

3.2 Deposit geology

The four Endeavour deposits are situated within 4km of each other along an aeromagnetically-defined linear structure, the Endeavour Linear (cf. Figure 2.5). E26 is the southern-most deposit (Figure 3.1). E48 is situated approximately midway between E26 and E22 and E27 ~1.5km north of E26 (Figure 3.1). The two open pit deposits, E22 and E27, are situated ~4km north of E26, ~1km apart, with E22 situated west of E27 (Figure 3.1).

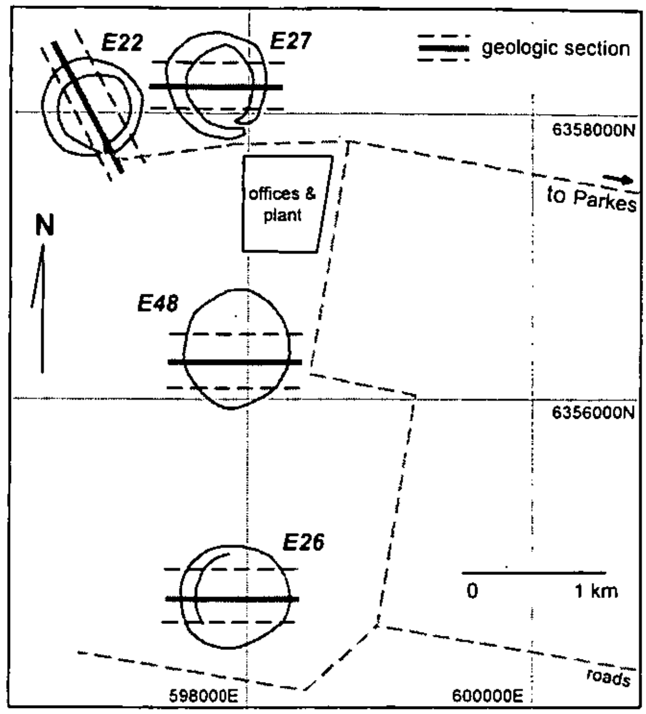

Figure 3.1 A location plan of the four deposits with respect to one another (Australian Map Grid co-ordinates) and the positions of the geologic sections through each deposit. The dashed lines parallel to the section lines represent the width of projection of the sections.

The Wombin Volcanics of the GVC host the E22, E26, E27 and E48 deposits (Simpson *et al.*, 2000; Crawford, 2001b). Thick (>300m) trachyandesite units interbedded with thin (<5M) massive to weakly-bedded, fine-grained volcanic sandstone units are the principal host rocks at E22 and E27 (Jones, 1985; Heithersay *et al.*, 1990). Similar host rocks are observed at E48 (Wolfe, 1994), whereas trachytic and trachyandesitic volcaniclastic sedimentary rocks and lavas host the E26 deposit (Heithersay *et al.*, 1990).

The Endeavour deposits are essentially concentrically zoned, cylindrical bodies of approximately coeval (~439Ma) quartz + sulphide stockwork veins centred on multiphase QMP complexes (Heithersay *et al.*, 1990; Perkins *et al.*, 1990). These vertically attenuated multiphase QMP complexes extend from 50 – 150m laterally and a minimum of 600 – 900m vertically (Jones, 1985; Heithersay *et al.*, 1990; Squires, 1992) and have corresponding ore zones of ~300m in diameter.

A sub-vertical fault system, trending 070°, has bisected the E22 deposit. A vertical movement of ~20m south-side-down is indicated by the displacement of one of the prominent volcanic marker horizons (Jones, 1985). A similar-trending sub-vertical fault system is evident at E27, however, displacement on this and other faults within the E27 deposit are thought to be minor (Jones, 1985). Other faults recognized at E22 also show little displacement (Jones, 1985). Faults at E26, typically showing minor displacements, trend preferentially towards the northwest (Harris, 1997). At E48, the host sequence is structurally intact and late-stage faults show only minor displacements, with one exception. The post-mineralisation, low angle Altona Fault has truncated the top of the ore body at depths of ~100m below surface (Wolfe, 1994; this study).

An oriented core analysis conducted by Harris (1997) demonstrated that the stockwork and sheeted veins associated with the main stages of mineralisation at all four of the Endeavour deposits have a preferred orientation of ~140 – 170°, which was shown to indicate dilation in the direction of ~10 – 265°. The implication of similar preferred vein orientations for the four deposits was interpreted by Harris (1997) to indicate a regional structural control on vein emplacement (cf. Jones, 1985).

3.3 Intrusions of the Endeavour deposits

3.3.1 Intrusion classification

Sillitoe (2000) listed a number of criteria that alone, or in combination, should be satisfied before different intrusions can be distinguished from one another in porphyry environments. They are 1) truncation of veins in older phases at contacts with younger phases; 2) narrow (<1cm) chilled margins in younger phases; 3) narrow (<2cm) zones of flow-aligned phenocrysts in younger phases along contacts with older phases; 4) xenoliths of older phases and/or quartz vein material in younger phases within a few 10's of centimetres of the contact with older phases; 5) better textural preservation and lower vein density in younger phases and 6) abrupt decrease in metal grade in younger intrusions.

Once different intrusions were established on the basis of these criteria at E22, E26, E27 and E48, they were described according to five textural characteristics as follows:

1. *phenocryst abundance (porphyritic rocks)* – uncrowded (20 - 50%) or crowded (50 - 70%);
2. *nature of the groundmass* – aphanitic, very fine-grained granular (microcrystalline with grains ranging in size from 20 – 50μm) or fine-grained granular (grains ranging in size from 50 – 100μm);
3. *mafic phenocrysts* – total proportion (<2 to ~15%) of biotite, magnetite, augite and/or hornblende phenocrysts population;

4. *non-mafic phenocrysts* – variable proportions of plagioclase and alkali-feldspar phenocrysts and accessory apatite, sphene and zircon microphenocrysts; and
5. *coarse-grained interstitial quartz* – the presence or absence of primary, 100 – 200μm sized, anhedral to euhedral, single or composite quartz grains within the groundmass.

Each intrusive phase has been classified according to its estimated original quartz, alkali-feldspar and plagioclase contents in accordance with the IUGS nomenclature proposed by Streckeisen (1973). Problems associated with secondary K-silicate minerals and other alteration assemblages have been taken into account when estimating the original alkali feldspar and quartz contents by discriminating between primary and secondary alkali feldspar and quartz on the basis of crystal size, form and mode of occurrence.

In addition to characteristically well-zoned phenocrysts, primary alkali feldspar typically occurs as small (20 – 100μm), euhedral to subhedral crystals intergrown with quartz (Figure 3.2a), whereas secondary K-feldspar commonly occurs as clusters of >1mm crystals (Figure 3.2b) or in very fine-grained (<20μm) massive zones that are not associated with quartz. Primary quartz is distinguishable in the groundmass because it typically occurs intergrown with anhedral grains of primary alkali feldspar (Figure 3.2c). In contrast, secondary quartz typically occurs as anhedral grains in discrete, continuous or non-continuous veinlets (<1mm – 5mm; Figure 3.2d).

Primary magnetite phenocrysts have distinctive euhedral crystal forms (octahedral grains 0.2 – 1mm across; Figure 3.2e) and obvious phenocryst nature in thin sections and are described below as part of the mafic phenocryst component of the intrusive phases. Secondary magnetite is common, particularly in the host volcanic rocks, as small (~50μm) anhedral grains (Figure 3.2f).

Both primary and secondary biotites occur in the Endeavour porphyry deposits, however, as with magnetite, secondary biotite typically occurs in the host volcanic rocks. Where it occurs in the intrusive phases, secondary biotite is distinguished from primary biotite phenocrysts by its fine grain size (20 – 50μm) and shreddy habit (Figure 3.2g). Primary biotite typically forms large (500 to >1000μm) euhedral, tabular crystals (Figure 3.2h).

Figure 3.2 Photomicrographs of the characteristic primary and secondary habits of common minerals in the QMP rocks associated with the Endeavour deposits. Sample numbers given in the format E26/284/68.0m refer to the drillcore samples; Deposit number/Drillhole number/Depth.

A Primary groundmass quartz intergrown with anhedral alkali feldspar is typical of the QMP intrusions and aplite intrusions. Photomicrograph of aplite from E26 in plane-polarised light (ppl); E26/284/68.0m.

B Large (>1mm), euhredral, secondary K-feldspar crystals in a biotite K-feldspar phyric-QMP intrusion (K-QMP) from E27; E27/386/241.1m.

C Quartz crystals with irregular contacts with groundmass alkali feldspar: photomicrograph of biotite phyric QMP (B-QMP) intrusion from E22 in ppl; E22/39/592.2m.

D The subhedral to euhedral quartz grains of a discontinuous quartz vein (arrow) are distinct from a primary quartz grain associated with K-feldspar (at position 1): photomicrograph of a augite-biotite K-feldspar QMP (KA-QMP) intrusion from E27 in cross-polarised light (xpl); E27/386/280.7m.

E Primary magnetite is typically octahedral, as shown in this example from a B-QMP intrusion from E22; E22/229/683.6m. Photomicrograph in transmitted and reflected light.

F Secondary magnetite (at positions 2) is distinctly smaller (<50μm) and commonly subhedral compared to primary magnetite. This example of a biotite quartz monzonite (BQM) intrusion at E26, taken in ppl, also show secondary biotite, a typical mineral accompanying secondary magnetite; E26/286/66.1m.

G The characteristic shreddy habit of secondary biotite is contrasted with the distinctly phenocryst nature of primary biotite in this photomicrograph in ppl, of a BQM intrusion from the same BQM intrusion from E26 as in (G).

H A photomicrograph in xpl, depicting the phenocryst nature of primary biotite and plagioclase in a B-QMP intrusion from E22; E22/229/683.6m.

Abbreviations:
afs - alkali feldspar; ap - apatite; bi - biotite; Kfs - K-feldspar; mt - magnetite; pl - plagioclase; qz - quartz

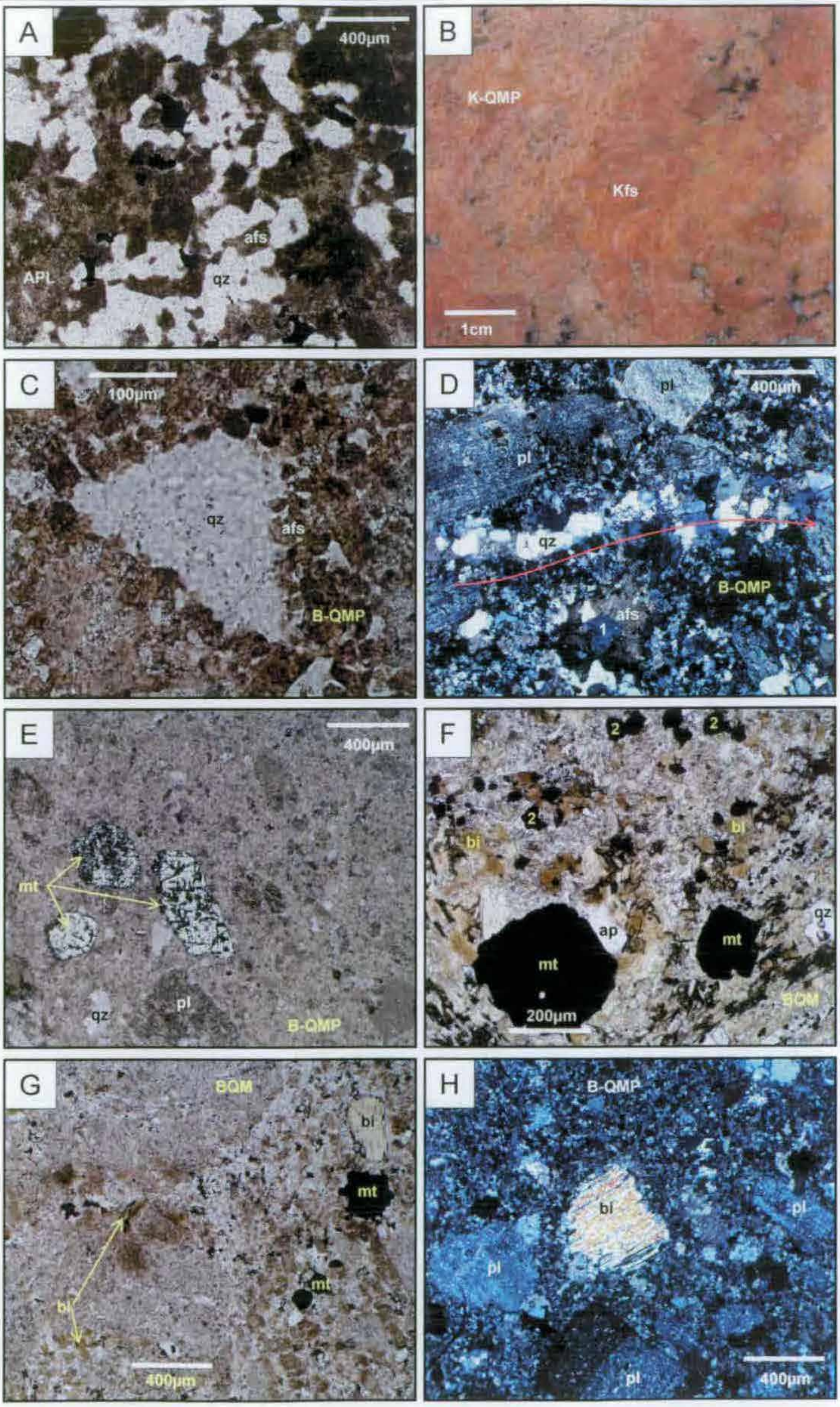
A
400µm
afs
APL
qz
B
K-QMP
Kfs
1cm
C
100µm
qz
afs
B-QMP
D
pl
400µm
pl
qz
B-QMP
afs
1
E
400µm
mt
qz
pl
B-QMP
F
2
2
2
bi
bi
ap
mt
mt
qz
200µm
BQM
G
BQM
bi
mt
bi
mt
400µm
H
B-QMP
bi
pl
pl
pl
400µm

3.3.2 Features common to porphyry intrusions of the QMP complexes

The porphyritic rocks of the QMP complexes at E22, E26, E27 and E48 share several common features, including ubiquitous plagioclase and alkali feldspar phenocrysts (Table 3.1; Figure 3.3a). Plagioclase generally comprises 40 – 80% of the rock and forms two varieties of phenocrysts: 1) subhedral crystals (4 x 6mm), and 2) euhedral tablets (~1 x2mm). Alkali feldspar occurs as zoned, euhedral phenocrysts and as anhedral grains within the groundmass of the QMP intrusions. The zoned phenocrysts generally contain poikilitic inclusions of plagioclase, biotite (Figure 3.3b) and/or apatite. Many plagioclase phenocrysts have been mantled by finer-grained, anhedral alkali feldspar, a texture typical of the monzonite intrusions (Figure 3.3c).

Quartz in the groundmass of the QMP intrusions generally occurs as 50μm grains intergrown with anhedral alkali feldspar (Figure 3.2a). In rare cases, quartz occurs as 150 – 200μm euhedral crystals that have irregular edges and are intergrown with smaller alkali feldspar crystals (Figure 3.2c).

Apatite, sphene and less commonly, zircon, are present as accessory microphenocrysts in all of the intrusive phases associated with the Endeavour deposits. Apatite is the most abundant microphenocryst and comprises up to 1% by volume of the rock. It typically forms ~80 – 160μm euhedral, tabular (Figure 3.3d) or hexagonal crystals (Figure 3.3c). It is closely associated with augite, magnetite and hornblende, and also occurs as inclusions in alkali feldspar, biotite (Figure 3.3b) and zircon (Figure 3.3e). Sphene is less abundant than apatite, with only one or two primary sphene microphenocrysts observed petrographically in most samples of the various intrusions (Figure 3.3f). Zircon is the least abundant microphenocryst phase. Where present, zircon occurs as subhedral to euhedral prismatic grains, typically ~100μm, but locally up to 400μm across (Figure 3.3e).

Almost all of the rocks in the Endeavour intrusive complexes have a distinctive rusty colour (e.g. Figure 3.3a). This is due to ubiquitous haematite dusting of the feldspars, both plagioclase and alkali feldspar, and secondary orthoclase. Blevin and Morrison (1997) proposed that the reddening was due to the formation of haematite from the exsolution of Fe, originally contained within the alkali feldspar as Fe^{+3}, as the primary alkali feldspars underwent exsolution and unmixing during cooling from magmatic temperatures.

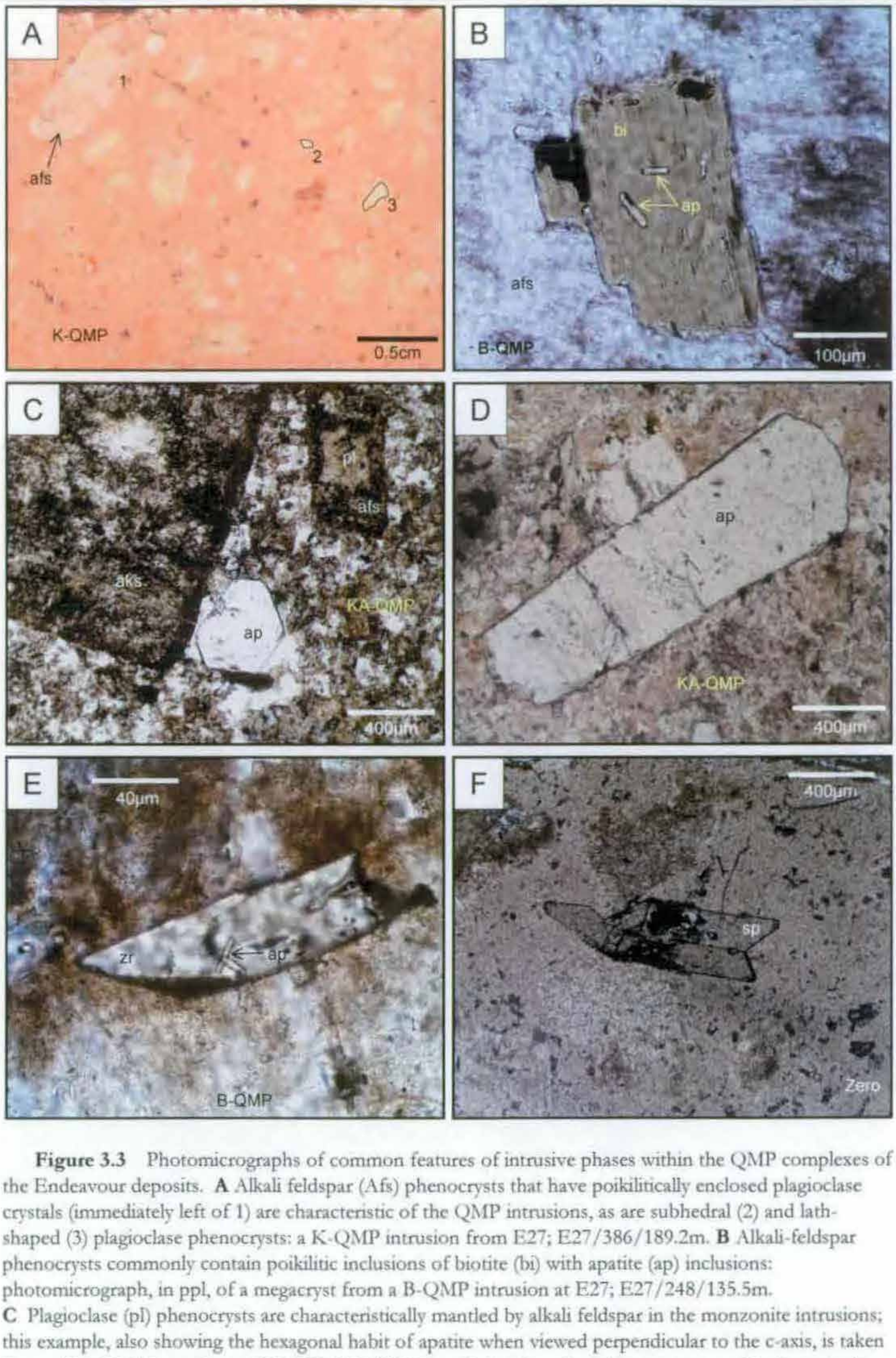

Figure 3.3 Photomicrographs of common features of intrusive phases within the QMP complexes of the Endeavour deposits. **A** Alkali feldspar (Afs) phenocrysts that have poikilitically enclosed plagioclase crystals (immediately left of 1) are characteristic of the QMP intrusions, as are subhedral (2) and lath-shaped (3) plagioclase phenocrysts: a K-QMP intrusion from E27; E27/386/189.2m. **B** Alkali-feldspar phenocrysts commonly contain poikilitic inclusions of biotite (bi) with apatite (ap) inclusions: photomicrograph, in ppl, of a megacryst from a B-QMP intrusion at E27; E27/248/135.5m. **C** Plagioclase (pl) phenocrysts are characteristically mantled by alkali feldspar in the monzonite intrusions; this example, also showing the hexagonal habit of apatite when viewed perpendicular to the c-axis, is taken from a KA-QMP intrusion at E27; E27/386/280.7m. **D** Apatite microphenocrysts are ubiquitous to the QMP intrusions: K-QMP intrusion from E27 in ppl; E27/7/213.9m. **E** Primary zircon (zr) with apatite inclusions in a B-QMP intrusion from E27, taken in ppl; E27/248/135.5m. **F** Sphene (sp) microphenocrysts are typical of the porphyry intrusions: zero porphyry at E26 in ppl; E26/46/1748.8m.

3.4 Intrusive history of the Endeavour deposits

Detailed pit mapping at E27 (Appendix A1) and drillcore logging (Appendix A2) of boreholes from all four of the Endeavour deposits have led to the identification of eight intrusive phases within the QMP complexes of E22, E26, E27 and E48. Each phase is described in terms of its spatial distribution, petrographic characteristics and temporal relationships. The intrusions are described in the interpreted chronological sequence from oldest to youngest.

The various intrusive phases associated with each Endeavour deposit are presented here on representative cross-sections, where the representative sections for E22, E26, E27 and E48 were selected to reflect maximum variability in terms of rock type, but at the same time, to retain, at least in two dimensions, the most accurate distribution of intrusive contacts. In excess of 7000m from 40 drillholes were logged over the four deposits (see Appendix A2 for details) and the cross-sections developed are based on true lithologic contacts and portray the intricate multiplicity of intrusive events exhibited in the QMP complexes. Figure 3.1 indicates the location of the four deposits with respect to one another and the positions of the cross sections for each deposit detailed below. For E22, all six drillholes logged have been projected onto a northwest – southeast section, mine grid 9700E/57000N to 9925E/56650N plus ~50m to the southwest and 200m to the northwest (Figure 3.4). All thirteen drillholes logged for E26 have been projected onto the mine grid 53050N plus 200m south; 300m north east – west section (Figure 3.5). An east – west cross section, mine grid 57050N plus 200m south: 200m north, included all thirteen boreholes logged for E27 (Figure 3.6), however, not all holes are presented on the section since some are oriented parallel to the section. The eight boreholes logged from E48 are projected onto the east – west section mine grid 53650N plus ~250m south, 250m north (Figure 3.7).

3.4.1 Monzodiorite

Two discrete intersections (38m and 78m long respectively) of coarse-grained (2 – 3mm), greenish-grey equigranular monzodiorite occur in the lower parts of the deepest drillhole at E26 (D46, Figure 3.5). This lithology is inferred to extend from a minimum of ~1300m below surface to the present day surface, where it crops out between 0.5 and 1km northwest of the E26 deposit (Figure 3.5).

The monzodiorite contains 10 – 20% mafic minerals, which are, in order of decreasing abundance, augite, biotite, magnetite and hornblende. These generally form sub- to euhedral grains up to 2mm across (Figures 3.8a). The abundances of alkali feldspar and mafic minerals decrease and increase respectively in the more mafic samples, whereas the plagioclase abundance remains approximately constant at ~60% (Table 3.1). Alkali feldspar intergrown with quartz and in rare cases, primary (?) anhydrite, comprise the interstitial material (~5%) of the monzodiorite (Figure 3.8b). Neither primary disseminated sulphides nor later porphyry-style quartz + sulphide veins are present in the monzodiorite, which is interpreted here to be a pre-mineral intrusion that was emplaced distal to the later QMP complexes associated with mineralisation.

The relative age of the monzodiorite cannot be proven because a narrow (<2m) sericitised shear zone (Figure 3.8c) totally obscures the contact between the monzodiorite and adjacent biotite quartz monzonite (described below). There appears to be clasts of monzodiorite in the biotite quartz monzonite within ~1m of the sheared contact between the two units, although sericite alteration assemblages associated with either intrusion emplacement or shearing have partially masked the clast boundaries. The monzodiorite is interpreted here to be the oldest known intrusion in the immediate vicinity of the Endeavour deposits.

3.4.2 Biotite quartz monzonite

Biotite quartz monzonite (BQM) intrusions are abundant in the lower portions of all four deposits, occurring at depths greater than ~650m below surface. There have been numerous drillcore intersections and underground exposures of the BQM at E26, whereas fewer intersections have been noted at E48 and only single intersections at both E22 and E27 (Figures. 3.4, 3.5, 3.6 and 3.7). The E31 stock, a biotite quartz monzonite intrusion, crops out ~2km northeast of the E26 deposit (Arundell, 1998) and occurs both above and below the Altona Fault near the E48 deposit (Wolfe, 1994; Kolkert, 1998; this study: cf. Figure 2.5). Heithersay and Walshe (1995) demonstrated similar geochemical compositions for the BQM of the E26 deposit and the E31 stock*. Based on the similar geochemical features, the E31 stock is interpreted here to be an example of a BQM intrusion.

* The E26 stock of Heithersay and Walshe (1995) was renamed the E31 stock by Arundell (1998).

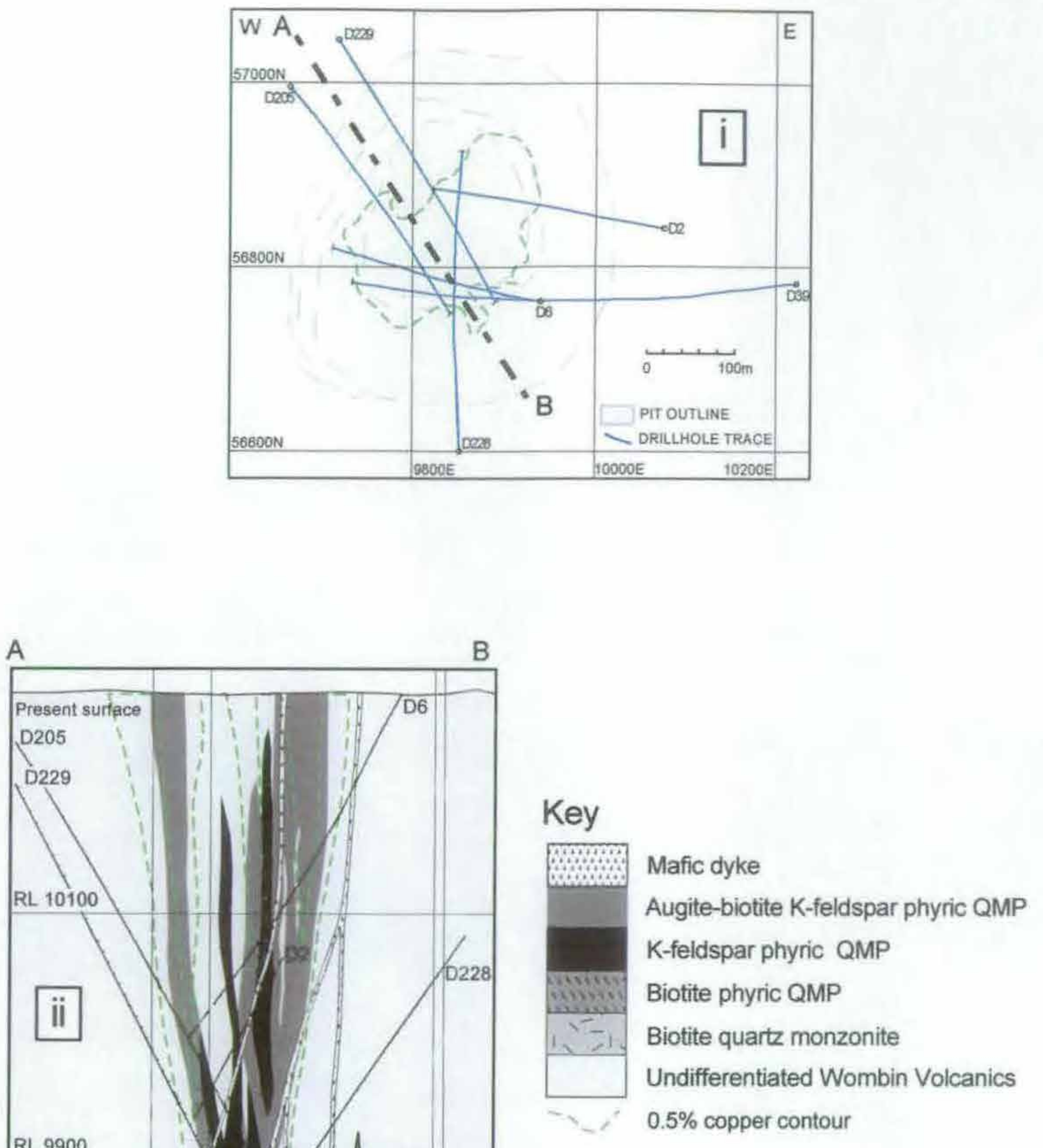

Figure 3.4 **i** Plan of E22 at surface showing drillhole traces that have been projected onto the section shown in (ii); **ii** E22 interpretive northwest - southeast section, mine grid 9700E/57000N to 9925E/56650N (A - B).

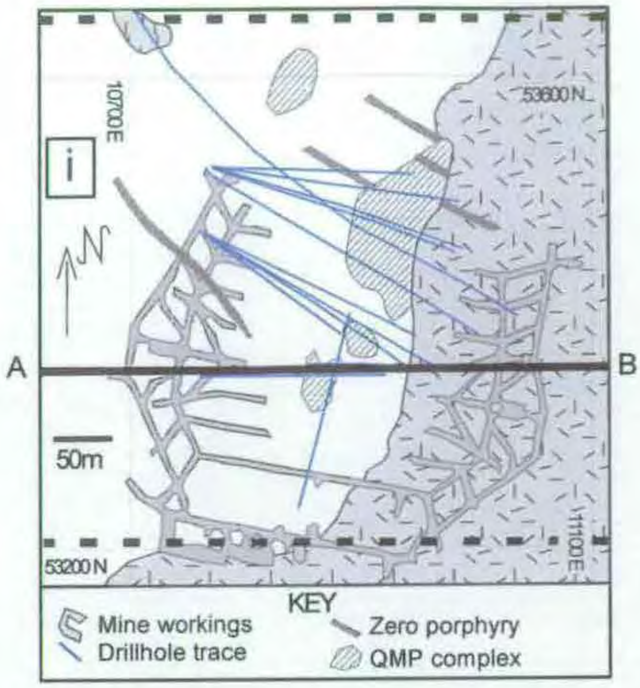

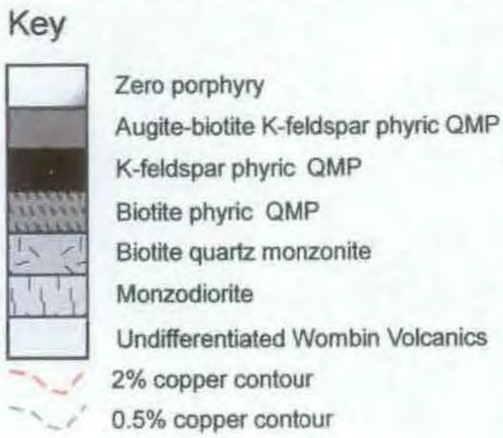

Figure 3.5 **i** Plan of E26 at 9800mRL showing the drillhole traces that are projected onto the east - west section in (ii);
ii E26 interpretive east - west section, mine grid 53050N (A - B).

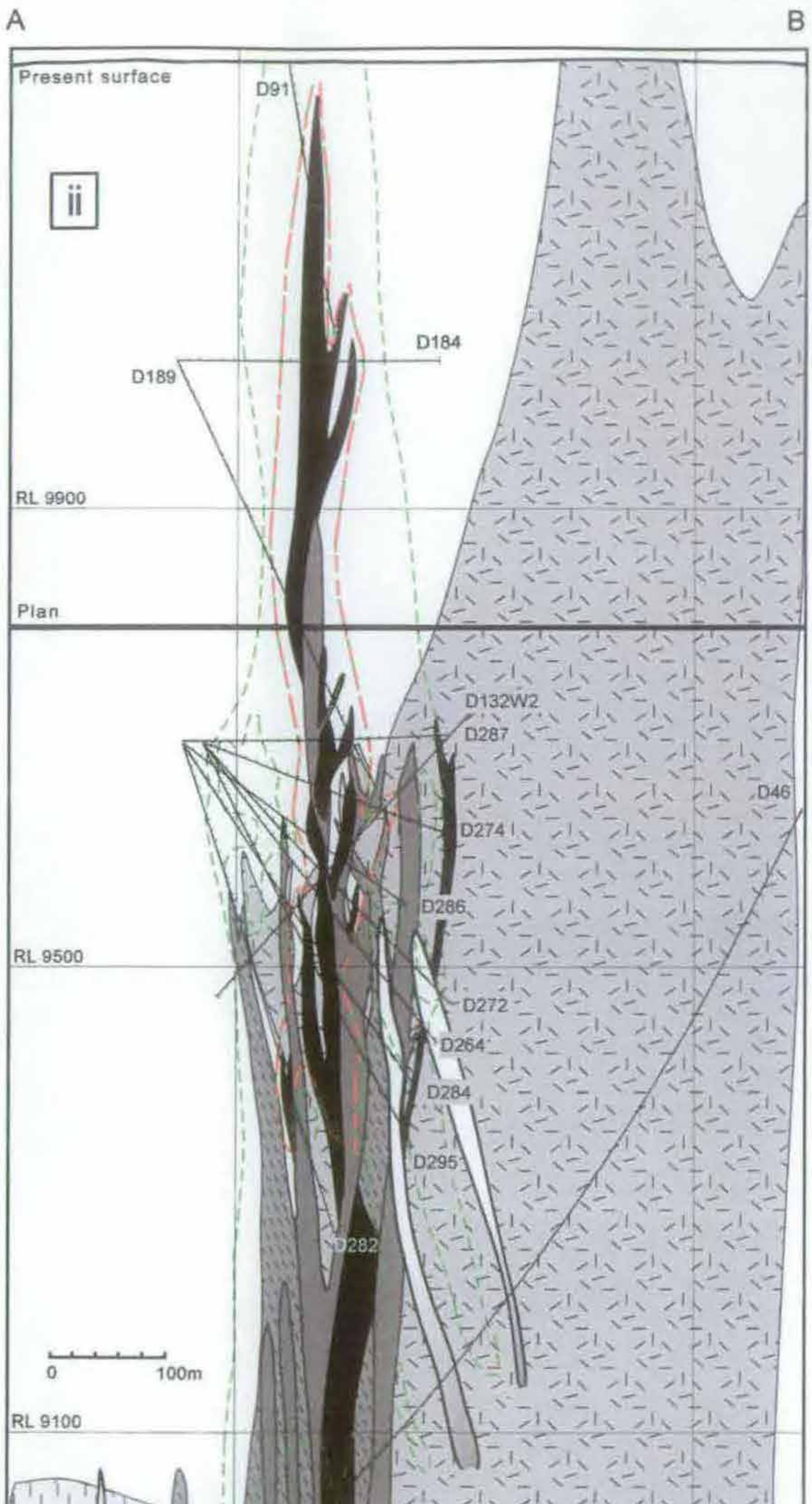

A
B
Present surface
ii
D91
D184
D189
RL 9900
Plan
D132W2
D287
D46
D274
D286
RL 9500
D272
D264
D284
D295
D282
0
100m
RL 9100
E11200

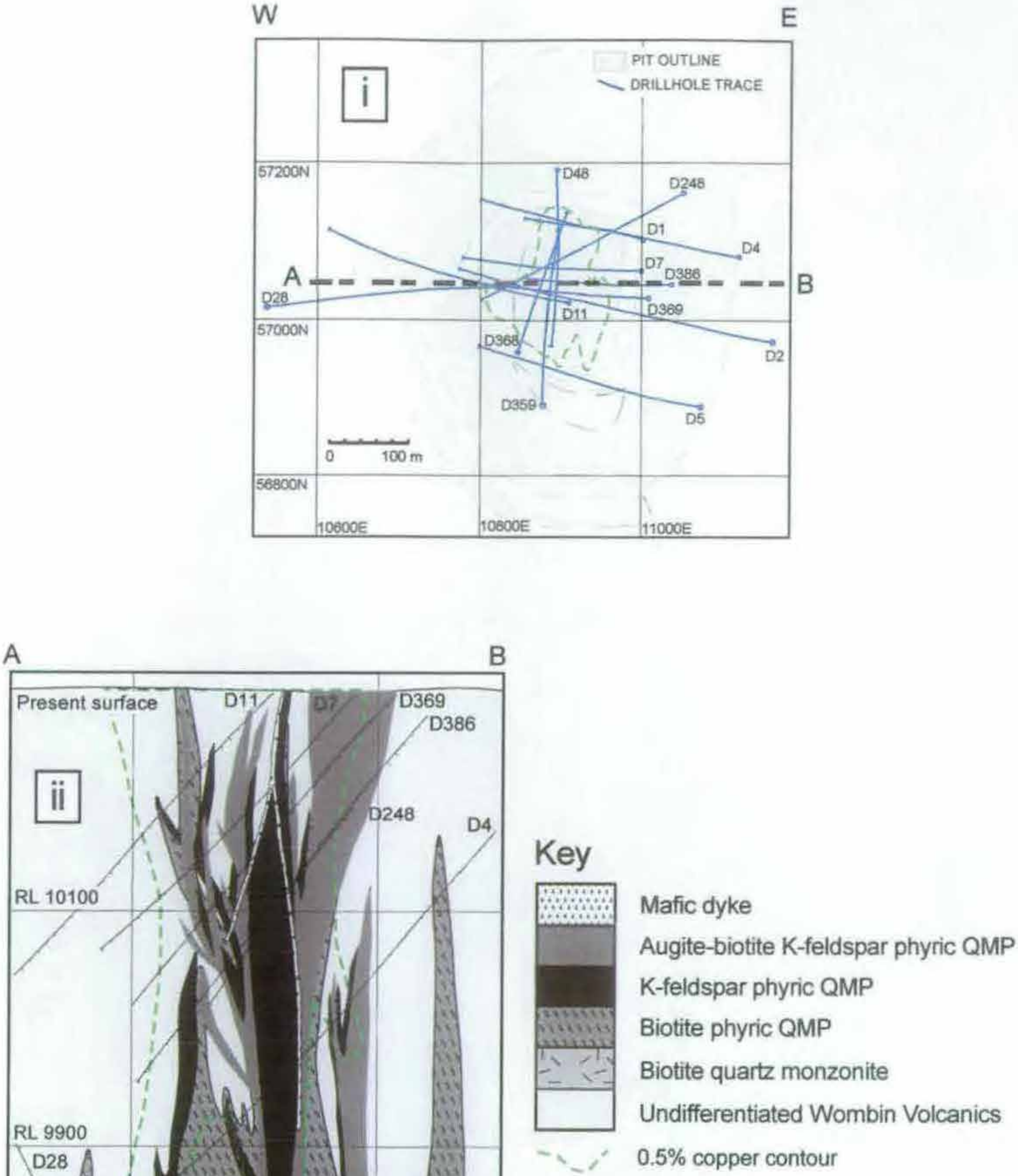

Figure 3.6 **i** Plan of E27 at surface showing the drillhole traces that are projected onto the east - west section in (ii); **ii** E27 interpretive east - west section, mine grid 57050N (A - B).

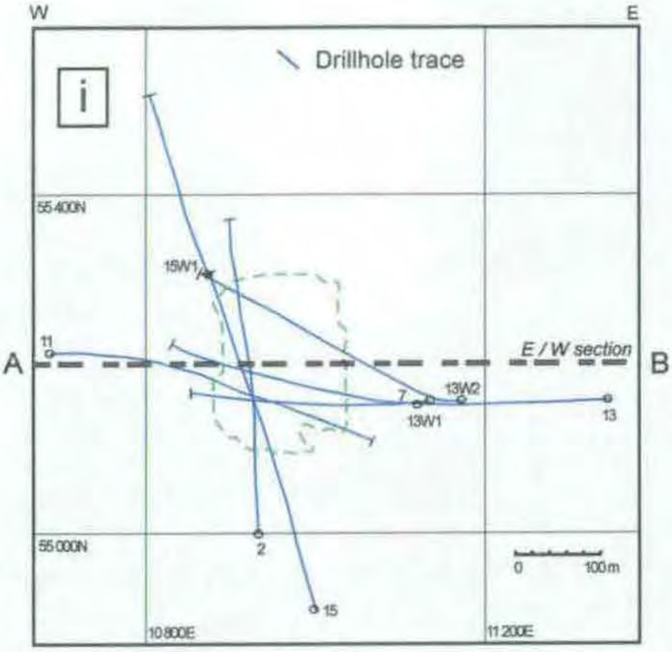

Key

- Mafic dyke
- Augite-biotite K-feldspar phyric QMP
- Microgranite
- K-feldspar phyric QMP
- Biotite phyric QMP
- Biotite quartz monzonite
- Undifferentiated Wombin Volcanics
- 2% copper contour
- 0.5% copper contour

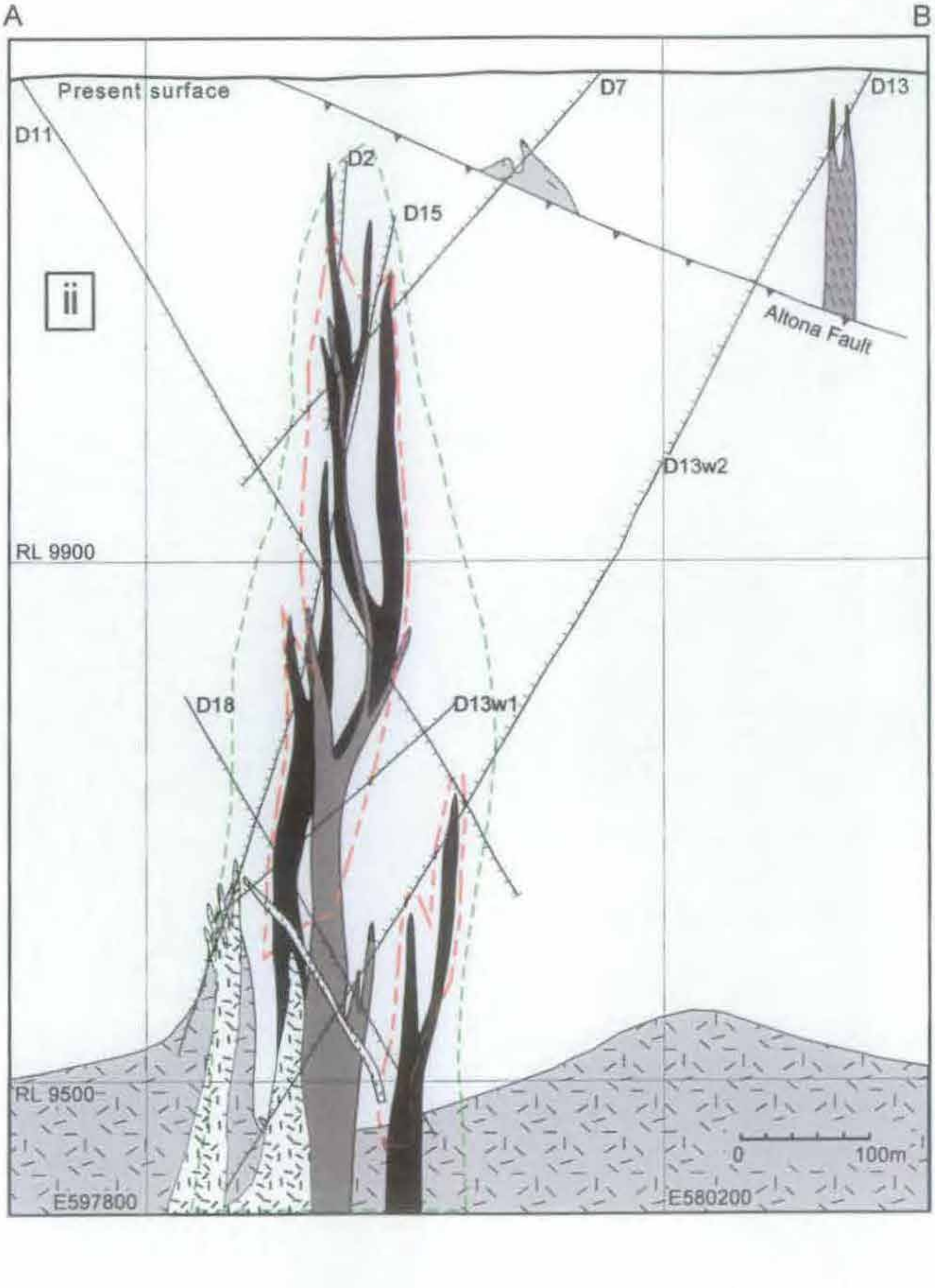

Figure 3.7 **i** A plan of E48 at 9 800mRL showing the drillhole traces that are projected onto the east - west section in (ii); **ii** E48 interpretive east - west section, mine grid 53650N of E48 (A - B).

BQM intrusions are commonly medium- to coarse-grained (~2mm), dark brick-red and equigranular to semi-porphyritic in texture (Figures 3.8d, e, f, g and h). They comprise mainly euhedral biotite, plagioclase and alkali feldspar crystals 1 – 2mm across and interstitial material (Table 3.1). The interstitial material in the BQM intrusions is fine-grained granular subhedral alkali feldspar intergrown with anhedral quartz and minor (<1%) anhydrite. In addition to crystals and groundmass, alkali feldspar occurs as rims around plagioclase. At E22, E26 and E27, alkali feldspar typically forms randomly oriented crystals in a groundmass of micrographic alkali feldspar and quartz (Figure 3.9a).

Bornite, chalcopyrite and lesser chalcocite exist as disseminated blebs (<1% by volume) within the BQM from E26, E27 and E48 (Figure 3.9b). Later porphyry-style quartz veins are uncommon, although some (<1% by volume) straight-walled, 2 – 5mm wide quartz + sulphides veins with K-feldspar ± biotite selvedges have been noted.

Erratic, but locally high Cu and Au grades occur at the margins of the E31 stock at the E31 prospect, indicating that the BQM intrusions introduced sub-economic mineralisation into the Endeavour systems (cf. Table 1.3).

BQM intrusions are interpreted to be younger than the monzodiorite (cf. section 3.3.1 above). In addition, clasts of the BQM are common in many of the QMP intrusions that define the QMP complexes (Figures 3.9c and d), implying that the BQM intrusions predate the multiphase QMP complexes.

3.4.3 Quartz monzonite porphyry intrusions

QMP intrusive complexes are central to each of the Endeavour deposits. These complexes, which form irregular 50 – 200m wide pipe-like bodies, are known to extend from surface to at least 1300m below surface at E26 (Figure 3.5). The BQM has been recognised from 900 to 600m below surface at the other deposits (Figures 3.4, 3.6 and 3.7). Three varieties of porphyritic intrusions define the QMP complexes at each deposit. Because timing relationships between the three phases are complex, the three intrusive phases are described before the timing relationships between them are discussed.

Figure 3.8 Photographs and photomicrographs of the monzodiorite of E26 and the BQM (biotite quartz monzonite) intrusions of E22, E26, E27 and E48.

A A photograph of the monzodiorite intrusions that occurs peripheral to the lower reaches of the E26 deposit; E26/46/1673.9m.

B Primary (?) anhydrite as interstitial material in the monzodiorite with quartz, plagioclase, alkali feldspar and magnetite; photomicrograph in ppl, E26/46/1590.0m.

C The sheared contact between the monzodiorite and BQM intrusions at E26 is shown here with clasts of what are interpreted to be the monzodiorite within the BQM intrusion; E26/46/1749.6m. Note the intense sericite alteration (dark grey) associated with the shear zone.

D The BQM intrusive phase at E22 is coarse-grained (2 - 3mm) equigranular and contains abundant alkali feldspar, biotite and plagioclase and rare quartz grains; E22/229/728.6m.

E An example of the BQM at E26 showing the mantling of plagioclase on alkali feldspar (1) and the equigranular texture typical of these intrusions; E26/282/396.3m.

F The BQM intrusion at E27 is virtually identical to many examples of similar intrusions at E26. The BQM at E27 (E27/28/708.6m) is finer-grained (~1mm) than the E22 example.

G At E48, the BQM intrusions are typically weakly porphyritic and finer-grained than the E22 and E26 examples; E48/13w2/1015.0m.

H A photomicrograph in xpl showing the typical equigranular to weakly porphyritic texture of the BQM intrusions, the rimming of plagioclase with primary alkali-feldspar and the interstitial nature of quartz; E26/284/318.0m.

Abbreviations:
afs - alkali feldspar; anh - anhydrite; bi - biotite; hb - hornblende; mt - magnetite; pl - plagioclase; qz - quartz

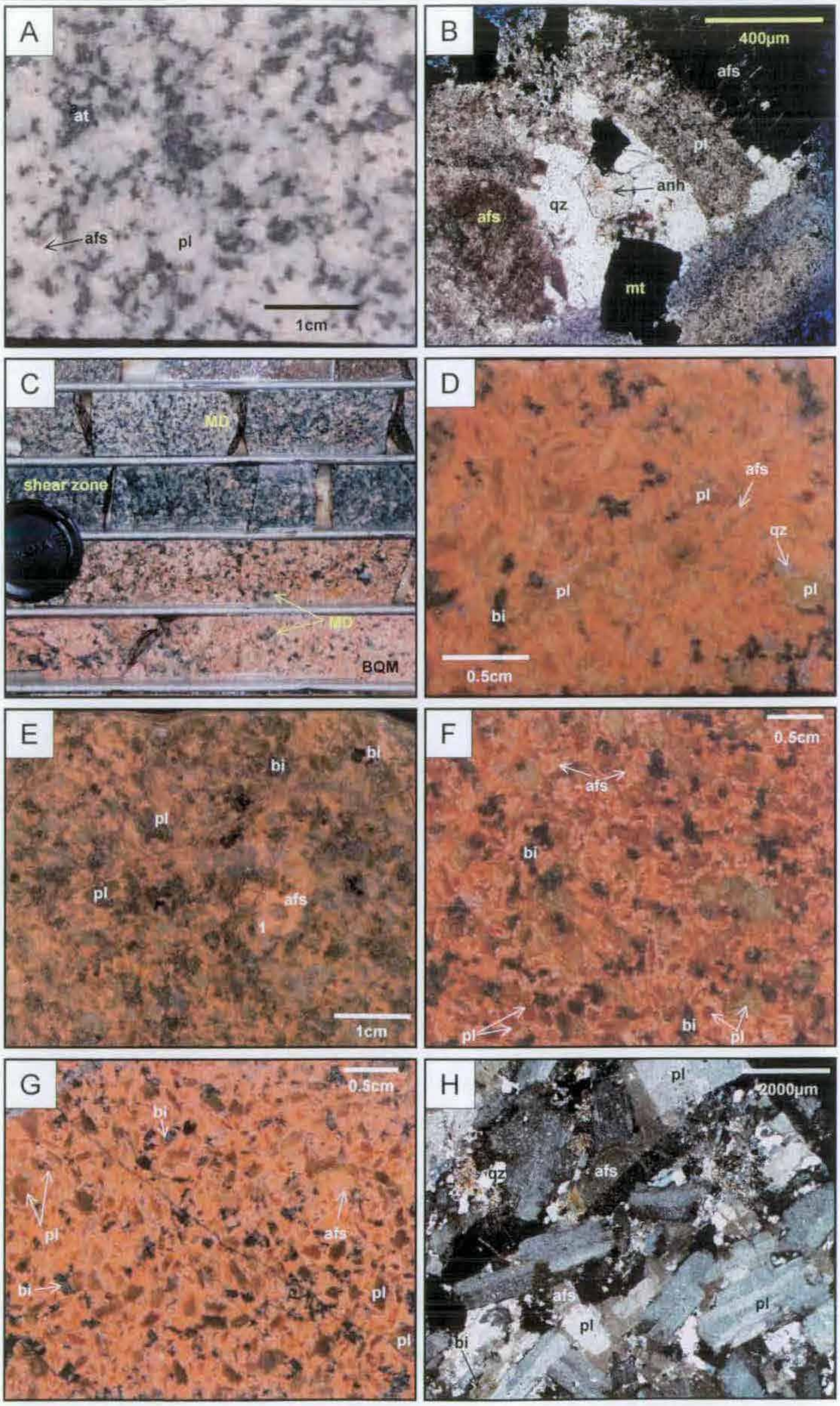
A
at
afs
pl
1cm
B
400µm
afs
pl
anh
qz
afs
mt
C
MD
shear zone
MD
BQM
D
afs
pl
qz
pl
pl
bi
0.5cm
E
bi
bi
pl
pl
afs
1cm
F
0.5cm
afs
bi
pl
bi
pl
G
0.5cm
bi
pl
afs
bi
pl
pl
H
pl
2000µm
qz
afs
afs
pl
pl
bi

Table 3.1 A summary of the textural characteristics and metal grades of the various intrusive phases of the Endeavour deposits.

Type	*Deposit*	*% Phenos*	*Groundmass (μm)*	*Afs:Qz*	*% Mafics*	*Hbl*	*Bi*	*Mag*	*Aug*	*Access/Trace*	*% Pl*	*Sub Pl*	*Euh Pl*	*% Afs*	*Afm*	*% Qz*	*Cu and Au grade*
MD	E26	cg, equi	2-5% int. mat. (~200μm)	~60:40	10-20	+	+	+	++	Zir, Spn, Apa, Anh	~60	=	=	10-20		~2	
	E22	cg, equi	~5% int. mat. (~80-100μm)	~50:50	~10	=	++	+		Apa, Zir	~40	++	+	40-50		2-5	
BQM	E26	mg - cg, equi	5-10% int. mat. (~80μm)	~60:40	10-15	=	++	=	=	Apa, Spn, Anh	~40	++	+	~40		~2	0.2 - 0.5%) Cu
	E27	semi-porph	10-20% int. mat. (~50μm)	~60:40	15	=	++	+	=	Apa, Zir, Ttn	30-40	++	+	40-50		2-5	<0.5g/t Au
	E48	mg - cg, equi	5-10% int. mat. (~80μm)	~60:40	10-15	=	++	=	=	Apa, Spn, Zir	~40	++	+	30-40		~2	
	E22	20-30	vfg-aph (10-20μm)	~80:20	5-10	=	+	+	+	Apa, Spn	~80	++	+	~10	+	<2	
B-QMP	E26	~50	fg (50-80μm)	~60:40	5-10	=	++	+	=	Apa, Spn	~70	++	+	~20	+	2-5	0.5 - 1.5% Cu
	E27	~50	fg (80-100μm)	~60:40	5-10	+	=	+	++	Apa, Spn	~70	++	+	~20	+	2-5	<1g/t Au
	E48	~50	fg (50-80μm)	~60:40	5-10	+	=	+	++	Apa, Spn, Fl	~70	++	+	~20	+	2-5	
	E22	20-30	vgf (20-40μm)	~50:50	~2	+	+	+		Apa +	~70	++	+	10 - 20	+ (P, Bi)	5-10	
K-QMP	E26	30-40	aph-vfg (10-20μm)	~60:40	<2	+	++			Apa =	60-70	++	+	20 - 30	++ (P, Pl)	5-10	1.5 - 2.5%, up to 4.5% Cu
	E27	~40	fg-vfg (30-60μm)	~50:50	<2	++	=	+		Apa +	60-70	+	+	20 - 30	++ (P, Pl)	5-10	0.5 - 2.5g/t, up to 8g/t au
	E48	30-40	vfg (~40μm)	~60:40	<2	+	+			Apa =	~70	++	+	~20	++ (P, Pl, Apa)	5-10	
	E22	20-30	vfg-aph (~20μm)	~80:20	2-5	+	=	=	++	Apa	~80	++	+	10 - 20	+ (P, Pl)	~2	
KA-QMP	E26	~50	fg (~80μm)	~60:40	2-3	+	++	=	=	Apa	~70	++	+	20 - 30	++ (P, Pl)	~5	0.3 - 0.8% Cu
	E27	~50	fg (60-100μm)	~60:40	2-3	+	=	+	++	Apa	~70	++	+	20 - 30	++ (P, Pl, Bi)	~5	<1g/t Au
	E48	~50	fg (50-90μm)	~60:40	2-3	+	=	=	++	Apa	~70	++	+	20 - 30	++ (P, Pl, Bi)	~5	
MG	E48	mg - cg, equi	Gr Afs+Qz	~70:30	<2		=			Zir, Apa	10-20			~50		30-40	0.3 - 0.5% Cu; ~0.4g/t Au
MMD	-	seriate - equi	fg - vfg (30 - 50μm)	~50:50	~5		++		+	Apa =	~60	++	+	~30		~5	
MS	-	10 - 20	Fth Afs (50 - 100μm)	~60:40	~2		=	=	=	Apa +	5-10			40-50		30-40	
Aplite	-	~5	Gr Afs+Qz (0.5 - 1mm)	~50:50	<2		+			Apa +	<1			~50		40-50	Locally high grade; Cu ~1%; Au ~1g/t
ZP	E26	30 - 40	aph, vfg (10-20μm)	~70:30	5-10	=	+	+	++	Anh phenos	60-70	=	+	10-20	++ (P, Pl, Anh)	<2	<0.1% Cu; <0.1g/t Au
Basalt	E22, E27	~20	Acicular pl (~80μm)		30-40			+*	+**		~60						

Abbreviations: MD - monzodiorite; MG - microgranite; MMD - micromonzodiorite; MS - microsyenite; ZP - zero porphyry; ; cg - coarse-grained (2 - 3mm); mg - medium-grained (1 - 2mm); fg - fine-grained granular (50 – 100μm); vfg - very fine-grained granular (20 – 50μm); aph - aphanitic; equi - equigranular; semi-porph - semi-porphyritic; int mat - interstitial material; Gr - graphic; Fth - feathery textured; Phenos - phenocrysts; Afs:Qz - alkali feldspar to quartz ratio; Hbl - hornblende; Bi - biotite; Mag - magnetite (* includes Fe-Ti oxides in basalt); Aug - augite (** includes olivine); Hyp - hypersthene; Access/Trace - accessory/trace minerals; Zir - zircon; Apa - apatite; Spn - sphene; Anh - anhydrite; Fl - fluorite; Pl - plagioclase; Sub - subhedral; Euh - euhedral; Afs - alkali feldspar; Afm - alkali feldspar megacryst (phenocryst >1cm); P - poikilitic inclusions; ++ dominant; + abundant; = present.

3.4.3.1 Biotite phyric QMP (B-QMP)

Volumetrically minor biotite and K-feldspar phyric quartz monzonite porphyry (B-QMP) intrusions occur at the margins of E22, E26 and E27. They have been intercepted in drillcore from ~1300m below surface at E26 (Figure 3.5) through to surface at E27 and E22 (Figures 3.4 and 3.6 respectively). Two ~5m thick intersections of B-QMP occur ~30 – 50m below surface at E48 (Figure 3.7). Rare B-QMP intrusions occur within the QMP complexes at E22 and E26 (Figures 3.4 and 3.5 respectively).

B-QMP intrusions are uncrowded (20 – 30% phenocrysts; Figures 3.9e and f) to crowded (50 – 60% phenocrysts; Figure 3.9g and h) porphyritic rocks that contain plagioclase (60 – 80%), alkali feldspar (10 – 20%) and mafic (5 – 10% biotite, augite and magnetite) phenocrysts in an aphanitic to fine-grained granular groundmass of alkali feldspar and quartz (Table 3.1). The groundmass of the B-QMP intrusions at E48 contains minor (<1%) fluorite in addition to alkali feldspar and quartz (Figure 3.10a). There is typically ~5% quartz in the B-QMP intrusions, which, in some samples from E22, occurs as singular euhedral crystals that have irregular boundaries with the surrounding alkali feldspar in the groundmass (Figure 3.2c).

Cu-sulphides occur as 10 – 50μm disseminations through the groundmass of the B-QMP intrusions and comprise ~1% of the total mineralogy. Bornite + chalcopyrite clots, from 1 – 8cm in diameter, are typical of some of the B-QMP intrusions, especially at E27 (Figure 3.10b). Porphyry-style bornite-mineralised quartz veins typically comprise <1% of the rock volume of B-QMP intrusions, although in some examples, no quartz – sulphide veins are present.

3.4.3.2 K-feldspar phyric QMP (K-QMP)

Pale pink (E26 and E48), through salmon pink (E27), to dark orange-red (E22) uncrowded, K-feldspar phyric quartz monzonite porphyry intrusions (K-QMP) occur in the central parts of the QMP complexes associated with all four Endeavour deposits (Figures 3.4, 3.5, 3.6 and 3.7). These intrusions are, volumetrically, the most abundant in the QMP complexes.

Figure 3.9 Photomicrographs of BQM intrusions and photographs of the B-QMP (biotite, K-feldspar phyric quartz monzonite) intrusions at E22, E26, E27 and E48.

A Micrographic quartz - alkali feldspar intergrowths are characteristic of BQM intrusions, this example from E26, E26/284/186.6m in ppl.

B A photomicrograph in ppl depicting bornite intergrown with quartz and alkali feldspar in a BQM intrusion from E26, the same sample as in (A).

C Clast of BQM within a B-QMP intrusion, indicating that the BQM predates the B-QMP; this example from E26, E26/46/1649.9m.

D In this photograph, a BQM clast totally surrounded by a K-QMP intrusion from E22, indicating the BQM intrusions also predate K-QMP intrusions; E22/205/360.1m.

E The uncrowded (20 - 30% phenocrysts) nature of the B-QMP intrusions at E22 is shown here in this example; E22/39/553.7m. Euhedral hornblende, biotite and plagioclase phenocrysts are typical of these intrusions.

F B-QMP intrusions at E26 are typically uncrowded to crowded - this photograph shows an uncrowded B-QMP (~30% phenocrysts); E26/46/1540.6m. Euhedral alkali feldspar, plagioclase and biotite phenocrysts are well depicted in this example.

G A photograph showing the typically crowded (~50% phenocrysts) character of the B-QMP intrusions at E27; E27/5/118.3m. Alkali feldspar, plagioclase, magnetite and biotite phenocrysts are visible.

H B-QMP intrusions at E48 are crowded (50% phenocrysts) and similar in texture to other B-QMP intrusions, however, phenocrysts, particularly alkali feldspar, are smaller, typically <0.5cm; E48/13/69.7m. Some phenocrysts appear aligned in this B-QMP sample (white arrow).

Abbreviations:
afs - alkali feldspar; bi - biotite; bor - bornite; pl - plagioclase; mt - magnetite; qz - quartz

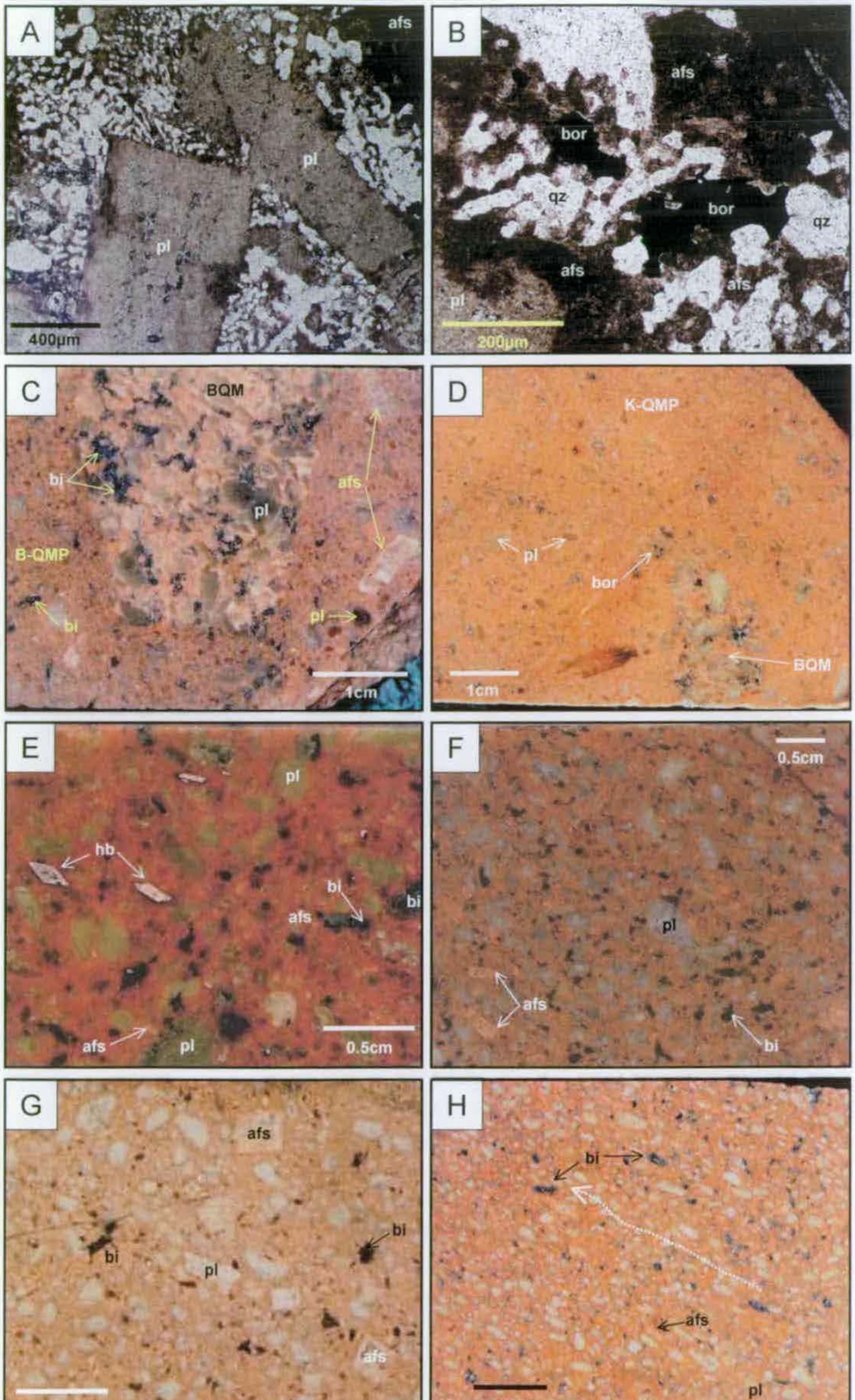
A
afs
pl
pl
400µm
B
afs
bor
qz
bor
qz
afs
afs
pl
200µm
C
BQM
bi
afs
pl
B-QMP
pl
bi
1cm
D
K-QMP
pl
bor
BQM
1cm
E
pl
hb
bi
bi
afs
afs
pl
0.5cm
F
0.5cm
pl
afs
bi
G
afs
bi
bi
pl
afs
1cm
mt
H
bi
afs
1cm
pl

Figure 3.10 Photographs of B-QMP and K-QMP (K-feldspar phyric quartz monzonite porphyry) intrusions at E22, R26, E27 and E48.

A This photomicrograph (ppl) shows apatite, quartz, alkali feldspar and fluorite (primary ?) later intergrown with chlorite in a B-QMP intrusion from E48; E48/13/69.7m.

B This late-mineral B-QMP intrusion on the periphery of E27 (pit, eastern wall) shows a bornite "clot" and two large (>2cm), angular clasts of Wombin Volcanics (WV). Two smaller (<1cm) angular clasts of Wombin Volcanics are also present. Alkali feldspar phenocrysts are clearly visible in this example.

C K-QMP intrusions from E22 are generally uncrowded (~20 phenocrysts) and contain abundant K-feldspar and plagioclase phenocrysts as well as disseminated bornite grains (~1mm); E22/6/254.6m.

D This photograph shows the typical uncrowded (~35% phenocrysts) nature of K-QMP intrusions at E26; E26/189/242.2m. Note the small (<1cm) bornite clot in the bottom centre of the photograph and the quartz vein immediately to its right (1).

E K-QMP intrusions at E27 are generally uncrowded (~30% phenocrysts) and contain abundant large (>1cm) alkali feldspar phenocrysts, or megacrysts, that often contain poikilitic inclusions of plagioclase (2); this example E27/386/189.2m. Disseminated bornite, and bornite clots are typical of these intrusions.

F E48 K-QMP intrusions are uncrowded (~20 - 30% phenocrysts) and contain ubiquitous alkali feldspar megacrysts, plagioclase phenocrysts and disseminated bornite; E48/13w2/703.8m.

G A larger-scale photograph of a bornite clot in a K-QMP intrusion at E27; this sample from the open pit. Note that bornite veinlets appear to crosscut this example (3 and 4).

H This photomicrograph (xpl) shows poikilitic inclusions of plagioclase within an alkali feldspar phenocryst, this example from an E27 pit sample (E27/W/15).

Abbreviations:
afs - alkali feldspar; ap - apatite; bor - bornite; chl - chlorite; fl - fluorite; pl - plagioclase; qz - quartz

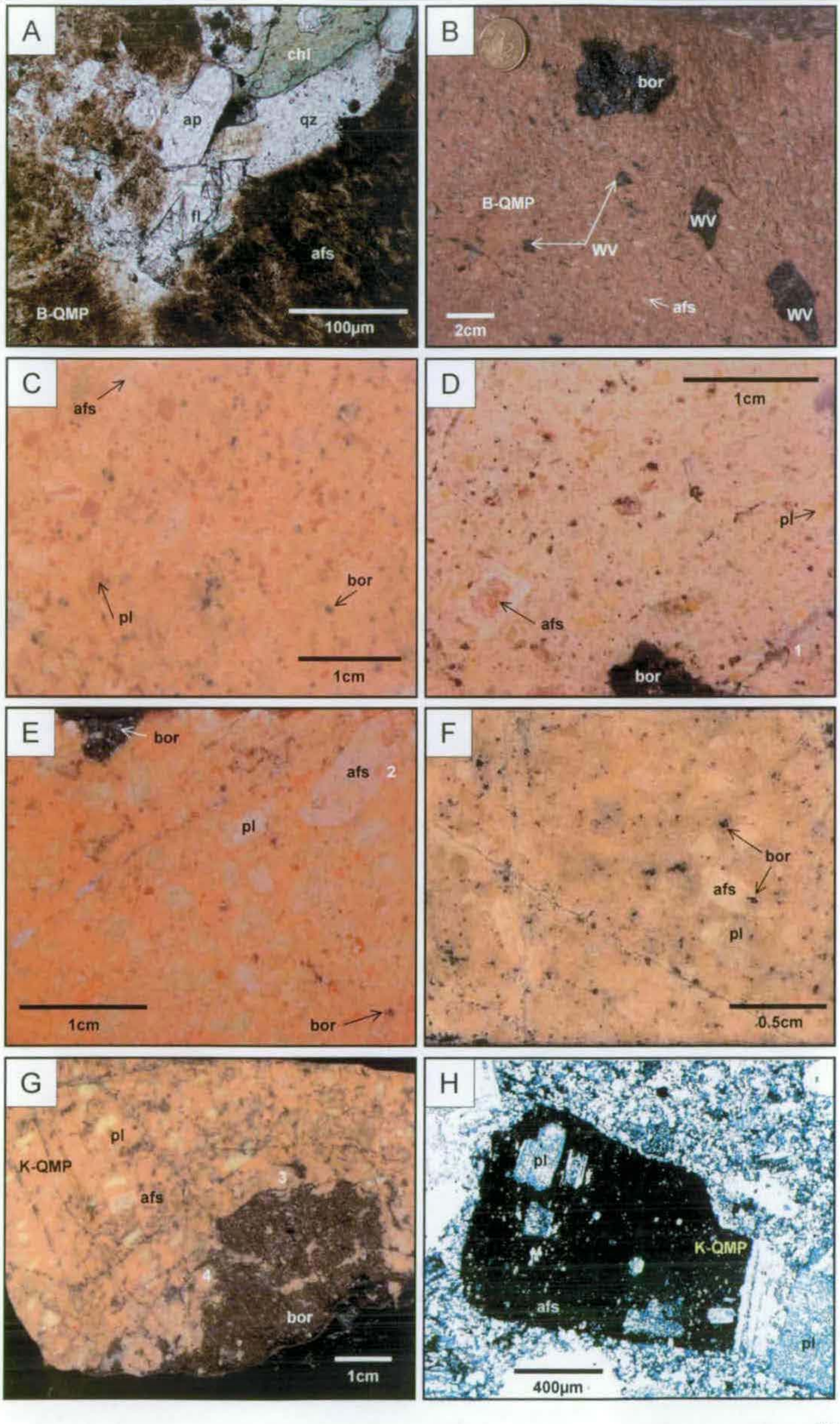
A
chl
ap
qz
fl
afs
B-QMP
100µm
B
bor
B-QMP
WV
WV
WV
afs
WV
2cm
C
afs
bor
pl
1cm
D
1cm
pl
afs
1
bor
E
bor
afs
2
pl
1cm
bor
F
bor
afs
pl
0.5cm
G
pl
K-QMP
3
afs
4
bor
1cm
H
pl
K-QMP
afs
pl
400µm

K-QMP intrusions are uncrowded porphyries (~30 - 40% phenocrysts) that contain mainly plagioclase, alkali feldspar and minor (<2%) magnetite + biotite hornblende phenocrysts in an aphanitic to very fine-grained granular groundmass of alkali feldspar and quartz (Table 3.1; Figures 3.10c, d, e, f and g). Large (>1cm) K-feldspar phenocrysts, locally called "megacrysts", are characteristic of this phase. The K-feldspar phenocrysts and megacrysts typically contain poikilitic inclusions of plagioclase (Figure 3.10h), biotite and/or apatite. The alkali feldspar:quartz ratio of the groundmass in K-QMP intrusions varies from ~50:50 to 70:30.

Up to 10% of the quartz occurs as micrographic intergrowths with alkali feldspar, as clusters of three or four anhedral grains or as "brain rock" and other anisotropic textures. The term "anisotropic textures" is used here to describe variable textures that are not "porphyritic" but still occur within the QMP phases. Brain rock, an anisotropic texture defined by thin (5 – 20mm), alternating bands of crenulated, coarse-grained prismatic quartz and microcrystalline aplite porphyry (Shannon *et al.*, 1982), is locally well-developed in K-QMP intrusions at E26 and E22 (Figures 3.11a and b respectively). Discontinuous chains of prismatic quartz crystals that form discrete zones within the porphyry or aplite porphyry rather than distinct quartz layers (Figure 3.11c) define another anisotropic texture, locally termed "partial brain rock". A third anisotropic texture is characterized by spherical, radial aggregates of alkali feldspar and quartz that appear to have nucleated on a substrate seed crystal at the centre of the aggregate (Figures 3.11d and e).. There are also clusters of three or four anhedral quartz grains that are reminiscent of what Candela and Blevin (1995) interpreted as miarolitic cavities. Many of these clusters contain solid inclusions of primary hornblende (Figure 3.11f).

Vein dykes in the Endeavour deposits were first described by Heithersay and Walshe (1995). They are thin (<1cm), composite quartz veins and aplite dykes. Two types are present: 1) aplite dykes with selvages of prismatic quartz (Figure 3.11g); and 2) aplite dykes containing randomly arranged prismatic quartz crystals (Figure 3.11h). The aplite within the vein dykes is similar in texture and composition to the igneous portions of brain rock.

Brain rock and partial brain rock textures generally occur at the margins of K-QMP intrusions. In contrast, miarolitic cavities and spherical, radial aggregates occur throughout these intrusions, typically within the groundmass and along the edges of alkali feldspar phenocrysts respectively. Vein dykes occur throughout the K-QMP intrusions

Figure 3.11 Photographs and photomicrographs of anisotropic textures in the QMP intrusions.

A Brain rock (alternating bands of crenulate quartz and aplite porphyry) at E22; E22/229/641.3. These alternating bands are commonly of variable thickness and have been ptygmatically folded in this example (1).

B At E26, brain rock (E26/189/235.8m) is characterised by alternating bands of aplite porphyry that contains visible small (1 - 2mm) phenocrysts of plagioclase and less commonly alkali feldspar and prismatic quartz crystals. Disseminated bornite is present in both components of brain rock in this example. Some of the prismatic quartz bands appear to have been broken at (2).

C Discontinuous chains of prismatic quartz crystals (3 and 4) intergrown with aplite, or very fine-grained alkali feldspar, define partial brain rock anisotropic textures in K-QMP intrusions; E26/91/136.7m. Note bornite in the partial brain rock quartz crystals (5) and disseminated in the K-QMP rock.

D Photomicrograph in ppl of spherical, radial aggregates of alkali feldspar and euhedral quartz in a B-QMP intrusion at E22; E22/39/570.5m.

E A photomicrograph showing discrete spherical shells of subhedral to euhedral quartz and very fined grained (~50μm) alkali feldspar in a K-QMP intrusion at E27; E27/248/182.0m.

F This photomicrograph (xpl) of a possible miarolitic cavity in the groundmass of a KA-QMP (augite-biotite K-feldspar phyric quartz monzonite porphyry) intrusion at E27. Discrete quartz crystals appear to have grown inward from the walls of the cavity, and contain solid inclusions of hornblende; E27/7/213.9m.

G A vein dyke containing randomly oriented prismatic quartz crystals and aplite porphyry in a K-QMP intrusion at E27; E27/248/206.4m. Disseminated bornite is also present in the vein dyke and as disseminations in the K-QMP rock.

H A photograph of a vein dyke in the Wombin Volcanics (WV) at E48, cut by a quartz - bornite vein. This type of vein dyke is characterised by a central seam of aplite and selvages of quartz. Note the disseminated bornite in the aplite, E48/13w1/711.2.

Abbreviations:
afs - alkali feldspar; apl - aplite or aplite porphyry; hb - hornblende; mt - magnetite; pl - plagioclase; qz - quartz;

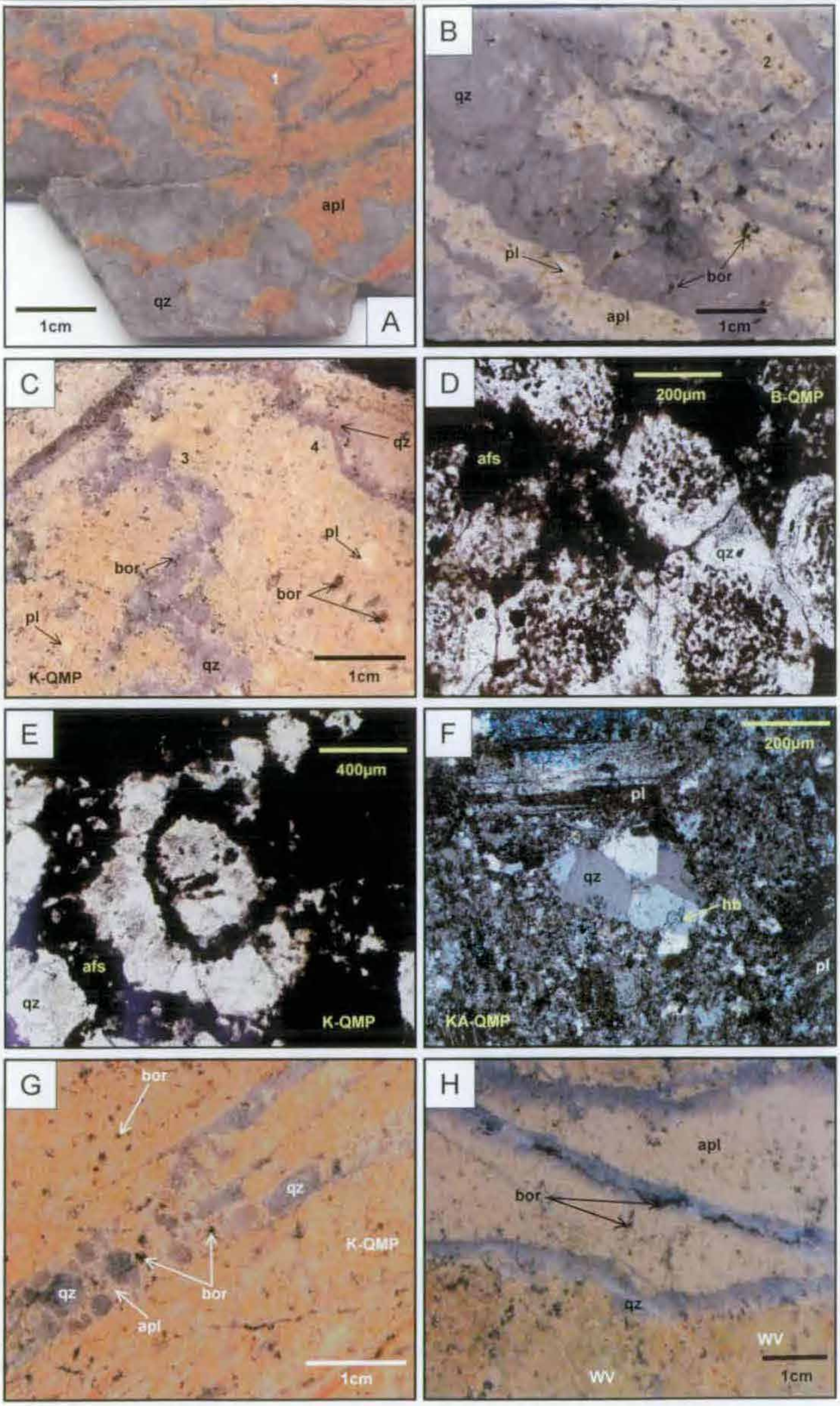
A
1
apl
qz
1cm
B
qz
2
pl
bor
apl
1cm
C
3
4
qz
pl
bor
bor
pl
K-QMP
qz
1cm
D
200μm
B-QMP
afs
qz
E
400μm
afs
qz
K-QMP
F
200μm
pl
qz
hb
pl
KA-QMP
G
bor
qz
K-QMP
bor
qz
apl
1cm
H
apl
bor
qz
WV
WV
1cm

and surrounding volcanic rocks at all four of the Endeavour deposits. These textures are abundant in the K-QMP intrusions (~5 – 10%), locally comprising >10% of the total rock volume.

Many workers have suggested that anisotropic textures such as those described above indicate quartz crystallization in the presence of a volatile-rich aqueous fluid (Shannon *et al.*, 1982; Kirkham and Sinclair, 1988; Lowenstern and Sinclair, 1996). This association of quartz crystallization in the presence of an aqueous fluid within the K-QMP intrusions is taken to indicate a close temporal relationship between the emplacement of the K-QMP intrusions and the peak development of magmatic – hydrothermal fluids in these systems. However, for these textures to have formed, it is thought that these fluids were not released at the time of brain rock formation.

Hydrothermal alteration zones in the four Endeavour deposits are centred on and most intense within the K-QMP intrusions. Straight-walled stockwork veins diminish in intensity with distance from the K-QMP intrusions and generally account for 5 – 20% by volume of the host rock, while disseminated sulphides account for ~2% of the same. Many samples of brain rock and other anisotropic textures within the K-QMP intrusions, including vein dykes, contain 1 – 2% very fine-grained (~10 – 50μm) disseminated bornite ± chalcopyrite. Alteration assemblages and veining are described in detail in Chapter 4.

3.4.3.3 Augite-biotite, K-feldspar phyric QMP (KA-QMP)

Dark rust-coloured, augite-biotite, K-feldspar phyric quartz monzonite porphyry (KA-QMP) intrusions occur over much of the vertical extent of the four deposits, close to both the B-QMP and K-QMP intrusions (Figures 3.4, 3.5, 3.6 and 3.7). Volumetrically, KA-QMP intrusions are the second most abundant intrusive phase in the QMP complexes.

The KA-QMP intrusions are crowded to uncrowded porphyries that contain plagioclase (70 – 80%) and alkali feldspar (10 – 30%) phenocrysts. Most KA-QMP intrusions contain 2 – 3%, rarely up to ~5%, augite + biotite + magnetite + hornblende phenocrysts. The fine-grained granular groundmass of the KA-QMP intrusions generally contains ~30 – 40% quartz, but locally contains as much as 50% in samples from E26, and as little as 10% in samples from E22 (Figures 3.12a, b, c and d). Anisotropic textures are also present in most KA-QMP intrusions, although they are less abundant (~2 – 3%, locally up to 5%) than they are in the K-QMP intrusions.

Disseminated grains of bornite and chalcopyrite, typically 10 – 50μm in diameter, occur throughout the groundmass, comprising ~1% of the total mineralogy. Porphyry-style mineralised quartz veins, with or without central K-feldspar seams locally account for ~5%, rarely up to 10%, by volume of the KA-QMP intrusions at each of the four deposits.

3.4.3.4 Timing relationships

B-QMP intrusions have sharp intrusive contracts with the host volcanic rocks and BQM intrusions. Clasts of K-QMP and KA-QMP intrusions are typically absent from the B-QMP intrusions. Since most B-QMP intrusions are distal to the central zones of the intrusive complexes within which porphyry-style veining is most intensely developed, the presence of hydrothermal veins (Figure 3.12e) and BQM clasts (Figure 3.9c) indicates that most of the B-QMP intrusions were emplaced after the BQM, but before the K- and KA-QMP intrusions. However, the absence of hydrothermal veins and late sericite alteration assemblages (described in section 4.4.6.1) in some examples implies that not all B-QMP intrusions were emplaced before the main hydrothermal events and are thus late-mineral intrusions. For example, on the eastern wall of the pit at E27, a B-QMP intrusion crosscuts thick (>1cm) quartz-sulphide veins associated with the main mineralising events (Figure 3.12f). Early- and late-mineral B-QMP intrusions are recognised at E22, E27 and E26. At E22, E26 and E27, the more abundant early-mineral B-QMP intrusions occur as dykes within the host volcanic rocks peripheral to the main QMP complexes. Late-mineral B-QMP intrusions at E22 and E26 occur as dykes (5 – 10m) within the complexes. In contrast, rare late-mineral B-QMP intrusions at E27 typically occur as dykes (up to 10m wide) outside the main QMP complex.

Contacts between K-QMP and KA-QMP, and between K-QMP and B-QMP intrusions are commonly sharp (Figure 3.13a), and those between B-QMP and KA-QMP intrusions are generally sharp, but rare gradational contacts over 20 – 30cm are observed (Figure 3.13b). Based on the lower phenocryst abundances and higher quartz contents of K-QMP compared to KA-QMP intrusions, the K-QMP and KA-QMP intrusions are interpreted here to be equivalent to Heithersay and Walshe's (1995) *QMP 1* and *QMP 2* intrusions respectively. Heithersay and Walshe (1995) interpreted 1) an abrupt drop in Cu grade from *QMP 1* to *QMP 2*, 2) the presence of quartz + sulphide vein fragments and bornite clots from *QMP 1* in *QMP 2* and 3) dykelets (<0.2m wide) of *QMP 2* crosscutting *QMP 1* on the northern margin of E26, to imply that *QMP 2* post-dates *QMP 1*.

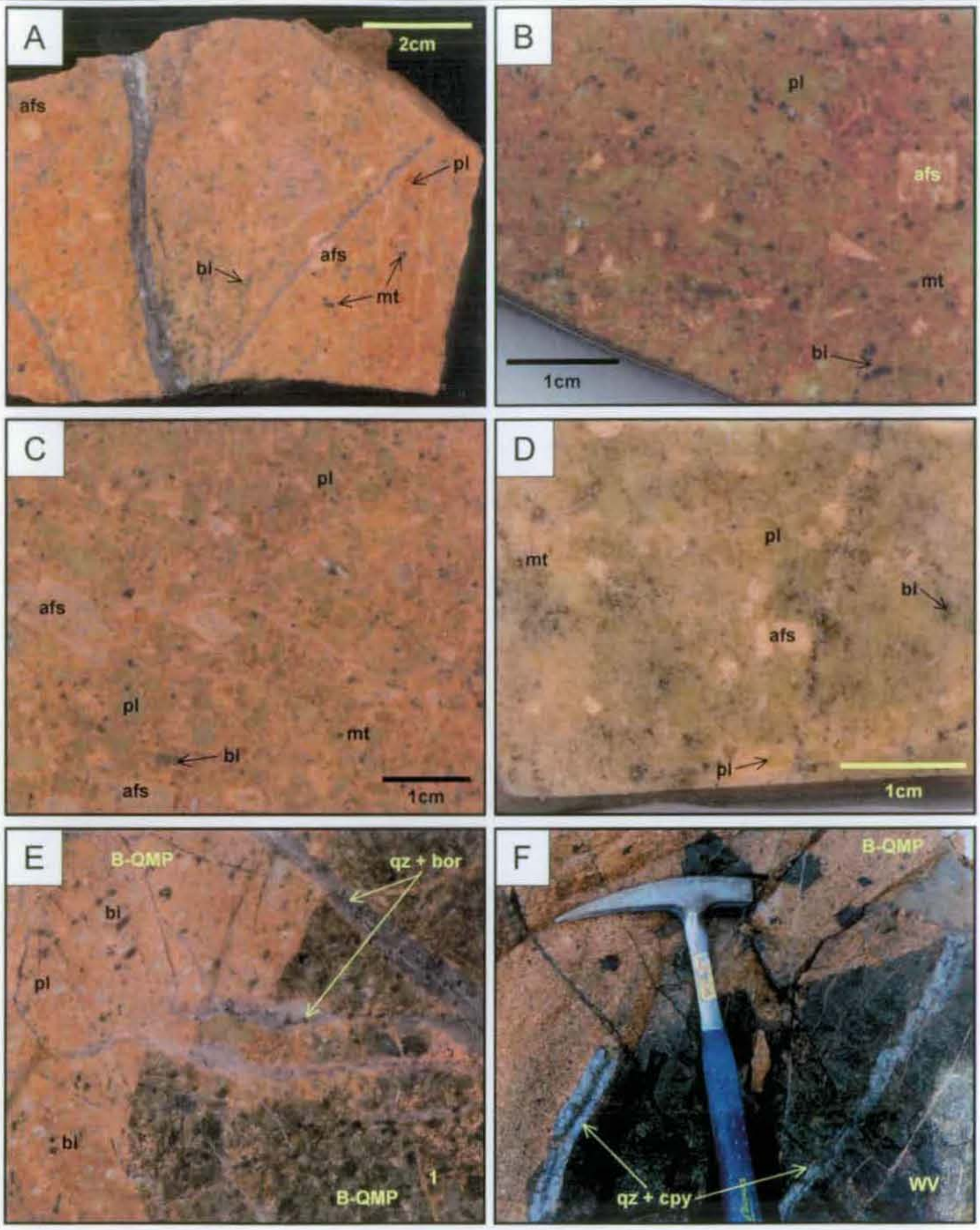

Figure 3.12 Photographs of KA-QMP (augite-biotite K-feldspar phyric quartz monzonite porphyry) intrusions at E22, E26, E27 and E48 and contact relationships within the QMP complexes. **A** A pit sample from E22 showing the uncrowded (~30% phenocrysts) nature of the KA-QMP intrusions at E22. Note the conspicuous alkali feldspar and plagioclase phenocrysts, are biotite and magnetite grains. The quartz vein through the left side of the rock contains chalcopyrite and bornite. **B** Similar features to those described for (A) above apply to KA-QMP rocks from E26; E26/46/1388.0m. **C** This KA-QMP intrusion from E27 shows the typical crowded porphyritic texture common to these rocks; E27/386/155.6m. Note also the conspicuous alkali feldspar and plagioclase phenocrysts. **D** A typical KA-QMP intrusion from E48; E48/2/306.0m with the same broadly similar characteristics as similar rocks described for E27 in (C). **E** The pre-mineral timing of some B-QMP intrusions is depicted here with early quartz - bornite veins crosscutting is intrusion on the periphery of E26; E26/284/80.1m. The B-QMP has intruded a BQM intrusion that has been affected by early biotite-magnetite alteration assemblages, giving the BQM a dark-grey appearance, and K-feldspar veinlets (1). **F** However, the post-mineral timing of other B-QMP intrusions is shown here, where a B-QMP intrusion crosscuts KA-QMP intrusion-related quartz - chalcopyrite veins and host Wombin Volcanics (WV) rocks on the eastern pit wall of E27.

For most cases at all four of the Endeavour deposits, this timing relationship of K-QMP predating KA-QMP intrusions, is true, and metal grades are seen to decrease markedly from K-QMP to KA-QMP intrusions. However, rare examples of K-QMP crosscutting KA-QMP intrusions are evidence that locally, both phases intruded each other. For example, Figure 3.13c shows a teardrop-shaped clast of KA-QMP totally enveloped by K-QMP.

In general though, the overall sequence of intrusions within the QMP complexes at E22, E26, E27 and E48 can be summarised as follows:

1. early-mineral B-QMP dykes and dykelets intruding the peripheries of the deposits;
2. central, volumetrically significant K-QMP intrusions;
3. KA-QMP intrusions; and
4. minor late-mineral B-QMP intrusions.

Sharp or gradational and locally contradicting contact relationships between B-QMP, K-QMP and KA-QMP intrusions within the QMP complexes, combined with the fact that K-QMP intrusions occur close to both B-QMP and KA-QMP intrusions, imply a close emplacement timing for all three phases.

3.4.3.5 Microgranite

Zones of "microgranite" up to 40m wide have been intersected within the BQM intrusions in drillholes at the base of E48 (Figure 3.4). The microgranite is distinguished by white, coarse-grained (~1mm), graphically intergrown alkali-feldspar and quartz and contains rare biotite (<2%) and plagioclase (<5) phenocrysts (Figure 3.13d).

Contacts between the BQM and microgranite intrusions are generally sharp (Wolfe, 1994; this study). This is interpreted to imply that the microgranite was emplaced after the BQM. There are, however, rare gradational contacts between the two intrusions, where these are interpreted to be the result of sericitic alteration assemblages having totally obscured the original intrusive contact. The presence of barren, sheeted veins crosscutting the microgranite (Figure 3.13e) can be used to further constrain the timing of its emplacement relative to the other intrusions of the E48, since it implies emplacement prior to or synchronous with a major veining event. However, because both K-QMP and KA-QMP intrusions were accompanied by major veining events (cf. section 4.4.5), it is not possible to further constrain the age of the microgranite based purely on crosscutting relationships. Wholerock geochemistry is used to correlate the microgranite with one of the QMP intrusions in Chapter 8 (section 8.3.6.2).

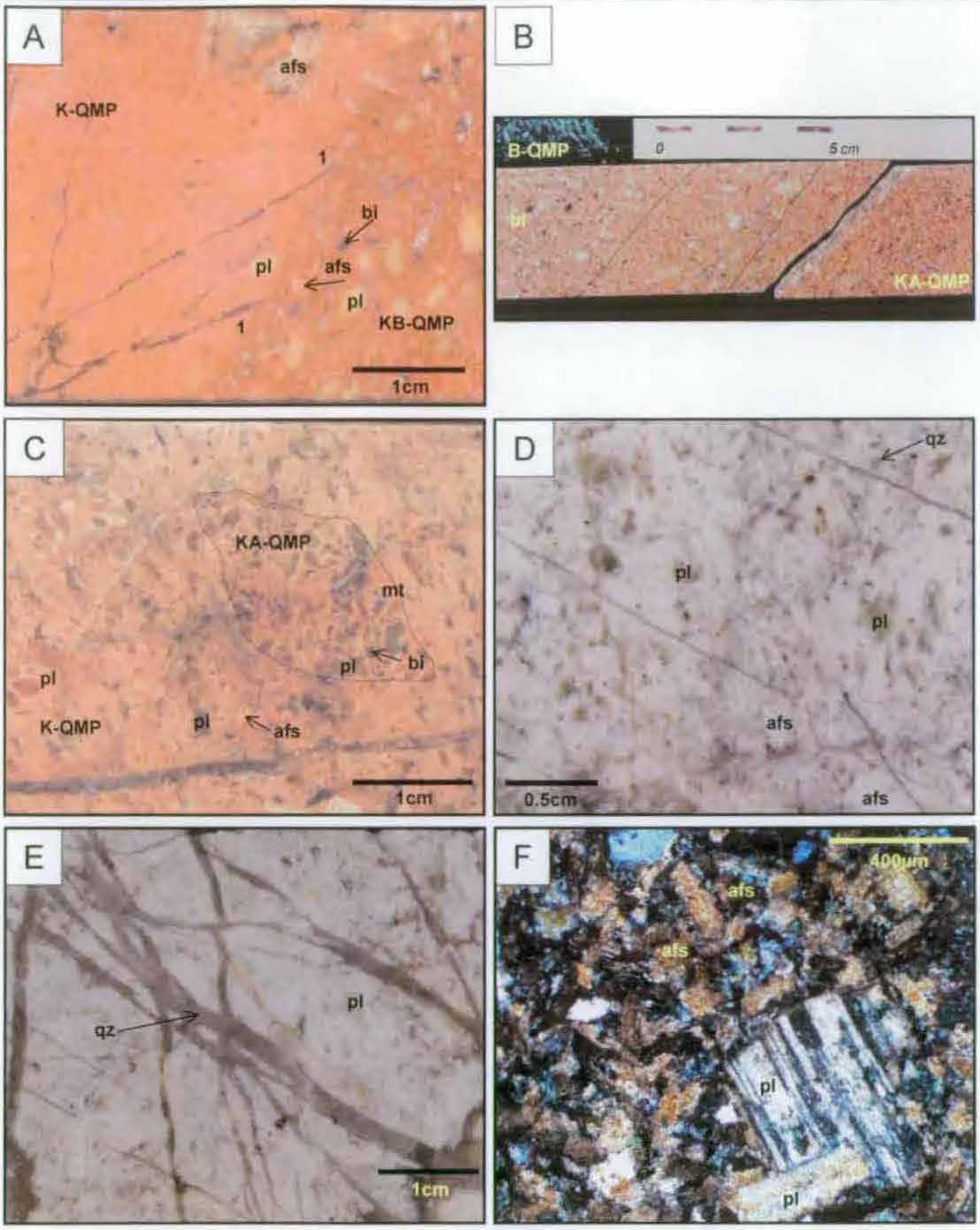

Figure 3.13 Photographs of contact relationships between the QMP phases of the Endeavour deposits, and textural features of other intrusive phases with the complexes. **A** An example of a KA-QMP intrusion intruding a veined K-QMP intrusion at E22; E22/2/303.7m. Note the truncated quartz veins at (1) **B** The gradational contact between a B-QMP and a KA-QMP intrusion at E26 is shown here; E26/46/1643.6m. Note, however, that this type of contact is rare compared to sharp contacts such as shown in (A). **C** A tear-drop shaped clast of KA-QMP within a K-QMP intrusion at E27 indicating that locally, KA-QMP intrusions pre-dated K-QMP intrusions; E27/386/241.3m. **D** The typically pale appearance of the "microgranite" intrusion at E48 is conspicuously different from other intrusions in the QMP complexes; E48/13w2/954.8m. This intrusion is finely equigranular (~1mm) to weakly porphyritic and contains abundant plagioclase, less abundant alkali feldspar and rare quartz. **E** Barren sheeted veins typically crosscut the microgranite intrusion at E48; E48/13w2/955.0m. **F** The microscopic feathery-texture of alkali feldspar crystals in microsyenite dykes is commonly defined by clusters of alkali feldspar in the groundmass, this example from E27; E27/368/289.0m. Note the cluster of plagioclase phenocrysts.

3.4.4 Minor dykes

Three varieties of early- to late-stage fine-grained, non-porphyritic dykes (0.2 – 2m wide) and dykelets (<0.2m wide) occur within volcanic and intrusive rocks of the Endeavour deposits. These are 1) seriate to equigranular micromonzodiorite, 2) microsyenite and 3) quartz microsyenite to microgranite (aplite) dykes.

3.4.4.1 Seriate to equigranular micromonzodiorite dykes

Seriate- to equigranular-textured micromonzodiorite dykes contain plagioclase + alkali feldspar + quartz with accessory biotite + augite and are typically biotite + magnetite altered. The absence of intense syn-mineral orthoclase alteration (cf. Chapter 4, section 4.4.5) in these micromonzodiorite dykes is interpreted to imply that they predate ore formation. This interpretation is consistent with their temporal relationships with the early intrusive phases, as micromonzodiorite dykes have only been observed in the monzodiorite and BQM intrusions in addition to the volcanic rocks.

3.4.4.2 Microsyenite dykes

Microsyenite dykes, distinguished in this study by a "feathery" texture defined by the K-feldspar in the groundmass (Figure 3.13f), contain 5 – 10% plagioclase with lesser (1 – 2%) alkali feldspar, biotite, augite and/or magnetite phenocrysts in a quartz and alkali feldspar (~95%) groundmass. Microsyenite dykes have been observed within all of the intrusions described above (Figure 3.14a). They appear to be fractionated derivatives of the various rocks into which they have intruded; and have no obvious unique timing in the sequence of intrusion emplacement.

3.4.4.3 Quartz microsyenite to microgranite (aplite)

Quartz microsyenite to microgranite (aplite) dykes and dykelets occur within all of the intrusions described above. They contain up to 95% graphically intergrown alkali feldspar and quartz and have a distinctive saccharoidal texture in hand specimen (Figure 3.14b). Most examples contain minor biotite microphenocrysts (Figure 3.14c). Many of the quartz microsyenite and aplite dykes contain 1 – 2% disseminated bornite ± chalcopyrite ± pyrite (Figure 3.14c), which is interpreted to imply that they are syn- or late-mineralisation intrusions. Intense K-silicate alteration has not been observed in the aplite dykes, possibly indicating a late-mineralisation timing for many of these dykes.

3.4.5 Post mineral zero porphyry dykes

Zero porphyries are volumetrically very minor post-mineral intrusions formed during the final phase of felsic intrusive activity recognized in the four Endeavour deposits studied. *Zero porphyry* is the mine term for a post-mineralisation mafic monzonite porphyry dyke, typically intruding the eastern and central parts of E26 (Figure 3.5). The local term describes one of the characteristic features of these rocks; zero Cu or Au grade.

There are two distinct rock types within the "zero porphyry" category; the "classic" zero porphyry, and what has been interpreted as a "chilled margin" phase to the zero porphyry dykes (Jones, 1985; Heithersay, 1991). All occurrences of this typically dark brown, aphanitic to weakly plagioclase-phyric (~2%) basaltic trachyandesite "chilled margin" phase are associated with "classic" zero porphyry material inward of the sharp outer intrusive contact. The "classic" zero porphyries are generally crowded (40 - 50% phenocrysts), brownish-red mafic monzonite porphyries (Table 3.1;Figure 3.14d) that contain plagioclase, alkali feldspar, augite + biotite + magnetite and anhydrite phenocrysts in a predominantly aphanitic to very fine-grained granular, alkali feldspar-rich (>95%) groundmass (Figure 3.14e). Alkali feldspar phenocrysts with poikilitic inclusions of plagioclase, apatite, augite and/or anhydrite (Figure 3.14f) are common.

In contrast to the mineralised intrusions of the Endeavour deposits, propylitic alteration assemblages (characterised by the presence of epidote) are present in the zero porphyries. In addition, zero porphyries contain no quartz – sulphide veins, K-silicate or phyllic alteration assemblages. Propylitic alteration assemblages and the absence of quartz + sulphide veins imply a post-mineral emplacement timing for both phases of the zero porphyry dykes (cf. Chapter 4, section 4.4.8).

Contacts between the "chilled" and "classic" phases are typically gradational over ~10 to 20cm (Figure 3.14g). However, differing proportions of rounded (Figure 3.14h) to angular clasts of the "chilled" phase are common in the "classic" phase within 30cm of the gradational contact. It is also significant that not all of the zero porphyry dykes have an associated "chilled margin" phases, e.g. E26/46/1747.6 – 1749.6 and E26/46/1773.0 – 1779.2m. These relationships combined indicate that the "chilled phase", or basaltic trachyandesite dykes, predate the zero porphyry dykes. The rounded nature of some of the clasts of basaltic trachyandesite within the zero porphyries possibly implies that the zero porphyries of E26 intruded along the cores of some of the basaltic trachyandesite dykes before they had totally crystallised.

Figure 3.14 Photographs of various intrusive rocks in the QMP complexes of the Endeavour deposits.

- **A** A photograph showing three separate intrusions at E27: BQM crosscut by a microsyenite dykelet. Both of these have been crosscut by a KA-QMP dykelet; E27/28/731.5m.
- **B** Saccharoidal-textured alkali feldspar and quartz is typical of pre- or syn-mineral aplite dykes. This example from E26 (E26/284/68.0m) is crosscut by numerous quartz + sulphide veins.
- **C** Biotite microphenocrysts are rare in aplite dykes (photomicrograph in ppl), but the saccharoidal texture visible in hand specimen (B) is also evident at the microscopic scale. Disseminated bornite and clusters of anhedral quartz are also characteristic of many aplite dykelets, this example from E26; E26/284/203.9m.
- **D** A typical example of a crowded zero porphyry rock from E26, comprising mainly plagioclase, alkali feldspar, clinopyroxene, magnetite and biotite phenocrysts in an aphanitic alkali feldspar-rich groundmass; E26/46/1294.2m.
- **E** A photomicrograph of part of the zero porphyry sample shown in (D) showing a primary anhydrite phenocryst with apatite inclusions and plagioclase phenocrysts in an aphanitic groundmass.
- **F** This photomicrograph in xpl shows primary anhydrite as a poikilitic inclusion, along with plagioclase, in a K-feldspar megacryst in the same zero porphyry sample as (D) and (E).
- **G** A photograph showing a gradational contact between the "chilled margin" and "classic" (crowded porphyritic) phases of the zero porphyry dykes at E26; E26/264/247.6m.
- **H** A rounded clast of the "chilled" phase within the "classic" phase of a zero porphyry intrusion; E26/264/263.0m. Note the sparse plagioclase phenocrysts in the basaltic trachyandesite "chilled" phase and the abundant plagioclase and alkali feldspar phenocrysts in the "classic" phase.

Abbreviations:
afs - alkali feldspar; anh - anhydrite; ap - apatite; apl - aplite; bi - biotite; bor - bornite; chilled - chilled margin phase of the zero porphyry dykes; cpx - augite; mt - magnetite; pl - plagioclase; qz - quartz; zero - classic phase of the zero porphyry

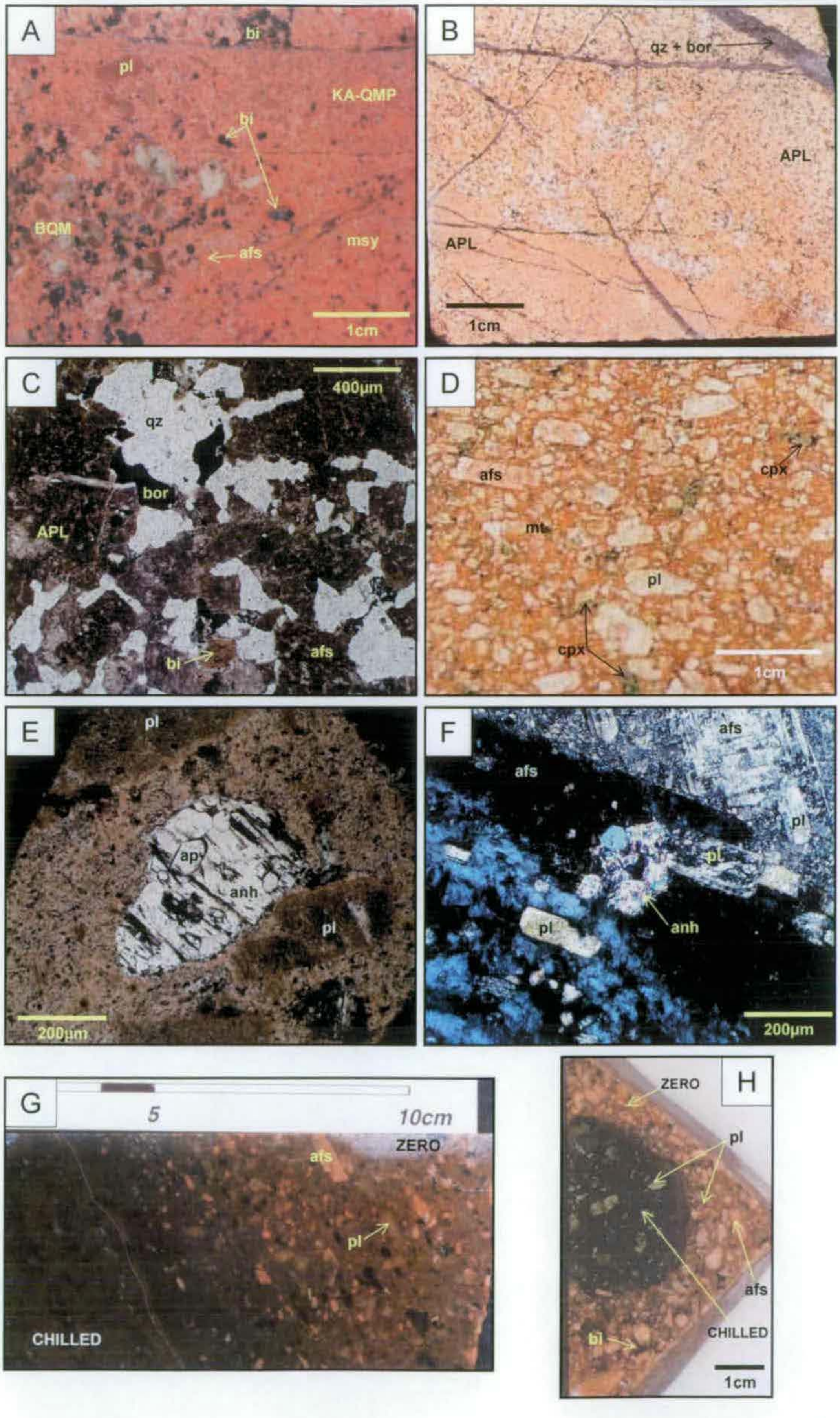
A
bi
pl
KA-QMP
bi
BQM
afs
msy
1cm
B
qz + bor
APL
APL
1cm
C
400μm
qz
bor
APL
bi
afs
D
afs
cpx
mt
pl
cpx
1cm
E
pl
ap
anh
pl
200μm
F
afs
afs
pl
pl
anh
pl
200μm
G
5
10cm
ZERO
afs
pl
CHILLED
H
ZERO
pl
afs
CHILLED
bi
1cm

It is important to note that the "classic" zero porphyry dykes are virtually texturally and mineralogically identical to the Gunningbland Forest monzonite porphyry intrusions ~15km south-southwest of the *Northparkes Mines* area (cf. Figure 2.5) and zero porphyry dykes at E37, with one notable exception. The Gunningbland Forest monzonite porphyry and E37 zero porphyry intrusions do not contain anhydrite phenocrysts (Figures 3.14e and 3.15a and b).

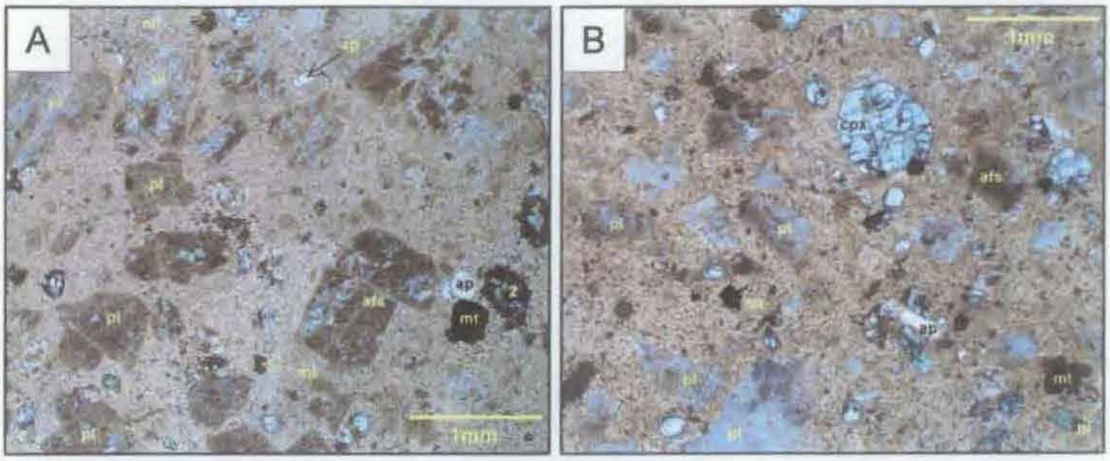

Figure 3.15 Photomicrographs showing the virtually identical texture and mineralogy of **A** the zero porphyries at E26 (E26/46/1294.3m) and **B** Gunningbland Forest monzonite porphyry, ~15km south-southeast of E26. With the exception of the groundmass being finer-grained in the zero porphyry, and the rock in general, a little more intensely altered, the biotite (1 on A; bi on B), augite (2 on A; cpx on B), magnetite (mt), plagioclase (pl), alkali feldspar (afs) phenocrysts and accessory apatite (ap) are present in both porphyritic rocks.

3.4.6 Mafic dykes

Several narrow (~1m wide) mafic dykes of basaltic composition are present at E22, E27 and E48 (Jones, 1985; Wolfe, 1994; this study). The dykes have a consistent northeasterly strike and near vertical dip and are typically coincident with variably altered zones of structural weakness. The relative age of the mafic dykes is unknown. Some have been faulted (Figure 3.16) and affected by late stage sericite alteration with associated variable chalcopyrite/pyrite (Jones, 1985), while others are not faulted and do not show signs of alteration. Considering the presence of sericite alteration in many examples, it is considered here that, although maybe not directly related to the QMP complexes and associated mineralisation, at least some of these mafic dykes may have been emplaced during the waning stages of Ordovician magmatism in the GVC. However, they may be completely unrelated to Ordovician magmatism and may be as young at Tertiary in age (Duggan *et al.*, 1999).

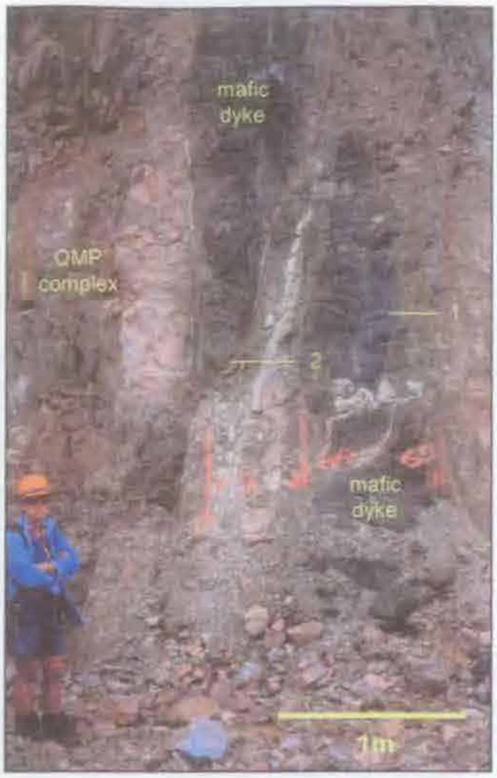

Figure 3.16 The view of the E27 pit looking northeast, showing a mafic dyke that has intruded the QMP complex. The mafic dyke has sericite-altered margins (1) and has been crosscut by faulting and sericite alteration (2).

3.4.7 Other rocks in the QMP complexes

3.4.7.1 Breccia pipes

What have been described as limited extent (~30m laterally x ~170m vertically) hydrothermal breccias occur at E27 and E22 (Jones, 1985). The pipe at E27 is a matrix-supported breccia, where the matrix is fine-grained, variably porphyritic- to non-igneous material (possibly rock flour?) and supports angular to sub-rounded clasts of variably altered and mineralised K-QMP, KA-QMP and veined Wombin Volcanics (Figure 3.17a). Its origin is unclear, however, it is proposed here that the breccia body at E27 possibly formed in response to a subsurface magmatic – hydrothermal explosion in the subvolcanic magma conduit associated with E27. Its formation can be restricted temporally to post-KA-QMP intrusions because rounded clasts of these rocks have been incorporated into the breccia.

3.4.7.2 Pebble dykes

Minor, volumetrically insignificant pebble dykes have been documented in the Endeavour deposits by several workers (e.g. Jones, 1985; Heithersay *et al.*, 1990;

Heithersay and Walshe, 1995; Harris, 1997) and additional examples have also been recognised during the current study. As with the breccia bodies described above, the origin of the pebble dykes remains unknown, however, the timing of their emplacement is restricted to post- zero porphyry intrusion because many examples from E26 contain variably rounded clasts of zero porphyry material, as well as other intrusions (Figure 3.17b).

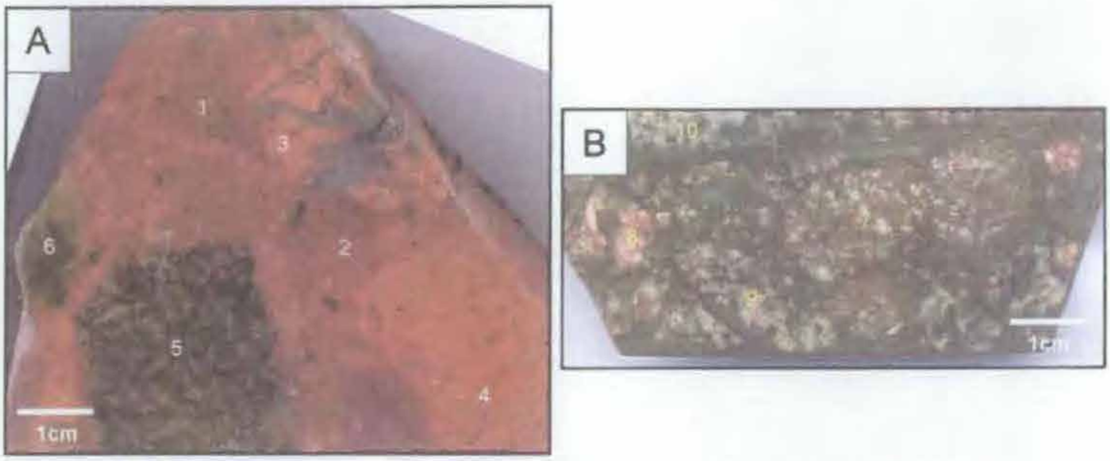

Figure 3.17 **A** An example of the hydrothermal breccia from E27 showing the variably porphyritic (1) to "non-igneous" (2) nature of the matrix, the presence of K-QMP (3) and KA-QMP (4) and altered Wombin Volcanics (5 and 6) clasts; E27/W/17 – pit sample). **B** A pebble dyke from E26 (E26/46/1693.9m) that indicates a post zero porphyry emplacement timing for its formation by the presence of variably rounded zero porphyry (7), mineralised (chalcopyrite) KA-QMP (8), BQM (9) and monzodiorite (10) clasts.

3.5 Discussion

Recognition of the different intrusive phases within the QMP complexes was undertaken to try and establish whether specific phases correspond with higher Cu and Au grades while others correspond with lower grades. The relationships between Cu grades and the different intrusive phases within the QMP complexes are shown on Figures 3.4, 3.5, 3.6 and 3.7 for E22, E26, E27 and E48 respectively. The 0.5% Cu contour extends into the host volcanic rocks at all four deposits. Jones (1985) showed that at E22, E26 and E27, zones of high Cu and Au grades in the host volcanic rocks coincide with zones of intense potassic, specifically K-feldspar, alteration. The most intense K-feldspar alteration at all four Endeavour deposits occurs within the K-QMP intrusions (described in Chapter 4). Figures 3.5 and 3.7 show that, at E26 and E48 respectively, the highest Cu grades (2% Cu contour) are broadly coincident with the K-QMP intrusions (House, 1994). The consistent relationship of high Cu and Au grades with K-QMP intrusions is well illustrated on Figure 3.18, where downhole plots show the obvious decrease in grade moving from K-QMP to other intrusions.

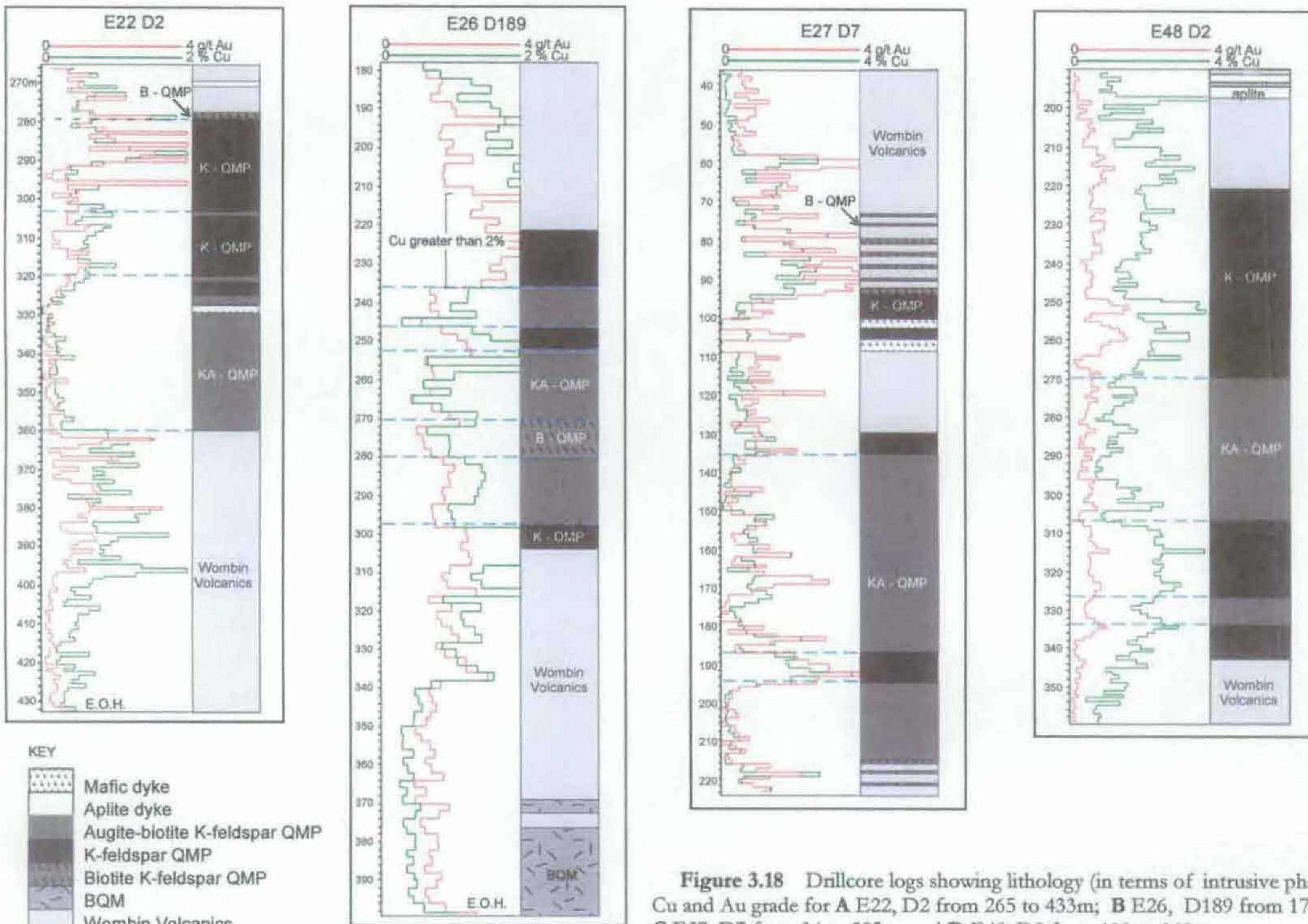

Figure 3.18 Drillcore logs showing lithology (in terms of intrusive phases) and Cu and Au grade for **A** E22, D2 from 265 to 433m; **B** E26, D189 from 178 to 399m; **C** E27, D7 from 34 to 225m; and **D** E48, D2 from 190 to 360m.

Based on the spatial and crosscutting relationships, K-silicate alteration and ore deposition in the Endeavour deposits is interpreted to be related to the emplacement of the K-QMP intrusions, which occurred early in the sequence of intrusive activity in the QMP complexes. There are numerous early-mineral B-QMP dykes and dykelets that predated K-QMP intrusions in the Endeavour deposits, but these are typically peripheral to the QMP complexes and are volumetrically minor. They may have been dilated during the K-QMP intrusive event, explaining their peripheral distribution.

The abundance of anisotropic textures in the K-QMP intrusions provides additional evidence that the main mineralising event accompanied this phase of intrusive activity. The development of anisotropic textures is thought to imply magma crystallisation in the presence of a magmatic – hydrothermal fluid (Shannon et al., 1982; Kirkham and Sinclair, 1988; London, 1992; Candela and Blevin, 1995; Lowenstern and Sinclair, 1996). The high (5 – 10%) abundance of anisotropic textures in the K-QMP intrusions is thus interpreted to indicate that volatile exsolution from the underlying magma chamber reached a peak during the emplacement of this phase, which is consistent with the close spatial association of K-QMP intrusions and the 0.5% Cu contour (Figures 3.4, 3.5, 3.6 and 3.7 and Figure 3.18). However, KA-QMP intrusions also occur within the 0.5% Cu contour; these intrusions too, contain anisotropic textures (although they are less abundant than in the K-QMP intrusions; 2 – 3%). Therefore, the syn-to late-mineral KA-QMP intrusions are interpreted to have added metal to the Endeavour porphyry Cu-Au deposits, consistent with the interpretation for E26 of Heithersay and Walshe (1995). Late-mineral B-QMP dykes and dykelets tend to occur outside the 0.5 Cu contour even though they typically contain bornite clots and are weakly mineralised. This is consistent with a late-mineral timing for this intrusive phase.

The inferred close timing of emplacement of all three QMP phases raises the question as to whether fractionation from the BQM produced the biotite-phyric porphyries at the margins of the QMP complexes and these then evolved to form more felsic varieties towards the centres of the intrusive complexes. These hypotheses are tested using whole rock igneous geochemistry in Chapter 8.

The post-mineral zero porphyry dykes of E26 contain abundant mafic and rare anhydrite phenocrysts, implying that less felsic igneous activity continued beyond the mineralising event. The presence of anhydrite phenocrysts indicates that the magma that produced the zero porphyries, which are less felsic than the QMP intrusions, contained sulphur that was mainly present as an oxidised species (Imai *et al.*, 1993).

A diagnostic characteristic of the K-QMP intrusions that distinguish them other QMP intrusions is the relative abundance of anisotropic textures. The type of volatile-rich fluid accumulation associated with these textures is generally typical of more evolved granitic rocks associated with Sn and Mo deposits (Kirkham and Sinclair, 1988). However, features similar to those interpreted to be indicative of crystallisation from an exsolved magmatic fluid have been noted in intrusions associated with some porphyry Cu deposits (Kirkham and Sinclair, 1988). These textures include pegmatitic bodies rich in K-feldspar, biotite and Cu minerals at Yerington, Questa and Copper Mountain and elongate cavities lined with sulphides and quartz at Bingham. Garwin (2002) documented similar textures from Batu Hijau. Kirkham and Sinclair (1988) suggested that most intrusions associated with porphyry Cu deposits would be too mafic to support the development of comb-layered quartz. However, they did suggest that at least some of the pegmatite bodies at Yerington, Questa and Copper Mountain might represent more mafic counterparts to comb-layered quartz associated with felsic Sn and Mo deposits. The intrusions associated with mineralisation in the Endeavour deposits are interpreted to be transitional between the calc alkaline, mafic intrusions associated with ore deposition in many porphyry Cu deposits, for example Batu Hijau, and the more granitic intrusions typically associated with porphyry Mo deposits, for example Henderson.

3.6 Summary

Eight different rocks types have been recognised in five intrusive events at E22, E26, E27 and E48. The five intrusive events are as follows:

1. A coarse-grained, equigranular monzodiorite intrusion, restricted to the deeper portions of E26;
2. Pre-mineral biotite quartz monzonite (BQM) intrusions, recognised at all four deposits.
3. A series of three successive QMP intrusions emplaced over a short period after the intrusion of the BQM comprise the QMP complexes central to each of the deposits, where the overall sequence of emplacement is early-mineral B-QMP dykes and dykelets → volumetrically dominant syn-mineral K-QMP → syn- to late-mineral KA-QMP intrusions → minor late-mineral B-QMP dykes.
4. Basaltic trachyandesite dykes and zero porphyry dykes at E26 have not been crosscut by quartz – sulphide veins and intense potassic alteration, and preserve propylitic alteration. These features imply that the zero porphyries were intruded late in the intrusive history of the Endeavour deposits.

5. Mafic dykes of uncertain age, may have been emplaced during the waning stages of Ordovician magmatism in the GVC.

The sequence of intrusion of the various phases within the QMP complexes of the Endeavour deposits is different from that of many other porphyry Cu deposits, e.g. the Laramide magmatic complexes of Arizona (Figure 3.19a). In the Arizona complexes, there is a distinct evolution in the intrusive phases from less to more felsic. In contrast, although the intrusive phases associated with the Endeavour deposits initially evolve to more felsic compositions, the later intrusive events are more considerably less felsic (Figure 3.19b) and possibly indicate that processes other than magmatic fractionation may have played a role in the formation of the Endeavour QMP complexes. This issue is discussed further in Chapter 8.

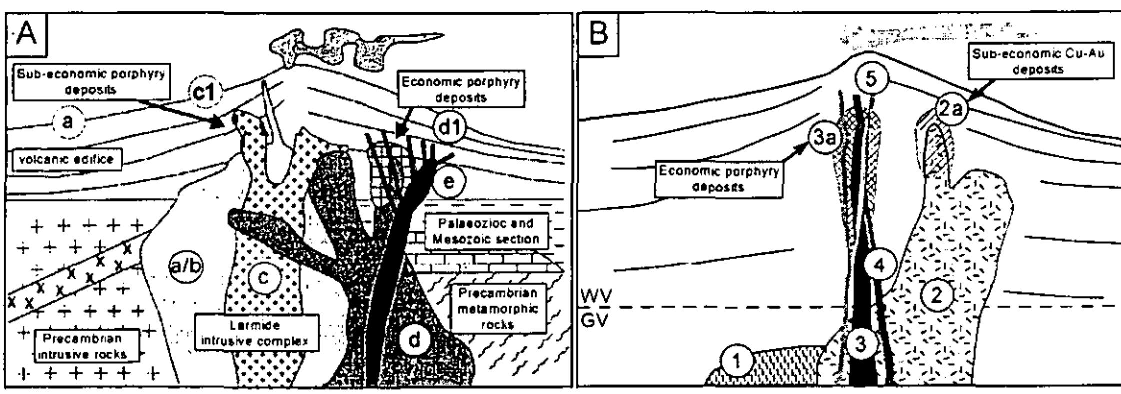

Figure 3.19 **A** Schematic representation of the characteristic sequence of intrusive activity in the Laramide magmatic complexes, Arizona (modified from Lang and Titley, 1998); **a** - mainly andesite; **a/b** - diorite/quartz diorite; **c** - monzodiorite/ granodiorite; **c1** - minor mineralisation; **d** - granodiorite/granodiorite/quartz monzonite /granite, **d1** - main stage mineralisation, **e** - quartz monzonite/granodiorite/granite. **B** Schematic illustration of the intrusive history in the Endeavour deposits, NSW; **1** - monzodiorite; **2** - biotite quartz monzonite; **2a** - minor mineralisation (e.g. E31 prospect); **3** - quartz monzonite porphyry complex; **3a** - main stage of mineralisation (e.g. E22, E26, E27 and E48); **4** - basaltic trachyandesite mafic monzonite porphyry dykes; **5** - mafic dykes; GV - Goonumbla Volcanics; WV - Wombin Volcanics.

In the same way to many other porphyry Cu deposits from around the world, intense K-silicate alteration assemblages and highest Cu and Au grades at E22, E26, E27 and E48 are associated with one of the earliest phases of porphyritic intrusions; the K-QMP intrusions. Additional ore deposition occurred in association with the emplacement of the later KA-QMP intrusions. This relationship of the highest Cu (and Au) grades being associated with the intrusion that generated the most intense K-silicate alteration is observed in many other porphyry Cu deposits, for example El Salvador (Gustafson and Hunt, 1975), Batu Hijau (Clode *et al.*, 1999) and Yerington (Carten, 1986; Dilles and Einaudi, 1992).

CHAPTER 4

Alteration and Mineralisation

4.1 Introduction

Porphyry-style ore deposits are characterised by sulphide mineralisation occurring in vein stockworks and associated hydrothermal alteration assemblages within the porphyry intrusions and surrounding host rocks (e.g. Titley, 1982). Geochemical studies have shown that the mineralising fluids are at least partly magmatic – hydrothermal in origin (e.g. Meyer and Hemley, 1967). The key to understanding porphyry-style alteration, veining and sulphide deposition lies in careful documentation of the spatial and temporal distribution of vein and alteration assemblages, which preserve evidence for hydrothermal fluid evolution. Hydrothermal alteration is a metasomatic process whereby the mineralogy, chemistry and texture of a rock change as a hydrothermal fluid reacts with its surroundings (Titley, 1994). In this way, fluid continuously modifies the volume of rock through which it moves by the dissolution of pre-existing phases and the precipitation of new phases. It is rare for the metasomatic hydrothermal reactions to proceed to completion in porphyry-style deposits. More commonly, these deposits preserve a complicated and inter-related series of partially completed metasomatic reactions that record the changing nature of the fluid with time (e.g. Gustafson and Hunt, 1975).

This chapter describes the alteration, veining and sulphide deposition of the E22, E26, E27 and E48 deposits, where the descriptions presented are mainly, although not exclusively, summarised from previous, detailed studies that have been conducted on individual deposits or prospects. Descriptions are augmented with observations from new, detailed drillcore logging undertaken from the four Endeavour deposits for this thesis. The generalised descriptions presented in the following sections are based on similarities in the secondary mineral assemblages that occur in the four Endeavour deposits. Deposit-specific characteristics are also discussed where extremes unique to a specific system need to be documented. Because sulphides are an integral component of the alteration and vein assemblages in the Endeavour deposits, they are included in these general descriptions. Following on from the descriptive sections, a detailed discussion of the sulphide mineralogy and related aspects of ore formation are presented, before a discussion and comparison of the Endeavour deposits with other porphyry-style deposits concludes the chapter.

Because several detailed alteration and vein paragenetic studies have already been conducted on the Endeavour deposits, the aim of this chapter is not to re-classify previous work. Instead, the aim is to synthesise all previous work and group it with new results from the current study, into a broad alteration and vein assemblage framework typical of the Endeavour deposits that takes into account the multiplicity of intrusive events detailed in Chapter 3. The intrusive, alteration and veining framework developed in this chapter then provides a temporal basis for fluid evolution studies, which is a main objective of this thesis.

4.2 Previous work

Several detailed studies of alteration and veining paragenesis have been conducted on the Endeavour deposits, beginning with a description of the hydrothermal alteration assemblages associated with E26 (Heithersay, 1986). Heithersay *et al.* (1990), and Heithersay and Walshe (1995) subsequently revised this paragenesis. Based on the detailed examination of the mutual relationships of veins and alteration haloes in drill core, Heithersay and Walshe (1995) proposed eleven stages of alteration and veining related to the intrusion of two quartz monzonite porphyry phases, *QMP 1* and *QMP 2*. The results of these studies by Heithersay and co-workers have formed the basis for most other studies of alteration and vein parageneses of the Endeavour deposits.

Wolfe (1994) described four and Howland-Rose (1996) described six main alteration and vein assemblages for the E48 deposit. Harris (1997) documented six stages of alteration and vein generation for E26 and related these temporally to the intrusion of four quartz monzonite porphyry intrusions, QM1 – QM4. Kolkert (1998) outlined six vein stages at the E28 prospect, some of which she interpreted as distal propylitic alteration associated with the E26 deposit. Squires (1992) described the alteration zones surrounding E27.

Figure 4.1 is a compilation of the alteration and vein parageneses of E26, E48 and E28 based on the studies of Heithersay (1986), Heithersay *et al.* (1990) and Heithersay and Walshe (1995) and Harris (1997) for E26; Wolfe (1994) and Howland-Rose (1996) for E48; and Kolkert (1998) for E28. These parageneses have been interpreted with respect

	Heithersay, 1986, 1990, 1995 - E26	Harris, 1997- E26	Wolfe, 1994 - E48	Howland-Rose, 1996 - E48	Kolkert, 1998 - E28	
Pre-mineral alteration	*Intrusion of BQM* **Stage 1** Vein dyking and incipient fine veining, precursor to *QMP 1*, quartz - K-feldspar - biotite - gypsum **Stage 2** Pervasive and selectively pervasive albitisation + sericitisation of feldspars; magmatic biotite → chlorite - quartz - carbonate - fluorite	*Intrusion of QM 1 with brain rock*	*Intrusion of BQM* **Stage 1** Selectively pervasive albitisation		*Intrusion of BQM* **Stages 1 and 2** equivalent to Wolfe (1994) Stages1 and 2 **Stage 3 - Distal propylitic alteration** - Selectively pervasice Albite alteration - Albite halos on distal carbonate - epidote veins - selectively pervasive epidote alteration	Pre-mineral alteration
Early K-Silicate alteration and mineralisation	*Intrusion of QMP 1* **Stage 3** Pervasive and vein controlled biotite development **Stage 3** - Patchy to pervasive K-feldspar alteration and veinlets, - haematite dusting of secondary K-feldspar **Stage 3** - quartz veining discontinuous and irregular with anhydrite ± albite ± K-feldspar ± magnetite ± sulphides; K-feldspar vein halos	**Stage 1A** Selectively pervasive alteration; K-feldspar (proximal) to biotite (distal) to intrusions **Stage 1A** Pervasive K-feldspar alteration and haematite dusting of feldspar **Stage 1B** K-feldspar ± quartz ± anhydrite ± bornite veinlets **Stage 1C** K-feldspar + biotite + magnetite ± quartz ± bornite alteration and veinlets *Intrusion of QM 2* **Stage 2A** Continuation of 1B and 1C veining with more quartz + bornite core + K-feldspar + magnetite ± bornite ± chalcopyrite selvages **Stage 2B** Thick banded quartz ± anhydrite (centre) veins ± Au ± chalcopyrite in sericite selvage	**Stage 1a** Selectively pervasive to pervasive biotite and magnetite alteration with magnetite veinlets **Stage 2A** quartz + calcite + anhydrite + K-feldapr + magnetite veinlets with proximal bornite > chalcopyrite → chalcopyrite > bornite → chalcopyrite distal **Stage 2B** quartz - K-feldspar - bornite (selvage) stockwork	**Stage 1 - Bi alteration** quartz + biotite + magnetite ± haematite veins and selvages **Stage 2** quartz + biotite + haematite + K-feldspar + (bornite > chalcopyrite) ± magnetite **Stage 3** quartz + muscovite + biotite ± white mica ± haematite + bornite + chalcocite + covellite + chalcopyrite ± sphalerite	**Stage 3A - epidote veins** zones of epidote + magnetite + carbonate alteration Patchy, selectively pervasive calcite alteration, notable for plag and mafic minerals Selective to pervasive (weak to intense) chlorite alteration of groundmass, plag and mafic minerals. Occurs in K-silicate, propylitic and lesser extent in phyllic zones **Stage 3B - Albite-Epidote alteration** quartz + carbonate + chlorite + sericite + pyrite veins	Early, distal propylitic alteration
Deep alteration features			*Intrusion of QMP* Grey irregular, discontinuous, anastomosing, to tubular Qz veins Vein dykes - quartz intergrown with aphanitic igneous material (brain rock) with haematite dusted feldspars Intrusion of 0.5 to 5cm monzonite dykelets - sacchroidal textured, vein dyke material Barren sheeted veins Patchy, pervasive, bleached sericite alteration Rare molybdenum veins			Deep alteration features
Main mineralising events	**Stage 4 - main mineralising vein event** quartz - K-feldspar + anhydrite + fluorite + apatite + rutile + bornite + chalcopyrite + haematite with selvages of quartz + K-feldspar + biotite **Stage 5 - stockwork vein event** quartz - K-feldspar + anhydrite + sericite + carbonate + bornite ± chalcopyrite + tellurides + lead selenides **Stage 6** quartz - K-feldspar + bornite ± chalcopyrite ± albite ± rutile veins *Intrusion of QMP 2* brain rock development magmatic - hydrothermal brecciation **Stage 7 - repeat of Stage 4 (*QMP 1*) for *QMP 2*** quartz + K-feldspar + biotite + anhydrite + (chalcopyrite > bornite) veins **Stage 8 - straight-walled, sheeted veins** milky quartz + fluorite + chalcopyrite + bornite	**Stage 2C - main mineralising event** Fine network of quartz + anhydrite + sulphides (proximal bornite → bornite > chalcopyrite → chalcopyrite > bornite → chalcopyrite distal) with thin sericite selvage **Stage 2DI - sheeted veins** quartz + sulphides ± anhydrite, with sericite + quartz selvage *Intrusion of QM 3 and QM 4?* **Stage 2DII** Sparse, irregular 2DI veins in QM3 and QM4 **Stage 2E - thick, banded quartz veins** quartz + sulphides + anhydrite with sulphides + magnetite + haematite + sericite + gypsum selvages **Stage 2F** quartz + anhydrite + sulphides veins, some spatial relationship to Qm4?	**Stage 3A - main mineralising event** quartz + bornite + chalcocite ± anhydrite veins **Stage 3B - stockwork veins** quartz + sulphides, multiple generations, intense pervasive sericite alteration (overprints early K-silicate alteration); bornite, chalcopyrite, chalcocite, covellite, tetrahedrite **Stage 3C** - Vein-controlled sericite + haematite alteration (mottled appearance) - carbonate + quartz + sulphides (bornite > chalcopyrite) **Stage 3D - carbonate veining** carbonate + chalcopyrite/pyrite (distal to Stage 3C)	**Stage 4 - Main mineralising event** quartz + sericite + calcite + biotite + bornite + sphalerite + galena + pyrite ± chalcopyrite **Stage 5** carbonate + quartz + bornite ± chalcocite ± enargite + covellite ± anhydrite	**Stage 4** equivalent to Wolfe (1994) Stage 3	Main mineralising events
Late sericite overprint		**Stage 3** Pebble dykes, where rock fragments often show pervasive sericite alteration	**Stage 3E - Pervasice Sericite + carbonate + quartz overprint** quartz + bornite + chalcocite + carbonate, with alunite (?) veinlets and alteration		**Stage 4C** Pervasive sericite overprint (Wolfe, 1994)	Late sericite overprint
Fault and shear zone alteration	**Stage 9 - quartz + sericite + pyrite ± chalcopyrite overprint** pervasive or vein/vein envelope controlled, intense to weak to not recognised	**Stage 4 - quartz + pyrite fracture fill** pyrite + anhydrite + sericite + talc + quartz shear, fracture fill; gypsum + carbonate selvage. Mineralisation is variable, bornite ± chalcopyrite ± galena ± sphalerite ± acanthite; possibly equivalent to Kolkert (1998) carbonate + base metal sulphide veins	**Indeterminate veins** sericite + pyrite + carbonate cut biotite + magnetite (Stage 3), cut by carbonate (Stage 4) **Fault Zone alteration** sericite + carbonate + pyrite alteration, quartz + sulphide vein fragments can be present		**Stage 5A - sericite + quartz alteration** carbonate + quartz + pyrite/chalcopyrite veins and patchy alteration, often with Altona Fault (Wolfe, 1994) **Stage 6A veins** quartz+carbonate+fluorite+altered rock fragments	Fault and shear zone alteration
Late phyllic alteration	**Stage 10** carbonaten + sulphate + zeolite veins **Stage 11** anhydrite to gypsum veins	**Stage 5A - post mineral** anhydrite + gypsum + sericite ± bornite ± chalcopyrite ± pyrite with sericite zones **Stage 5B** sericite + chalcopyrite, variation of above?	**Stage 4 - Carbonate alteration** carbonate "crackle breccia" + gypsum + fluorite + pyrite	**Stage 6** carbonate + clay alteration of sericite + sulphides	**Indeterminate veins** - carbonate + base-metal sulphide veins - carbonate + sericite + quartz + anhydrite veins	Late phyllic alteration
Late porpylitic alteration		*Intrusion of zero porphyries* **Stage 6 - Selective Propylitic alteration** - epidote + chlorite + calcite + haematite ± pyrite - thin haematite veinlets **Selective haematite ± carbonate alteration** epidote + chlorite + calcite + pyrite alteration	**Propylitic alteration** - distal epidote + chlorite + carbonate + pyrite + apatite alteration - epidote + carbonate + chlorite alteration replaced early biotite alteration - Patchy pervasive silica alteration - Distal pyrite veinlets with haematite selvages			Late porpylitic alteration

Figure 4.1 An interpreted synthesis of previous vein and alteration paragenetic studies of the Endeavour deposits (compiled from Heithersay, 1986; Heithersay *et al.*, 1990; Heithersay and Walshe, 1995; Wolfe, 1994; Howland-Rose, 1996; Harris, 1997; Kolkert, 1998.

to the intrusive histories established by the relevant studies, to show a generalised temporal framework of alteration and mineralisation of the Endeavour deposits as a whole. Squires' (1992) work is not included since it did not classify the alteration zones at E27 in temporal terms. Details of vein and alteration paragenesis in terms of intrusive activity have not been previously documented for E22 and E27.

4.3 Terminology

The following terms used in this chapter describe the various alteration styles and vein characteristics (Titley, 1982):

- selectively pervasive alteration – only specific minerals within the rock are altered;
- pervasive alteration – intense, texturally destructive alteration converting all minerals to a new mineral assemblage;
- patchy alteration – selective or pervasive alteration that is localised or patchily developed;
- weak, moderate or intense – describes the relative intensity of the alteration based on visual estimates;
- vein alteration – typically a vein selvage or vein of one mineral or a simple mineral assemblage;
- halo – the full spatial extent of an alteration mineral or mineral assemblage, typically adjacent to veins (vein envelope);
- vein – fracture filled by hydrothermal minerals, minimum width 5mm; and
- veinlet – fracture (<5mm wide) filled by hydrothermal minerals.

4.4 Alteration and vein paragenesis

Hydrothermal alteration at the Endeavour deposits is typically restricted to the intrusive and host volcanic rocks within a ~750m radius of the QMP complexes. The different alteration zones recognised are largely discontinuous and non-symmetrical and some alteration assemblages do not occur in every deposit. The "classic" porphyry-style alteration zoning as described by Lowell and Guilbert (1970) (potassic core – phyllic halo – peripheral propylitic zone) is complicated in the Endeavour deposits due to the multiplicity of intrusions and their associated hydrothermal alteration assemblages, and to fault controls on the late stage phyllic overprint. Although each of the deposits is unique in terms of its alteration zonation and paragenesis, there are many common features, and it is these common features that have been combined to develop the overall alteration and vein paragenesis presented below.

Figure 4.2 is a schematic space – time plot of the envisaged alteration and vein paragenesis of the Endeavour deposits. It takes into account the intrusive history established for the Endeavour deposits during this study and integrates this with previous paragenetic findings. In particular, the emphasis of the current study has been on the textures indicative of the transition from magmatic to hydrothermal conditions, i.e. vein dykes, brain rock, partial brain rock, miarolitic cavities, etc., (cf. section 3.4.3.2). Figure 4.2 establishes a broad temporal framework for the alteration and veining paragenesis that groups several previously defined stages into four main stages; an early stage, a transitional stage, a main mineralisation stage and a late mineralisation stage; pre- and post-mineralisation stages are also defined. The following sections describe each of these stages in detail.

4.4.1 Pre-mineral alteration

Heithersay *et al.* (1990) and Heithersay and Walshe (1995) defined the earliest vein and alteration stage at E26 as a series of vein-dykes with minor Cu-sulphides that appear to have formed prior to early K-silicate alteration. They suggested that these vein-dykes represent part of the alteration halo associated with the intrusion of the BQM (Figure 4.3a).

Pre-mineral, weak to intense, selectively pervasive to pervasive albitisation and sericitisation of plagioclase and K-feldspar (Figure 4.3b), with concomitant alteration of magmatic biotite to chlorite + quartz + carbonate ± fluorite (Figure 4.3c) mainly affected the volcanic host rocks and the BQM intrusions of the Endeavour deposits (Heithersay *et al.*, 1990; Wolfe, 1994; Kolkert, 1998).

4.4.2 Early Stage

Figure 4.2 indicates that in this study, early biotite and magnetite alteration, K-feldspar alteration, magnetite veinlets and K-feldspar + quartz ± biotite ± magnetite + Cu-sulphides ± anhydrite ± calcite veins and veinlets are grouped into the **Early Stage** of the temporal framework of the Endeavour deposits. Veins including quartz and sulphides within the early K-silicate alteration assemblage are defined as E1 veins. It is interpreted here that early stage K-silicate alteration assemblages are associated with the intrusion of the K-QMP intrusions at each of the deposits (Heithersay and Walshe, 1995; this study).

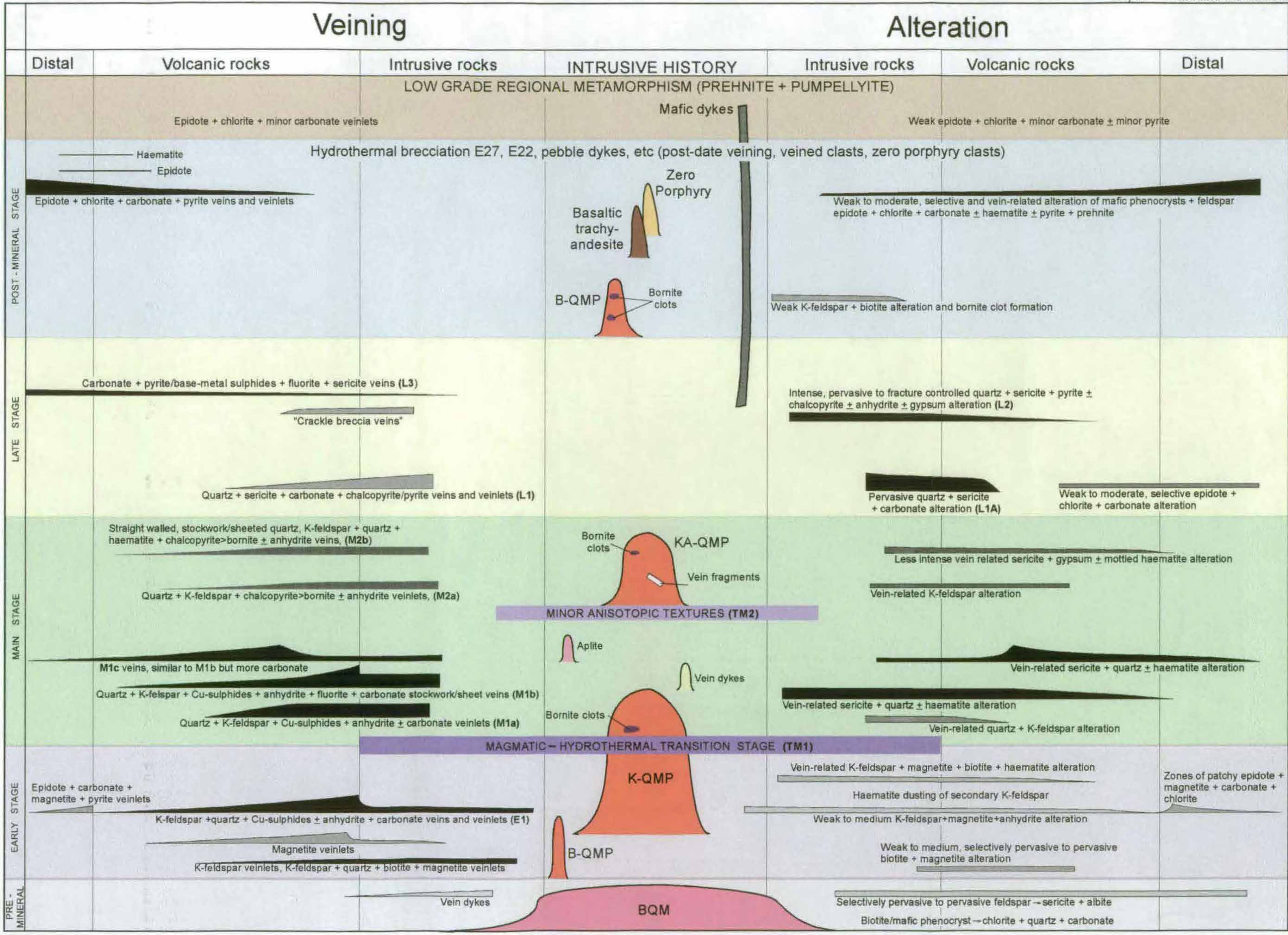

Figure 4.2 A schematic space - time illustration of the vein and alteration paragenesis in relation to the various intrusive events in the Endeavour deposits.

Figure 4.3 Photographs and photomicrographs of alteration assemblages from the Endeavour porphyry Cu-Au deposits.

- **A** An example of a pre-BQM vein dyke in Wombin Volcanics from E48 (E48/13w2/730.5m). Note the early stage E1 quartz + sulphide (1) and K-feldspar (2) veinlets that have crosscut the vein dyke.
- **B** Photomicrograph in crossed-polarised light showing selectively pervasive albitisation and sericitisation of feldspars (BQM of E48, E48/13w2/1015.0m).
- **C** Weak to moderate, selectively pervasive chlorite replacement of primary mafic phenocrysts (BQM from E26, E26/46/1759.6m).
- **D** Photomicrograph showing pervasive replacement of groundmass and mafic and feldspar phenocrysts by biotite and magnetite (Wombin Volcanics at E48; Wolfe, 1994).
- **E** Early formed secondary biotite + magnetite "spots" in Wombin Volcanics distal (~100m) to the E48 QMP complex; E48/7/111.4m.
- **F** The dark grey appearance of this BQM rock is due to pervasive biotite and magnetite alteration (E26/272/150.1m). K-feldspar veinlets also crosscut the sample.
- **G** Reddening of Wombin Volcanics by haematite dusting of feldspar (E27/368/294.1). Thin (~1mm) orthoclase veinlets crosscut the sample.
- **H** A typical early stage E1 veinlet, comprising K-feldspar + quartz + biotite ± magnetite, in the Wombin Volcanics close to E48 (Wolfe, 1994).
- **I** A photomicrograph of the same E1 vein in (G) under crossed-polarised light showing a central seam of quartz , grading out into magnetite and then into K-feldspar + biotite.

Abbreviations:
ab - albite; bi - biotite; chl - chlorite; epi - epidote; Kfs - K-feldspar; mt - magnetite; pl - plagioclase; qz - quartz

Early K-silicate alteration associated with the Endeavour deposits comprises selectively pervasive biotite and magnetite alteration and irregular magnetite veinlet formation distal to the QMP complexes, and proximal pervasive K-feldspar alteration and veinlet development (Heithersay *et al.*, 1990; Wolfe, 1994; Harris, 1997). These workers also suggested that there were both spatial and lithological controls on the early K-silicate alteration mineralogy, with early, secondary biotite and magnetite alteration typically best developed in the host volcanic rocks, and later pervasive K-feldspar alteration more common in the BQM intrusions.

Selectively pervasive to pervasive replacement of mafic phenocrysts, feldspar phenocrysts and groundmass material by biotite and magnetite (Figure 4.3d) has occurred in 50 – 200m aureoles around the central QMP complexes at each deposit (Heithersay *et al.*, 1990). Fine (<0.5mm) intergrowths of shreddy biotite and subhedral magnetite typically form clusters, which gives intensely biotite + magnetite altered rocks a spotted appearance (Figure 4.3e). Although this alteration style is best preserved in the volcanic host rocks, weak to moderate biotite + magnetite alteration is rarely recognisable in some BQM samples, particularly at E26, where the altered rocks appear dark grey (Figure 4.3f). Magnetite veinlets are also typically associated with biotite and magnetite alteration (Wolfe, 1994). These veinlets comprise "chains" of subhedral, 1 – 2mm magnetite grains that resemble the "chains of magnetite grains" described by Gustafson and Hunt (1975) from El Salvador. Wolfe (1994) provided textural evidence for magnetite veinlets having crosscut biotite clots, indicating that at least some secondary magnetite formed after biotite alteration.

A narrow (<10m) transition zone from biotite + magnetite to K-feldspar alteration is present at each deposit (Heithersay *et al.*, 1990; Wolfe, 1994; Heithersay and Walshe, 1995; Harris, 1997). The K-feldspar alteration zone is distinguished by reddening of the rocks proximal to the cores of the deposits (Figure 4.3g). The reddening is thought to result from haematite dusting of secondary K-feldspar (Heithersay and Walshe, 1995; Blevin and Morrison, 1997). The early K-feldspar alteration event produced weak to intense, selectively pervasive to pervasive K-feldspar ± anhydrite ± magnetite alteration assemblages and E1 type irregular, commonly discontinuous, K-feldspar + quartz ± biotite ± magnetite veinlets (Heithersay *et al.*, 1990: Wolfe, 1994; Heithersay and Walshe, 1995; Harris, 1997: Figures 4.3h and i).

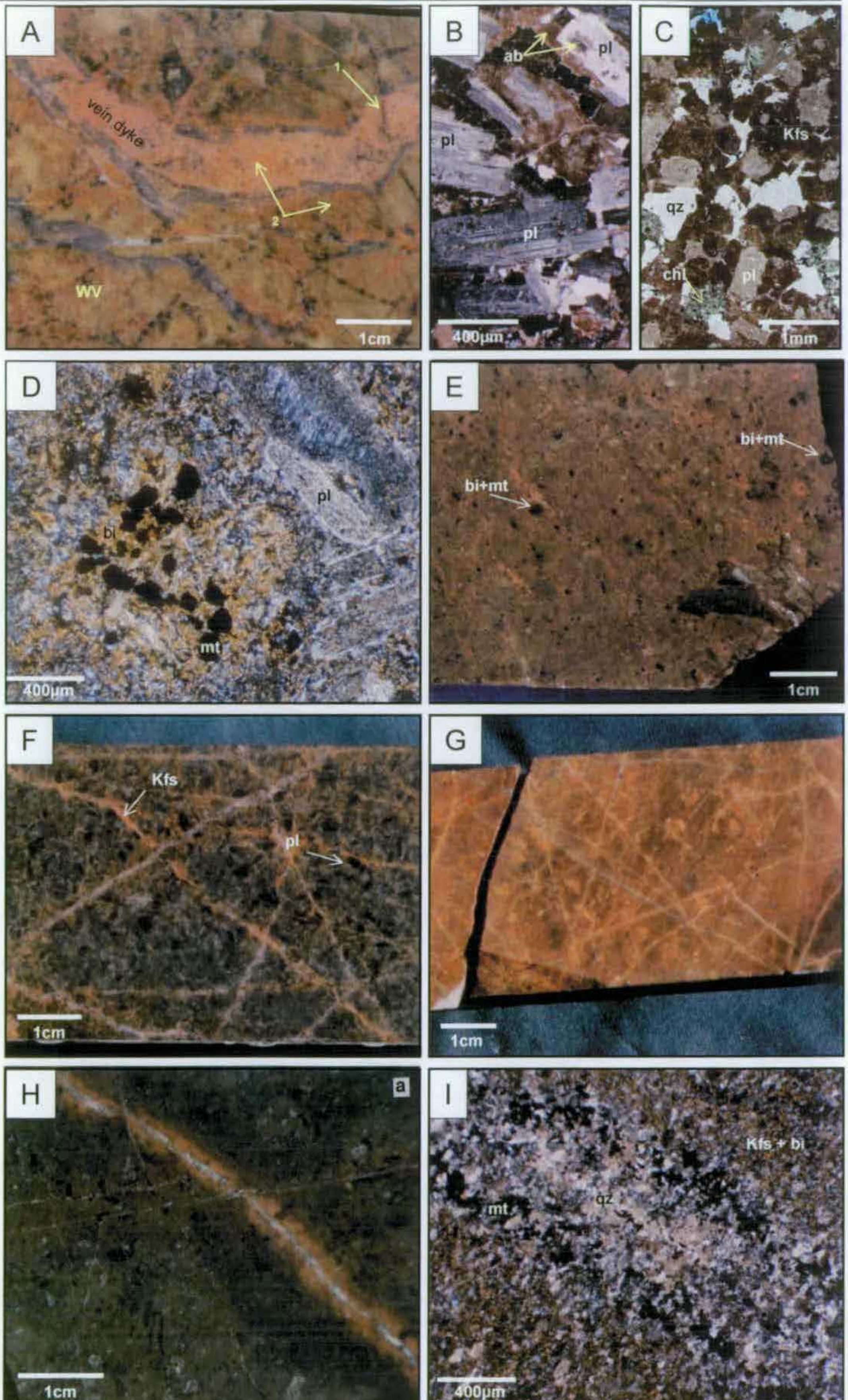
A
vein dyke
1
2
wv
1cm
B
ab
pl
pl
pl
400µm
C
Kfs
qz
chl
pl
1mm
D
pl
bi
mt
400µm
E
bi+mt
bi+mt
1cm
F
Kfs
pl
1cm
G
1cm
H
a
1cm
I
Kfs + bi
mt
qz
400µm

Within the early K-silicate alteration assemblages, Cu-sulphides occur in continuous to discontinuous E1 quartz + Cu-sulphides + K-feldspar ± anhydrite ± calcite veins and veinlets with associated K-feldspar ± magnetite ± biotite ± calcite vein-related alteration (Heithersay *et al.*, 1990; Wolfe, 1994; Harris, 1997; this study). These E1 veins typically crosscut selective to pervasive biotite – magnetite or K-feldspar alteration (Figure 4.4a). Sulphide mineralogy changes from proximal bornite-dominant, though roughly equal proportions of bornite and chalcopyrite, to distal chalcopyrite-dominant assemblages, and the sulphides generally occupy interstitial spaces between subhedral to euhedral quartz crystals. Quartz characteristically occurs as crustiform crystals that increase in size towards the centre of the veins and veinlets and oriented perpendicular to the vein walls. Quartz + sulphide veins of this sort have crosscut both the early-mineral, distal B-QMP intrusions (Figure 4.4b) and K-QMP intrusions, however, their presence is minor compared to later vein generations.

4.4.3 Distal propylitic alteration

Distal propylitic alteration assemblages that have overprinted secondary biotite + magnetite have been recognised at E48 (Wolfe, 1994) and at E28 (Kolkert, 1998). The propylitic alteration assemblage has mainly affected the volcanic host rocks, although some samples of the BQM intrusions have also been affected.

In addition to selectively pervasive albite alteration of feldspars (which is not restricted to the propylitic alteration zone), propylitic alteration associated with the Endeavour deposits is characterised by 1) moderate to intense, selectively pervasive to patchy replacement of feldspar, biotite and hornblende by epidote ± calcite (Figure 4.4c), and 2) selective to pervasive chlorite alteration of mainly biotite, hornblende and interstitial material (Wolfe, 1994; Kolkert, 1998). Veins (<1cm wide) of epidote ± carbonate ± magnetite are also associated with this alteration assemblage (Wolfe, 1994). Quartz – chlorite ± sericite ± pyrite and/or chalcopyrite veins and veinlets have been interpreted as the distal equivalents of the proximal E1 quartz + Cu-sulphides + K-feldspar veins and veinlets (Wolfe, 1994; Figure 4.2)

Low temperature, low pressure prehnite – pumpellyite metamorphic assemblages have been recognised in the vicinity of the Endeavour deposits (Jones, 1985; Radclyffe, 1995).

Figure 4.4 Photographs and photomicrographs of alteration assemblages from the Endeavour porphyry Cu-Au deposits.

A Early stage E1 quartz + sulphide veinlets (in Wombin Volcanics) that have crosscut selectively pervasive biotite + magnetite and K-feldspar alteration (E48; reproduced from Wolfe, 1994). In many places, epidote (green mineral) is intergrown with K-feldspar, or has replaced plagioclase crystals in the volcanic rock.

B Early stage E1 quartz + sulphide veinlets that have crosscut a B-QMP intrusion and a biotite + magnetite altered BQM intrusion on the periphery of E26 (E26/284/79.6m).

C Biotite + magnetite spots rimmed by epidote (E48; reproduced from Wolfe, 1994).

D Spherical aggregates of quartz and alkali feldspar in a zone of partial brain rock from a K-QMP intrusions at E27 (E27/248/182.0m).

E This sample of a K-QMP intrusion from the pit at E27 shows a variety of quartz textures: 1) discontinuous chain of prismatic quartz crystals - or partial brain rock; 2) irregular intergrown masses of K-feldspar and quartz in diffuse contact with the quartz monzonite porphyry; and 3) a typical, main mineralising stage, quartz + sulphide (chalcopyrite) vein.

F A sample of Wombin Volcanics (E48/27/570.8m) that has been crosscut by (1) a vein dyke, (2) several quartz + sulphide veins. Note the contradicting timing relationships of vein dyke emplacement indicated at i (pre- quartz + sulphide vein) and ii (post- quartz + sulphide vein).

G and H Irregular, tubular quartz veins are typical of anisotropic textures at E48. G and H display each side of a 1cm thick section of drillcore (E48/13w2/965.8). Sheeted quartz veins associated with KA-QMP crosscut the section (1). The host rock is the microgranite of E48, which has undergone intense phyllic alteration.

Abbreviations:
afs - alkali feldspar; bi - biotite; bor - bornite; epi - epidote; Kfs - K-feldspar; mt - magnetite; qz - quartz; WV - Wombin Volcanics

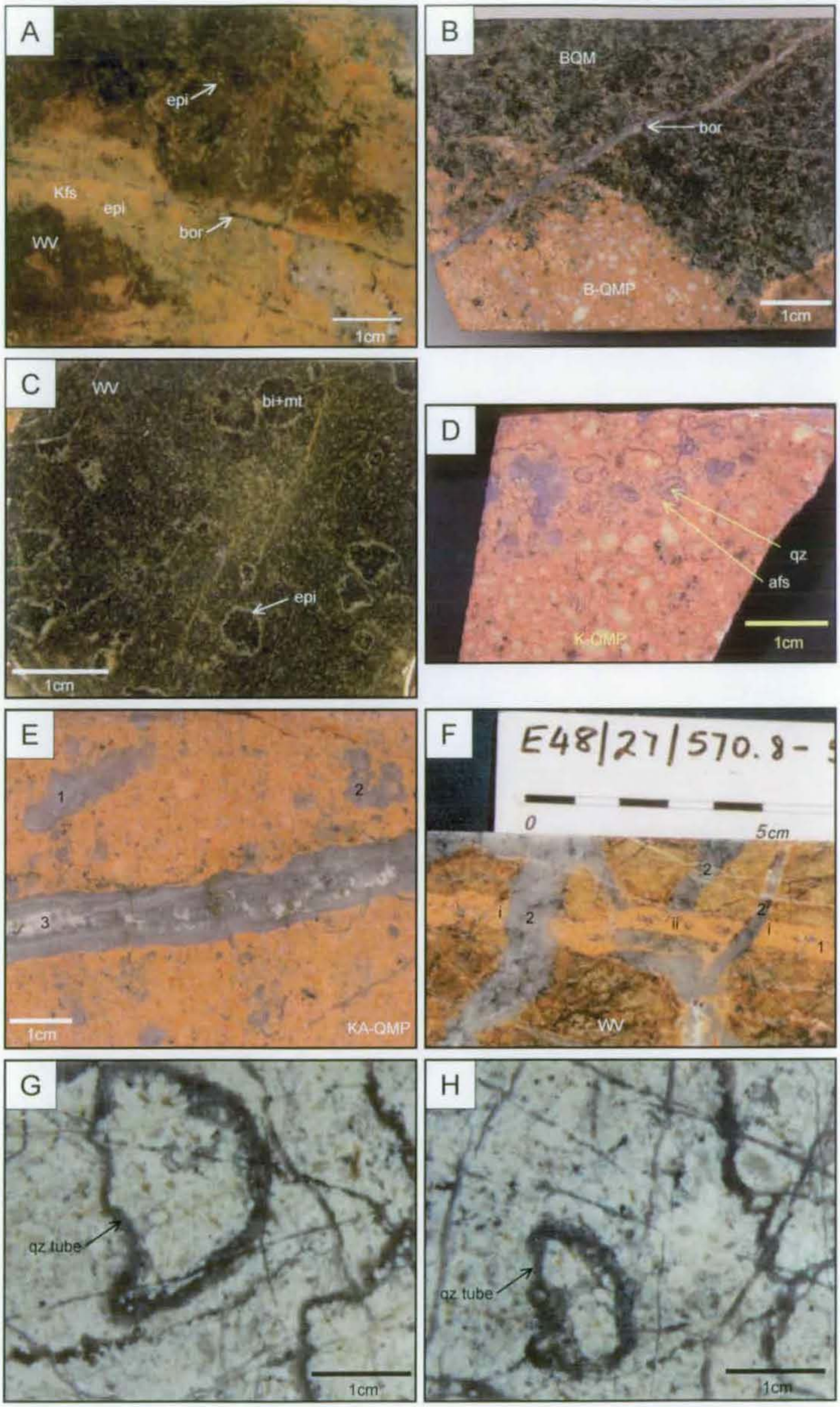
A
epi
Kfs
epi
bor
WV
1cm
B
BQM
bor
B-QMP
1cm
C
WV
bi+mt
epi
1cm
D
qz
afs
K-QMP
1cm
E
1
2
3
1cm
KA-QMP
F
E48/27/570.8-
0
5cm
2
i
2
ii
2
i
1
WV
G
qz tube
1cm
H
qz tube
1cm

The metamorphic assemblage is characterised by the presence of prehnite + pumpellyite + minor carbonate ± albite? and the absence of sulphides. It is distinguished mineralogically from the distal propylitic alteration assemblage because the latter is characterised by the presence of epidote + chlorite + albite + calcite + pyrite ± chalcopyrite (Kolkert, 1998).

4.4.4 Brain rock and anisotropic textures – Transitional Stage

Anisotropic textures are described as the **Transitional Stage** on the schematic space-time plot of the Endeavour deposits (Figure 4.2) to indicate the transition from magmatic to hydrothermal conditions. The main Transitional Stage is associated with the K-QMP intrusion (TM1). Anisotropic textures associated with KA-QMP intrusions (cf. section 3.4.3.3), define a second, less intensely developed Transitional Stage (TM2; Figure 4.2).

Brain rock and anisotropic textures are an integral component of K-QMP intrusions, and were discussed in section 3.4.3.2. These textures are interpreted to have formed due to quartz crystallisation from an aqueous fluid within an igneous melt (e.g. Shannon *et al.*, 1982; Kirkham and Sinclair, 1988; Lowenstern and Sinclair, 1996). Based on their occurrence (5 – 10% by volume), they are interpreted here to imply a close temporal relationship between the emplacement of the K-QMP intrusions and the peak production of magmatic – hydrothermal fluids. Anisotropic textures are thus thought to be representative of the transition from magmatic to hydrothermal conditions at the Endeavour porphyry deposits.

In addition to the typical brain rock textures documented at E22 and E26, textures such as spherical aggregates of quartz and alkali feldspar (Figure 4.4d), partial brain rock (Figure 4.4e), miarolitic cavities and vein dykes (Figure 4.4f) occur in K-QMP intrusions within 300m and 600m of the present-day surface at E27 and E22. Vein dykes and irregular, discontinuous, anastamosing to tubular grey quartz veins characterise the anisotropic textures at E48 (Wolfe, 1994; Figure 4.4g and h), where they typically occur deeper in the system than the other deposits, 800 – 1000m below the current surface. The irregular morphology, folded appearance and grey nature of the quartz of many examples of anisotropic textures from the Endeavour deposits are similar in some ways to the early, grey, ptygmatic "A" veins described by Gustafson and Hunt (1975) from El Salvador, although they are not continuous, through-going structures.

4.4.5 Main Stage

M1 and M2 veins, associated respectively with K-QMP and KA-QMP intrusions, are referred to as **Main Stage** events on Figure 4.2. They have been grouped together as the main mineralising stage in the Endeavour systems. Many of the characteristics of M1 and M2 veins are broadly similar, and, as Heithersay and Walshe (1995) demonstrated, distinguishing between veins associated with the two different intrusions at each deposit can rarely be achieved with confidence. In addition, many of the features of the M1 and M2 veins are spatially variable, which makes distinguishing them more difficult.

The main sulphide precipitation events at each of the Endeavour deposits are associated with quartz veining, early orthoclase and late sericite – haematite alteration related to the intrusion of the K-QMP intrusions (Jones, 1985, Heithersay and Walshe, 1995; this study). These alteration events are related to multiple generations of quartz + orthoclase + sulphide veins and veinlets (Jones, 1985; Heithersay, 1986; Heithersay *et al.*, 1990; Wolfe, 1994; Heithersay and Walshe, 1995; Harris, 1997; Kolkert, 1998).

From the detailed descriptions of previous studies, there are three groups of veins and veinlets in the main stage associated with the K-QMP intrusions (M1): 1) thin (<1cm) veins and veinlets of quartz + sulphide + orthoclase ± anhydrite (M1a); 2) stockwork or sheeted veins of quartz + sulphide ± anhydrite + carbonate veins together with vein-related and pervasive, locally mottled, sericite + quartz ± haematite alteration (M1b); and 3) milky quartz + chalcopyrite > bornite + calcite (M1c) veins (Figure 4.2).

In detail, M1a veins and veinlets contain abundant quartz, with minor bornite in excess of chalcopyrite, orthoclase, calcite ± anhydrite ± apatite ± rutile. M1a veins typically have thin (<0.5cm) alteration haloes of quartz + orthoclase (Figure 4.5a). Anhydrite is a common component of M1a veins in E26 and E48 (Figure 4.5b), a lesser component in E27 examples and minor component in E22 examples. In contrast, calcite is abundant in M1a veins at E22. Sulphide mineralogy changes from bornite-dominant proximal to the QMP complexes, through medial chalcopyrite-dominant, to distal pyrite-dominant assemblages in the M1a veins (Heithersay *et al.*, 1990; Wolfe, 1994; Heithersay and Walshe, 1995; Harris, 1997).

Stockwork (E27 and E22) and sheeted (E26 and E48 – preferential orientation north-northeast) quartz + sulphide + anhydrite + calcite + K-feldspar veins (M1b) contain the

Figure 4.5 Photographs and photomicrographs of alteration assemblages from the Endeavour porphyry Cu-Au deposits.

- **A** The onset of the main mineralisation event at each deposit is marked by M1a veinlets of quartz + K-feldspar + bornite (1), depicted here in Wombin Volcanics at E48 (E48/2/172.9m). An irregular vein of haematite dusted secondary K-feldspar has formed prior to the M1a veinlets (2).
- **B** Anhydrite is a common component in the M1a quartz + K-feldspar + bornite veinlets. This example is in a K-QMP intrusion from E26 (E26/282/305.0m).
- **C** A phyllic-altered K-QMP intrusion hosting the sheeted vein network at E48; this example from E48/2/312 - 321m.
- **D** M1b quartz + bornite + anhydrite veins in a K-QMP intrusion at E26 (E26/132w2/886.2m).
- **E** M1b veins in the BQM intrusion adjacent to the K-QMP intrusion depicted in (C) above (E26/132w2/860.3).
- **F** Parallel laminations of quartz and sulphides are characteristic of many stockwork veins in the Endeavour deposits. This example is from E22 (E22/2/286.7m) and shows laminated quartz + bornite M1b veins that have crosscut a K-QMP intrusion.
- **G** Crosscutting stockwork veins associated with KA-QMP intrusions at E27 (E27/368/152.4). These M2b veins are notably more chalcopyrite-rich than the similar M1b veins associated with K-QMP intrusions.
- **H** Two distinct generations of veining, alteration and mineralisation at E26 (underground sample, courtesy of D. Cooke). An earlier generation of L1 quartz + pyrite veins with distinct phyllic alteration haloes associated with K-QMP intrusions (1). These have been crosscut by straight-walled, quartz + bornite veins (M2b) associated with KA-QMP intrusions (2). The host rock is a trachyte of the Wombin Volcanics.

Abbreviations:
anh - anhydrite; cpy - chalcopyrite; bor - bornite; hm - haematite; Kfs - K-feldspar; qz - quartz; volc - volcanic rock clast

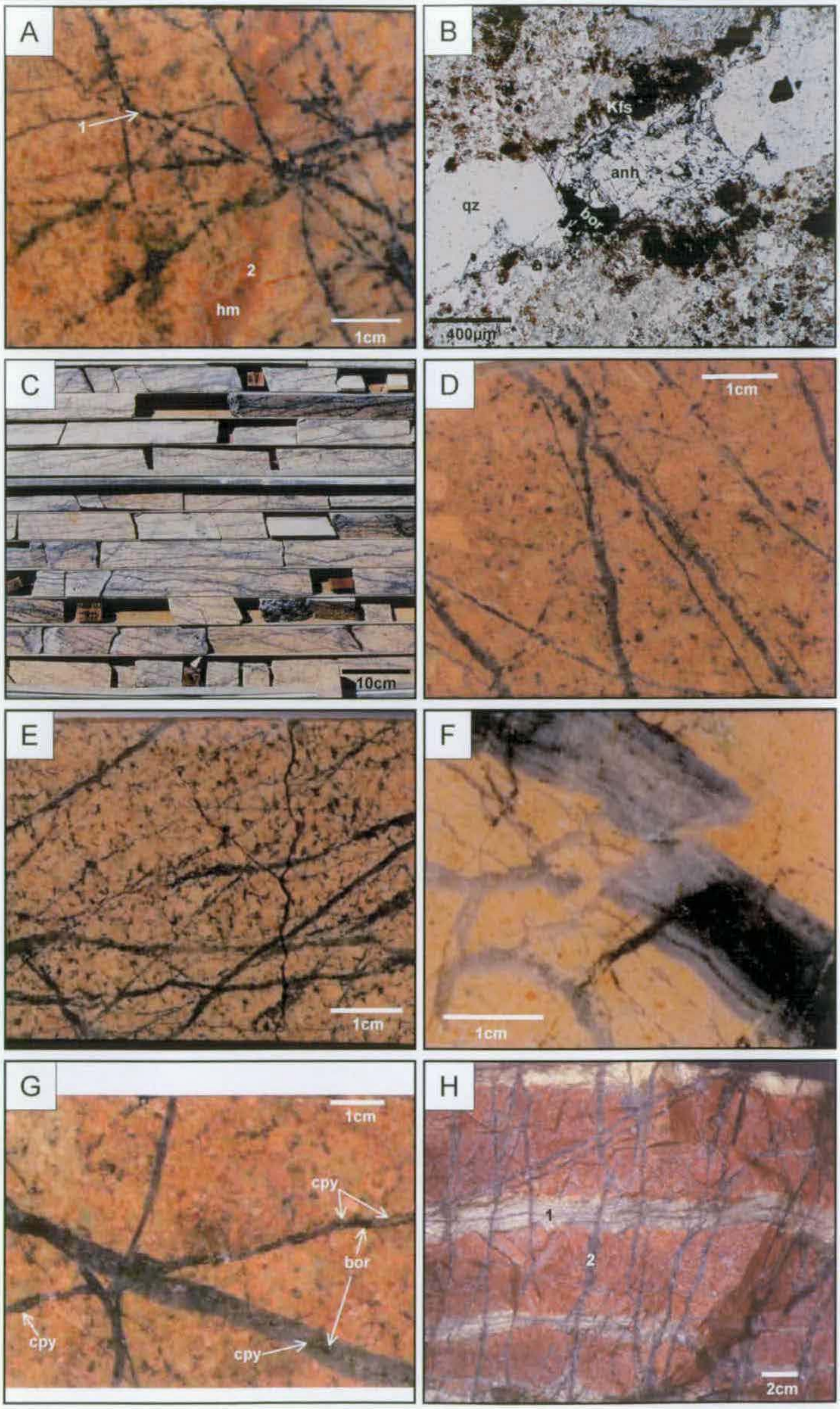
A
1
2
hm
1cm
B
Kfs
anh
qz
bor
400µm
C
10cm
D
1cm
E
1cm
F
1cm
G
1cm
cpy
bor
cpy
cpy
H
1
2
2cm

bulk of the sulphides associated with the Endeavour deposits (Heithersay *et al.*, 1990; Wolfe, 1994; Heithersay and Walshe, 1995). M1b veins, which are characteristically straight-walled and linear, and range in width from 0.5 to 2cm, typically account for 30 - 90% of the total rock volume (Figures 4.5c, d and e). Many of the stockwork veins are laminated parallel to the walls, with fine trains of sulphides defining the lamellae (Figure 4.5f). The lamellae are suggestive of repeated fracturing and deposition. As well as bornite and chalcopyrite, tetrahedrite – tennantite, covellite, chalcocite, tellurides and/or Pb-selenides are also locally present in M1b veins (e.g. Jones, 1985; House, 1994).

Distal (~50m from the QMP complexes) M1c veins are characterised by higher calcite and lower quartz contents (Heithersay et al., 1990; Wolfe, 1994). A change in the sulphide mineralogy is also apparent. The M1c veins are chalcopyrite- to pyrite-rich, whereas bornite is the dominant sulphide in the proximal M1b stockwork veins associated with the K-QMP intrusions (Heithersay et al., 1990; Wolfe, 1994; Heithersay and Walshe, 1995; this study).

Two vein generations, M2a and M2b, are associated with the KA-QMP intrusions at each of the Endeavour deposits. The vein generation resemble the M1a and M1b veins associated with the K-QMP intrusions described above. In detail, the M2a veinlets contain quartz with chalcopyrite in excess of bornite, and minor orthoclase and anhydrite. M2b veins associated with the KA-QMP intrusions are typically 0.5 – 1cm thick and contain quartz, chalcopyrite in excess of bornite and minor calcite, fluorite, with or without anhydrite (Heithersay and Walshe, 1995).

When comparing the vein generations associated with K-QMP and KA-QMP intrusions, it is apparent that M2a veins are morphologically identical to M1a veins, and can only be recognised confidently where they have crosscut K-QMP intrusions (Heithersay and Walshe, 1995; Figure 4.5g). Orthoclase alteration haloes are less intensely developed around M2a veins and veinlets compared to M1a veins. M2b stockwork veins typically contain clearer quartz than M1a veins. M2b veins also contain less abundant anhydrite and have chalcopyrite rather than bornite as the dominant sulphide (Heithersay *et al.*, 1990, Heithersay and Walshe, 1995). Figure 4.5h shows two different vein generations in a trachytic Wombin Volcanics host rock from E26, where L1 veins and vein-related quartz + sericite + haematite alteration have been crosscut by M2b veins. M1 veins and associated vein-related alteration assemblages are much more intensely developed than M2 vein generations.

Sericite + haematite alteration is commonly associated with M1b, M2a and M2b quartz + sulphide veins (Wolfe, 1994). This alteration style, which is typically selectively pervasive to vein-controlled, commonly manifests as yellow to red-brown alteration zones, which has a locally mottled appearance (Figure 4.6a). It is possible that this sericite + haematite alteration maybe related to Late stage sericite assemblages.

4.4.6 Late Stage

Three late stage phyllic alteration assemblages and related veins have been identified (Figure 4.2). Only one of these, L1, is mineralised.

4.4.6.1 Selective sericite overprint (L1)

Late stage phyllic alteration has been documented for E48 (Wolfe, 1994; Wolfe *et al.*, 1996) and E26 (Harris, 1997; Harris and Golding, 2001). This alteration style has also been recognised at E22 and E27 during this study (Figures 4.5c, 4.6b and c). It is characterised by widespread, intense to moderate, pervasive quartz + sericite + carbonate ± haematite replacement of feldspar phenocrysts and groundmass material. The end product of this alteration is a fine-grained (<100μm) sericite + carbonate + quartz matrix that hosts relict sericite-pseudomorphed feldspar phenocrysts (Wolfe, 1994; Harris, 1997: Figure 4.6d). The pervasive phyllic alteration is best developed in the K-QMP and KA-QMP intrusions, where it has locally overprinted 50 – 80% of the intrusions and gives rise to a distinctive pale, bleached appearance (Figures 4.6e and f). Pale green to dull grey zones also occur locally. Minor chalcopyrite in excess of bornite is disseminated in the sericite + quartz + carbonate matrix in K-QMP and KA-QMP intrusions at E22, E26 and E27. In contrast, chalcocite + bornite + tennantite – tetrahedrite occur evenly distributed throughout the fine-grained secondary quartz + sericite + carbonate groundmass at E48 (Wolfe, 1994; Figure 4.6g). Quartz + carbonate + sericite + chalcopyrite/pyrite veins are also associated with this pervasive sericite overprint (Wolfe, 1994; Harris, 1997). Wolfe (1994) and Wolfe *et al.* (1996), and Harris (1997) and Harris and Golding (2001), used oxygen isotopic compositions of sericite from these late phyllic alteration zones at E48 and E26 respectively, to confirm a magmatic – hydrothermal origin for these assemblages.

Since the KA-QMP intrusions at all four deposits have been overprinted by pervasive phyllic alteration, and the hydrothermal breccia at E27 contains clasts of intensely sericite altered Wombin Volcanics (cf. Figure 3.17a), it is interpreted that this assemblage (L1A)

Figure 4.6 Photographs and photomicrographs of alteration assemblages from the Endeavour porphyry Cu-Au deposits.

A Mottled appearance (sericite + haematite alteration) of a KA-QMP intrusion with a number of angular clasts (volc) of Wombin Volcanics; E48/13w2/846.2m.

B Pervasive sericite alteration of a KA-QMP intrusion at E22 (E22/6/248.9m). Minor bornite occurs as disseminated grains in pervasively sericite altered rocks (1). The typically fine-grained granular groundmass of QMP intrusions has been obliterated by pervasive sericite alteration, and has been replaced by a fine-grained mass of carbonate + calcite + quartz (2). A vein of quartz + bornite + chalcocite with a halo of quartz + sericite has crosscut the sample.

C Pervasive sericite alteration has given rise to a bleached, pale appearance for parts of the K-QMP intrusions at E27, depicted here in a pit sample (E27/E/43). Minor bornite occurs as disseminated grains in the pervasively sericite altered rock (1).

D This photomicrograph from a section of an E27 pit sample of K-QMP (E27/W/36) depicts the pervasive sericite alteration assemblage in detail. It is characterised by quartz + carbonate + sericite replacement of feldspar, both in the groundmass and phenocrysts. Minor sulphide disseminations are present (1), as are patches of sericite (2), carbonate (3) and K-feldspar + sericite.

E Typical sericite alteration in a K-QMP intrusion at E26, E26/91/137.7m. Bornite in excess of chalcopyrite sulphide disseminations are abundant (1).

F An example of the pervasive sericite overprint at E48, E48/13w2/854.8m. Note how the sericite alteration assemblage gives the rock pale green to grey appearance, especially the plagioclase phenocrysts phenocrysts (1). Bornite + chalcocite ± tetrahedrite-tennantite (2) typically occur as disseminations in this assemblage at E48.

G Where pervasive sericite alteration has occurred, the groundmass and phenocrysts of QMP intrusions are completely replaced by fine-grained sericite (1), minor carbonate (2) and quartz (3). Opaque grains in this photomicrograph (4) are chalcocite + bornite with minor tetrahedrite-tennantite (E48; photomicrograph reproduced from Wolfe, 1994).

H Intense, pervasive, fault-controlled sericite alteration assemblages are exemplified in this photograph of BQM at E48 (E48/15/580.9m), where plagioclase (1) has been dissolved from the completely detextured, grey to dark-grey rock.

Abbreviations
bor - bornite; cc - chalcocite; Kfs - K-feldspar; qz - quartz; ser - sericite

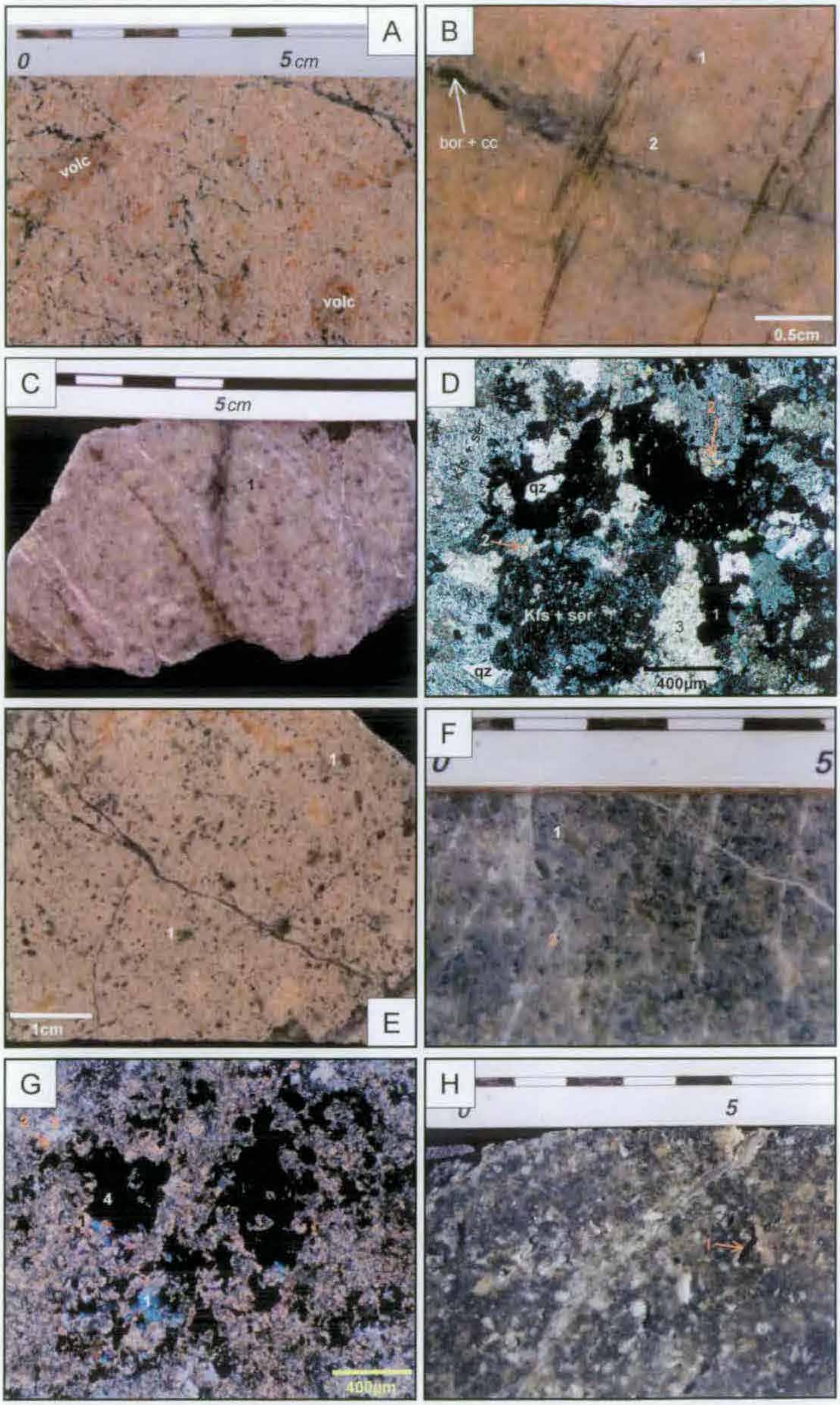
A
0
5 cm
volc
volc
B
1
bor + cc
2
0.5cm
C
5 cm
1
D
2
3
1
qz
2
Kfs + ser
3
1
qz
400µm
1
1
1cm
E
F
1
5
G
4
1
400µm
H
5
1

formed after the emplacement of the K-QMP intrusions (Figure 4.2) and became more intense with time, continuing beyond the emplacement of the KA-QMP intrusions. L1 quartz + carbonate + sericite + chalcopyrite/pyrite veins are associated with the pervasive sericite alteration assemblage (Figure 4.2).

4.4.6.2 Fault-related phyllic alteration (L2 and L3)

Extensive fault- and fracture-related sericite alteration (L2) and less abundant carbonate – base-metal sulphide vein assemblages (L3) formed after the main stages of Cu-sulphide deposition (M1, M2 and L1 on Figure 4.2: Heithersay, 1986; Heithersay *et al.*, 1990; Wolfe, 1994; Heithersay and Walshe, 1995; Harris, 1997; Kolkert; 1998). The L2 fault- and fracture-related phyllic assemblage, comprising sericite + carbonate + quartz + pyrite ± anhydrite alteration, has overprinted late stage pervasive sericite alteration (L1) and typically extends into the host rock for 0.01 – 10m from the fracture plane (Figure 4.6h). In detail, the L2 alteration assemblage comprises a fine-grained (<50μm) groundmass of subhedral sericite, with larger anhedral masses of carbonate and quartz, which has completely obliterated primary textures.

Carbonate + sericite + quartz + gypsum + base-metal sulphides ± fluorite veins with carbonate ± quartz ± gypsum haloes are characteristic features of late stage L3 alteration and veining (Heithersay *et al.*, 1990; Wolfe, 1994; Harris, 1997; Kolkert, 1998: Figure 4.7a). The presence of sulphides in these carbonate veins varies from abundant to non-existent. Sulphides commonly include pyrite ± sphalerite ± galena ± chalcopyrite. Locally, L3 veins contain rock fragments ± quartz/sulphide vein fragments, which give many examples the appearance of a "crackle breccia" (Wolfe, 1994; Kolkert, 1998; Figure 4.7b).

Zero porphyry dyke emplacement at E26 is inferred to have post-dated the development of pervasive phyllic alteration because the dykes preserve only a propylitic alteration assemblage. Since L2 fault- and fracture-related sericite alteration has overprinted some of the mafic dykes, L2 and L3 can be further constrained to a pre- to syn-mafic dyke emplacement.

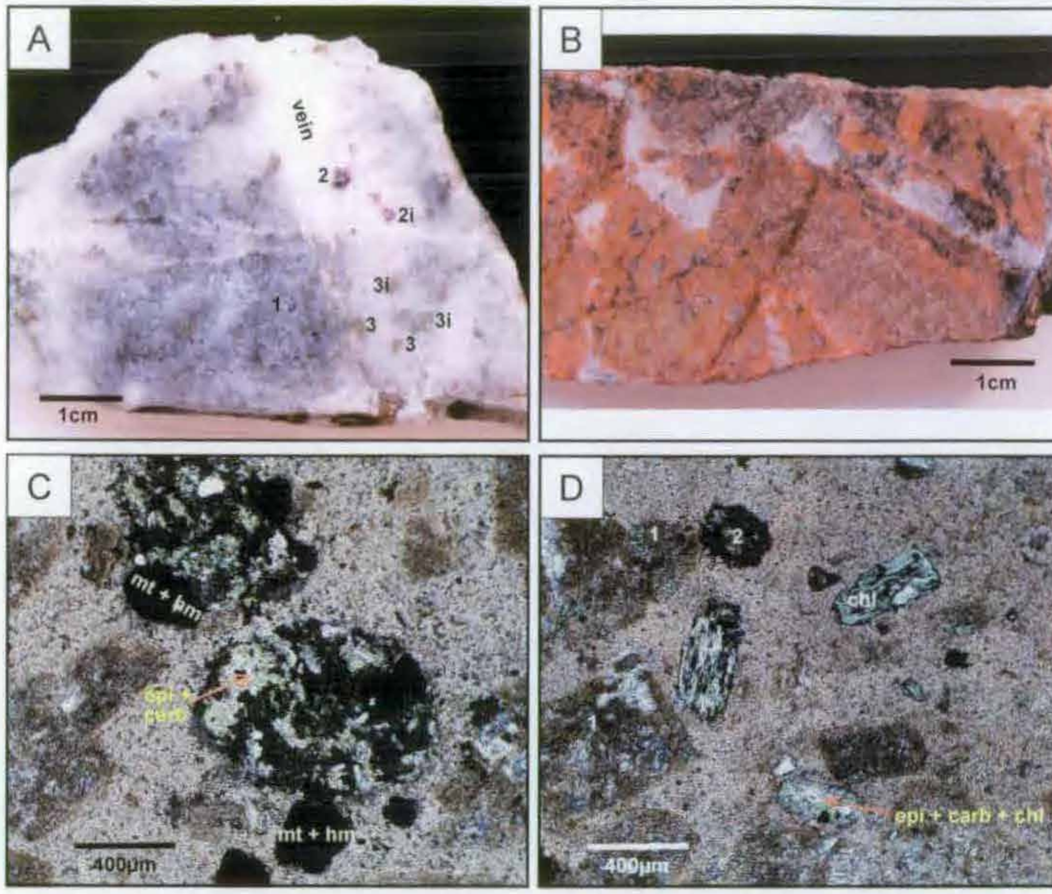

Figure 4.7 Photographs and photomicrographs of alteration assemblages from the Endeavour porphyry Cu-Au deposits.

A Fault-related (L2) sericite alteration (1) and L3 carbonate + sericite + quartz + fluorite (2) + pyrite (3) veins, taken from E27 pit (E27/S/29). Note fluorite (2i) and pyrite (3i) also occur in the L2 assemblage.

B Many L3 carbonate + sericite + quartz + gypsum veins contain fragments of wallrock and have been described as "crackle breccia" veins (Wolfe, 1994; Kolkert, 1998). This example is in Wombin Volcanics in the pit at E27 (E27/W/18).

C Late propylitic alteration is best preserved in the zero porphyries of E26. This photomicrograph (ppl), shows the weak to moderate, selectively pervasive nature of the propylitic assemblage; clinopyroxene has been altered to epidote + carbonate; E26/46/1294.3m.

D Photomicrograph (ppl) of a zero porphyry dyke from E26 showing that chlorite has replaced a primary biotite phenocryst. Weak chlorite + epidote replacement of feldspar (1) and epidote replacement of an unknown mafic precursor has also occurred (2); E26/46/1294.3m.

Abbreviations:

carb - carbonate; chl - chlorite; epi - epidote; hm - haematite; mt - magnetite

4.4.7 Post-mineral propylitic alteration

Weak to moderate, selective propylitic alteration has produced distinct haloes around the E22 and E27 deposits. A propylitic alteration assemblage is only patchily and weakly developed around E26, whereas E48 has a propylitic alteration halo outboard of the early pervasive biotite + magnetite zone (Jones, 1985; Heithersay *et al.*, 1990; Wolfe, 1994; Heithersay and Walshe, 1995; Harris, 1997; Kolkert, 1998). The timing of the propylitic alteration assemblage is constrained in part, by the fact that it has overprinted the zero porphyry dykes at E26.

The post-mineral propylitic alteration assemblage is characterised by selective replacement of feldspars and mafic minerals by epidote + chlorite + albite + carbonate ± haematite ± pyrite ± chalcopyrite (Jones, 1985; Heithersay *et al.*, 1990; Wolfe, 1994; Heithersay and Walshe, 1995; Harris, 1997; Kolkert, 1998; Figures 4.7c and d). Small (<1cm) clots of epidote + carbonate + chlorite have given a spotty appearance to some of the volcaniclastic rocks. Thin (<1mm) haematite veinlets are also present locally.

4.5 Sulphide mineralogy

Sulphides are an integral part of the early, main and late stage assemblages of the Endeavour deposits (Figure 4.2). Their texture and zonation are described below.

4.5.1 Sulphide minerals

Bornite is the principal host of gold in the Endeavour porphyry deposits. Gold typically occurs as <25μm inclusions along fractures within bornite grains (Figure 4.8a) and along bornite grain boundaries (Jones, 1985; House, 1994; Wolfe, 1994; Heithersay and Walshe, 1995). In rare examples, gold occurs as inclusions in chalcocite. In addition to gold, silver also occurs as inclusions in bornite (Jones, 1985) and the average silver grades for the Endeavour deposits are 3g/t at E22, E27 and E48 and 3.5 – 4g/t at E26 (North Limited, pers. comm., 2000). Bornite occurs either with chalcocite, where the two minerals are typically intergrown (Figure 4.8b and c), or with chalcopyrite, where chalcopyrite is characteristically found along fractures and cleavage planes within the bornite (Figure 4.8d) or is mutually intergrown with bornite (Figure 4.8e).

Figure 4.8 Photomicrographs (reflected light) of disseminated and vein sulphide minerals in the Endeavour porphyry Cu-Au deposits.

A An example of a gold inclusion in bornite from E26. This is taken from a stage M1 sheeted quartz vein (reproduced from House, 1994).

B Typical intergrowth of chalcocite (grey) and bornite (mauve) in a disseminated sulphide grain in BQM from E26 (E26/282/427.7m). Note the myrmekitic intergrowth at (1).

C Bornite (mauve) and chalcocite (grey) in a thick (drill core intersection of >0.5m) bornite + anhydrite + aplite vein, E26/272/197.1m. Chalcocite is interpreted to have precipitated after bornite because it surrounds subhedral bornite crystals.

D Chalcopyrite (yellow) along fracture planes and at the margin of a bornite (mauve) grain in a stage M1 quartz + sulphide ± K-feldspar vein that crosscuts a K-QMP intrusion at E27 (E27/369/159.6m). Replacement of bornite by covellite (blue) along fractures is typical.

E Co-existing bornite (mauve) and chalcopyrite in a bornite clot within a K-QMP intrusion at E27 (E27/E/25).

F Two co-exiting types of bornite in a stage M1 vein that has crosscut a QMP intrusion at E26: 1) - mauve bornite shown here intergrown with chalcocite (grey); and 2) orange bornite (reproduced from House, 1994).

G Co-existing bornite (mauve) and chalcocite (grey) with tetrahedrite - tennantite in a disseminated sulphide grain in a brain rock zone of a K-QMP intrusion at E48 (E48/11/507.0m).

H Disseminated sulphide grains in a K-QMP intrusion at E26 (E26/282/305.0m). Minerals present include anhydrite (1), quartz (2) and rutile (3). chalcopyrite (4), bornite (5) and bornite intergrown with chalcocite (6).

Abbreviations:
Au - gold; bor - bornite; cc - chalcocite; cpy - chalcopyrite; cov - covellite; tet-ten - tetrahedrite - tennantite

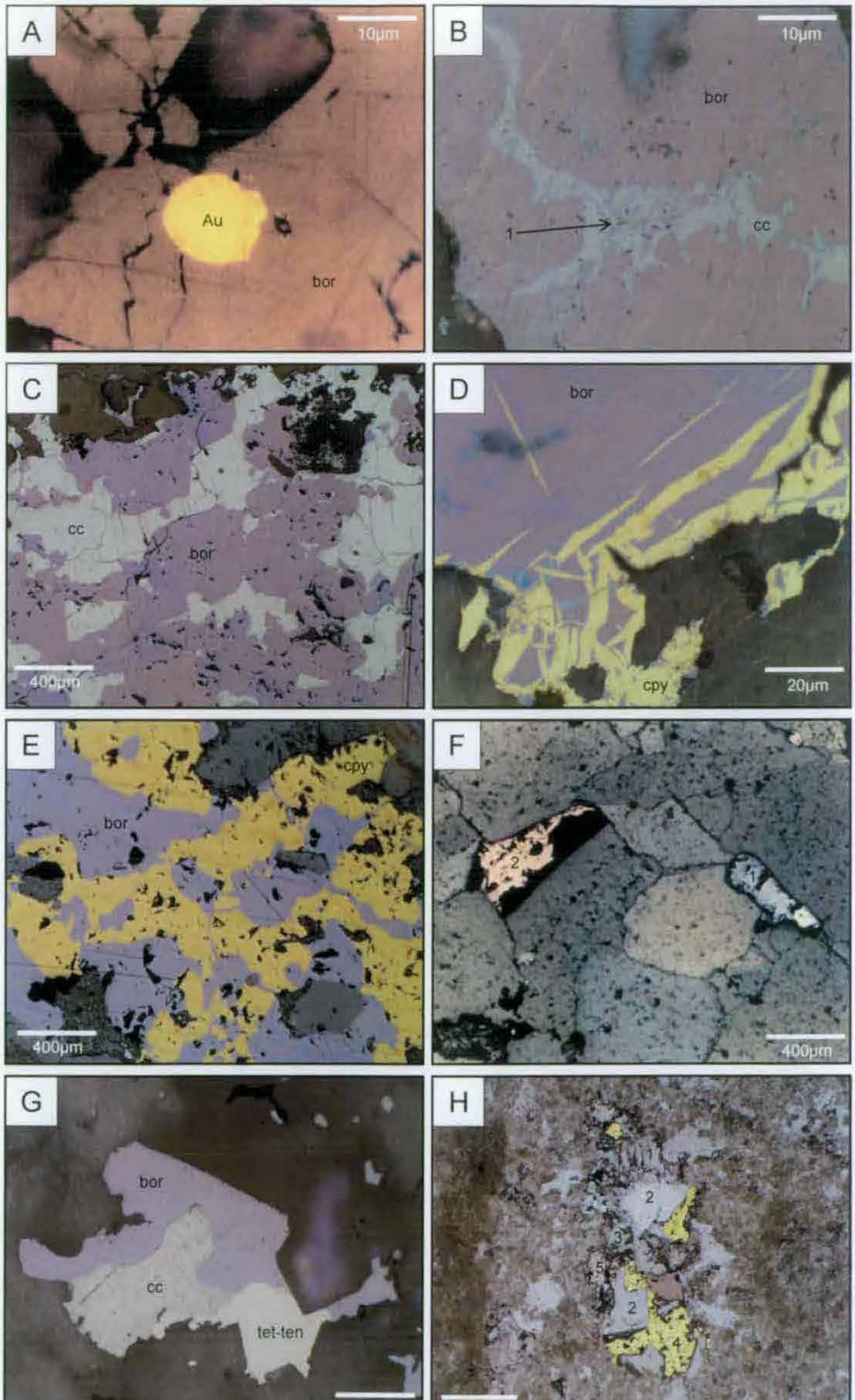
A
10µm
Au
bor
B
10µm
bor
1
cc
C
cc
bor
400µm
D
bor
cpy
20µm
E
cpy
bor
400µm
F
2
400µm
G
bor
cc
tet-ten
40µm
H
2
3
5
2
4
400µm

Two varieties of bornite have been recognized petrographically in the disseminated ores and quartz – sulphide veins; i). mauve and ii) orange-brown bornite (Jones, 1985; Heithersay *et al.*, 1990; House, 1994; Wolfe, 1994). Ramdohr (1969) noted that bornite is typically pinkish-brown to brown, but tarnishes quickly to violet-blue, particularly if intergrown with chalcocite. Based on this, one might argue that the two varieties of bornite recognized at the Endeavour deposits are simply the result of tarnishing, particularly given the compositional similarities (House, 1994). House (1994) observed that both mauve and orange-brown bornite varieties are compositionally similar in terms of stoichiometry ($Cu_{4.8-4.9}Fe_{0.9-1.0}S_4$). However, the constant colour of the two varieties after re-polishing; the orange bornite/chalcopyrite and mauve bornite/chalcocite associations; and the occurrence of both varieties in a single thin section (Figure 4.8f) led House (1994) to conclude that the colour distinctions are a function of minor variations in trace element compositions. Even though the trace element compositions of the mauve and orange-brown bornite varieties are similar (House, 1994), trace elements causing the colour variation may not be present in high enough concentrations to be detected by the electron microprobe (less than several hundred ppm).

Chalcopyrite inclusions within bornite and secondary chalcopyrite that occurs along bornite grain boundaries comprise only a small proportion of the total chalcopyrite within the veins and alteration assemblages of the Endeavour deposits. Chalcopyrite occurs more commonly as discrete grains in veins and alteration assemblages peripheral to the central bornite-rich deposit cores of each deposit (House *et al.*, 2002). Chalcopyrite is also associated with the veins and alteration assemblages related to the emplacement of the younger KA-QMP intrusions, and minor chalcopyrite occurs with pyrite in the outer propylitic halo.

Minor tellurides and selenides, tennantite, tetrahedrite and enargite are also present as inclusions in bornite and chalcopyrite in the ore zones of the deposits (House, 1994; Wolfe, 1994) and as intergrowths with bornite, and less commonly, chalcopyrite and chalcocite (Figure 4.8g). Locally bornite has been replaced by covellite (Figure 4.8d) and digenite (Jones, 1985; Heithersay *et al.*, 1990; House, 1994; Wolfe, 1994).

In the M1 and M2 veins, bornite and chalcopyrite are commonly intergrown with anhydrite (Figure 4.8h). Bornite also occurs rims around magnetite (Figure 4.9a) and coexists with haematite (Heithersay and Walshe, 1995). Magnetite is a minor but significant phase in the early K-silicate alteration assemblage at all four Endeavour deposits. However, proximal to the QMP complexes, most of the magnetite has been destroyed by pervasive K-silicate alteration and veining events. Main-stage orthoclase alteration at E22 and E27 is mostly fracture-controlled and resulted in comparatively less intense magnetite destruction than at E26 and E48, where more pervasive orthoclase alteration occurred. Where it has been preserved, magnetite has been replaced to varying degrees by bornite ± chalcopyrite, always in association with haematite (House, 1994). Haematite is also a primary alteration mineral in some of the M1 and M2 veins (Heithersay *et al.*, 1990; Wolfe, 1994; Heithersay and Walshe, 1995; Harris, 1997; Cooke *et al.*, 2000). In some examples, especially in the sericite overprint at E48, bornite is commonly intergrown with needles of sericite (Figure 4.9b).

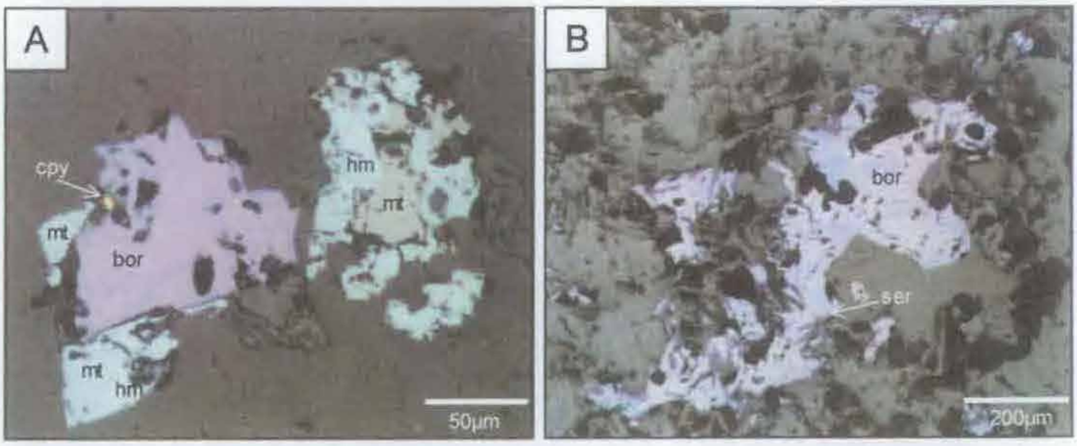

Figure 4.9 Photomicrographs (reflected light) of disseminated and vein sulphide minerals in the Endeavour porphyry Cu-Au deposit continued. **A** Disseminated bornite in association with magnetite in a B-QMP intrusion at E26 (E26/286/170.6m). Note that much of the magnetite has been replaced by haematite. **B**– Disseminated bornite intergrown with needles of sericite in a patch of intense, pervasive sericite alteration in a K-QMP intrusion at E26 (E26/184/129.3m).

4.5.2 Sulphide zoning

Previous studies (Jones, 1985; Heithersay *et al.*, 1990; House, 1994; Heithersay and Walshe, 1995) have shown that sulphides associated with the Endeavour deposits are zoned, with bornite the most abundant sulphide in the deposit cores. With increasing distance from the deposit cores, there is a transition to bornite + chalcopyrite, and then to chalcopyrite > bornite and finally to pyrite-dominant peripheral regions (Jones, 1985; Heithersay *et al.*, 1990; House, 1994).

House (1994) studied the sulphide zonation and metal distribution of E26 in detail. Figures 4.10a and b, show the distribution of sulphides with respect to K-QMP and KA-QMP intrusions (*QMP 1* and *QMP 2* respectively of Heithersay and Walshe, 1995). The inner bornite-dominant zones correspond with zones of most intense K-silicate alteration, while the outer pyrite-rich zones correspond with the inner zones of propylitic alteration associated with the QMP intrusions. It is also evident on Figure 4.10, that chalcopyrite is mainly associated with the KA-QMP intrusions. House (1994) noted the same relationships for E22, E27 and E48.

At E26, House (1994) found that Au and Cu are concentrically distributed about *QMP 1*. He also showed that the core of *QMP 2* is anomalously low in both Cu and Au at E26 (Figure 4.11a). There is a vertical zonation in the metal distribution at E26, where the highest Au grades are located deeper within the deposit, whereas high Cu grades are typically found closer to the surface (Figure 4.11b). Similar lateral and vertical zonation patterns of Cu and Au distributions occur at E48 (House, 1994). Cu/Au ratios vary within E26 and E48, and with the exception of the deeper portions of E26 and E48, where roughly equal proportions of Cu and Au occur, Cu to Au ratios are ~2:1. The highest Cu and Au grades occur at the peripheries of at E22 and E27 (House, 1994). House (1994) found that there is no clear vertical zonation to Cu and Au distribution at these two deposits. There is a strong correlation with Cu and Au at E22 and E27, with an almost 1:1 Cu to Au ratio (Jones, 1985).

4.5.3 Bornite clots

Bornite clots are associated with many B-QMP, some KA-QMP and several K-QMP intrusions throughout the Endeavour deposits. These clots are typically spherical to irregular masses of ~98% bornite, with several other mineral phases, including chalcopyrite, quartz, carbonate, apatite, albite, K-feldspar, biotite, chlorite and prehnite (?). The clots occur in rocks that have been overprinted by K-silicate alteration assemblages, but have no obvious association with any (cf. Figures 3.10b, d, e and g). Sericite alteration assemblages are not associated with the bornite clots.

Several of the B-QMP intrusions that contain bornite clots have a weakly developed propylitic mineral assemblage in addition to the secondary orthoclase alteration assemblage (Figure 4.12a). In one example, secondary biotite situated immediately adjacent to the bornite clot has been completely altered to chlorite, and carbonate has been engulfed by bornite (Figure 4.12b). Sub- to euhedral quartz crystals, typically containing hornblende and augite inclusions (Figure 4.12c), and primary hornblende crystals (Figure 4.12d), are preserved within the bornite.

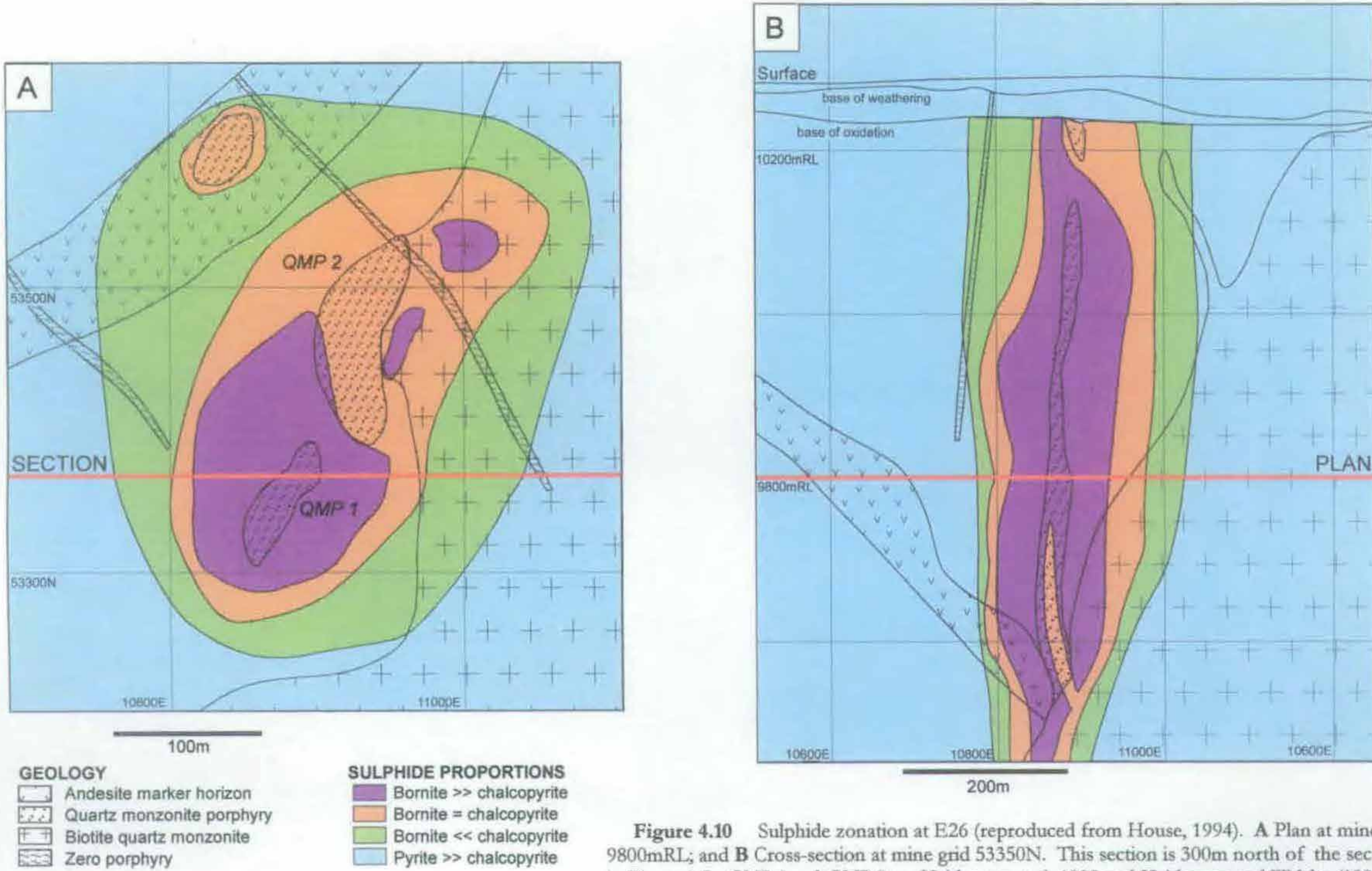

Figure 4.10 Sulphide zonation at E26 (reproduced from House, 1994). **A** Plan at mine grid 9800mRL; and **B** Cross-section at mine grid 53350N. This section is 300m north of the section shown in Figure 3.5. *QMP 1* and *QMP 2* are Heithersay *et al.*, 1990 and Heithersay and Walshe (1995) terms, that are equivalent to the K-QMP and KA-QMP intrusions defined in this thesis respectively.

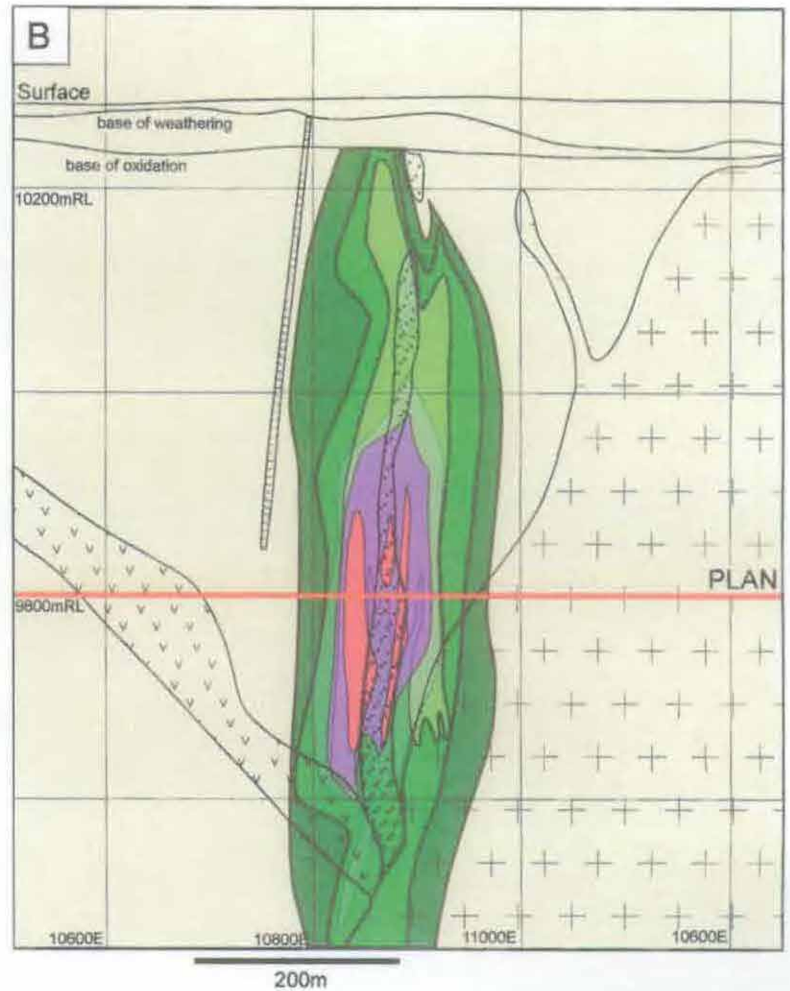

Figure 4.11 Metal distribution at E26 (reproduced from House, 1994). **A** Plan at mine grid 9800mRL; and **B** Cross-section at mine grid 53350N. This section is 300m north of the section shown in Figure 3.5. *QMP 1* and *QMP 2* are Heithersay *et al.*, 1990 and Heithersay and Walshe (1995) terms, that are equivalent to the K-QMP and KA-QMP intrusions defined in this thesis respectively.

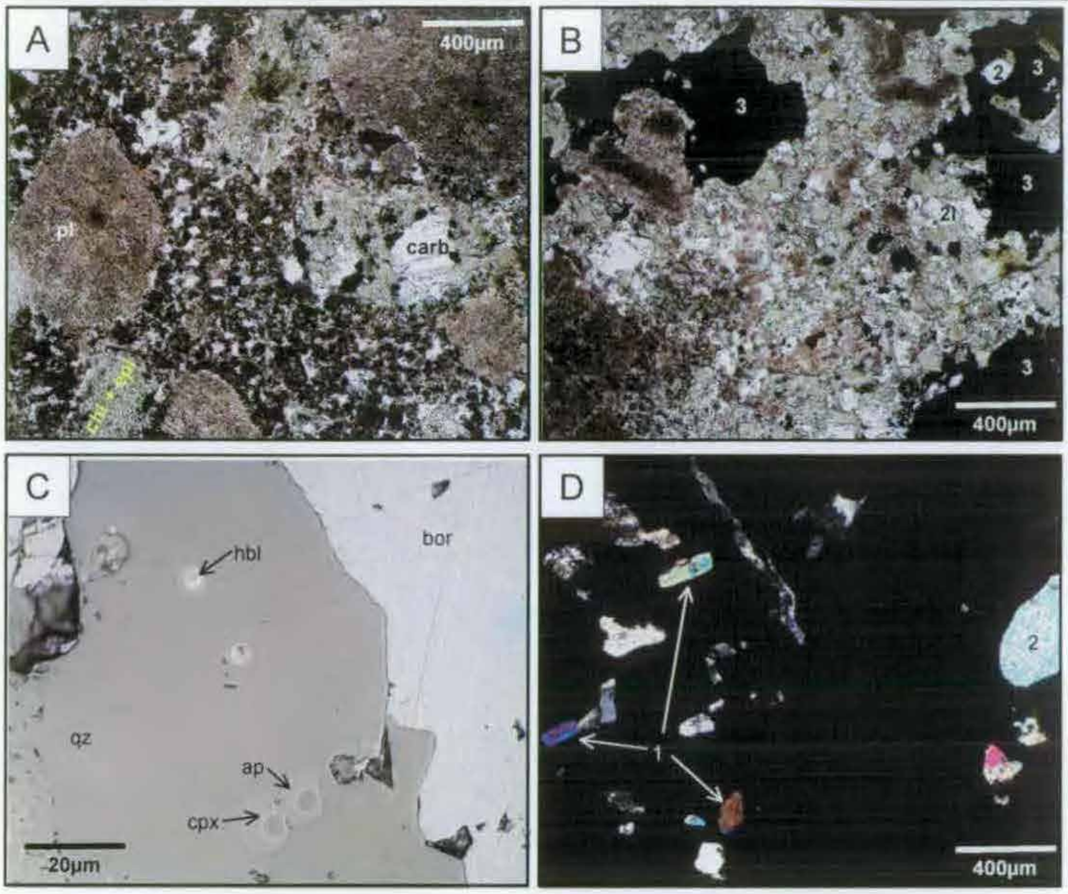

Figure 4.12 Photomicrographs of alteration and sulphide mineralogy of bornite clots.

A A photomicrograph (ppl) of a weakly developed propylitic assemblage in a late-mineral B-QMP intrusion from the pit at E27 (E27/E/25). Carbonate has replaced part of the groundmass, while epidote and chlorite have replaced precursor mafic minerals.

B A photomicrograph of secondary biotites situated adjacent to the bornite clot that has been completely replaced by chlorite (1). Carbonate, probably associated with early K-silicate alteration, it engulfed by bornite (2) and is notably rounded (2i). Large, irregular black areas are bornite (3), and collectively they form a clot at the hand specimen scale. This is from the same sample as A.

C This photomicrograph (reflected light) shows parts of a subhedral quartz crystal, which is totally engulfed by bornite (part of the bornite clot of A and B above) The quartz crystal contains primary clinopyroxene, hornblende and apatite inclusions. The circular marks are from the electron microprobe.

D In a different view of the same sample as E, this photomicrograph (xpl) shows that bornite has totally surrounded euhedral hornblende crystals (1) and rounded carbonate grains (2). The opaque parts of the field of view are bornite

Abbreviations:

ap - apatite; bor - bornite; carb - carbonate; chl - chlorite; cpx - clinopyroxene; epi - epidote; hm - haematite; mt - magnetite; pl - plagioclase; qz - quartz

4.6 Discussion

4.6.1 Alteration and mineralisation assemblages

Alteration and ore deposition at E22, E26, E27 and E48 is typically vein controlled and is intimately associated with the emplacement of multiple QMP intrusions. The multiple vein generations and overprinting alteration styles record an evolution in fluid chemistry from; 1) early biotite – magnetite (proximal) and propylitic (distal); through 2) orthoclase; 3) phyllic; to 4) late propylitic assemblages. Because of the complex intrusive, and therefore vein and alteration history, classic Eastern Pacific models of alteration zonation such as Lowell and Guilbert (1970) are simply not applicable to the Endeavour deposits. The alteration assemblages described by Lang *et al.* (1995) for the Canadian alkaline porphyry deposits are similar to those characteristic of the Endeavour deposits.

Widespread (up to ~200m) altered biotite – magnetite haloes are present in the host volcanic rocks and the BQM intrusions. Early biotite and magnetite aureoles, similar to those recognised at all four of the Endeavour deposits, have been documented at a number of porphyry deposits; including El Salvador, Chile (Gustafson and Hunt, 1975), Ann-Mason, Nevada, USA (Dilles and Einaudi, 1992) and Bingham, Utah, USA (Moore, 1978). A more spatially restricted orthoclase alteration assemblage has overprinted the secondary biotite and magnetite assemblages closer to the QMP complexes, and is intimately associated with early stage mineralisation.

Early propylitic (chlorite + carbonate + epidote) alteration is evident in the BQM intrusions at all four deposits and at E28, a prospect in the peripheral zones of E26 (Kolkert, 1998). Although propylitic alteration is typically indicative of thermal decline in the Goonumbla area (see below), inconsistent crosscutting relationships between propylitic assemblages and early K-silicate assemblages led Kolkert (1998) to propose that these two alteration styles were broadly concomitant. Concomitant distal propylitic alteration and proximal early K-silicate alteration has been documented for other porphyry deposits, e.g. Ann-Mason, Nevada, USA (Dilles and Einaudi, 1992) and many of the porphyry deposits in British Columbia, Canada (Lang *et al.*, 1995).

Fracture-controlled orthoclase alteration is characteristic of the main stage ore forming events in the Endeavour deposits. Early veinlets and thin veins of quartz + sulphide + K-feldspar give way temporally to multistage stockwork and sheet veining of a similar nature.

Both of these styles are associated with two QMP intrusions. With the first QMP intrusion, K-QMP, these veins and veinlets are bornite-dominant. With the second intrusion, KA-QMP, they are chalcopyrite-dominant. The development of transitional stage brain rock and associated textures is typical of these QMP intrusions and confirms and highlights the production of magmatic – hydrothermal fluids at this time in the evolution of the Endeavour deposits.

Zones of intense, pervasive phyllic alteration at E48 and E26 have been attributed to high temperature – high salinity magmatic fluids (Wolfe *et al.*, 1996; Harris and Golding, 2001). The concept that phyllic alteration, traditionally viewed as a result of the influx and mixing of low temperature – low salinity meteoric fluids with the magmatic fluid, can be attributed to magmatic fluid alone is not new (e.g. Panguna; Ford and Green, 1977). Indeed, recent literature indicates that there is increasing evidence relating at least some phyllic alteration assemblages to magmatic rather than meteoric fluids, e.g. Porgera (Richards *et al.*, 1998) and Far Southeast (Hedenquist *et al.*, 1998). Wolfe *et al.* (1996) proposed that the pervasive phyllic overprint at E48 represents what remains of a feeder to high level, high sulphidation epithermal-style alteration and vein + sulphide assemblages that has subsequently been faulted and/or eroded away, similar to what has occurred at El Salvador (Hedenquist, 2000).

Notwithstanding Kolkert (1998)'s observations that early propylitic alteration is associated with E26, at least some of the propylitic alteration assemblages formed late in the evolution of the systems, especially at E22 and E27. Late-stage propylitic alteration is interpreted to reflect the thermal collapse of the hydrothermal system (cf. Sander and Einaudi, 1990).

4.6.2 Sulphide mineralogy

The association of gold with bornite in the potassic alteration assemblages is common to many copper porphyry deposits, e.g. Granisle (Cuddy and Kesler, 1982), Panguna (Clark, 1990), Batu Hijau (Clode *et al.*, 1999) and Grasberg (Kavalieris, 1994). In many examples, there is an additional association of gold with potassic alteration assemblages dominated by biotite and magnetite (Sillitoe, 1990). In contrast to deposits such as Batu Hijau, Granisle and Panguna, the Endeavour deposits do not show the association of bornite and gold with magnetite. Comparison with other deposits shows that Au-rich Cu-sulphide deposition usually occurs without the haematitisation of magnetite. At the Endeavour deposits, the association of Cu-enrichment and relative Au-depletion with haematisation of magnetite was interpreted by House (1994) to imply that this association was just one of many possible mechanisms that enhance copper in Cu-Au porphyry deposits. Magnetite destruction can be coincident with gold deposition (House, 1994). This is the case for E26 and E48, where alteration of this style is pervasive; it is also less intense in the deeper portions of the two deposits where the gold grade is the highest. In contrast to E26 and E48, main stage orthoclase alteration associated with ore deposition at E22 and E27 is more fracture-controlled than it is pervasive, resulting in much less intense magnetite destruction in the latter two deposits. Compared to E22 and E27, E26 and E48 are relatively gold-depleted (Cu:Au ratios typically >1), which was interpreted by House (1994) to indicate that relative Au-depletion in the Endeavour deposits is enhanced by the haematisation of magnetite.

Of the two varieties of bornite present in the Endeavour deposits, the mauve bornite is typically myrmekitically intergrown with chalcocite, which is interpreted to imply co-precipitation of the two sulphides resulting from the decomposition of a bornite solid exsolution on cooling (Vaughan and Craig, 1997). At E26 and E48, the mauve bornite is restricted to the cores of the hydrothermal systems (House, 1994; Wolfe, 1994). In contrast, the more abundant orange bornite is generally intergrown with chalcopyrite along cleavage planes and fractures within bornite grains, which is consistent with it being exsolved from a bornite – chalcopyrite solid solution on cooling (Vaughan and Craig, 1997). The fact that gold is associated with both bornite varieties, but is not found in chalcopyrite is significant. This is interpreted to imply that gold remained in a high temperature bornite or bornite-chalcocite solid solution when chalcopyrite separated, and exsolved later with further cooling (House, 1994; Heithersay and Walshe, 1995; Simon *et al.*, 2000). The two bornite varieties maintain a constant stoichiometry throughout the E26 deposit, which led House (1994) to suggest that this was achieved by the incorporation of excess Fe and S into chalcopyrite and excess Cu into chalcocite on cooling. The occurrence of tellurides and selenides is interpreted to imply that the bornite solid solution/s locally achieved Te and Se saturation.

4.6.3 Ore distribution

Au is interpreted to have been retained in a high temperature bornite or bornite-chalcopyrite solid solution when chalcopyrite separated, and exsolved from this solid solution later with cooling. The varying Cu/Au ratios of the Endeavour deposits, from approximately equal proportions of both metals at E22 and E27, to generally higher Cu at E26 and E48 is possibly related to relative levels of erosion. Because the deeper portions of both E26 and E48 have higher Au contents than their respective upper levels, it is possible that the higher Au proportions at E22 and E27 relates to deeper levels of erosion at these two deposits.

It is possible that the mostly fracture-controlled main stage orthoclase alteration at E22 and E27 resulted in comparatively less magnetite destruction than at E26 and E48, where more pervasive orthoclase alteration occurs. The fact that E22 and E27 are also relatively more Au-rich than E26 and E48 possibly indicates that Au enrichment may be enhanced by the haematitisation of magnetite (House, 1994).

4.6.4 Origin of bornite clots

The origin of bornite the clots is enigmatic. It appears that magmatic quartz crystals that contain clinopyroxene and hornblende inclusions occur within the bornite. Bornite is also intergrown with hydrothermal biotite (now chlorite) and carbonate; minerals typical of the early orthoclase alteration assemblages.

Bornite clots occur mainly in K-QMP and late-mineral B-QMP intrusions, although they are also present, to a much lesser extent, in KA-QMP intrusions. Early-mineral B-QMP intrusions do not contain bornite clots. Given the occurrence of bornite clots, it is possible that they could have formed by the assimilation of previously deposited sulphides. This assimilated sulphide could then have been "sweated" out from the successive intruding melts as immiscible sulphide droplets on crystallisation. This is proposed because bornite occurs in pre-mineral veins (E1) and thereafter, K-QMP and KA-QMP added sulphide to the systems. Thus, every intrusion after the first early-mineral B-QMP intrusions could contain some sulphides assimilated from early-crystallised intrusions.

The sub- to euhedral quartz crystals that occur together with the bornite clots are not present in any of the QMP intrusions within the deposits, except where they are associated with anisotropic textures. Since anisotropic textures are thought to be indicative of the coexistence of aqueous fluid and silicate melt, it is possible that the aqueous fluid produced the biotite and carbonate associated with the bornite clots. In addition, given that the bornite clots occur intergrown with magmatic quartz and K-silicate alteration minerals, it is possible that local pockets of immiscible sulphide melt may have coexisted with both the silicate melt and magmatic aqueous fluid to form the bornite clots.

4.7 Summary

Pre-mineral, weak to intense, selective to pervasive albitisation and sericitisation of plagioclase and K-feldspar and alteration of biotite to chlorite, quartz and carbonate, is recognised in the BQM and host volcanic rocks. The early stage of hydrothermal activity comprises selectively pervasive biotite + magnetite alteration assemblages, which affected mainly the host volcanic rocks, and proximal pervasive K-feldspar alteration assemblages and veinlets, which mostly affected the intrusive rocks. Distal propylitic alteration, characterised by the patchy replacement of feldspar and mafic minerals by epidote and carbonate, has also been noted. The main phase of sulphide deposition was spatially and temporally related to the emplacement of the K-QMP intrusions and the associated orthoclase alteration assemblages, which are characterised by multiple generations of quartz, K-feldspar and sulphide veins at the various deposits. At E26 and E48, anhydrite is also commonly part of this alteration assemblage. Multiple main stage sulphide-bearing vein generations also formed in association with KA-QMP intrusions. The late stage mineralised phyllic overprint, typified by intense, pervasive, quartz, sericite, carbonate and sulphide assemblages, is best developed in the K-QMP and KA-QMP intrusions and has been interpreted to be magmatic – hydrothermal in origin. Late stage fault-related carbonate, sericite and quartz alteration assemblages and carbonate, base-metal sulphide veins predate the intrusion of the basaltic trachyandesite and zero porphyry dykes at E26. Weak to moderate pervasive propylitic alteration assemblages associated with thermal collapse of the Endeavour systems are the last alteration event related to the QMP intrusive complexes.

CHAPTER 5

Fluid Inclusions

5.1 Introduction

Fluid inclusion analyses can provide useful information regarding fluid compositions, temperatures, pressures and volatile evolution in magmatic – hydrothermal systems. Many workers believe that ore metals in porphyry systems are derived from the crystallising magma and transported in magmatic – hydrothermal fluids into the upper portions of the magma chamber and adjacent areas, where they can precipitate in economic concentrations (e.g. Henley and McNabb, 1978; Burnham, 1979; Candela, 1989a and b; Beane and Bodnar, 1995). The volume of aqueous fluid will be determined, in part, by the initial concentration of H_2O in the magma and the amount of crystallisation that has taken place in the magma chamber (Roedder, 1992). Evidence for the passage of this fluid can locally be found in fluid inclusions trapped in veins and altered wallrock.

The initial volatile content of most felsic magmas is ~2 – 7% H_2O; (Burnham, 1979), but because most of the crystals forming from the magma have only trace volatile constituents in their structures (e.g. F, Cl, OH^-, CO_2, etc), the volatile concentration of the residual melt increases as crystallisation continues (Roedder, 1992). Pressure – depth constraints play an important role in determining whether or not a magmatic fluid will exsolve. This is because at deep crustal levels, H_2O is typically incorporated into hydrous magmatic minerals and not released as an immiscible fluid.

In this study, fluid inclusions have been analysed in different vein stages from each of the Endeavour porphyry deposits with the following aims:

1) to track hydrothermal fluid evolution in the systems and establish the P-T-X condition of these fluids;
2) to determine if a common sequence of fluid evolution occurred at each of the four deposits; and
3) to determine when during their histories, volatiles separated from the magmas as immiscible fluids.

Previous fluid inclusion studies have been conducted by Heithersay and Walshe (1995) and Harris (1997) on E26 and by Howland-Rose (1996) on E48. Data from these studies have been incorporated into the present study to augment the relevant data sets.

5.2 Methods

A total of 660 quartz-hosted fluid inclusions from twenty-six ~150μm thick doubly polished sections have been analysed during this study. These samples were selected to provide maximum spatial and temporal coverage of the alteration and mineralisation paragenesis at E22, E26, E27 and E48. Figures 5.1 shows the spatial distribution of samples from the four deposits. Details of sample location, host medium and paragenetic stage are summarised in Table 5.1; full details are provided in Appendix B1.

The paragenetic framework developed in Chapter 4 has formed the basis for the fluid inclusion study (cf. Figure 4.2). Early Stage veins (E1) are indicated here as early quartz (EQ); Transitional Stages TM1 and TM2 anisotropic textures are denoted as transitional quartz; Main Stage M1 and M2 veins as main quartz (MQ) and Late Stage veins (L1) as late quartz (LQ). Transitional quartz is further subdivided into transitional'magmatic quartz (TMQ), for quartz within the magmatic/aplitic portion of the anisotropic texture, and transitional hydrothermal quartz (THQ) for quartz from the comb quartz layers of brain rock or partial brain rock.

5.2.1 Fluid inclusion classification

Fluid inclusions have been classified as primary, pseudo-secondary or secondary according to Roedder's (1984) and Shepherd *et al.*'s (1985) definitions. Primary fluid inclusions are those incorporated into the host during mineral growth, while pseudo-secondary inclusions are those that were incorporated within the host mineral along sealed fractures during mineral growth (Figures 5.2a and b). Primary growth zones in many quartz grains from the Endeavour deposits are defined by submicron-sized fluid inclusions (Figure 5.2c). Secondary inclusions are those that were incorporated along healed fractures that crosscut or terminate against grain boundaries (Figures 5.2d). The alignment of fluid inclusions along the long axis of the mineral, different fluid inclusion densities in adjacent crystals and the concentration of fluid inclusions at the edges of crystals are additional features of primary fluid inclusions.

Table 5.1 Summary of fluid inclusion samples, including deposit (total number of sections analysed), number of polished slides analysed (some sections contain quartz from more than one paragenetic stage), paragenetic stage; early (EQ), transitional magmatic (TMQ), transitional hydrothermal (THQ), main (MQ) and late (LQ) and host medium; Qz – quartz; Kfs – K-feldspar; Carb – carbonate; Anh – anhydrite; Fl – fluorite.

Deposit	*Samples*	*Paragenetic Stage*	*Host medium*
E22 (6)	1	EQ	Early Qz+Kfs+sulphide veinlet in volcanic rock
	3	TMQ	Magmatic Qz in brain rock in K-QMP
	2	THQ	Comb-layered (hydrothermal) quartz in brain rock in K-QMP
E26 (9)	2 (+1)	EQ	Early Qz + Kfs + sulphide veinlets in volcanic rock
	5 (+1)	TMQ	Magmatic Qz in brain rock (1), anisotropic textures in K-QMP (3) and KA-QMP (1)
	1 (+1)	MQ	Sheeted Qz + sulphide ± Anh ± Kfs veins in K-QMP and KA-QMP
	1 (+1)	LQ	Qz in late Qz + Py + Carb vein
E27 (5)	1 (+1)	EQ	Early Qz + Kfs + sulphide veinlets in volcanic rock
	1 (+1)	TMQ	Magmatic Qz in anisotropic texture in K-QMP (1) and KA-QMP (1)
	1	THQ	Comb-layered (hydrothermal) quartz in partial brain rock in K-QMP
	1 (+2)	MQ	Sheeted Qz + sulphide ± Anh ± Kfs veins in K-QMP and KA-QMP
	1 (+1)	LQ	Qz in late Qz + Py + Carb vein
E48 (6)	2 (+2)	EQ	Early Qz + Kfs + sulphide veinlets in volcanic rock
	1 (+2)	TMQ	Magmatic Qz anisotropic textures in K-QMP
	2	MQ	Sheeted Qz + sulphide ± Anh ± Kfs veins in K-QMP and KA-QMP
	1 (+1)	LQ	Qz in late Qz + Py + Carb vein

Three main types and five subtypes of fluid inclusions have been recognised based on phase relationships at 25°C (Figure 5.3). These inclusion types are listed in Table 5.2 and typical examples of each fluid inclusion type from the Endeavour deposits are presented in Figure 5.4. In summary, the fluid inclusion types and their homogenisation behaviour are as follows:

- Type 1a inclusions are two phase inclusions that contain liquid and <60% vapour (L + V);
- Type 1b inclusions are similar to Type 1a inclusions but contain an additional opaque phase (L + V + op). Both Type 1 fluid inclusions homogenise to liquid at elevated temperatures.
- Type 2 inclusions are similar to Type 1 inclusions in that they contain two phases however, they are vapour-rich and homogenise to the vapour phase at elevated temperatures (Type 2a V + L; Type 2b V + L + op). Type 2 inclusions are less common than both Type 1 and Type 3 inclusions.
- Type 3 inclusions are hypersaline inclusions that contain liquid, vapour (5 – 50% volume) and a variety of daughter crystals. They are subdivided according to the daughter crystals present:

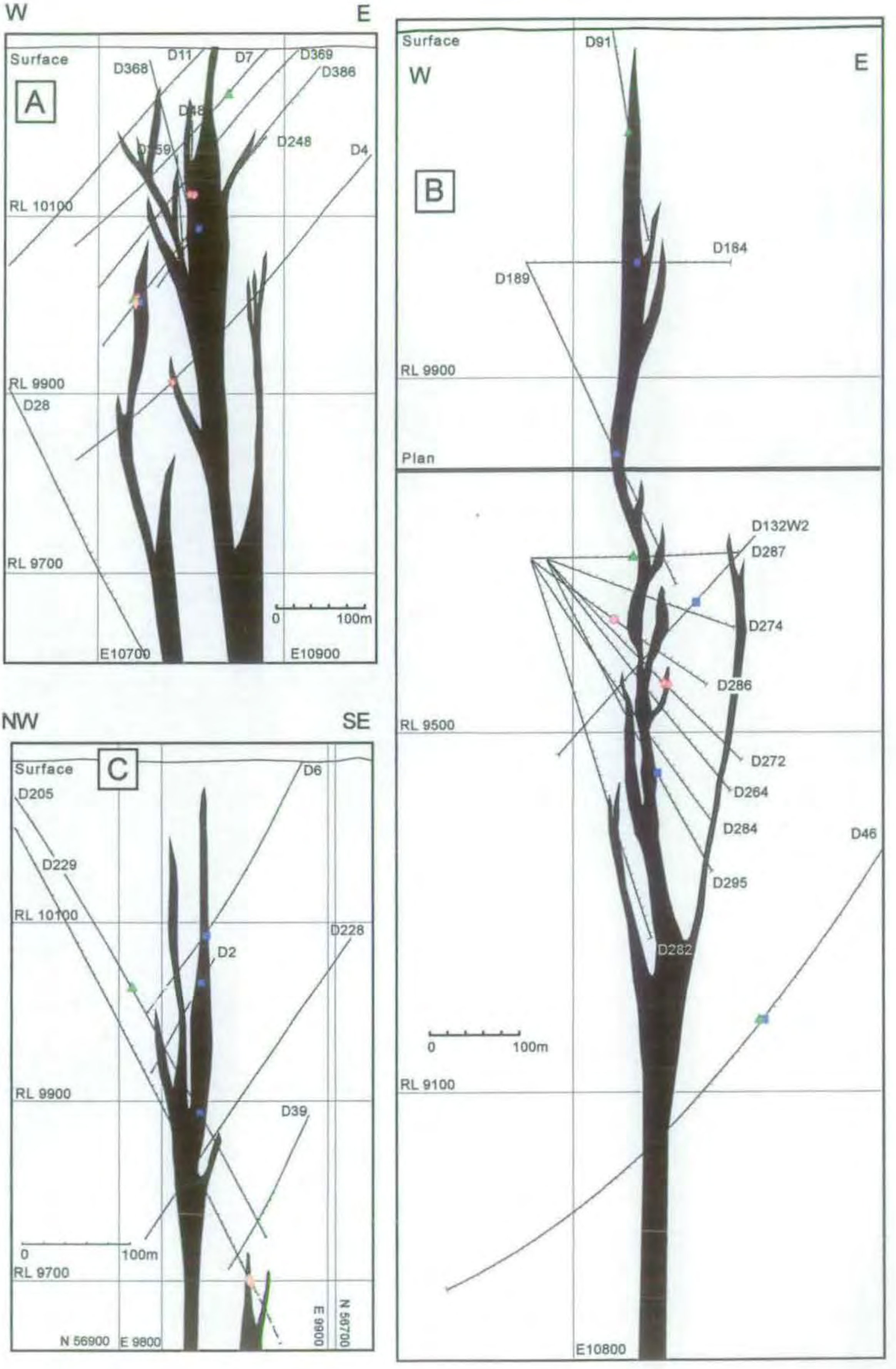

W
E
Surface
A
D368
D11
D7
D369
D386
D248
D4
RL 9900
D28
RL 9700
0
100m
E10900
Surface
D91
W
E
B
D184
D189
RL 9900
Plan
D132W2
D287
D274
D286
RL 9500
D272
D264
D284
D46
D295
D282
0
100m
RL 9100
E10800
NW
SE
Surface
C
D6
D205
D229
RL 10100
D228
D2
RL 9900
D39
0
100m
RL 9700
N 56900
E 9800
E 9900
N 56700

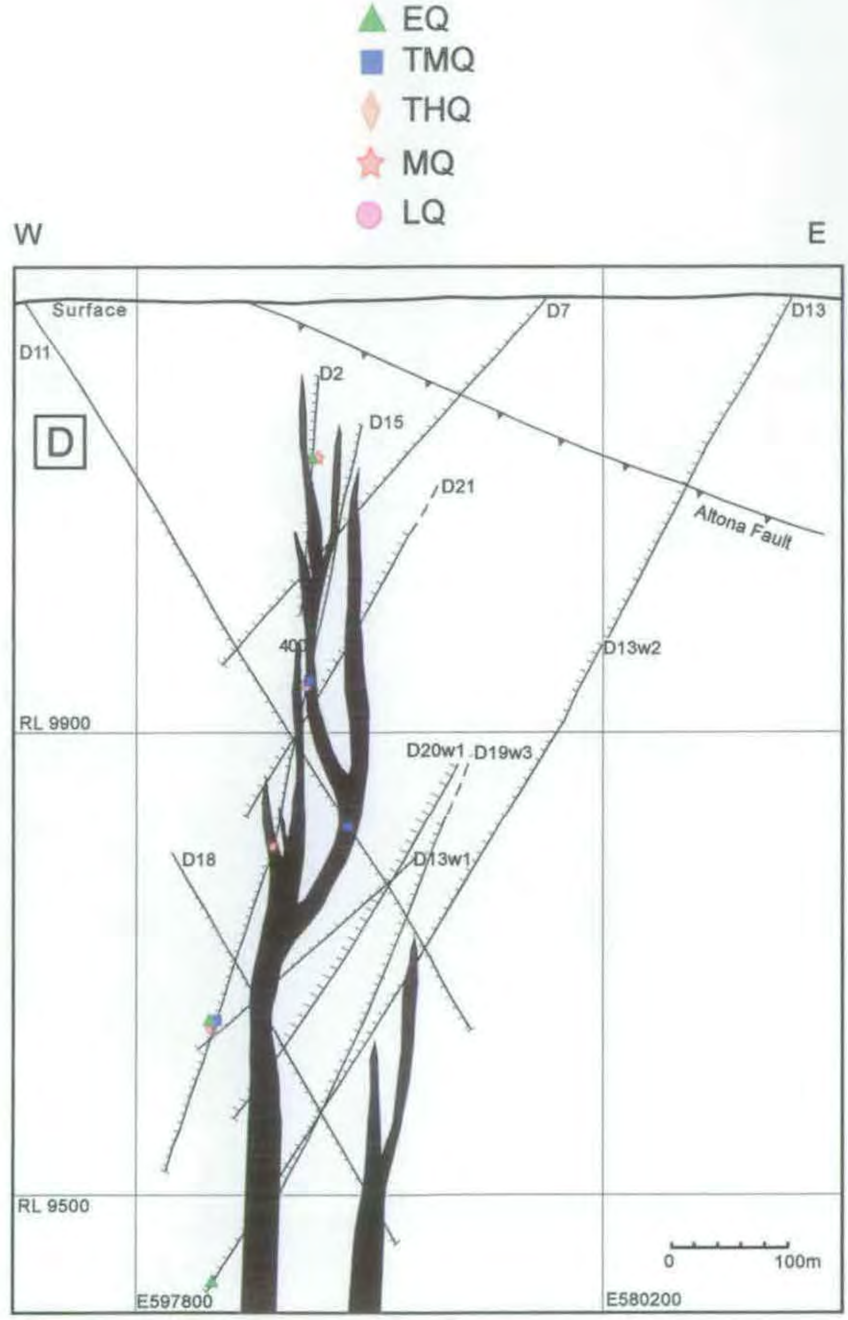

Figure 5.1 Cross-sections through **A** E22, **B** E26, **C** E27 and **D** E48 showing the spatial and temporal distribution of fluid inclusion samples (and K-QMP intrusions for reference). Section locations are shown on Figures 3.4, 3.5, 3.6 and 3.7 respectively.

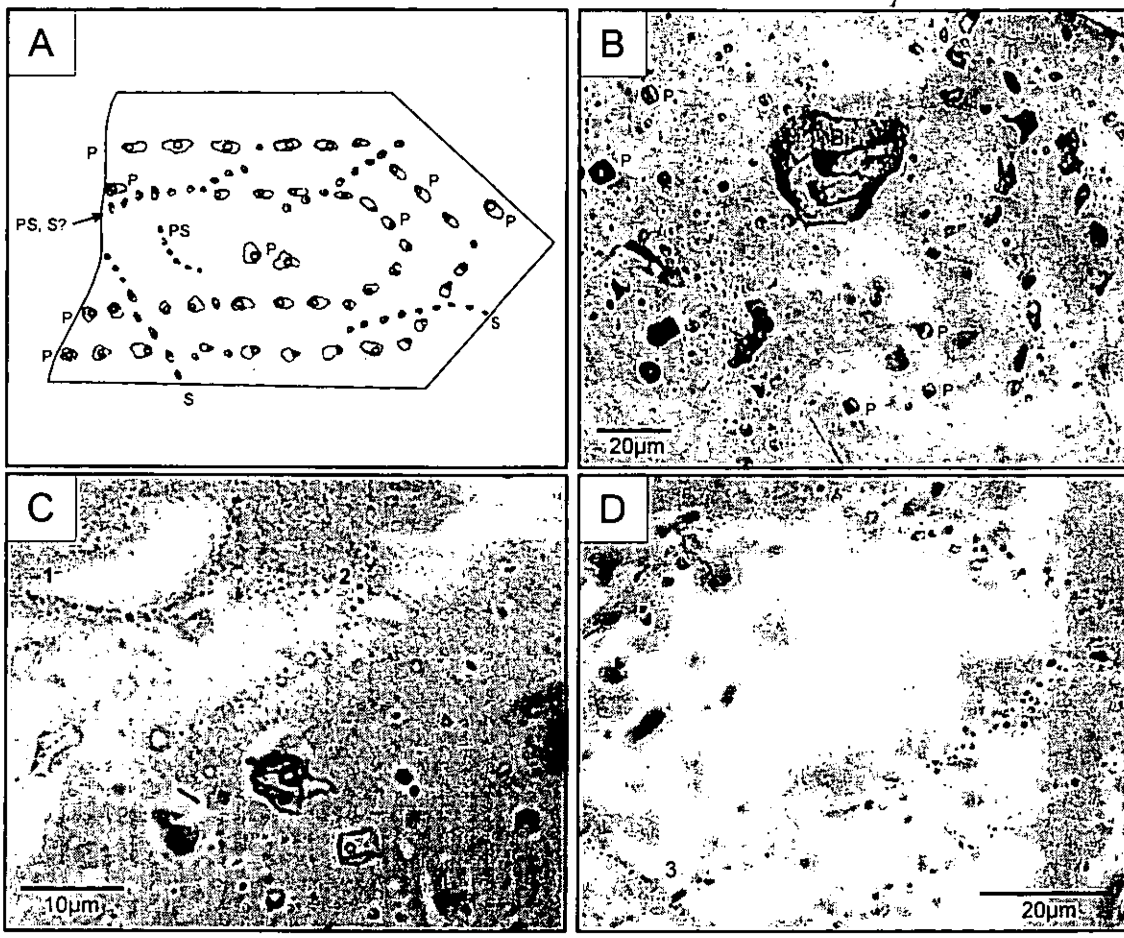

Figure 5.2 **A** Primary (P), pseudo-secondary (PS) and secondary (S) classification of fluid inclusions (after Shepherd *et al.*, 1985). **B** One of the characteristics of primary fluid inclusions (P) is their alignment along growth planes; Bi – solid biotite inclusion, TMQ from E27. **C** Growth zones (1 and 2) are typically defined by submicron-sized fluid inclusions, EQ from E48. **D** Cross-cutting secondary fluid inclusion trails (3) in TMQ from E22.

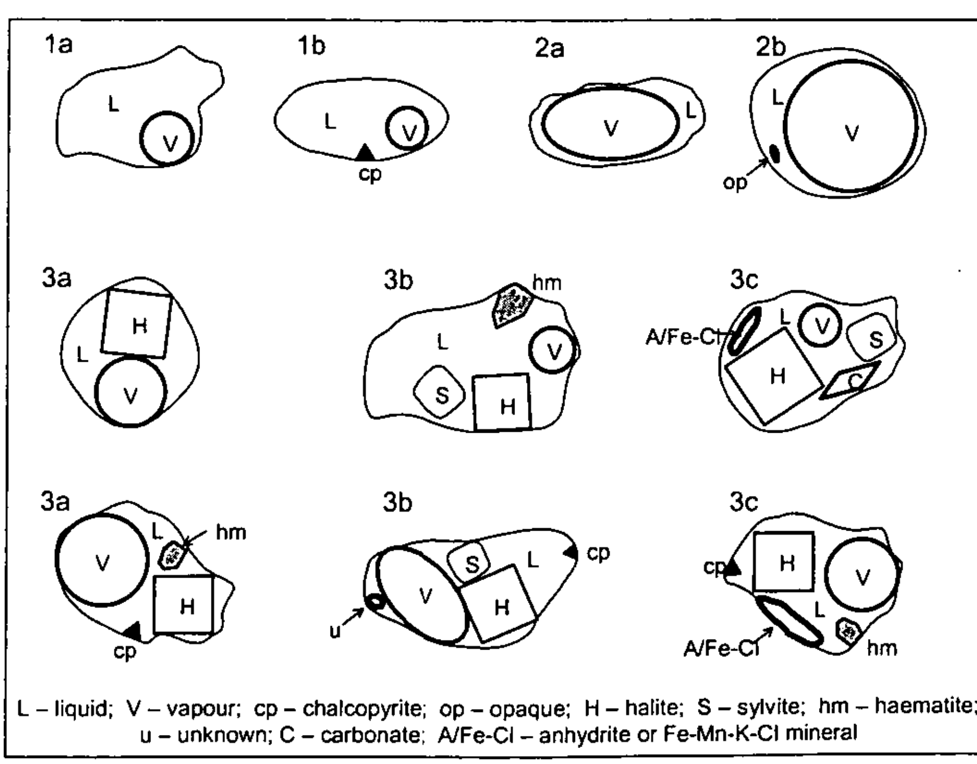

Figure 5.3 Sketches of the various fluid inclusion types occurring the different quartz generations in the Endeavour deposits.

Figure 5.4 Photomicrographs of typical fluid inclusions in the different quartz generations from the Endeavour deposits.

A Secondary two-phase Type 1a in THQ from E22;
B Primary two-phase Type 2a in TMQ from E26;
C Primary multiphase Type 3a in MQ from E27, which contains halite, haematite and chalcopyrite daughter crystals;
D Primary multiphase Type 3b in THQ in E22 with halite, sylvite and an opaque daughter crystals;
E Primary multiphase Type 3c in MQ from E27, which contains halite, an opaque and either anhydrite or a Fe-Mn-K chloride daughter crystals;
F A cluster of primary multiphase Type 3a and 3b fluid inclusions and a secondary inclusion trail (1) in MQ from E27. Halite, sylvite, haematite, chalcopyrite, opaque and anhydrite or Fe-Mn-K chloride daughter phases are present in the multiphase Type 3a and 3b fluid inclusions;
G Primary multiphase Type 3 inclusions in MQ from E27, which contain halite, sylvite, opaque phases and unknown daughter crystals; and
H Primary Type 3 fluid inclusion in MQ from E27 with halite, sylvite, anhydrite or Fe-Mn-K chloride and two unknown daughter crystals.

Abbreviations
A/Fe-Cl - anhydrite/Fe-Mn-K-chloride; cpy - chalcopyrite; L - liquid; H - halite; Hm - haematite; op - opaque; S - sylvite; u - unknown; V - vapour

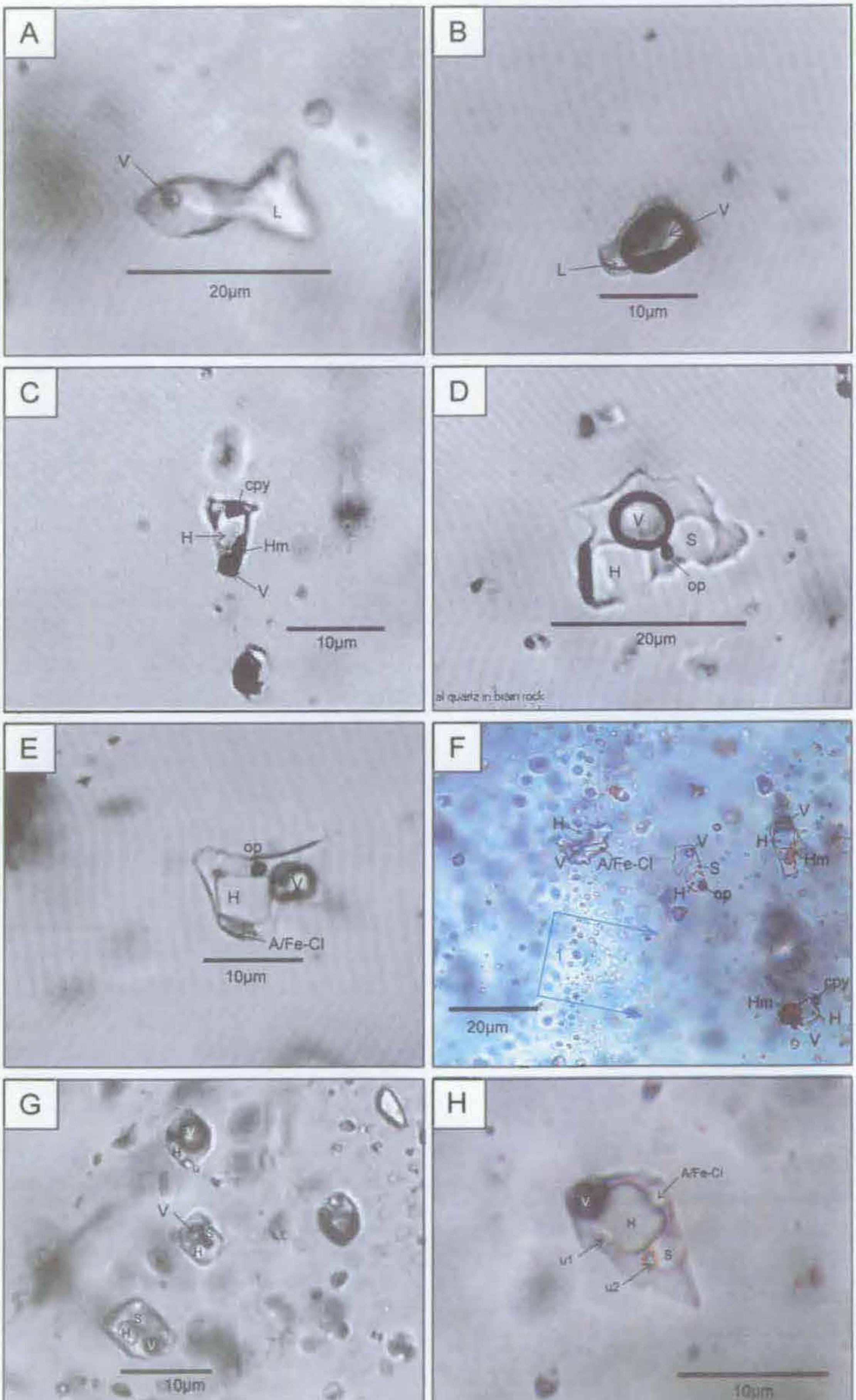
A
V
L
20µm
B
V
L
10µm
C
cpy
H
Hm
V
10µm
D
V
S
H
op
20µm
E
op
V
H
A/Fe-Cl
10µm
F
H
V
A/Fe-Cl
V
S
H
op
V
H
Hm
cpy
Hm
H
V
20µm
G
V
H
V
S
H
S
H
V
10µm
H
V
A/Fe-Cl
H
u1
S
u2
10µm

- Type 3a contain L + V + **halite** (H) ± op ± haematite (hm),
- Type 3b L + V + H + **sylvite** (S) ± hm ± op ± others, and
- Type 3c L + V + H ± **anhydrite or Fe-Mn-K chloride** (A/Fe-Cl) ± S ± hm ± op ± others.

Chalcopyrite occurs as a daughter crystal in many of the Type 1 and 3 fluid inclusions. Type 3a and 3b inclusions homogenise by halite dissolution or vapour homogenisation, while Type 3c inclusions homogenise exclusively by halite dissolution. Halite and sylvite in Type 3 fluid inclusions account for 10 – 50% and ~10% volume respectively. Where present, anhydrite or Fe-Mn-K chlorides typically account for 5 – 10% volume of Type 3c fluid inclusions.

Homogenisation behaviour is classified by adding a suffix to the inclusion type ("subtype" in Table 5.2). **L** is added for vapour disappearance, **V** for liquid disappearance or **H** for halite dissolution, **S** for sylvite dissolution, **O** for Fe-Mn-K chloride or unidentified salt dissolution, **M** for metastable (bubble not reappearing after cooling), **D** for decrepitation before homogenisation, or **N** for no homogenisation observed up to the maximum operating temperature of the fluid inclusion stage (600°C). For example, a Type 3aL inclusion is a Type 3a inclusion that homogenises by halite dissolution followed by homogenisation of the vapour bubble to the liquid phase and a Type 3aH inclusion is a Type 3a fluid inclusion that homogenises by bubble disappearance followed by halite dissolution. Halite, sylvite, haematite and chalcopyrite daughter crystals have been identified from physical and optical properties according to Table 5 in Cline and Bodnar (1994). Several other phases with optical properties similar to those described by Cline and Bodnar (1994) may be present. Cooke and Bloom (1990) identified Fe-Mn chloride, Fe-chloride, K-Fe chloride, anhydrite and calcite as daughter crystals in porphyry-related fluid inclusions from the Acupan gold mine in the Philippines. Fe-Mn chloride is typically present as elongate hexagonal, high relief, birefringent crystals, while Fe-chloride generally forms elongate to irregular, high relief, strongly birefringent, colourless to light green crystals (Cooke and Bloom, 1990). They tentatively identified the latter phase as erythrosiderite ($K_2FeCl_5.H_2O$) as it is similar in all aspects to a daughter crystal identified at Granisle and Bell porphyry copper deposits by Wilson *et al.* (1980). Anhydrite has similar optical properties (Cline and Bodnar, 1994) to the Fe-Mn-K chloride phases recognised by Cooke and Bloom (1990), but does not dissolve on heating, whereas erythrosiderite does. Carbonate daughters crystals, recognised by their typical translucent, birefringent, rhombic crystal form (Cline and Bodnar, 1994), are present in few Type 3c inclusions.

Table 5.2 Summary of fluid inclusion types including phases present at room temperature and typical homogenisation behaviour. L - liquid; V - vapour; H - halite; S - sylvite; A - anhydrite; Fe-Cl - Fe-Mn-K chloride, op - opaque, hm - haematite, cpy - chalcopyrite.

Type	*Subtype*	*Phases*	*Homogenisation behaviour*
1a	1aL	L + V	V → L
1b	1bL	L + V + op	V → L
2a	2aV	V + L	L → V
2b	2bV	V + L + op	L → V
3a	3aH	L + V + H ± op ± hm ± cpy	V → L, H → L
	3aL	L + V + H ± op ± hm ± cpy	H → L, V → L
3b	3bH	L + V + H + **S** ± op ± hm ± cpy	V → L, S → L, H → L / S → L, V → L, H → L
	3bS	L + V + H + **S** ± op ± hm ± cpy	V → L, H → L, S → L
	3bL	L + V + H + **S** ± op ± hm ± cpy	S → L, H → L, V → L
3c	3cA	L + V + H + **A** ± S ± op ± hm ± cpy	V → L, H → L, A → L
	3cH	L + V + H + **A/Fe-Cl** ± S ± op ± hm ± cpy	V → L, A → L, H → L
	3cS	L + V + H + **A/Fe-Cl** ± S ± op ± hm ± cpy	V → L, H → L, S → L

5.2.2 Microthermometry

Microthermometric measurements were obtained from heating and cooling experiments conducted on a *Linkam MDS600* stage (-196 to 600°C) mounted on an *Olympus BX60* microscope. All measurements were made using the 100-times magnification lens. Wherever possible, the following observations and microthermometric measurements were recorded:

5.2.2.1 Undersaturated (<23.3 wt% NaCl eq.) fluid inclusions (Types 1 and 2)

- mode of occurrence; primary (p), pseudo-secondary (ps) or secondary (s)
- inclusion shape and size,
- volume percent liquid (L), vapour (V) and if appropriate, opaque phase (op),
- lowest temperature attained by the liquid before it froze (T_{min}), eutectic melting point of liquid ($T_{eutectic}$) and temperature of final ice melting ($T_{m\ ice}$),
- temperature of homogenisation (T_hF) and homogenisation behaviour,
- salinity in wt% NaCl eq. based on freezing point depression using Potter *et al.*'s (1978) equation (5.1) for the NaCl-H_2O system:

$$\text{wt\% NaCl eq.} = 1.76958T_{m\ ice} - 0.042384T_{m\ ice}^2 + 0.00052778T_{m\ ice}^3 \quad \ldots\ldots\ 5.1$$

5.2.2.2 Hypersaline (>23.3 wt% NaCl eq.) fluid inclusions (Type 3)

- mode of occurrence; primary (p), pseudo-secondary (ps) or secondary (s)
- inclusion shape and size,

- volume percent liquid (L) and vapour (V), as well as identification and volume percent of daughter phases (halite, sylvite, anhydrite, Fe-Mn-K chlorides, haematite ± others),
- temperature of homogenisation (T_hF) and homogenisation behaviour,
- salinity in wt% NaCl eq. based on either the temperature of halite dissolution using Potter *et al.*'s (1977) equation for the NaCl-H_2O system (Equation 5.2), or the temperatures of halite and sylvite dissolution using Bodnar *et al.*'s (1989) SALTY computer algorithm:

$$\text{wt\% NaCl eq.} = 26.218 + 0.0072T_hH + 0.000106T_hH^2 \qquad \ldots\ldots\ 5.2$$

5.2.3 PIXE analysis

Three fluid inclusions in transitional magmatic quartz (TMQ) from an E48 vein dyke sample were analysed by proton induced X-ray emission (PIXE) at CSIRO, Canberra. PIXE analysis is a non-destructive analytical technique that can provide quantitative compositional information on the contents of fluid inclusions (Heinrich *et al.*, 1992). Fluid inclusions chosen for PIXE analysis were within 10µm of the surface of the host grain to minimise attenuation of X-ray signals from S, Cl and K as they pass though quartz; Na is not detectable by PIXE analysis (pers. comm., T.T. Win, CSIRO, Canberra, 2001).

5.2.4 Decrepitation analysis

Fluid inclusion chips (~0.5cm x 0.5cm) containing large (>10µm) primary fluid inclusions close to the surface were selected for decrepitation analysis. Chips were put in platinum crucibles on a porcelain tray and then put in a preheated (1000°C) furnace for 20 minutes. They were then cooled, mounted on glass slides and carbon-coated as quickly as possible to prevent sublimation of salt crystals. Solid phases produced by decrepitation were then analysed on the Cameca SX50 microprobe at the University of Tasmania's Central Science Laboratory (CSL). The probe was set with a beam current of 5nA, acceleration voltage of 15kV and spot size of ~10µm to minimise destruction of the inclusion decrepitate during analysis. Atomic percentages were used for ratio calculations because the microprobe software normalises these percentages to carbon, thereby negating a normalisation process in data reduction (pers. comm., D.S. Steele, 2001). Full analytical results are presented in Appendix B2.

5.3 Microthermometric results

Of the 660 fluid inclusions analysed during this study, 358 have been classified as primary or pseudo-secondary and the remainder as secondary fluid inclusions. Of the primary and pseudo-secondary fluid inclusions, 309 yielded both salinity and homogenisation temperature data, whereas the remaining yielded either salinity or homogenisation temperature information. Sylvite and halite dissolution temperatures were obtained from 53 of the 62 Type 3b fluid inclusions analysed and from 8 of the 9 analysed Type 3c fluid inclusions that contained both daughter salts.

Fluid inclusions studied range in size from ~3μm x 2μm up to 36μm x 13μm, with an average size of ~9 μm x 6μm. Inclusions of dimensions less than 3μm x 2μm were not analysed because phase changes could not be observed readily. The fluid inclusions studied were mainly negative crystal-shaped or elongate to regular in form.

5.3.1 Fluid inclusions in early quartz (EQ)

Fifty-four primary and pseudo-secondary fluid inclusions in selected quartz crystals from Early Stage E1 quartz + bornite + K-feldspar veins (EQ) were analysed microthermometrically. The quartz in these veins is typically fine-grained (<200μm) and subhedral. Crystals have nucleated on the vein walls and grain sizes increase towards the centre of the vein. EQ contains abundant secondary inclusion trails. Primary growth zones are present in many samples. Quartz grains with abundant isolated primary fluid inclusions and those with only minor secondary trails were chosen for analysis.

In EQ, Type 3 fluid inclusions homogenised mainly by halite dissolution at temperatures from 450 to >600°C, with most homogenising above 550°C (Figure 5.5). Calculated salinities for these fluid inclusions range from 50 to 75 wt% NaCl ± KCl eq., with a mode at 60 – 65 wt% NaCl ± KCl eq. (Figure 5.5). Type 1 (15 – 25 wt% NaCl eq. calculated salinity) and Type 2 fluid inclusions homogenised by vapour and liquid disappearance respectively at temperatures between 450 to 500°C (Figure 5.5). Based on dissolution temperatures of sylvite and halite in Type 3b inclusions (137 – 368° and 502 – 571°C respectively), NaCl:KCl:H_2O compositions of 43 – 61:13 – 30:17 – 29 (average 55:19:26) have been calculated (Figure 5.6). Calculated Na/Na + K ratios range from 0.67 to 0.85 (average ~0.79). All Type 3c inclusions in EQ contain either anhydrite or Fe-Mn-K chloride; salinities of these fluid inclusions have been estimated on wt% NaCl eq. concentrations. Results are summarised in Table 5.3.

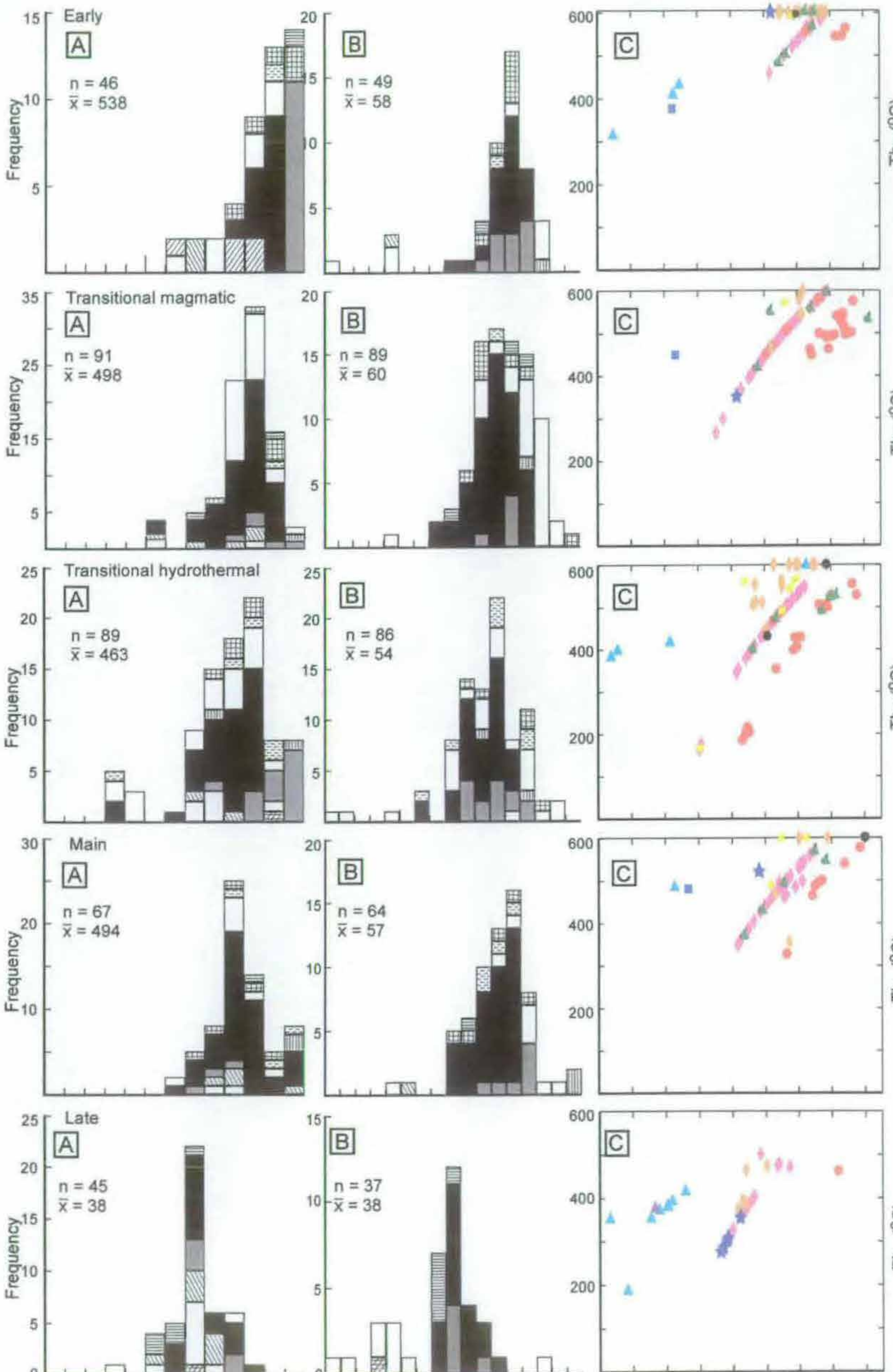

Early
A
n = 46
x̄ = 538
B
n = 49
x̄ = 58
C
Transitional magmatic
A
n = 91
x̄ = 498
B
n = 89
x̄ = 60
C
Transitional hydrothermal
A
n = 89
x̄ = 463
B
n = 86
x̄ = 54
C
Main
A
n = 67
x̄ = 494
B
n = 64
x̄ = 57
C
Late
A
n = 45
x̄ = 38
B
n = 37
x̄ = 38
C
Frequency
Th_F (°C)
Salinity (eq. wt% NaCl ± KCl)

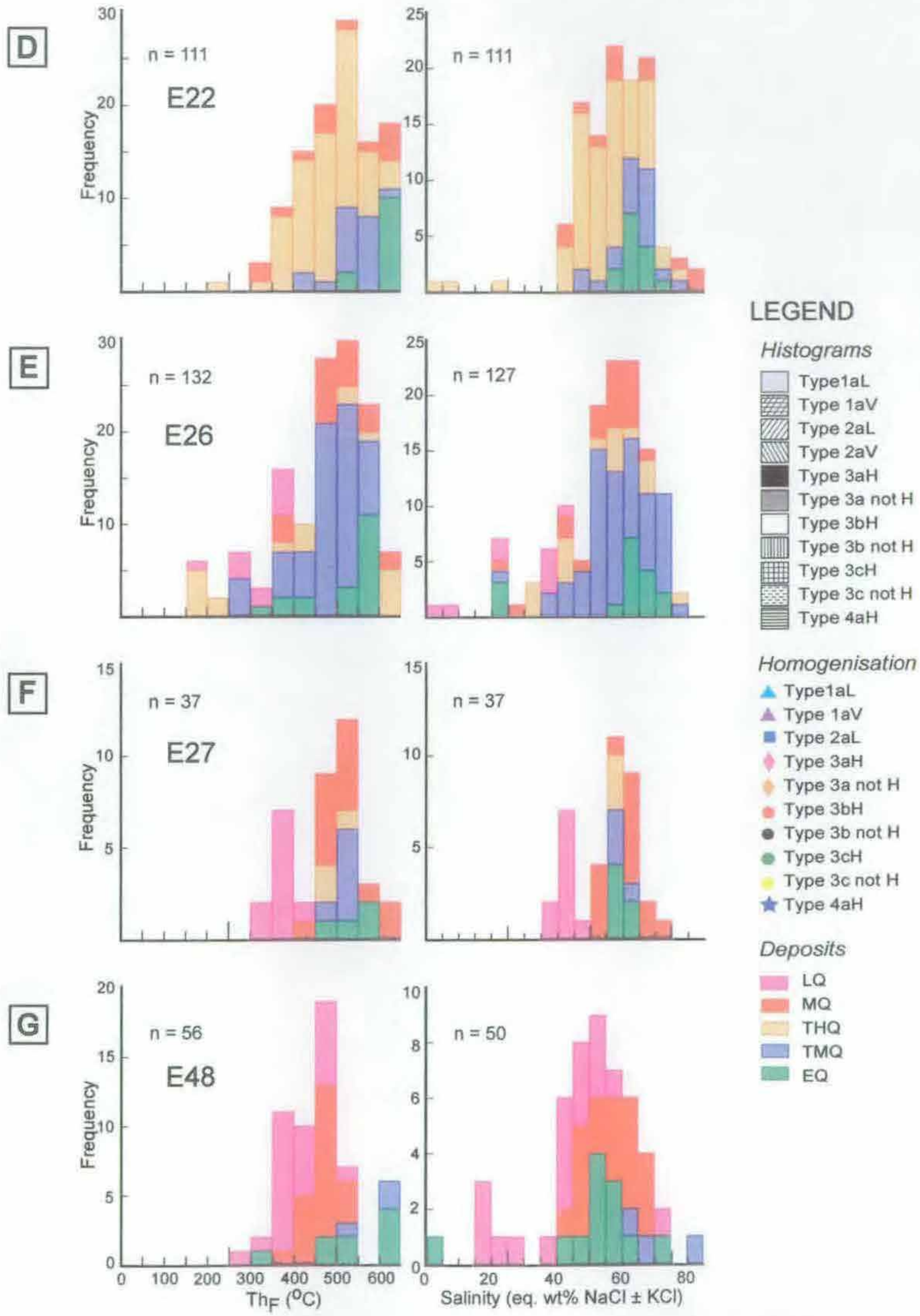

Figure 5.5 Cumulative frequency histograms of **A** homogenisation temperatures, **B** salinity and **C** homogenisation temperature vs salinity graphs of fluid inclusions for early, transitional magmatic, transitional hydrothermal, main and late stage quartz. **D**, **E**, **F** and **G** are cumulative histograms of homogenisation temperatures and salinities for E22, E26, E27 and E48 respectively.

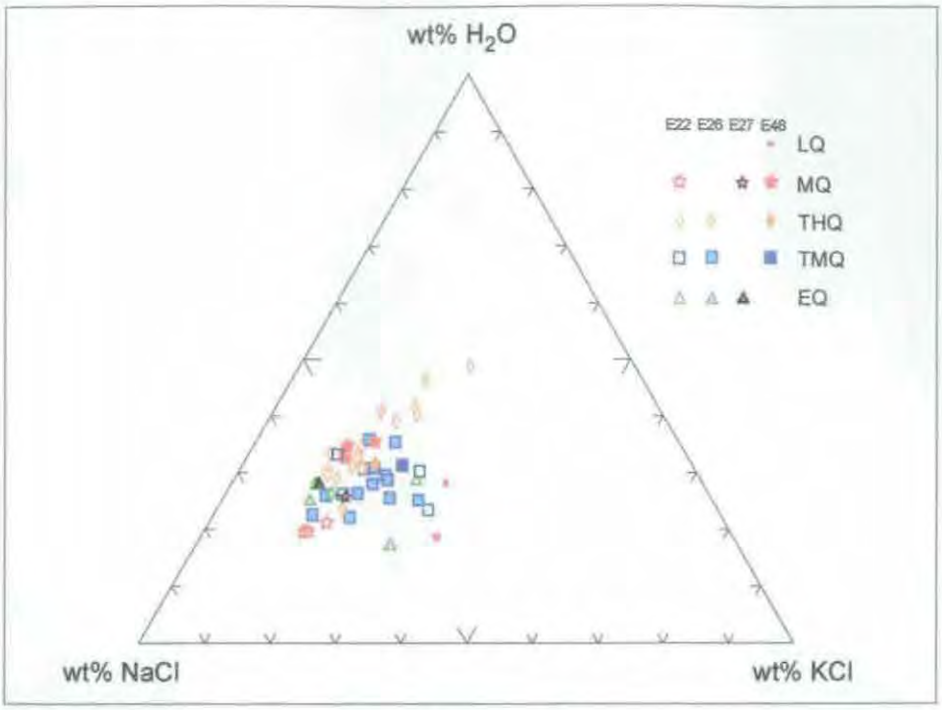

Figure 5.6 NaCl-KCl-H_2O compositions of Type 3b fluid inclusions from this study (all paragenetic stages at E22, E26, E27 and E48), as determined from calculations using SALTY (Bodnar *et al.*, 1989).

Table 5.3 Summary of fluid inclusion characteristics for each paragenetic stage in terms of constituent inclusion types, homogenisation temperature (T_hF), salinity, NaCl:KCl:H_2O composition and Na/Na + K. Homogenisation temperatures are presented uncorrected for pressure and salinities are reported as wt% NaCl eq. expect where T_{mKCl} was recorded, where they are reported as wt% NaCl + KCl eq.

Stage	*Types*	*T_hF (°C)*	*Salinity (wt% NaCl ± KCl eq.)*	*Average NaCl:KCL:H_2O*	*Average Na/Na+K*	*Comments*
EQ	3a + 3b < 3c 2a + 1a	450 - >600, mode >550 450 - >600	50 - 75, mode 60 - 65 15 - 25 (Type 1)	55:19:26 -	0.79 -	-
TMQ	3a + 3b > 3c 2a	350- >600, mode 500-550 300 - >550	50 - 75, mode 55 - 60 -	50:22:28 -	0.74 -	V < 20%
THQ	3a + 3b = 3c 2a	350 - 550, mode 450-500 400 - 500	45 - 70, peak 55 - 60 -	47:18:35 -	0.76 -	V 20 - 50%, cpy/hm
MQ	3a + 3b = 3c 2a	450 - 550, mode 450 - 500 ~450	45 - 70, peak 60 - 65 -	56:16:28 -	0.81 -	V 20 - 50%, cpy/hm
LQ	3a 1a/b	340-500, mode 350-400 350 - 400,	35 - 55, peak 40 - 45 20 - 25	42:34:24 -	0.61	-

EQ fluid inclusions from E22, E26 and E27 have similar homogenisation temperatures and calculated salinities (Figures 5.5d, e and f respectively). EQ from E48 have salinities up to 5 wt% NaCl ± KCl eq. lower than the other deposits (Figure 5.5g). Two of the three sylvite-bearing fluid inclusions in EQ from E22 are rich in KCl compared to those from the other deposits (Figure 5.6).

5.3.2 Fluid inclusion in transitional quartz

5.3.2.1 Fluid inclusions in transitional magmatic quartz (TMQ)

Fluid inclusions contained within transitional magmatic quartz (TMQ) from anisotropic textural features (vein dykes and brain rock) were analysed for this study. TMQ grains with the fewest secondary fluid inclusion trails and those that contained solid inclusions of magmatic minerals (clinopyroxene, hornblende, biotite, etc), were chosen preferentially to other grains, since the presence of magmatic inclusions is a distinguishing feature of TMQ.

Ninety-seven primary and pseudo-primary fluid inclusions in TMQ were analysed. Co-exiting Type 3 (a + b > c) and lesser abundant Type 2a fluid inclusions occur within TMQ (Table 5.3). Homogenisation temperatures for Type 3 fluid inclusions range from 350 to >600°C, although most of the fluid inclusions analysed homogenised between 450 and 600°C, with a mean of 540°C (Figure 5.5). Measured halite and sylvite dissolution temperatures range from 388 to >600°C and from 122 to 267°C respectively. These dissolution temperatures correlate to calculated salinities of between 50 and 75 wt% NaCl ± KCl eq., with a mode at 55 – 60 wt% NaCl ± KCl eq. (Figure 5.5). The halite and sylvite dissolution temperatures also correlate to an average, calculated NaCl:KCl:H_2O composition of 50:22:28 (Figure 5.6) and Na/Na + K ratio of 0.74. NaCl:KCl:H_2O compositions range between 42 – 62:14 – 32:22 – 36 and Na/Na + K between 0.63 and 0.84. Only homogenisation temperatures could be measured for Type 2 fluid inclusions in TMQ; they range from 300 to >550°C. Results are summarised in Table 5.3.

Fluid inclusions in TMQ from all four of the Endeavour deposits studied have similar homogenisation temperatures, although those from E26 show the broadest range (Figures 5.5d, e, f and g). TMQ from E26 also have the broadest range in calculated salinities. The highest calculated salinities occur in TMQ from E48.

5.3.2.2 Fluid inclusions in transitional hydrothermal quartz (THQ)

The comb-textured quartz of transitional hydrothermal quartz (THQ) comprises bands of euhedral, prismatic quartz crystals that grew on sub-planar substrates, where each crystal is oriented with its c-axes perpendicular to layering, and the spaces between each crystal is filled by igneous rock (aplite or porphyritic aplite).

Ninety-one primary and pseudo-secondary fluid inclusions have been analysed in THQ, mainly from E22 and E26. Co-existing Type 2 and 3 fluid inclusions are common in THQ. The Type 3 fluid inclusions in THQ typically contain higher vapour contents (20 – 50%) than in other quartz generations, and many contain haematite ± chalcopyrite daughter crystals. Type 3 inclusions in THQ homogenised either by halite dissolution or vapour disappearance at temperatures mainly between 350 and 550°C. Sylvite and halite dissolution temperatures range from 106 to 388°C and from 287 to 597°C respectively. These translate to calculated salinities of 45 – 70 wt% NaCl ± KCl eq., with a mode at 55 – 60 wt% NaCl ± KCl eq. (Figure 5.5). The average calculated NaCl:KCl:H_2O composition and Na/Na + K ratio of Type 3b and 3c fluid inclusions in THQ are 47:18:35 (Figure 5.6) and 0.76 respectively. NaCl:KCl:H_2O compositions range between 24 – 49:12 – 26:25 - 57 and Na/Na + K between 0.53 and 0.85. Type 3b and 3c fluid inclusions from THQ at E22 are generally more KCl-rich than those from E26 (Figure 5.6). Homogenisation of Type 2 fluid inclusions to the vapour phase in THQ occurred at temperatures from 400 to 480°C (Figure 5.5). No ice melting temperatures were measured for Type 2 fluid inclusions. Results are summarised in Table 5.3.

5.3.3 Fluid inclusions in main quartz (MQ)

Main stage quartz (MQ) occurs in 0.2 – 3cm wide, sheeted quartz veins that host most of the ore in the Endeavour systems. These veins contain coarse-grained (>200μm to ~5mm), grey and vitreous quartz crystals that are elongated perpendicular to the vein walls. Most of the veins also contain thin trails of sulphides, anhydrite and sericite parallel to the vein walls, which is interpreted to indicate repeated fracturing, fluid flow and mineral deposition through single veins (Heithersay, 1991; Wolfe, 1994; Harris, 1997). Quartz grains containing the most abundant fluid primary inclusions and the fewest secondary trails were selected for analysis.

Seventy-one primary and pseudo-secondary fluid inclusions were analysed in MQ. Co-existing Type 2 and 3 fluid inclusions are common in MQ. Type 2 fluid inclusions homogenised to the vapour phase at temperatures close to 450°C (Figure 5.5); no ice melting temperatures were measured for Type 2 fluid inclusions. The Type 3 inclusions in MQ contain similar vapour contents (20 – 50%) to those of THQ and many inclusions contain haematite ± chalcopyrite daughter crystals. Homogenisation in MQ Type 3 inclusions occurred chiefly by halite dissolution or vapour disappearance at temperatures between 450 and 550°C, with a mode from 450 – 500°C. Halite and sylvite dissolution temperatures range from 464 to 597°C and from 121 to 240°C respectively, which correlate to calculated salinities of between 45 and 70 wt% NaCl ± KCl eq., average salinity of 57 wt% NaCl ± KCl eq. (Figure 5.5). Based on the dissolution temperatures of sylvite and halite, NaCl:KCl:H_2O compositions between 46 – 65:14 – 19:20 – 36 (average 56:16:28) have been calculated (Figure 5.6). Calculated Na/Na + K ratios vary from 0.76 to 0.84 (average 0.81). Results are summarised in Table 5.3.

Calculated salinities and homogenisation temperatures for MQ from all four deposits are similar, however, those from E22 show a wider range than the other deposits (Figures 5.5d, e, f and g).

5.3.4 Fluid inclusions in late quartz (LQ)

Late stage quartz (LQ) from L1 veins in the Endeavour deposits consist mainly of quartz, anhydrite, carbonate and chalcopyrite, pyrite and rare chalcopyrite. Quartz within these veins is generally coarse-grained (>200μm), euhedral and is crosscut by fewer secondary trails than in the other stages.

Forty-five primary and pseudo-secondary fluid inclusions were analysed in LQ grains. Types 3a, 1a/b and lesser abundant Type 2a fluid inclusions are typical of LQ. Type 1 and Type 2 fluid inclusions homogenised to liquid and vapour respectively at temperatures from 350 to 400°C (Figure 5.5). Type 1 fluid inclusions have ice-melting temperatures from -12 to -24°C, corresponding to calculated salinities from 20 to 25% wt% NaCl eq. (Figure 5.5). Homogenisation temperatures similar to those for Type 1 and 2 fluid inclusions have been measured for Type 3 fluid inclusions in LQ (Figure 5.5). The latter typically homogenised by halite dissolution and have calculated salinities from 35 to 55 wt% NaCl ± KCl eq., mostly between 40 and 45 wt% NaCl eq. (Figure 5.5). Only a few Type 3b and 3c inclusions from LQ were analysed due to their rare occurrence. Two from E48 have an average NaCl:KCl:H_2O composition of ~42:34:24 and Na/Na + K ratio of 0.61 (Figure 5.6). Results are summarised in Table 5.3.

LQ fluid inclusions have similar homogenisation temperatures for E26, E27 and E48, although those for E48 have the widest range (Figures 5.8e, f and g respectively). LQ from E48 also show the widest range in calculated salinities.

5.4 PIXE results

Proton-induced X-ray emission (PIXE) analysis was conducted on three fluid inclusions in TMQ from a vein dyke sample from E48. The fluid inclusions are hosted in subhedral quartz grains within the aplitic material of the vein dyke (Figure 5.7). Two of the three fluid inclusions analysed are interpreted to be primary TMQ generation inclusions (E48_5_1a and 3a), while the third, E48_5_2b, is interpreted to be a post-TMQ secondary fluid inclusion. PIXE-determined fluid inclusion compositions are presented in Table 5.4. Element distributions within the individual fluid inclusions are displayed in Figures 5.8 and 5.9, and the PIXE spectra are presented in Figure 5.10.

The PIXE analyses have shown that the two primary fluid inclusions (1a and 3a) comprise predominantly K, Cl (several weight percent each) and Na (based on the presence of halite daughter crystals since PIXE cannot detect Na). Fluid inclusion 3a contains >4 wt% Ca. In addition to Na, K, Cl ± Ca, these two primary TMQ fluid inclusions contain 100's to 1 000's of ppm Ti, Mn, Fe, Cu and Zn. Fluid inclusion 1a contains >500ppm Rb and S as well as higher concentrations of Al and Ba than the host (Figure 5.8); these elements reside primarily in daughter minerals at 25°C.

The post-TMQ fluid inclusion (2a) comprises mainly Cl, (>5wt%; Table 5.4). Ca and Ti concentrations in fluid inclusion 2a are similar to those in fluid inclusion 1a. Significantly lower concentrations of Fe (by more than an order of magnitude), Cu, Mn and Zn are noted for fluid inclusion 2a. The Pb concentration is the highest of all three fluid inclusions in the post-TMQ inclusion 2a. Br concentrations are low (~25 – 60ppm) for all three fluid inclusions analysed.

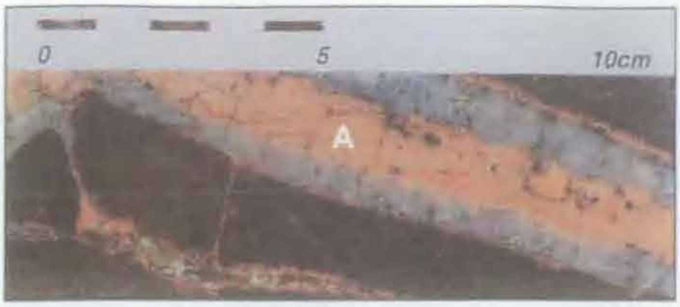

Figure 5.7 A photograph of the vein dyke sample from E48 (R48/15/449.0m) that was thick-sectioned for PIXE analysis of fluid inclusions. TMQ grains containing fluid inclusions were taken from an area similar to that marked A on the figure.

Table 5.4 **A** Microthermometric data for PIXE-analysed fluid inclusions. Salinity is a calculated estimate using Equation 5.1 and 5.2, and SALTY for fliud inclusions 1a, 2b and 3a respectively. Density is calculated using the method outlined in Roedder and Bodnar (1980) and data of Skinner (1966) and Haas (1976). **B** Fluid inclusion compositions as determined by PIXE analysis. ND reflects not determined. Note that Cl concentrations are most likely low due to attenuation of the Cl signal with depth as the beam passes through the host quartz grain.

A

F.I. Name	*Tm_{ice}*	*Th V*	*Tm H*	*Tm S*	*Th F*	*wt% NaCl*	*wt% KCl*	*Salinity*	*Density*	*Comments*
E48/5/1a	-2.5	>200.1	-	-	>200.1	4.2	-	4.2	-	Decrepitated before homogenisation
E48/5/2b	-0.1	125.6	-	-	125.6	0.2	-	0.2	-	Late-stage secondary inclusion
E48/5/3a	-	340.6	490.2	198.0	490.2	48.3	20.3	68.6	1.38 or 1.21*	Halite + sylvite + other

*1.38 - density calculated using the NaCl eq. salinity as 68.6 (including sylvite)

1.21 - density calculated using the final homogenisation temperature of halite only

B

F.I. Name	*E48-5-1a*	*E48-5-2b*	*E48-5-3a*
Element	*conc. (ppm)*	*conc. (ppm)*	*conc. (ppm)*
Cl	35731	56909	ND
K	257000	1649.3	85698
Ca	1822.6	1890.9	44656
Ti	2266.6	2346.8	3929.6
Mn	566.5	209.77	7550.7
Fe	22612	907.88	23172
Cu	2090.3	1365.6	654.06
Zn	210.54	80.73	897.56
As	105.9	4.91	ND
Br	23.65	46.09	60.1
Rb	526.33	38.41	114.49
Sr	701.89	254.19	170.33
Pb	73.63	210.59	437.31

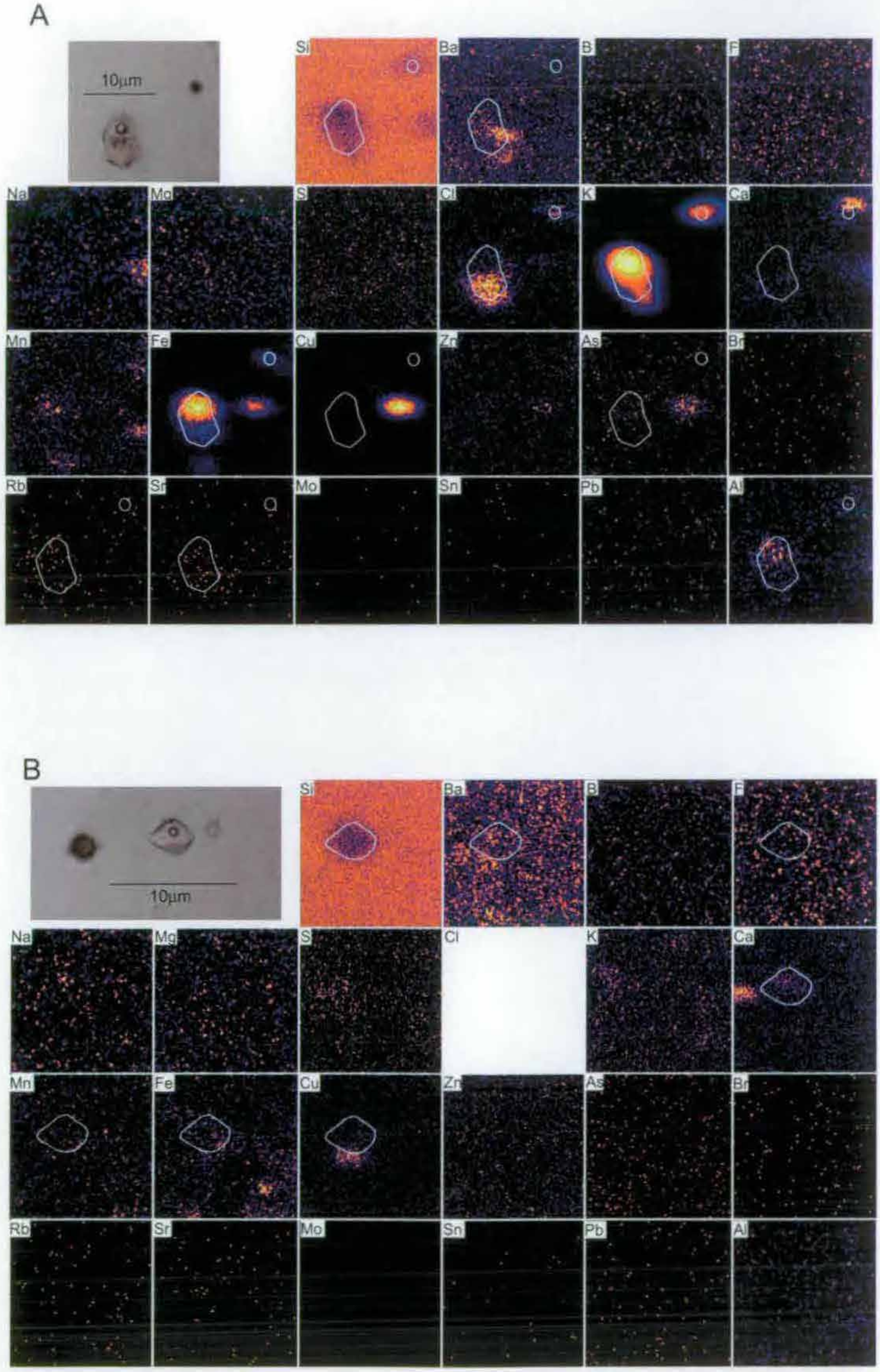

Figure 5.8 Photographs showing the distribution of elements (PIXE) in fluid inclusion **A** E48_5_1a and **B** E48_5_2b.

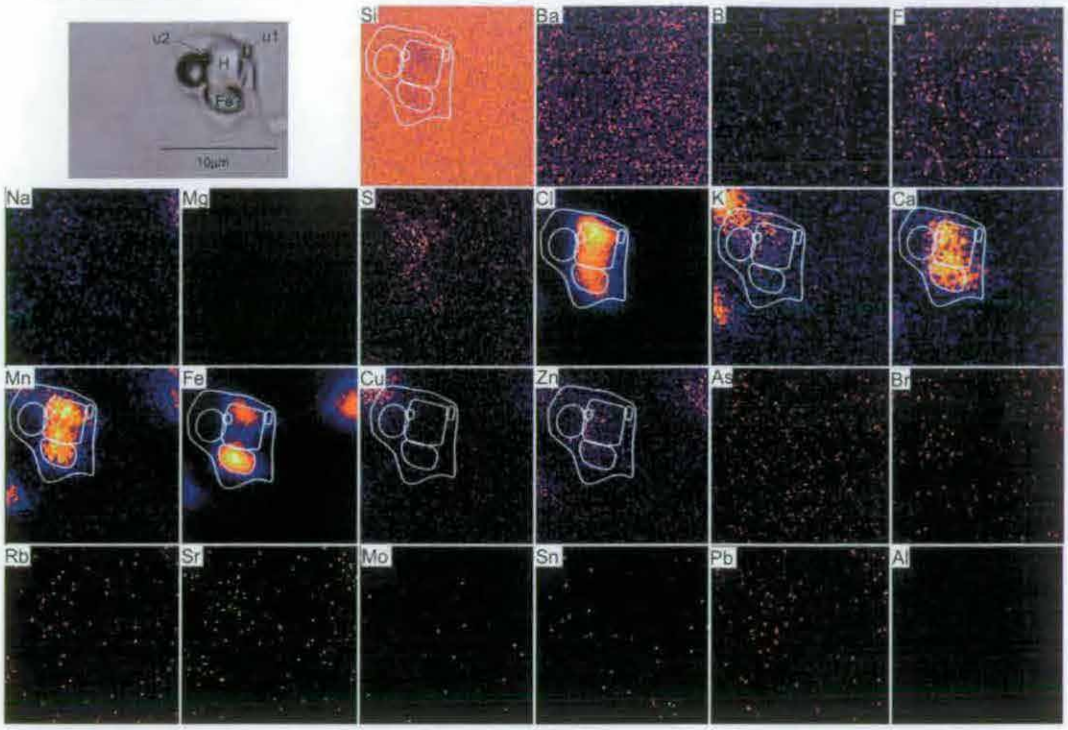

Figure 5.9 Photographs showing the distribution of elements (PIXE) in fluid inclusion E48_5_3a. The fluid inclusion contains liquid, vapour (V), halite (H), Fe-Mn-K-chloride? (Fe?) and two unknown minerals (u1 and u2).

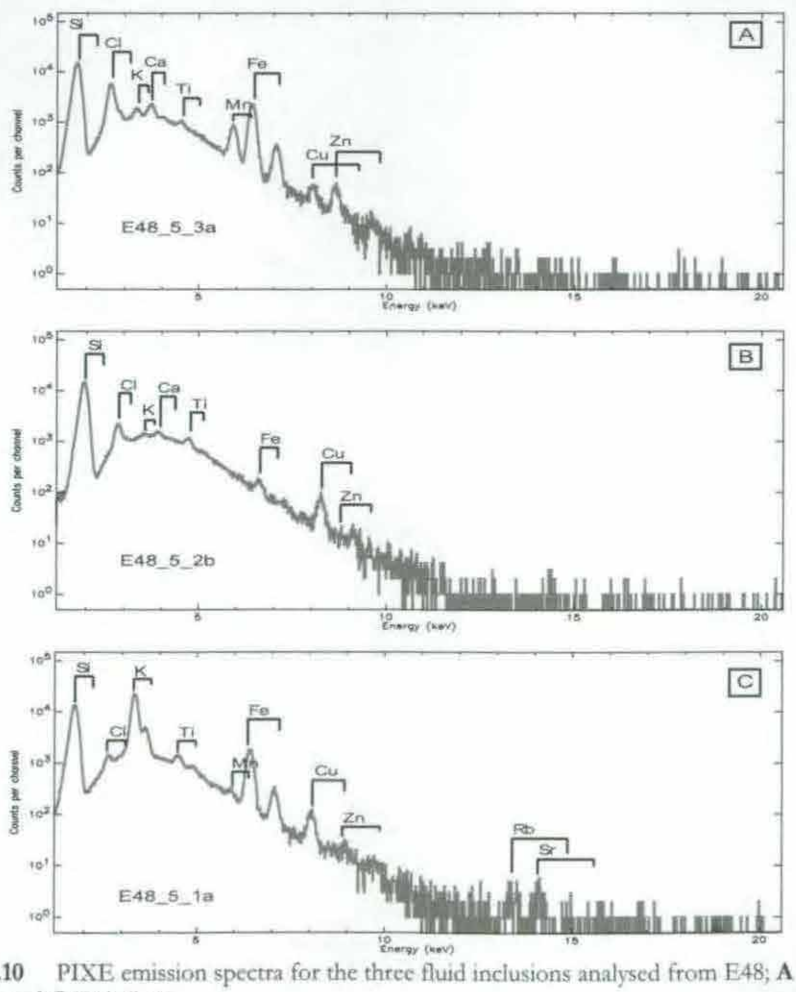

Figure 5.10 PIXE emission spectra for the three fluid inclusions analysed from E48; **A** E48_5_3a, **B** E48_5_2b and **C** E48_5_1a.

5.5 Decrepitation results

After the completion of microthermometric analyses, several fluid inclusions were decrepitated in order to ascertain the ratios of selected cations, anions and metals in the salt residues (decrepitates) by electron microprobe analysis (Appendix B2). The diameter of the electron beam was too large for only the salts to be analysed and as a result, between 80 and 95% quartz was included in the probe analyses (Figure 5.11). It was therefore not possible to determine the actual salt concentrations from the fluid inclusion decrepitates. Consequently, relative abundances, expressed as element ratios, are discussed below. It was also not possible to determine which species, if any, volatilised during the decrepitation process, or during the time between decrepitation and microprobe analysis.

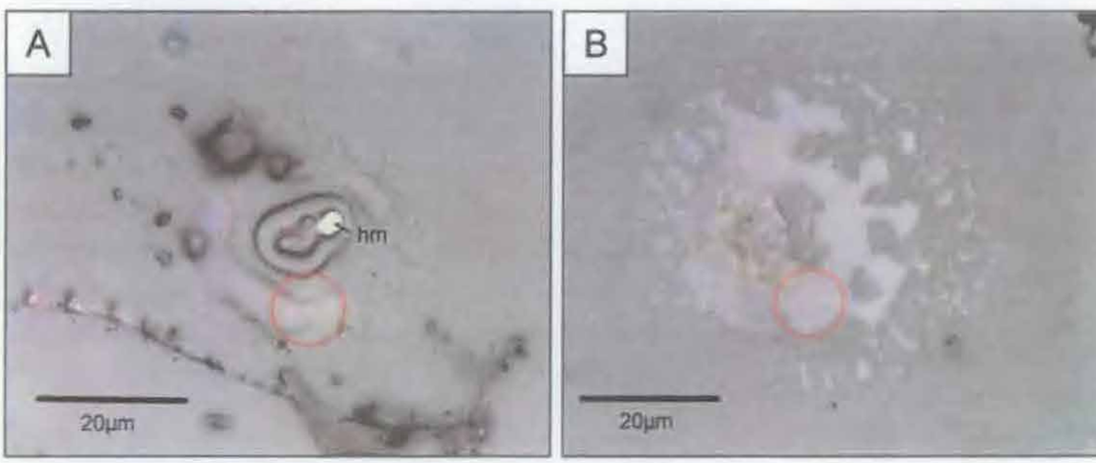

Figure 5.11 **A** and **B** Salt residue of decrepitated fluid inclusions showing the probe analysis spot (red circle); hm – haematite.

A series of element ratio plots have been generated for the 44 residual salt decrepitates analysed from the different generations of quartz (Table 5.5; Figure 5.12). Fe/Na and Mn/Na, and to a lesser extent, Al/Na and Mg/Na in TMQ decrease relative to EQ. These ratios increase significantly in THQ and MQ, before diminishing to similar values as EQ in LQ (Figures 5.12a). MQ generally has higher cation ratios than other quartz generations. Al/Na is relatively high in LQ compared to others quartz generations. Concomitant changes in the Ca/Na and K/Na ratios accompany the changes in the Fe/Na, Mn/Na, Al/Na and Mg/Na ratios in LQ. With the exception of EQ, both Ca/Na and K/Na increase with time from THQ, so that these ratios attain their highest values in LQ.

S/Cl and F/Cl increase sharply from EQ to TMQ and THQ before decreasing markedly in MQ (Figures 5.12b). There is an overall increase in these ratios in LQ. EQ has significantly lower anion:Cl ratios than other quartz generations, whereas THQ,

Table 5.5 Minimum, maximum and average cation, anion and metal and cation to anion ratios calculated for 48 decrepitated fluid inclusions (based on electron microprobe data).

Stage	EQ: 1 sample, 2 analyses			TMQ: 4 samples, 10 analyses			THQ: 3 samples, 24 analyses			MQ: 3 samples, 5 analyses			LQ: 2 samples, 3 analyses		
Ratio	*Minimum*	*Maximum*	*Average*	*Minimum*	*Maximum*	*Average*	*Minimum*	*Maximum*	*Average*	*Minimum*	*Maximum*	*Average*	*Minimum*	*Maximum*	*Average*
Ca/Na	0.3	0.4	0.4	0.2	1.7	1.0	0.3	18.1	4.0	1.6	15.4	4.1	1.6	12.9	6.4
K/Na	1.5	1.9	1.7	0.4	2.2	1.4	0.2	8.5	1.7	0.5	7.1	1.8	0.5	8.0	3.4
Mn/Na	2.9	3.3	3.1	0.0	2.8	0.6	0.1	111.5	14.8	1.7	84.3	27.8	1.7	2.5	2.1
Mg/Na	0.1	0.1	0.1	0.0	0.3	0.1	0.0	2.6	0.5	0.0	3.5	1.5	0.0	0.5	0.3
Al/Na	3.0	3.1	3.0	0.0	4.4	0.7	0.1	19.9	2.5	0.5	12.8	4.4	0.5	60.9	22.2
Fe/Na	11.7	13.2	12.5	1.3	9.3	2.9	6.1	129.1	34.2	10.4	220.9	99.6	10.4	28.7	20.3
S/Cl	6.3	6.9	6.6	0.0	287.0	60.0	0.0	466.0	67.8	0.0	1.5	0.8	0.0	4.4	2.0
F/Cl	0.0	0.0	0.0	0.0	5.0	1.5	0.0	331.0	17.9	0.0	0.4	0.1	0.0	0.2	0.1
Cu/Cl	11.5	13.1	12.3	2.3	16695.0	3228.1	0.7	262.0	69.2	0.5	2.4	1.4	1.6	2.6	2.1
Fe/Cl	98.8	102.1	100.4	3.4	24770.0	3916.4	38.5	48007.0	8129.7	8.8	346.9	112.0	1.0	105.6	48.9
Cu/S	1.8	1.9	1.9	12.5	2120.0	484.0	0.1	1932.0	325.6	1.4	12.7	5.2	0.4	1.8	1.1
Fe/S	14.8	15.6	15.2	10.1	11623.0	3199.3	12.1	80931.0	13492.1	6.8	724.8	282.7	23.7	249.0	99.8
Fe/Cu	7.8	8.6	8.2	0.6	14.2	4.0	6.1	458.1	90.3	17.2	272.1	115.5	15.2	67.2	41.2

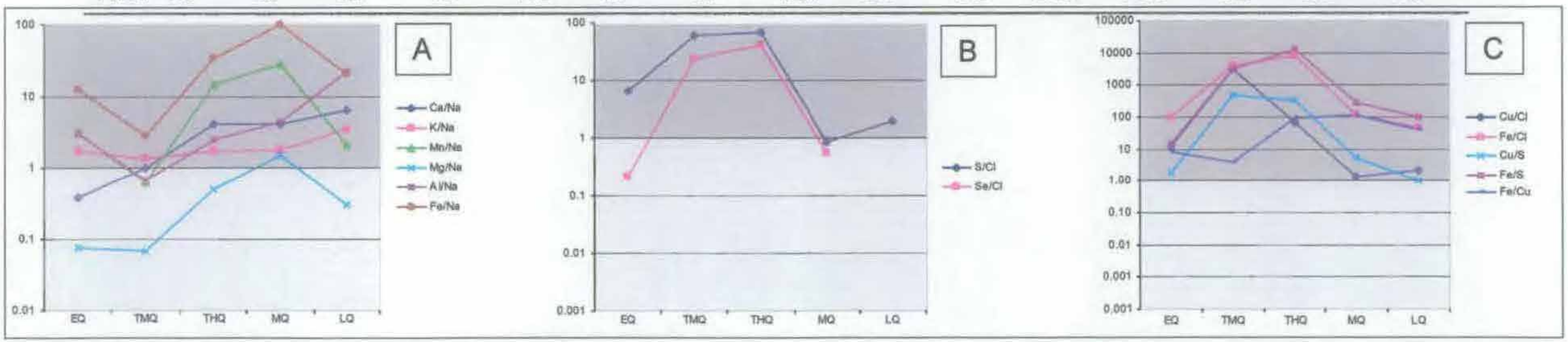

Figure 5.12 A Plots of various **A** cation ratios, **B** anion ratios and **C** metals and cation to anion for EQ, TMQ, THQ, MQ and LQ. Dark shaded areas indicate enrichment, pale shaded areas indicate depletion.

and to a lesser extent, TMQ, have high anion:Cl ratios. The F/Cl ratio decreases sharply in MQ and LQ compared to THQ, although it is still higher in MQ than in EQ. The changing F/Cl ratio of the fluid from THQ to MQ is reflected in the compositions of certain minerals associated with MQ and is discussed in detail in Chapter 7.

Metal and cation to anion ratios are ubiquitously higher in TMQ and THQ compared to EQ, MQ and LQ (Figures 5.12c). Cu/Cl, Fe/Cl, Cu/S, Fe/S and Fe/F ratios attain their lowest values in LQ. The Fe/Cu ratio is variable for the different quartz generations. Note, however, that this ratio is similar for THQ and MQ, and that these similar ratios are significantly higher than the Fe/Cu ratios in TMQ and EQ.

The ratio plots on Figure 5.12, however, infer for example, that Cu, Fe and S are more concentrated than Cl in the fluids. These inferences are considered unlikely given the fluid inclusion PIXE data (Table 5.4). It is thus considered here, that partial volatilisation of Cl (and possibly other elements such as Na and S) occurred during the experiments and that this partial volatilisation possibly accounts for the errors. However, it is also likely that the errors would be a factor in all of the analyses. In addition, comparable results are obtained if non-volatile element ratios are used for actual data rather than the average values used for the ratio plots (Table 5.6). For example, on a plot of K/Cu vs Cu/Ca (Figure 5.13a), a relative decrease in the Cu content of THQ, MQ and LQ fluids is implied from the overall negative correlation of ratios when these are compared to EQ and TMQ fluids. Similarly, when data points are plotted on a graph of Fe/Cu vs Cu/Ca (Figure 5.13b), an overall increase in the Ca content of THQ, MQ and LQ fluids relative to the EQ and TMQ fluids can be inferred. Thus, even with probable volatilisation, several trends in the data are consistent through the analyses of residual salts from the various generations of quartz, and are thought to be a reflection of changes in fluid compositions with time.

Notwithstanding likely volatilisation, the decrepitation results are interpreted to infer that Fe, Mn, Al and Mg concentrations, initially variable in EQ, decrease in TMQ before increasing in THQ and MQ. An overall increase with time, from EQ to LQ, in the relative abundances of Ca and K is also inferred. Changes in anion ratios are thought to indicate that S and F abundances decrease from TMQ and THQ to MQ. Since it is inferred that S decreased substantially in MQ, the decrease in Cu/S in MQ and LQ compared to TMQ and THQ, is thought to infer a sharp decrease in the relative Cu abundance in MQ. This decrease in Cu from TMQ to MQ is also indicated by the relative increase in Fe/Cu from TMQ to MQ.

Table 5.6 Non-volatile element ratios for fluid inclusion decrepitation analyses.

Stage	*No*	*Fe/Ca*	*Cu/Ca*	*Fe/Cu*	*Al/Fe*	*K/Cu*
EQ	139	32.14	3.74	8.59	0.22	1.23
EQ	140	34.97	4.49	7.80	0.26	1.03
TMQ	28	1.13			0.25	
TMQ	31	2.18	0.40	5.48	0.03	2.23
TMQ	33	1.96	1.09	1.80	0.05	0.44
TMQ	131	2.62	2.51	1.04	0.05	0.65
TMQ	132	7.04	4.75	1.48	0.03	0.35
TMQ	134	2.68	1.90	1.41	0.04	1.03
TMQ	40	2.71	0.93	2.92	2.63	1.98
TMQ	41	1.28	2.00	0.64	0.61	0.41
TMQ	129	8.01	1.07	7.46	0.02	4.27
TMQ	130	3.38	0.24	14.15	0.02	9.31
THQ	48	14.12	0.08	181.31	0.04	4.09
THQ	57	6.23	0.43	14.54	0.01	1.35
THQ	58	11.60	0.37	30.96	0.02	0.92
THQ	60	12.03	0.31	38.91	0.08	3.44
THQ	61	4.59	0.02	238.79	0.02	7.55
THQ	49	19.33	0.28	70.21	0.02	1.22
THQ	50	7.70	0.52	14.70	0.14	0.92
THQ	51	3.48	0.57	6.13	0.11	0.22
THQ	123	2.84	0.06	47.34	0.04	1.37
THQ	124	8.26			0.05	
THQ	126	6.58			2.44	
THQ	127	19.96	1.42	14.06	0.03	0.75
THQ	115	16.69			0.05	
THQ	120	5.09	0.04	128.71	0.61	75.63
THQ	121	16.80			0.00	
THQ	122	3.98			0.03	
THQ	66	42.72			0.11	
THQ	67	1.48			0.12	
THQ	100	12.85	0.27	47.97	0.01	0.41
THQ	112	12.06	1.82	6.61	0.02	0.07
THQ	113	6.73			0.10	
THQ	101	67.07	1.19	56.22	0.02	0.24
THQ	104	8.93	0.02	458.11	0.14	45.18
THQ	105	13.37			0.03	
MQ	34	6.38			0.40	
MQ	98	14.33	0.05	272.13	0.02	0.34
MQ	76	15.98	0.93	17.23	0.71	0.80
MQ	75	15.29	0.05	283.84	0.01	1.02
MQ	86	78.69			0.01	
LQ	18	2.22	0.03	67.19	0.18	1.19
LQ	22	2.20			5.87	
LQ	92	3.25	0.05	71.90	0.03	2.05
LQ	10	13.55	0.89	15.15	0.02	1.30

THQ and MQ display similar patterns for all ratios plotted on Figures 5.12. This is interpreted to indicate that, despite the lower relative abundance of Cu in MQ and higher relative Fe abundance in THQ, these two fluids are similar. Homogenisation temperatures for the two fluids are broadly comparable, however, THQ fluid inclusions typically homogenise at temperatures ~50°C higher than MQ fluid inclusions. Calculated salinities of the two fluids are similar with an average of ~55 wt% NaCl eq. The relatively lower abundance of Cu in MQ, and relatively higher abundance of Fe in THQ possibly indicate a decrease in the Cu abundance in MQ compared to THQ.

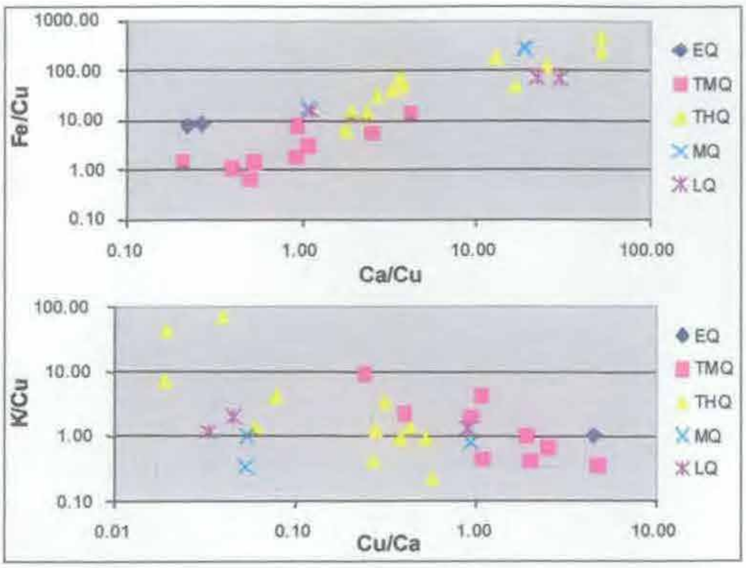

Figure 5.13 Plots of non-volatile element ratios for fluid inclusion decrepitation analyses.

5.6 Pressure-depth estimates

In fluid inclusions where the homogenisation temperatures of halite (T_hH) and vapour (T_hV) are the same, the solution can be assumed to on the liquid-vapour-solid phase boundary, allowing a pressure to be obtained from Haas's (1976) data (Roedder and Bodnar, 1980) and Bodnar *et al.*'s (1985) H_2O-NaCl projection. No identical T_hH and T_hV values were obtained, but values within 15°C were recorded for 10 Type 3a fluid inclusions from TMQ, THQ, MQ and LQ (Table 5.7), yielding the following minimum pressure estimates: 1) 1 TMQ ~290bar; 2) 3 THQ 260 to 370bar, 3) 2 MQ 315 – 325bar and 4) 4 LQ 130 – 160bar (Figure 5.14a). Three Type 3a fluid inclusions in EQ and two in MQ dissolved halite between 590 and 600°C, even though vapour was still present at 600°C. This is interpreted to imply that minimum trapping pressures for EQ and MQ were greater than ~400 bar, using Bodnar *et al.*'s (1985) H_2O-NaCl projection diagram (Figure 5.14a; I and II).

Assuming lithostatic pressure and an estimated rock density of 2.7g/cm^3, calculated depths range from ~1000 to 1400m for EQ, TMQ, THQ and MQ. Assuming hydrostatic pressure, depths for EQ, TMQ, THQ and MQ yield depths from ~2900 to 3800m. For LQ, lithostatic pressures yield significantly shallower (550 – 650m) depth estimates for the group of 4 fluid inclusions that yielded estimated pressures of 130 – 160bar. Assuming hydrostatic pressure for this group yields depth estimates from ~1350 to 1600m for LQ. These latter depth estimates are close to the lithostatic pressure depth estimates for EQ, TMQ, THQ and MQ.

Equal vapour homogenisation temperatures (T_hV) of co-existing Type 1 and Type 2 inclusions can also be used to estimate minimum pressures using a portion of the H_2O phase diagram with 10 and 25 wt% NaCl eq. solution liquid-vapour curves (Roedder and Bodnar, 1980). Using this method, four fluid inclusion pairs from THQ, MQ and LQ yield minimum trapping pressures of 285 (1 pair), 445 (1 pair) and 190 to 245 (2 pairs) bar respectively (Table 5.8; Figure 5.14b). Assuming lithostatic pressure, these pressures yield estimated depths of ~1100 to 1700m for THQ and MQ and ~750 – 800m for LQ. If hydrostatic conditions are assumed for LQ, estimated depths are from ~2000 – 2100m. These hydrostatic pressure depth estimates are similar to lithostatic pressure depth estimates for THQ and MQ. Suitable inclusion pairs for this method were not observed in EQ and TMQ.

Table 5.7 Pressure and depth estimates from Type 3a fluid inclusions from EQ, TMQ, THQ, MQ and LQ (Roedder and Bodnar, 1980; Bodnar *et al.*, 1985). T_hV and T_hH – homogenisation temperature of vapour and halite respectively, ΔT_h – difference between T_hV and T_hH; av. T – average temperature used in pressure estimate; Est. D_{lith} and D_{hyd} – estimated depths using lithostatic and hydrostatic pressure respectively.

Sample	*Stage*	*ThV (°C)*	*ThH (°C)*	*ΔTh*	*av. T (°C)*	*Est. P (bar)*	*Est. D_{lith} (m)*	*Est. D_{hyd} (m)*
E22/25	EQ/MQ	>600	590-599	~10		~400	min. 1633	min. 4082
E26/74	TMQ	469.8	466.5	3.3	468.2	287.1	1085	2930
E22/6	THQ	525.5	540.1	14.6	532.8	370.0	1398	3776
E22/6	THQ	529.1	532.2	3.1	530.7	365.0	1379	3724
E22/6	THQ	447.4	446.1	1.3	446.8	258.5	977	2638
E27/90	MQ	495.8	480.5	15.3	488.2	315.4	1192	3218
E26/80	MQ	493.9	508.3	14.4	501.1	326.2	1233	3329
E27/90	LQ	365.1	377.0	11.9	371.1	141.5	535	1444
E27/90	LQ	351.2	364.9	13.7	358.1	131.3	496	1340
E27/90	LQ	380.4	383.4	3.0	381.9	157.4	595	1606
E27/90	LQ	389.1	374.2	14.9	381.7	157.2	594	1604

Table 5.8 Pressure and depth estimates from co-existing Type 1 – Type 2 fluid inclusion pairs with similar T_hF values from THQ, MQ and LQ (Roedder and Bodnar, 1980). Est D_{lith} and D_{hyd} – estimated depths using lithostatic and hydrostatic pressure respectively.

Sample	*Stage*	*Type*	*T_h (°C)*	*Salinity*	*Est. P (bar)*	*Est. D_{lith} (m)*	*Est. D_{hyd} (m)*
E22/8	THQ	2aV	399.3	ND			
E22/8	THQ	1aL	417.7	21.5	283	1070	2888
E26/72	MQ	2aV	480.7	ND			
E26/72	MQ	1aL	485.2	22.7	444	1678	4531
E48/25	LQ	2aV	387.9	ND			
E48/25	LQ	1aL	378.2	20.2	195	737	1990
E48/27	LQ	2aV	388.2	ND			
E48/27	LQ	1aL	380.3	17.8	205	775	2092

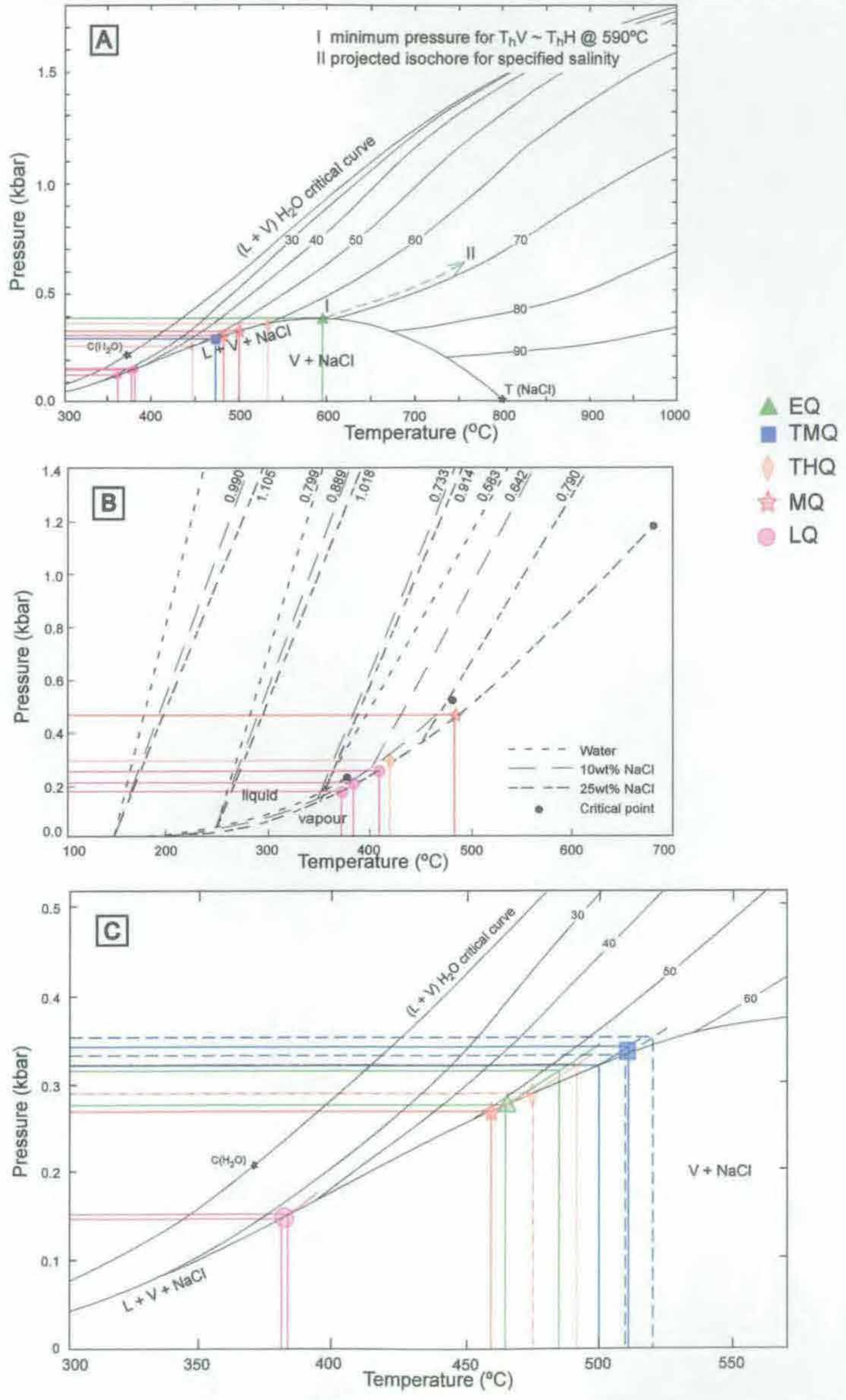

Figure 5.13 Pressure estimates based on **A** equal ThV and ThH in Type 3a inclusions using Bodnar *et al.*'s (1985) NaCl-H_2O projection; **B** equal ThV for Type 1 and Type 2 fluid inclusions using a variety of solution liquid-vapour curves (Roedder and Bodnar, 1980); and **C** similar ThF for co-existing Type 2 and Type 3a fluid inclusions using Bodnar *et al.*'s (1985) NaCl-H_2O projection.

The two methods outlined above could only be applied to fourteen fluid inclusions or fluid inclusion pairs, because it is much more common in porphyry environments for hypersaline inclusions to homogenise by halite disappearance than by vapour disappearance. Applying extrapolated vapour – liquid fields for various salinity fluids (Bodnar *et al.*, 1985) to co-existing Type 3 – Type 2 fluid inclusions pairs that homogenised at similar temperatures (within ~15°C) by halite and bubble disappearance respectively also yields estimated pressures (Table 5.9).

Table 5.9 Pressure and depth estimates from co-existing Type 2 – Type 3aH (homogenisation by halite dissolution) fluid inclusion pairs with similar T_hF values (T_hV_{2a} and T_hH_{3a}) from EQ, TMQ, THQ, MQ and LQ (Bodnar *et al.*, 1985). Est D_{lith} and Est D_{hyd} – depth estimates using lithostatic and hydrostatic pressure respectively.

Sample	*Stage*	T_hV_{2a} (°C)	T_hH_{3a} (°C)	ΔTh	*Salinity*	*Est. P (bar)*	*Est.* D_{lith} *(m)*	*Est.* D_{hyd} *(m)*
E27/87	EQ	489.4	463.2	-26.2	52.3	280 - 330	1058 - 1247	2857 - 3367
E27/87	TMQ	519.7	508.7	-11.0	57.7	335 - 355	1266 - 1341	3418 - 3622
VL S24	TMQ	500.0	511.9	11.9	57.7	320 - 345	1209 - 1303	3265 - 3520
E22/8	THQ	481.6	472.8	-8.8	53.3	290 - 320	1096 - 1209	2959 - 3265
E48/12	MQ	461.0	472.5	11.5	53.3	270 - 290	1020 - 1096	2755 - 2959
E27/90	LQ	380.0	384.1	4.1	44.6	145 - 155	547 - 586	1480 - 1582

This method was applied to six such pairs from all five quartz generations and the estimated pressures are 280 – 330bar for EQ (1 pair); 320 – 355bar for TMQ (2 pairs); 290 – 310bar for THQ (1 pair); 260-290bar for MQ (1 pair) and 145 – 155bar for LQ (1 pair). Assuming lithostatic pressures, these pressure estimates correlate with depths from ~1060 – 1250m for EQ, ~1200 – 1350m for TMQ, ~1100 – 1300m for THQ and 1020 to 1100m for MQ (Figure 5.14c). These depth estimates compare well with those estimated by the other methods above. For LQ, similar depths are estimated using hydrostatic pressure; 1480 – 1580m.

In summary, fluid inclusion data from E22, E26, E27 and E48 have been used to estimate pressures of entrapment of ~300 – 450bar for EQ, TMQ, THQ and MQ and ~150 – 200bar for LQ fluids. These pressures yield depths estimates from ~1000 to ~1700m using lithostatic pressure for EQ, TMQ, THQ and MQ. Similar depth estimates are obtained for LQ using hydrostatic pressure. It is thus likely that a transition from lithostatic to hydrostatic pressure occurred synchronous with the change from MQ to LQ.

5.7 Discussion

5.7.1 Comparison with previous studies of the Endeavour deposits

The microthermometric data obtained from this study are broadly consistent with those of obtained for E26 by Heithersay and Walshe (1995) and Harris (1997). Homogenisation temperatures recorded for EQ in this study are similar to Harris's (1997) Stage IIB veins from E26 (370 – 490°C, mode ~470°C) and Heithersay and Walshe's (1995) Stage 3 veins (T_hF 410 to 720°C). Calculated salinities for EQ in this study are 10 – 15 wt% NaCl ± KCl eq. lower than those estimated by Heithersay and Walshe (1995); 75 – 80 wt% NaCl ± KCl eq. Heithersay and Walshe (1995) make no distinction between magmatic and hydrothermal quartz in their vein stages 4 and 6 (TMQ equivalents), however, the high homogenisation temperatures (up to 760°C) and common presence of magmatic textures such as graphic intergrowths of K-feldspar and quartz, are thought to justify this interpretation. Halite melting temperatures for fluid inclusions in TMQ of this study (190 to 595°C, mode 550 to 600°C) are comparable with Heithersay and Walshe's (1995) results (410 to 670°C, mode 580°C). Sylvite dissolution temperatures in Type 3b and 3c inclusions in the current study range from 120 to 390°C (mean 233°C), while those of Fe-Mn-K chlorides range from 230 to 590°C (mean 463°C). The sylvite dissolution temperatures are 100 to 200°C lower than the range of 350 to 590°C reported by Heithersay and Walshe (1995). Their data are more consistent with measured dissolution temperatures of Fe-Mn-K chlorides from this study (Appendix D1). Because of this discrepancy in sylvite dissolution temperatures, the calculated average NaCl:KCl:H_2O composition of TMQ of this study is 50:22:28, compared to 55:32:13 from Heithersay and Walshe's (1995) study (Figure 5.15; grey area ii). It may be that Heithersay and Walshe (1995) misidentified sylvite for Fe-Mn-Cl daughter salts. This would account for the discrepancies in sylvite dissolution temperatures and average NaCl:KCl:H_2O composition.

Type 3 fluid inclusions with haematite ± chalcopyrite ± anhydrite are abundant in Harris's (1997) main stage quartz veins and these have homogenisation temperatures of 450 to 560°C (mode 520 – 560°C), which are similar to the results of this study. Heithersay and Walshe (1995) show similar homogenisation temperatures for their main stage fluid inclusions; 460 – 560°C. These authors have calculated salinities for main stage fluids from 40 – 55 wt% NaCl eq. The decrease in salinity for MQ, as recorded by Heithersay and Walshe (1995), was not found to be as large in the current study. Instead, a change in the NaCl:KCl:H_2O ratios was detected.

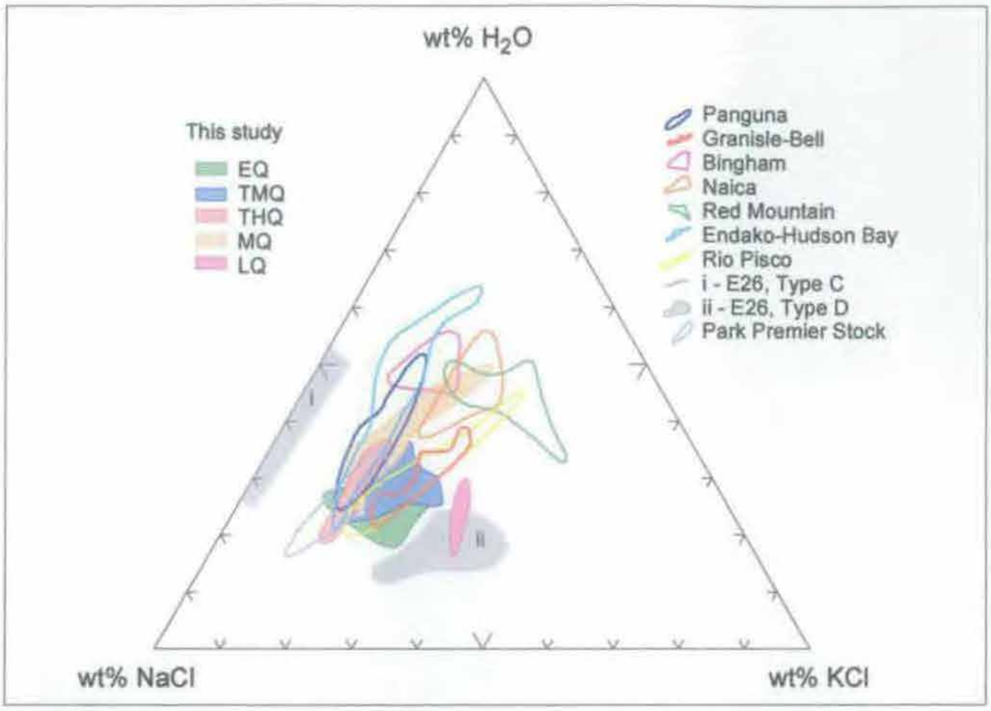

Figure 5.15 A ternary diagram of fluid inclusion NaCl:H_2O:KCl compositions from this study compared to 1) results from Heithersay and Walshe (1995) – grey areas i and ii, and 2) other porphyry Cu-Au deposits (modified after Roedder, 1984).

Fluid inclusions in Heithersay and Walshe's (1995) late stage veins homogenise mainly by halite dissolution at temperatures from 310 to 490°C and have calculated salinities from ~45 to 60 wt% NaCl eq. Homogenisation temperatures in this study are similar to those of Heithersay and Walshe (1995), whereas salinities are lower. The discrepancies between calculated salinities of this study and those of Heithersay and Walshe (1995) for all quartz generations are thought to be related to the different sylvite dissolution temperatures recorded for the two studies. Harris's (1997) late stage fluid inclusions have lower homogenisation temperatures than the current study; 240 – 320°C. The disparity between Harris's (1997) late stage fluid inclusions and those from LQ of this study may indicate that Harris (1997) sampled a lower temperature portion of late stage mineralisation and alteration than the current study, possibly Late Stage L3 veins.

With the exception of the EQ and TMQ fluids of E22 being slightly more KCl-rich, the fluids represented by the different generations of quartz studied, are broadly similar for all four of the Endeavour deposits.

5.7.2 *Comparison with other porphyry deposits*

Early veins in porphyry environments typically contain abundant co-existing vapour-rich (Type 2) and hypersaline (Type 3) fluid inclusions (Gustafson and Hunt, 1975; Henley and McNabb, 1978; Reynolds and Beane, 1985; Hedenquist *et al.*, 1998; Selby *et al.*, 2000). Co-existing Type 2 and Type 3 inclusions occur in EQ at all four Endeavour deposits; they also occur in TMQ, THQ and MQ. Type 1b inclusions containing chalcopyrite daughter crystals that homogenise at similar temperatures to primary Type 3 inclusions are also present in the Endeavour deposits; another common feature of early veins in porphyry environments (Bodnar, 1995). EQ and TMQ fluid inclusions are typically more KCl-rich than later fluid inclusions, except LQ, and have compositions similar to fluid inclusions from Rio Pisco and Granisle-Bell porphyry deposits (Figure 5.15). Hypersaline fluid inclusions that contain haematite ± chalcopyrite ± other daughter crystals are typical most porphyry deposits; in the Endeavour deposits they characterise the fluid inclusions in THQ and MQ. THQ and MQ fluid inclusions are typically more dilute than TMQ and EQ fluid inclusions and less KCl-rich than LQ fluid inclusions. The NaCl:H_2O:KCl compositions to THQ and MQ fluid inclusions are similar to those of many other porphyry deposits. The KCl-rich LQ fluid inclusions in the Endeavour deposits are more KCl-rich than fluid inclusions from many other porphyry deposits (Figure 5.15). This aspect is discussed below.

Fluid inclusion studies on the Endeavour systems have highlighted the presence of several fluid phases and the metal-carrying capacity of high temperature magmatic – hydrothermal brines. This is consistent with the results of fluid inclusion studies on many other porphyry deposits, e.g. Eastoe (1982), Reynolds and Beane (1985), Cline and Bodnar (1994) and Rowland and Wilkinson (1999).

In terms of comparing the four Endeavour deposits with each other, it is evident that with the exception of minor (~200 – 300m) changes in the estimated depths of emplacement, fluid evolution in these deposits was remarkably similar. This is not considered surprising given the similar intrusive histories, and similar associations of mineralisation and alteration with the various intrusions.

5.7.3 Fluid evolution in the Endeavour systems

From the results above there is some evidence for a decrease in fluid temperatures with time in the Endeavour deposits; from 550 to >600°C in EQ to 350 – 400°C in LQ. This probably reflects the overall thermal decay of these magmatic – hydrothermal systems after the evolution of volatile-rich fluids (Cathles, 1981; Hanson, 1995). Despite the overall decrease in temperature with time from TQM, THQ and MQ, the multiplicity of emplacement, exsolution of an aqueous fluid, expulsion of that fluid and associated alteration and mineralisation related to the K-QMP and KA-QMP intrusions, probably accounts for the wide range in temperatures for each paragenetic stage.

There is an apparent initial increase in salinity from EQ to TMQ fluids, before a gradual decrease in salinity in the fluids associated with THQ, MQ and LQ. EQ fluids have salinities of ~55 wt% NaCl eq., whereas TMQ fluids have higher and more variable salinities around 60 wt% NaCl ± KCl eq. THQ and MQ have an average salinity of ~55 wt% NaCl eq., but have lower KCl concentrations than EQ fluids. LQ have salinities of ~45 wt% NaCl eq. Therefore, as for other well-documented porphyry systems, the mineralising fluids of the Endeavour deposits became less saline with time. However, an important distinction is that hypersaline fluid inclusions have been recognised in all quartz generations in the Endeavour deposits, in contrast to deposits such as Santa Rita (Reynolds and Beane, 1985), where late stage fluid inclusions are undersaturated with respect to salts. This implies that hypersaline magmatic – hydrothermal fluids were dominant throughout the evolution of the Endeavour deposits. This dominance of magmatic – hydrothermal fluid throughout the evolution of the porphyry systems contrasts with many porphyry deposits, where a convective phase of late stage meteoric fluid overwhelmed the early magmatic hydrothermal events (e.g. Taylor, 1974; Sheppard and Gustafson, 1976; Henley and McNabb, 1978).

Experimental evidence has demonstrated that partitioning of volatiles, especially Cl, between co-existing aqueous fluids and silicate melts is a function of pressure, and as a result, a greater proportion of Cl and volatiles partition into the aqueous fluids at higher pressures (Shinohara *et al.*, 1989). In addition, numerical modelling (Candela, 1989b; Cline and Bodnar, 1991) has indicated that the first fluids to exsolve from a typical calc-alkaline to alkaline melt at pressures below ~1.3kbar have low Cl contents (Cline and Bodnar, 1994). However, as crystallisation proceeds, Cl and other volatiles become concentrated in the silicate melts and more volatiles are fractionated into exsolving aqueous fluids

(Cline and Bodnar, 1994). In the Endeavour systems being studied, continuing crystallisation in the magma chamber over the time period separating EQ and TMQ fluids might have allowed the latter fluids to become more enriched in volatiles other than H_2O, and hence become more saline than the EQ fluids. Assuming that Heithersay and Walshe's (1995) high (~760°C) homogenisation temperatures relate to TMQ, these fluids homogenise at temperatures that extend well into the magmatic range. This possibly implies that fluid inclusions in TMQ were incorporated into the host quartz under magmatic conditions. Given the typical magmatic textures and ubiquitous presence of igneous solid inclusions in quartz precipitated during TMQ, it is suggested that TMQ fluids represent the approximate transition from magmatic to hydrothermal conditions in the Endeavour porphyry copper deposits (450 to >600°C, mean 540°C; 50 – 75 wt% NaCl ± KCl eq., mode 55 – 60 wt% NaCl ± KCl eq.).

The microthermometric analysis of fluid inclusions from the Endeavour deposits yielded pressure estimates of ~300 – 450bar for EQ, TMQ, THQ and MQ. At these pressures, an exsolving magmatic – hydrothermal fluid would immediately separate into two immiscible phases according to Bodnar *et al.*'s (1985) NaCl – H_2O projection; a low salinity vapour-rich phase and a highly saline liquid phase. This immiscibility would be indicated by the presence of co-existing vapour-rich (Type 2) and hypersaline (Type 3) fluid inclusions. Co-existing Type 2 and Type 3 fluid inclusions are present in EQ, TMQ, THQ and MQ quartz generations of the Endeavour deposits. The rare occurrence of co-existing high salinity (15 – 25 wt% NaCl eq.) liquid-rich (Type 1) and vapour-rich (Type 2) fluid inclusions is interpreted to indicate local heterogeneity in the high salinity phase of the magmatic aqueous fluid. Phase equilibria constraints preclude the co-existence of Type 2 and Type 3 fluid inclusions that homogenise by halite dissolution (Cline and Bodnar, 1994). As predicted by Bodnar *et al.* (1985), the co-existence of Type 2 and Type 3 fluid inclusions is interpreted to imply that a melt + vapour + high-salinity liquid co-existed at the time of trapping (Dilles, 1987; Cline and Bodnar, 1994; Heithersay and Walshe, 1995).

Based on the low Br concentrations and orders of magnitude higher concentrations of Cl in all three fluid inclusions analysed on the PIXE probe, it is likely that Cl was the primary ligand in the high-temperature magmatic – hydrothermal fluid associated with TMQ (and by inference other fluids), and that this fluid was a Na – K ± Ca brine that contained significant concentrations of Fe, Mn, Cu, Ti and Zn. It is probable that Cu (and Au) were transported as Cl-complexes in the magmatic – hydrothermal fluids associated with ore deposition in the Endeavour deposits.

Consistent trends in the decrepitation results are interpreted to imply that relatively higher Cu and lower Fe abundances in THQ compared to MQ reflect a decrease in the Cu concentrations from THQ to MQ. There is also a decrease in homogenisation temperatures of ~50°C from THQ to MQ (~550 to ~500°C), even though THQ and MQ have comparable salinities of ~55 wt% NaCl ± KCl eq. These features combined are thought to imply that the cooler MQ fluids associated with the main mineralising stages at the Endeavour deposits reflect the precipitation of sulphides from cooling THQ fluids.

Both microthermometry and decrepitation analyses show that there is an overall increase in the relative abundances of Ca and K in the fluids with time, so that fluids associated with LQ are the most Ca- and K-rich. The average Na/Na + K ratio of early fluids (0.79) most likely represents the primary fluid that exsolved from the magmas associated with the Endeavour deposits. As crystallisation progressed, the Na/Na + K ratio of the fluid changed, particularly with regard to K. The gradual increase in Na/Na + K from 0.74 in TMQ through 0.76 in THQ to 0.81 in MQ possibly reflects the gradual loss of K from the fluids with the onset of increasingly intense potassic alteration associated with ore deposition. Heithersay and Walshe (1995) showed that it is reasonable to assume that the early high temperature magmatic – hydrothermal fluids associated with E26 were equilibrated with two feldspars + melt + vapour + saline brine at magmatic temperatures. They also showed that, initially, cooling of this fluid could lead to the development of potassic alteration zones. Subsequent cooling could allow muscovite precipitation (Burnham, 1979) and reaction along the K-feldspar – muscovite boundary with falling temperature would raise the K-content of the fluid. This interpreted wall rock buffering (possibly locally limited to, but not exclusive to, pre-existing alteration zones) probably also accounts for the increase in Ca of the LQ fluids compared to the earlier fluids studied in the Endeavour deposits. Wall rock buffering from the host Wombin Volcanics might be a significant feature towards the deposit peripheries since the average atomic Na/Na + K ratio for the host Wombin Volcanics is 0.48, based on whole rock geochemical analysis (Crawford, 1999).

The pressure-depth estimates based on microthermometric data are interpreted to indicate a change from lithostatic to hydrostatic pressure regimes synchronous with the change from MQ to LQ. It is likely that this transition to hydrostatic conditions led to increased gas production as the magmatic – hydrothermal fluid was connected to the palaeo-surface (or water table). It is possible that the inferred increased gas production led to an increase in fluid acidity, which might have enhanced the capacity of LQ fluids to leach K and Ca from the surrounding, altered rocks.

The inference that LQ fluids are similar to MQ fluids in terms of Cu/S, Cu/Cl, Fe/Cu and other metal/anion ratios is thought to indicate that they may have been significant in terms of ore deposition in the Endeavour systems. Indeed, Wolfe (1994) and Wolfe *et al.* (1996) first argued for a magmatic – hydrothermal origin for late stage phyllic alteration and mineralisation at E48. More recently work by Harris (1997) and Harris and Golding (2001) provided further evidence for a magmatic – hydrothermal origin for late stage phyllic alteration and mineralisation at E26 and similar late stage phyllic alteration is observed in E22 and E27 (this study). The magmatic – hydrothermal origin of these late stage fluids may account for their abundances of copper – including the high-grade core associated with pervasive sericite alteration in the E48 deposit.

5.8 Summary

The four main paragenetic stages at E22, E26, E27 and E48 contain hypersaline Type 3 and less abundant vapour-rich Type 2 and liquid-rich Type 1 fluid inclusions. EQ fluid inclusions homogenise at temperatures typically above 550°C and have an average calculated salinity of 58 wt% NaCl ± KCl eq. TMQ fluid inclusions have homogenisation temperatures typically between 500 and 550°C and average calculated salinities of 60 wt% NaCl ± KCl eq. The homogenisation temperatures of THQ fluid inclusions are ~50°C higher (average ~500°C) than those in MQ (average ~460°C), although the average calculated salinities of fluid inclusions in THQ and MQ are similar; ~ 55 wt% NaCl ± KCl eq. LQ fluid inclusion have the lowest homogenisation temperatures (350 – 400°C) and the lowest average calculated salinity (38 wt% NaCl ± KCl eq.) of all those studied.

Microthermometric data yield trapping pressures of ~300 – 450bar for EQ, TMQ, THQ and MQ and ~150 – 200bar for LQ fluids. Depth estimates based on these pressure are from ~1000 to ~1700m using lithostatic pressure for EQ, TMQ, THQ and MQ. Similar depth estimates are obtained for LQ using hydrostatic pressure. This is interpreted to indicate a transition from lithostatic to hydrostatic regimes synchronous with the change from MQ to LQ fluids, which may have been associated with an increase in acidity and associated increase in K and Ca concentrations in the LQ fluids compared to earlier fluids. There is an overall increase in the KCl content of the fluid inclusions with time so that the LQ fluid inclusions are the richest in KCl. An increase with time of the Ca content of the fluids accompanies the increasing K content. These features are consistent with wall rock buffering of the magmatic – hydrothermal fluids as they cooled.

The cooler, Cu-depleted MQ fluids associated with the main mineralising stages of the Endeavour deposits are inferred to have evolved via the precipitation of sulphides from cooling THQ fluids. Cl was the dominant ligand in the high-temperature magmatic – hydrothermal fluids associated with mineralisation at the Endeavour deposits. These fluids were most likely Na – K ± Ca brines that contained significant concentrations of Fe, Mn, Cu, Au and Zn as Cl-complexes.

CHAPTER 6
Sulphur Isotopes

6.1 Introduction

Sulphur isotope geochemistry can be used in ore deposit research to provide information on the temperature of mineralisation, the chemical conditions and mechanisms of ore deposition, and the source of sulphur. In this chapter, sulphur isotopic compositions of bornite, chalcopyrite, pyrite, anhydrite and gypsum are investigated to confirm whether isotopic zonation, typical of some porphyry deposits, is evident in the Endeavour systems, and if so, to explain this zonation. In addition, changes in sulphide and sulphate isotopic compositions are modelled to determine the $H_2O:SO_2$ ratio of the systems, particularly with the view of determining whether this ratio changed as a function of paragenesis or spatial location.

Several previous workers in the Goonumbla district have conducted sulphur isotope studies. Heithersay and Walshe (1995), Radclyffe (1995) and Harris (1997) described lateral and vertical zonation in $\delta^{34}S$ values around E26, while Howland-Rose (1996) described the same around E48. These studies focused on a variety of sulphides and sulphates, and where appropriate, their data are incorporated into the present study.

The four broad paragenetic stages established in Chapter 4 are used so that sulphur isotopic compositions are discussed in terms of the early (EQ), transitional magmatic (TMQ) transitional hydrothermal (THQ)/ main (MQ) and late (LQ) stages.

6.2 Methods

Fifty-three bornite grains and five anhydrite grains from the different paragenetic stages of the Endeavour deposits were analysed for sulphur isotopes using both conventional (hand drilling) and laser ablation methods at the Central Science Laboratory of the University of Tasmania. The results are summarised in Appendix C1, and all $\delta^{34}S$‰ values are reported relative to Canyon Diablo Troilite (CDT), calculated as follows:

$$\delta^{34}S_{sample}\ (‰) = [(^{34}S/^{32}S)_{standard} \times 1000] \ / \ (^{34}S/^{32}S)_{standard}$$

Coarse-grained bornite and anhydrite were hand drilled and analysed according to the conventional sulphur isotope techniques of Robinson and Kusakabe (1975). An analytical uncertainty of ±0.1‰ is estimated from internal standards of homogeneous galena from Broken Hill ($\delta^{34}S$ = +3.40‰) and Rosebery ($\delta^{34}S$ = +12.40‰) that were run with an SO_2 reference gas of $\delta^{34}S \approx$ CDT. These internal standards were calibrated against international sphalerite standards IAEA NZ1 ($\delta^{34}S$ = +1.83‰) and NBS 123 ($\delta^{34}S$ = +4.34‰). Isotope measurements were performed on a VG Sira Series II mass spectrometer.

Samples of finely intergrown sulphides (<1mm) could not be hand drilled. Nineteen samples of fine-grained sulphides were analysed using the laser ablation method of Huston *et al.* (1995) on ~200μm thick polished sections. Ablations were conducted using an 18W Quantronix 117Nd:YAG model laser in an oxidising atmosphere (at 25 torr oxygen pressure) and a ~35mA current for 2 seconds on single or multiple sites (up to 5) to yield sufficient SO_2 for analysis. The total gas was passed from the sample chamber through two different purification circuits (H_2O and CO_2) before the SO_2 gas was collected and analysed using a VG Sira Series II mass spectrometer.

For comparison between conventional and laser ablation-derived $\delta^{34}S$ values, the laser ablation samples have to be corrected with an empirical factor, because the method of concentrating SO_2 in the ablation method results in a small fractionation (~0.15‰) in $\delta^{34}S$. The empirical $\delta^{34}S$ laser correction factors for pyrite and chalcopyrite have been documented by Huston *et al.* (1995), but no values were available for bornite. The empirical correction factor for bornite was determined by analysing "homogeneous" bornite from four polished bornite chips that gave repeatable $\delta^{34}S$ values. The four chips were from a 5cm diameter bornite clot at E27. Initially, the four chips were ablated (2 spots per grain) and the average $\delta^{34}S$‰ calculated to be -6.226‰. The chips were then crushed with CuO_2 and oxidised on the conventional line; the measured and corrected $\delta^{34}S$ value was calculated to be -2.405‰. Therefore, the overall correction factor for bornite using laser ablation is the difference between the two measurements, i.e. -2.405 - (-6.226) = +3.281‰. The accuracy of this measurement is ±0.4‰.

Because similar bornite populations were analysed by both techniques in this investigation, the distributions of $\delta^{34}S$ values were expected to be similar for the two populations. However, using the +3.281‰ correction factor, the distribution of $\delta^{34}S$

values for the laser ablation population was skewed towards lighter $\delta^{34}S$ by ~0.75‰ when compared with the one for the conventional method population. This difference is thought to be due to minor fluctuations in homogeneity of the bornite standard.

Adjusting the empirical correction factor to +4.571‰ (+3.821 + 0.75‰) corrects the skewness and is thought to be within analytical error and technique accuracy (Keith Harris, CSL, pers. comm., 2001). Thus, the empirical $\delta^{34}S$ laser correction factor used for bornite is +4.571‰ (Appendix C2 contains additional details on the determination of the empirical factor for bornite).

6.3 Results

6.3.1 Early sulphides

The $\delta^{34}S$ values from early stage (EQ) bornite and chalcopyrite (n = 17) are between -6.1 and -1.1‰ (Figure 6.1), although most are between -4.5 ± 1.4‰. No EQ sulphates were analysed for sulphur isotopes. There are insufficient data to comment on vertical or lateral zonation in the $\delta^{34}S$ values for EQ at E22, E26 and E27 (Table 6.1) and there is no systematic spatial variation in $\delta^{34}S$ values for early sulphides at E48 (Figures 6.2).

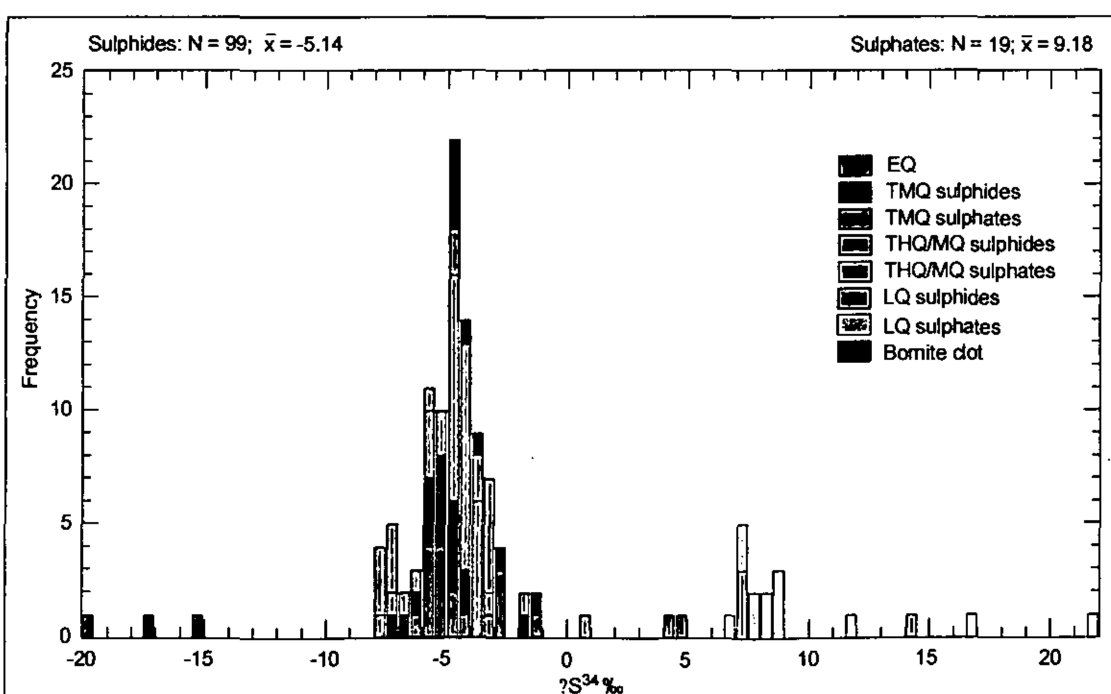

Figure 6.1 Cumulative frequency histogram of δS^{34} values for EQ, TMQ, THQ/MQ and LQ sulphides (mainly bornite, some chalcopyrite and pyrite) and sulphates (mainly anhydrite, some gypsum). All data is tabulated in Appendix C1.

Table 6.1 Summary of fluid inclusion and S isotope compositions (sulphides) for EQ, TMQ, THQ/MQ and LQ fluids.
Abbreviations: bor - bornite; cpy - chalcopyrite; py - pyrite
PH - Heithersay and Walshe, 1995; JHR - Howland-Rose, 1996; AH - Harris, 1997; VL - this study; Th_F - final homogenising temperature (cf. Chapter 5).

Stage	*$\delta^{34}S$ (mean ± 1σ)*	*Th_F (mean ± 1σ)*	*Salinity (mean ± 1σ)*	*Deposit*	*Analyses*	*Vertical zonation*	*Lateral zonation*
Early (EQ)	-4.5 ± 1.4 ‰ (n = 17)	555 ± 50 °C (n = 44)	60 ± 5 wt% NaCl ± KCl eq. (n = 49)	E22	1 (VL) bor	Insufficient data	Insufficient data
				E26	3 (VL) + 1 (PH) bor	Insufficient data	Insufficient data
				E27	2 (VL) bor	Insufficient data	Insufficient data
				E48	1 (VL) + 5 (JHR) bor 4 (JHR) cpy	No systematic vertical variation	No systematic lateral variation
Transitional magmatic (TMQ)	-4.7 ± 1.6 ‰ (n = 21)	500 ± 75 °C (n = 91)	60 ± 10 wt% NaCl ± KCl eq. (n = 89)	E22	3 (VL) bor	Heavier towards surface	Heavier towards periphery
				E26	11 (VL) + 1 (PH) bor	No systematic vertical variation	Heavier towards periphery
				E27	3 (VL) bor	Heavier towards surface	Heavier towards periphery
				E48	3 (VL) bor	No systematic vertical variation	Heavier towards periphery
Transitional hydrothermal and main (THQ/MQ)	-4.8 ± 1.0 ‰ (n = 34)	465 ± 100 °C (n = 156)	55 ± 15 wt% NaCl ± KCl eq. (n = 150)	E22	2 (VL) bor	Heavier towards surface	Heavier towards periphery
				E26	6 (VL) + 6 (PH) bor 3 (PH) cpy	No systematic vertical variation	No systematic lateral variation
				E27	3 (VL) bor	Heavier towards surface	Heavier towards periphery
				E48	4 (VL) + 6 (JHR) bor 3 (JHR) cpy	No systematic vertical variation	No systematic lateral variation
Late (LQ)	-4.9 ± 2.3 ‰ (n = 20)	375 ± 65 °C (n = 45)	40 ± 15 wt% NaCl ± KCl eq. (n = 37)	E22	1 (VL) bor	Insufficient data	Insufficient data
				E26	3 (VL) bor 4 (PH) + 3 (DR) + 2 (AH) py	Heavier towards surface	Heavier towards periphery
				E27	-	No data	No data
				E48	2 (VL) bor 3 (JHR) py	No systematic vertical variation	No systematic lateral variation

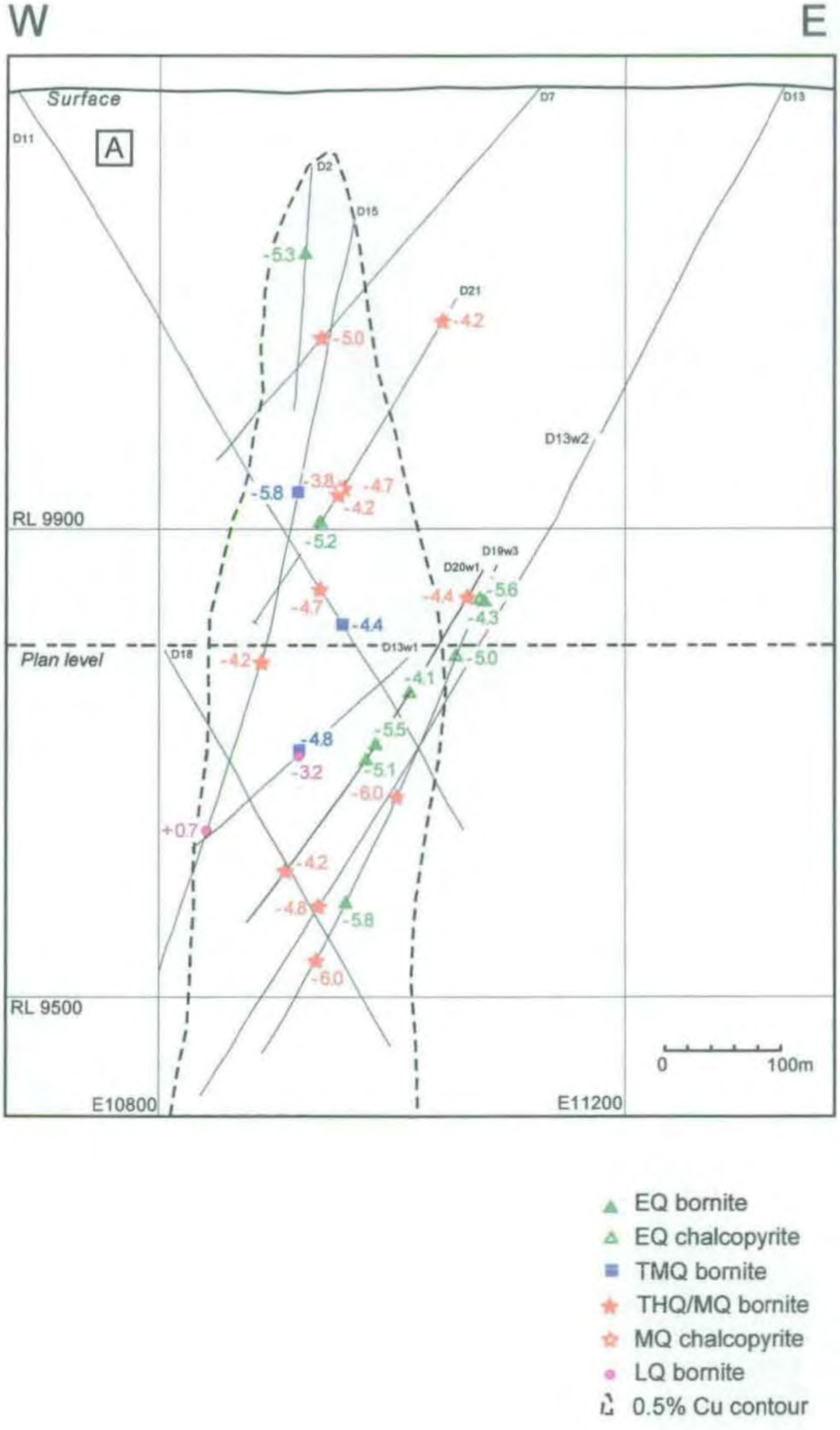

W
E
Surface
A
D11
D2
D15
D7
D13
D21
D13w2
D19w3
D20w1
D13w1
D18
RL 9900
RL 9500
Plan level
E10800
E11200
0
100m
-5.3
-5.0
-4.2
-5.8
-3.8
-4.7
-4.2
-5.2
-4.7
-4.4
-4.4
-5.6
-4.3
-5.0
-4.2
-4.1
-4.8
-3.2
-5.5
-5.1
-6.0
+0.7
-4.2
-4.8
-5.8
-6.0
EQ bornite
EQ chalcopyrite
TMQ bornite
THQ/MQ bornite
MQ chalcopyrite
LQ bornite
0.5% Cu contour

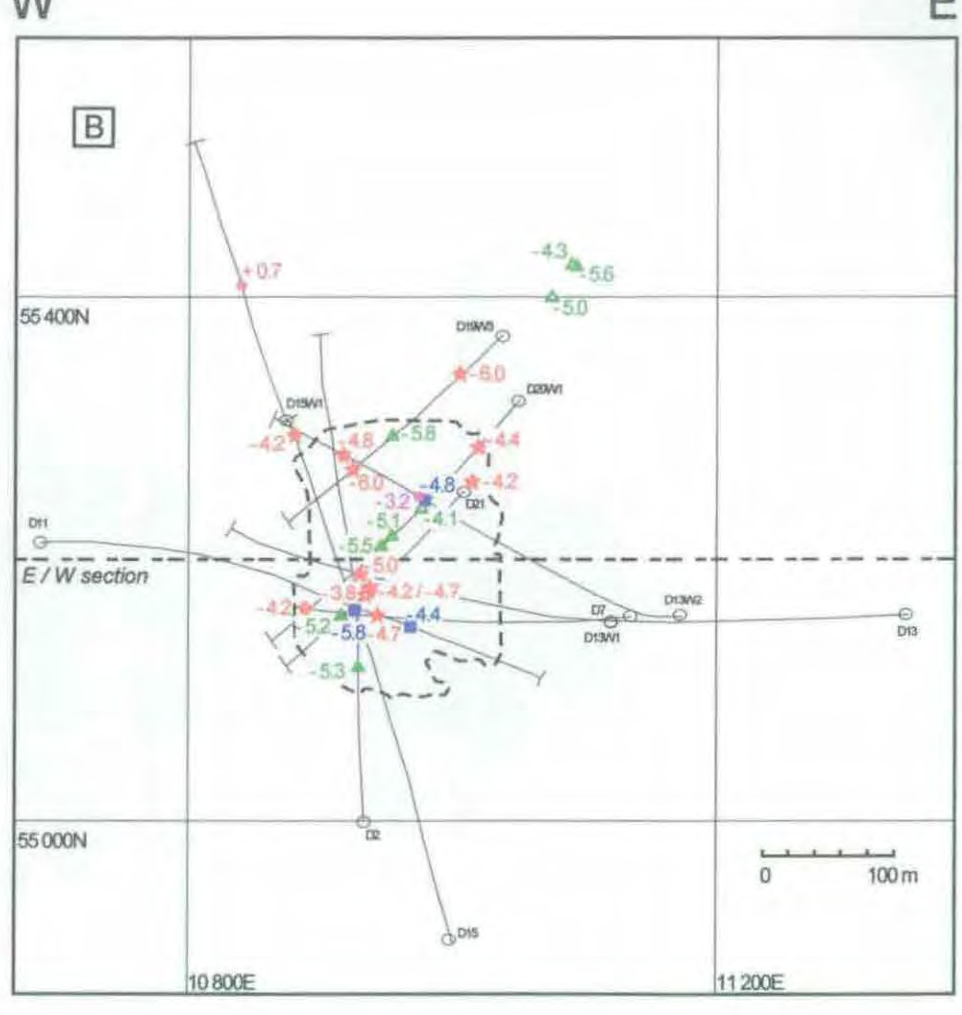

Figure 6.2 **A** E48 east-west section, mine grid 53650N and **B** plan - 9800mRL showing $\delta^{34}S$ values for sulphides in early (EQ), transitional magmatic (TMQ), transitional hydrothermal and main (THQ/MQ) and late stage (LQ) quartz veins (cf. Figure 3.7 for geology).

6.3.2 Transitional magmatic sulphides and sulphates

$\delta^{34}S$ values from transitional magmatic stage (TMQ) bornite are between -19.7 and -1.2‰ (n = 21), with most between -6.3 and -3.1‰ (Figure 6.1; Appendix C1). Extreme negative values of -17.4, -19.7 and -15.4‰ were obtained from single samples from E22, E27 and E26 respectively, skewing the $\delta^{34}S$ distribution of TMQ sulphides (Figure 6.1). These very negative $\delta^{34}S$ values are from bornite collected from the basal, peripheral regions of the three systems (Figure 6.3, 6.4 and 6.5 respectively).

Two analyses of TMQ anhydrite from E26 yielded $\delta^{34}S$ values of +4.4 and +4.8‰. The latter sample is intergrown with bornite, which has a $\delta^{34}S$ value of -1.9‰. The anhydrite and intergrown bornite is interpreted to represent a co-precipitated sulphate – sulphide pair.

Vertical and lateral zoning in $\delta^{34}S$ values in TMQ sulphides is evident at E22 and E27 (Figures 6.3 and 6.4 respectively), where values become less negative towards the surface and with increasing distance from the cores of the deposits (Table 6.1). Only the lateral component of this zonation is evident at E26 and E48 (Figures 6.5 and 6.2 respectively).

6.3.3 Transitional hydrothermal/main sulphides and sulphates

Transitional hydrothermal (THQ)/main stage (MQ) bornite and lesser chalcopyrite (n = 34) have $\delta^{34}S$ values ranging between -8.0 and -3.4‰ (Figure 6.1), but mainly between -4.8 ± 1.0‰ (Appendix C1).

Anhydrite for these stages from E26 has $\delta^{34}S$ values of around +7.3‰ (n = 4), with one value of +14.3. A co-precipitated anhydrite - bornite pair from a MQ vein yielded $\delta^{34}S$ values of +7.4 and -3.8‰ respectively. Heithersay and Walshe (1995) report MQ anhydrite – bornite and anhydrite – chalcopyrite pairs having $\delta^{34}S$ values of +14.1 and -5.0‰, and +7.3 and-4.2‰ respectively.

There is no systematic spatial zonation in $\delta^{34}S$ values for THQ/MQ sulphides at E26 and E48 (Figures 6.5 and 6.2 respectively). In contrast, as with TMQ sulphides, $\delta^{34}S$ values of THQ/MQ sulphides at E22 and E27 (Figures 6.3 and 6.4 respectively), become heavier towards the surface and with increasing distance from the cores of the deposits (Table 6.1). TMQ Sulphates do not show any systematic spatial variation at E26.

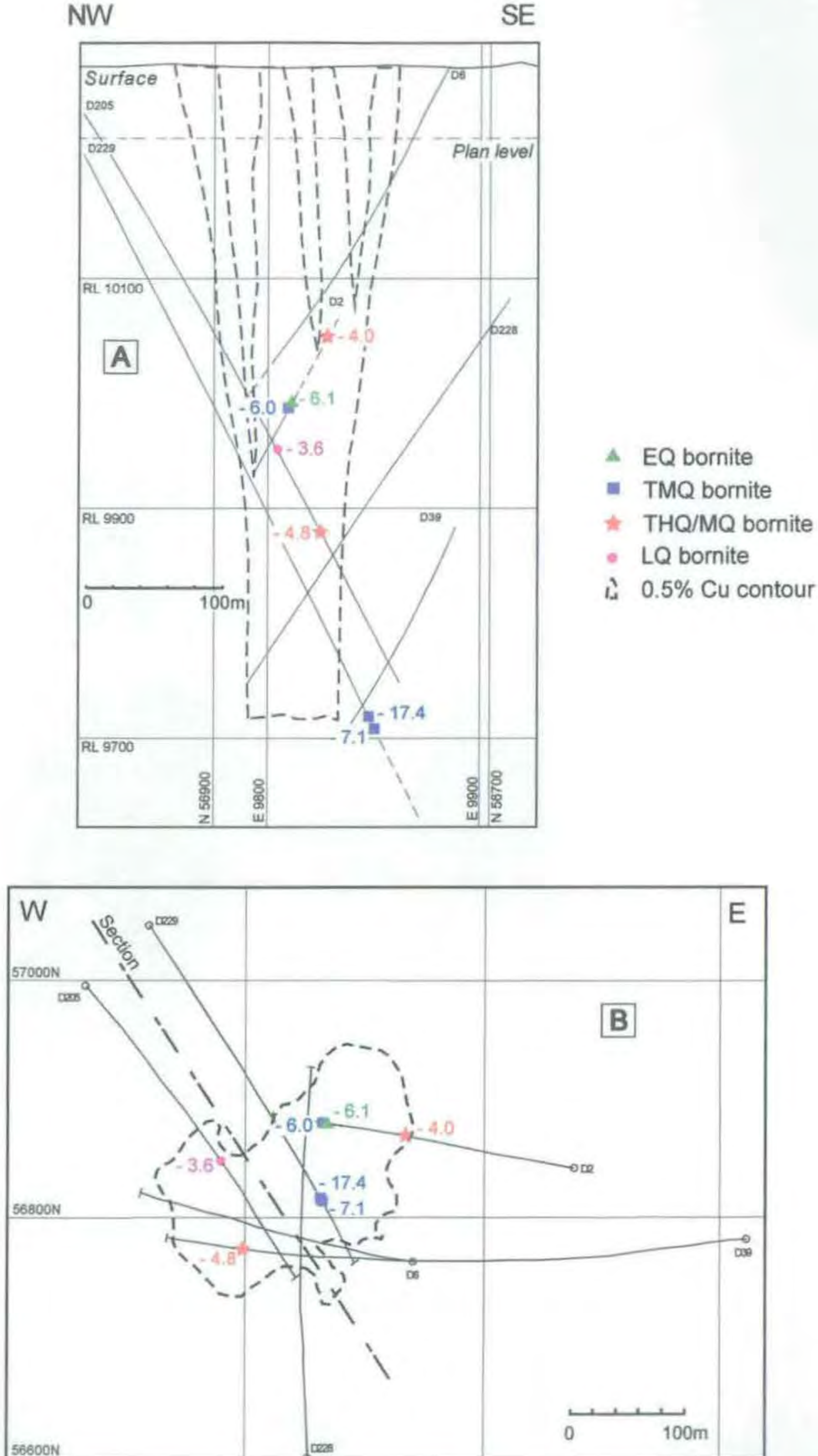

Figure 6.3 **A** E22 oblique section, mine grid 9 700E/57 000N to 9 925E/56 650N and **B** plan - surface showing $\delta^{34}S$ values for sulphides in EQ, TMQ, THQ/MQ and LQ veins (cf. Figure 3.4 for geology). All data presented in Appendix C1.

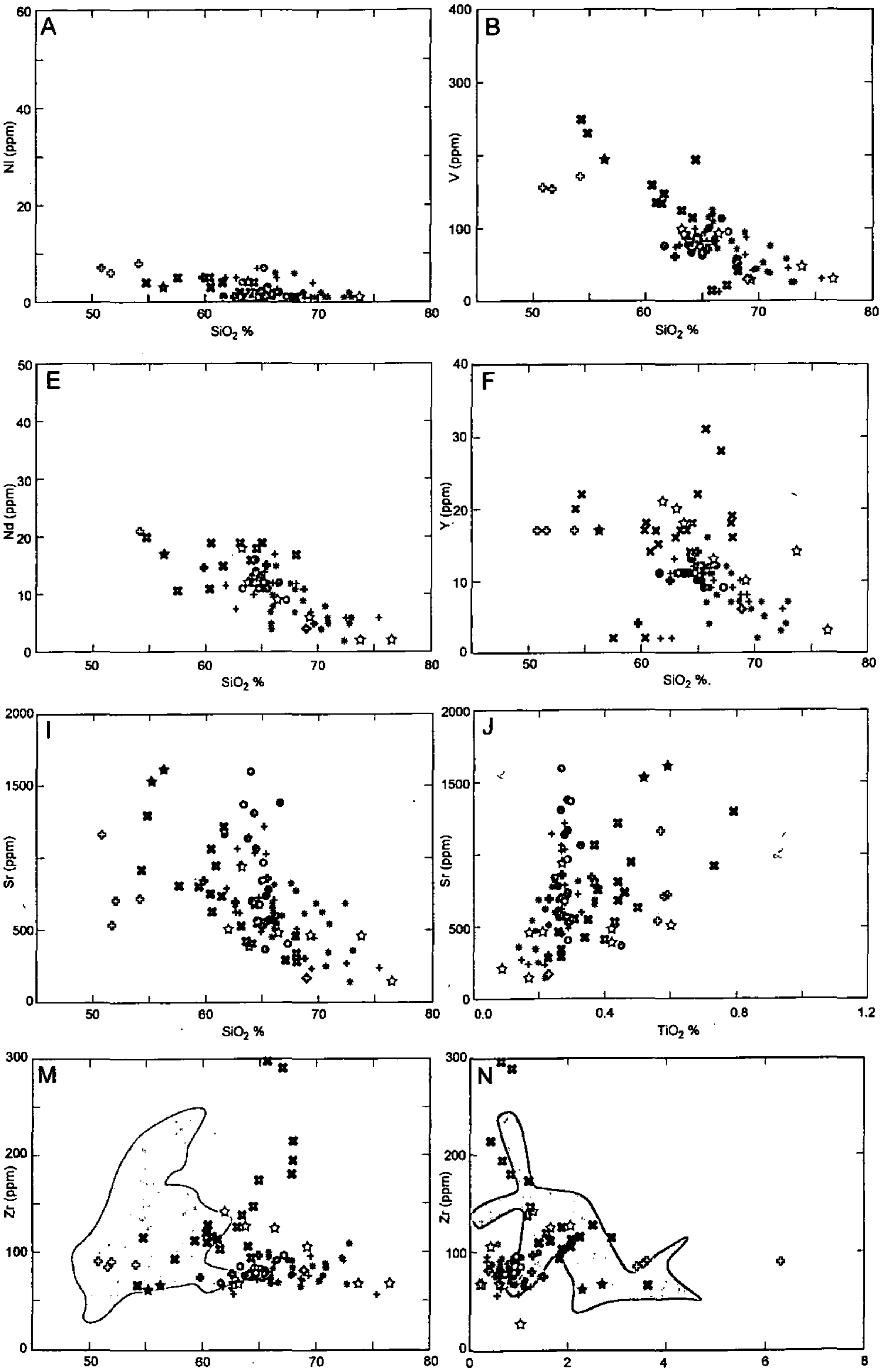

A
Ni (ppm)
SiO2 %
B
V (ppm)
SiO2 %
E
Nd (ppm)
SiO2 %
F
Y (ppm)
SiO2 %.
I
Sr (ppm)
SiO2 %
J
Sr (ppm)
TiO2 %
M
Zr (ppm)
SiO2 %
N
Zr (ppm)
MgO %

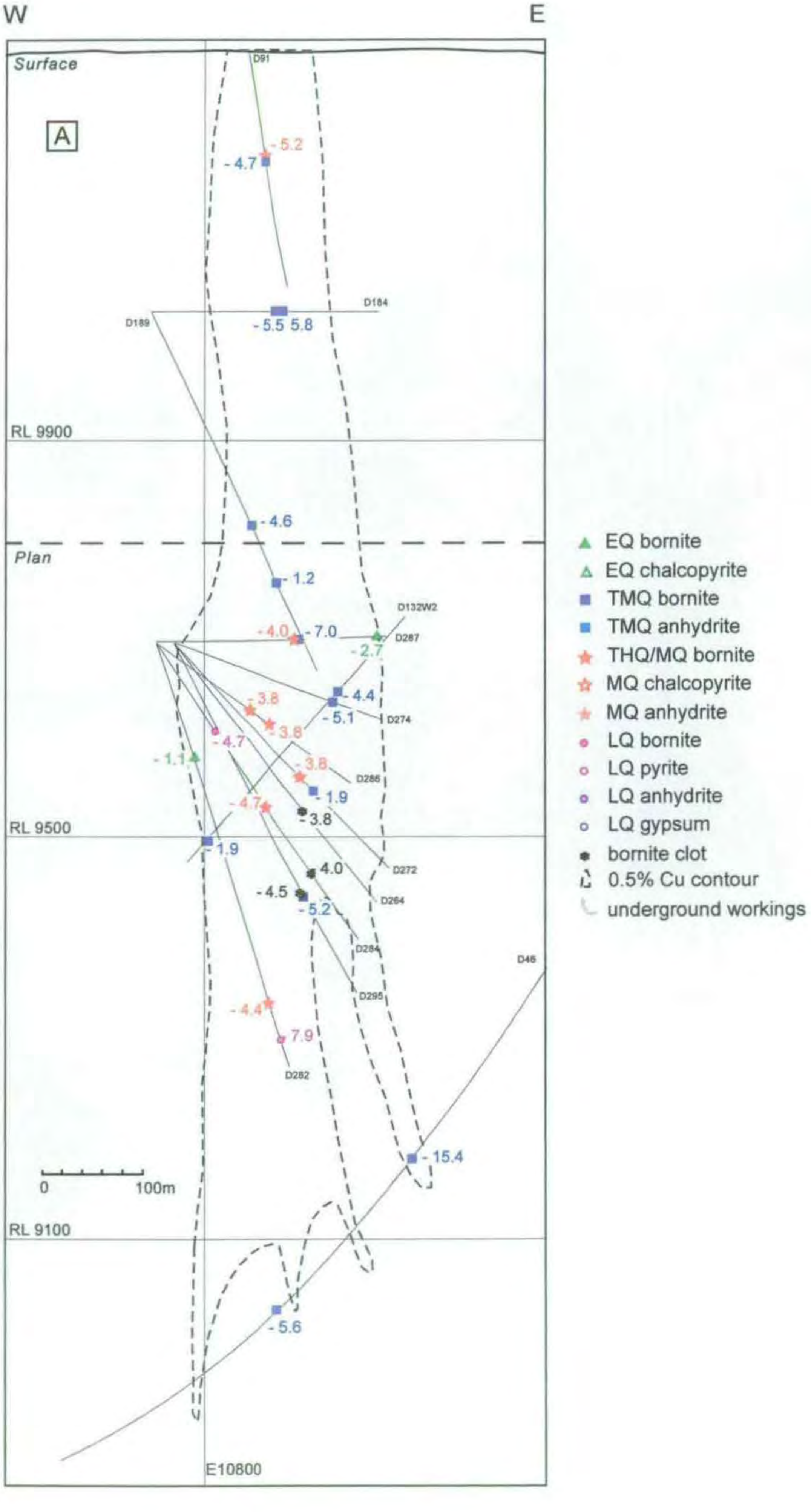

W
E
Surface
A
RL 9900
Plan
RL 9500
RL 9100
E10800
0
100m
D91
D184
D189
D132W2
D287
D274
D286
D272
D264
D284
D295
D282
D46
- 5.2
- 4.7
- 5.5 5.8
- 4.6
- 1.2
- 4.0
- 7.0
- 2.7
- 4.4
- 5.1
- 3.8
- 3.8
- 4.7
- 1.1
- 3.8
- 1.9
- 4.7
- 3.8
- 1.9
4.0
- 4.5
- 5.2
- 4.4
7.9
- 15.4
- 5.6
EQ bornite
EQ chalcopyrite
TMQ bornite
TMQ anhydrite
THQ/MQ bornite
MQ chalcopyrite
MQ anhydrite
LQ bornite
LQ pyrite
LQ anhydrite
LQ gypsum
bornite clot
0.5% Cu contour
underground workings

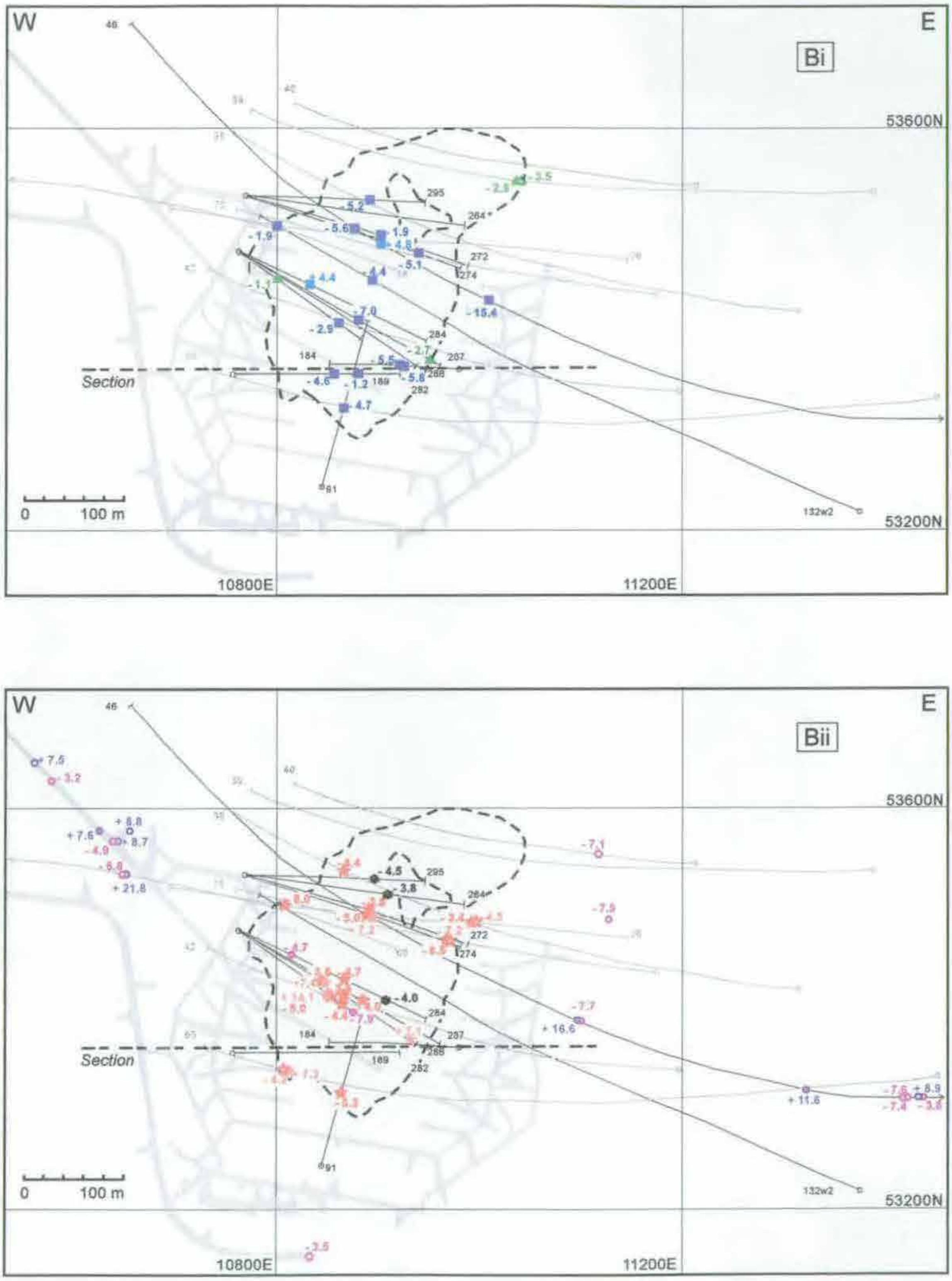

Figure 6.5 **A** E26 east-west section, mine grid 53050N. showing $\delta^{34}S$ values for sulphides and sulphates for EQ, TMQ, THQ/MQ and LQ from this study (cf. Figure 3.5 for geology); and **B** plan - 9800mRL showing $\delta^{34}S$ values for sulphides and sulphates in EQ and TMQ (**Bi**), and THQ/MQ and LQ (**Bii**) from this study (black boreholes), Heithersay, 1991 (grey drillholes) and Radclyffe, 1995 (mine workings).

6.3.4 Late sulphides and sulphates

Late stage (LQ) pyrite and lesser bornite (n = 20; Figure 6.1) have $\delta^{34}S$ values ranging between -7.9 and +0.7‰, with most between -4.9 and -3.0‰ (Appendix C1).

Anhydrite and gypsum from E26 have been analysed for sulphur isotopes in LQ veins (n = 13); they have $\delta^{34}S$ values between +6.9 and +21.8‰, with a mean value of 10.0‰ (Appendix C1). Anhydrite – pyrite pairs from Heithersay and Walshe (1995) and Harris (1997) yielded $\delta^{34}S$ values of +8.3 and -5.0‰, +7.5 and -5.9‰, and +16.6 and -7.7‰ respectively.

There are insufficient data to comment on the vertical and lateral zonation in $\delta^{34}S$ values for late sulphides at E22 and E27 (Figures 6.3 and 6.4 respectively; Table 6.1) and there is no obvious spatial variation in the $\delta^{34}S$ values in late stage sulphides at E48 (Figure 6.2). However, at E26, $\delta^{34}S$ values for LQ sulphides become heavier towards the surface and with increasing distance from the centre of the deposit (Figure 6.5).

6.4 Discussion

6.4.1 $\delta^{34}S$ values for sulphate - sulphide pairs

Two reasons for determining $\delta^{34}S$ values of co-precipitated sulphate – sulphide pairs are 1) to establish the source of sulphur in the magmatic – hydrothermal fluid and 2) to understand the precipitating mechanism of sulphur-bearing minerals from the exsolved magmatic fluid. The variation in $\delta^{34}S$ in sulphates and sulphides commonly exhibit a linear relationship on a $\delta^{34}S$ vs $\Delta^{34}S_{sulphate - sulphide}$ diagram (Field and Gustafson, 1976). They proposed that the $\Delta^{34}S_{sulphate - sulphide}$ would vary with temperature and would converge to a point that would reflect the initial $\delta^{34}S$ of the exsolved fluid provided, that during the life of the system, isotopic equilibrium was maintained, there was a constant H_2S:SO_2 ratio and there was an infinite sulphur reservoir to maintain a constant $\delta^{34}S$. Plotting the isotopic differences against fluid inclusion homogenisation temperature allows comparison of the data for paired sulphides and sulphates that are constrained by fluid inclusion geothermometry. This addresses, to some extent, the concern raised by Ohmoto (1986) that correlations on $\delta^{34}S$ vs $\Delta^{34}S$ diagrams are a mathematical artifact.

To test whether $\delta^{34}S$ of sulphides and sulphates co-vary with temperature in the Endeavour systems, sulphur isotope pairs from Heithersay and Walshe (1995), Harris (1997) and this study have been plotted on a $\delta^{34}S$ vs temperature diagram (Figure 6.6), which is analogous to the $\delta^{34}S$ vs $\Delta^{34}S$ of Field and Gustafson (1976). Temperatures for paired data on this diagram were calculated using the equations of Ohmoto and Rye (1979) and Ohmoto and Lasaga (1982):

$$T\,^{o}C_{\text{(anhydrite – bornite)}} = 2591/((\Delta^{34}S - 0.56)^{1/2}) \quad .... \; 6.1$$

$$T\,^{o}C_{\text{(anhydrite – pyrite)}} = 2462/((\Delta^{34}S - 0.56)^{1/2}) \quad .... \; 6.2$$

$$T\,^{o}C_{\text{(anhydrite – chalcopyrite)}} = 2552/((\Delta^{34}S - 0.56)^{1/2}) \quad ...... \; 6.3$$

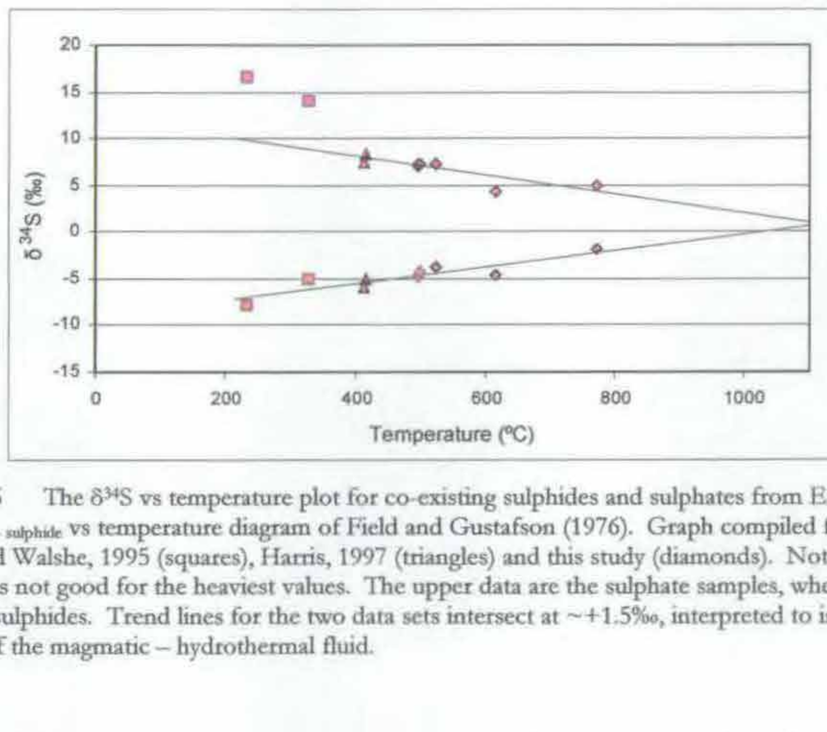

Figure 6.6 The $\delta^{34}S$ vs temperature plot for co-existing sulphides and sulphates from E26, based on the $\Delta^{34}S_{\text{sulphate - sulphide}}$ vs temperature diagram of Field and Gustafson (1976). Graph compiled from Heithersay and Walshe, 1995 (squares), Harris, 1997 (triangles) and this study (diamonds). Note the fit for sulphate data is not good for the heaviest values. The upper data are the sulphate samples, whereas the lower are the sulphides. Trend lines for the two data sets intersect at ~+1.5‰, interpreted to indicate the initial $\delta^{34}S_{\Sigma S}$ of the magmatic – hydrothermal fluid.

Actual and theoretical temperatures for sulphate and sulphide pairs have been modelled in an attempt to establish the $H_2S:SO_2$ ratio of the Endeavour systems. The actual temperatures obtained from applying equations 6.1, 6.2 and 6.3 to sulphate and sulphide pair $\delta^{34}S$ values from this study are represented on Figure 6.7 as *actual*. The theoretical temperatures (*theoretical* on Figure 6.7) have been calculated using the same $\delta^{34}S$ values and equations, however, various $H_2S:SO_2$ ratios have been used to find the "best fit" in an attempt to model the $H_2S:SO_2$ of the Endeavour systems. The "best-fit" model for the higher temperature sulphates and sulphides (>400°C) were obtained for an initial $H_2S:SO_2$ ratio of 1:1. There is good correlation between *actual* and *theoretical* $\delta^{34}S$ values (Table 6.2) for TMQ and THQ/MQ sulphur minerals on a plot of $\delta^{34}S$ vs temperature using calculated H_2S and SO_2 $\delta^{34}S$ data (Figure 6.7).

Table 6.2 Actual $\delta^{34}S$ values for sulphate – sulphide pairs for E26, and calculated (theoretical) H_2S and SO_2‰ (>400°C) and H_2S and SO_4‰ (<400°C) values based on different $H_2S:SO_2$ ratios. Plot compiled from VL – this study; PH – Heithersay and Walshe (1995) and AH – Harris (1997); bor – bornite; cpy – chalcopyrite; py – pyrite; anh – anhydrite. Temperature calculations based on equations from Ohmoto and Rye (1979) and Ohmoto and Lasaga (1982).

Sample	Stage	$\delta^{34}S_{anh}$	$\delta^{34}S_{sulphide}$	$\Delta^{34}S$	T°C	$H_2S:SO_2$	$H_2S‰_{calc}$	$SO_4‰_{calc}$	$H_2S‰_{calc}$	$SO_2‰_{calc}$	Source
VLS55/BnStd	TMQ	4.9	-1.9	6.7	773	1	-	-	-0.4	3.4	VL
VLS53/VL S7	TMQ	4.4	-4.7	9.08	615	1	-	-	-1.2	4.2	VL
VLS54/VL S13	MQ	7.4	-3.8	11.16	523	1	-	-	-2.0	5.0	VL
VLS56/x main	MQ	7.2	-4.8	12.04	495	1	-	-	-2.2	5.2	VL
VLS57/x main	MQ	7.1	-4.8	11.91	495	1	-	-	-2.2	5.2	VL
PH14/PH15(cpy)	MQ	7.3	-4.2	11.5	499	1	-	-	-2.2	5.2	PH
AH661/AH663	LQ	8.3	-5.0	13.3	417	1	-	-	-3.2	6.2	AH
AH9700A/B	LQ	7.5	-5.9	13.4	414	1	-	-	-3.2	6.2	AH
PH12/PH13	MQ	14.1	-5.0	19.1	329	1	-7.7	10.7	-4.7	7.7	PH
PH16/PH17(py)	LQ	16.6	-7.7	24.3	232	1	-11.5	14.5	-7.5	10.5	PH
PH12/PH13	MQ	14.1	-5.0	19.1	329	1.5	-5.9	12.5	-3.5	9.0	PH
PH16/PH17(py)	LQ	16.6	-7.7	24.3	232	1.5	-8.9	17.0	-5.7	12.3	PH
PH12/PH13	MQ	14.1	-5.0	19.1	329	1.75	-5.2	13.2	-3.0	9.4	PH
PH16/PH17(py)	LQ	16.6	-7.7	24.3	232	1.75	-7.9	18.0	-5.0	12.9	PH
PH12/PH13	MQ	14.1	-5.0	19.1	329	2	-4.6	13.8	-2.7	9.0	PH
PH16/PH17(py)	LQ	16.6	-7.7	24.3	232	2	-7.1	18.8	-4.5	12.3	PH

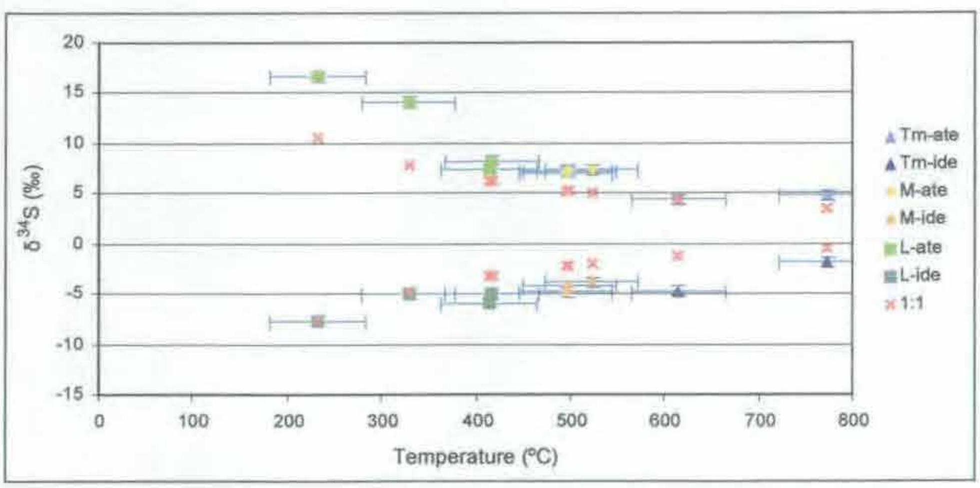

Figure 6.7 A $\delta^{34}S$ vs temperature diagram for actual and theoretical (H_2S and SO_2) values based on an $H_2S:SO_2$ of 1:1 and an initial $\delta^{34}S_{\Sigma S}$ = 1.5‰. Tm-ate –TMQ sulphate; Tm-ide –TMQ sulphide; M-ate – MQ sulphate; M-ide – MQ sulphide; L-ate – LQ sulphate; L-ide – LQ sulphide. Error bars indicate the range of homogenisation temperatures from fluid inclusions within each paragenetic stage.

Very little isotopic fractionation occurs between anhydrite and dissolved sulphate at temperatures greater than 200°C and between different sulphides (bornite and chalcopyrite) and H_2S in solution at temperatures between 200 and 600°C (Sakai, 1968; Ohmoto and Rye, 1979). It is thus reasonable to assume that the $\delta^{34}S$ values of anhydrite reflect the $\delta^{34}S_{SO_2}$ and that the $\delta^{34}S$ values of the corresponding sulphides reflect the $\delta^{34}S_{H_2S}$ of the original magmatic – hydrothermal ore fluid above 400°C. Previous studies have used this feature to estimate the initial $H_2S:SO_2$ ratio of the primary magmatic –

hydrothermal fluid (Heithersay and Walshe, 1995; Harris, 1997). Two E26 anhydrite – bornite pairs from this study; the TMQ pair at the calculated temperature of 773°C (+4.9 and -1.9‰ respectively) and the main stage pair at 523°C (+7.4 and -3.8‰ respectively), can be compared with sulphate – sulphide pairs from previous studies. By simple calculation, based on the assumption that the anhydrite and bornite $\delta^{34}S$ values reflect the $\delta^{34}S_{SO_2}$ and $\delta^{34}S_{H_2S}$ of the magmatic – hydrothermal fluid respectively, and an initial $\delta^{34}S_{\Sigma S}$ of +1.5‰ (Figure 6.6), the ore fluid would have a $H_2S:SO_2$ ratio of ~1:1 at temperatures >400°C. This result is consistent with calculations by Heithersay and Walshe (1995) and Harris (1997).

In contrast to the higher temperature stages, correlation between actual and theoretical $\delta^{34}S_{sulphate - sulphide}$ values below 400°C is poor. The poor correlation between these values in LQ fluids is thought to imply one of four things: 1) the lower temperature sulphate – sulphide pairs were not co-precipitated in isotopic equilibrium; 2) there was a limited sulphur reservoir that became depleted in sulphur with time; 3) there was a change in the $H_2S:SO_2$ ratio of the fluid with time (e.g. Field and Gustafson, 1976); or 4) sulphate was precipitated in equilibrium with SO_4 rather than SO_2. Because sulphur isotopic exchange kinetics indicate that equilibrium between aqueous SO_2 and H_2S is expected at temperatures above ~250°C (Ohmoto and Lasaga, 1982; Ohmoto and Goldhaber, 1997) it is reasonable to assume that the sulphate – sulphide pairs were co-precipitated in isotopic equilibrium. In addition, approach to equilibrium is also indicated because sulphate – sulphide isotopic fractionations increase with time (Taylor, 1987).

The presence of anhydrite phenocrysts in the post-mineral zero porphyries of E26 (cf. Chapter 3) is thought to preclude the possibility that a limited sulphur reservoir explains the deviation away from predicted $\delta^{34}S$ values at temperatures <400°C. A change in the $H_2S:SO_2$ ratio of the fluid might explain this deviation however. Theoretical values for $H_2S:SO_2$ ratios of 1.5 and 2 for pairs at temperatures of <400°C are plotted on Figure 6.8 (Table 6.2). Because of the strong correlation between theoretical and actual points, it is plausible to argue that a change in the $H_2S:SO_2$ ratio, from ~1 to between 1.5 and 2, might account for the observed deviation from theoretical $\delta^{34}S$ values in the lower temperature sulphate – sulphide pairs.

One way of producing H_2S, i.e. increasing the $H_2S:SO_2$ ratio, in hydrothermal systems is the hydrolysis of SO_2, which generates more H_2S with decreasing temperature according to the following equation (Ohmoto, 1986):

$$4H_2O + 4SO_2 \rightleftarrows H_2S + 3HSO_4^- + 3H^+$$

The observed changes in $\delta^{34}S$ in both sulphates and sulphides at temperatures <400°C in the Endeavour systems can be adequately explained by proposing an increase in the production of H_2S according to the equation above during the precipitation of LQ sulphates and sulphides.

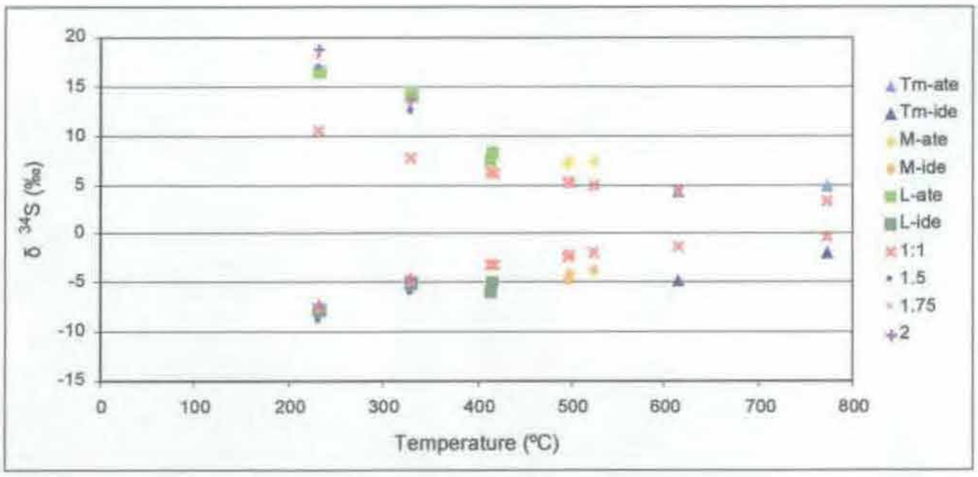

Figure 6.8 A $\delta^{34}S$ vs temperature diagram for actual and theoretical H_2S and SO_2 values for temperatures >400°C and H_2S and SO_4 values for temperatures <400°C based on an initial $\delta^{34}S_{\Sigma S}$ = 1.5‰ and an $H_2S:SO_2$ of 1:1. Tm-ate – TMQ sulphate; Tm-ide – TMQ sulphide; M-ate – MQ sulphate; M-ide – MQ sulphide; L-ate – LQ sulphate; L-ide – LQ sulphide. In addition to an $H_2S:SO_2$ of 1:1, values below 400°C were modelled at ratios of 1.5, 1.75 and 2. Note the good fit for modelled and actual data for $H_2S:SO_2$ ratios of between 1.5 and 2.

6.4.2 Spatial and temporal $\delta^{34}S$ zonation

The mode of the $\delta^{34}S$ values increases with time from EQ through TMQ, THQ/MQ and LQ stage sulphides in the Endeavour deposits (Figures 6.9). At the same time, an overall increase in $\delta^{34}S$ values with increasing distance from the cores of each deposit was detected for several of the paragenetic stages (Table 6.2; Figures 6.2, 6.3, 6.4, 6.5). These patterns are especially pronounced at E26, where although no systematic vertical variation in $\delta^{34}S$ is evident in the core of the deposit, there is a distinct increase in $\delta^{34}S$ towards the periphery of the deposit (Figure 6.5b: Heithersay and Walshe, 1995; Radclyffe, 1995; this study).

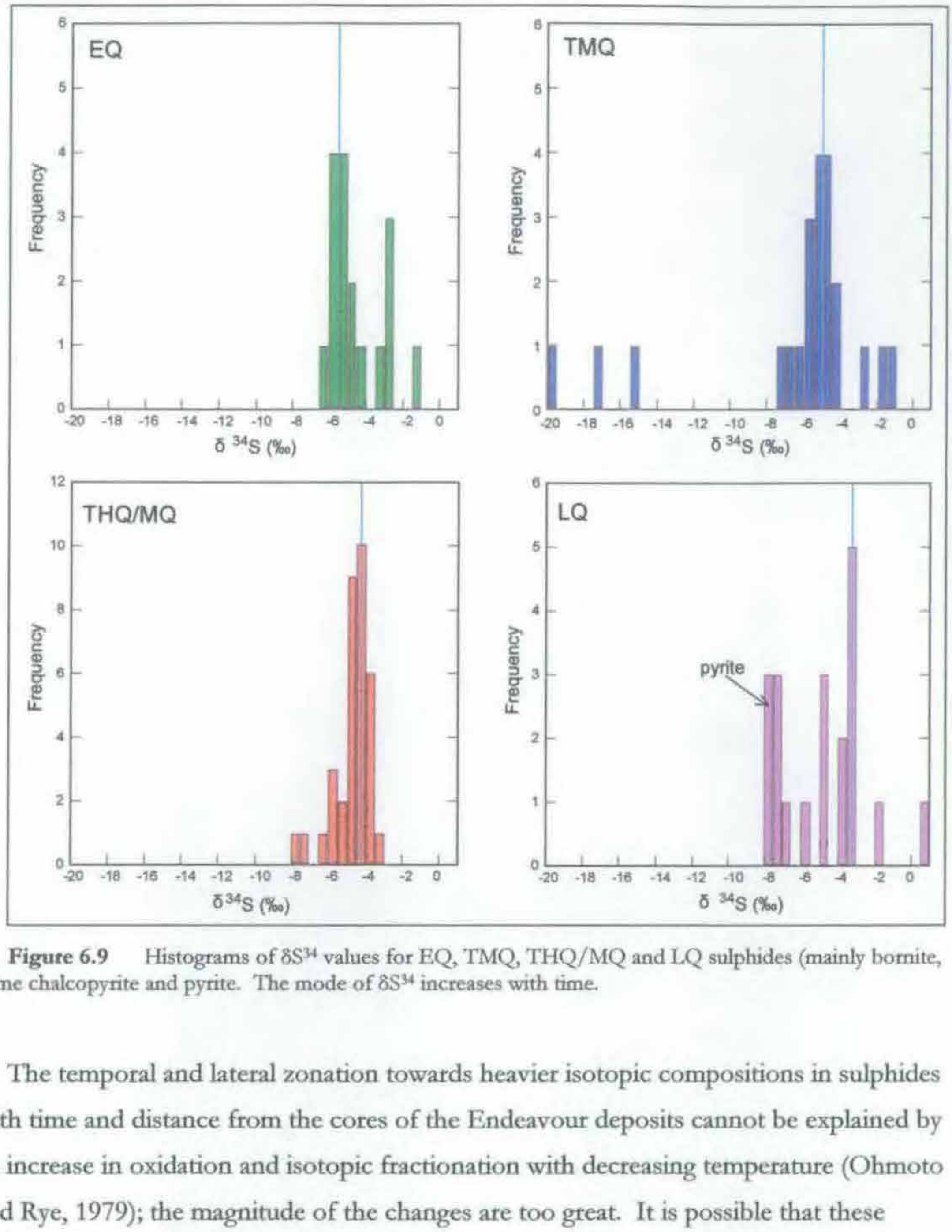

Figure 6.9 Histograms of δS[34] values for EQ, TMQ, THQ/MQ and LQ sulphides (mainly bornite, some chalcopyrite and pyrite. The mode of δS[34] increases with time.

The temporal and lateral zonation towards heavier isotopic compositions in sulphides with time and distance from the cores of the Endeavour deposits cannot be explained by an increase in oxidation and isotopic fractionation with decreasing temperature (Ohmoto and Rye, 1979); the magnitude of the changes are too great. It is possible that these patterns reflect wallrock leaching of isotopically heavy sulphur, and this being incorporated into the magmatic – hydrothermal fluids, which would have its greatest effects on the peripheries of the deposits. Evaporites are the most common source of isotopically heavy sulphur (Taylor, 1987). Since the host rocks to the Endeavour deposits are volcanic sediments and coherent, shallow-level sill-like intrusions of trachyandesitic to rhyolitic composition, the probability of the host volcanic sequences being a supply of heavy sulphur is minimal (although the possibility that seawater sulphate may have been present as pore water cannot be eliminated). Instead, it is more likely that δ^{34}S values in the Endeavour deposits reflect wallrock buffered systems in which oxidising ore fluids reacted with reduced volcanic host rocks. This possibly resulted in a net decrease in isotopic fractionation and consequent increase in $\delta^{34}S$ values as the wallrock to fluid ratio increased with time and distance away from the deposits (cf. section 5.8.3). An alternative explanation could be that the reduction of a small amount of sulphate added isotopically heavier sulphur and increased the isotopic compositions in the late stage sulphides.

The increase in isotopic fractionation vertically towards the top of E26 proposed by Heithersay and Walshe (1995) and Radclyffe (1995) is not confirmed in this study. Instead, there appears to be no systematic vertical zonation to $\delta^{34}S$ values at E26 and E48 and only indistinct vertical zonation at E22 and E27 (Figures 6.2 – 6.5).

6.4.3 Comparison with other deposits

$\delta^{34}S$ values for sulphides from most porphyry deposits are between -5.5 and +6.5‰ (Figure 6.10) and do not appear to be systematically related to either size of deposit, tectonic setting (oceanic vs continental crust) or associated intrusive rock type (Taylor, 1987). The $\delta^{34}S$ values for the Endeavour sulphides range from -19.7 to +0.7‰ with a mean of -5.1‰ and standard deviation of 2.7‰. Sulphates from the Endeavour deposits range between +4.4 and +21.8‰ with a mean of +9.2‰ and standard deviation of 4.2‰. The sulphur isotope compositions of both the sulphides and sulphates are broadly consistent with those of other porphyry deposits.

Of the deposits shown in Figure 6.10, two show a distinctive "negative tail" similar to the one produced by the three very negative $\delta^{34}S$ values from TMQ bornite in this study (Figures 6.1 and 6.9). El Salvador in Chile has sulphide $\delta^{34}S$ values ranging from -10.1 to -0.3‰ (mean -3.0‰) and Galore Creek in British Columbia, Canada, has $\delta^{34}S_{sulphide}$ values ranging from -13 to -7‰ (mean -10‰). The -10.1‰ $\delta^{34}S$ value for El Salvador was reported for isolated, peripheral pyrite from an unaltered rhyolite sample: probably consistent with low temperature fractionation effects (Field and Gustafson, 1976). The very negative $\delta^{34}S$ values at Galore Creek, as with those from several other alkaline-suite related porphyry copper deposits in northern USA and Canada (-2.7 and -8.2‰), have been explained by the incorporation of some sedimentary (biogenic) sulphur (Shannon *et al.*, 1983). Since the very negative $\delta^{34}S$ values of this study are from central, early stage bornite, and there are no marine sediments near the Endeavour deposits to account for the light $\delta^{34}S$ values by wallrock contamination, an alternative explanation is necessary.

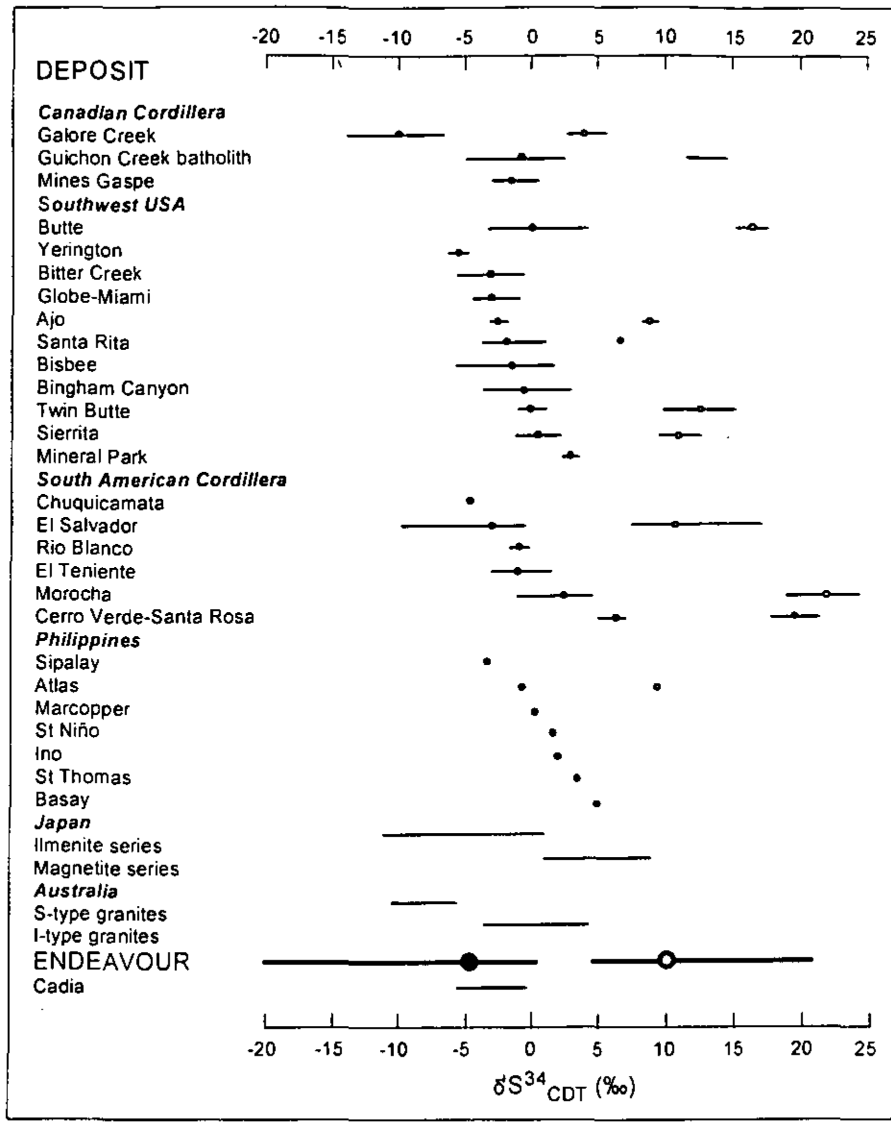

Figure 6.10 A plot of $\delta^{34}S$ for sulphides and sulphates from porphyry copper deposits around the world (compiled from Ohmoto and Rye, 1979 and Taylor, 1987).

There are several possible explanations for the very negative $\delta^{34}S$ values (much lower than the those expected for the deduced $H_2S:SO_2$ ratio ~1:1) of some TMQ sulphides. They may be accounted for by sulphide precipitation from local, atypical batches of hyper-oxidised fluid. Under hyper-oxidised conditions, sulphides acquire abnormally light isotopic compositions (Ohmoto, 1986). Phase separation is one mechanism for forming locally derived hyper-oxidised fluid (Taylor, 1987). Since these sulphides are interpreted to have precipitated at the magmatic – hydrothermal transition, probably in the presence of a volatile-rich aqueous fluid (cf. Chapter 3), it is possible that these very negative $\delta^{34}S$ values reflect sulphide precipitation from local hyper-oxidised ore fluid with $H_2S:SO_2$ ratios much lower than the bulk composition of the magmatic – hydrothermal fluids.

Another way of explaining the very negative $\delta^{34}S$ values of some TMQ sulphides is by the interaction of the ore fluid with intensely haematite-altered wall rocks. Haematite dusting of feldspars is a common feature of all the intrusive rocks associated with the Endeavour deposits. Because most sulphide samples for isotope analysis are from quartz + sulphide veins that crosscut intrusive rocks, strongly negative numbers would be expected for more of the population if interaction with haematite-altered wall rock is to explain this feature. Since only three of the 99 sulphides have these very low $\delta^{34}S$ values, it is unlikely that interaction with haematite-altered rocks caused hyper-oxidation and consequent extreme sulphur isotope fractionation. Although haematite is also an alteration mineral in some assemblages (cf. Chapter 4), the fact that haematite-bearing alteration assemblages post-date TMQ makes it unlikely for haematite to have acted as an oxidant to produce these extremely negative $\delta^{34}S$ values.

The deduced $H_2S:SO_2$ of ~1:1 and $\delta^{34}S_{\Sigma S}$ of ~1.5‰ for the ore fluids of the Endeavour deposits compare well with similar values for these parameters determined for many other porphyry deposits of the world. The two Frieda sub-deposits in Papua New Guinea have $H_2S:SO_2$ ratios of 1:4 and 1:1 and $\delta^{34}S_{\Sigma S}$ of 1 and 2‰ respectively (Eastoe, 1983). St Niño and Atlas porphyry deposits in the Philippines also have $H_2S:SO_2$ ratios of ~1:1, as do several porphyry copper deposits in Chile, e.g. Chuquicamata, El Salvador and Rio Blanco (Sasaki *et al.*, 1984). Field and Gustafson (1976) determined that early anhydrite – chalcopyrite – bornite assemblages at El Salvador were formed from a sulphur reservoir having $\delta^{34}S_{\Sigma S}$ of ~1.6‰. Thus it is evident that the overall $H_2S:SO_2$ ratio of ~1:1 and the $\delta^{34}S_{\Sigma S}$ of ~1.5‰ deduced for the primary ore fluids of the Endeavour deposits are comparable to those of other porphyry deposits.

Spatial and temporal zonation in $\delta^{34}S$ values in sulphides from other porphyry deposits is variable. Spatial zonation in $\delta^{34}S$ in sulphides is not evident at either the Panguna or Frieda porphyry copper deposits in Papua New Guinea (Eastoe, 1983). Sulphides and sulphates from the Sungun porphyry copper deposit in Iran also show no systematic spatial or temporal isotopic variation (Hezarkhani and Williams-Jones, 1998). There is no systemic vertical or lateral zonation in $\delta^{34}S$ values away from the centre of the deposit at the Silver Creek porphyry Mo deposit in Colorado (Wareham *et al.*, 1998). However, at Bingham, Field (1966) concluded that $\delta^{34}S$ values decrease with distance away from the deposit. $\delta^{34}S$ values around porphyry deposits in the western Pacific tend to be zoned towards lighter values away from the cores of deposits (Cooke, 1997), similar to Bingham. The non systematic vertical variation but systematic lateral and temporal decrease in fractionation with time and distance from the centre of the Endeavour systems is most comparable to the $\delta^{34}S$ values in sulphides from the Cadia Ridgeway deposit in New South Wales, Australia, which is also hosted in Ordovician volcanic host rocks. Most sulphides at the Cadia Ridgeway deposit have $\delta^{34}S$ values between -6 and -1‰ and the lateral (and temporal?) zonation have been attributed to increased interaction with reduced wallrock with increasing distance from the deposit (Harper, 2000). It is proposed here that the lateral and temporal increase in $\delta^{34}S$ values in the Endeavour systems possibly resulted from a net decrease in isotopic fractionation and consequent increase in $\delta^{34}S$ values as the wallrock to fluid ratio increased with time and distance away from the deposits.

6.5 Summary

$\delta^{34}S$ values for the Endeavour sulphides range from -19.7 to +0.7‰ with a mean of -5.1‰ and standard deviation of 2.7‰, while those for sulphates range between +4.4 and +21.8‰ with a mean of +9.2‰ and standard deviation of 4.2‰. The isotopic compositions of sulphate – sulphide pairs and temperature estimates from the fluid inclusion study were used to establish that the initial $\delta^{34}S_{\Sigma S}$ of the magmatic – hydrothermal ore fluid was ~+1.5‰. Actual $\delta^{34}S$ values of the sulphate – sulphide pairs were compared with modelled data and the "best fit" H_2S:SO_2 ratio, using the initial $\delta^{34}S_{\Sigma S}$ of +1.5‰, was determined to be ~1 for temperatures >400°C and between 1.5 and 2‰ for temperatures <400°C. The deduced change in H_2S:SO_2 ratio is thought to be due to an increased production of H_2S via the hydrolysis of SO_2 with decreasing temperature.

There is a broad temporal and lateral zonation towards heavier isotopic compositions in sulphides with time and distance away from the cores of the Endeavour deposits. This zonation is attributed to the interaction of oxidised ore fluid with reduced volcanic host rocks, which resulted in a decrease in isotopic fractionation and consequent increase in $\delta^{34}S$ values with time and distance from the ore deposits.

Very negative $\delta^{34}S$ values for some transitional-magmatic sulphides are thought to reflect bornite precipitation from locally developed hyper-oxidised fluids, which led to abnormally light isotopic compositions.

CHAPTER 7

Mineral Chemistry

7.1 Introduction

Volatile elements, particularly F and Cl are important to the formation of magmatic – hydrothermal ore deposits, because the relative concentrations of these halogens can affect a variety of processes, such as the timing of vapour saturation and separation of a volatile-rich aqueous fluid from a melt (Loferski and Ayuso, 1995). Because of their significance, much attention has been given to determining the relative fugacities of F and Cl in magmatic – hydrothermal systems in order to better understand their role on ore-forming processes in these environments (e.g. Munoz and Ludington, 1974; Gunow *et al.*, 1980; Chivas, 1981; Keith and Shanks, 1988). Minerals that incorporate halogens and crystallise with variable F:Cl ratios, such as biotite and apatite, are thus useful indicators of fluid and/or magma compositions if the partitioning behaviour of F and Cl are known. Biotite and apatite are especially useful in this regard because of their occurrence in a wide compositional range of igneous rocks (Loferski and Ayuso, 1995). In addition to halogens, sulphur can also be incorporated into apatite as a sulphate molecule. Thus, as well as providing insight into the halogen evolution in magmas, apatite is useful in monitoring the availability of sulphur during crystallisation (Streck and Dilles, 1998).

The abundances and ratios of F and Cl in biotite and apatite, and the S contents of apatite are used in this chapter to investigate the relationship between the unmineralised regional intrusions in the Goonumbla Volcanic Complex (GVC) and the various mineralised intrusions at E22, E26, E27 and E48. Initially, this chapter discusses the halogen ratios and fugacities of biotite from the four common intrusions to each of the Endeavour deposits, namely BQM, B-QMP, K-QMP and KA-QMP. It also describes the same for hydrothermal biotite associated with the main mineralising events in these systems. Thereafter, the compositions of apatite from the Endeavour-related intrusive rocks and other intrusive rocks within the GVC are presented. The chapter is concluded with a discussion of the implications of these results for the mineralised and unmineralised intrusive rocks of the GVC.

7.2 Biotite

F and Cl occur in biotite by replacing hydroxyl anions according to the following equation (Munoz, 1984):

$$\text{bi(OH)} + \text{HX} \rightleftarrows \text{bi(X)} + H_2O, \text{ where X} = \text{F or Cl}$$

The extent of halogen replacement in micas is governed by 1) the activity of the halogen ion or halogen acid present during crystallisation; 2) the cation population of the octahedral sheet in the biotite crystal; and 3) the temperature of F or Cl for OH replacement (Munoz, 1984). The model equation of halogen exchange in micas given above can be manipulated in such a way that the mole fractions of F, Cl and OH of biotite can be used to calculate the activities of these components in magmas or hydrothermal fluids. Thus, the relative fugacities of HF and HCl of the melts and of the magmatic – hydrothermal fluids may be investigated by studying the F:Cl ratios of primary and secondary biotite respectively.

7.2.1 Methods

All elemental analyses were obtained from polished thin sections using a Cameca SX50 electron microprobe (probe) at the University of Tasmania's Central Science Laboratory. The probe was set with a beam current of 25nA, acceleration voltage of 15kV and spot size of ~5μm and counting times were set to 30 seconds. F and K were analysed first on different spectrometers to minimise alkali and halogen migration. The OH values are calculated based on 11 oxygen formula units.

Probe analyses were obtained from 74 igneous and hydrothermal biotite grains from the four Endeavour deposits (Appendix D1). Of the 74 analyses, 25 are of vein or alteration-related secondary biotite grains, 10 are of biotite inclusions within magmatic – hydrothermal quartz, and the remainder are of primary biotite phenocrysts (30) or of poikilitic biotite inclusions (9) within K-feldspar phenocrysts.

7.2.2 Biotite compositions

Primary magmatic biotites from BQM, B-QMP, K-QMP and KA-QMP intrusions associated with the Endeavour deposits have 1) lower X_{Mg}, [Mg/(Mg+Fe)], Si, and F; 2) variable but generally lower Al^{IV}; 3) erratic Cl; 4) inconsistent but commonly higher

Mn^{+2}; and 5) higher Ti, than hydrothermal biotites specifically related to ore deposition (Figure 7.1). Biotite inclusions have the highest X_{Mg}, Si, and F and lowest Ti composition of all the biotites analysed.

Biotites from BQM, B-QMP and KA-QMP intrusions (n = 29) have a narrow X_{Mg} range from 0.64 to 0.68 (average 0.66). X_{Mg} is generally higher and more variable for hydrothermal biotites (n = 27), with values ranging from 0.68 to 0.76 (average 0.71). Biotites from K-QMP intrusions (n = 5) have X_{Mg} values that straddle the two compositional fields; values range from 0.72 to 0.75 (average 0.73). The highest X_{Mg} values, from biotite inclusions in magmatic – hydrothermal quartz, range from 0.76 to 0.83 (average 0.79).

Atomic proportions of the cations and anions have been calculated according to the structural formula for biotite using 22 oxygen and 4 halogen sites. At a mineral scale, these atomic proportions (atomic percentages) are a better reflection of where certain elements sit in the crystal lattice. Thus atomic percentages (at %) are used for discriminating the different types of biotites rather than weight percentages.

F contents throughout the range of biotite compositions increase steadily with increasing X_{Mg}, from 0.47 at% associated with the lower X_{Mg} to 1.67 at% for the highest X_{Mg} (Figure 7.1c). Similarly, although more scattered, Cl decreases with increasing X_{Mg} from 0.01 to 0.04 at% (Figure 7.1d). The higher F and generally lower Cl with higher X_{Mg} values are interpreted to reflect the crystal-chemical effects referred to "Fe-F" and "Mg-Cl" avoidance respectively (Munoz, 1984).

BQM, B-QMP and KA-QMP intrusion biotites, through K-QMP intrusion and hydrothermal biotites, to magmatic – hydrothermal biotite inclusions, show steadily increasing Si contents (Figure 7.1a), from 5.24 to 6.00 at%, with increasing X_{Mg}. Al^{IV} and Ti decrease with increasing X_{Mg} from 2.00 to 2.76 at% and 0.26 to 0.54 respectively for the same sequence (Figure 7.1e). Mn^{+2} contents of the different types of biotites are variable with increasing X_{Mg} and range from 0.004 to 0.078 at% (Figure 7.1f).

Figure 7.1 Major element and halogen compositions of biotites from the Endeavour deposits. **A** X_{Mg} vs atomic Si; **B** X_{Mg} vs atomic Al^{IV}; **C** X_{Mg} vs atomic F; **D** X_{Mg} vs atomic Cl; **E** X_{Mg} vs atomic Ti and **F** X_{Mg} vs atomic Mn plots for magmatic, inclusion and hydrothermal biotites from the Endeavour deposits. The same biotites are plotted with respect to the **G** F and F/Cl intercept values and **H** the Cl and F/Cl intercept values. See text for details on intercept value calculation parameters.

Legend

- ■ inclusion in THQ
- ¤ phenocryst in B-QMP
- ▲ vein/alteration hydrothermal
- ✚ phenocryst in K-QMP
- • phenocryst in BQM
- ♦ phenocryst in KA-QMP
- o poikilitic inclusion in K-feldspar phenocryst in BQM
- ◇ poikilitic inclusion in K-feldspar phenocryst in B-QMP
- • phenocryst in vein dyke

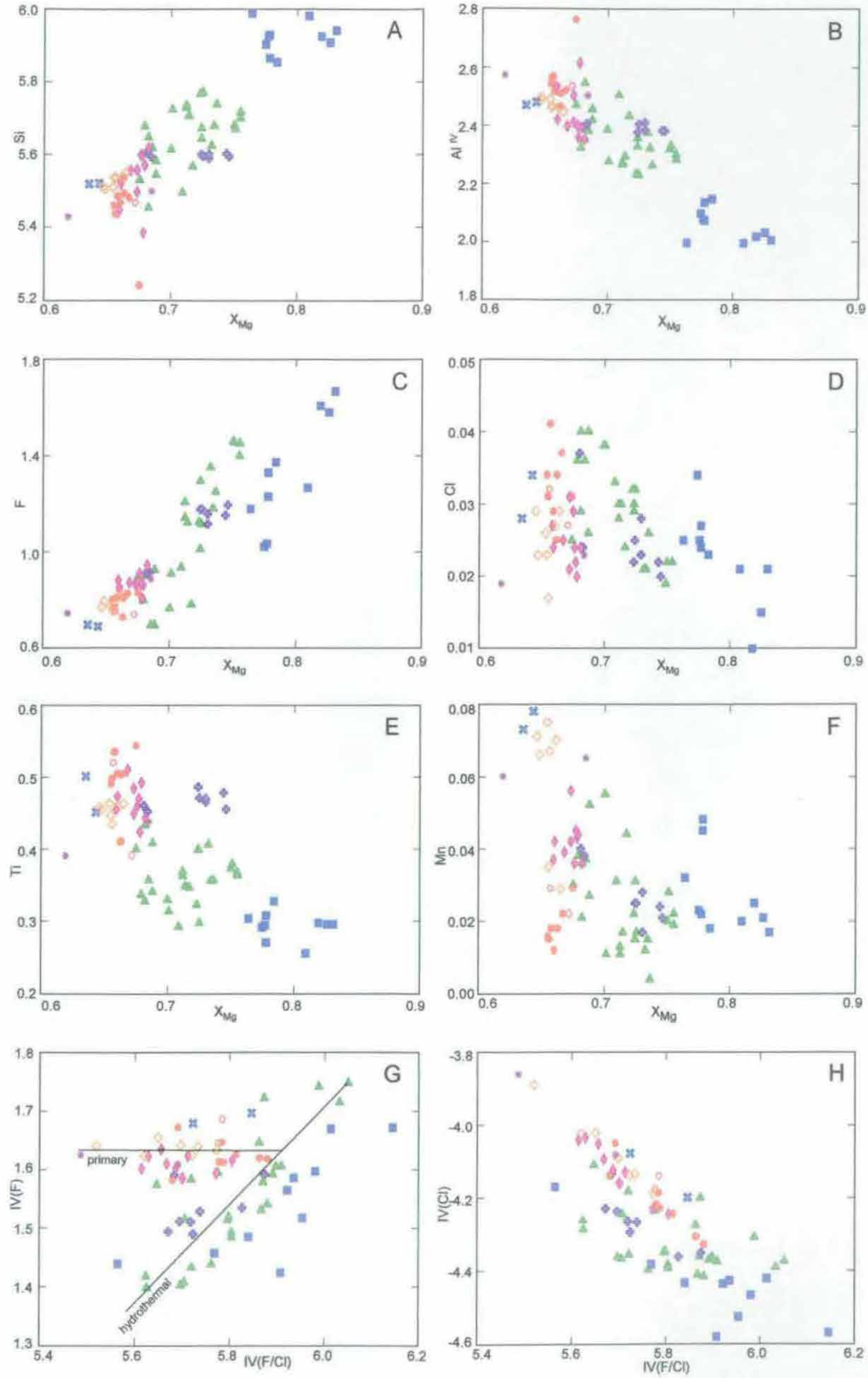
A
Si
X_{Mg}
B
Al IV
X_{Mg}
C
F
X_{Mg}
D
Cl
X_{Mg}
E
Ti
X_{Mg}
F
Mn
X_{Mg}
G
IV(F)
IV(F/Cl)
primary
hydrothermal
H
IV(Cl)
IV(F/Cl)

7.2.3 *Biotite halogen chemistry*

In order to compare the relative enrichment in F and Cl of biotite, Munoz (1984) defined F and Cl "intercept values" to overcome the effects of Fe-F and Mg-Cl avoidance and correct the F content for the Mg:Fe ratio. The F and Cl intercept values are:

$IV(F) = 1.52X_{phlog} + 0.42X_{ann} + 0.20X_{sid} - \log(X_F/X_{OH})$; and

$IV(Cl) = -5.01 - 1.93X_{phlog} - \log(X_{Cl}/X_{OH})$ respectively,

where $X_{phlog} = Mg/\Sigma$ octahedral cations (Al^{VI}); $X_{sid} = [(3\text{-}Si/Al)/1.75](1 - X_{phlog})$; and $X_{ann} = 1 - (X_{phlog} + X_{sid})$ (Gunow *et al.*, 1980): X_F, X_{Cl} and X_{OH} are the mole fractions of these components in the hydroxyl site. The F/Cl intercept value is further defined as IV(F/Cl) = IV(F) – IV(Cl), and because the term for OH is effectively omitted, calculation of IV(F/Cl) is not affected by uncertainties in OH contents, which are difficult to determine in biotite. Note that smaller intercept values for IV(F) correlate with higher degrees of F enrichment, while more negative values for IV(Cl) imply higher degrees of Cl enrichment. Lower IV(F/Cl) correspond to higher F:Cl ratios (Munoz, 1984).

The IV(F/Cl) for all of the biotites analysed range from 5.49 to 6.14 and IV(F/Cl) higher than ~5.9 are restricted to hydrothermal biotites and biotite inclusions (Figures 7.1g and h). Hydrothermal biotites and biotite inclusions also have generally lower IV(F) (1.40 to 1.75) than primary magmatic biotite phenocrysts associated with BQM, B-QMP and KA-QMP intrusions (1.58 – 1.70). IV(F) for magmatic biotites associated with K-QMP intrusions (1.49 – 1.60) are more similar to hydrothermal biotites and biotite inclusions (Figure 7.1g). It is significant that IV(F) for primary biotites define a flat trend with increasing IV(F/Cl), since this indicates progressively decreasing Cl contents in the source fluids (melts). B-QMP, KA-QMP and rare K-QMP biotites show the most depleted Cl levels (Figure 7.1g). In contrast, the IV(F) of hydrothermal biotites and biotite inclusions define a positive slope of ~1, indicating more variable, though typically increasing F and Cl contents in the fluids associated with their formation (Figure 7.1g). It is evident in Figure 7.1h that IV(Cl) for biotites from B-QMP and KA-QMP intrusions are higher (-3.88 to -4.29) than those for biotites from K-QMP and BQM intrusions and hydrothermal biotites and biotite inclusions (-4.07 to -4.48). The higher IV(Cl) for primary biotite phenocrysts from B-QMP and KA-QMP intrusions is consistent with lower Cl concentrations in the source melts, compared to the Cl-rich, lower IV(Cl) fluids that produced the hydrothermal biotites and biotite inclusions.

7.2.4 *Fugacity ratios*

Biotite F and Cl contents can be used to approximate the relative halogen fugacity ratios in the associated magmas or fluids (Munoz, 1992). Figure 7.2a shows compositions of magmatic and hydrothermal biotites as well as biotite inclusions associated with the Endeavour deposits plotted in terms of log $(X_F/X_{Cl})^{bio}$ and X_{phlog}. There is a steady increase in $\log(X_F/X_{Cl})^{bio}$ with increasing X_{phlog} from the magmatic biotites through the hydrothermal biotites to the biotite inclusions (Figure 7.2a). Note, however, that there is a change in slope of the $\log(X_F/X_{Cl})^{bio}$ / X_{phlog} trend from QMP intrusion primary biotites to hydrothermal biotites and biotite inclusions from the Endeavour deposits (Figure 7.2b). The slope steepens from primary, through K-QMP intrusion biotites to hydrothermal biotites and biotite inclusions.

Fugacity ratios for magmatic, inclusion and hydrothermal biotites from the Endeavour systems have been calculated according to the equations of Munoz (1992) above using 700°C for magmatic, 550°C for inclusion and 450°C for hydrothermal biotite (cf. Chapter 5). These equations are:

$$\log (f_{HF}/f_{HCl})^{fluid} = -1000/T(1.22 + 1.65X_{Mg})^{bio} + 0.25 + \log(X_F/X_{Cl})^{bio}$$
$$\log (f_{H2O}/f_{HF})^{fluid} = -1000/T(2.37 + 1.1X_{Mg})^{bio} + 0.43 - \log(X_F/X_{OH})^{bio}; \text{ and}$$
$$\log (f_{H2O}/f_{HCl})^{fluid} = -1000/T(1.15 + 0.55X_{Mg})^{bio} + 0.68 - \log(X_{Cl}/X_{OH})^{bio},$$

where fluid is melt or aqueous fluid, depending on the nature of the biotite, and T is temperature in degrees Kelvin.

Fugacity ratios of magmatic biotites from the BQM, B-QMP and KA-QMP intrusions range from -0.82 to -0.45 for log $(f_{HF}/f_{HCl})^{fluid}$ and from 4.12 to 4.51 for log $(f_{H2O}/f_{HCl})^{fluid}$ respectively (Figure 7.2c). On a similar trend, but at a lower temperature, the biotite inclusions from within magmatic – hydrothermal quartz have marginally lower $(f_{HF}/f_{HCl})^{fluid}$ values (-1.31 to -0.67), but markedly higher log $(f_{H2O}/f_{HCl})^{fluid}$ values (4.50 to 5.00). The lowest log $(f_{HF}/f_{HCl})^{fluid}$ and highest log $(f_{H2O}/f_{HCl})^{fluid}$ values are for hydrothermal biotites, with values ranging from -1.77 to -1.26 and from 4.67 to 4.96 respectively. With the exception of the hydrothermal biotites, biotites from the Endeavour deposits are within a range similar to biotites from Bingham (Selby and Nesbitt, 2000). Magmatic biotites partially overlap the Los Pelambres porphyry Cu deposit biotite compositional field, while the hydrothermal biotites have similar but greater log $(f_{HF}/f_{HCl})^{fluid}$ and log $(f_{H2O}/f_{HCl})^{fluid}$ values than the Deboullie syenite and granodiorite biotites (Loferski and Ayuso, 1995; Selby and Nesbitt, 2000).

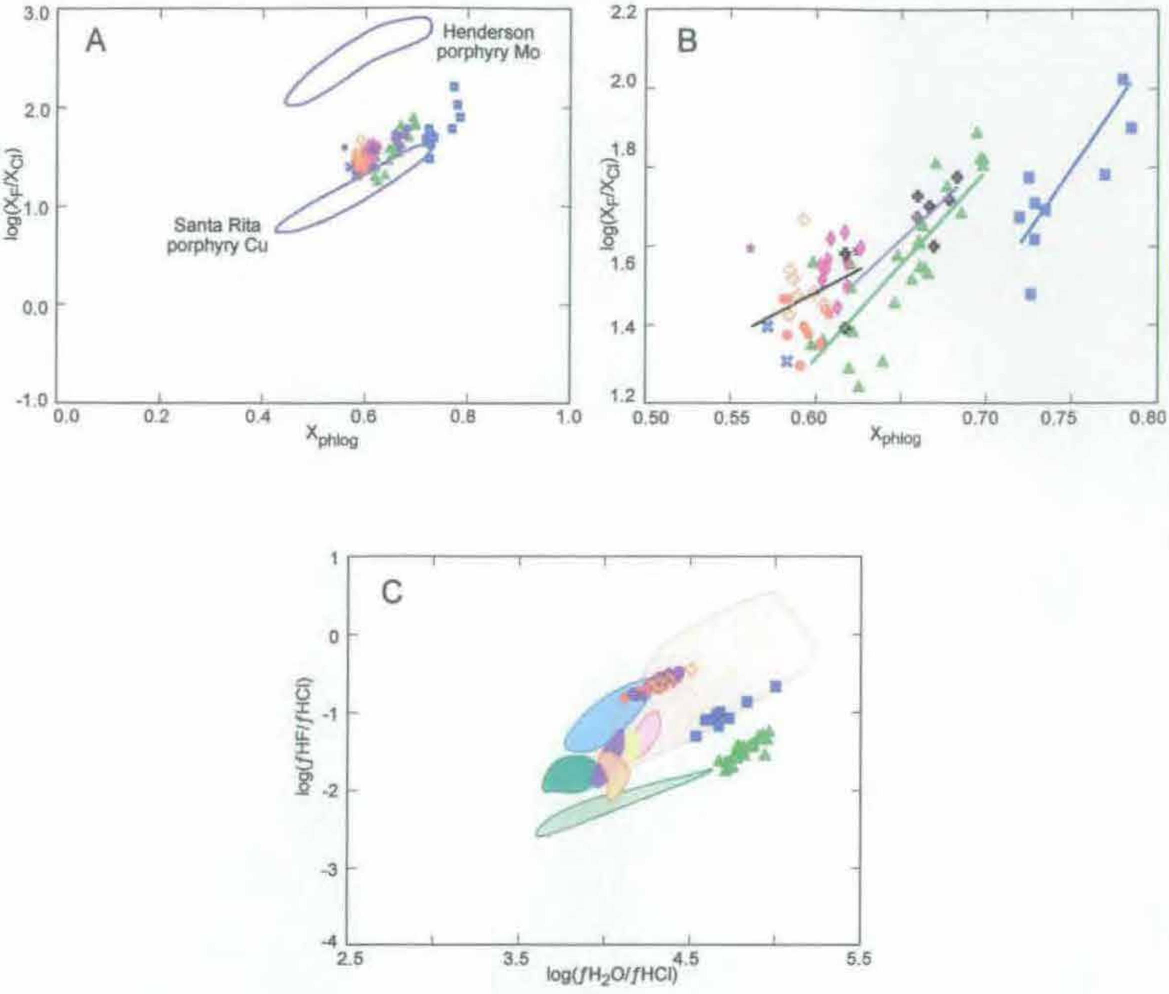

Figure 7.2 **A** Plot showing log (X_F/X_{Cl}) vs X_{phlog} for magmatic, inclusion and hydrothermal biotites from the Endeavour deposits, compared with biotites from Santa Rita and Henderson porphyry deposits (from Loferski and Ayuso, 1995). **B** An enlargement of plot (A), and including trend lines for the various types of biotite. **C** log (fHF/ fHCl) and log (fH_2O/ fHCl) values for the various types of biotite compared with other deposits. Fields for other porphyry deposits are included from Selby and Nesbitt (2000) and references cited therein.

Legend

- inclusion
- phenocryst in B-QMP
- hydrothermal
- phenocryst in K-QMP
- phenocryst in BQM
- phenocryst in KA-QMP
- microphenocryst in K-feldspar phenocryst in BQM
- microphenocryst in K-feldspar phenocryst in B-QMP
- phenocryst in vein dyke

Bingham, USA · Santa Rita, USA · Hanover, USA · Casino, Canada

Babine Lake, Canada · Los Pelambres, Chile · Bakircay, Turkey · Deboullie, USA

7.2.5 Discussion

The chemical characteristics of biotites from the Endeavour deposits are similar to those described for primary and secondary biotites from many other porphyry Cu ± Au ± Mo systems (e.g. Dilles and Einaudi, 1992; Sheets and Nesbitt, 1994; Loferski and Ayuso, 1995; Frei, 1996; Sheets, 1996; Selby and Nesbitt, 2000). Although absolute concentrations of halogens, other elements and X_{Mg} differ widely among the many deposits studied, Selby and Nesbitt (2000) proposed that $X_{Mg} \geq 0.55$ are generally indicative of altered magmatic or hydrothermal biotite. The biotite data for the Endeavour deposits are consistent with this hypothesis.

The change in slope of the IV(F):IV(F/Cl) trend, from broadly flat for most primary QMP intrusion biotites, to ~+1 for hydrothermal biotites and biotite inclusions, is thought to imply a change in the relative F:Cl of the fluids (melts) producing the different biotites. This could be achieved either by the addition of F to, or the removal of Cl from, the respective fluids (melts). The IV(Cl) indicates that primary QMP biotite phenocrysts are the most Cl-depleted, and that hydrothermal biotites and biotite inclusions are the most Cl-enriched. It thus seems reasonable to suggest that the relative decrease in Cl in the magma (and associated relative increase in F) that produced the phenocrysts, and corresponding increase in Cl in the fluid that produced the secondary biotites, reflects the exsolution of a Cl-rich magmatic aqueous phase.

Two K-QMP biotites plot in the IV(F):IV(F/Cl) field for BQM, B-QMP and KA-QMP intrusions, while the remaining K-QMP biotites plot midway between the primary and hydrothermal biotite fields. This is interpreted to imply that a Cl-rich hydrothermal fluid overprinted primary, Cl-poor biotite phenocrysts during the formation of the Endeavour deposits; this fluid is taken to be that which produced the relatively Cl-rich hydrothermal biotites and biotite inclusions presented here.

Thus the primary biotite phenocrysts from the QMP intrusions directly associated with the Endeavour deposits are thought to record the evolution a Cl-rich magmatic – hydrothermal fluid that overprinted some of the existing primary biotites in the K-QMP intrusions and crystallised relatively Cl-rich secondary biotites and Cl-rich and F-rich biotite as inclusions in magmatic – hydrothermal quartz (cf. section 5.6).

7.3 Apatite

Apatite, a mineral that is highly resistant to weathering, alteration and diffusion processes (Peng *et al.*, 1997), is ubiquitous in both the volcanic and igneous rocks of the GVC. Sulphur can be accommodated in apatite because of a coupled substitution reaction of Si and S for P (Rouse and Dunn, 1982). Frei (1996) concluded that magmatic S content and magmatic fO_2 are the major controls on the SO_3 content in igneous apatite, since apatite can incorporate oxidised sulphur from the melt into its lattice. Streck and Dilles (1998) demonstrated that individual apatite grains from the Yerington batholith were consistently zoned from SO_3-rich cores to SO_3-poor rims. They proposed that the notable drop in SO_3 towards the rims of apatite crystals was due to a competition for SO_3 that developed in the melt once anhydrite crystallisation commenced after the magma had cooled significantly. Because of its sulphur-bearing capacity, and because sulphur is an essential component of magmatic – hydrothermal fluids, apatite is an especially useful mineral to study in an attempt to unravel volatile evolution in porphyry systems.

F, Cl and OH are essential components of apatite. In a similar way to how F, Cl and OH compositions can be studied in primary and secondary biotites, these components have been studied in apatites in an attempt to understand the evolution of magmatic volatiles in the Endeavour systems. S contents of apatites have also been studied in this regard. In addition to studying apatites from the intrusions associated with mineralisation, apatites from regional unmineralised volcanic and intrusive rocks of the GVC have been studied for comparative purposes.

7.3.1 Methods

Four hundred and fifty-two probe analyses were obtained from 158 grains of apatite from the GVC (Appendix D2; Figure 7.3). Four types of apatite have been distinguished: 1) primary apatite phenocrysts from ore-related intrusions, host volcanic rocks and regional intrusive rocks (120 grains; 387 analyses); 2) secondary apatites in quartz veins from the Endeavour deposits (17 grains; 29 analyses); 3) apatite inclusions in K-feldspar, hornblende or sphene phenocrysts from regional and ore-related intrusions (5 grains, 18 analyses); and 4) apatite inclusions in magmatic – hydrothermal quartz (THQ) associated with K-QMP intrusions (16 grains, 18 analyses).

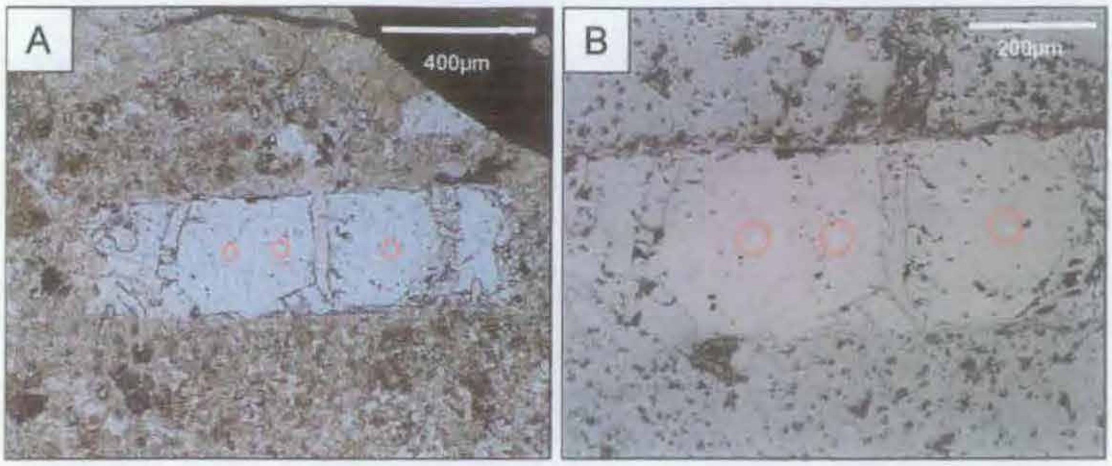

Figure 7.3 **A** Photomicrograph of a typical primary apatite phenocryst in ppl; E48/4/3, and **B** the same grain at twice the magnification in reflected light. Red circles highlight probe marks.

All elemental analyses were obtained from polished thin sections using a Cameca SX50 microprobe at the University of Tasmania's Central Science Laboratory. Because analysing elements such as Na, F, Cl, etc., in apatite accurately on the electron microprobe can be problematic (Stormer *et al.*, 1993), several precautionary measures were taken to ensure data integrity:

- microprobe analyses were restricted to apatite crystals oriented in thin section parallel to the c-axis;
- F, Na, Cl, Ca and Mn were analysed using a 15nA beam current, a 20kV acceleration voltage and a ~10µm nominal spot size; all remaining elements were analysed using a 60nA beam current, a 25kV acceleration voltage and a ~5µm nominal spot size; and
- F, Cl and Na were analysed first to minimise halogen loss and alkali migration respectively.

7.3.2 Apatite compositions

7.3.2.1 Apatites from the intrusions related to the Endeavour deposits

As a result of apatite being a more robust mineral than biotite, apatite has been better preserved in the prehnite – pumpellyite facies metamorphosed regional volcanic and intrusive rocks of the GVC (cf. Chapter 2). In light of this, a comparative study of apatites has been undertaken to establish whether apatites associated with the mineralised intrusions are chemically distinct from apatites in the unmineralised regional intrusive and volcanic rocks of the GVC.

Because of the broad ranges in composition and overlaps in compositional fields for the different apatites, the remaining description focuses initially on coupled substitution reactions that can occur in all apatites. It then goes on to compare the compositions of apatites from the intrusions associated with mineralisation, B-QMP, K-QMP and KA-QMP, and apatites of regional intrusive and volcanic rocks.

7.3.2.2 Coupled substitution reactions

The SO_3 concentrations of apatites from intrusive and volcanic rocks of the GVC range from <0.01 to 1.15wt% (Figure 7.4a), spanning almost the entire range of previously reported SO_3 concentrations for apatites in felsic igneous rocks (Streck and Dilles, 1998). For the majority of apatites analysed, there is a steady increase in SO_3 with increasing SiO_2. This broadly linear relationship between S and Si is also evident on a plot of atomic S vs Si (Figure 7.4b), and is consistent with the incorporation of sulphur into the apatite crystal structure according to the coupled substitution reaction $S^{+6} + Si^{+4} \rightleftharpoons 2P^{+5}$ (Rouse and Dunn, 1982; Streck and Dilles, 1998). However, if the S content of apatite is controlled solely by the $S^{+6} + Si^{+4} \rightleftharpoons 2P^{+5}$ substitution reaction, an intercept of 0 and a slope of 1 is expected. Thus the trend of S:Si on Figure 7.4b, intercepting the y-axis at 0.03 and having a slope of <1, is interpreted to imply that the above substitution reaction is not the only factor affecting the S content of apatites in the GVC rocks.

Two other coupled substitution reactions are thought to influence the S:Si ratio in apatite; $REE^{+3} + Si^{+4} \rightleftharpoons Ca^{+2} + P^{+5}$ (Rønsbo, 1989) and $S^{+6} + Na^{+} \rightleftharpoons P^{+5} + Ca^{+2}$ (Liu and Comodi, 1993), where REE = rare earth elements. The significance of the latter exchange reaction, which is particularly important for higher S concentrations (Liu and Comodi, 1993), is supported by the positive correlation between S and Na in apatites from the GVC (Figure 7.4c). Thus, considering all three coupled substitution reactions, a combined correlation expression can be written: $S \approx Si - REE^{+3} + Na$ (Streck and Dilles, 1998). Using Ce as a proxy for REE because its concentration is approximately half of the total REE concentration in igneous apatite (Rønsbo, 1989), this correlation expression can be rewritten as $S^* \approx Si - Ce + Na$ (Streck and Dilles, 1998). When S* for each GVC apatite analysis is plotted against S, the slope is ~1 (Figure 7.4d). This feature was suggested by Streck and Dilles (1998) to confirm that the correlation expression of S* closely resembles actual behaviour of these elements in apatite.

Figure 7.4 Compositions of apatites from mineralised intrusive rocks and unmineralised intrusive and volcanic rocks of the GVC.

A SO_3% vs SiO_2% for all analysed GVC apatites: Condobolin Road monzodiorite (▲); Wombin intrusion (♦); Gunningbland Forest monzonite porphyry intrusions (◇); zero porphyry(+); primary (○), secondary (★) and inclusion (■) apatite. **B** Atomic S vs Si; **C** Atomic S vs Na and **D** Atomic S vs S* (Si-Ce+Na) plots of all analysed GVC apatites. **E** Atomic S vs Na with the intrusions specified, see legend below. **F** Select analyses showing per grain variation from 1) E48 host Wombin Volcanics - E48/18/168.3 (◊ ♦); 2) E27 BQM, E27/58/1; 3) E27 B-QMP, E27/64/b; 4) E48 KA-QMP, E48/4/3 and 5) E48 K-QMP, E48/11/5. **G** Select analyses showing per sample variation from 1) E26 BQM, E26/14; 2) E27 B-QMP, E27/64; 3) E22 KA-QMP, E22/26 and 4) E48 K-QMP, E48/11. **H** All B-QMP apatites from E22 and E27. For E, F, G and H - open symbols represent rim analyses whereas filled symbols represent core analyses.

Legend

■ apatite inclusions	□ secondary apatites	○● primary B-QMP apatites
✱● primary K-QMP apatites	+● primary KA-QMP apatites	⌘✖ primary BQM apatites
★ primary E26 monzodiorite	◇♦ primary zero porphyry apatite	☆ aplite (for E only)
◇ Gunningbland Forest, Cooks Myalls and Woods		

compositional field for apatites from the Condobolin Road monzodiorite
compositional field for apatites from Wombin Volcanics
compositional field for apatites from a Wombin intrusions
compositional field for apatites from BQM intrusions
compositional field for apatites from zero porphyries

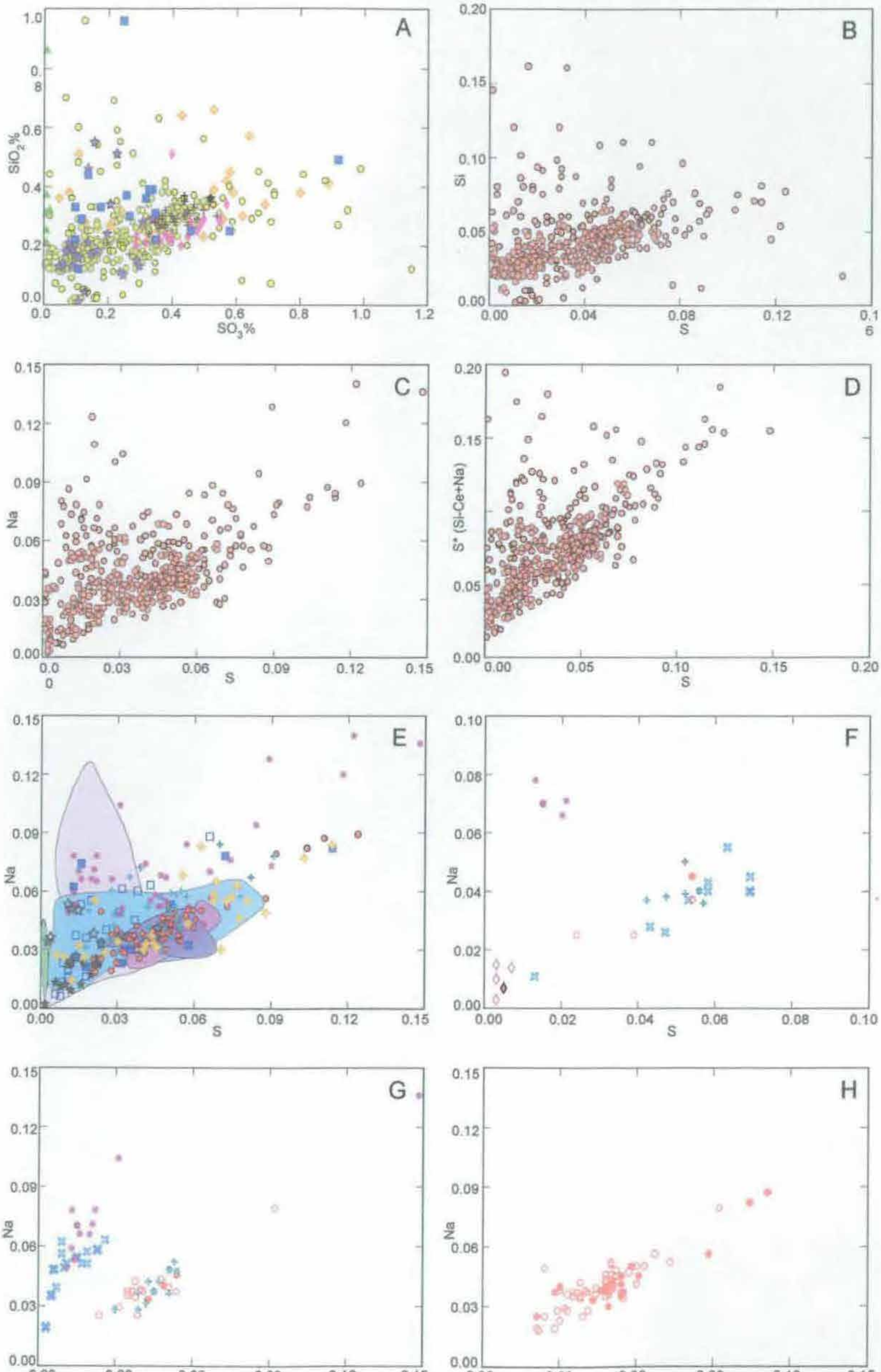
A
SiO_2%
SO_3%
B
Si
S
C
Na
S
D
S* (Si-Ce+Na)
S
E
Na
S
F
Na
S
G
Na
S
H
Na
S

7.3.2.3 Comparison with regional volcanic and intrusive rocks of the GVC

Apatites from intrusive rocks within the Wombin Volcanics overlap entirely the S and Na compositions of apatite from the BQM intrusions associated with the Endeavour deposits (Figure 7.4e). In contrast, apatite from the Condobolin Road monzodiorite (cf. Figure 2.5) intrusion in the Nelungaloo Volcanics has markedly lower S contents than other apatites in the GVC. Apatites from Wombin Volcanics, which host the Endeavour deposits, have lower S and higher Na contents than most other apatites analysed, whereas apatites from the ore-related QMP intrusions are characterised by higher S and Na contents (Figure 7.4e). It is interesting to note that the S and Na compositions of apatites from the Gunningbland Forest, Cooks Myalls and Woods (in order of decreasing S content) monzonite porphyry intrusions overlap entirely those of apatites from the B-QMP and KA-QMP intrusions and partially overlap those of the zero porphyries of E26 (Figure 7.4e). The apatites from the monzodiorite intrusion at E26 have low S and Na contents, whereas those from the zero porphyries of E26 have similar Na, but lower S contents than those from the QMP intrusions associated with mineralisation (Figure 7.4e). Secondary apatites have similar S and Na compositions to apatites from K-QMP intrusions. However, in contrast, apatite inclusions within magmatic – hydrothermal quartz span much of the S and Na range for apatites from the GVC as a whole.

Streck and Dilles (1998) reported a marked decrease in S from the cores to the rims of individual apatite grains within the Yerington batholith. A similar line of investigation was undertaken on apatite grains within the GVC rocks, and although most individual grains analysed show variation in S content (Figure 7.4f), the distinct zoning described by Streck and Dilles (1998) is not a common feature of GVC apatite. In addition, the variation in the S content of different apatite grains within a given sample (Figure 7.4g), and within a given intrusion type (e.g. B-QMP; Figure 7.4h), is inconsistent.

Apatites from intrusions directly associated with ore deposition at the Endeavour deposits are characterised by higher F:Cl ratios (~20 – 40) than apatites from other intrusive and volcanic rocks within the GVC (~20; Figure 7.5a). Apatite inclusions in magmatic – hydrothermal quartz have similar F:Cl ratios to secondary apatites, which are within the lower range of F:Cl ratios for the GVC apatites (~20; Figure 7.5a). The compositions of apatites from E22, E26, E27 and E48 ore-related intrusions are compared to apatites from the zero porphyries of E26 and the regional Gunningbland Forest, Cooks Myalls and Woods monzonite porphyry intrusions in Figures 7.5b, c, d and e respectively.

Figure 7.5 Compositions of apatites from mineralised intrusive rocks and unmineralised intrusive and volcanic rocks of the GVC.
A Atomic S vs F:Cl for all apatites analysed in the GVC rocks: Condobolin Road monzodiorite (▲); Wombin intrusion (♦); Gunningbland Forest, Cooks Myalls and Woods monzonite porphyry intrusions (◇); zero porphyry intrusions (+); primary (∘), secondary (☆) and inclusion (■) apatites. **B** Intrusions specific atomic S vs. F:Cl for E22, **C** E26, **D** E27 and **E** E48 - see legend below. For E48, all BQM analyses that fall within the regional monzonite porphyry field are from one sample; E48/17. **F** Plot of atomic S vs Cl for all GVC apatites analysed (see legend below). **G** Atomic F:Cl vs F^{+3} for all apatites analysed in the GVC rocks; and **H** Atomic F^{+3} vs F for apatites from selected intrusions as well as hydrothermal apatites and apatite inclusions.

Legend

- ■ apatite inclusions
- ▫ secondary apatites
- • primary B-QMP apatite
- * primary K-QMP apatite
- + primaryKA-QMP apatite
- ✖ primary BQM apatite
- ★ primary E26 monzodiorite
- ☆ primary aplite apatite
- ◊ primary volcanic apatite
- ◇ Gunningbland Forest, Cooks Myalls and Woods
- ♦ Wombin intrusion (H only)

compositional field for apatites from the Condobolin Road monzodiorite
compositional field for apatites from Wombin Volcanics
compositional field for apatites from a Wombin intrusions
compositional field for apatites from BQM intrusions
compositional field for apatites from zero porphyries

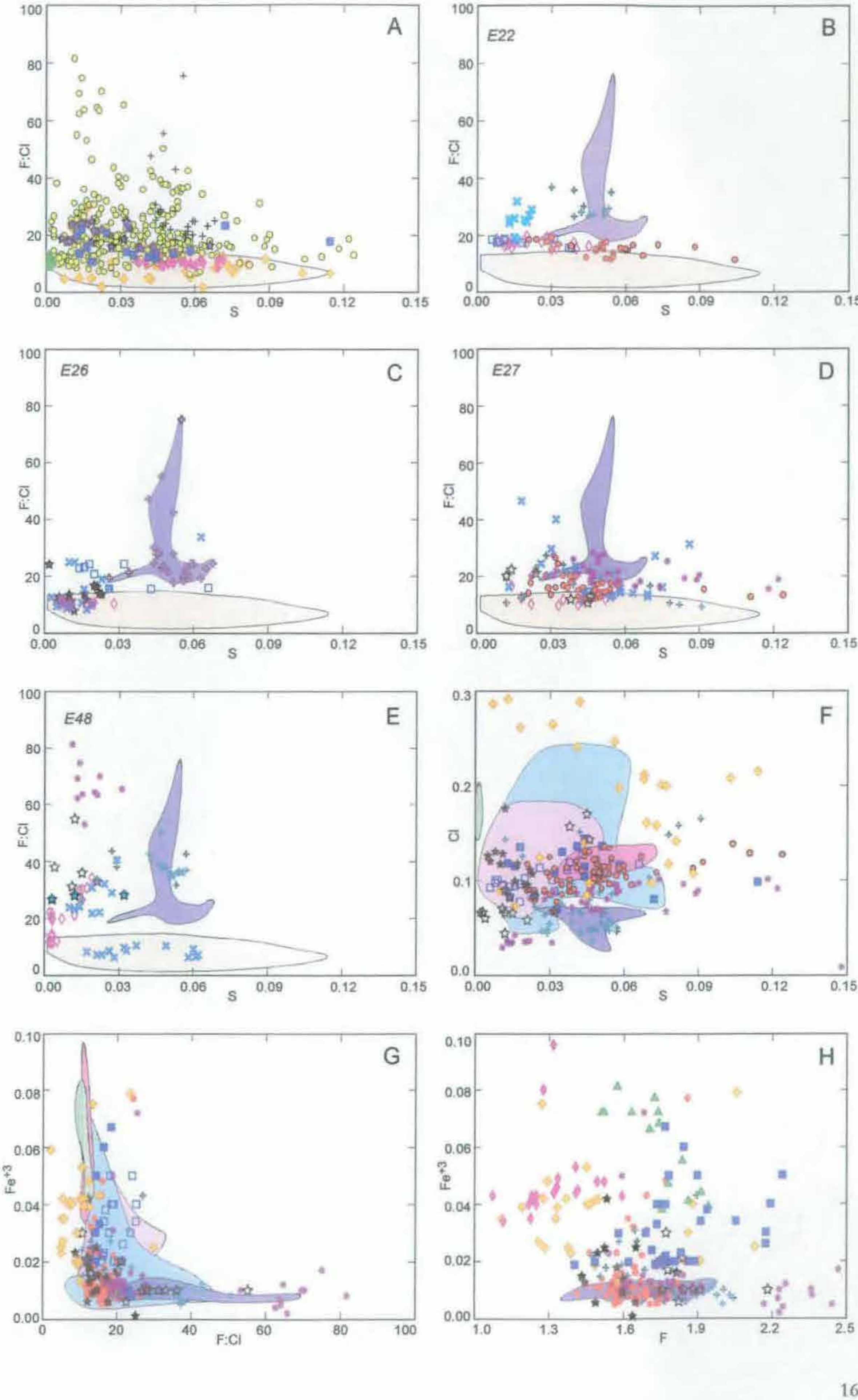
A
B
E22
C
E26
D
E27
E
E48
F
G
H
F:Cl
S
Cl
Fe+3
F

There is a notable increase in the F:Cl ratio in apatites from the E48 intrusions compared with the same ratio in apatites from E22, E26 and E27 intrusions. Apatites from K-QMP rocks at E48 have F:Cl ratios up to 80 (Figure 7.5e). The F:Cl ratios of apatites from the zero porphyry intrusions of E26 are indistinguishable from apatite from the Endeavour-related intrusions. Apatites in the regional monzonite porphyry intrusions have distinctly lower F:Cl ratios than apatites in the ore-related intrusion, which reflects either a relative increase in Cl or a decrease in F contents. A plot of S vs Cl illustrates that the likely cause for lower F:Cl ratios in apatite from the regional monzonite porphyries is a relative increase in Cl (Figure 7.5f).

The Fe^{+3} contents of apatites from the various GVC volcanic and intrusive rocks vary with F:Cl and F contents (Figure 7.5g and h). It is evident that apatites from B-QMP, K-QMP and KA-QMP intrusions associated with the Endeavour deposits typically have Fe^{+3} contents of <0.01 at%, whereas apatites in the host volcanic rocks, the BQM and the regional Gunningbland Forest and Cooks Myalls monzonite porphyry intrusions have Fe^{+3} contents from 0.02 to 0.08 at% (Figure 7.5g). Also, secondary apatites and apatite inclusions within magmatic – hydrothermal quartz are distinctly Fe-rich (0.02 – 0.08) compared to primary apatites in the Endeavour-related intrusions. Note that in addition to being Fe-rich, many of the hydrothermal apatites are Cl-rich as well.

In summary, compositional ranges for the different groups of apatites are typically broad and overlapping. Nonetheless, three characteristics discriminate apatites from the QMP intrusions associated with the Endeavour deposits, B-QMP, K-QMP and KA-QMP, from those in the regional unmineralised intrusive and volcanic rocks of the GVC, including the BQM intrusions:

1) S and Na contents are typically higher in apatites from mineralised intrusions;
2) Apatites from the mineralised QMP intrusions have higher F:Cl ratios and lower Fe^{+3} contents than other rocks; and
3) Secondary apatites associated with alteration and veining in the Endeavour deposits, have lower F:Cl ratios and higher Fe^{+3} contents than primary apatite phenocrysts in the QMP intrusions; characteristics similar to apatites from regional volcanic and intrusive rocks from the GVC.

7.3.3 Discussion

Frei (1996) suggested that apatite SO_3 contents could be used as a vector to ore deposits, with high (>0.2wt%) SO_3 indicating potentially mineralised rocks. His proposal is not strongly supported by the data from this study. This is mainly because apatites from the Gunningbland Forest and Cooks Myalls monzonite porphyries, intrusions that are not associated with known mineralisation, also have high SO_3 contents. In addition, apatites from the zero porphyries of E26 are indistinguishable in terms of SO_3 contents, from other intrusions associated with mineralisation at the Endeavour deposits, e.g. KA-QMP. In fact, high SO_3 contents are anticipated for the zero porphyries since they contain anhydrite phenocrysts (cf. section 3.4.5).

Unlike Streck and Dilles (1998), who showed distinct zoning in individual apatite grains, GVC apatites are not zoned with respect to SO_3. Instead, the F:Cl ratio distinguishes apatites from ore-related and unmineralised intrusions. The results thus indicate that S-enrichment in apatite is not unique to the ore-related intrusions, despite the fact that sulphide ores formed at the Endeavour deposits. Since Cl is inferred to be higher in apatites from the regional monzonite porphyry intrusions, and typically lower in apatites from the ore-related intrusive rocks, the change in F:Cl probably indicates a relative increase in F in the ore-related apatites compared to the regional intrusive and volcanic apatites. This relative increase in F of the ore-related apatites is possibly an effect of fractionation, since the regional intrusive rocks are not as fractionated as those associated with the Endeavour deposits (Chapter 8) and the F:Cl of a melt will increase with increasing fractionation (Taylor and Fallick, 1997).

When whole rock geochemistry is taken into account (cf. Chapter 8), it is evident that the least evolved intrusive rocks within the Wombin Volcanics, the regional Woods slightly more fractionated Gunningbland Forest and Cooks Myalls monzonite porphyry intrusions, contain apatites richest in Cl and Fe^{+3}, and that the more evolved intrusions, those associated with the Endeavour deposits, contain apatites poorest in Cl and Fe^{+3}. Similar whole rock geochemistry and other characteristics were interpreted by Loferski and Ayuso (1995) and Dilles (1987) to indicate that the decrease of Cl in apatites from intrusions with increasing SiO_2 and decreasing Fe_2O_3 contents, reflects a decrease in Cl with increasing fractionation/differentiation. Other porphyry complexes (e.g. Sheets and Nesbitt, 1994; Sheets, 1996) also show a decrease in Cl content in apatite with increasing F, which is in accord with Lang *et al.* (2001), who suggested that Cl drops markedly in apatites with increasing fractionation/differentiation. Dilles (1987) proposed that because Cl preferentially partitions into magmatic fluids, the decrease of Cl in apatites from increasingly fractionated intrusions was due to the evolution of greater and greater amounts of aqueous magmatic fluid.

Dilles (1987) described the F and Cl contents of biotites and apatites from the Yerington batholith. He showed that F in these minerals is generally high in intrusions associated with mineralisation relative to the surrounding stocks, and increases with increasing Si contents; trends that are mimicked by apatites from the GVC. In contrast, Cl contents of biotites and apatites from the Yerington batholith are low relative to the surrounding rocks, and decrease with increasing Si contents. At magmatic temperatures, Cl preferentially partitions into volatile-rich aqueous phases relative to granitic magma (Kilinc and Burnham, 1972), whereas F partitions into magma (Burnham, 1979). Because of these features, Dilles (1987) ascribed a decreasing Cl:F trend in Yerington batholith apatites to a trend of evolution of increasing amounts of magmatic aqueous fluid during crystallisation (and fractionation), as proposed in a more general sense by Candela (1983).

Since Cl readily partitions into the aqueous phase at magmatic temperatures and Cl decreases in apatites from increasingly fractionated intrusions within the Endeavour systems, it is proposed here that the decreasing Cl through the B-QMP, KA-QMP to K-QMP records the evolution of a Cl-rich fluid from the parent magma that produced the QMP complexes of the Endeavour deposits. The increased Fe^{+3} and Cl contents of apatites from the Gunningbland Forest and Cooks Myalls and to a lesser extent Woods monzonite porphyries is interpreted here to imply two things. First, the magma that generated these intrusions did not fractionate to the same degree as those associated with the Endeavour deposits and thus had excess Fe^{+3} available to the melt crystallising apatite. Second, the magma had not yet exsolved a Cl-rich aqueous fluid and thus retained Cl, which was then incorporated into apatite.

It is inferred from the above discussion that the magmas associated with the QMP intrusions of the Endeavour deposits had elevated F contents. Elevated F contents increase the H_2O solubility of a melt (Holtz *et al.*, 1993), decrease the liquidus temperature of a melt (Dingwell, 1988) and decrease the melt viscosity (Dingwell *et al.*, 1993). Thus, as predicted by Taylor and Fallick (1997), F serves as a catalyst for the production of small volumes of unusually low viscosity felsic magma that can fractionate further than is typical of felsic magmatic systems. It is considered here that the elevated F contents of the QMP parent magma facilitated the formation of relatively small volumes of highly fractionated melt to form the QMP intrusions central to the Endeavour deposits. These concepts are discussed in detail in Chapter 8.

7.4 Summary

Biotites from the intrusions associated with the Endeavour deposits show a steady increase in Si and decrease in Ti and Al^{IV} with increasing Mg/Mg+Fe (X_{Mg}). The high X_{Mg} for many of the biotites is consistent with biotites from several other porphyry copper deposits. The F and Cl contents of biotite from the these intrusions indicate that the melt from which they were produced was depleted in Cl and enriched in F relative to the Cl-rich magmatic – hydrothermal fluid that produced Cl-rich secondary biotite. The Cl-rich magmatic – hydrothermal fluid most likely Cl-enriched many of the primary biotites in the ore-related K-QMP intrusions.

Apatites directly associated with the Endeavour deposits are characteristically enriched in S, Si and Na relative to the host Wombin Volcanics and other rocks from the GVC. They are, however, similar in composition to apatites from unmineralised regional intrusions such as the Gunningbland Forest monzonite porphyry. In addition to being enriched in S, apatites directly associated with the Endeavour intrusions have higher F:Cl ratios than apatites from other intrusive and volcanic rocks in the GVC. It is likely that the lower F:Cl ratios in apatites from regional intrusive rocks are a function of higher Cl contents. Apatites from regional intrusive and volcanic rocks of the GVC are relatively enriched in Fe compared to those from intrusive rocks directly associated with the Endeavour deposits. This Fe enrichment is also evident in secondary apatites and apatite inclusions within magmatic – hydrothermal quartz. Overall, the Cl-rich character of secondary biotite and apatite in the QMP complexes is consistent with the evolution of a Cl-rich magmatic – hydrothermal fluid from the crystallising intrusions.

CHAPTER 8

Geochemistry and Petrogenesis

8.1 Introduction

How do the intrusions associated with mineralisation at the Endeavour Cu-Au porphyry deposits different from unmineralised intrusions elsewhere in the region? Volcanic and intrusive rocks from the GVC west of the Parkes Thrust, extending from south of Nelungaloo to west of Peak Hill (cf. Figure 2.5), have been studied geochemically in an attempt to answer this question. Rocks in the GVC east of the Parkes Thrust are not included in this discussion; these are described in detail in Crawford (2001b).

The 281 whole rock XRF major element and XRD trace element analyses listed in Appendix E1 come from numerous sources. Clarke (1990), Heithersay (1991), Müller *et al.* (1994), Blevin and Morrison (1997), Crawford *et al.* (2001), *Northparkes Mines* and various Honours theses (Squires, 1992; Hall, 1993; Wolfe, 1994; Radclyffe, 1995; Howland-Rose, 1996; Harris, 1997) provided data for most of the regional volcanic and intrusive rocks. Most of the whole rock analyses for intrusive rocks associated with Endeavour deposits are from samples collected by the author (n = 56), with a further 15 from Blevin and Morrison (1997) and a few from various Honours theses (Squires, 1992; Wolfe, 1994; Radclyffe, 1995). In addition to whole rock XRD and XRF analyses, solution ICP-MS whole rock rare earth element analyses were conducted at the University of Tasmania on 23 ore-related intrusive rocks collected by the author and 22 regional intrusive and volcanic rocks sampled by Crawford *et al.* (2001); these results are presented in Appendix E2. Pb isotope data are from Carr and Dean (1990), Carr *et al.* (1995) and Kolkert (1998). Reconnaissance Sr-Nd data comes from Whitford *et al.* (1992). Pb and reconnaissance Sr-Nd isotope data is compiled in Appendix E3. Additional Nd data comes from Crawford *et al.* (2001).

Initially, this chapter details the geochronology of the GVC. It then goes on to describe the whole rock major and trace element geochemistry of the regional volcanic and intrusive rocks in the GVC before describing the same for the intrusive rocks associated with the Endeavour deposits. A study of the rare earth element abundances in the ore-related and regional GVC rocks, and an assessment of existing radiogenic isotope data conclude the chapter.

8.2 Geochronology

Radiogenic isotopic dating of rocks from the GVC is limited. Available ages are summarised in Table 8.1

Table 8. 1 A summary of the dating work done for intrusive rocks of the GVC. * is interpreted to be a Wombin intrusion rather than a Nelungaloo intrusion (as interpreted by Perkins *et al.*, 1990). Sample numbers, e.g. E26/287/220.6m, pertain to Deposit/drillhole/depth; (p) – primary phenocryst; (s) – secondary phase; [1] denotes a correlation age, [2] a plateau age, [3] an integrated age and [4] a maximum age.

Sample	*Mineral*	*Method*	*Age (Ma)*	*Reference*
Alteration/mineralisation	Sericite	$^{40}Ar/^{39}Ar$	439.2 ± 1.2	Perkins *et al.*, 1990
Wombin intrusion *	Zircon	U-Pb (SHRIMP)	438.5 ± 3.6	Perkins *et al.*, 1990
Condobolin Road monzodiorite	Zircon	U-Pb (SHRIMP)	484.3 ± 2.9	Butera *et al.*, 2001
Goonumbla Siding monzodiorite	Zircon	U-Pb (SHRIMP)	450.8 ± 4.2	Butera *et al.*, 2001
Wombin intrusion	Zircon	U-Pb (SHRIMP)	438.9 ± 4.7	Butera *et al.*, 2001
Wombin intrusion	Zircon	U-Pb (SHRIMP)	439.1 ± 4.5	Butera *et al.*, 2001
E37 Zero porphyry	Zircon	U-Pb (SHRIMP)	437 ± 6.0	Crawford *et al.*, 2001
BQM E26 (E26/287/220.6m)	Zircon	U-Pb (SHRIMP)	445.2 ± 3.9	This study
Monzodiorite E26 (E26/46/1720.2m)	Hornblende (p)	$^{40}Ar/^{39}Ar$	495.6 ± 26.4 [1]	This study
late-mineral B-QMP, E26 (E26/46/1161.6m)	Biotite (p)	$^{40}Ar/^{39}Ar$	444.3 ± 4.1 [1]	This study
			444.0 ± 6.3 [2]	
early-mineral B-QMP, E22 (E22/39/581.0m)	Biotite (p)	$^{40}Ar/^{39}Ar$	448.6 ± 7.0 [3]	This study
BQM, E26 (E26/284/318.0m)	Biotite (p)	$^{40}Ar/^{39}Ar$	439.0 ± 5.2 [2]	This study
Alteration/mineralisation, E26 (E26/286/153.9)	Biotite (s)	$^{40}Ar/^{39}Ar$	449.0 ± 6.2 [4]	This study

Five new $^{40}Ar/^{39}Ar$ age determinations of hornblende and biotite separates from the Endeavour deposits have been generated in the current study. The samples were analysed at Queens University in Canada, and the results are presented in Appendix E4. Primary biotite phenocrysts from an early-mineral B-QMP intrusion from E22 yielded an $^{40}Ar/^{39}Ar$ integrated age of 448.6 ± 7.0Ma. A late-mineral B-QMP intrusion at E26 yielded an $^{40}Ar/^{39}Ar$ correlation age of 444.3 ± 4.1Ma, and a plateau age of 444.0 ± 6.3Ma from primary biotite phenocrysts. Primary biotite phenocrysts from a BQM sample from E26 yielded an $^{40}Ar/^{39}Ar$ plateau age of 439.0 ± 5.2Ma, whereas secondary biotite associated with main stage mineralisation from E26, yielded an $^{40}Ar/^{39}Ar$ maximum age of 449.0 ± 6.2Ma. This latter age is older than that reported by Perkins *et al.* (1990), who dated late stage sericite mineralisation at 439.2 ± 1.2Ma. The secondary biotite sample of this study was weakly chloritised, therefore it is likely that the isotopic system may have been disturbed, and the $^{40}Ar/^{39}Ar$ can be considered as a maximum age for main stage mineralisation (T. Ulrich, pers. comm., Queens University, 2001). Hornblende from the monzodiorite intrusion at E26 yielded an $^{40}Ar/^{39}Ar$ correlation age of 495.6 ± 26.4Ma. The large error and absence of a plateau age probably reflects moderate chloritisation of the hornblende, and it is likely that this age is meaningless, since it is considerably older than the host volcanic rocks (~462 – 451Ma, Figure 8.1: Duggan *et al.*, 1999; Crawford *et al.*, 2001; Butera *et al.*, 2001).

In addition to the $^{40}Ar/^{39}Ar$ dating, this study obtained one new U-Pb (SHRIMP) age from zircons from an E26 BQM intrusion at the Australian National University, Canberra. The U-Pb (SHRIMP) age of 445.2 ± 3.9Ma is within error of the biotite $^{40}Ar/^{39}Ar$ age for a similar sample (Table 8.1). The NSW SPIRT project U-Pb (SHRIMP) dated zircons from a zero porphyry dyke at Endeavour 37 (E37), which yielded an age of 437 ± 6.0Ma (Crawford *et al.*, 2001).

It is thus clear that much of the intrusive activity and magmatic – hydrothermal alteration associated with the Endeavour deposits occurred around 445 – 437Ma (Figure 8.1). However, these ages are not accurate enough to yield definitive evidence of the sequence of emplacement of the various intrusions within the QMP complexes, or to constrain the duration of discrete mineralising events.

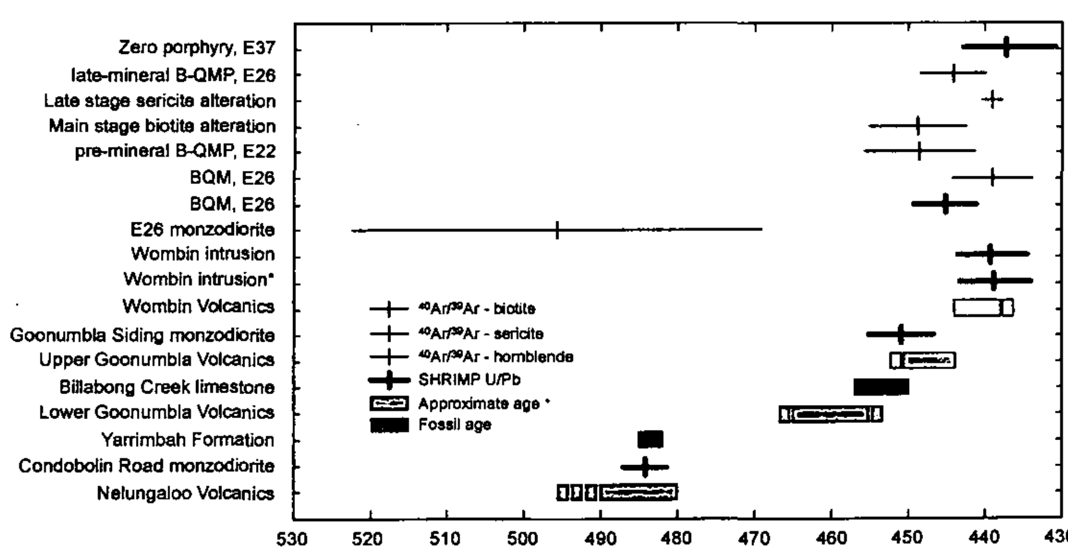

Figure 8.1 The geochronology of the GVC, compiled from dates in Table 8.1 and additional information (approximate ages of the volcanic rocks and fossil ages) from Crawford et al., 2001 and Duggan et al., 1999. Rock units are listed in terms of their relative ages from oldest to youngest; * is interpreted to be an intrusion into the Wombin Volcanics (Perkins et al., 1990); + approximate age is constrained by fossil and intrusions ages.

8.3 Whole rock major and trace element geochemistry of the GVC

The GVC is part of the Junee-Narromine Ordovician volcanic belt. Notwithstanding the different tectonic settings proposed (cf. section 2.2.1), most workers agree that the volcanic belts are the remnants of the Early Ordovician to Early Silurian Macquarie Island Arc (Glen and Walshe, 1999). Examining the whole rock major and trace element data available for the volcanic and intrusive rocks in the GVC can test this hypothesis. The geochemical aspects of each of the three major units of the GVC, the Nelungaloo, Goonumbla and Wombin Volcanics, are discussed below. Intrusions within each of the units are also discussed.

8.3.1 Regional GVC rocks

8.3.1.1 Major elements

Volcanic rocks

The volcaniclastic sandstones and siltstones and lavas of the Nelungaloo Volcanics can be classified as calc-alkaline to high-K calc-alkaline rocks when plotted on a K_2O vs SiO_2 discrimination diagram (Figure 8.2a). On a discrimination diagram that includes Na_2O, they can be classified mainly as basaltic andesites to andesites (Figure 8.2b). Similarly, the mainly lavas or shallow intrusive sills of the Goonumbla Volcanics, and ignimbrites, volcaniclastic rocks and lavas of the Wombin Volcanics can be classified mainly as high-K calc-alkaline to shoshonite rocks, and as trachybasalts through trachyandesites to trachytes respectively, on the same two discrimination diagrams. There is a steady increase in K_2O and K_2O + Na_2O with increasing SiO_2 from the Nelungaloo Volcanics through the Goonumbla to the Wombin Volcanics. The least-altered samples available were collected for these analyses. As such, although alkali mobility due to alteration might be expected, the strikingly consistent compositional fields on Figures 8.2a and 8.2b indicates that geochemical affinity may be determined with confidence for these rocks (Crawford, 2001b).

The Harker diagrams illustrate a number of other features. The most significant of these is that despite the ~40Ma age spread from ~480Ma to ~440Ma (Figure 8.1), the fields defined by the Nelungaloo, Goonumbla and Wombin Volcanics are particularly coherent, showing the characteristic smooth TiO_2, Fe_2O_3 and CaO depletion with fractionation that typifies calc-alkaline suites (Figures 8.2c, d and e respectively).

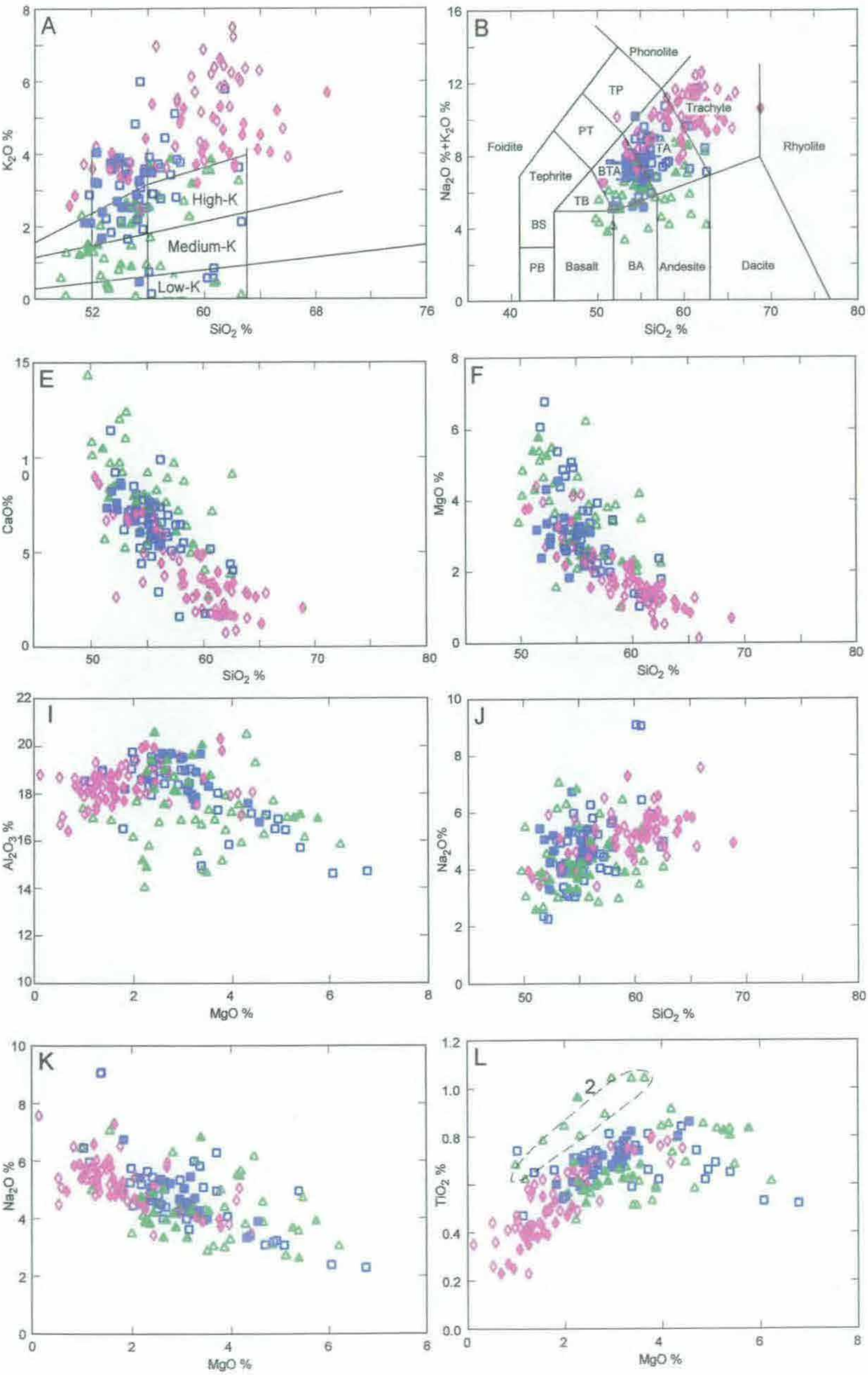
A
B
E
F
I
J
K
L
K_2O %
SiO_2 %
High-K
Medium-K
Low-K
Na_2O % + K_2O %
Phonolite
TP
PT
Foidite
Tephrite
Trachyte
TA
BTA
TB
BS
PB
Basalt
BA
Andesite
Dacite
Rhyolite
CaO%
MgO %
Al_2O_3 %
Na_2O%
Na_2O %
TiO_2 %
2

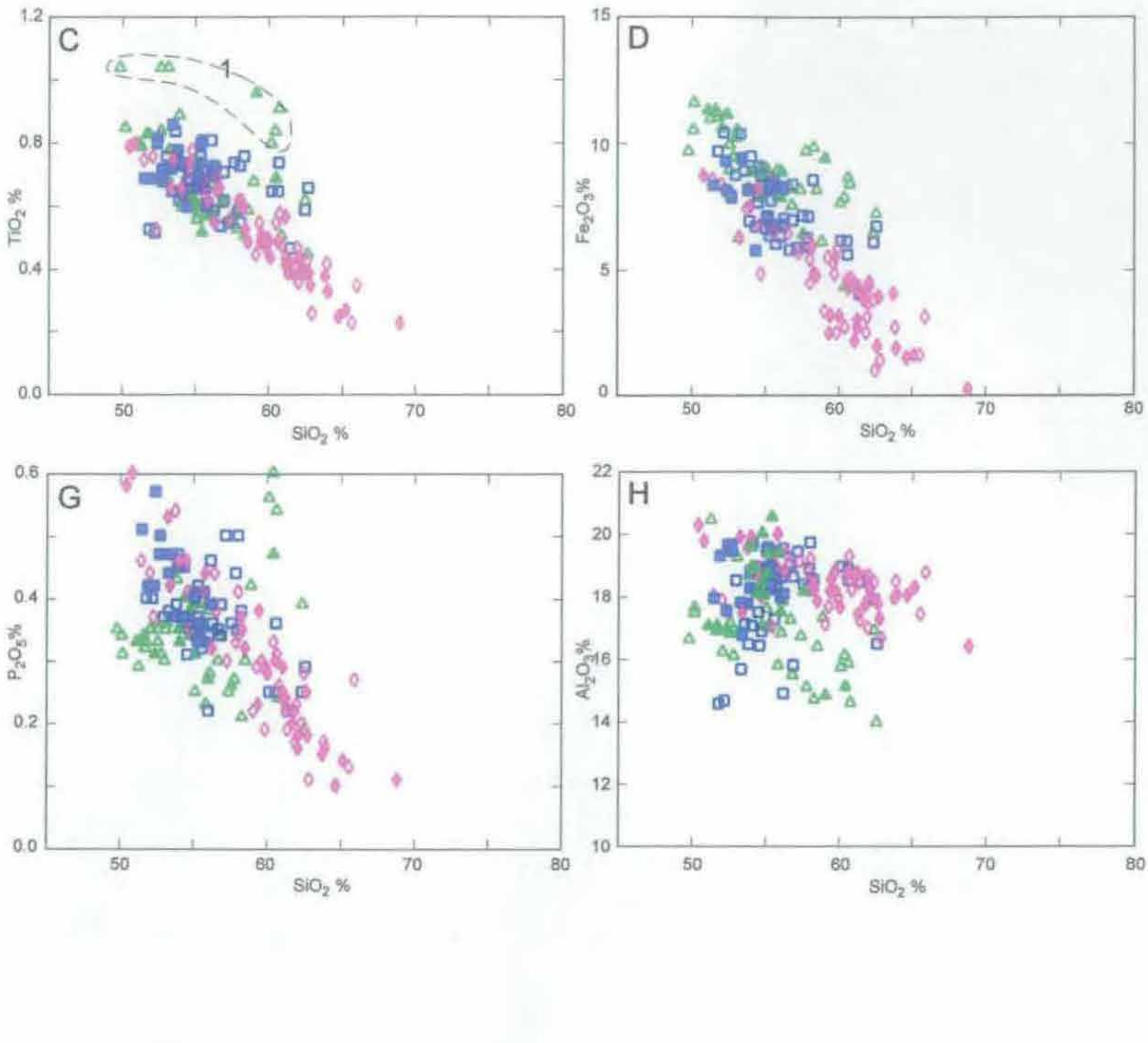

Figure 8.2 Harker diagrams for the volcanic and intrusive rocks of the Goonumbla Volcanic Complex. **A** K_2O% vs SiO_2%, after Peccerillo and Taylor, 1976; **B** Na_2O% + K_2O% vs SiO_2%, after Le Bas *et al.*, 1986; **C** TiO_2% vs SiO_2%; **D** Fe_2O_3% vs SiO_2%; **E** CaO% vs SiO_2%; **F** MgO% vs SiO_2%; **G** P_2O_5% vs SiO_2%; **H** Al_2O_3% vs SiO_2%; **I** Al_2O_3% vs MgO%; **J** Na_2O% vs SiO_2%; **K** Na_2O% vs MgO% and **L** TiO_2% vs MgO%. 1 and 2 on (C) and (L) respectively represent the high TiO_2 suite of the Nelungaloo Volcanics.

Legend

- Nelungaloo Volcanics
- Nelungaloo intrusions
- Goonumbla Volcanics
- Goonumbla intrusions
- Wombin Volcanics
- Wombin intrusions

Abbreviations:
BA - basaltic andesite; BS - basanite; BTA - basaltic trachyandesite; PB - picrobasalt; PT - phonotephrite; TA - trachyandesite; TB - trachybasalt; TP - tephriphonolite

MgO also decreases with increasing SiO_2 from the Nelungaloo through the Goonumbla to the Wombin Volcanics (Figure 8.2f). On average, the Wombin Volcanics extend to notably more evolved compositions than the Nelungaloo and Goonumbla Volcanics, many being trachyandesites and trachytes with 60 – 65% SiO_2 and <2% MgO. Basaltic composition rocks in the Goonumbla and Wombin suites have the highest P_2O_5 contents (Figure 8.2g), which then decrease with fractionation. This indicates apatite-saturation at the basaltic stage of magmatic evolution and suggests, by comparison with Southwest Pacific arc suites, shoshonitic affinities of these suites (Crawford, 2001b). In contrast, most of the Nelungaloo rocks at 50 – 53% SiO_2 have notably lower P_2O_5 than their later counterparts, and apatite-saturation appears at ~56% SiO_2, which is consistent with medium-K to high-K calc alkaline affinities.

Not all of the Harker diagrams show consistent trends with increasing SiO_2 contents; for example, Na_2O and Al_2O_3 show greater complexity. The Nelungaloo Volcanics have low and variable Al_2O_3 contents with respect to increasing SiO_2 (Figure 8.2h) and decreasing MgO (Figure 8.2i) and the Nelungaloo andesites have distinctly lower Al_2O_3 than the Goonumbla and Wombin andesites. In the Goonumbla Volcanics, there is a distinct increase in Al_2O_3 with decreasing MgO contents to ~2%, reflecting little removal of plagioclase. For MgO <2%, there is a sharp decrease in Al_2O_3 contents for the Wombin Volcanics, reflecting significant plagioclase extraction. The field for Na_2O-SiO_2 is more scattered than for other elements, which probably reflects limited Na_2O mobility during pervasive low-grade metamorphism. However, there is a distinct increase in Na_2O with increasing SiO_2 and decreasing MgO contents for the Goonumbla and Wombin Volcanics (Figures 8.2j and k respectively).

Plots of TiO_2 against SiO_2 (Figure 8.2c) and MgO (Figure 8.2l) indicate that there may be two distinct suites, with higher and lower TiO_2 contents, in the Nelungaloo Volcanics. The change in slope of the Nelungaloo trend at ~4% MgO probably reflects the appearance of Fe-Ti oxides as a major fractionating phase. There is a distinct increase in TiO_2 as MgO contents decrease from ~7 to ~5% in the Goonumbla Volcanics; thereafter there is a decrease in TiO_2 with decreasing MgO contents for the Wombin Volcanics.

Intrusive rocks

Whole rock major element contents of the intrusive rocks within the Nelungaloo, Goonumbla and Wombin Volcanics overlap their volcanic counterparts on the same discrimination and Harker diagrams (Figures 8.2). They also show similar trends of decreasing TiO_2, MgO, CaO, and Fe_2O_3 and increasing K_2O with increasing SiO_2 contents.

8.3.1.2 Trace elements

Volcanic rocks

Ni abundances are higher in the Nelungaloo and basal unit of the Goonumbla Volcanics than they are in the remaining Goonumbla and all of the Wombin Volcanics (Figure 8.3a), commensurate with the presence of olivine phenocrysts in these more mafic units. There is an overall decrease in V (Figure 8.3b) with increasing SiO_2 contents from the Nelungaloo through the Goonumbla to the Wombin Volcanics, paralleling the changes in Fe_2O_3 contents.

Light REE (La, Ce, Nd) abundances in the Nelungaloo Volcanics are considerably higher than in the Goonumbla and Wombin Volcanics despite the higher P_2O_5 and K_2O contents of the latter suites (Figure 8.3c, d and e respectively). This possibly reflects a mantle source feature (Glen *et al.*, 2001). In contrast, there are no consistent differences between the three suites on the SiO_2 vs Y plot (Figure 8.3f).

Ba and Rb show the expected general increase with increasing SiO_2, while Nb and Sr abundances are more variable (Figure 8.3g, h, i and j respectively). High Sr abundances (1200 – 1800ppm) in many of the Goonumbla and Wombin andesites are notable.

Intrusive rocks

Whole rock trace element contents for the intrusive rocks within the Nelungaloo, Goonumbla and Wombin Volcanics overlap their volcanic counterparts in terms of relationships with SiO_2, MgO and TiO_2 in a similar manner to the major elements (Figure 8.3). However, several of the trace elements are significant for the intrusive rocks, especially with respect to those that intrude the Wombin Volcanics, e.g. Nb and Zr.

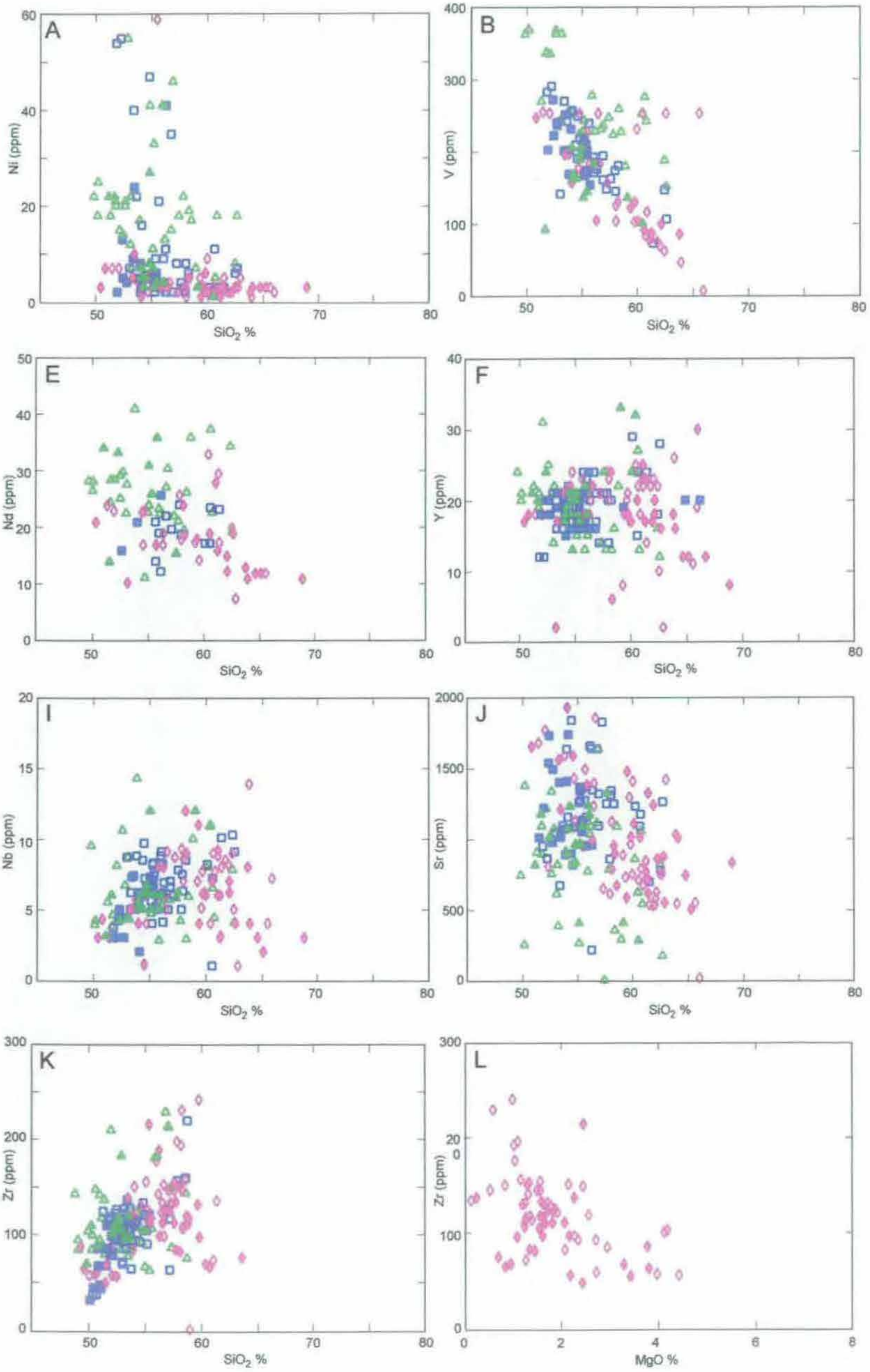
A
Ni (ppm)
SiO$_2$ %
B
V (ppm)
SiO$_2$ %
E
Nd (ppm)
SiO$_2$ %
F
Y (ppm)
SiO$_2$ %
I
Nb (ppm)
SiO$_2$ %
J
Sr (ppm)
SiO$_2$ %
K
Zr (ppm)
SiO$_2$ %
L
Zr (ppm)
MgO %

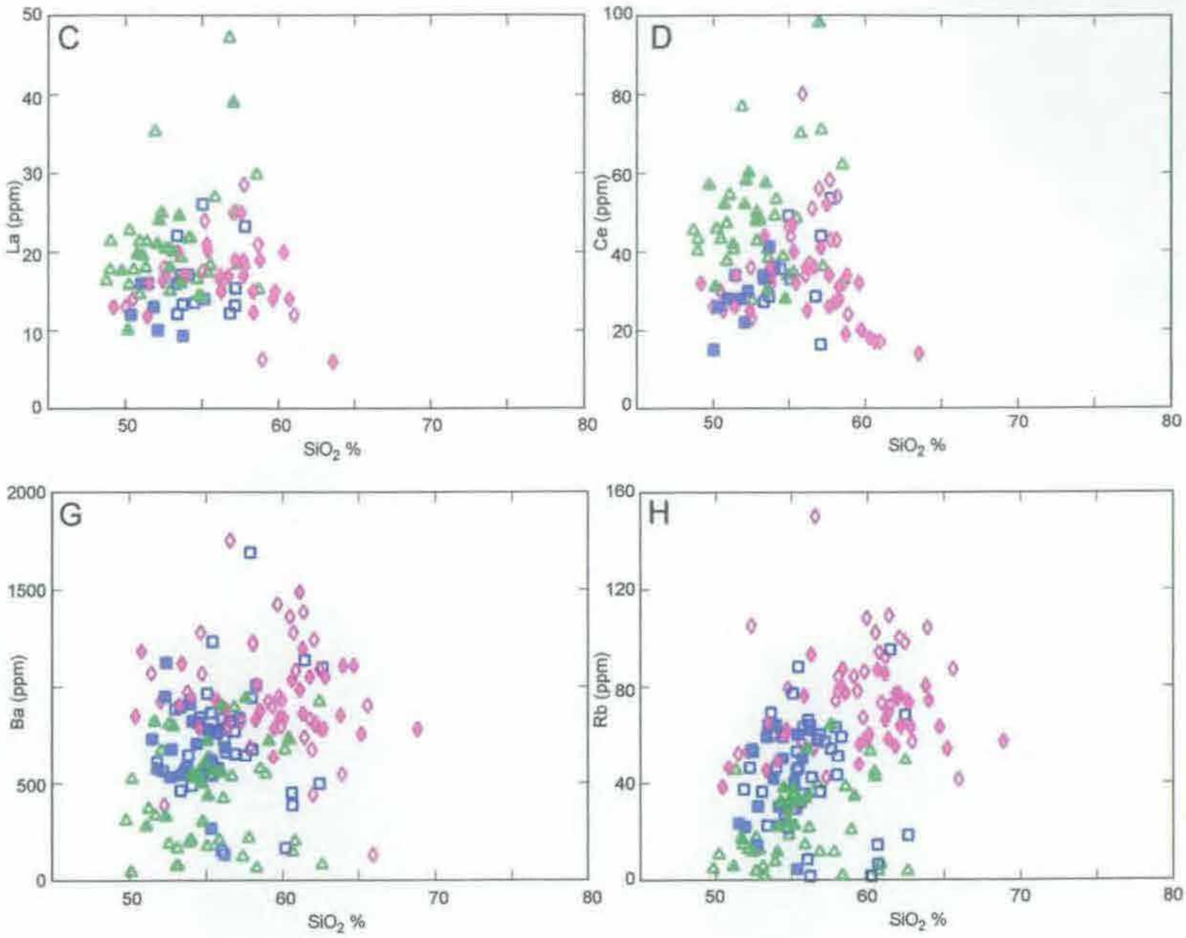

Figure 8.3 Harker diagrams for the volcanic and intrusive rocks of the Goonumbla Volcanic Complex. **A** Ni (ppm) vs SiO_2%; **B** V (ppm) vs SiO_2%; **C** La (ppm) vs SiO_2%; **D** Ce (ppm) vs SiO_2%; **E** Nd (ppm) vs SiO_2%; **F** Y (ppm) vs SiO_2%; **G** Ba (ppm) vs SiO_2%; **H** Rb(ppm) vs SiO_2%; **I** Nb (ppm) vs SiO_2%; **J** Sr (ppm) vs SiO_2%; **K** Zr (ppm) vs MgO% and **L** Zr (ppm) vs MgO%.

Legend

- △ Nelungaloo Volcanics
- ▲ Nelungaloo intrusions
- □ Goonumbla Volcanics
- ■ Goonumbla intrusions
- ◇ Wombin Volcanics
- ◆ Wombin intrusions

As with other incompatible elements, Zr increases with increasing SiO_2 contents. However, there is a distinct decrease in the rate of Zr increase with respect to SiO_2 when SiO_2 increases beyond ~58% (Figure 8.3k), notably in some of the intrusive rocks within the Wombin Volcanics. The change in rate of increase in Zr, marked by a distinct break in the slope of increasing Zr at SiO_2 ~58%, defines the beginning of a "depleted Zr trend". Heithersay and Walshe (1995) also recognised this "depleted Zr trend" for intrusions within the Wombin Volcanics close to the Endeavour deposits although they did not describe extrusive equivalents for these Zr-depleted intrusive rocks. However, Crawford (2001b) showed that several volcanic rocks plot on the depleted Zr trend (Figure 8.3k). Many of the intrusions associated with the Wombin Volcanics plot on the "undepleted" Zr trend, including the Gunningbland Forest monzonite porphyries. The depleted Zr trend is also evident on the MgO vs Zr plot (Figures 8.3l), and probably reflects the onset of zircon crystallisation at ~58 wt% SiO_2 and 3 – 3.5 wt% MgO.

8.3.2 Ore-related E22, E26, E27 and E48 intrusions

This section describes the geochemistry of the intrusions common to all of the deposits in the same order as they are interpreted to intrude at each of the Endeavour deposit; BQM (biotite quartz monzonite) followed by early-mineral biotite phyric QMP, syn-mineral K-feldspar phyric QMP and augite-biotite – K-feldspar phyric QMP, and late-mineral biotite phyric QMP (early-mineral B-QMP, K-QMP, KA-QMP and late-mineral B-QMP respectively; cf. Chapter 3). The geochemistry of the microgranite intrusions at E48 and the monzodiorite intrusion and zero porphyry dykes at E26 are addressed at the end of the section.

8.3.2.1 Major elements

In terms of the whole rock major elements, the ore-related QMP intrusions have similar, though more felsic compositions than the rocks of the GVC as a whole. Due to noteworthy hydrothermal alteration, reflected by the abundant brick-red K-feldspar, the mineralised intrusions are too enriched in K_2O to plot on a K_2O vs SiO_2 discrimination diagram (Figure 8.4a), whereas on the $Na_2O + K_2O$ vs SiO_2 discrimination diagram, the intrusive rocks associated with ore deposition range from trachyte and trachydacite to rhyolite (Figures 8.4b). On these plots, increasing K_2O and $Na_2O + K_2O$ contents with increasing SiO_2 contents are obvious for the ore-related intrusions. On SiO_2 vs TiO_2,

Fe_2O_3, CaO and MgO plots (Figures 8.4c, d, e and f respectively), the QMP intrusions are thought to continue the fractionation trends noted in the Goonumbla Volcanics, but more specifically in the Wombin Volcanics and associated intrusive rocks. In other words, the trends of decreasing TiO_2, Fe_2O_3, CaO and MgO with increasing SiO_2 contents shown in the Wombin rocks continue in the BQM and then continue through the QMP intrusions. It is evident that most of the BQM samples overlap many of the Wombin intrusions in terms of these major elements; however, the QMP intrusions are generally the most fractionated of the ore-related intrusions. Note that although there is some scatter in the data, the later KA-QMP intrusions are generally not as fractionated, or SiO_2-rich as the K-QMP intrusions. It is also important to note that the early- and late-mineral B-QMP intrusions cannot be distinguished on these plots. The B-QMP intrusions as a whole are the least evolved of the QMP intrusions associated with the Endeavour deposits.

Variations in P_2O_5 concentrations clearly illustrate the overlap and continuing fractionation trends of some of the regional intrusive rocks and those directly associated with the Endeavour deposits (Figures 8.4g). The decrease in P_2O_5 with increasing SiO_2 contents continues through the intrusions associated with ore formation. Al_2O_3 contents decrease with increasing SiO_2 through the intrusive rocks associated with the Wombin Volcanics and continue to decrease through the sequence of ore-related QMP rocks (Figure 8.4h). Al_2O_3 contents also decrease with decreasing MgO (Figure 8.4i), with a notable change in slope at ~1% MgO, which is the upper limit of MgO contents of the QMP intrusions. Na_2O contents increase to SiO_2 ~62% (Figure 8.4j); thereafter, there is a sharp decrease in Na_2O as SiO_2 increases. This decrease in NaO_2 is also evident on the Na_2O vs MgO plot (Figure 8.4k), where NaO_2 initially increases as MgO decreases to ~1% and thereafter it decreases with decreasing MgO contents. The changes of slope in the Al_2O_3 and Na_2O trends at MgO ~1% possibly indicate albite alteration and/or subsequent K-feldspar replacement of albite in some QMP samples. Variable Na_2O/K_2O contents at MgO contents less than ~1% support this proposal (Figure 8.4l).

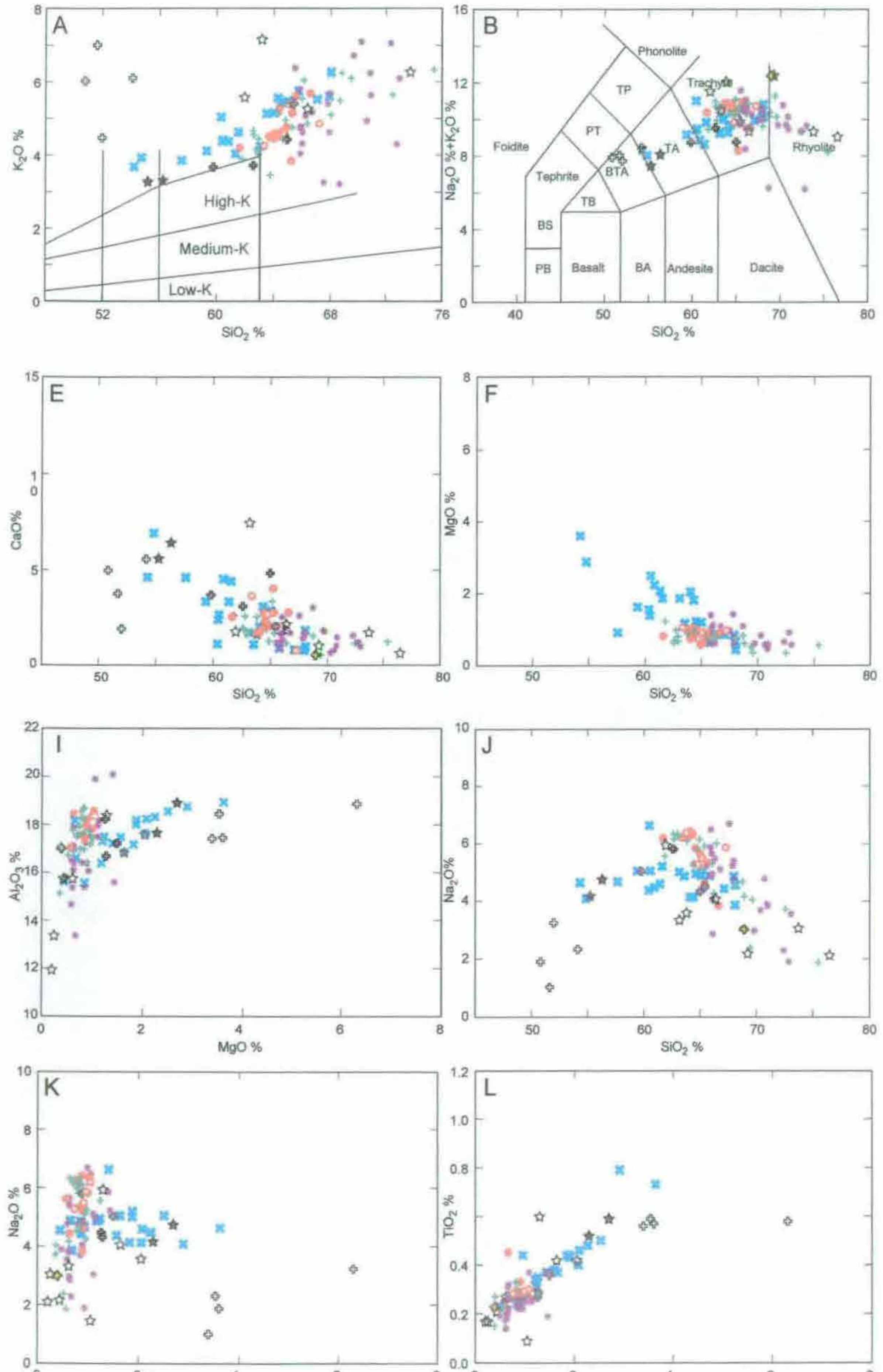

A
K_2O %
SiO_2 %
High-K
Medium-K
Low-K
B
Na_2O %+K_2O %
SiO_2 %
Phonolite
TP
PT
Foidite
Tephrite
BTA
TA
Trachyte
Rhyolite
TB
BS
PB
Basalt
BA
Andesite
Dacite
E
CaO%
SiO_2 %
F
MgO %
SiO_2 %
I
Al_2O_3 %
MgO %
J
Na_2O%
SiO_2 %
K
Na_2O %
MgO %
L
TiO_2 %
MgO %

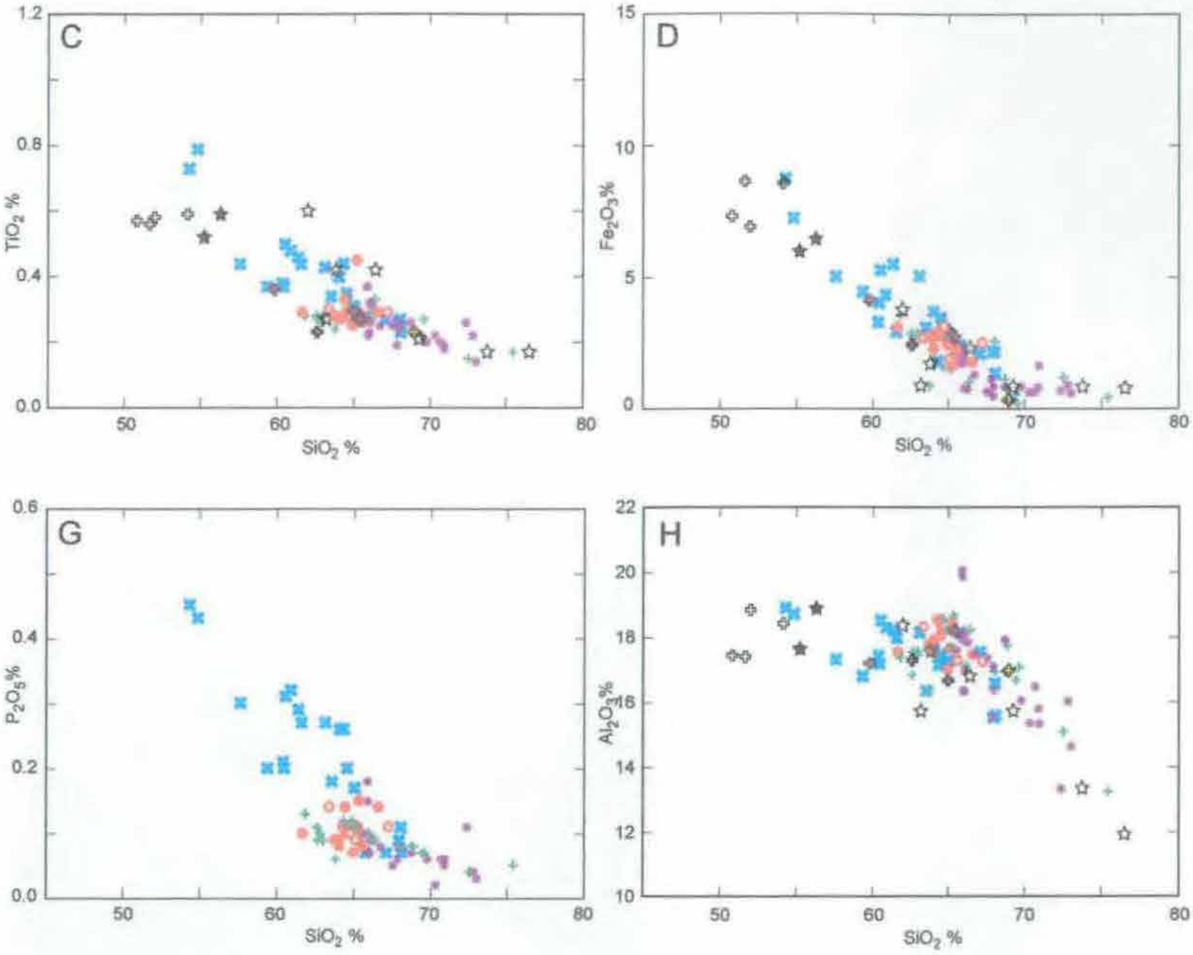

Figure 8.4 Harker diagrams for the intrusive rocks associated with the Endeavour deposits. **A** K_2O% vs SiO_2%, after Peccerillo and Taylor, 1976; **B** Na_2O% + K_2O% vs SiO_2%, after Le Bas *et al.*, 1986; **C** TiO_2% vs SiO_2%; **D** Fe_2O_3% vs SiO_2%; **E** CaO% vs SiO_2%; **F** MgO% vs SiO_2%; **G** P_2O_5% vs SiO_2%; **H** Al_2O_3% vs SiO_2%; (I) Al_2O_3% vs MgO%; **J** Na_2O% vs SiO_2%; **K** Na_2O% vs MgO% and **L** TiO_2% vs MgO%.

Legend

BQM
early-mineral and late-mineral B-QMP
K-QMP
KA-QMP

Aplitic rocks
E26 monzodiorite
E48 microgranite
Basaltic trachyandesite
Zero porphyry

Abbreviations:
BA - basaltic andesite; BS - basanite; BTA - basaltic trachyandesite; PB - picrobasalt; PT - phonotephrite; TA - trachyandesite; TB - trachybasalt; TP - tephriphonolite

8.3.2.2 Trace elements

The overlap in major element compositions between some of the regional intrusive rocks within the Wombin Volcanics and those associated with ore formation is also evident in many of the whole rock trace elements. The low Ni contents of the regional Wombin intrusive and volcanic rocks also characterises the intrusive rocks associated with the Endeavour deposits (Figure 8.5a).

The overall decrease in V abundances with increasing SiO_2 that is characteristic of the intrusive rocks within the Wombin Volcanics is also evident for the BQM intrusions and the QMP sequence of ore-related intrusions (Figure 8.5b). Similar trends are evident for many of the incompatible trace elements; La, Ce and Nd abundances decrease with SiO_2 contents increasing beyond ~60%, especially in the early- and late-mineral B-QMP, K-QMP and KA-QMP intrusions (Figures 8.5c, d and e respectively). The relationship between SiO_2 and Ce is noteworthy. Ce abundances decrease slightly for the BQM intrusions, however; they decrease markedly with increasing SiO_2 >~60% for the QMP intrusions. Y abundances mimic Ce abundances with increasing SiO_2, although they are higher and more variable in the BQM intrusions than they are in the ore-related QMP intrusions associated with the Endeavour deposits (Figure 8.5f).

Ba abundances in the BQM intrusions are distinct from those of the ore-related QMP intrusions, with typically lower Ba abundances for similar SiO_2 and TiO_2 contents in the B-QMP, K-QMP and KA-QMP rocks (Figures 8.5g and h respectively). Similar patterns are evident for Sr abundances in the BQM and QMP intrusions (Figures 8.5i and j respectively). BQM intrusions typically have higher Rb and Nb abundances than the QMP intrusions for similar SiO_2 contents (Figures 8.5k and l respectively).

The depleted Zr trend is more pronounced in the ore-related QMP intrusions than it is in the BQM intrusions and the regional intrusive and volcanic rocks (Figure 8.5m). Zr abundances in the QMP intrusions decrease with decreasing MgO contents (Figure 8.5n), whereas they increase with decreasing MgO contents in most of the BQM samples. This latter pattern is similar for the majority of the regional Goonumbla and Wombin rocks. It is also significant that some of the BQM intrusive rocks fall on the same "undepleted" Zr trend as most of the Wombin and Goonumbla volcanic and intrusive rocks.

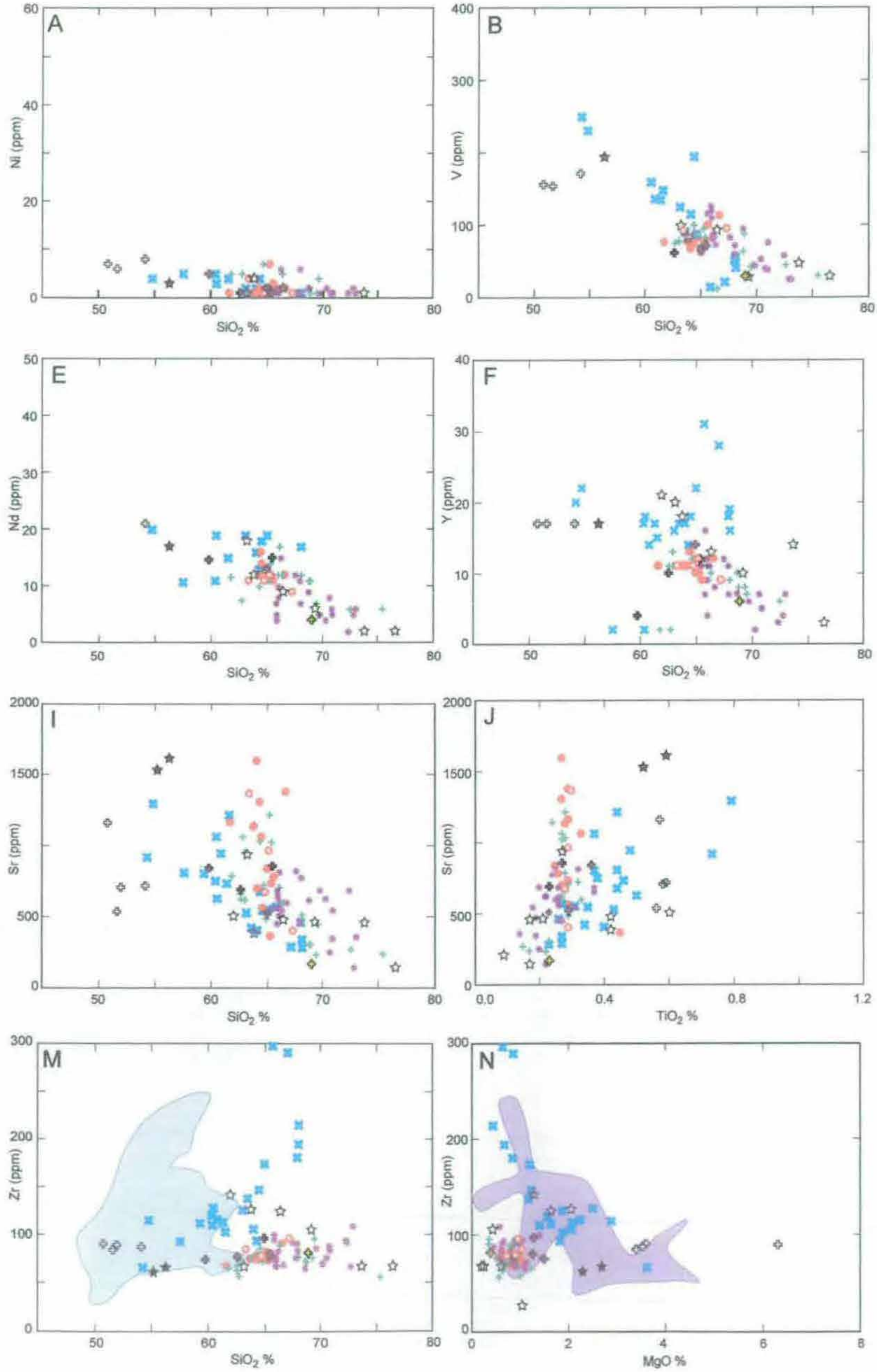
A
Ni (ppm)
SiO2 %
B
V (ppm)
SiO2 %
E
Nd (ppm)
SiO2 %
F
Y (ppm)
SiO2 %
I
Sr (ppm)
SiO2 %
J
Sr (ppm)
TiO2 %
M
Zr (ppm)
SiO2 %
N
Zr (ppm)
MgO %

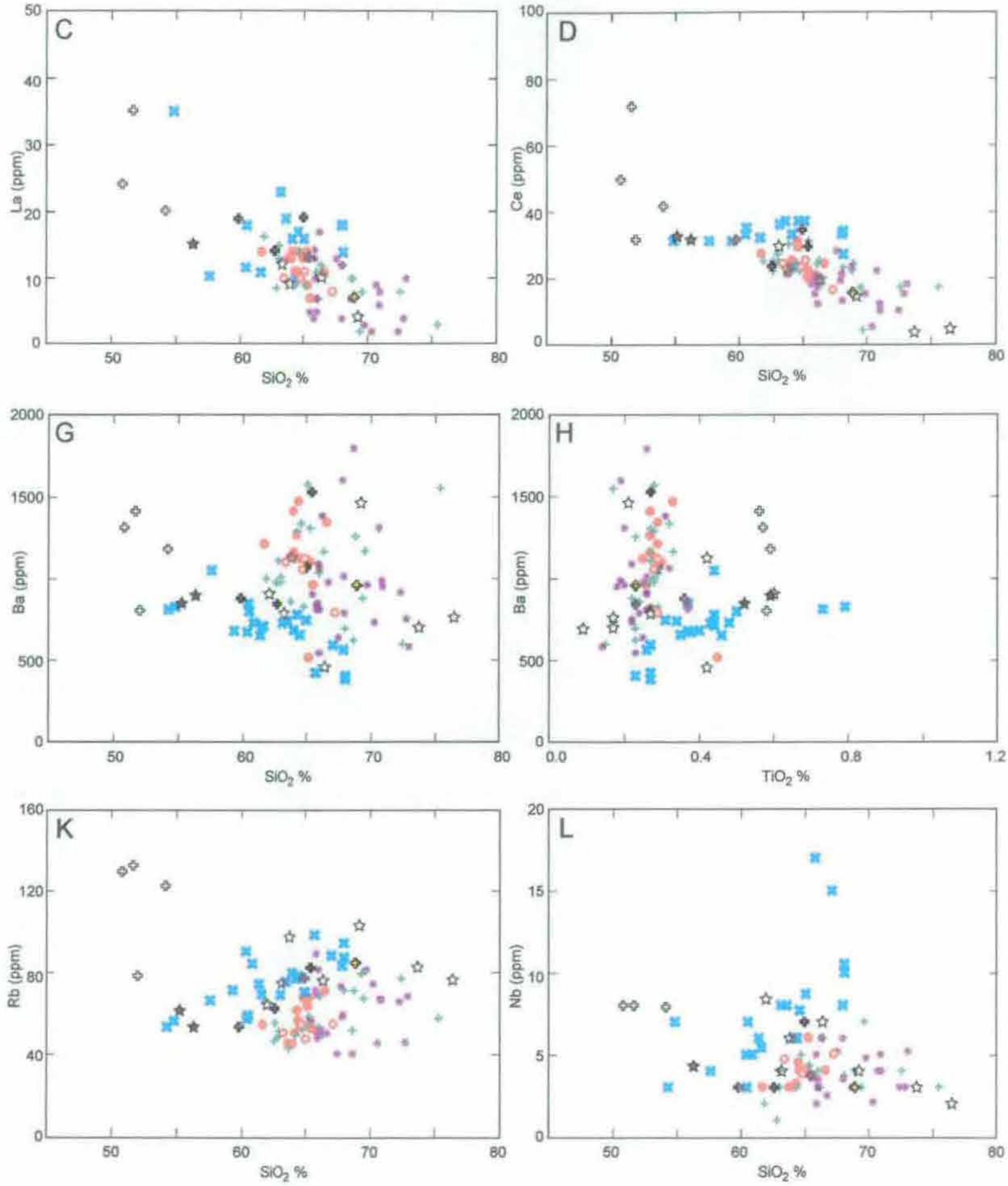

Figure 8.5 Harker diagrams for the intrusive rocks associated with the Endeavour depostis. **A** Ni (ppm) vs SiO_2%; **B** V (ppm) vs SiO_2%; **C** La (ppm) vs SiO_2%; **D** Ce (ppm) vs SiO_2%; **E** Nd (ppm) vs SiO_2%; **F** Y (ppm) vs SiO_2%; **G** Ba (ppm) vs SiO_2%; **H** Ba (ppm) vs MgO%; **I** Nb (ppm) vs SiO_2%; **J** Sr (ppm) vs SiO_2%; **K** Rb (ppm) vs SiO_2%; **L** Nb (ppm) vs SiO_2%; **M** Zr (ppm) vs SiO_2% and **N** Zr (ppm) vs MgO%. Shaded areas in (M) and (N) represent the fields for the Goonumbla Volcanic Complex rocks.

Legend

- BQM
- early-mineral and late-mineral B-QMP
- K-QMP
- KA-QMP
- Aplitic rocks
- Basaltic trachyandesite
- E26 monzodiorite
- Zero porphyry
- E48 microgranite

It is thus evident that there is a striking divergence in trace element abundances with fractionation between the BQM and the QMP intrusions associated with mineralisation. The BQM has notably higher Y, Rb, Nb and Zr and lower Ba and Sr for 60 – 70% SiO_2, than any of the QMP intrusions. These trace element characteristics are similar to most of the intrusions into the Wombin Volcanics.

8.3.3 Normalised multi-element plots

One way of comparing trace element enrichments and depletions in rock suites is to plot abundances of elements, from most to least incompatible during mantle melting (Sun and McDonough, 1989), normalised to their abundances in well-characterised mid ocean ridge basalts (MORB). On such plots, arc-type magmas are typically enriched in large ion lithophile elements (LILE) such as Rb, Ba, Sr, Th and LREE relative to MORB. They also show pronounced negative Nb-Ta anomalies relative to K and La and Ce and positive Sr and Pb anomalies relative to Ce and Pr (Sun and McDonough, 1989).

On the N-MORB normalised multi-element plots presented here, samples collected mainly by the author and by Crawford (2001b) have been selected to represent the compositional range of each subset of rocks to ensure minimum analytical variation, since these two data sets were collected using the same techniques at the same laboratory.

8.3.3.1 Regional volcanic and intrusive rocks of the GVC

Patterns for the GVC volcanic and intrusive rocks show the typically spiked pattern characteristic of island arc rocks (Figures 8.6a, b and c). All samples show the characteristic enrichment in LILE and concomitant Nb depletion associated with subduction-related magmatism. In addition to LILE enrichment, all of the GVC rocks are relatively enriched in Pb compared to N-MORB. There is an overall negative slope to the multi-element plots of the GVC volcanic and intrusive rocks.

In general, the multi-element plots illustrate an overall progressive enrichment in LILE, e.g. Ba and K, and depletion in Nb, Zr and Ti, with time. However, the Nelungaloo rocks are notably enriched in La, Ce and P compared to the Goonumbla and Wombin rocks (Figure 8.6d). Similar trends are observed for the intrusive rocks; however, the data are more scattered.

Figure 8.6 Multi-element plots for the volcanic and intrusive rocks of the Goonumbla Volcanic Complex normalised to N-MORB after Sun and Mc Donough (1989). **A** Nelungaloo Volcanics (shaded) and intrusions ( ); **B** Goonumbla Volcanics (shaded) and intrusions ( ); **C** Wombin Volcanics (shaded) and intrusions ( ); **D** Comparative patterns for the Nelungaloo, Goonumbla and Wombin Volcanics; **E** BQM intrusions ( ) relative to the Wombin Volcanics; **F** B-QMP intrusions (early- and late-mineral) relative to the Wombin Volcanics; **G** K-QMP intrusions ( ) relative to the Wombin Volcanics; and **H** KA-QMP intrusions ( ) relative to the Wombin Volcanics.

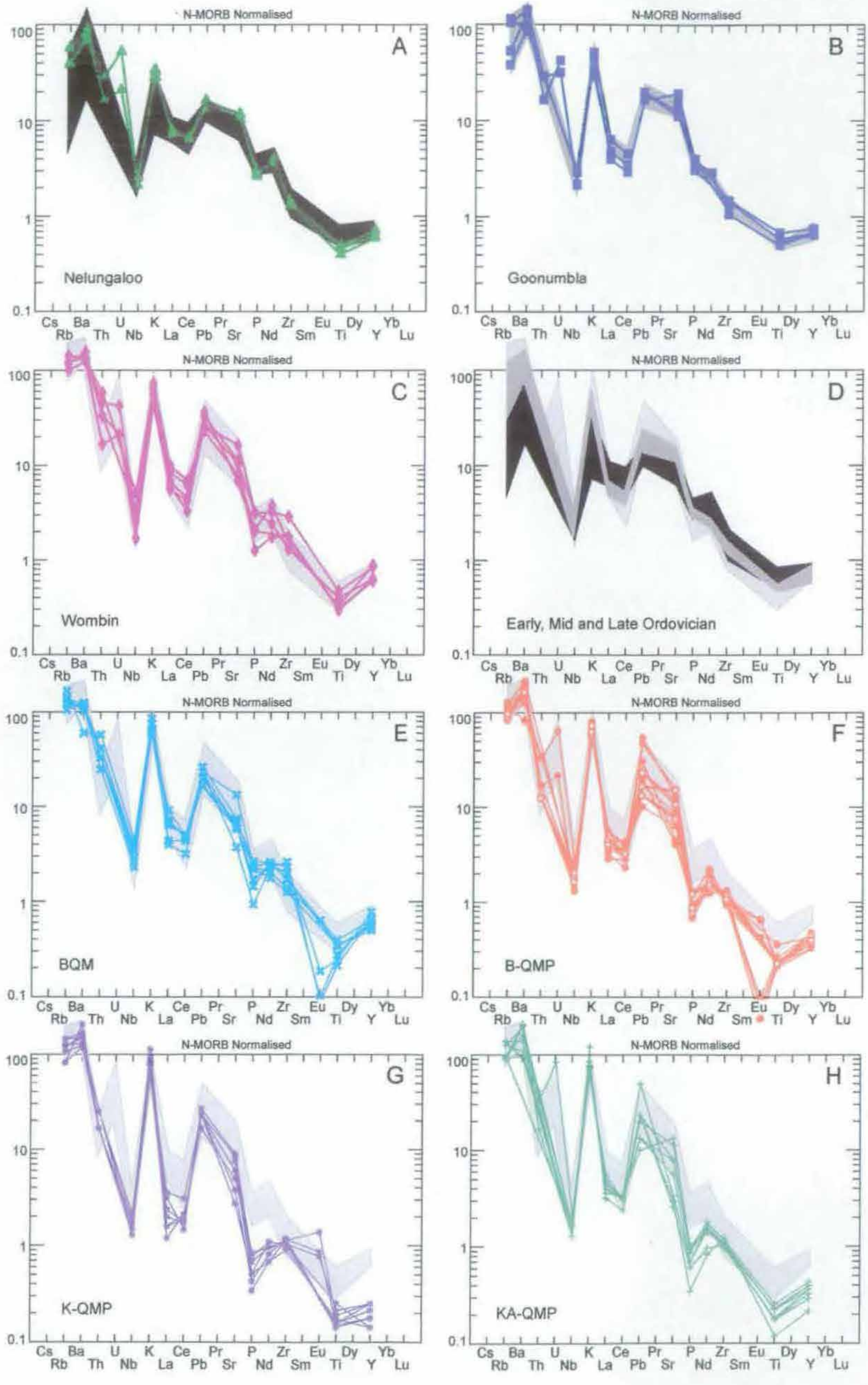

N-MORB Normalised
A
Nelungaloo
B
Goonumbla
C
Wombin
D
Early, Mid and Late Ordovician
E
BQM
F
B-QMP
G
K-QMP
H
KA-QMP
100
10
1
0.1
Cs Ba U K Ce Pr P Zr Eu Dy Yb
Rb Th Nb La Pb Sr Nd Sm Ti Y Lu

8.3.3.2 Intrusions associated with ore deposition

The multi-element plots of the intrusions related to the Endeavour deposits illustrate that with the exception of the Eu anomaly, the BQM intrusions are virtually identical to many of the intrusions associated with the Wombin Volcanics (Figure 8.6e). Note that the Eu anomaly might be an analytical artifact, since many of the GVC rocks used for these plots were not analysed for Eu. See Section 8.4.4.2 below for a detailed discussion.

It is evident that the progressive fractionation of the incompatible and compatible elements from the Mid- to Late Ordovician Goonumbla and Wombin Volcanics and associated intrusions (including the BQM) becomes more pronounced through the QMP intrusions associated with the Endeavour deposits, reflecting the temporal increase in fractionation of magmas across this range (Figures 8.6f, g and h respectively). Figures 8.7a, b, c and d illustrate the multi-element patterns for BQM, B-QMP, K-QMP and KA-QMP for E22, E26, E27 and E48 respectively.

8.3.4 Interpretation

The consistent overlap and similar character of geochemical trends for most of the major and trace elements with respect to SiO_2, MgO and TiO_2 are inferred to reflect the broadly co-magmatic nature of the intrusive and volcanic rocks of the Mid- to Late Ordovician, evolving, high-K calc-alkaline to shoshonitic GVC.

The Early Ordovician Nelungaloo Volcanics are probably a high-K calc-alkaline suite. However, their notably higher LREE contents preclude any comagmatic relationship with the later Ordovician rocks. This is not unexpected given the 30 – 40 million-year age difference between these two suites (Figure 8.1).

In terms of major elements, the Goonumbla and Wombin Volcanics, including the ore-related BQM intrusions, show a coherent trend from basaltic trachyandesite through trachyte, with increasing K_2O and decreasing TiO_2, Al_2O_3, Fe_2O_3, CaO and MgO contents with increasing SiO_2 contents. These trends continue from the regional volcanic and intrusive GVC rocks through the QMP intrusions associated with the Endeavour deposits.

Multi-element plots of the regional volcanic and intrusive rocks show the spiked pattern typical of magmas generated in subduction-related tectonic settings. This feature, and the pronounced Fe-depletion with increasing SiO_2 are characteristic of calc-alkaline

Figure 8.7 Multi-element plots for the intrusive rocks associated with the Endeavour deposits compared to the Wombin Volcanics (shaded); **A** E22; **B** E26; **C** E27; **D** E48; **E** aplitic rocks from all four deposits; **F** the microgranite of E48; **G,** the monzodiorite of E26; and **H** the basaltic trachyandesite zero porphyry dykes of E26.

Legend

BQM — early-mineral and late-mineral B-QMP — K-QMP — KA-QMP

Aplitic rocks — E48 microgranite — E26 and other monzodiorite intrusions into the Goonumbla Volcanics

Basaltic trachyandesite — Zero porphyry

KA-QMP of E22 and E48 — B-QMP intrusions

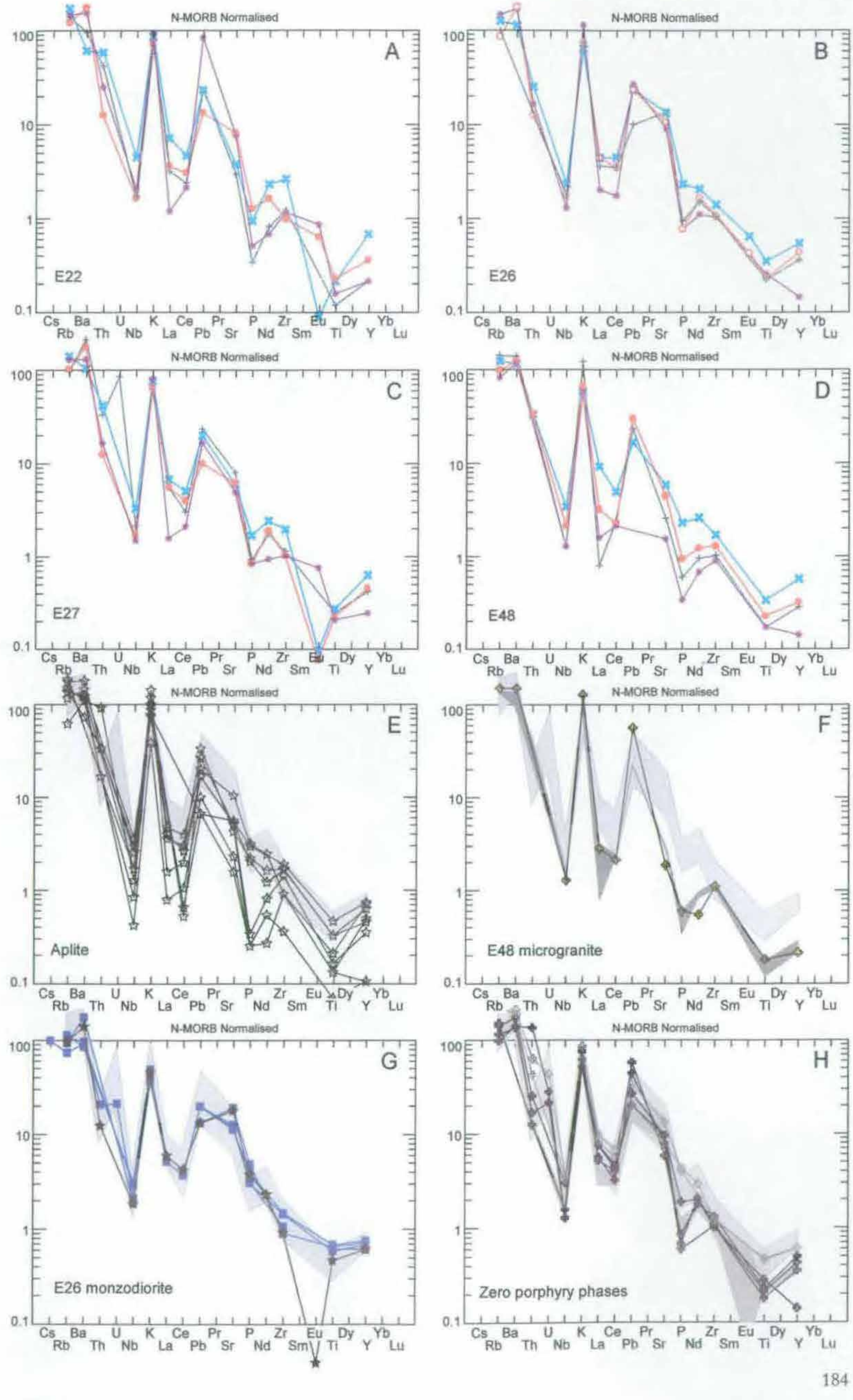
N-MORB Normalised
A
E22
B
E26
C
E27
D
E48
E
Aplite
F
E48 microgranite
G
E26 monzodiorite
H
Zero porphyry phases
100
10
1
0.1
Cs Ba U K Ce Pr P Zr Eu Dy Yb
Rb Th Nb La Pb Sr Nd Sm Ti Y Lu

and shoshonitic suites generated in subduction-related environments. These features are characteristic of early, low pressure fractionation of olivine and clinopyroxene, followed by later fractionation of Fe-Ti oxide and plagioclase (Gill, 1981).

Within the Goonumbla and Wombin Volcanics and their comagmatic intrusive counterparts, there is a general increase in the extent of fractionation, and in the extent of LILE enrichment, from Mid- to Late Ordovician, with the ore-related QMP intrusions being the most evolved and LILE-enriched rocks.

The difference in trace element abundances with fractionation between the BQM and the ore-related QMP intrusions (higher Y, Nb and Zr and lower Ba in the BQM than in the QMP intrusions) is good evidence that the BQM did **not** fractionate to the porphyry-type compositions characteristic of the QMP intrusions related to the Endeavour deposits. Therefore, the BQM intrusions do not represent the parent stock of the ore-related QMP intrusions, in contrast to the claim of Heithersay and Walshe (1995). The proposal that fractional crystallisation alone could not have produced the QMP intrusions from the BQM magma is also in contrast to the model suggested by Lang and Titley (1998) for the evolution of the intrusions associated with the calc-alkaline-related porphyry deposits in the Laramide region of Arizona, USA. They suggested that the earliest intrusions in the Laramide magmatic complexes were mainly andesitic to rhyolitic and unmineralised. With time, the intrusions became more felsic so that the later intrusions, which are associated with mineralisation, are the most felsic, reaching compositions of quartz monzonite and granite. The fact that the KA-QMP and late-mineral B-QMP intrusions are generally less fractionated than the older K-QMP intrusions provides additional evidence for the BQM not being representative of the parent stock, since if the BQM magma was the parent stock, successive intrusions should be progressively more felsic. However, the overall strong trends of increasing K_2O and decreasing TiO_2, MgO, etc., with increasing SiO_2 from the BQM to the QMP intrusions as a whole, do indicate that fractionation from a BQM-type magma did play some role in the formation of the ore-related QMP intrusions.

8.3.5 Other intrusions in the Endeavour porphyry complexes

8.3.5.1 Aplitic rocks

Most of the aplitic rocks studied are compositionally indistinguishable from the rest of the sample suite (Figures 8.4 – 8.5). This is interpreted to imply that they are comagmatic, and that they probably developed as late-stage differentiates of the rocks that they intruded. This comagmatic nature is demonstrated in the multi-element plots, which although variable due to the inclusion of examples of aplites associated with intrusions through the BQM – KA-QMP range, still broadly resemble the major intrusive rocks (Figure 8.7e).

8.3.5.2 E48 microgranite

Geochemically, the E48 microgranite intrusion most closely resembles the KA-QMP intrusions, particularly the E22 and E48 examples, on the Harker diagrams (Figures 8.4 – 8.5) and on the multi-element plot (Figure 8.7f). It is possible that the microgranite is a late-stage derivative of the KA-QMP phase at E48 that intruded prior to the hydrothermal alteration and veining related associated with the emplacement of the KA-QMP intrusion at this deposit.

8.3.5.3 E26 monzodiorite

In all geochemical aspects, the monzodiorite intrusion in the lower portions of E26 is similar to both the Nelungaloo and Goonumbla volcanic and intrusive rocks (Figures 8.2 – 8.5). It cannot be distinguished geochemically from these rocks.

Radiometric ($^{40}Ar/^{39}Ar$) dating on weakly to moderately chloritised hornblende from the monzodiorite at E26 yielded a correlation age of 495.6 ± 26.4Ma (Figure 8.1). U-Pb (SHRIMP) dating of zircons from the Goonumbla Siding monzodiorite intrusions yielded an age of 450.8 ± 4.2Ma (Butera *et al.*, 2001; Figure 8.1). Since the oldest volcanic rocks in the region of the Endeavour deposits are interpreted as the Mid Ordovician Goonumbla Volcanics, the $^{40}Ar/^{39}Ar$ age is thought to be erroneous due to the moderate chloritisation of the hornblende dated. Instead, because the E26 monzodiorite has a virtually identical multi-element pattern to that of the regional Goonumbla Hill and "Cardiff" (cf. Figure 2.5) monzodiorite intrusions (Figure 8.7g), it is considered to be of a similar age to these regional intrusions, which is more likely given the age of the host volcanic sequence (Figure 8.1).

8.3.5.4 Post-mineral zero porphyry dykes

There are two distinct groups of rocks within the volumetrically minor post-mineral "zero porphyry" category; the relatively older basaltic trachyandesite dykes and the K-feldspar phyric mafic monzonite zero porphyry dykes (cf. section 3.3.5).

Basaltic trachyandesite dykes

It is obvious on the whole rock major and trace element plots that the trachyandesites are compositionally distinct from the zero porphyry rocks (Figures 8.4 – 8.6). The trachyandesites plot as shoshonites, or as basaltic trachyandesites in the area that Keith *et al.* (1998) defined as "mafic alkaline" rocks: more mafic than andesite and trachyandesite and more alkali-rich than basalt or picrobasalt. In addition to the significant SiO_2 gap between these two rock types, Figure 8.7h shows that the basaltic trachyandesites are relatively more enriched in K, Ba, La, Ce and Sr and less depleted in Nb, Th, P and Ti than the zero porphyry dykes and the other ore-related intrusive rocks.

It is considered here that these small volume shoshonitic basaltic trachyandesitic dykes are probably the result of magmatism associated with the waning stages of extension in the GVC. This magmatism is thought to represent a "last gasp" of shoshonitic magmatism of Latest Ordovician age, probably related to the ultimate cessation of regional extension responsible for the generation of the entire GVC.

Zero porphyry monzonite dykes

The zero porphyry monzonites plot entirely within the compositional fields defined by the intrusive rocks associated with the Endeavour deposits, and the multi-element plot (Figure 8.7h) shows that they most closely resemble B-QMP intrusions. Since the zero porphyry dykes post-date ore-related QMP intrusions, it is interpreted here that the zero porphyries are further examples, next to the late-mineral B-QMP intrusions, of renewed, "less-fractionated" igneous activity in the vicinity of the Endeavour deposits. However, from the lower SiO_2 contents (and associated lesser evolved character of the other major and trace elements), it is apparent that the late-mineral B-QMP intrusions and zero porphyries did not evolve and fractionate more felsic end-members and as a result their potential for exsolving the ore-bearing magmatic – hydrothermal fluids was diminished.

The zero porphyry monzonites of E26 are geochemically, texturally and mineralogically similar to zero porphyry dykes at E37 and to the Gunningbland Forest monzonite porphyries. It is possible that the zero porphyry dykes at E26 represent near-mine examples of regional scale intrusive activity in the Latest Ordovician GVC, in which significant fractionation and the subsequent exsolution of magmatic – hydrothermal fluids and associated mineralisation did not occur.

8.4 Rare earth element geochemistry

The rare earth elements (REE) are particularly useful in petrogenetic studies of igneous rocks because they show systematic geochemical behaviour during geochemical/magmatic processes. The chondrite-normalised REE patterns for volcanic and intrusive rocks of the GVC and thereafter, those for the intrusions associated with the Endeavour deposits, are discussed below.

8.4.1 Regional GVC rocks

Normalised whole rock REE abundances for Nelungaloo Volcanics and Condobolin Road monzodiorite samples show strong light REE (LREE) enrichment, with $(La/Sm)_N$ values between 1.86 – 2.79 (average 2.26) and La abundances 75 – 110 times chondrite. The REE patterns slope continuously towards Lu (Figure 8.8a). $(Gd/Yb)_N$ values (1.67 – 2.14) are higher than any other GVC rocks, reflecting the slope of the Nelungaloo patterns relative to the essentially flat HREE levels of all but the most evolved GVC rocks. The wide range of HREE levels, with $(Yb)_N$ ranging from 7 to 18, is considerably more than could be produced by fractionation from a single parent in this lava suite, which is limited to the basaltic andesite and andesite range of compositions. Different parental magmas, with significantly varying $(La/Yb)_N$, from 4.2 to 10.5, are thus indicated for the Nelungaloo lavas (Crawford, 2001b).

The Goonumbla Volcanics and comagmatic Goonumbla Hill and Goonumbla Siding monzodiorite intrusions (cf. Figure 2.5) have coherent LREE enriched patterns with flat HREE relative to the Nelungaloo rocks (Figure 8.8b). They show moderate LREE enrichment, with $(La/Sm)_N$ ranging from 2.11 – 3.01 (average 2.49), and have $(Gd/Yb)_N$ values from 0.91 to 1.62, average 1.57. The Goonumbla Volcanics and associated comagmatic intrusions lack any significant Eu anomaly. Wombin Volcanics show REE patterns that are close to those of the Goonumbla Volcanics, with similar $(La/Sm)_N$ and $(Gd/Yb)_N$ value ranges; 2.53 – 3.90, average 3.10 and 0.98 – 1.62, average 1.28 respectively (Figure 8.8c). The most evolved of the Wombin Volcanics show a significant dip in middle REE (MREE). The similar REE pattern of the Wombin intrusions and the Wombin Volcanics confirms their comagmatic character.

Figure 8.8 Chondrite-normalised REE diagrams for the volcanic and intrusive rocks of the Goonumbla Volcanic Complex and intrusive rocks associated with the Endeavour deposits compared to Wombin rocks (shaded). **A** Nelungaloo Volcanics ( ) and intrusions ( ); **B** Goonumbla Volcanics ( ) and intrusions ( ); **C** Wombin Volcanics ( ) and intrusions ( ); **D** Comparative patterns for the intrusive rocks associated with E22, E26, E27 and E48; **E** BQM intrusions ( ); **F** B-QMP intrusions (early- and late-mineral); **G** K-QMP intrusions ( ); and **H** KA-QMP intrusions ( ).
Normalisation values are from Sun and Mc Donough (1989).

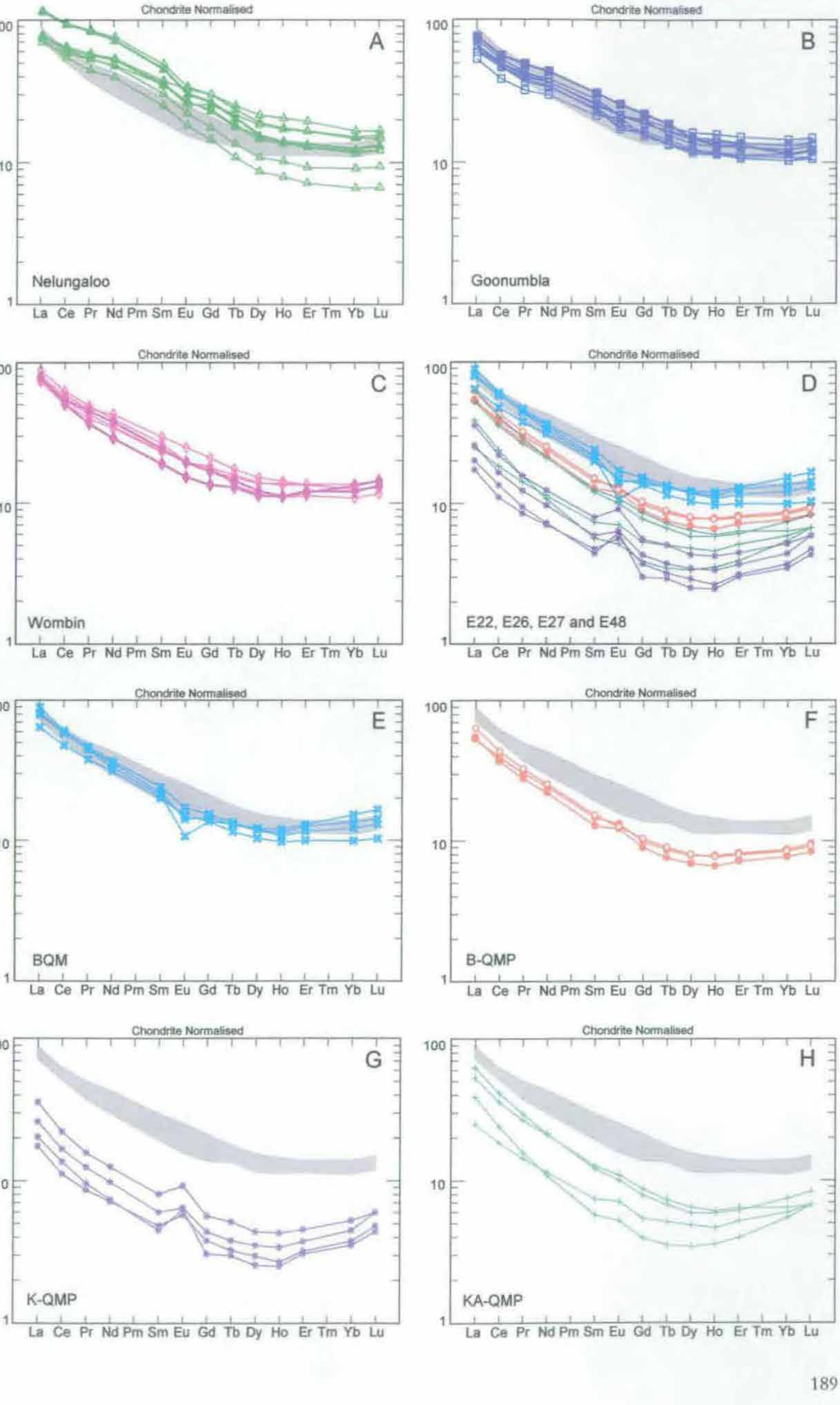
Chondrite Normalised
A
Nelungaloo
B
Goonumbla
C
Wombin
D
E22, E26, E27 and E48
E
BQM
F
B-QMP
G
K-QMP
H
KA-QMP
100
10
1
La Ce Pr Nd Pm Sm Eu Gd Tb Dy Ho Er Tm Yb Lu

8.4.2 Intrusive rocks associated with the Endeavour deposits

Chondrite normalised whole rock REE patterns for most of the intrusive rocks associated with the Endeavour deposits are different from those of the regional intrusive rocks of the GVC (Figures 8.8e – 8.8h).

BQM intrusions are virtually identical to the intrusions associated with the Wombin Volcanics with the exception of a slightly stronger negative Eu anomaly (Figures 8.8e). The Eu anomalies (Eu/Eu*, where Eu* = $(Sm_N \cdot Gd_N)^{1/2}$; Taylor and McLennan, 1985) for the Wombin Volcanics intrusions are 0.97, while those for the BQM range from 0.64 to 0.92, averaging 0.82. There is, however, a significant change in the Eu anomaly for the ore-related QMP intrusions; it becomes progressively more positive from B-QMP to K-QMP and then becomes less positive again in KA-QMP intrusions. Eu/Eu* range from 1.01 – 1.14 (average 1.09) for the B-QMP intrusions, between 1.28 – 1.71 (average 1.44) for the K-QMP intrusions and between 1.05 – 1.14 (average 1.10) for the KA-QMP intrusions (Figures 8.8f, g and h respectively).

LREE enrichment becomes progressively more pronounced through the ore-related intrusive sequence, which is reflected in the steepening LREE profiles in Figures 8.8e through h. The average $(La/Sm)_N$ value for the Wombin intrusions is 3.10, whereas it increases to 3.41 (range 3.05 – 3.67) in the BQM intrusions, through 3.81 (range 3.45 – 4.04) for the B-QMP intrusions, 4.01 (3.44 – 4.27) for K-QMP intrusions to 4.60 (3.17 – 6.36) for the KA-QMP intrusions.

Besides the Eu anomaly and steepening LREE slopes, the most obvious difference between the regional intrusive rocks and those associated with the Endeavour deposits is the progressive decrease in overall REE abundances through the sequence of BQM (which is similar to the Wombin Volcanics) through B-QMP to K-QMP. This trend is reversed by the KA-QMP, which are typically not as depleted in REE as K-QMP intrusions (Figure 8.9). La abundances are typically 80 – 90 times chondrite, decreasing systematically to 18 – 20 times chondrite in the most evolved QMP rocks. At the same time, REE patterns become more "u-shaped" as a trough develops between Eu and Ho with increasing fractionation, and HREE depletion occurs at a slower rate than LREE depletion. $(Gd/Yb)_N$ values, although somewhat variable, decrease from an average of 1.12 for BQM intrusions (Wombin intrusions average, 1.17) to an average of 0.98 for the KA-QMP intrusions. These features are evident for all four of the Endeavour deposits (Figures 8.9).

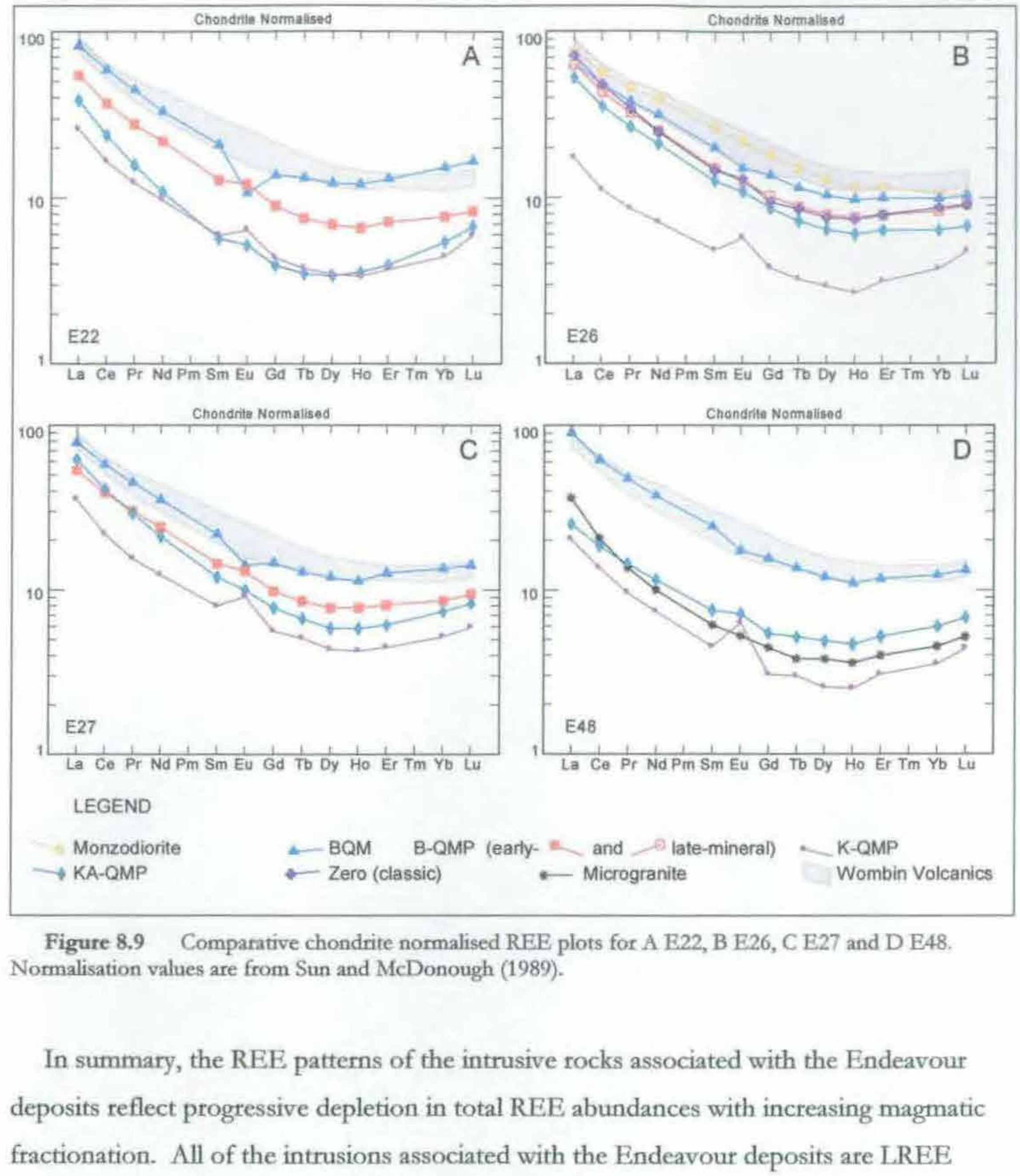

Figure 8.9 Comparative chondrite normalised REE plots for A E22, B E26, C E27 and D E48. Normalisation values are from Sun and McDonough (1989).

In summary, the REE patterns of the intrusive rocks associated with the Endeavour deposits reflect progressive depletion in total REE abundances with increasing magmatic fractionation. All of the intrusions associated with the Endeavour deposits are LREE enriched; however, relative LREE enrichment becomes more pronounced though the ore-related QMP intrusions. From the BQM intrusions, which have virtually identical REE patterns, with the exception of the slightly stronger negative Eu anomaly, to the regional monzonite intrusions associated with the Wombin Volcanics, the QMP intrusions are progressively depleted in MREE and in HREE with increasing fractionation. However, HREE depletion has occurred at a slower rate than MREE depletion, which gives rise to the characteristic "u-shaped" patterns with increasing fractionation.

8.4.3 Interpretation

Below follows a discussion of the mineralogical and igneous processes that are envisaged to have controlled REE fractionation in the intrusive rocks of the GVC and more specifically, those related to the Endeavour deposits. In particular, it addresses possible explanations for the decrease in overall REE abundances from the BQM to the more fractionated ore-related QMP intrusions, the changing Eu anomaly, LREE enrichment and the development of the "u-shaped" patterns of the ore-related QMP intrusions.

8.4.3.1 REE abundances

The most striking feature of the REE patterns of the ore-related intrusions compared to those of the regional GVC rocks is the progressive decrease in the relative abundance of REE with increasing fractionation, where K-QMP are the most fractionated rocks even though they predate KA-QMP intrusions. Major and trace element geochemical characteristics of the regional GVC rocks, as well as those of the ore-related intrusions, define a systematic trend more consistent with high-temperature magmatic fractionation than with intense hydrothermal alteration. Thus, processes other than alteration and consequent dilution (by quartz veining) must be invoked to explain the progressive decrease in REE abundances in the QMP intrusions.

Accessory phases such as apatite, sphene and zircon strongly fractionate REE in magmatic systems; LREE and MREE are important components of apatite and sphene, and HREE are significant in zircon and less so in apatite (Bea, 1996). Thus, fractionation and removal of these minerals may result in variable and significant REE depletion in the residual melt. Since most of the intrusive rocks of the GVC, including those associated with ore deposition, contain these REE-rich accessory phases; it is likely that the fractionation of these minerals may have affected the overall abundances of REE in these rocks. However, the absolute effect of this fractionation cannot be established. In addition, the apatite-, sphene- and zircon-bearing, geochemically similar, though less fractionated Wombin intrusions, e.g. the Gunningbland Forest monzonite porphyries, do not show the REE depletion characteristic of the ore-related intrusions, including the late-mineral B-QMP and zero porphyries of E26 (Figure 8.10).

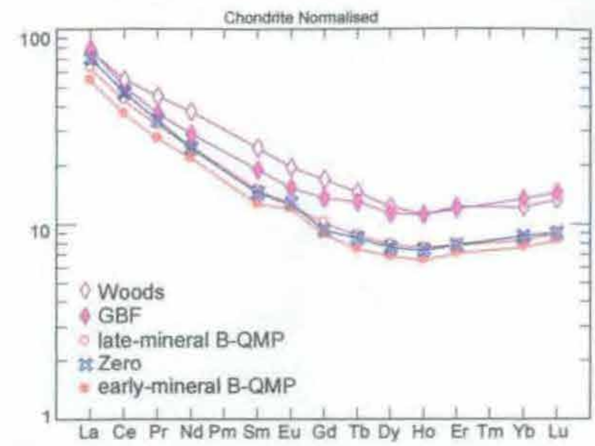

Figure 8.10 REE plots for pre- and late-mineral B-QMP intrusions (E22 and E26 respectively), E26 zero porphyry (Zero) and the Gunningbland Forest (GBF) and Woods monzonite porphyries.

Modelled fractionation effects

The possible effects of fractionation of the REE-rich and other phases have been modelled in an attempt to explain the distinct decrease in REE abundances from the BQM (and other intrusions into the Wombin Volcanics) to the QMP rocks directly associated with mineralisation.

Even though arguments presented above preclude the BQM from being the direct parent magma of the QMP intrusions, given the typical monzodioritic to monzonitic intrusions into the Wombin Volcanics, it is likely that fractionation of a BQM-type monzodiorite magma had some role in generating the more fractionated ore-related QMP intrusions. Since the regional monzodioritic to monzonitic intrusions within the GVC have remarkably concordant REE patterns to the BQM, the BQM intrusion of E27 is used in this modelling exercise to be *representative* of the parent magma. Fractionation from BQM-type magma to K-QMP-type would involve probably 20 – 30% fractionation by weight of a feldspar + hornblende-dominant assemblage (see Lindsay *et al.* (2001) for a typical model). Assuming a parent – daughter relationship between BQM-type magma and K-QMP-type magma, and given the measured REE abundances in E27 of these rocks, Figure 8.11 shows the REE patterns of the bulk fractionate required to drive BQM to K-QMP if it corresponded to 10%, 30% and 50% by weight fractionation. Taking the 30% bulk fractionate, the REE pattern has a pronounced negative Eu anomaly, a marginally concave HREE pattern, with $(Dy/Yb)_N$ of 0.95, and strong LREE enrichment, where the LREE pattern is more convex than is typical for GVC monzodiorites. This pattern is different from other GVC intrusive rocks in having higher HREE levels (25 – 30 times chondrite).

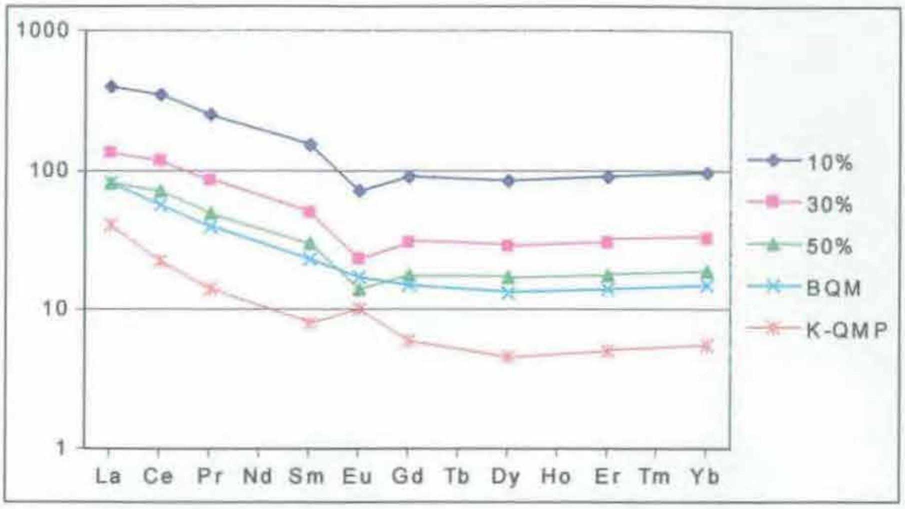

Figure 8.11 REE plots for E27 BQM modelled as a parent magma, and K-QMP as a daughter, showing REE patterns of a bulk fractionated required to be extracted from BQM to make K-QMP if the fractionation involved was 10%, 30% and 50%.

If fractionation of BQM to K-QMP involved perhaps 40 – 50% removal of a bulk crystal extract, how much of this extract was hornblende, and could hornblende be responsible for producing the saucer-shaped K-QMP REE patterns? In terms of MgO, BQM rocks contain, on average, ~2% MgO, whereas typical dioritic hornblende contain 12 – 14% MgO (Roberts *et al.*, 2000). Thus, if hornblende was the only mafic (MgO-affecting) phase crystallising through this interval, dropping the ~2% MgO of BQM-type magma to the ~0.5% MgO of K-QMP-type magma requires ~10 – 12% by weight fractionation of hornblende if hornblende alone was fractionating. However, if hornblende comprised only ~10% of the 30% bulk fractionate (the remainder being plagioclase, K-feldspar and quartz), the same drop in MgO to ~0.5% can be achieved. This indicates that probably no more than ~10% hornblende fractionation could have been involved in the fractionation scheme linking a BQM-type parent magma to the evolved K-QMP.

Simple REE modelling calculations are shown in Figure 8.12 with the aim of testing hornblende's effect on REE if it was removed from the BQM to produce the K-QMP intrusions. The hornblende (**hlb1**) was taken from a study of diorite – granodiorite fractionation with compositions close to the rocks studied herein (Fourcade and Allegre, 1981). Subtraction patterns are shown for the removal of 10% of hbl1 from the BQM. The hornblende fractionation has virtually no effect, with the exception of the development of a weak positive Eu anomaly. Note, however, that plagioclase, K-feldspar and quartz were also fractionating over this interval. The calculated fractionation pattern for the removal of 10% hornblende along with 20% of a typical feldspar separate (also from Fourcade and Allegre, 1981) from the BQM produced a REE pattern very close to the BQM pattern (not shown in Figure 8.12 for clarity). This modelling implies that hornblende was not a key factor in dropping the REE patterns from the BQM to the K-QMP melts, and that accessory phases and/or other factors must have been involved.

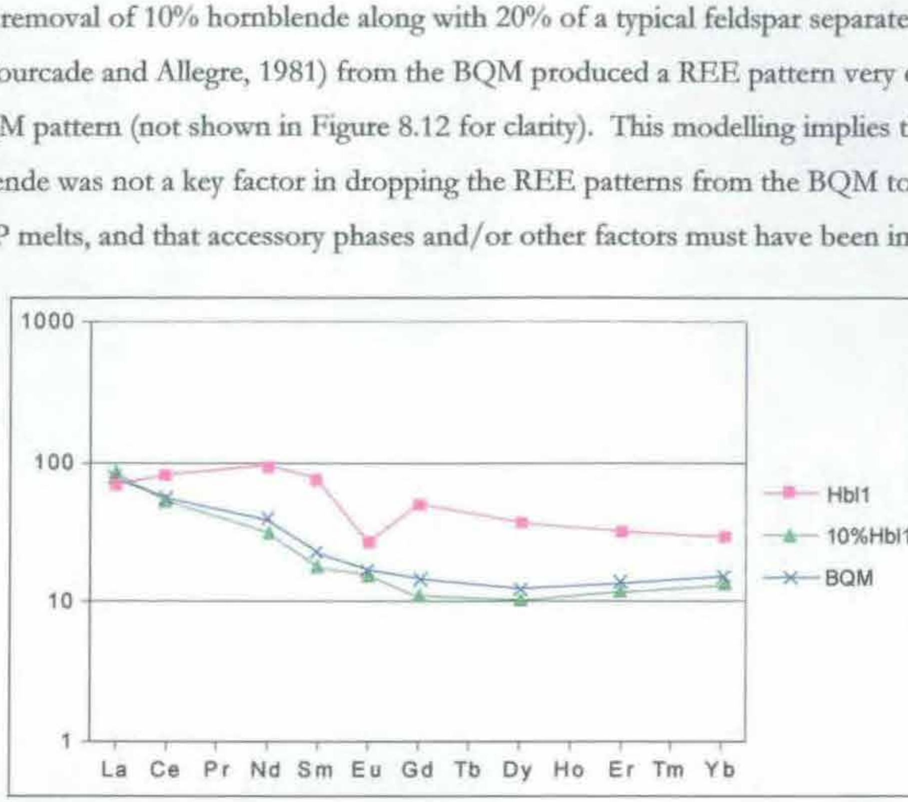

Figure 8.12 REE plots for the E27 BQM, hornblende (**hbl1**) (from Fourcade and Allegre, 1981), showing the effects of fractionating 10% of **hlb1** from a BQM-type magma.

The progressive decrease in P_2O_5 from BQM to K-QMP shows unambiguously that apatite was a fractionating phase over this interval. The decrease in Zr (depleted Zr trend) indicates the same for zircon fractionation. Another REE-rich phase to consider is sphene, which has REE patterns virtually identical to hornblende in such rocks, but 1 – ~1.5 orders of magnitude higher (Fourcade and Allegre, 1981). The effect of sphene would be much like that of hornblende, but 10 – 50 times less sphene is required. Only a very small (<0.1%) amount of sphene fractionation could have been involved because it depletes the residual melt in MREE too rapidly. In addition to apatite, zircon and sphene, allanite would probably also have been fractionating in such evolved rocks. Although not searched for exhaustively in the GVC intrusions, it is reported from a number of detailed mineralogical studies of diorite – granodiorite fractionation (e.g. Fourcade and Allegre, 1981; Roberts *et al.*, 2000).

Using typical diorite REE patterns from Fourcade and Allegre (1981) for hornblende, apatite, zircon, sphene and allanite, three different proportions of these phases were added to the plagioclase, K-feldspar and quartz dominant 30% bulk fractionate to see which would "best fit" the BQM to K-QMP drop in REE abundances by fractionation (Figure 8.13). The three models were:

1) BQM = 10% plag + 10% K-feldspar + 10% Hbl + 0.1% All + 1% Zir + 0.1% Apa;

2) BQM = 10% plag + 10% K-feldspar + 10% Hbl + 0.15% All + 2% Zir + 0.2% Apa;

3) BQM = 10% plag + 10% K-feldspar + 10% Hbl + 0.15% All + 2% Zir + 0.25% Apa

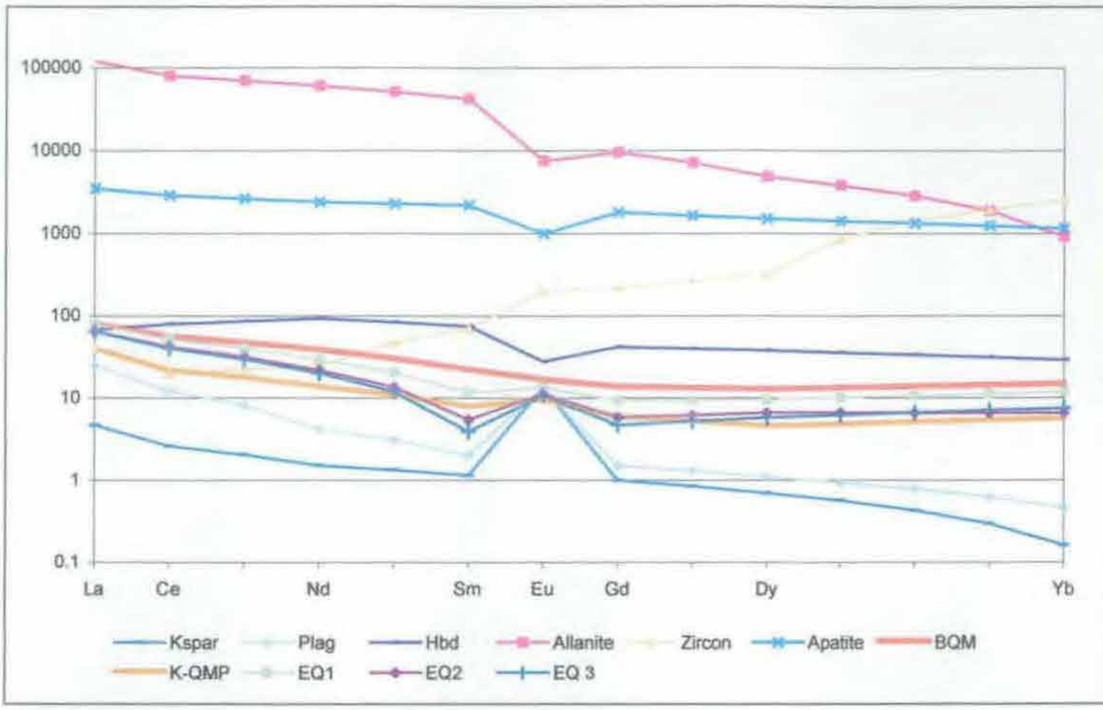

Figure 8.13 REE patterns for E27 BQM, E27 K-QMP and Equations 1, 2 and 3 above using typical dioritic REE patterns for hornblende, apatite, zircon, sphene and allanite from Fourcade and Allegre (1981).

It is clear from Figure 8.13 that HREE patterns can be matched for reasonable amounts of fractionation typical of monzodioritic to monzonitic – quartz monzonitic compositions, as can the generation of the positive Eu anomaly. However, all three models produce patterns that are too enriched in LREE for fractionation alone to account for the overall depletion in LREE abundances in the more evolved K-QMP rocks. Although it is possible that choice of different REE patterns for the accessory phases might produce better matches for LREE, those selected were from a suite very similar to the GVC, and are considered to be reasonable and representative. Therefore, it is interpreted that the shortfall in the LREE is real, and requires another explanation.

Magmatic fluid exsolution

A shallow crustal process such as magma devolatilisation can greatly influence REE abundances. This is suggested because it has been shown experimentally that REE, especially the LREE and MREE can partition into the volatile-rich fluid during phase separation associated with pressure reduction or crystallisation (Reed *et al.*, 2000). The separation of an aqueous phase is thought to be a relatively common feature of late-stage crystallisation in magmatic – hydrothermal systems, as suggested by experimental work on volatile exsolution from Cl-enriched granitic magmas (Webster, 1997) and the results of modelling of simultaneous exsolution of Cl-bearing vapour and liquid from a silicate melt by Shinohara (1994). Since pervasive alteration and ore deposition within the later porphyritic intrusions in porphyry-style deposits is compatible with the loss of most of such a volatile-rich fluid into the surrounding host rocks (Henley and McNabb, 1978; Lang and Titley, 1998), it seems a feasible mechanism to investigate for the Endeavour deposits.

The melt-fluid experiments of Webster *et al.* (1989) demonstrated that aqueous fluids containing Cl ± F play a significant role in the fractionation of lithophile trace elements, such as REE, in halogen-enriched, water-saturated magmas. Smith *et al.* (1999) proposed that the release of a F-rich volatile phase could contribute to modifying the abundances of LREE and Y (and HREE) in some granitic magmas. Other workers have also invoked the evolution and subsequent loss of an aqueous phase as a cause of REE abundance modification, e.g. Candela (1984; 1990) and, specific to the Chilean porphyry deposits, Baldwin and Pearce (1982). Candela (1984) proposed that in the presence of a volatile-rich phase, LREE and to a lesser extent MREE, partition preferentially into the volatile-rich phase, leaving the residual melt relatively depleted in LREE and to a progressively lesser extent, MREE and HREE.

There are several field examples that demonstrate the role of volatile-induced REE mobilisation in magmatic – hydrothermal environments. Carten *et al.* (1988) proposed that the presence of fluorite and REE-bearing minerals such as monazite, zircon, apatite and xenotime, in high temperature veins in the Seriate Stock of the Henderson porphyry Mo deposits, confirmed the mobility of these elements in magmatic – hydrothermal fluids. This was proposed by Carten *et al.* (1988) because stable fluoride complexes involving these elements have been suggested by numerous authors, e.g. Flynn and Burnham (1978), Alderton *et al.* (1980) and Taylor *et al.* (1981). It has also been proposed for the Homrit Waggat granite ring complex in Egypt, that volatile transfer with the formation of REE-halogen complexes may have resulted in variable REE fractionation (Hassanen, 1997). A similar scenario of REE-halogen complexing and REE mobility was proposed to explain the variable REE fractionation in the potassic arc magmas of the Indonesian Lewotolo volcano (de Hoog and van Bergen, 2000). This experimental and field data is taken as reasonable evidence that the presence of a Cl- ± F-bearing volatile-rich fluid can influence the REE abundances of the residual melt in fractionating magmatic systems.

The presence of primary accessory F-rich phlogopite and fluorapatite phenocrysts in the QMP intrusions associated with the Endeavour deposits (cf. Chapter 7) and fluorite in the early and main stage alteration assemblages (cf. section 4.4.1 and 4.4.5 respectively) is indicative of fluorine having an important function in these systems. It has also been established that Cl-rich brines were important for ore formation at the Endeavour deposits (cf. section 5.8.3). Thus, F and Cl are inferred to have played a significant role in REE mobility in the Endeavour porphyry systems.

Eu anomaly

Eu anomalies in igneous rocks are principally controlled by two factors, feldspar fractionation and oxygen fugacity. Feldspars have low partition coefficients for all REE except Eu, and as a consequence, the presence of feldspars has a minor effect on the overall REE pattern, except for the production of an Eu anomaly. The removal of feldspar from a felsic melt by crystal fractionation will give rise to a negative Eu anomaly (Green, 1980). Conversely, accumulation of feldspar will give rise to a positive Eu anomaly. The Eu anomaly can also be controlled by the oxygen fugacity of the magma, where the magnitude of the anomaly is inversely proportional to the prevailing oxygen fugacity conditions during partial melting and fractional crystallisation (McKay, 1989). In other words, increasing oxygen fugacities during fractional crystallisation or partial melting result in increasingly positive Eu anomalies. However, in addition to these two major factors, from the REE modelling presented above, it is evident that the fractionation of variable amounts of REE-rich accessory phases can also generate a positive Eu anomaly.

Eu anomalies in the regional volcanic and intrusive rocks of the GVC are negligible. However, all intrusive rocks associated with the Endeavour deposits are characterised by either positive or negative Eu anomalies. Initially, a variably negative Eu anomaly characterises the BQM intrusions. Since the removal of feldspar from a felsic melt can result in the formation of a negative Eu anomaly, its removal from the parental magma to the BQM during fractional crystallisation may have been important. However, the anomaly becomes progressively more positive with fractionation in the more evolved QMP intrusions. Because feldspars are important phases in all rocks of the GVC, including the QMP intrusions, it is thought unlikely that feldspar fractionation (or accumulation) alone could account for the variable nature of the Eu anomaly in the latter rocks, especially the less positive anomaly characteristic of the post K-QMP intrusions.

It is thus proposed here that the Eu anomaly in the ore-related intrusions has been greatly influenced by an increasing oxygen fugacity during fractional crystallisation. This is suggested because the dusting of the feldspars with haematite in all of the intrusive rocks associated with mineralisation is strong evidence that high oxygen fugacities prevailed during crystallisation of the ore-related intrusions. The destruction of magnetite to haematite during main stage alteration and mineralisation (cf. sections 4.4.5) is also interpreted to imply that conditions of increasing oxygen fugacities dominated the magmatic – hydrothermal systems at the time of maximum ore deposition.

Discussion

From the REE fractionation modelling presented above and the experimental evidence that the evolution of a magmatic – hydrothermal fluid influences LREE abundances, it is considered here that a combination of the two processes were responsible for the overall decrease in REE abundances through the BQM → QMP fractionation sequence associated with the Endeavour deposits. It is thought that initially, crystal fractionation associated with a BQM-type magma, which included the fractionation of REE-rich accessory phases such as zircon, apatite, sphene and allanite, resulted in a general decrease in the REE abundances for progressively more fractionated QMP intrusions. However, in addition to this fractionation, the K-QMP intrusions were further depleted in LREE by the exsolution of a magmatic – hydrothermal fluid. This combination of processes satisfactorily explains the LREE depletion and generally lesser REE depletion of the KA-QMP intrusions, since the latter intrusions are typically less fractionated, but also evolved a magmatic – hydrothermal fluid. The less LREE-depleted REE patterns of the more mafic B-QMP intrusions and zero porphyry dykes are probably the result of fractionation of a BQM-type magma, since these intrusions are not associated with the exsolution of magmatic – hydrothermal fluids. It is proposed here that the REE patterns of the ore-related intrusions have been greatly influenced by an increasing oxygen fugacity (indicated by haematite dusting of feldspars) during fractional crystallisation. This is likely to have resulted in the production of progressively more positive Eu anomalies in the ore-related QMP intrusions.

8.5 Radiogenic isotopes

Magma will inherit the isotopic composition of its source during partial melting. This isotopic composition will remain constant during subsequent fractional crystallisation processes provided the magma does not become contaminated by interaction with isotopically different sources like wall rock or other magmas. Thus, estimates of the present-day isotopic characteristics of the mantle as a source region for basaltic magmas may be obtained from young MORB and ocean island basalts, since these rocks have not been significantly contaminated en route to the surface. Because continental crustal material has radiogenic isotopic compositions that are measurably different from those of the mantle, radiogenic isotopic studies of volcanic and igneous rocks provides an effective method of establishing the role of crustal contamination in magma generation.

Radiogenic isotope data is lacking for the Ordovician intrusive rocks in the Goonumbla region and its usefulness is compromised by the fact that samples for radiogenic isotope studies have been collected in isolation from samples collected for geochemical and petrographic work. Because of this, isotope-based petrogenetic models are not well constrained by petrology and petrography. Despite this, several authors have made important contributions to our understanding of the probable petrogenetic processes that led to the isotopic signatures of these rocks.

Three detailed studies of radiogenic isotopes have been conducted in the Goonumbla area; Carr and Dean (1990), Whitford *et al.* (1992) and Carr *et al.* (1995). Additional Pb data were generated by Kolkert (1998).

Carr and Dean (1990) concluded that the Pb isotopic signatures of Au deposits in the western Lachlan Fold Belt reflect the mixing of two mantle sources; one with MORB-like U, Th and Pb abundances and one relatively depleted in Pb. Magmatic feldspars and ore-stage sulphides from E26 were found to have similar Pb isotope signatures, which was interpreted to indicate that both the ore and host rocks of E26 were from the same mantle-derived magmatic source. Of the two mantle sources proposed by Carr and Dean (1990), the E26 Pb isotopic signatures are typical of the depleted Pb source, which is characterised by low $^{207}Pb/^{206}Pb$ ratios (Figure 8.14).

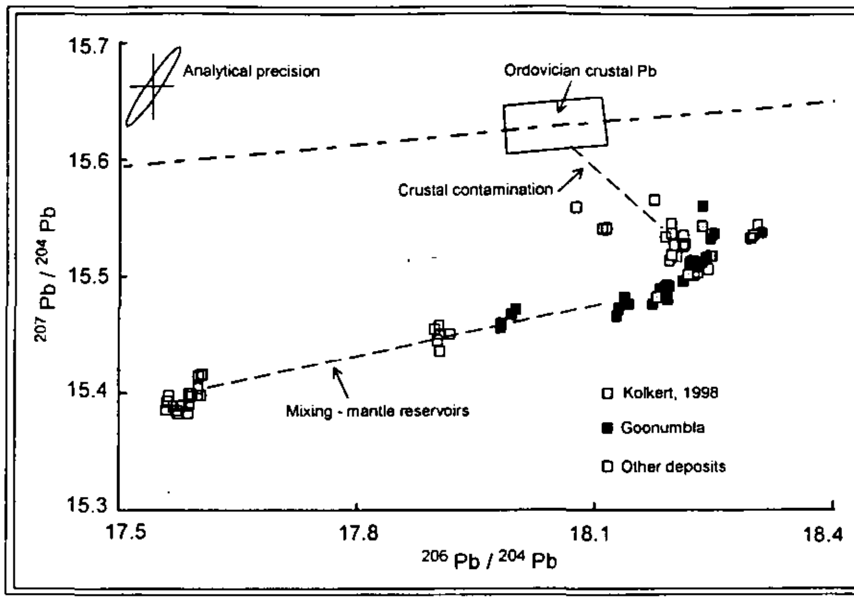

Figure 8.14 A Pb isotope ratio plot of high-Pb sulphides from E26 together with other Ordovician basaltic volcanic rocks from the Lachlan Fold Belt (modified from Carr and Dean, 1990; Whitford *et al.*, 1992).

A reconnaissance Sr and Nd isotopic study of the Goonumbla district has also been conducted (Whitford *et al.*, 1992). These authors sampled (monzo)diorite and monzonite from outcrops along the margins of the "caldera" (assumed here to be some of the intrusions that intrude the Wombin Volcanics, cf. Figure 2.5) and quartz monzonite porphyry intrusions from the Endeavour deposits. One sample of the Early Ordovician Nelungaloo Volcanics was also analysed for Sr and Nd isotopes. Apart from the Nelungaloo example, samples were found to be enriched in Sr, with low Rb/Sr ratios and a fairly wide range of $^{87}Sr/^{86}Sr$ ratios (0.7042 – 0.7061); all features characteristic of shoshonitic rocks. Using Perkins *et al.* (1990) intrusion and alteration age of ~439Ma, calculated initial $^{87}Sr/^{86}Sr$ ratios for the Late Ordovician samples gave a restricted range from 0.70404 to 0.70426; the Nelungaloo sample gave a higher initial $^{87}Sr/^{86}Sr$ ratio of 0.70464. The higher initial $^{87}Sr/^{86}Sr$ ratio for the Nelungaloo sample was interpreted to reflect minor crustal contamination. Nd isotopes were also measured and Whitford *et al.* (1992) calculated that the Goonumbla rocks had $\varepsilon_{Nd(i)}$ values ranging from +5.8 to +7.9, where the sample with the highest $\varepsilon_{Nd(i)}$ value had the lowest initial $^{87}Sr/^{86}Sr$ ratio. These $\varepsilon_{Nd(i)}$ values are within the range of the ~440Ma MORB reservoir and preclude significant contamination by radiogenic continental crust.

Whitford *et al.* (1992) concluded that the Sr and Nd isotopic data complemented the Pb isotopic data of Carr and Dean (1990) and confirmed the primitive isotopic character of the Endeavour host rocks. The high $\varepsilon_{Nd(i)}$ values, low initial $^{87}Sr/^{86}Sr$ ratios and the low

^{207}Pb/^{206}Pb ratios were interpreted by Whitford *et al.* (1992) to be consistent with a mantle source with little or no crustal input. These characteristics are typical of the rocks and sulphides from E26, which is consistent with a magmatic origin for the Cu-Au. They suggested that variations in the Nd isotopic composition could reflect either variation in the mantle source or minor crustal contamination (Figure 8.15).

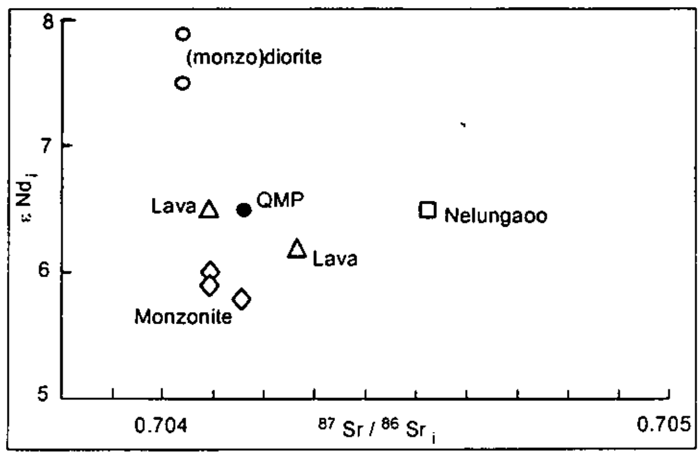

Figure 8.15 Plot of initial ^{87}Sr/^{86}Sr vs εNd$_{(i)}$ for intrusive and volcanic rocks of the GVC. Initial ratios calculated at 470Ma for Nelungaloo and 439Ma for all other samples (Whitford et al., 1992).

Carr *et al.* (1995) showed that most of the Ordovician Au (and Cu) deposits of the Lachlan Fold Belt are characterised by low ^{207}Pb/^{204}Pb ratios but variable ^{206}Pb/^{204}Pb ratios. Based on the Pb isotopic data, they concluded, " .... it was difficult to propose that there is even a minor crustal Pb component within the ore deposits studied".

Specific to the Goonumbla region, Carr *et al.* (1995) showed that Pb isotopic compositions of whole rock and feldspar concentrates from E26 were similar (high ^{206}Pb/^{204}Pb ratios, 18.204 – 18.215), confirming a magmatic origin for the Cu-Au mineralisation. Kolkert (1998) analysed Pb isotopes in galena from late stage L3 veins (cf. Figure 4.2) distal to the E26 and E28 systems and found that they had identical isotopic compositions to Carr *et al.*'s (1995) whole rock and feldspar analyses (Figure 8.14), precluding any local scavenging of Pb on the periphery of the systems.

As with Whitford *et al.* (1992), there is a dilemma concerning the role of crustal (radiogenic) Pb. Initially Carr *et al.* (1995) suggested little or no crustal input. However, they later suggested that deviation (higher ^{207}Pb/^{204}Pb ratios) from the mixing line between the two proposed mantle components, described in Carr and Dean (1990), in a group of samples from the Endeavour deposits, represented varying degrees of crustal contamination. This crustal contamination, they proposed, was most likely to have involved hydrothermal mixing of magmatic Pb with more fractionated, radiogenic crustal Pb, and that the timing of this mixing was early in the intrusive history of the deposits. They suggested that early hydrothermal fluids circulated through the Early Ordovician sedimentary and volcanic sequence and leached crustal Pb that then mixed with magmatic Pb during later ore deposition.

Recent studies have shown that the Nelungaloo Volcanics were derived from subduction-related processes in an oceanic island arc environment (Glen *et al.*, 2001). This precludes the Nelungaloo Volcanics as a source for crustal Pb, and an alternative source is required to explain the crustal Pb signature on the Endeavour deposits. It is proposed here that Latest Ordovician, craton-derived sediments such as the Girliambone Group (REF??) could have been a source of radiogenic Pb. The probability of a crustal component is also inferred from $\varepsilon_{Nd(i)}$ values. $\varepsilon_{Nd(i)}$ values decrease with time in all of the Ordovician volcanic belts of New South Wales (Figure 8.16). This decrease has been interpreted to reflect the gradual appearance of a crustal component in the island arc derived melts towards the Late Ordovician as the arc migrated towards the craton (Crawford *et al.*, 2001).

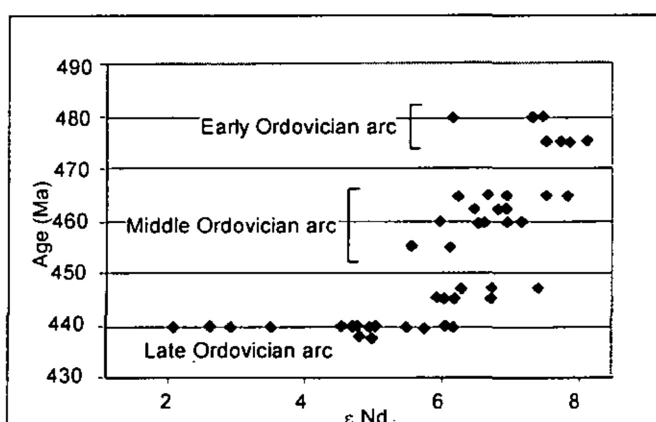

Figure 8.16 Age-corrected $\varepsilon_{Nd(i)}$ values for Ordovician igneous rocks from the Junee-Narromine and Molong volcanic belts of New South Wales (Crawford *et al.*, 2001).

8.6 Summary

The Early Ordovician Nelungaloo Volcanics and intrusions are a high-K calc-alkaline suite that is not comagmatic with the later Ordovician rocks. The Goonumbla and Wombin Volcanics and intrusions, including the BQM intrusions, show a coherent trend from basaltic trachyandesite through trachyte, with increasing K_2O and decreasing TiO_2,

Al_2O_3, Fe_2O_3, CaO and MgO contents with increasing SiO_2 contents. These trends continue through to the QMP intrusions associated with the Endeavour deposits. The consistent overlap and similar character of trends in most of the major and trace elements with respect to SiO_2, MgO and TiO_2 indicate the comagmatic nature of these intrusive and volcanic rocks in the evolving, high-K calc-alkaline to shoshonitic GVC of the Mid- to Late Ordovician. Spiked patterns on multi-element plots typical of magmas generated in subduction-related tectonic settings, and the pronounced Fe-depletion with increasing SiO_2 are characteristic of calc-alkaline suites generated in subduction-related environments and fractionation of early olivine and clinopyroxene, and later Fe-Ti oxide and plagioclase.

The obvious increase in SiO_2 and K_2O with decreasing MgO, CaO and FeO indicates that the QMP intrusions are more fractionated than the BQM intrusions. Contrary to previous models, this study suggests that the BQM is not the parent magma, but that BQM-like magma did play some role in the formation of the more fractionated QMP intrusions associated with mineralisation at the Endeavour deposits.

REE fractionation modelling has shown that fractionating a BQM-type magma may account for the decrease in overall REE abundances recognised in the more evolved KA- and K-QMP intrusions compared to the BQM intrusions, however it inadequately explains excessive LREE loss in the same. This may have been the result of LREE stripping due to the exsolution of a magmatic – hydrothermal fluid from the QMP magmas.

The high $\varepsilon_{Nd(i)}$ values, low initial $^{87}Sr/^{86}Sr$ ratios and the low $^{207}Pb/^{206}Pb$ ratios of the rocks and sulphides associated with E26 are consistent with a mantle source with little or no crustal input. These characteristics are typical of the rocks and sulphides from E26, which is consistent with a magmatic origin for the Cu-Au. Variations in the Nd isotopic composition are interpreted to indicate an increased crustal component in the Latest Ordovician magmatism in the Macquarie Arc, although the reason for this remains unclear.

CHAPTER 9

Conclusions and Genetic Model

9.1 Introduction

Theories of ore formation in porphyry deposits are well documented in the literature. All porphyry metal systems share the common feature of one or more subvolcanic porphyritic intrusion(s) that are spatially and temporally related to mineralisation. However, as Gustafson and Hunt (1975) pointed out, porphyry deposits tend to be variations on a theme, with each deposit/district having its own distinctive combination of geological features that help set it apart from others in the porphyry continuum. Based on the results of the previous chapters, this chapter presents a new genetic model for the Endeavour porphyry Cu-Au deposits, which incorporates the generic features, together with the geological elements that help to characterise this group of deposits. First, however, models of fluid exsolution and migration through magma chambers are reviewed. In addition, the connection between Au-rich porphyry deposits and island arcs, and the possible role(s) of mafic alkaline, or shoshonitic magmas in porphyry deposits are discussed. This chapter concludes with a brief summation of potential exploration implications and recommendations for future work.

9.2 Volatile exsolution and migration in magma chambers

Many workers have argued that metals are carried as chloride complexes within aqueous magmatic – hydrothermal fluids in porphyry systems, and that most of the metals partition more readily into this aqueous fluid than they do into the silicate melt (Holland, 1972; Kilinc and Burnham, 1972; Henley and McNabb, 1978; Candela, 1984; Candela and Holland, 1986; Candela, 1989; Candela and Piccoli, 1995). There is little doubt that during emplacement, calc-alkaline and alkaline magmas can have the capacity to exsolve an aqueous fluid that can precipitate porphyry-style ore (Henley and McNabb, 1978; Burnham, 1979; Hedenquist and Lowenstern, 1994). However, two fundamental processes have to operate in a shallow crustal magma chamber to cause volatile exsolution and the subsequent formation of a magmatic – hydrothermal ore deposit. Firstly, the melt must become supersaturated with respect to volatiles (which is a function of depth of emplacement, initial melt composition and crystallisation history), and secondly, the aqueous fluid must separate physically from the magma, and be able to migrate and accumulate in the apices of the magma chamber in a focused manner (Burnham, 1979; Candela, 1991; Shinohara and Kazahaya, 1995).

Magmatic volatile exsolution is commonly the result of two sequential processes (Burnham, 1997). Initially, volatile exsolution may be the result of crystallisation of anhydrous minerals from the magma (second boiling), which results in an overall increase in the relative proportion of volatiles remaining in the melt such that the melt exceeds critical volatile saturation. This process is typically enhanced as a consequence of decompression (first boiling) of the magma chamber as it ascends through the crust (Burnham, 1979; Candela, 1991). Once generated, the aqueous fluid forms as bubbles that are dispersed throughout the magma. For the formation of an ore deposit, this dispersed aqueous fluid must buoyantly migrate and accumulate in the apical portions of the intrusion so that it can be focused on expulsion from the magma chamber (Burnham, 1979; Candela, 1991; Hedenquist and Lowenstern, 1994). Instantaneous decompression can be triggered by brittle failure in the roof zone of the magma chamber if hydrostatic pressure associated with the accumulation of an aqueous fluid within the apices of the magma chamber exceeds the lithostatic pressure and tensile rock strength (Henley and McNabb, 1978). Additional fluid can be released from the melt during the decompression event.

Various mechanisms have been proposed for the migration, accumulation and egress of this aqueous fluid in shallow crustal melts (e.g. Henley and McNabb, 1978, Candela, 1991 and Shinohara *et al.*, 1995). These mechanisms are outlined below.

Henley and McNabb (1978) proposed that a magma chamber crystallising along its walls and floor would eventually exsolve an aqueous fluid by second boiling. Convection within the crystallising magma chamber would then deliver the aqueous fluid to the apical parts of the magma chamber due to the density contrast between it and the silicate melt from which it exsolved. Once transported, the fluid would then be expelled from the magma chamber through fractures in its subsolidus roof as a buoyant magmatic vapour plume, from which a higher density, high salinity brine would condense with decreasing pressure. Due to buoyancy controls, the brine would then pond in the core of the plume, where it could produce potassic alteration and associated stockwork vein mineralisation (Henley and McNabb, 1978). The buoyant vapour phase would rise further into the overlying country rocks and possibly form high sulphidation epithermal deposits on interaction with groundwater.

The rising magmatic vapour plume model of Henley and McNabb (1978) relies on a convecting magma. This is considered a distinct limitation, since convection within a magma chamber is only possible if the magma chamber has undergone less than ~25% crystallisation (Candela, 1991). Henley and McNabb's (1978) plume model also relies on the magma chamber crystallising primarily along its wall and does not take into account crystallisation in other parts of the magma chamber.

Based on these limitations, Candela (1991) suggested possible mechanisms of fluid/vapour transport and accumulation within a magma chamber under three different sets of conditions: 1) exsolution of an aqueous fluid at <<20% crystallisation, e.g. at high initial H_2O concentrations or low pressure; 2) exsolution at >~25% crystallisation, e.g. at moderate initial H_2O concentrations or moderate pressures; or 3) volatile exsolution occurs in an immobile crust at >>25% crystallisation, e.g. at lower initial H_2O concentrations or at higher pressures. Candela (1991) determined that volatiles would successfully reach the apical parts of a magma chamber in Cases 1 and 2 and suggested that the critical factor determining the behaviour of the aqueous fluid in a given system is the rate of change of the density of the bubble + melt + crystal systems as crystallisation proceeds, which in turn is controlled by the timing of volatile evolution.

In Case 1 (shallow magmas, or deep, wet magmas; Candela and Holland, 1986), vapour saturation and the subsequent rise of a significantly buoyant aqueous plume occurs early in the crystallisation history where there is a high proportion of only moderately fractionated residual melt. In this case, the residual melt has a relatively low viscosity and the aqueous fluid may rise from a subvertical border zone at the edge of a magma chamber as a buoyant plume in much the same fashion as suggested by Henley and McNabb (1978). This effect is enhanced at shallow depths because of the associated enhanced buoyancy of volatiles. For deeper magmas, or shallow, dry magmas (Candela and Holland, 1986), Case 2 above, vapour evolution typically occurs later in the crystallisation history, at which stage the viscosity of the residual melt is much higher (Candela, 1991). In this instance, the higher viscosity (March, 1981) might preclude plume rise even though volatiles do exsolve. Here, Candela (1991) proposed that critical percolation and the delivery of the volatiles to the top of the magma chamber probably occurs by advection through a three-dimensional spanning cluster of vapour bubbles.

Candela's (1991) Case 3 considers vapour exsolution in an immobile crust such that critical percolation (as outlined in Case 2 above) is not achieved and the aqueous phase is dispersed through the subsolidus cracking front. It will remain in pores, vesicles and miarolitic cavities in this case, instead of accumulating in the apical regions of the chamber. This scenario is unlikely to lead to porphyry ore formation.

Several textural characteristics indicate the mode of volatile migration. For example, quenching of the buoyant aqueous plume, which also contains trapped melt and crystals, might result in the formation of aplites, miarolitic granites and porphyries with fine-grained groundmasses. In contrast, advection of volatiles through a spanning cluster of bubbles to the apical parts of a magma chamber might result in hydrothermal alteration centred on the apical parts of the chamber; however, textural diversity in the resulting rocks is not envisaged (Candela, 1991).

Similarly to Candela (1991), Shinohara and Kazahaya (1995) proposed that the mechanism of aqueous fluid migration through a crystallising magma is likely to be dependent on the volume ratio of bubbles to melt to crystals. They proposed that bubbles would ascend buoyantly through a magma containing dispersed crystals provided the crystal content was low enough to ensure free convection within the magma chamber. With increasing crystal content, bubble ascent would be slowed by interference between bubbles and crystals, and the bubbles would likely be trapped in the crystallisation zone by capillary force. A further increase in the crystal content would result in a net increase in the volume ratio of bubbles to melt, which is likely to cause bubble coalescence. When these bubbles become large enough to overcome the capillary force, bubble ascent will resume. Shinohara and Kazahaya (1995) proposed that in fully crystalline magma chambers, aqueous fluid migration might continue along grain boundaries within the crystallised melt.

Based on the fact that many volcanic eruptions produce large emissions of gas during intervals when only negligible magma is actually erupted, Kazahaya *et al.* (1994) suggested that quiescent degassing of volcanoes is caused by magma convection within a subvolcanic column of magma, which results in the transportation of volatiles from a large reservoir to the top of the magma column. Shinohara *et al.* (1995) modelled this scenario for the formation of the Pine Grove porphyry Mo deposit and proposed that water-rich magma rises, and as a consequence, vesiculates at the top of a magma chamber to produce a denser, degassed magma. The degassed magma would then descend through the non-degassed (rising, water-rich) magma because of its lower H_2O content and consequent higher density, thereby setting up a convection system within the magma chamber. In this way, volatiles from a large proportion of the underlying magma chamber could be delivered to the apical parts of the magma chamber. In their model, ore deposits are typically associated with magma chambers where the egress of the magmatic vapour plume is focused within a subdeposit conduit that develops as a result of bubble accumulation and the consequent increase in pressure within the magma chamber, which induces fracturing of the wall rock. They suggested that once the subdeposit conduit geometry is created, if sufficiently wide and long-lived, it will permit convective overturn of magma and continued focusing of degassed volatiles (Shinohara *et al.*, 1995).

9.3 Island arcs

Although Au-rich porphyry deposits occur in continental arcs, they are more common in island arcs (e.g. Wyborn, 1996; Sillitoe, 1997; Keith *et al.*, 1998; Jensen and Barton, 2000). Many island arc porphyry Cu-Au deposits are associated with low- or medium-K calc-alkaline magmas, e.g. the tonalite porphyry associated with Batu Hijau (Clode *et al.*, 1999) and the diorites at Panguna (Clark, 1990) and many Cu-Au deposits in the Philippines (Sillitoe and Gappe, 1984). However, Au-rich porphyry deposits associated with high-K calc-alkaline to shoshonitic magmas are also known in island arcs, e.g. Dinkidi in the Philippines (Wolfe *et al.*, 1999) and Grasberg in Indonesia (Kavalieris, 1994).

There are several reasons why K- and incompatible element-rich magmas generated in island arcs are associated with Au deposits and are hence thought to make effective mineralising sources (Wyborn, 1996):

- higher K implies a more metasomatised mantle, which is a potential source of metals, S, F, Cl, CO_2, H_2O, etc. Furthermore, larger amounts of melting can take place because of the lower liquidus temperature of the metasomatised mantle, thus allowing larger, more robust magma bodies to rise into the upper crust (Wyborn, 1996);
- higher proportions of water in the extensively metasomatised mantle implies more water available for earlier fluid saturation and greater fluid evolution (Wyborn, 1994);
- the presence of low melting point K-phases increases the chances of fractional crystallisation in upper crustal magma chambers by processes such as convective fractionation, thereby speeding up volatile evolution (Sparks *et al.*, 1984);

- magmas with higher alkali contents have intrinsically higher Fe^{+3}:Fe^{+2} ratios. This favours the development of magnetite and anhydrite over pyrrhotite and increases the sulphur solubility of the melt, with S occurring as SO_2 rather than H_2S (Sack and Carmichael, 1980; Kilinc *et al.*, 1983); and
- higher sulphur solubility increases the chances of the resulting magma remaining undersaturated with respect to sulphur until emplacement into the upper crust.

One of the most important pre-requisites for the formation of porphyry Cu-Au deposits is that the parent magma remains undersaturated with respect to H_2S until it is emplaced into the shallow crust (Wyborn, 1996). This would ensure that available Cu, Au, other chalcophile elements and S are transported in the melt to the upper crust. If sulphur saturation is achieved at any stage prior to emplacement, these elements would be incorporated into an immiscible magmatic sulphide phase that would be retained in the source (Wyborn, 1996; Cooke *et al.*, 1998), leaving the emplaced melt devoid of these vital ore-forming components.

9.4 Mafic shoshonitic magmas

Mantle-derived mafic alkaline magmas and shoshonites have been suggested to contribute metals (especially Au) and volatiles to a large spectrum of magmatic – hydrothermal ore deposits (e.g. Sillitoe, 1997; Keith *et al.*, 1998; Rowland and Wilkinson, 1999; Jensen and Barton, 2000). These deposits include some porphyry Cu and Mo deposits, such as Bingham, Henderson and Climax (Keith *et al.*, 1993; Keith *et al.*, 1997), as well as some porphyry Cu-Au deposits, e.g. Porgera (Richards, 1997) and Grasberg (Pollard and Taylor, 2002). In many of the porphyry systems, it appears that the silicic and mafic alkaline magmas may have coexisted and that ore-forming components may have been derived from both magmas (Keith *et al.*, 1998; Maughan *et al.*, 2002).

Recent volcanic eruptions highlight the probable operation of convective volatile transfer mechanisms between basaltic magmas and overlying silicic magmas (Kress, 1997; Keith *et al.*, 1998). Anders *et al.* (1991) demonstrated that in the recent eruptions of two Chilean volcanoes, 50 to 100 times more S was emitted than could be accounted for by the volume of silicic magma erupted. Additional examples of recent volcanic eruptions emitting excess S (at least 20 times greater than melt solubility) are those of Ruiz (Fournelle, 1990) and Pinatubo, where in the latter case, excess S was present as SO_2

vapour and anhydrite crystals (Pasteris, 1996). Kazahaya *et al.* (1994) documented excess SO_2 and H_2O emissions in recent eruptions of the Izu-Oshima volcano in Japan and suggested that since the Izu-Oshima magma was water-undersaturated and relatively reduced (containing no anhydrite), degassing of excess SO_2 and H_2O may have relied on magma convection driven by the increase in density of the magma after degassing (cf. Shinohara *et al.*, 1995 above). It has been suggested that convective volatile transfer related to 1) the commingling of silicic magma with; 2) the injection of; or 3) the volatile transfer from, S-rich underplated basaltic magma to overlying rhyolitic magma most likely explains the excess SO_2 in these volcanic systems (Anders *et al.*, 1991; Hattori, 1993; Kazahaya *et al.*, 1994). Keith *et al.* (1998) investigated the possibility that this process of convective volatile transfer from mafic alkaline magma to intermediate or silicic magma could be a vital process in delivering magmatic volatiles to the apical parts of magma chambers related to several porphyry Mo deposits.

It is appropriate at this stage to define the term "mafic alkaline magma" as used by Keith *et al.* (1998). Mafic alkaline magmas are primitive, mantle-derived magmas that are more mafic or basic than andesite and trachyandesite, and more alkali-rich than basalt or picrobasalt using the Le Bas *et al.* (1986) total alkali – SiO_2 classification. Although this definition includes the Na-rich members of the IUGS classification (Streckeisen, 1973), such as hawaiite and mugearite, the K-rich varieties, such as trachybasalts, shoshonites and basaltic trachyandesites are more common in the extensional tectonic settings associated with the porphyry deposits they were investigating (Keith *et al.*, 1998).

Keith *et al.* (1998) suggested that the higher than normal Mo content of the rhyolitic parental melts and/or the evidence of commingling of rhyolitic and mafic alkaline magma in five out of eight of the major Mo deposits in North America (Bookstrom, 1988; Keith *et al.*, 1993) indicates that mantle-derived mafic alkaline magmas are an integral part of Climax-type porphyry Mo deposits. Following detailed studies of these deposits, Keith *et al.* (1998) proposed a model that could account for these characteristics. Initially, a rhyolitic melt crystallising along the walls and floor of a magma chamber can induce the formation of an aqueous fluid by second boiling. This fluid is rich in S, metals, Cl and other incompatible elements. They suggested that subsequent to the initial fractionation and segregation of a rhyolitic-derived aqueous fluid, underplated or injected, wet oxidised mafic alkaline magma might have entered the chamber, with several possible consequences. The mafic alkaline magma may provide heat, which would promote convection and the subsequent turnover of magma to deliver undissolved volatiles from the rhyolitic magma to the top of the magma chamber. This heat might also cause assimilation of the roof rocks and the cores of any older stocks present or extend the life of the chamber to allow for the generation of large volumes of rhyolitic magma and the emplacement of multiple intrusions. In addition to providing heat, the mafic alkaline magma may quench on contact with the cooler rhyolitic magma, which would initiate the formation of a buoyant stream of volatile-rich magma and bubbles from the mafic alkaline magma, thereby augmenting the supply of volatiles (and metals) to the top of the magma chamber. Even though evidence for the operation of these processes in cupola regions of rhyolitic magma chambers is rare, they suggested that commingling or interaction of mafic alkaline magmas with rhyolitic magma in the parental magma chambers might have operated in many of the porphyry Mo systems.

It is considered here that mafic alkaline magma is not an appropriate term for the K-rich, shoshonitic rocks of the GVC. As such, Keith *et al.*'s (1998) term "mafic alkaline magma" has been replaced by "mafic shoshonitic magma" from here onwards, since it is deemed more appropriate for the GVC.

9.5 Previous models for the Endeavour deposits

Previous models for the genesis of the Endeavour deposits have been presented by Jones (1985), Heithersay *et al.* (1990), Heithersay and Walshe (1995) and Blevin and Morrison (1997). The Heithersay and Walshe (1995) model is summarised below because it is the most comprehensive model compiled prior to 1997 and combines Jones's (1985) and Heithersay *et al.*'s (1990) work. Thereafter, a summary of the Blevin and Morrison (1997) model is given.

9.5.1 Heithersay and Walshe, 1995

Heithersay and Walshe (1995) interpreted the Goonumbla and Wombin Volcanics to represent an ancient volcanic edifice that was built on a substrate of Early Ordovician sediments and volcanic rocks. This volcano, they suggested, was initially submarine but became subaerial and limestone-fringed with time. A large (~20km diameter) roughly circular feature in the ground magnetics had been interpreted to represent the outer limits a caldera associated with this volcano in the Goonumbla region. Many of the widespread monzodioritic to monzonitic intrusions associated with the Wombin Volcanics were thought to be subvolcanic intrusions that had been emplaced around the rim of the caldera during a period of resurgent magmatism.

Heithersay and Walshe (1995) proposed that the SiO_2-poor volcanic and subvolcanic intrusive rocks of the upper Goonumbla and Wombin Volcanics demonstrate that low pressure olivine fractionation occurred within the monzodiorite magma chamber as melts ponded at the base of the igneous complex prior to eruption or emplacement at higher levels. They interpreted this trend of lower SiO_2 – higher K_2O to indicate anhydrous fractionation under conditions of continued loss of volatiles during volcanic eruptions. The higher SiO_2 – lower K_2O trend of the intrusions associated with mineralisation was ascribed by Heithersay and Walshe (1995) to imply plagioclase and biotite fractionation rather than plagioclase, olivine and pyroxene fractionation. They suggested that the relative SiO_2 enrichment in rocks associated with mineralisation reflects fractionation under conditions such that most of the volatiles were contained within the systems and it was this retention of volatiles until late stage magmatism that led to the development of Endeavour porphyry Cu-Au deposits.

The alignment of the four Endeavour deposits along the "Endeavour Linear" (cf. section Figure 9.1a), as well as the location of other prospects such as E31, led Heithersay and Walshe (1995) to hypothesise that the pipe-like porphyry intrusions associated with the Endeavour deposits occur as satellite bodies located on the shoulders of the monzodiorite- to monzonite-zoned E31 stock* (BQM) and crosscut the stock at depth (Figure 9.1b). The pipe-like porphyry intrusions were interpreted as "valves" that provided focused egress points for the exsolved aqueous fluid + melt from the evolving E31 magma chamber. Heithersay and Walshe (1995) suggested that the position of these pipe-like porphyry intrusions on the shoulders of the main magma chamber reflected two things. Firstly, that greater cooling on the walls of the stock at depth would lead to the accumulation of the aqueous fluid on the shoulders of the magma chamber rather than in the apical regions. Secondly, they suggested that the position of the pipe-like intrusions was controlled to some extent by the Endeavour Linear structural corridor (cf. section 2.4.1.3).

* The E31 stock was originally called the E26 stock by Heithersay and Walshe (1995) but was renamed the E31 stock by Arundell (1998).

In terms of the overall model, using E26 as their type example, Heithersay and Walshe (1995) suggested that the early biotite – magnetite alteration assemblage surrounding the deposit reflects a relict alteration column associated with a valve zone on the southwest margin of the E31 stock and that this alteration predated the intrusion of the QMP complex. With continued fractionation of the E31 stock (BQM), Heithersay and Walshe (1995) envisaged the exsolution and migration of an aqueous plume similar to the scenario presented by Henley and McNabb (1978), which ponded in this valve zone. Fine fractures were believed to have developed in this alteration column during times of high fluid pressure, allowing the evolved aqueous fluid, together with some silicate melt and crystals (QMP) to egress the E31 stock in a focused manner by the pressure difference between lithostatic pressure within the chamber and hydrostatic pressure above the ascending column of fluid. At the emplacement depths they calculated (~1900m assuming lithostatic pressure), Heithersay and Walshe (1995) suggested that the aqueous fluid would have immediately split into two immiscible phases, and that the radius of the two-phase region would decrease with depth as the critical pressure and temperature increased (e.g. Eastoe, 1982). At E26, the upper part of the aqueous plume probably behaved similarly to the vapour plume of Henley and McNabb (1978), whereas the lower part of the column probably behaved like a reflux column in which diluted, cooled, gas-buffered saline brines condensed from the upper part of the plume (Figure 9.2c). This condensed fluid then mixed with high temperature and highly saline fluids (+ melt) being episodically expelled from the stock as fluid pressure exceeded the minimum principal stress and the tensile strength of the rocks. These processes resulted in the formation of *QMP 1* (and *QMP 2* when it intruded the core of *QMP 1*) and the stockwork and sheeted vein networks that accompany these intrusions at E26. They suggested that the higher proportions of muscovite in the K-silicate alteration assemblages associated with E48 indicate that this deposit formed higher up the column. Since E48 is characteristically more Au-rich than E26 (cf. Table 1.2), Heithersay and Walshe (1995) took its interpreted height of formation in the column to imply that Au is preferentially mobilized through the lower parts of the column and is more fixed in the upper parts of the column.

9.5.2 Blevin and Morrison, 1997

Blevin and Morrison (1997) suggested that the model presented by Heithersay and Walshe (1995) adequately explains the textural and compositional evolution of the Goonumbla area. However, they suggested that one fractionation trend is adequate and that any divergence in the K_2O – SiO_2 relationship is probably due to varying degrees of potassic alteration. Blevin and Morrison (1997) proposed that the Endeavour systems are classic examples of magmatic – hydrothermal deposits where progressive phases of mineralisation can be linked to specific alteration assemblages and to multiple igneous phases, all emanating from the same, shallow, zoned source. Successive pulses of both melt and magmatic volatiles emanate from progressively deeper parts of the systems as fractional crystallisation proceeds and the remaining fluids become more refined. They suggested that as a result, the intrusions within the QMP complexes also become progressively more felsic.

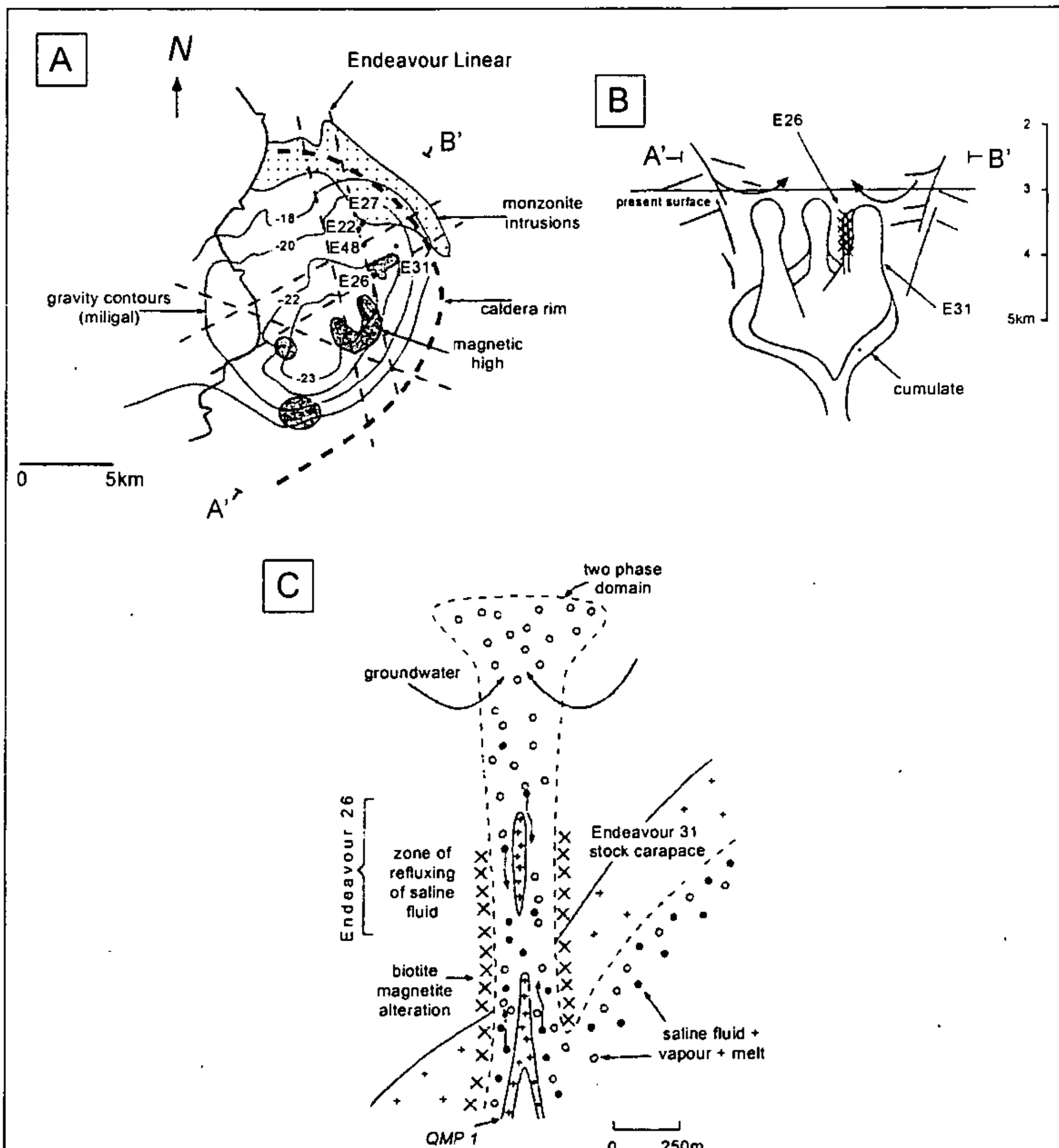

Figure 9.1 **A** A sketch of the structural and geophysical features of the northern GVC; **B** the geological interpretation of the geophysical features of the E26 area; and **C** a simplified model for the development of E26 at the time of *QMP 1* (modified after Heithersay and Walshe, 1995).

The unmineralised regional intrusions were suggested by Blevin and Morrison (1997) to be the mafic and possibly cumulate phases of the more felsic, mineralised intrusions. They proposed that these barren intrusions represent either the deeper, more eroded portion of the magmatic systems, or that they represent intrusions that failed to fractionate to more evolved compositions.

9.5.3 Limitations of previous models

The obvious increase in SiO_2 and K_2O with decreasing MgO, CaO and Fe_2O_3 indicates that the QMP intrusions are more fractionated than the BQM intrusions, and at first glance, proposing that the BQM is the parent stock from which the QMP complexes emanate seems feasible. However, the marked divergence in trace element abundances (higher Rb, Nb, Zr – lower Ba, Sr) with fractionation between the BQM and the porphyry intrusions implies that the BQM was probably unlikely to fractionate to the compositions characteristic of the QMP intrusions related to ore deposition at the Endeavour deposits (cf. section 8.3.4). Neither the Heithersay and Walshe (1995) nor Blevin and Morrison (1997) model can account for these divergences. The fact that the inwardly crystallising stock (E31 stock/BQM) may have played some role in the genesis of the Endeavour deposits is not in question. However, in light of the above, it is evident that factors other than fractional crystallisation and subsequent aqueous fluid exsolution must have been operational to produce the trace element patterns characteristic of the QMP intrusions.

Heithersay and Walshe's (1995) two fractionation trends cannot explain the presence of abundant biotite in the unmineralised Wombin-related Gunningbland Forest monzonite porphyries and in the zero porphyry dykes associated with E26 (and E37). If two fractionation trends were responsible for the regional unmineralised versus near-mine mineralised intrusions, then it follows that biotite should not be an abundant phase in the regional porphyry intrusions, which it clearly is. Blevin and Morrison (1997) proposed that one fractionation trend would be sufficient. This study confirms that one fractionation trend sufficiently explains the geochemical character of the Late Ordovician GVC rocks, and quantifies it to be the low pressure trend of early fractionation of olivine and clinopyroxene followed by Fe-Ti oxide and later by the fractionation of plagioclase (cf. section 8.3.4), a typical calc-alkaline and shoshonitic crystallisation sequence.

Both Blevin and Morrison's (1997) and Heithersay and Walshe's (1995) models proposed that continued crystallisation of the BQM would generate progressively more felsic melt fractions such that each successive QMP intrusion should be more felsic than the preceding melt batch. Although this might account for the felsic nature of the K-QMP intrusions, neither model can explain why the later KA-QMP, late-mineral B-QMP and mafic monzonite "zero" porphyry intrusions are less felsic than many of the BQM samples from which they are supposed to be the fractionated derivatives. These models also fail to account for the presence of post-mineral basaltic trachyandesite dykes and the commingling of these with the zero porphyry dykes. In addition, if, as Blevin and Morrison (1997) suggested, the regional intrusions represent the more mafic or cumulate phases of the more felsic mineralised intrusions, why do they not contain disseminated sulphides like some of the late-mineral B-QMP intrusions?

Clearly then, although the fractionated nature of the K-QMP intrusions can partly be explained by fractionation and the subsequent release of magmatic volatiles and melt in valve zones off the shoulders of the BQM (or E31 stock), these models do not satisfactorily explain the less felsic character of post K-QMP intrusions or the significant geochemical differences between the BQM and QMP intrusions as a group. In addition, they do not adequately account for the similarities and differences between the regional intrusions and zero porphyries and the regional intrusions and some of the weakly mineralised B-QMP intrusions associated with the Endeavour deposits. Thus it seems that the character of the intrusions associated with the Endeavour deposits required a distinctive set of conditions for their formation.

A revised 4-stage genetic model for the Endeavour porphyry deposits is thus presented below that takes into account the limitations of the previous models as well as differences and similarities of the regional unmineralised intrusions within the Wombin Volcanics and the intrusions associated with the Endeavour deposits. It is integrated with the geological evolution of the GVC as a whole.

9.6 Geological evolution of the Endeavour deposits – a new genetic model

The GVC is the principal component of the Early to Late Ordovician Macquarie Island Arc in the Parkes region. It records the evolution of the western portion of the Macquarie Arc from Early Ordovician, high-K calc alkaline magmatism (Nelungaloo Volcanics), through Mid Ordovician basaltic trachyandesitic to trachyandesitic, mainly shoshonitic magmatism (Goonumbla Volcanics), to Late Ordovician trachyandesitic to trachytic shoshonitic magmatism (Wombin Volcanics). The Goonumbla and Wombin Volcanics are interpreted as the thick (>1km), subaqueous volcaniclastic apron developed on the flanks of a shallow marine to subaerial stratovolcano (Simpson *et al.*, 2000). Monzodioritic intrusions were emplaced during the Mid Ordovician, comagmatic with the Goonumbla Volcanics. Additional monzonites intruded the Wombin Volcanics in the Late Ordovician. The change from trachyandesitic (Goonumbla Volcanics) to trachytic shoshonitic magmatism (Wombin Volcanics) was possibly triggered by regional extension and rotation of the arc lithosphere away from an active subduction zone during the Late Ordovician (Crawford, 2001a). The pipe-like QMP complexes associated with the Endeavour deposits, and other monzonites in the Goonumbla region were emplaced into the Wombin Volcanics between ~445 and ~437Ma.

Jones (1985) suggested that the preferred orientation of the Endeavour deposits indicates a structural control on the location of the mineralised centres and the probable presence of a deep-seated crustal weakness in the area. The north-northwest-trending, aeromagnetically defined "Endeavour Linear" structural corridor has been interpreted as this deep-seated structure (Jones, 1985; Heithersay and Walshe, 1995). In addition, east – west extensional stresses active prior to and during ore deposition facilitated the formation of possibly shallow crustal northwest- and northeast-trending fractures. The pipe-like QMP complexes central to each of the Endeavour deposits were probably emplaced at intersections of these fractures (Harris, 1997; North, 1999). Glen and Walshe (1999) argued that the Endeavour deposits formed at the intersection of the arc-parallel (?) Endeavour Linear, and the arc-normal (?) Lachlan Transverse Zone (LTZ), the latter a regional-scale west-northwesterly-trending structure that extends across much of NSW (cf. Figure 2.4).

9.6.1 Stage 1 – Monzodiorite emplacement

A monzodiorite that intruded the upper Goonumbla Volcanics (?) at the base of E26 is the oldest intrusion recognised in the four economic Endeavour deposits. Based on virtually identical geochemical characteristics, this monzodiorite is considered a near-mine example of the Middle Ordovician monzodiorite intrusion that crop outs ~5km to the southeast at Goonumbla Hill (cf. Figure 2.5), and is considered unrelated to mineralisation.

9.6.2 Stage 2 – Intrusion of the BQM magma chamber

Late Ordovician shoshonitic magmatism in the GVC is related to the extrusion of the Wombin Volcanics, and includes all of the intrusions associated with the Endeavour deposits. The BQM intrusions are the oldest intrusive phase associated with mineralisation. They strongly resemble several equigranular to weakly porphyritic biotite monzonite intrusions within the Wombin Volcanics that crop out 5 – 10km south of *Northparkes Mines* at The Woods and Cooks Myalls, and east of the mine area around E31 (cf. Figure 2.5). It is thus likely that the BQM intrusions associated with the Endeavour deposits represent near-mine equivalents of the more widespread biotite monzonite intrusions in the northern GVC that are inferred to be of the same age.

Widespread, weak to moderate, albite – sericite alteration of plagioclase in the BQM intrusions and the host Wombin Volcanics is thought to be have been associated with contact (thermal) metamorphism and/or minor K-silicate and sodic metasomatism around the BQM intrusions due to the conductive heating and subsequent circulation of heated pore water (seawater?) in the host volcanic rocks.

9.6.3 Stage 3 – QMP emplacement and ore formation

9.6.3.1 Stage 3a – QMP complex emplacement

The three early to syn-mineral phases comprising the pipe-like QMP complexes central to each Endeavour deposit, early-mineral B-QMP → K-QMP → KA-QMP, were emplaced following the intrusion of the BQM magma chamber. These phases were followed by the intrusion of minor late-mineral B-QMP dykes.

The QMP complexes intimately associated with the Endeavour deposits (including E37) have not been recognised elsewhere in the GVC. Besides being intimately associated with K-silicate alteration assemblages and Cu-Au mineralisation, there are several differences between the intrusive phases associated with the QMP complexes and the unmineralised regional intrusions:

- the intrusive rocks associated with the Endeavour deposits are distinctly more fractionated than any of the regional intrusions; many contain up to 10% quartz;
- anisotropic textures, which are abundant in K-QMP and less so in KA-QMP intrusions, are not developed in regional intrusions;

- Cl contents of primary apatite microphenocrysts from regional intrusions are higher than they are in apatite microphenocrysts from intrusions associated with the Endeavour deposits; the latter are F-rich and also depleted in Fe compared to regional examples. These characteristics most likely indicate that the regional intrusions are less fractionated than the intrusions associated with mineralisation;
- intrusions associated with the Endeavour deposits are relatively enriched in K, Ba and Sr and depleted in Rb, Nb and Zr compared to the BQM and other regional intrusions that are interpreted to be of a similar age;
- B-QMP, KA-QMP and K-QMP intrusions show increasing LREE depletion compared to the regional intrusions; a characteristic that cannot be entirely accounted for by fractionation from BQM-like intrusions; and
- basaltic trachyandesite dykes, which are commingled with mafic monzonite porphyry intrusions at E26, have not been recognised elsewhere in the GVC.

It is envisaged that the combination of 1) crosscutting northwest- and northeast-trending shallow crustal structures; 2) a fractionating BQM-like magma chamber interacting with a mafic shoshonitic magma; and 3) deep-crustal structure(s) that tapped the shoshonitic melts from the mantle, were the ingredients essential for the formation of the Endeavour deposits within the Late Ordovician GVC. Widespread, BQM-like magmatism was almost certainly occurring on a district scale during the Late Ordovician, and northwest- and northeast-trending fractures were probably not restricted to the near-mine area during regional extension. Thus, the presence of the LTZ and/or "Endeavour Linear" structure(s), and the presence of commingled mafic shoshonitic magma and more felsic magma are interpreted to be the key features to understanding the formation of the Endeavour porphyry Cu-Au deposits. Speculations on the formation of fertile magmas in such a regime are discussed further in section 9.7.

9.6.3.2 Stage 3b – Ore formation

Cu and Au mineralisation in the Endeavour deposits is intimately associated with the K-silicate alteration and sheeted or stockwork veins related to the K- and KA-QMP intrusions. Sulphide precipitation probably occurred as the aqueous fluid cooled from >600°C to 550 – 500°C and became Cu-saturated, possibly also partly due to wallrock interaction. This is indicated by the abundance of chalcopyrite daughter crystals in the fluid inclusions in quartz from the main stage veins. Veins and alteration assemblages associated with the KA-QMP intrusions are more chalcopyrite-rich than those associated with the K-QMP intrusions, which are bornite-dominant. According to phase equilibrium constraints on high temperature porphyry deposits, Simon *et al.* (2000) suggested that a changeover to chalcopyrite-dominant assemblages reflects cooling of the magmatic – hydrothermal system.

K-silicate alteration assemblages and quartz – Cu-sulphide veins formed at lithostatic pressures of 300 – 450bar, which correspond to depths of between 1000 and 1700m below the palaeo-surface. The fluids evolved from very high temperature (>550°C) highly saline (~60wt% NaCl eq.) brines during the early stages, to 500 – 550°C, 55 – 60wt% NaCl + KCl eq. brines at the time of simultaneous fluid + melt emplacement associated with the K-QMP intrusions. At these pressures and depths, the exsolving magmatic volatile-rich aqueous fluid immediately separated into two immiscible phases (Bodnar *et al.*, 1985); which is indicated by the presence of co-existing vapour-rich and hypersaline fluid inclusions in quartz from the early, transitional and main hydrothermal paragenetic stages. The fluids associated with the quartz in transitional anisotropic textures were metal- and Cl-rich and precipitated Cu, with Au, as sulphides as they cooled to ~500°C during the main stage of mineralisation. The Cl-rich nature of the fluids that produced the secondary biotite associated with intense K-silicate alteration assemblages is indicated by the lower F:Cl ratios of these biotites compared to primary biotite phenocrysts in the intrusions associated with mineralisation.

The exsolution of an aqueous phase from the K- and KA-QMP intrusions is also inferred from the REE patterns. B-QMP, KA-QMP and K-QMP intrusions show increasingly LREE depletion, a feature that is not consistent with crystal fraction alone (cf. section 8.4.4.1). Instead, since it has been demonstrated experimentally that a magmatic aqueous fluid can partition LREE preferentially to the remaining REE, the excessive LREE depletion is thought to be due to the exsolution from these intrusions of progressively larger amounts of aqueous fluid.

9.6.3.3 Stage 3c – Sericite overprint and distal propylitic alteration

Oxygen isotope studies on sericite from E48 (Wolfe, 1994; Wolfe *et al.*, 1996) and E26 (Harris, 1997; Harris and Golding, 2001) have confirmed a magmatic – hydrothermal origin for late stage sericite – quartz – haematite – carbonate – sulphide alteration assemblages. During this study, similar phyllic alteration assemblages were recognised at E22 and E27 and a similar origin is assumed for these assemblages.

The presence of haematite and sericite in this phyllic alteration assemblage indicates that the associated fluids were respectively more oxidised and more acidic (by the hydrolysis reaction $3KAlSi_3O_8 + 2H^+ — KAl_3Si_3O_{10}(OH)_4 + 2K^+ + 6SiO_2$) compared to those related to the intense quartz – K-feldspar – Cu-sulphide assemblages associated with the K- and KA-QMP intrusions. Similar features in the alteration assemblages at the Dinkidi porphyry Cu-Au deposit in the Philippines led Wolfe (2001) to suggest that any changes in the oxidation state, sulphur activity, pH and temperature with time may reflect the evolution to cooler, acidic, sericite-stable fluids compared to the earlier K-feldspar-stable fluids. The higher oxidation state and acidity of the magmatic – hydrothermal phyllic alteration assemblages of the Endeavour deposits could have been the result of SO_2 and HCl condensation back into the brine (Eastoe, 1980) as it cooled. Fluid inclusions investigated during this study show that the fluids circulating during the late magmatic – hydrothermal stages were cooler (350 – 400°C), less saline (~45wt% NaCl eq.) and relatively K- and Ca-rich compared to those associated with the main stage intense K-silicate alteration and mineralisation assemblages (500 – 550°C and 60 – 65wt% NaCl + KCl eq.).

Microthermometric data from fluid inclusions in late stage quartz yielded similar depths of emplacement (1350 – 1600m) under a hydrostatic regime (130 – 160bar) compared to those for early, transitional and main stage quartz under a lithostatic regime. This is thought to imply that late stage brittle faults connected the magmatic – hydrothermal system to the palaeo-surface, which probably led to the formation of phyllic alteration assemblages as escalated gas production increased fluid acidity through condensation and disproportionation reactions.

Distal propylitic alteration zones extend to ~1km from the QMP complexes and include epidote – chlorite – albite – carbonate – chalcopyrite – pyrite assemblages as well as carbonate – base-metal sulphide veins (Kolkert, 1998). Kolkert (1998) concluded from her fluid inclusion and stable isotope studies that the carbonate – base-metal sulphide veins at E28 (distal to E26) were formed during distal phyllic-equivalent propylitic alteration associated with QMP mineralisation by interaction and mixing of magmatic – hydrothermal fluids with pore water (seawater?) in the host Wombin Volcanics.

Wallrock buffering, or the interaction of oxidised ore fluids with reduced volcanic host rocks, is interpreted to have produced an increase in $\delta^{34}S$ values with time and distance from the centre of the deposits. The very negative $\delta^{34}S$ values (-19 to -15‰) for some transitional magmatic sulphides are thought to reflect bornite precipitation from locally hyper-oxidised fluids, which led to the formation of abnormally light isotopic compositions.

9.6.4 Stage 4 – Post-mineral alteration assemblages and intrusions

Commingled basaltic trachyandesite and mafic monzonite "zero" porphyry dykes, which have a post-mineral timing, were intruded into the QMP complex at E26 after the Cu-Au stockwork vein mineralisation, magmatic – hydrothermal phyllic (and propylitic?) alteration, and a second generation of fault- and fracture-related phyllic alteration, which is well developed at all four of the Endeavour deposits. The zero porphyry dykes at E26 are interpreted to represent near-mine examples of widespread mafic shoshonitic magmatism in the Late Ordovician, which is inferred from the occurrence of similar rocks at E37 and at the Gunningbland Forest.

In addition, various mafic dykes of uncertain age were also emplaced at E22, E27 and E48. Since several of these mafic dykes have been faulted (cf. Figure 3.16) and have fault-related phyllic alteration haloes, whereas others remain unaltered and unfaulted, their relation to the Endeavour mineral deposits is unknown, but at least some could have been emplaced during the waning stages of Late Ordovician magmatism in the GVC.

The origin of the limited extent breccia bodies at E22 and E27 and numerous pebble dykes at E26 is unclear. The post-mineral timing of these bodies is well-constrained by the clasts of mineralised and veined KA-QMP and zero porphyry dyke material (cf. section 3.4.7). It may be that these volumetrically minor rocks represent different scales of magmatic – hydrothermal brecciation – the lack of penetrative fabrics or any alignment of clasts argues against a tectonic brecciation process.

Weak, selectively pervasive propylitic alteration assemblages were produced within the zero porphyries, and possibly as part of well-developed propylitic haloes around at least E22 and E27 in the waning stages of magmatic activity associated with the Endeavour deposits. It is possible that low permeability of the unaltered basaltic trachyandesite dykes protected them from this post-mineral propylitic alteration.

9.7 Fertile melt production in the Endeavour QMP complexes

The preceding section outlined the sequence of events that combined to produce the Endeavour porphyry deposits. The following sections speculate on why the QMP complexes associated with the deposits were endowed with metals relative to the regional intrusive rocks of the GVC.

9.7.1 BQM magmatism

The Late Ordovician magmatism in the GVC is interpreted to be the product of high degrees of partial melting of metasomatised lithospheric mantle in an evolved island arc. This partial melting led to the generation of large volumes of shoshonitic melt, which, under the extensional regime interpreted for the GVC at this time, was emplaced high into the crust, possibly facilitated by local, deep-seated structures (1 and 2 on Figure 9.2). The equigranular texture of the BQM implies that the magma chamber was emplaced at depths sufficient to prevent aqueous phase separation (~4km?). The low levels of Ni, Cr and Mg in the BQM (and regional equivalent) intrusions (cf. section 8.3.2.2) imply that low-pressure olivine, clinopyroxene and plagioclase fractionation had occurred prior to emplacement. This low pressure fractionation may have led to the formation of cumulate phases associated with this magma chamber deeper in the crust (cf. Figure 9.1b), which could account for the ~20km wide gravity low in the central parts of the GVC. The BQM and equivalent regional intrusions may be smaller apophyses from this large, central magma chamber.

With continued fractional crystallisation of anhydrous phases along the walls and floor of the BQM magma chamber, it is proposed that the pluton became zoned from monzodiorite at its margins to monzonite in its interior (4 on Figure 9.3) and the process of second boiling triggered volatile exsolution when the residual melt achieved volatile saturation. Continued second boiling probably facilitated the formation of locally developed "froths" at the top of the magma chamber (5 on Figure 9.2; Candela, 1991) and aqueous plumes along shoulders of the magma chamber, where more fractionated, biotite quartz monzonite stocks were emplaced (6 and 7 on Figure 9.2; Candela, 1991). Available metals and ligands from the fractionating BQM melt were then partitioned into the aqueous fluid (Candela and Holland, 1986), and the release of this fluid into the surrounding volcanic host rocks and rigid edges of the pluton probably occurred when the hydrostatic pressure of the aqueous fluid exceeded the lithostatic pressure plus the

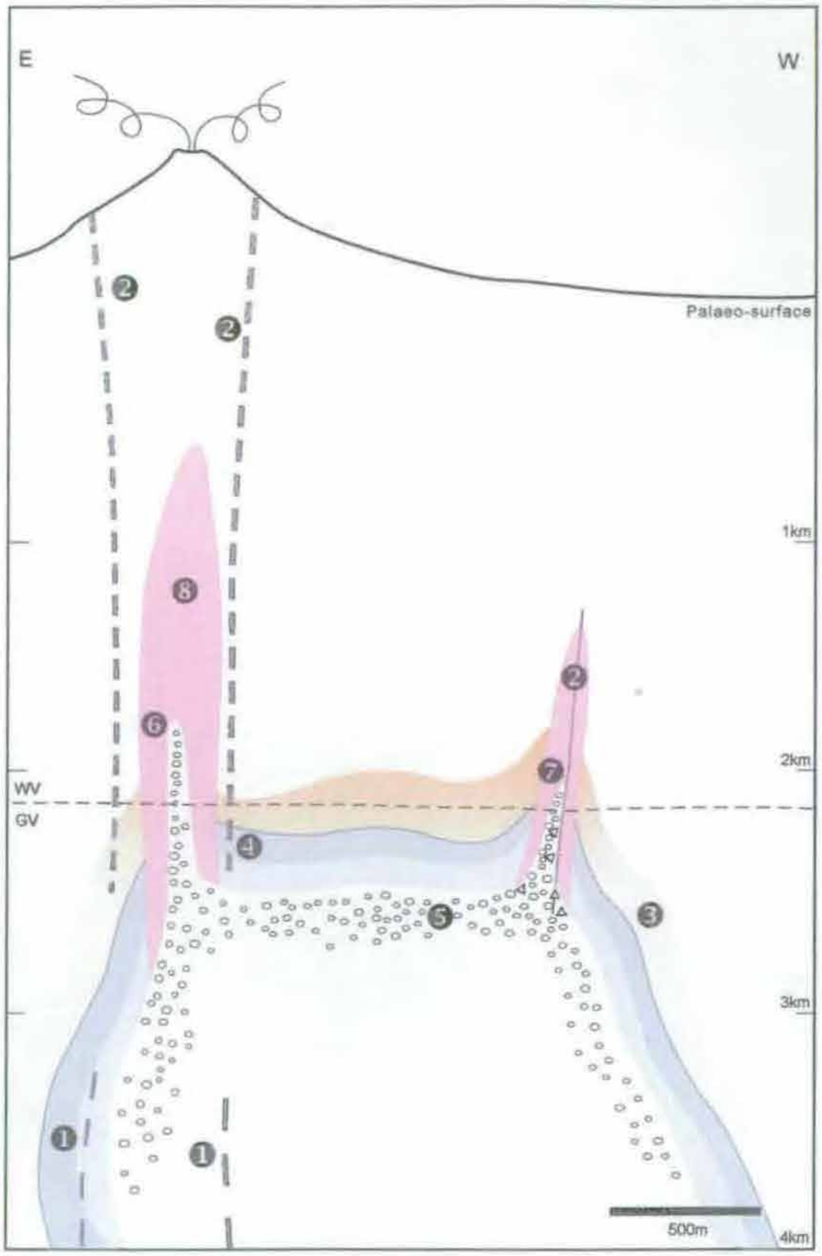

Figure 9.2 Late Ordovician magmatism and the intrusion of the BQM magma chamber

Movement on deep-seated crustal structures (1) and local northwest and northeast-trending fractures (2) facilitated the intrusion of a subvolcanic trachytic magma chamber. The BQM magma chamber was emplaced into the shallow crust (~4km), possibly where it achieved neutral buoyancy. Interaction with intrusion-induced, conductively-heated pore water (seawater?) in the host rocks is interpreted to have initiated the formation of widespread albite - sericite alteration assemblages around the magma chamber (3). Continued crystallisation led to the formation of a zoned magma chamber at depth (4). It also induced volatile build-up in pluton due to second boiling (5). When hydrostatic pressure exceeded lithostatic pressure plus tensile rock strength, fracturing occurred and caused the magma chamber to propagate into the surrounding volcanic rocks and emplace more fractionated biotite quartz monzonite stocks (6 and 7) along its margins (Candela, 1991). Metals and ligands were preferentially partitioned into the aqueous fluid and when this was released, it formed the strong magnetite-biotite - K-feldspar alteration assemblages (7 and 8) and sub-ore grade Cu-Au (and Zn) anomalies associated with the BQM stocks of the Endeavour deposits.

tensile rock strength of the host rocks. Upon its release, the magmatic – hydrothermal fluid formed the haloes of biotite – magnetite – K-feldspar alteration and associated sub-ore grade Cu-Au and Zn mineralisation (7 and 8 on Figure 9.2) that surround the BQM intrusions close to the Endeavour deposits (e.g. E31).

9.7.2 QMP melt production and Cu-Au porphyry-style mineralisation

For the intrusion of the main phase hosting mineralisation, K-QMP, it is proposed that movement along some deep-seated structure(s), such as the Endeavour Linear and/or LTZ, might have allowed the tapping and delivery of mafic shoshonitic melt to the base of the BQM magma chamber that was already exsolving an aqueous fluid. In this way, it is thought that additional volatiles and metals were probably transferred from the mafic shoshonitic melt to the BQM melt, thereby enhancing the metal productivity of the magma chamber as a whole (1 – 3 on Figure 9.3). Associated movements on shallow crustal fault systems above the magma chamber, such as the northwest- and northeast-trending fractures, is thought to have caused almost immediate magma chamber decompression (4), which resulted in the simultaneous egress of an aqueous fluid together with QMP melt into dilatant zones (brain rock (5) and anisotropic texture (6) development). Localised fracturing and additional volatile exsolution from the QMP melt (7 and 8) is thought to have led to the formation of the narrow, K-QMP intrusions and associated stockwork and sheeted veins (10) and K-silicate alteration (11) related to the Cu-Au ore bodies (Figure 9.3).

It is envisaged that episodic movement along the deep-seated (mantle-tapping?) structure(s) could have allowed repeated emplacement of mafic shoshonitic magmas into the BQM magma chamber. Related movements on shallow faults above the magma chamber could also have resulted in episodic, near instantaneous magma chamber decompression and associated aqueous fluid exsolution and repeated egress of varying amounts of aqueous fluid and melt into dilatant zones, and probably led to the emplacement of the KA-QMP intrusions (12) and associated stockwork veins (13) and K-silicate alteration (14) into the narrow, pipe-like K-QMP intrusions. It is envisaged that after a period of time, during which phyllic and propylitic alteration assemblages were developed (15 and 16), the sequence of mafic shoshonitic magma emplacement through K-silicate alteration, led to the rise of minor late-mineral B-QMP intrusions (17 on Figure 9.3) and associated disseminated Cu-sulphides and assimilation-derived bornite clots.

Figure 9.3 QMP melt production and Cu-Au porphyry-style mineralisation

Movement on the deep-seated structures (❶) triggered the emplacement of mafic shoshonitic magma into the base of the crystallising BQM magma chamber (❷). On contact with the cooler BQM melt, the mafic shoshonitic magma was quenched, which initiated the formation of a buoyant stream of volatile-rich magma and volatile bubbles (❸). Prior to widespread depressurisation-induced aqueous fluid exsolution by first boiling, B-QMP dykes and dykelets were intruded on the periphery of the system due to the initial build up of a small MVA plume and rise of mixed shoshonitic - BQM melt (❹). Related movement on the shallow crustal northwest- and northeast-trending fractures probably caused near-instantaneous depressurisation and first boiling of the relatively more fractionated (B-QMP removal and minor crystallisation) BQM + mafic shoshonitic mixed melt, which led to the simultaneous egress of aqueous fluid and K-QMP melt into dilatant zones and the formation of brain rock (❺) in the apices of the conduit and other anisotropic textures throughout K-QMP (❻). Localised fracturing and continued aqueous fluid exsolution, possibly driven by the density contrast between buoyant, ascending volatile-rich magma (❼) and descending, relatively dense degassed magma (❽) (Shinohara *et al.*, 1995) is proposed to have led to the formation of the narrow, K-QMP intrusions and associated sheet and stockwork K-feldspar - quartz - Cu-sulphide vein networks (❾) and intense K-silicate alteration assemblages (❿). Repeated, episodic movement on the deep- and shallow- (⓫) crustal structures and the addition of mafic shoshonitic melt shortly after the intrusion of K-QMP led to the emplacement of KA-QMP intrusions (⓬), with their own stockwork vein systems (⓭) and slightly less intense K-silicate alteration (⓮) assemblages. The initially hot magmatic - hydrothermal fluid associated with K- and KA-QMP intrusions became oxidised and more acidic as it cooled, which was probably due to increased gas production from the cooling aqueous fluid. This sericite-stable fluid is thought to have led to the formation of phyllic alteration and Cu-sulphide assemblages that overprinted K- and KA-QMP intrusions in the proximal regions (⓯) of the Endeavour deposits. Distal propylitic assemblages, possibly related to the proximal magmatic-related phyllic alteration, and associated carbonate - base-metal veins in the distal regions of the QMP complex (⓰) occurred prior to the emplacement of late-mineral B-QMP intrusions (⓱).

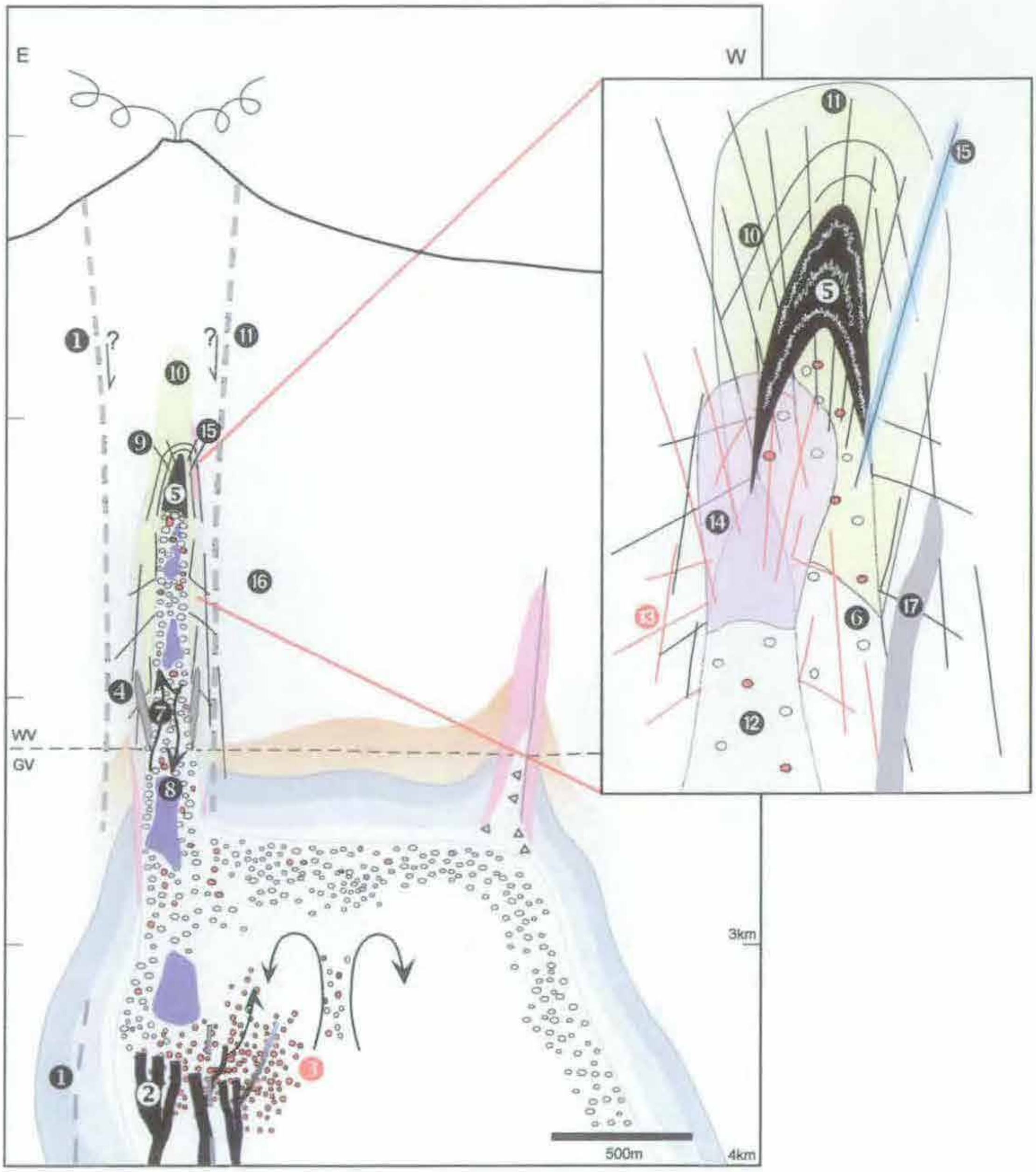

E
W
WV
GV
3km
4km
500m
?
?
1
2
3
4
5
6
7
8
9
10
11
12
13
14
15
16
17

Local conditions at E48, possibly adiabatic pressure quenching (Candela, 1991), are inferred to have led to the further fractionation of the KA-QMP phase at this deposit to form the microgranite intrusion.

Given the successively decreasing metal grade, intensity of K-silicate alteration and associated stockwork or sheeted veining associated with successive QMP phases, it is possible that successive batches of shoshonitic magma added to the magma chamber were similar in composition, however, the first batch had the greatest proportion of incompatible metals and volatiles which it added to the BQM magma. Although not considered essential for the production of increasingly more mafic intrusions from the monzodioritic BQM – shoshonitic mixed magma, it is thought that successive batches of mafic shoshonitic magma might have been required to explain the decrease in the overall felsic nature of the successive intrusions within the QMP complexes.

The addition of batches of mafic shoshonitic melt can adequately explain the relative enrichment of Ba and Sr and depletion of Rb, Nb and Zr in the QMP intrusions compared to the BQM, since mafic shoshonitic magmas are respectively enriched in Ba and Sr and depleted in Rb and Nb (Gill, 1981; Keith *et al.*, 1998). The F-rich character of the apatite and biotite phenocrysts in both the QMP and BQM intrusions associated with the Endeavour deposits can also be explained by the addition of a fertile mantle component, since F could have been added to the crystallising BQM magma chamber from the mafic shoshonitic melt. An increase in the F content of the melt would also have inhibited crystallisation by lowering the solidus temperature of the melt (Dingwell, 1988). Hence, later crystallisation of apatite and biotite in the BQM magma chamber could have incorporated F from the enriched, mixed magma. With the interpreted increase in F content of the mixed magma and associated inhibition of crystallisation, it is thought that successive batches of mafic shoshonitic magma would have been able to interact with the BQM magma over an extended period of time.

9.7.3 Commingled basaltic trachyandesite and mafic monzonite porphyry

The sharp intrusive contacts between the basaltic trachyandesite dykes and the surrounding BQM at E26 indicates that the BQM magma was mostly crystalline at the time of basaltic trachyandesite intrusion. However, gradational contacts between the basaltic trachyandesite and monzonitic zero porphyry dykes, and the presence of rounded to angular clasts of basaltic trachyandesite within the younger zero porphyry intrusions indicates that the zero porphyry melt intruded the cores of the basaltic trachyandesite dykes before they were completely crystalline. These latter contact relationships are indicative of magma commingling (Keith *et al.*, 1998).

Commingling implies the simultaneous intrusion of different magmas. Within the confines of the extensional setting of the evolving Macquarie Island Arc in the Latest Ordovician, basaltic trachyandesite and monzonitic melts may represent different magmas derived from a broadly similar parental shoshonitic (basaltic) magma by different extents of fractionation (although with variable K_2O; cf. Figure 8.3). In this scenario, episodic movement on the deep-seated crustal structures(s) (1 on Figure 9.4) may have triggered the roughly simultaneous intrusion of basaltic trachyandesitic (2) and monzonitic magmas (3) from (adjacent?) magma chambers, and possibly prompted near instantaneous first boiling and consequent emplacement of the zero porphyries (4) into shallow fault-controlled dilatant zones. Given the intrusive contact relationships, it is envisaged that the two magmas ascended mainly through the same fracture network, which led to the commingling of the basaltic trachyandesitic and monzonitic magmas at, or close to the site of their solidification.

It is considered likely that the mafic shoshonitic magma underplated into the nearly crystalline mixed magma chamber at this time had become saturated with respect to sulphur, possibly due to slower rates of ascent through the crust than previous batches of mafic shoshonitic melt. Because of this, it is envisaged that a magmatic sulphide phase developed prior to its emplacement into the upper crust, thereby precluding the new batch of mafic shoshonitic magma from adding sulphur and metals to the system. Geochemically, S-saturated mafic shoshonitic magmas still contain some volatiles and elements such as K, Ba and Sr (Wyborn, 1996), which were probably added to the small amount of mixed melt that remained in the chamber at this time.

The addition of S-saturated mafic alkaline melt into a nearly crystalline mixed BQM magma chamber can account for the shoshonitic geochemical signatures of, and presence of anhydrite in, the zero porphyries associated with E26. This is proposed since it is considered here that the zero porphyries at E26 were partially sourced from a magma chamber that had additional SO_2 from previously intruded volatile-rich mafic shoshonitic melts. At the same time, the presence of the QMP complexes may have aided closed-system conditions by providing greater confining pressures, which allowed sulphate to remain in the magma chamber. In contrast, the similar zero porphyries at E37 and mafic

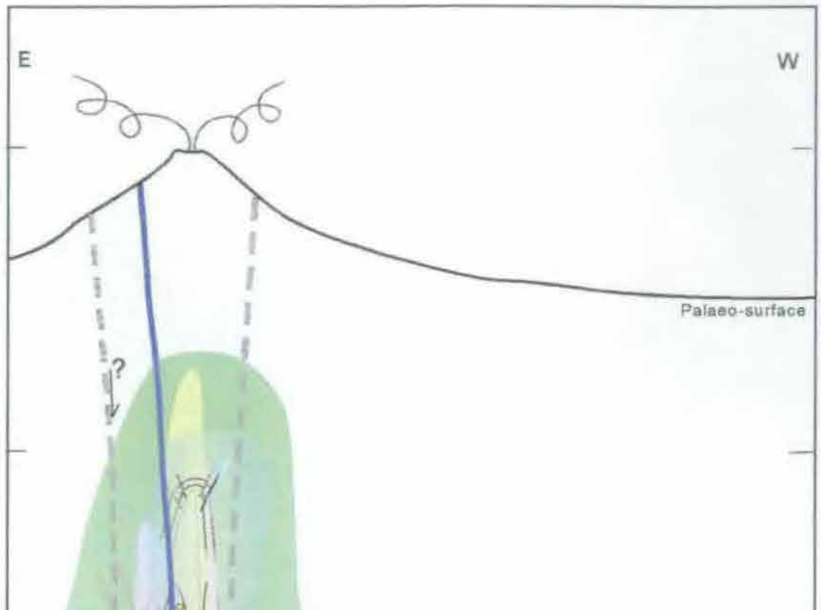

Figure 9.4 Commingled basaltic trachyandesite and mafic monzonite porphyry

During the waning stages of Latest Ordovician extension, episodic movement on the deep crustal structure(s) possibly led to the near simultaneous intrusion of basaltic trachyandesite (1) and trachytic melts (2) sourced from a broadly similar parental magma, but residing in two adjacent(?) magma chambers. The movement possibly prompted near instantaneous first boiling (and migration of the aqueous fluid by advection through spanning clusters because of the high viscosity of the near-crystalline mixed BQM - shoshonitic magma chamber (3)), and consequent emplacement of the zero porphyries into shallow crustal fracture-controlled dilatant zones. The intrusive contact relationships between the basaltic trachyandesite (4) and zero porphyries (5) is interpreted to imply that the two magmas ascended through the same fracture network, which led to the commingling of the two magmas at, or close to, the site of their solidification. Widespread late-stage propylitic alteration was developed around the Endeavour porphyry deposits during the waning stages of magmatic activity (6). Zero porphyries are restricted to E26 in the vicinity of *Northparkes*, however, their occurrence at E37 and Gunningbland Forest indicates a GVC-wide scale of sulphur-saturated shoshonitic subvolcanic intrusive activity at this time. Mafic dykes of uncertain age may or may not be related to the mineralising systems. However, the fact that some of these mafic dykes are faulted and surrounded by late-stage phyllic alteration haloes is thought to indicated that some may have been emplaced during the waning stages of Latest Ordovician magmatism in the GVC.

monzonite porphyries at the Gunningbland Forest do not contain anhydrite. This could be due to open-system degassing and consequent loss of SO_2 from the intruding magmas, which in effect, left them devoid of anhydrite.

Zero porphyries do not occur at E22, E27 and E48, but do occur at E26, E37 and at the Gunningbland Forest. The zero porphyries are thus inferred to be part of a more regional magmatic event than the intrusion of the QMP complexes, which are associated solely with the Endeavour deposits (including E37). This is supported by the available geochronology: 1) the BQM and B-QMP intrusions were emplaced between 445 and 440Ma; 2) alteration and mineralisation at E26 is ~439Ma and 3) a zero porphyry from E37, which has strong geochemical, mineralogical and textural similarities to the zero porphyry dykes at E26 and the Gunningbland Forest monzonite porphyries has been dated at ~437Ma (cf. Table 8.1). Overall, the magmatic evolution of the Endeavour deposits occurred over approximately 8 million years, with hydrothermal activity occurring as discrete events towards the end on this period.

Thus, the preferred genetic model for the formation of the QMP complexes and associated alteration and mineralisation assemblages at E22, E26, E27 and E48 centres on the emplacement of a series of mafic shoshonitic melts into the base of a crystallising, zoned monzodiorite to monzonite magma chamber. The emplacement of these mafic shoshonitic melts was probably triggered by episodic movement along one or more deep-seated mantle-tapping structure(s), such as the LTZ or (less likely?) the Endeavour Linear, during Latest Ordovician extensional tectonic setting of the evolving Macquarie Island Arc.

9.8 Recommendations for further work

Work undertaken for this thesis has highlighted several key features for exploration and raised questions for further research in the GVC in central-west New South Wales.

- Several textural and geochemical features, e.g. variably developed anisotropic textures, higher degree of fractionation and abnormally high LREE depletion, distinguish the mineralised intrusions associated with the Endeavour deposits from the unmineralised regional intrusions in the GVC. These criteria could be readily applied to exploration within the GVC to help establish the mineral potential of regional intrusive rocks.
- Given the similarity of the mafic monzonite porphyry intrusions of the Gunningbland Forest with the E26 and E37 zero porphyry dykes, where the latter are

both associated with QMP complexes and mineralisation, it is considered that further exploration around the Gunningbland Forest area is warranted. The location of Pb-Zn skarn prospects of E6, E7 and E44 is thought to be significant in this regard.

- It has been established that both apatite and biotite in the intrusive rocks associated with mineralisation are enriched in F. Even though most of the regional intrusions within the GVC have been affected by weak, low-grade prehnite – pumpellyite metamorphism, relict biotite phenocrysts are still preserved. Determining the halogen contents of biotite in the regional intrusions may be another way of establishing their potential for hosting mineralisation.
- Detailing the distribution, mineralogy, alteration, geochemistry, crosscutting relationships and geochronology of the different mafic dykes within the Endeavour deposits would considerably enhance our understanding of the influence(s) these (and similar?) rocks might have had on the development of the mineralised systems.
- A detailed study of the propylitic alteration haloes that surround E22 and E27 may broaden our understanding of the temporal manifestations of this alteration assemblage, since it is envisaged that propylitic alteration assemblages were developed throughout the life of the Endeavour magmatic – hydrothermal systems.
- By conducting additional paragenetically-constrained research on the S isotopic compositions of sulphides and sulphates in the E22, E27 and E48 deposits, the extent of wallrock buffering in these systems could be assessed to establish whether a zonation towards heavier $\delta^{34}S$ values with time and distance from the centre of the deposits exists or not. Further research into the generation of the anomalously negative $\delta^{34}S$ values (-19 to -15‰) in sulphides associated with the transition from magmatic to hydrothermal conditions may provide insight into the conditions of the magma at this time.
- A detailed structural study that integrates deposit-scale and district-scale data is required, so that the evolution of the stress regime with time, and the structural controls on porphyry emplacement and vein formation can be better understood.
- The preferred model presented in this thesis would greatly benefit from a detailed radiogenic isotope study to further constrain the proposed mafic shoshonitic magma as the fertile component in these Endeavour systems, which is currently based on the presence of commingled basaltic trachyandesite and mafic monzonite porphyry melts in the waning stages of magmatism at E26, and the presence of variable altered mafic dykes at the other deposits.

CHAPTER 10

References

- Alderton, D. H. M., Pearce, J. A. and Potts, P. J., 1980. Rare earth mobility during granite alteration: evidence from southwest England: Earth and Planetary Science Letters; 49, 149-165.

- Anders, R. J., Rose, W. I., Kyle, P. R., Desilva, S., Francis, P., Gardeweg, M. and Moreno, R., H., 1991. Excessive sulfur dioxide emissions from Chilean volcanoes: Journal of Volcanology and Geothermal Research; 46, 323-329.

- Arundell, M. C., 1997. Goonumbla: 25 years, four deposits, 52 prospects and still drilling...: Third international Mining Geology Conference, proceedings, 183-187.

- Arundell, M. C., 1998. The geology and mineralisation of the E31 copper-gold prospect, Goonumbla, N.S.W.: Unpub. Master of Economic Geology thesis, University of Tasmania, 82 p.

- Baldwin, J. A. and Pearce, J. A., 1982. Discrimination of productive and non-productive porphyritic intrusions in the Chilean Andes: Economic Geology; 77, 664-674.

- Bea, F., 1996. Residence of REE, Y, Th and U in granites and crustal protoliths; implications for the chemistry of crustal melts: Journal of Petrology; 37, 521-552.

- Beane, R. E. and Bodnar, R. J., 1995. Hydrothermal fluids and hydrothermal alteration in porphyry copper deposits, *in* Pierce, F. W., and Bohm, J. G., eds., Porphyry copper deposits of the American cordillera, 20: Tucson, Arizona Geological Society Digest.

- Blevin, P. L. and Chappell, B. W., 1995. Chemistry, origin, and evolution of mineralized granites in the Lachlan fold belt, Australia; the metallogeny of I- and S-type granites: Economic Geology; 90, 1604-1619.

- Blevin, P. L. and Morrison, G. W., 1997. Magmatic and hydrothermal evolution of major intrusive related gold deposits: AMIRA, P425, final report, Parts 11 and 14.

- Bodnar, E., 1995. Fluid-inclusion evidence for a magmatic source of metals in porphyry copper deposits: Mineralogical Association of Canada Short Course Series; 23, 139-152.

- Bodnar, R. J., Burnham, C. W. and Sterner, S. M., 1985. Synthetic inclusions in natural quartz. III. Determination of phase equilibrium properties in the system H_2O-NaCl to 1000°C and 1500 bars: Geochimica et Cosmochimica Acta; 49, 1861-1873.

- Bodnar, R. J., Sterner, S. M. and Hall, D. L., 1989. SALTY: A Fortran program to calculate the compositions of fluid inclusions in the system NaCl-KCl-H_2O: Computers and Geosciences; 15, 14-41.

- Bookstrom, A. A., 1988. Tectonic setting and generation of Rocky Mountain porphyry molybdenum deposits, *in* Dickinson, W. R., and Payne, W. D., eds., Relations of tectonics to ore deposits in the southern Cordillera, 14, Arizona Geological Society Digest, 215-226.

- Bowman, H. N., Richardson, S. J. and Dolanski, J., 1982. Narromine 1:250 000 Metallogenic Map SI 55-3 - mine data sheets and metallogenic study: New South Wales Geological Survey, 337.

- Burnham, C. W., 1979. Magmas and hydrothermal fluids, *in* Barnes, H. L., ed., Geochemistry of hydrothermal ore deposits, 2nd Edition: New York, Wiley Interscience, 71-136.

- Burnham, C. W., 1997. Magmas and hydrothermal fluids, *in* Barnes, H. L., ed., Geochemistry of hydrothermal deposits, 3rd edition: New York, John Wiley and Sons, Inc, 63-123.

- Butera, K. M., Williams, I. S., Blevin, P. L. and Simpson, C. J., 2001. Zircon U-Pb dating of Early Palaeozoic monzonitic intrusives from the Goonumbla area, New South Wales: Australian Journal of Earth Sciences; 48, 457-464.

- Candela, P. A., 1983. Halogen trends in apatite as an indicator of magmatic vapor evolutions: EOS, Transactions, American Geophysical Union; 64, 343.

- Candela, P. A., 1984. A partitioning model for the rare earth elements and other polyvalent, chloride-complexed metals in melt-vapor systems: *in* Anonymous, ed., Geological Society of America, 97th Annual Meeting, Reno, Nevada, USA, 1984, 462.

- Candela, P. A., 1989a. Felsic magmas, volatiles, and metallogenesis, *in* Whitney, J. A., and Naldrett, A. J., eds., Reviews in Economic Geology, 4, 223-233.

- Candela, P. A., 1989b. Magmatic ore-forming fluids: thermodynamic and mass transfer calculations of metal concentrations, *in* Whitney, J. A., and Naldrett, A. E., eds., Ore deposition associated with magmas: Reviews in Economic Geology, 4, 203-221.

- Candela, P. A., 1990. Theoretical constraints on the chemistry of the magmatic aqueous phase, *in* Stein, H. J., and Hannah, J. L., eds., Ore-bearing granite systems; Petrogenesis and mineralizing processes, Special paper 246: Boulder, Colorado, Geological Society of America, 11-20.

- Candela, P. A., 1991. Physics of aqueous phase evolution in plutonic environments: American Mineralogist; 76, 1081-1091.

- Candela, P. A., 1994. Combined chemical and physical model for pluton devolatilisation: a non-Rayleigh fractionation algorithm: Geochimica et Cosmochimica Acta; 58, 2157-2167.

- Candela, P. A. and Blevin, P. L., 1995. Do some miarolitic granites preserve evidence of magmatic volatile phase permeability?: Economic Geology; 90, 2310-2316.

- Candela, P. A. and Holland, H. D., 1986. A mass transfer model for Cu and Mo in magmatic hydrothermal systems: The origin of porphyry-type ore deposits: Economic Geology; 81, 1-19.

- Candela, P. A. and Piccoli, P. M., 1995. Model ore-metal partitioning from melts into vapor and vapor/brine mixtures, *in* Thompson, J. F. H., ed., Magmas, fluids and ore deposits: Short course series (Mineralogical Association of Canada), 23: Victoria, B.C., Mineralogical Association of Canada, 101-127.

- Carne, J. E., 1908. The copper mining industry and the distribution of copper ores in New South Wales: Sydney, New South Wales Geological Survey, Mineral Resources, 280 p.

- Carr, G. R. and Dean, J. A., 1990. Mantle and crustal lead isotope signatures of Au mineralization in the western tectonic domains of the Lachlan fold belt, NSW: *in* Compston, W., ed., Seventh international conference on Geochronology, cosmochronology and isotope geology, Canberra, 1990, 15 p.

- Carr, G. R., Dean, J. A., Suppel, D. W. and Heithersay, P. S., 1995. Precise lead isotope fingerprinting of hydrothermal activity associated with Ordovician to Carboniferous metallogenic events in the Lachlan Fold Belt of New South Wales: Economic Geology; 90, 1467-1505.

- Carten, R., 1986. Sodium-calcium metasomatism: chemical, temporal, and spatial relationships at the Yerington, Nevada, porphyry copper deposit: Economic Geology; 81, 1495-1519.

- Carten, R. B., Walker, B. M. and Geraghty, E. P., 1988. Comparison of field-based studies of the Henderson porphyry molybdenum deposit, Colorado, with experimental and theoretical models of porphyry systems, *in* Taylor, R. P., and Strong, D. F., eds., Recent advances in the geology of granite-related mineral deposits, Special volume 39: Ottawa, Canadian Institute of Mining and Metallurgy, 351 - 366.

- Cathles, L. M., 1981. Fluid flow and genesis of hydrothermal ore deposits, *in* Skinner, B. J., ed., Economic Geology; 75th anniversary volume: Boulder, Colorado, Econ. Geol. Publ. Co., U.S.A., 424-457.

- Chappell, B. W., White, A. J. R. and Hine, R., 1988. Granite provinces and basement terranes in the Lachlan Fold Belt, southeastern Australia: Australian Journal of Earth Science; 35, 505-521.

- Chivas, A. R., 1981. Geochemical evidence fort magmatic fluids in porphyry copper mineralization: Contributions to Mineralogy and Petrology; 78, 389-403.

- Clark, G. H., 1990. Panguna copper-gold deposit, *in* Hughes, F. E., ed., Geology of the mineral deposits of Australia and Papua New Guinea: Melbourne, The Australian Institute of Mining and Metallurgy, 1807-1816.

- Clarke, I., 1990. Igneous petrology, *in* Clarke, I., and Sherwin, L., eds., Geological setting of gold and copper deposits in the Parkes area, New South Wales, 23. Records of the Geological Survey of N.S.W., New South Wales Geological Survey, 95-136.

- Cline, J. S. and Bodnar, R. J., 1991. Can economic porphyry copper mineralisation be generated by a typical calc-alkaline melt?: Journal of Geophysical Research; 96, 8113-8126.

- Cline, J. S. and Bodnar, R. J., 1994. Direct evolution of brine from a crystallizing silicic melt at the Questa, New Mexico, molybdenum deposit: Economic Geology; 89, 1780-1802.

- Clode, C., Profett, J., Mithcell, P. and Munajat, I., 1999. Relationships on intrusion, wall-rock alteration and mineralisation in the Batu Hijau copper-gold porphyry deposit: *in* Weber, G., ed., Pacrim '99, conference proceedings, Bali, Indonesia, 1999, 485-498.

- Cooke, D. R., 1991. Styles and controls of mineralisation, Acupan Gold Mine, Baguio District, Philippines: Unpub. PhD thesis, Monash University, 396 p.

- Cooke, D. R., 1997. Case studies of western Pacific porphyry Cu-au deposits in Indonesia, *in* Thompson, J. T. F., Cooke, D. R., and Gemmell, J. B., eds., Porphyry and epithermal deposits of the circum-Pacific, CODES Short Course, September 1997, University of Tasmania, 131-144.

- Cooke, D. R. and Bloom, 1990. Epithermal and subjacent porphyry mineralization, Acupan, Baguio District, Philippines; a fluid-inclusion and paragenetic study: Journal of Geochemical Exploration; 35, 297-340.

- Cooke, D. R., Heithersay, P. S., Wolfe, R. and Calderon, A. L., 1998. Australian and western Pacific porphyry Cu-Au deposits: AGSO Journal of Australian Geology and Geophysics; 17, 97-104.

- Cooke, D. R., House, M. J., Smith, S.G. and Wolfe, R. C., 2000. Oxidized magmas, oxidized fluids and their controls on alteration assemblages and metal distribution in the porphyry Cu-Au deposits of Goonumbla, NSW, Australia: *in* Anonymous, ed., Geological Society of America Annual Meeting, Summit 2000, Reno, Nevada, USA, 2000, A-113.

- Crawford, A. J., 1999. Lithogeochemistry and correlations of the Junee-Parkes-Narromine belt: an update: Hobart, Centre for Ore Deposit Research, 44 p.

- Crawford, A. J., 2001a. Tectono-magmatic development of the Ordovician volcanic belts in central western NSW, and the timing and location of porphyry-style mineralisation within the Macquarie Arc, *in* Crawford, A. J., Cooke, D. R., and Glen, R. A., eds., NSW Ordovician SPIRT Report: Hobart, Centre for Ore Deposit Research, 7.41 - 7.52.

- Crawford, A. J., 2001b. Lithostratigraphy and lithochemistry of volcanic and intrusive rocks, Parkes-Narromine belt, *in* Crawford, A. J., Cooke, D. R., and Glen, R. A., eds., NSW Ordovician SPIRT Report: Hobart, Centre for Ore Deposit Research, 2.19-2.41.

- Crawford, A. J. and Berry, R. F., 1992. Tectonic implications of Late Proterozoic-Early Palaeozoic igneous rock associations in western Tasmania: Tectonophysics; 214, 37-56.

- Crawford, A. J., Cooke, D. R. and Glen, R. A., 2001. NSW Ordovician SPIRT Report: Hobart, Centre for Ore Deposit Research, 510 p.

- Crawford, A. J. and Direen, N. G., 1998. Late Proterozoic-early Palaeozoic evolution of the eastern Adelaide Foldbelt and western Lachlan Foldbelt; the real breakup, and subsequent continental crust-forming events: *in* Bird, R. T., Powell, C. M., and Wingate, M. T. D., eds., 14th Australian Geological Congress, 1998, 15-16.

- Crook, K. A. W., 1980. Fore-arc evolution in the Tasman Geosyncline: the origin of southeast Australian continental crust: Geological Society of Australia Journal; 27, 215-232.

- Cuddy, A. S. and Kesler, S. E., 1982. Gold in the Granisle and Bell porphyry copper deposits: *in* Levinson, A. A., ed., Precious metals in the Northern Cordillera, Vancouver, British Columbia, 1982, 139-155.

- de Hoog, J. C. M. and van Bergen, M. J., 2000. Volatile-induced transport of HSFE, REE, Th and U in arc magma: evidence from zirconolite-bearing vesicles in potassic lavas of Lewotolo volcano (Indonesia): Contributions to Mineralogy and Petrology; 139, 485-502.

- Degeling, P. R., Corbett, G. J. and Leach, T. M., 1995. The Peak Hill high sulphidation gold deposit, NSW: *in* Mauk, J. L., ed., PACRIM Congress - Exploring the rim, 1995, 175-180.

- Dilles, J. H., 1987. Petrology of the Yerington batholith, Nevada: evidence for evolution of porphyry copper ore fluids: Economic Geology; 82, 1750-1789.

- Dilles, J. H. and Einaudi, M. T., 1992. Wall-rock alteration and hydrothermal flow paths about the Ann-Mason porphyry copper deposit, Nevada - a 6km vertical reconstruction: Economic Geology; 87, 1963-2001.

- Dingwell, D. B., 1988. The structures and properties of fluorine-rich magmas: a review of experimental studies, *in* Taylor, R. P., and Strong, D. F., eds., Recent advances in the geology of granite-related mineral deposits, Special volume 39: Ottawa, Canadian Institute of Mining and Metallurgy, 1-12.

- Dingwell, D. B., Knoche, R. and Webb, S. L., 1993. The effect of F on the density of haplogranite: American Mineralogist; 78, 325-330.

- Direen, N. G., 1999. Geology and geophysics of the Koonenberry Belt, far western NSW: Unpub. PhD thesis, 339 p.

- Downes, P. M. and Burton, G. R., 1999. Mineral occurrences in the Forbes district: *in* Lyons, P., and Wallace, D., eds., Geology and metallogenesis of the Parkes - Grenfell - Wyalong - Condobolin region, New South Wales, Forbes, 1999, 37-53.

- Duggan, M. B., Lyons, P., Raymond, O. L., Wallace, D. A., Wyborn, D., Young, G. C., Krynen, J. P., Scott, M. M. and Sherwin, L., 1999. Forbes Geology - Sheet S155-7: Australian Geological Survey Organisation.

- Eastoe, C., 1980. Chemistry of magmatic fluids in the Panguna (Bougainville) porphyry copper deposit, International Geological Congress, Abstracts, 1980, 929.

- Eastoe, C. J., 1982. Physics and chemistry of the hydrothermal system at the Panguna porphyry copper deposit, Bougainville, Papua New Guinea: Economic Geology; 77, 127-153.

- Eastoe, C. J., 1983. Sulfur isotope data and the nature of the hydrothermal systems at the Panguna and Frieda porphyry copper districts, Papua New Guinea: Economic Geology; 78, 201-213.

- Fergusson, C. L. and Coney, P. J., 1992a. Implications of a Bengal fan-type deposits in the Paleozoic Lachlan Fold Belt of southeastern Australia: Geology; 20, 1047-1049.

- Fergusson, C. L. and Coney, P. J., 1992b. Convergence and intraplate deformation in the Lachlan Fold Belt of southeastern Australia: Tectonophysics; 214, 417-440.

- Field, C. W., 1966. Sulfur isotope abundance data, Bingham district, Utah: Economic Geology; 61, 850-871.

- Field, C. W. and Gustafson, L. B., 1976. Sulfur isotopes in the porphyry copper deposit at El Salvador, Chile: Economic Geology; 71, 1533-1548.

- Flynn, R. T. and Burnham, C. W., 1978. An experimental determination of rare earth partitioning coefficients between a chloride containing vapor phase and silicate melts: Geochimica et Cosmochimica Acta; 42, 685-701.

- Ford, J. H. and Green, D. C., 1977. An oxygen and hydrogen isotope study of the Panguna porphyry deposit, Bouganville: Geological Society of Australia Journal; 24, 63-80.

- Foster, D. A., Gray, D. R. and Bucher, M., 1999. Chronology of deformation within the turbidite-dominated, Lachlan Orogen; implications for the tectonic evolution of eastern Australia and Gondwana: Tectonics; 18, 452-485.

- Fourcade, S. and Allegre, C. J., 1981. Trace elements behavior in granite genesis: A case study The calc-alkaline plutonic association from the Querigut Complex (Pyrénées, France): Contributions to Mineralogy and Petrology; 76, 177-195.

- Fournelle, J., 1990. Anhydrite in Nevada del Ruiz November 1985 pumice: relevance to the sulfur problem: Journal of Volcanology and Geothermal Research; 42, 189-201.

- Frei, R., 1996. Sulfur in bulk rock and igneous apatite; tracing mineralized and barren trends in intrusions: Schweiz. Mineral. Petrogr. Mitt.; 76, 57-73.

- Garwin, S., 2002. The geological setting of intrusion-related hydrothermal systems near the Batu Hijau porphyry copper-gold deposit, Sumbawa, Indonesia, *in* Goldfarb, R., ed., Global Exploration - Integrated methods for discovery, Society of Economic Geologists, Special Publication No 9 (in Press).

- Gill, J. B., 1981. Orogenic andesites and plate tectonics: Berlin, Springer-Verlag, 390 p.

- Glen, R. A., 1992. Thrust, extensional and strike-slip tectonics in an evolving Palaeozoic orogen - a structural synthesis of the Lachlan Fold Belt of southeastern Australia: Tectonophysics; 214, 341-380.
- Glen, R. A., Percival, I. G., Barron, L. M. and Crawford, A. J., 2001. The Early Ordovician Nelungaloo Volcanics and Yarrimbah Formation, *in* Crawford, A. J., Cooke, D. R., and Glen, R. A., eds., NSW Ordovician SPIRT Report: Hobart, Centre for Ore Deposit Research, 2.1-2.17.
- Glen, R. A. and Walshe, J. L., 1999. Cross-structures in the Lachlan Orogen: the Lachlan Transverse Zone example: Australian Journal of Earth Sciences; 46, 641-658.
- Glen, R. A., Walshe, J. L., Barron, L. M. and Watkins, J. J., 1998. Ordovician convergent-margin volcanism and tectonism in the Lachlan sector of east Gondwana: Geology; 26, 751-754.
- Glen, R. A. and Wyborn, D., 1997. Inferred thrust imbrication, deformation gradients and the Lachlan Transverse Zone in the eastern belt of the Lachlan Orogen, New South Wales: Australian journal of Earth Science; 44, 49-68.
- Gordon, M. J., 1990. The geology of E.L. 2908, Molong; and mineralisation of the Endeavour 37 prospect, Goonumbla, N.S.W.: Unpub. BSc Honours thesis, Australian National University, 109 p.
- Gray, D. R. and Foster, D. A., 1997. Orogenic concepts - application and definition: Lachlan Fold Belt, eastern Australia: American Journal of Science; 297, 859-891.
- Gray, N., Mandyczewsky, A. and Hine, R., 1995. Geology of the zoned gold skarn at Junction Rees, New South Wales: Economic Geology; 90.
- Green, T. H., 1980. Island arc and continent-building magmatism; a review of petrogenic models based on experimental petrology and geochemistry: Tectonophysics: Orthodoxy and creativity at the frontiers of earth sciences (Carey symposium); 63, 367-385.
- Gunow, A. J., Ludington, S. and Munoz, J. L., 1980. Fluorine in micas from the Henderson molybdenite deposit, Colorado: Economic Geology; 75, 1127-1137.
- Gustafson, L. B. and Hunt, J. P., 1975. The porphyry copper deposit at El Salvador, Chile: Economic Geology; 70, 857-912.
- Haas, J. L. J., 1976. Physical properties of the coexisting phases and the thermochemical properties of the H_2O component in boiling NaCl solutions, US Geological Survey Bulletin, 1421-A, 73 p.
- Hall, M. C., 1993. The stratigraphy and palaeovolcanology of the Late Ordovician Goonumbla Volcanics, Goonumbla, N.S.W.: Unpub. BSc Honours thesis, Monash University, 158 p.
- Hanson, H. R., 1995. The hydrodynamics of contact metamorphism: Geological Society of America Bulletin; 107, 595-611.
- Harper, B., 2000. Hydrothermal alteration at the Ridgeway porphyry gold-copper deposit, NSW: Unpub. BSc Honours thesis, University of Tasmania, 130 p.
- Harris, A. C., 1997. Vein emplacement, E26N porphyry Cu-Au deposit, Goonumbla, New South Wales: Unpub. BSc Honours thesis, University of Queensland, 102 p.
- Harris, A. C. and Golding, S. D., 2001. A magmatic fluid source for phyllic alteration in some porphyry-related mineralisation: *in* Williams, P. J., ed., 2001: A hydrothermal odyssey - extended conference abstracts, Townsville, Australia, 2001, 70-71.
- Hassanen, M. A., 1997. Post-collision, A-type granites of Homrit Wagga Complex, Egypt: petrological and geochemical constraints on its origin: Precambrian Research; 82, 211-236.
- Hattori, K., 1993. High-sulfur magma, a product of fluid discharge from underlying mafic magma: Evidence from Mt Pinatubo, Philippines: Geology; 21, 1083-1086.
- Hedenquist, J. W., 2000. Stable isotopic zonation of alteration minerals over a porphyry Cu-Mo deposit, El Salvador, Chile: *in* Anonymous, ed., Geological Society of America Annual Meeting, Summit 2000, Reno Nevada, USA, 2000, A-138.
- Hedenquist, J. W., Arribas, A. J. and Reynolds, T. J., 1998. Evolution of an intrusion-centred hydrothermal system: Far Southeast Lepanto porphyry and epithermal Cu-Au deposits, Philippines: Economic Geology; 93, 373-404.
- Hedenquist, J. W. and Lowenstern, J. B., 1994. The role of magmas in the formation of hydrothermal ore deposits: Nature; 370, 519-527.

- Heinrich, C. A., Ryan, C. G., Mernagh, T. P. and Eadington, P. J., 1992. Segregation of ore metals between magmatic brine and vapor; a fluid inclusion study using PIXE microanalysis: Economic Geology; 87, 1566-1583.

- Heithersay, P. S., 1986. Endeavour 26 North copper-gold deposit, Goonumbla, N.S.W. - paragenesis and alteration zonation: *in* Berkman, D. A., ed., The 13th Congress of the Council of Mining and Metallurgical Institutions, Melbourne, 1986, 181-189.

- Heithersay, P. S., 1991. The shoshonite-associated Endeavour 26 North porphyry copper-gold deposit, Goonumbla, NSW: Unpub. PhD manuscript, Australian National University, 187 p.

- Heithersay, P. S., 1994. The central west New South Wales Cu-Au province: Porphyry copper-gold deposits, Master of Economic Geology Unpub. Course Manual 1, 1.1-1.26.

- Heithersay, P. S., O'Neill, W. J., van der Helder, P., Moore, C. R. and Harbon, P. G., 1990. Goonumbla porphyry copper district - Endeavour 26 North, Endeavour 22 and Endeavour 27 copper-gold deposits, *in* Hughes, F. E., ed., Geology of the mineral deposits of Australia and Papua New Guinea.: Melbourne, Australasian Institute of Mining and Metallurgy, 1385-1398.

- Heithersay, P. S. and Walshe, J. L., 1995. Endeavour 26 North: A porphyry copper-gold deposit in the Late Ordovician shoshonitic Goonumbla Volcanic Complex, New South Wales, Australia: Economic Geology; 90, 1506-1532.

- Henley, R. W. and McNabb, A., 1978. Magmatic vapor plumes and ground-water interaction in porphyry copper emplacement: Economic Geology; 73, 1-20.

- Hezarkhani, A. and Williams-Jones, A. E., 1998. Controls of alteration and mineralisation in the Sungun porphyry copper deposit, Iran: evidence from fluid inclusions and stable isotopes: Economic Geology; 93, 651-670.

- Holland, H. D., 1972. Granites, solution and base metal deposits: Economic Geology; 67, 281-301.

- Holliday, J. R., Wilson, A. J., Blevin, P. L., Tedder, I. J., Dunham, P. D. and Pfitzner, M., 2002. Porphyry gold-copper mineralisation in the Cadia district, eastern Lachlan Fold Belt, New South Wales, and its relationship to shoshonitic magmatism: Mineralium Deposita; 37, 100-116.

- Holtz, F., Dingwell, D. B. and Harald, B., 1993. Effects of F, B_2O_3 and P_2O_5 on the solubility of water in haplogranite melts compared to natural silicate melts: Contributions to Mineralogy and Petrology; 113, 492-501.

- Hooper, B., Heithersay, P. S., Mills, M. B., Lindhorst, J. W. and Freyberg, J:, 1996. Shoshonite-hosted Endeavour 48 porphyry copper-gold deposit, Northparkes, central New South Wales: Australian Journal of Earth Sciences; 43, 179-288.

- Hooper, B. and Stoltz, N., 1994: Discovery of the shoshonite hosted E48 porphyry deposit, North Parkes, N.S.W., 12th Australian Geological Convention, Perth, 1994, 188.

- House, M. J., 1994. Gold distribution at the E26 porphyry copper-gold deposit, N.S.W.: Unpub. MSc thesis, University of Tasmania, 125 p.

- House, M. J., Cooke, D. R., Smith, S. and Lickfold, V., 2002. Hypogene oxidation & metal distribution in the porphyry Cu-Au deposits of Goonumbla, NSW: Mineralium Deposita; In prep.

- Howland-Rose, J. S., 1996. Fluid evolution at the Endeavour 48 porphyry Cu-Au deposit, Parkes, NSW: Unpub. BSc Honours thesis, University of Newcastle, 87 p.

- Huston, D. L., Power, M., Gemmell, J. B. and Large, R. L., 1995. Design, calibration and geological application of the first operational Australian laser ablation sulphur isotope microprobe: Australian Journal of Earth Sciences; 42, 549-555.

- Imai, A., Listanco, E. L. and Fujii, T., 1993. Petrologic and sulfur isotopic significance of highly oxidized and sulfur-rich magma of Mt. Pinatubo, Philippines: Geology; 21, 699-702.

- Jensen, E. P. and Barton, M. D., 2000. Gold deposits related to alkaline magmatism: Society of Economic Geologists Reviews; 13, 279-314.

- Johnson, M. C., Anderson, A. T. J. and Rutherford, M. J., 1994. Pre-eruptive volatile contents of magmas, *in* Carrol, M. R., and Holloway, J. R., eds., Volatiles in magmas, 30. Reviews in Mineralogy: Chelsea, Michigan, Mineralogical Society of America.

- Jones, B. M., 1991. Geological setting and genesis of the Endeavour 44 Au, Pb, Zn skarn, Parkes, NSW: Unpub. BSc Honours thesis, Australian National University, 72 p.

- Jones, G. J., 1985. The Goonumbla porphyry copper deposits, New South Wales: Economic Geology; 80, 591-613.

- Kavalieris, I., 1994. The Grasberg superporphyry, Ore deposit studies and exploration models - porphyry copper-gold deposits, Unpub. Short Course Manual 5.1: Hobart, CODES SRC, University of Tasmania, 3.1-3.29.

- Kazahaya, K., Shinohara, H. and Saito, G., 1994. Excessive degassing of Izu-Oshima volcano: Magma convection in a conduit: Bulletin of Volcanology; 56, 207-216.

- Keith, J. D., Christiansen, E. H. and Carten, R. B., 1993. The genesis of giant porphyry molybdenum deposits, *in* ???, ed., Giant Ore Deposits, Special Publication 2: Boulder, Colorado, Society of Economic Geologists, 285-317.

- Keith, J. D., Christiansen, E. H., Maughan, D. T. and Waite, K. A., 1998. The role of mafic alkaline magmas in felsic porphyry Cu and Mo systems, *in* Lentz, D. R., ed., Mineralized intrusion-related skarn systems, Short Course Series, Volume 26: Québec, Mineralogical Association of Canada, 211-243.

- Keith, J. D. and Shanks, W. C. I., 1988. Chemical evolution and volatile fugacities of the Pine Grove porphyry molybdenum and ash-flow tuff system, southwestern Utah, *in* Taylor, R. P., and Strong, D. F., eds., Recent advances in the geology of granite-related mineral deposits, Special volume 39: Ottawa, Canadian Institute of Mining and Metallurgy, 402-423.

- Keith, J. F., Whitney, J. A., Hattori, K., Ballantyne, G. H., Christiansen, E. H., Barr, D. L., Cannan, T. M. and Hook, C. J., 1997. The role of magmatic sulfides and mafic alkaline magmas in the Bingham and Tintic mining districts, Utah: Journal of Petrology; 38, 1679-1690.

- Kilinc, A., Carmichael, I. S. E., Rivers, M. L. and Sack, R. O., 1983. The ferric-ferrous ration of natural silicate liquids equilibrated in air: Contributions to Mineralogy and Petrology; 83, 136-140.

- Kilinc, I. A. and Burnham, C. W., 1972. Partitioning of chloride between a silicate melt and coexisting aqueous phase from 2 to 8 kilobars: Economic Geology; 67, 231-235.

- Kirkham, R. V. and Sinclair, W. D., 1988. Comb quartz layers in felsic intrusions and their relationship to porphyry deposits, *in* Taylor, R. P., and Strong, D. F., eds., Recent advances in the geology of granite-related mineral deposits, Special volume 39: Ottawa, Canadian Institute of Mining and Metallurgy, 50-71.

- Kolkert, R., 1998. Carbonate-base metal veins peripheral to the Goonumbla Cu-Au deposits - vectors to mineralised centres?: Unpub. BSc Honours thesis, University of Tasmania, 144 p.

- Kress, V., 1997. Magma mixing as a source for Pinatubo sulfur: Nature; 389, 591-593.

- Krynen, J. P., Sherwin, L. and Clarke, I., 1990a. Geological setting of gold and copper mineralisation in the Parkes area, *in* Clark, I., and Sherwin, L., eds., Records of the Geological Survey of New South Wales, 23, Part 1, 1-76.

- Krynen, J. P., Sherwin, L. and Clarke, I., 1990b. Parkes Special 1:100 000 Geological Sheet (parts 8431, 8432, 8531 and 8532): Sydney, Department of Minerals and Energy.

- Lang, J. R., Stanley, C. R. and Thompson, J. F. H., 1995. Porphyry copper-gold deposits related to alkalic igneous rocks in the Triassic-Jurassic arc terranes of British Columbia: Arizona Geological Society Digest; 20, 219-236.

- Lang, J. R., Thompson, J. F. H., Moreton, J., Baker, T., Coulson, I., Maloof, T., James, J., Friedman, R. and Lepitre, M., 2001. Regional and system-scale controls on the formation of copper and/or gold magmatic-hydrothermal mineralization: Vancouver, BC, Canada, MDRU, 105 p.

- Lang, J. R. and Titley, S. R., 1998. Isotopic and geochemical characteristics of Laramide magmatic systems in Arizona and implication for the genesis of porphyry copper deposits: Economic Geology; 93, 138-170.

- Le Bas, M. J., Le Maitre, R. W., Streckeisen, A. and Zanettin, B., 1986. A chemical classification of volcanic rocks based on the total alkali-silica diagram: Journal of Petrology; 27, 745-750.

- Leach, T. L., 1995. Petrological evaluation of processes of copper-gold mineralisation in the Goonumbla district: North Limited; Unpublished North Limited Company Report, 72.

- Lindhorst, J. W. and Cook, W. G., 1990. Gidginbung gold-silver deposit, *in* Hughes, F. E., ed., Geology of the mineral deposits of Australia and Papua New Guinea, 2: Melbourne, Australasian Institute of Mining and Metallurgy, 1365-1370.

- Lindsay, J. M., Schmitt, A. K., Trumbull, R. B., de Silva, S. L., Siebel, W. and Emmermann, R., 2001. Magmatic evolution of the La Pacana caldera system, central Andes, Chile: Compositional variation of two cogenetic large-volume felsic ignimbrites: Journal of Petrology; 42, 459-486.

- Liu, Y. and Comodi, P., 1993. Some aspects of the crystal-chemistry of apatites: Mineralogical Magazine; 57, 709-719.

- Loferski, P. J. and Ayuso, R. A., 1995. Petrography and mineral chemistry of the composite Deboullie pluton, northern Maine, U.S.A.: implication for the genesis of Cu-Mo mineralization: Chemical Geology; 123, 89-105.

- London, D., 1992. The application of experimental petrology to the genesis and crystallisation of granitic pegmatites: The Canadian Mineralogist; 30, 499-540.

- Lowell, J. D. and Guilbert, J. M., 1970. Lateral and vertical alteration-mineralisation zoning in porphyry ore deposits: Economic Geology; 65, 373-408.

- Lowenstern, J. B., 1995. Applications of silicate-melt inclusions to the study of magmatic volatiles, *in* Thompson, J. F. H., ed., Magmas, fluids and ore deposits, 23, Mineralogical Society of Canada Short Course, 71-99.

- Lowenstern, J. B. and Sinclair, W. D., 1996. Exsolved magmatic fluid and its role in the formation of comb-layered quartz at the Cretaceous Logtung W-Mo deposit, Yukon Territory, Canada: Transactions of the Royal Society of Edinburgh: Earth Sciences; 87, 291-303.

- March, B. D., 1981. On the crystallinity, probability of occurrence, and rheology of lava and magma: Contributions to Mineralogy and Petrology; 78, 85-98.

- Maughan, D. T., Keith, J. D., Christiansen, E. H., Pulsipher, T., Hattori, K. and Evans, N. J., 2002. Contributions from mafic alkaline magmas to the Bingham porphyry Cu-Au-Mo deposit, Utah, USA: Mineralium Deposita; 37, 14-37.

- McInnes, P., Miles, I., Radclyffe, D. and Brooker, M., 1998. Endeavour 42 (E42) gold deposit, Lake Cowal, *in* Berkman, D. A., and Mackenzie, D. H., eds., Geology of Australian and Papua New Guinean minerals deposits: Melbourne, Australiasian Institute of Mining and Metallurgy, 581-586.

- McKay, G. A., 1989. Partitioning of rare earth elements between major silicate minerals and basaltic melts, *in* Lipin, B. R., and McKay, G. A., eds., Geochemistry and mineralogy of rare earth elements, 21. Reviews in Mineralogy: Washington, D.C., The Mineralogical Society of America, 348.

- Meyer, C. and Hemley, J. J., 1967. Wall rock alteration, *in* Barnes, H. L., ed., Geochemistry of hydrothermal ore deposits: New York, Holt, Rinehart and Winston, 166-235.

- Moore, W. J., 1978. Chemical characteristics of hydrothermal alteration at Bingham, Utah: Economic Geology; 73, 1260-1269.

- Müller, D., Heithersay, P. S. and Groves, D. I., 1994a. Geochemical discrimination between shoshonitic and potassic volcanic rocks in different tectonic settings: a pilot study: Mineralogy and Petrology; 46, 259-289.

- Müller, D., Heithersay, P. S. and Groves, D. I., 1994b. The shoshonite porphyry Cu-Au association in the Goonumbla district, N.S.W., Australia: Mineralogy and Petrology; 51, 299-321.

- Munoz, J. L., 1984. F-OH and Cl-OH exchange in micas with applications to hydrothermal ore deposits, *in* Bailey, S. W., ed., Micas, 13. Reviews in Mineralogy: Chelsea, Michigan, Mineralogical Society of America, 469-494.

- Munoz, J. L., 1992. Calculation of HF and HCl fugacities from biotite compositions; revised equations: *in* Anonymous, ed., Geological Society of America Annual Meeting, Cincinnati, Ohio, 1992, A221.

- Munoz, J. L. and Ludington, S. D., 1974. Fluoride-hydroxyl exchange in biotite: American Journal of Science; 274, 396-413.

- North, 1999. Structural evolution and controls on Cu-Au mineralisation, Goonumbla Region, Confidential Company Report, 14 p.

- Ohmoto, H., 1986. Stable isotope geochemistry of ore deposits, *in* Valley, J. W., Taylor, H. P. J., and O'Neill, J. R., eds., Stable isotopes in high temperature geological processes, 16. Reviews in Mineralogy: Boulder, Colorado, Mineralogical Society of America, 491-559.
- Ohmoto, H. and Goldhaber, M. B., 1997. Sulfur and carbon isotopes, *in* Barnes, H. L., ed., Geochemistry of hydrothermal ore deposits: New York, John Wiley and Sons, 517-612.
- Ohmoto, H. and Lasaga, A. C., 1982. Kinetics of reactions between aqueous sulfates and sulfides in hydrothermal systems: Geochimica et Cosmochimica Acta; 46.
- Ohmoto, H. and Rye, R. O., 1979. Isotopes of sulfur and carbon, *in* Barnes, H. I., ed., Geochemistry of hydrothermal ore deposits: New York, Wiley, 509-567.
- Pasteris, J. D., 1996. Mount Pinatubo volcano and "negative" porphyry copper deposits: Geology; 24, 1075-1078.
- Peccerillo, A. and Taylor, S. R., 1976. Geochemistry of Eocene calcalkaline volcanic rocks from the Kastamonu area, northern Turkey: Contributions to Mineralogy and Petrology; 58, 63-81.
- Pemberton, J. W. and Offler, R., 1985. Significance of clinopyroxene compositions from the Cudgegong Volcanics and Toolamanang Volcanics: Cudgegong-Mudgee district, NSW Australia: Mineralogical Magazine; 49, 591-599.
- Peng, G., Luhr, J. F. and McGee, J. J., 1997. Factors controlling sulphur concentration in volcanic apatite: American Mineralogist; 82, 1210-1224.
- Percival, I. G., 1998. Fossils from the Billabong Creek Limestone Member in the area west of Parkes and Peak Hill, NSW: Orange, Geological Survey of New South Wales, 5 p.
- Perkins, C., McDougall, I. and Claoué-Long, J., 1990. 40Ar/39Ar and U-Pb geochronology of the Goonumbla porphyry Cu-Au deposits, New South Wales, Australia: Economic Geology; 85, 1808-1824.
- Pollard, P. J. and Taylor, R. G., 2002. Paragenesis of the Grasberg Cu-Au deposit, Irian Jaya, Indonesia: results from logging section 13: Mineralium Deposita; 37, 117-136.
- Potter, R. W. I., Babcock, R. S. and Brown, D. L., 1977. A new method for determining the solubility of salts in aqueous solutions at elevated temperatures: Journal of Research, U.S. Geological Survey; 5, 389-395.
- Potter, R. W. I., Clynne, M. A. and Brown, D. L., 1978. Freezing point depression of aqueous sodium chloride solutions: Economic Geology; 73, 284-285.
- Radclyffe, D., 1995. Regional-scale propylitic alteration in the Goonumbla mineral field, Parkes, NSW: Unpub. BSc Honours thesis, University of Tasmania, 118 p.
- Ramdohr, P., 1969. The ore minerals and their intergrowths: Heidelberg, Permagon Press, 1205 p.
- Reed, M. J., Candela, P. A. and Piccoli, P. M., 2000. The distribution of rare earth elements between monzogranitic melt and the aqueous volatile phase in experimental investigations at 800°C and 200MPa: Contributions to Mineralogy and Petrology; 140, 251-262.
- Reynolds, T. J. and Beane, R. E., 1985. Evolution of hydrothermal fluid characteristics at the Santa Rita, New Mexico, porphyry copper deposit: Economic Geology; 80, 1328-1347.
- Richards, J. P., 1997. Controls on scale of Porgera-type porphyry/ epithermal gold deposits associated with mafic, alkalic magmatism: Transactions of the Institution of Mining and Metallurgy; 106, B1-B8.
- Richards, J. P., Ronacher, E. and Johnston, M., 1998. New mineralization styles at the Porgera gold deposit, Papua New Guinea: *in* Anonymous, ed., Geological Society of America Annual Meeting, 1998, 302.
- Richardson, S., 1976. Geology and mineralization of the Cargo area: International Geological Congress - ore deposits of the Lachlan fold belt, New South Wales, Sydney, 10-12.
- Roberts, M. P., Pin, C., Clemens, J. D. and Paquette, J. L., 2000. Petrogenesis of mafic to felsic plutonic rock associations: the calc-alkaline Quérigut Complex, French Pyrenees: Journal of Petrology; 41, 809-844.
- Robinson, B. W. and Kusakabe, M., 1975. Quantitative preparation of sulphur dioxide, for $^{34}S/^{32}S$ analyses, from sulphides by combustion with cuprous oxide: Analytical Chemistry; 47, 1179-1181.

- Rock, N. M. S., Groves, D. I. and Perring, C. S., 1989. Gold, lamprophyres, and porphyries: What does their association mean?, Economic Geology Monograph 6. The geology of gold deposits: the perspective in 1988: Boulder, Colorado, Society of Economic Geologists, 609-625.

- Roedder, E., 1984. Fluid inclusions: Chelsea, Michigan, Mineralogical Society of America, 644 p.

- Roedder, E., 1992. Fluid inclusion evidence for immiscibility in magmatic differentiation: Geochimica et Cosmochimica Acta; 56, 5-20.

- Roedder, E. and Bodnar, R. J., 1980. Geologic pressure determinations from fluid inclusion studies: Annual Review of Earth and Planetary Sciences; 8, 263-301.

- Rønsbo, J. G., 1989. Coupled substitutions involving REEs and Na and Si in apatites in alkaline rocks from the Ilimaussaq intrusion, south Greenland, and the petrological implications: American Mineralogist; 74, 896-901.

- Rouse, R. C. and Dunn, P. J., 1982. A contribution to the crystal chemistry of ellestadite and the silicate sulfate apatites: American Mineralogist; 67, 90-96.

- Rowland, M. G. and Wilkinson, J. J., 1999. Significance of intermediate stage veins at Quebrada Blanca, Chile: *in* Stanley, C. J. *et. al.*, ed., Mineral Deposits: Processes to processing, Rotterdam, 1999.

- Rutland, R. W. R., 1976. Orogenic evolution of Australia: Earth Science Reviews; 12, 161-196.

- Sack, R. O. and Carmichael, I. S. E., 1980. Ferric-ferrous equilibrium in silicate melts at 1 bar: EOS, Transactions, American Geophysical Union; 61, 1152.

- Sakai, H., 1968. Isotopic properties of sulfur compounds in hydrothermal processes: Geochemical Journal; 2, 2-9.

- Sander, M. V. and Einaudi, M. T., 1990. Epithermal deposition of gold during transition from propylitic to potassic alteration at Round Mountain, Nevada: Economic Geology; 85, 285-311.

- Sasaki, A., Ulriksen, C. E., Sato, K. and Ishihara, S., 1984. Sulfur isotope reconnaissance of porphyry copper and manto-type deposits in Chile and the Philippines: Bulletin of the Geological Survey of Japan; 35, 615-622.

- Scheibner, E., 1973. A plate tectonic model of the Palaeozoic tectonic history of New South Wales: Geological Society of Australia Journal; 20, 405-426.

- Scheibner, E., 1993. Structural framework of New South Wales: Geological survey of New South Wales, Quarterly Notes; 93, 1-36.

- Scheibner, E. and Basden, H., 1998. Geology of New South Wales - synthesis: Sydney, Geological Survey of New South Wales.

- Scott, K. M., 1978. Geochemical aspects of the alteration-mineralisation at Copper Hill, New South Wales, Australia: Economic Geology; 73, 966-976.

- Scott, R. J., 1999. Structural interpretation of transects in the Parkes area, NSW SPIRT 1999, 1999, 1-14.

- Selby, D. and Nesbitt, B. E., 2000. Chemical composition of biotite from the Casino porphyry Cu-Au-Mo mineralization, Yukon, Canada; evaluation of magmatic and hydrothermal fluid chemistry: Chemical Geology; 171, 77-93.

- Selby, D., Nesbitt, B. E. and Muehlenbachs, K., 2000. Hydrothermal alteration and fluid chemistry of the Endako porphyry molybdenum deposit, British Columbia: Economic Geology; 95, 183-201.

- Shannon, J. R., Walker, B. M., Carten, R. B. and Geraghty, E. P., 1982. Unidirectional solidification textures and their significance in determining relative ages of intrusions at the Henderson mine, Colorado: Geology; 10, 293-297.

- Shannon, S. S. J., Finch, R. J., Ikramuddin, M. and Mutschler, F. E., 1983. Possible sedimentary sources of sulfur and copper in alkaline-suite porphyry-copper systems: *in* Anonymous, ed., Geological Society of America, 96th Annual meeting, Indianapolis, 1983, 684.

- Sheets, R. W., 1996. Comparative geochemistry of porphyritic intrusions of the Babine Lake area, west-central B.C.: implication for porphyry Cu exploration: *in* Anonymous, ed., Geological Society of America, 28th Annual meeting, 1996, A-93.

- Sheets, R. W. and Nesbitt, B., 1994. Differences in biotite and apatite chemistry from barren and mineralized porphyritic intrusions of the Babine Lake area, west-central B.C., Geological Association of Canada; Mineralogical Association of Canada; Canadian Geophysical union, joint meeting, 1994, 102.
- Shepherd, T., Rankin, A. H. and Alderton, D. H. M., 1985. A practical guide to fluid inclusion studies: Glasgow, Blackie, 235 p.
- Sheppard, S. M. F. and Gustafson, L. B., 1976. Oxygen and hydrogen isotopes in the porphyry copper deposit at El Salvador, Chile: Economic Geology; 71, 1549-1559.
- Sherwin, L., 1996. Narromine 1:250 000 Geological sheet.: Geological Survey of New South Wales.
- Sherwin, L., 1999. Regional geological overview, *in* Lyons, P., and Wallace, D., eds., Geology and metallogenesis of the Parkes - Grenfell - Wyalong - Condobolin region, New South Wales, AGSO Record 1999/20: Forbes, Australian Geological Survey Organisation, 108 p.
- Shinohara, H., 1994. Exsolution of immiscible vapor and liquid phases from a crystallizing melt: implications for chlorine and metal transport: Geochimica et Cosmochimica Acta; 58, 5215-5221.
- Shinohara, H., Iiyama, J. T. and Matsuo, S., 1989. Partition of chlorine compounds between silicate melt and hydrothermal solutions: I. Partition of NaCl-KCl: Geochimica et Cosmochimica Acta; 53, 2617-2630.
- Shinohara, H. and Kazahaya, K., 1995. Degassing processes related to magma-chamber crystallization, *in* Thompson, J. F. H., ed., Magmas, fluids and ore deposits: Short course series (Mineralogical Association of Canada), 23: Victoria, B.C., Mineralogical Association of Canada, 47-70.
- Shinohara, H., Kazahaya, K. and Lowenstern, J. B., 1995. Volatile transport in a convecting magma column: implications for porphyry Mo mineralisation: Geology; 23, 1091-1094.
- Sillitoe, R. H., 1990. Gold-rich porphyry copper deposits of the Circum-Pacific region - an updated overview, Pacific Rim Congress 90, 1990, 119-126.
- Sillitoe, R. H., 1997. Characteristics and controls of the largest porphyry copper-gold and epithermal gold deposits in the circum-Pacific region: Australian Journal of Earth Science; 44, 373-388.
- Sillitoe, R. H., 2000. Gold-rich porphyry deposits: Descriptive and genetic models and their role in exploration and discovery: Society of Economic Geologists, Reviews; 13, 315-345.
- Sillitoe, R. H. and Gappe, I. M. J., 1984. Philippine porphyry copper deposits: geologic setting and characteristics, CCOP/TP14, RAS/81/120, UNDP Technical support for regional offshore prospecting in East Asia, 89 p.
- Simon, G., Kesler, S. E., Essene, E. J. and Chryssoulis, S. L., 2000. Gold in porphyry copper deposits: experimental determination of the distribution of gold in the Cu-Fe-S system at 400^{o} to 700^{o}C.: Economic Geology; 95, 259-270.
- Simpson, C., Cas, R. A. F. and Arundell, M. C., 2000. The Goonumbla Caldera, Parkes, NSW: fact or fiction?: *in* Skilbeck, C. G., and Hubble, T. C. T., eds., Understanding planet earth: Searching for a sustainable future. Abstracts for the 15th Australian Geological Convention, University of Technology, Sydney, Australia, 2000, 452.
- Simpson, C. J. and Cas, R. A. F., 1999. The stratigraphy, volcanology and palaoegeographic interpretation of the Goonumbla Volcanic Complex, Parkes region, NSW: Clayton, Monash University, 113 p.
- Simpson, C. J., Cas, R. A. F. and Arundell, M. C., 2002. Volcanology and paleaogeography of the Ordovician mafic volcanic succession hosting the Northparkes Cu-Au deposits, central NSW, Australia: Journal of Volcanology and Geothermal Research, in prep.
- Skinner, B. J., 1966. Thermal expansion, Section 6, Memoir - Geological Society of America: Boulder, Geological Society of America, 75-96.

- Smith, D. R., Noblett, J., Wobus, R. A., Unruh, D. M., Douglass, J., Beane, R., Davis, C., Goldman, S., Kay, G., Gustavson, B., Saltoun, B. and Stewart, J., 1999. Petrology and geochemistry of late-stage intrusions of the A-type, mid-Proterozoic Pikes Peak Batholith (central Colorado, USA); implications for petrogenetic models: Precambrian research; 98, 271-305.
- Sparks, R. S., Huppert, H. E. and Turner, J. S., 1984. The fluid dynamics of evolving magma chambers: Royal Society of London Philosophical Transactions; A310, 511-534.
- Squires, V. E., 1992. The mineralisation and alteration of the Endeavour 27 porphyry copper-gold deposit, Goonumbla, New South Wales: Unpub. BSc Honours thesis, University of Sydney, 123 p.
- Stormer, J. C. J., Pierson, M. L. and Tacker, R. C., 1993. Variation of F and Cl X-ray intensity due to anisotropic diffusion in apatite during electron microprobe analysis: American Mineralogist; 78, 641-648.
- Streck, M. J. and Dilles, J. H., 1998. Sulfur evolution of oxidised arc magmas as recorded in apatite from a porphyry copper batholith: Geology; 26, 523-526.
- Streckeisen, A. L., 1973. Plutonic rocks: classification and nomenclature recommended by the IUGS Subcommission on the systematics of igneous rocks: Geotimes; 18, 26-30.
- Stuart-Smith, P. G., Hill, R. I., Rickard, M. J. and Etheridge, M. A., 1992. The stratigraphy and deformation history of the Tumut region: implications for the development of the Lachlan Fold Belt: Tectonophysics; 214, 211-237.
- Sun, S.-s. and McDonough, W. F., 1989. Chemical and isotopic systematics of oceanic basalts; implications for mantle composition and processes, *in* Saunders, A. D., and Norry, M. J., eds., Magmatism in the ocean basins, Geological Society Special Publication 42: London, Geological Society of London, 313-345.
- Sun, S.-s. and Wyborn, D., 1994. Source character and magmatic processes in some Au, Cu and Sn provinces: a trace elements and isotope approach: *in* ??, ed., 12th Australian Geological Convention, Perth, 1994, 421.
- Suppel, D. W., Barnes, R. G. and Scheibner, E., 1998. The Palaeozoic in New South Wales; geology and mineral resources: AGSO Journal of Australian Geology and Geophysics; 17, 87-105.
- Suppel, D. W. and Scheibner, E., 1990. Lachlan Fold Belt in New South Wales - regional geology and mineral deposits, *in* Hughes, F. E., ed., Geology of the mineral deposits of Australia and Papua New Guinea.: Melbourne, Australasian Institute of Mining and Metallurgy, 1321-1327.
- Taylor, B. E., 1987. Stable isotope geochemistry of ore-forming fluids, *in* Kyser, T. K., ed., Short course in stable isotope geochemistry of low temperature fluids, 13: Saskaton, Mineralogical Association of Canada, 337-445.
- Taylor, H. P. J., 1974. The application of oxygen and hydrogen isotope studies to problems of hydrothermal alteration and ore deposition: Economic Geology; 69, 849-883.
- Taylor, R. P. and Fallick, A. E., 1997. The evolution of fluorine-rich felsic magmas: source, dichotomy, magmatic convergence and the origins of topaz granite: Terra Nova; 9, 105-108.
- Taylor, R. P., Strong, D. F. and Fryer, B. J., 1981. Volatile control of contrasting trace element contributions in peralkaline granitic and volcanic rocks: Contributions to Mineralogy and Petrology; 77, 267-271.
- Taylor, S. R. and McLennan, S. M., 1985. The continental crust: its composition and evolution: Oxford, Blackwell Scientific, 312 p.
- Titley, S. R., 1982. The style and progress of mineralization and alteration in porphyry copper systems, *in* Titley, S. R., ed., Advances in geology of the porphyry copper deposits, southwestern North America: Tucson: Tucson, Arizona, University of Arizona Press, 93-116.
- Titley, S. R., 1994. Evolutionary habits of hydrothermal and supergene alteration in intrusion-centred ore systems, southwestern North America, *in* Lentz, D. R., ed., Alteration and alteration processes associated with ore-forming systems, 11. Short Course Notes, Geological Association of Canada, 237-260.
- Vaughan, D. J. and Craig, J. R., 1997. Sulfide ore mineral stabilities, morphologies, an intergrowth textures, *in* Barnes, H. L., ed., Geochemistry of hydrothermal ore deposits: New York, John Wiley and Sons Inc., 367-434.

- Walshe, J. L., Heithersay, P. S. and Morrison, G. W., 1995. Toward an understanding of the metallogeny of the Tasman Fold Belt system: Economic Geology; 90, 1382-1401.

- Wareham, C. D., Rice, C. M., Boyce, A. J. and Rogers, G., 1998. S, C, Sr and Pb sources in the Pliocene Silver Creek porphyry Mo system, Rico, Colorado: Economic Geology; 93, 32-46.

- Webster, J. D., 1997. Exsolution of magmatic volatile phases from Cl-enriched mineralising granitic magmas and implication for ore metal transport: Geochimica et Cosmochimica Acta; 61, 1017-1029.

- Webster, J. D., Holloway, J. R. and Hervig, R. L., 1989. Partitioning of lithophile trace elements between H2O and H2O- CO2 fluids and topaz rhyolite melt: Economic Geology; 84, 116-134.

- Whitford, D. J., Sun, S.-s., Carr, G. R. and Heithersay, P. S., 1992. Strontium, neodymium and lead isotope geochemistry of Ordovician igneous rock from Goonumbla: a reconnaissance, CSIRO Centre for Isotope Studies Research Report, 1991-1992: Sydney, 81-84 p.

- Wilson, J. W. J., Kesler, S. E., Cloke, P. L. and Kelly, W. C., 1980. Fluid inclusion geochemistry of the Granisle and Bell porphyry copper deposits, British Columbia: Economic Geology; 75, 45-61.

- Wolfe, R. C., 1994. The geology, paragenesis and alteration geochemistry of the Endeavour 48 Cu-Au porphyry, Goonumbla N.S.W.: Unpub. BSc Honours thesis, University of Tasmania, 102 p.

- Wolfe, R. C., 2001. Dinkidi Cu-Au porphyry: Geology of the Didipio region and paragenesis of the Dinkidi Cu-Au porphyry deposit: Unpub. PhD thesis, University of Tasmania, 200 p.

- Wolfe, R. C., Cooke, D. R., Hooper, B. and Heithersay, P. S., 1996. A magmatic origin for late-stage sericite-alunite alteration at the Endeavour 48 Cu-Au porphyry deposit, Goonumbla, NSW, Geological Society of Australia Abstracts, Canberra, 1996, 480.

- Wolfe, R. C., Cooke, D. R. and Joyce, P., 1999. Geology, mineralisation and genesis of the alkaline Dinkidi Cu-Au porphyry, north Luzon, Philippines: *in* Weber, G., ed., Pacrim '99, conference proceedings, Bali, Indonesia, 1999, 509-516.

- Wyborn, D., 1992. The tectonic significance of Ordovician magmatism in the eastern Lachlan Fold Belt: Tectonophysics; 214, 177-192.

- Wyborn, D., 1994. Mantle magmatism and large gold-copper deposits, Ore deposit studies and exploration models, Unpub. Short Course Manual 5.1: Hobart, CODES SRC, University of Tasmania, 5.1-5.4.

- Wyborn, D., 1996. Porphyry copper-gold potential in New South Wales, Minfo, 50, 4-6 p.

Appendices

A1 Pit maps

A2 Borehole logs

B1 Fluid inclusion data – microthermometric results

B2 Fluid inclusion data – decrepitation results

C1 Sulphur isotope analyses

C2 Empirical correction for bornite

D1 Electron microprobe analyses – biotite

D2 Electron microprobe analyses – apatite

E1 Whole rock XRD and XRF analyses

E2 Whole rock ICP-MS REE analyses

E3 Radiogenic isotope data

E4 $^{40}Ar/^{39}Ar$ dating

Appendix A

Pit maps and Drillholes logs

APPENDIX A1 – Pit maps

Maps of the northern, eastern, western and southern walls of the E27 open pit are presented in Appendix A1.

APPENDIX A2 – Drillhole logs

A list of boreholes logged for this thesis, including the number of samples collected. An asterisk indicates which of these logs are included in this appendix, Appendix A2. All remaining logs are available on request.

Borehole	Final Depth	Logged	Metres	Samples
E22/D2	433.0	263.0 - 433.0	170.0	15
E22/D6 *	367.4	141.8 - 367.4	225.6	8
E22/D39	800.0	536.5 - 624.3	87.8	8
E22/D205	612.0	288.4 - 525.5	237.1	16
E22/D228	708.4	567.8 - 649.0	81.2	7
E22/D229 *	728.9	634.1 - 728.9	94.8	19
E26/D46 *	1806.6	1194.8 - 1806.6	611.8	25
E26/D91	295.0	64.3 - 295.0	230.7	8
E26/D132W2	1002.0	717.0 - 1002.0	285.0	17
E26/D184	229.6	0 - 229.6	229.6	10
E26/D189 *	398.5	126.5 - 398.5	272.0	12
E26/D264	333.4	122.6 - 333.4	210.8	10
E26/D272	278.5	141.7 - 278.5	136.8	10
E26/D274	231.0	114.5 - 195.3	80.8	7
E26/D282	456.0	167.7 - 456.0	288.3	28
E26/D284	372.1	0 - 372.1	372.1	40
E26/D286	265.4	0 - 265.4	265.4	31
E26/D287	258.2	85.0 - 258.2	173.2	14
E26/D295	398.8	252.0 - 398.8	146.8	6
E27/D1	348.6	44.5 - 348.6	304.1	6
E27/D2	450.0	320.0 - 450.0	130.0	4
E27/D4 *	596.0	204.4 - 596.0	391.6	12
E27/D5	398.6	109.4 - 398.6	289.2	5
E27/D7	222.7	0 - 222.7	222.7	22
E27/D11	206.5	70.2 - 206.5	136.3	8
E27/D28	750.0	515.0 - 750.0	235.0	8
E27/D48	310.0	69.7 - 310.0	240.3	5
E27/D248	431.9	125.0 - 431.9	306.9	12
E27/D359	404.1	146.7 - 404.1	257.4	7
E27/D368	300.3	137.1 - 300.3	163.2	7
E27/D369 *	336.5	140.0 - 264.3	124.3	17
E27/D386	300.6	149.5 - 300.6	151.1	11
E48/D2 *	600.0	101.9 - 360.0	258.1	12
E48/D7	423.0	75.4 - 423.0	347.6	12
E48/D11	702.0	200.0 - 590.0	390.0	11
E48/D13	382.3	22.5 - 80.0	57.5	1
E48/D13w1	837.7	621.0 - 820.0	199.0	7
E48/D13w2	1035.5	352.0 - 1035.5	683.5	16
E48/D15	662.5	150.0 - 662.5	512.5	10
E48/D15w1 *	1016.7	638.8 - 1016.7	377.9	21
OVERALL TOTAL			***7025.9***	***381***

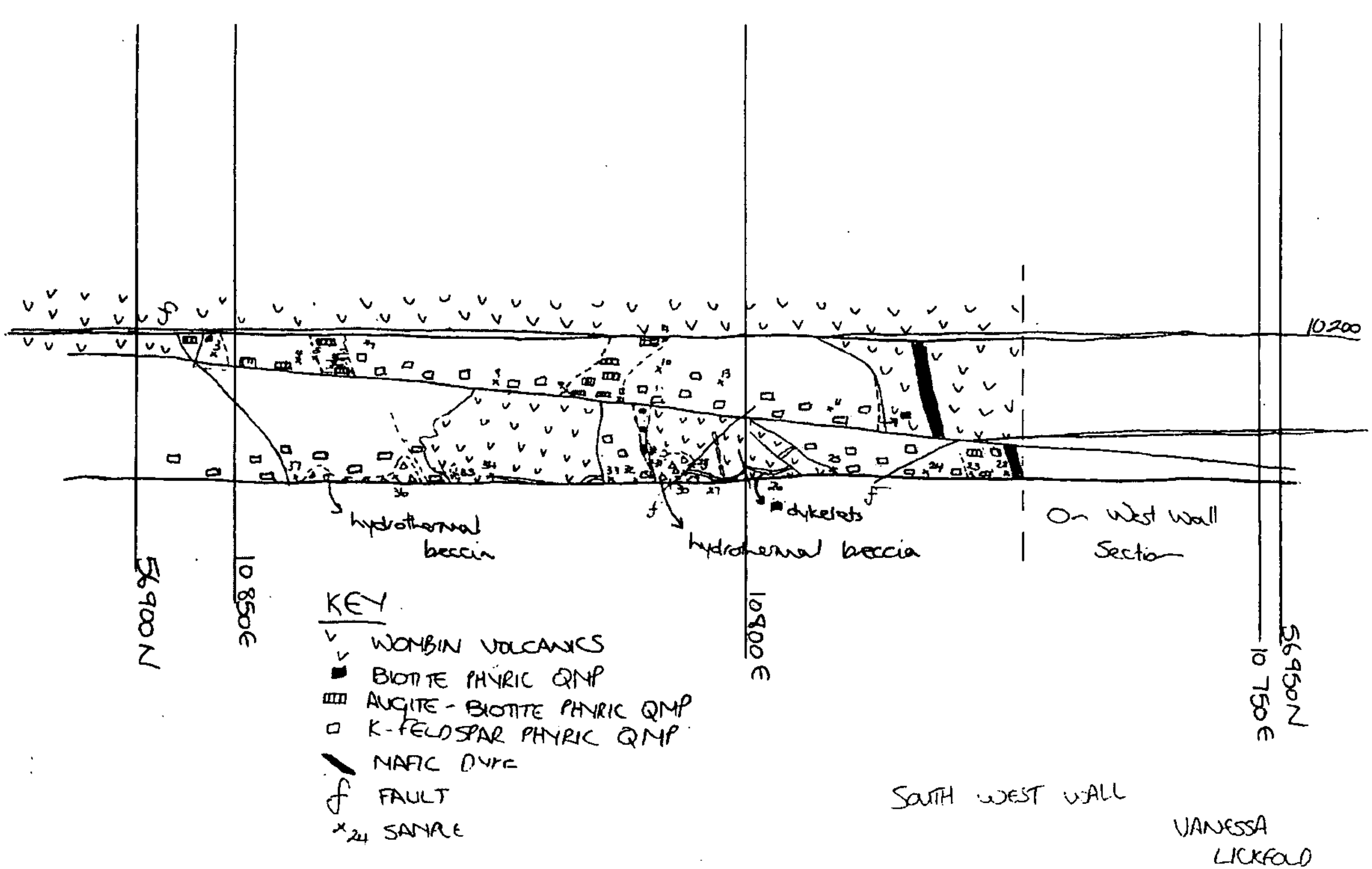
10200
hydrothermal breccia
dykelets
hydrothermal breccia
On West Wall Section
56900N
10 850E
10800E
10 750E
56950N
KEY
WOMBIN VOLCANICS
BIOTITE PHYRIC QMP
AUGITE - BIOTITE PHYRIC QMP
K-FELDSPAR PHYRIC QMP
MAFIC DYKE
FAULT
24 SAMPLE
SOUTH WEST WALL
VANESSA LICKFOLD

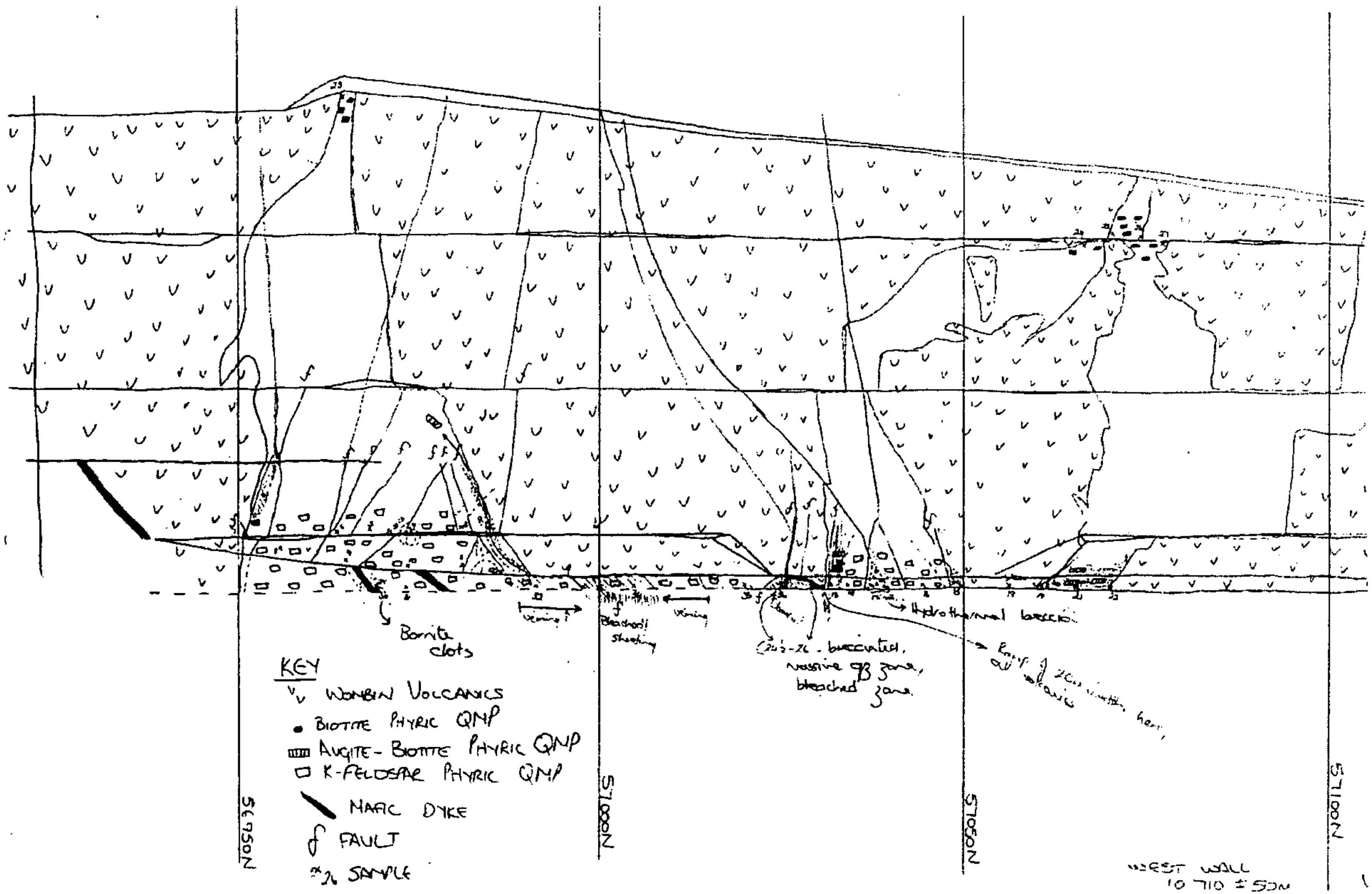

Bornite clots
Veining
Bleached/ Sheeting
Veining
Hydrothermal breccia
breccciated, massive qz zone, bleached zone.
KEY
WOMBIN VOLCANICS
BIOTITE PHYRIC QMP
AUGITE-BIOTITE PHYRIC QMP
K-FELDSPAR PHYRIC QMP
MAFIC DYKE
FAULT
SAMPLE
5695ON
5700ON
5705ON
5710ON
WEST WALL
10 710 ± 5OM

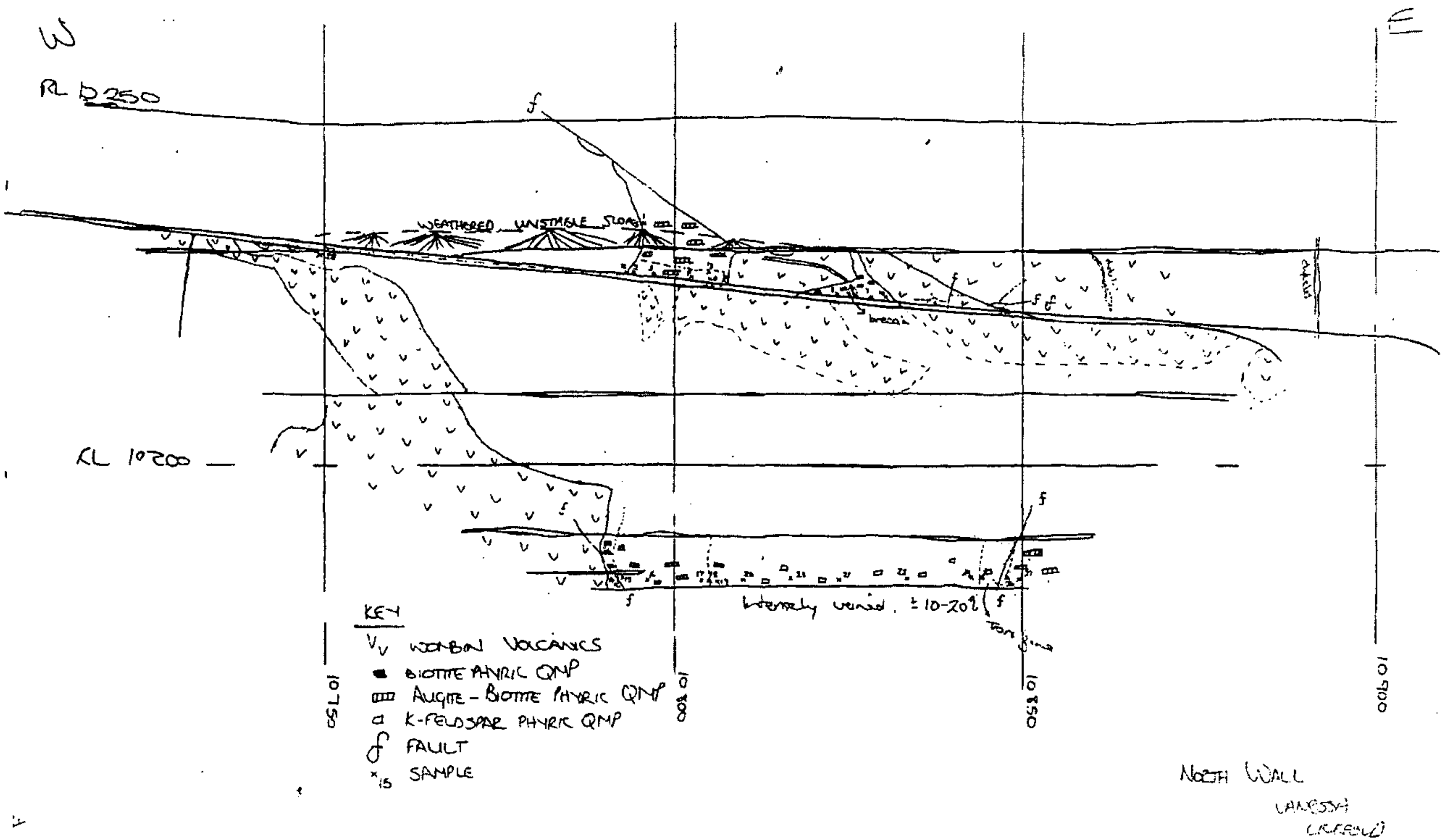
W
E
RL 10250
WEATHERED UNSTABLE SLOPE
breccia
RL 10200
Intensely veined, ±10-20%
KEY
Vv WONBON VOLCANICS
BIOTITE PHYRIC QMP
AUGITE - BIOTITE PHYRIC QMP
K-FELDSPAR PHYRIC QMP
f FAULT
x15 SAMPLE
10750
10800
10850
10900
NORTH WALL

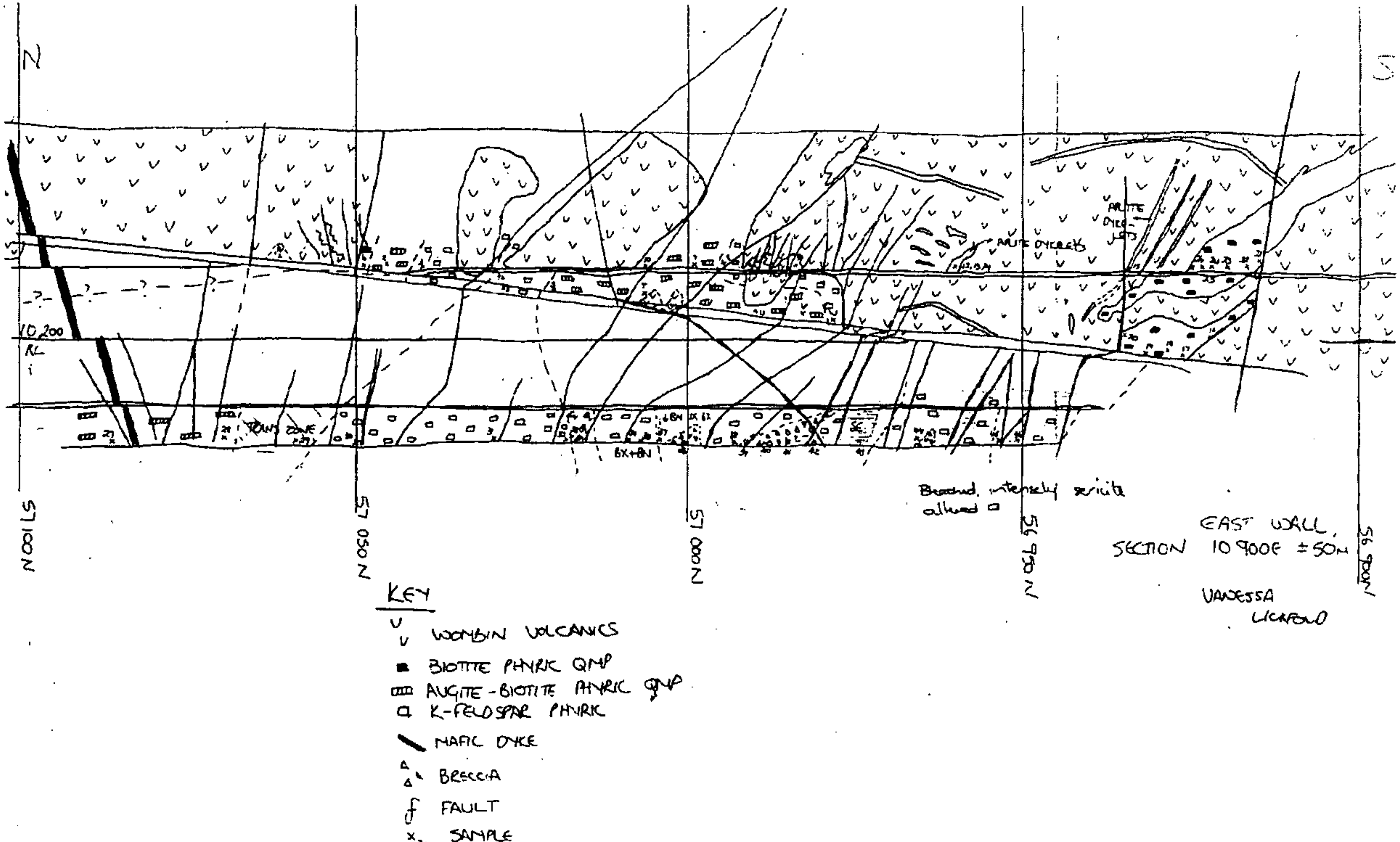
N
10,200
RL
APLITE DYKE JETS
APLITE DYKELETS
BX+BN
57 100 N
57 050 N
57 000 N
56 950 N
56 900 N
Brecciated, intensely sericite altered
EAST WALL,
SECTION 10 900E ± 50m
VANESSA LICKFOLD
KEY
WOMBIN VOLCANICS
BIOTITE PHYRIC QMP
AUGITE - BIOTITE PHYRIC QMP
K-FELDSPAR PHYRIC
MAFIC DYKE
BRECCIA
FAULT
SAMPLE

E22/229 (1 of 2)

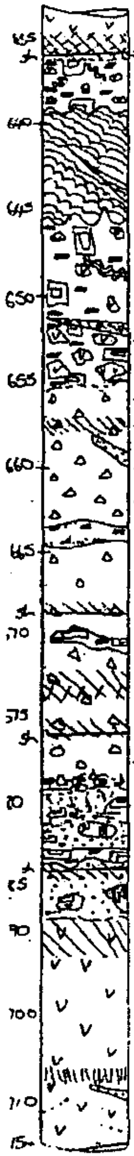

634.1 - 634.9m — Unaltered, black, fine grained volcanics

634.8 - 635.9m — discontinuous qz veins — Sericitised Vv with discontinuous qz veins (30-40%). Olive green. Shear 635.8 - 635.9. Possibly [illegible] aplite veins?

635.9 - 637.0m — Nasty [illegible]. Uncorroded (40-50%). Mafics 5-10%. Blebs 30-40% [illegible] 30%, Kfs 20-30%. Dissem [illegible]. Abundant altered Vv (avg 2-3cm, (5%) BR bands 636.9-637.0 & 637.5-637.7. Qz in [illegible]

MGMB

637.0 - 645.5m — Brain rock. Variable proportions of massive qz & aplitic porphyry from >99% qz to ±100% aplite / Orange, finely granular qz with qz eyes in places, v sparse (10-20% plane) >80% plag (altn Kfs [illegible] blebs not), Kfs 10-30% - small & single, v rare mags. Possible [illegible]? Addition [illegible]. Waning of veins only occas. MMP from 643.7 - 643.9. Contacts 'indistinct'

Direction to margin ↑

[illegible] crystal quality

15/4/00

645.5 - 655.0m — [illegible] with BR in core to 649.5m. Few waning qz veins of 2mm (<1%). Abundant Vv clasts - 652 to 652 (x̄ 2-3cm range 1-10). V little qz in qm - usually as discrete Xtals (<<1%). BR unit 647.3 - 648.7 - Massive qz 90% aplite ±10

652.3 - 652.0 — Sharp U&L contacts of Vv bx; sericite altered, aplite BR matrix

Distinct increase in Vv clasts below 652 - to 20-30% indistinct lower contact

656.0 - 663.4m — Intrusive bx with aplitic porphyry of BR as matrix - with varying amounts of qz dissolved. Matrix ±60%, Vv clasts ±40%. Qz dissolved 2-5% & blotchy, angular, discontinuous veins. Structures with chlorite [illegible]. Variably [illegible]. Ser zone 657 - 658 and aplite [illegible] 658.8 - 658.9. Main difference below 652-655 and below 655 is dramatic increase in qz in matrix & slight ↑ in clast

intrusive bx ≠ qz black, altered, crystalline volcanic fragments. Might be "pseudo bx" but in some of the matrix. 15/4/00

Magic [illegible] 663.4 - 664.7m 15/4/00 — Sharp U&L contacts. NO CLASTS, chlorite [illegible] - some [illegible] 657.9 - 658.7 [illegible] sparse (±20%) [illegible] Kfs. Zones of MMP

664.7 - 678.6m — Intrusive bx (as for 656 - 663.4) excluding qz + [illegible] Ser zones 669 - 669.7 - sh 668.6 - 668.7. Qz throughout varies in matrix as discontinuous veins, blotchy, [illegible] ±1-2%, up to 5% 373.4 - 373.6. MMP as [illegible] 670.8 - 670.7 and 671.5 - 671.7. Ser 672 - 673.7

Aplite, might be microdiorite?

Ser 675.4 - 676.2 sh 675.6 - 676.5

Brecciated lower contact

678.6 - 679.0m — 20cm MMP with abundant Vv then [illegible] with mixed MMP. Murky aplite as matrix → ORE ONE (17/4/00)

681.0 - 682.7m — Murky aplite intrusion ≠ clasts of MMP AND fine grained [illegible] upper contact - can't determine

682.7 - 683.3m — MMP, v sharp lower contact, sericite [illegible] 18/4/00

683.3 - 685.5m — Murky aplite porph, blotchy Kfs - v little Xtals. MMP clasts, [illegible] clasts. Shear 683.8 - 684.7: Below shear - appears same through [illegible] & blotchy - may be diff matrix (still mixed) [illegible] not as [illegible]

Probably ore

685.5 - 693.0m — Ser Vv, sheared upper contact

693.0 - 720.4m — Vv, generally unaltered, to 695.0 ≠ [illegible]? Qz veining < 1%. Sheared lower contact

Murky (carb; ser?) all 706.2 - 707.1

* Aplite (BR ≡ ?) 709.4 - 5cm, 710 (1cm) 713.3 (2cm)

* but can resolve lower contact ≠ aplite - aplite later ∴ breaks [illegible] MMP aplite comes in AFTER and aplite porph comes in after [illegible]

15/4/00

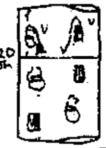

720.4 - 728.8m

E.O.H. 728.8m

Parts of the BGM is very red, others v like pale parent of RGB, the LOTS of fine Qz

E22/229 (2 of 2)

Fragments of fine grained 725m material 717.5 - 717.8 ≠ 719.9 - 720.2 (≠ Vv xenos)

Bi Plag Monz. Variably altered (bleached) Pale orange to 725 then gradually redden to brick red by 727 ≡ EC7/750. Bi ≤10% blotchy plag in equigranular Kfs + Qz matrix. Possible Kfs phenos <5%

Age Relationships

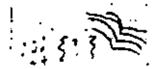

Uncertain, porph ≠ [illegible] may, not [illegible] of others

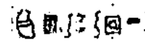

→ evidence of age in D39 [illegible] 592.2

Vv

Appendices

4 ... 5

E22/6 (1 of 2)

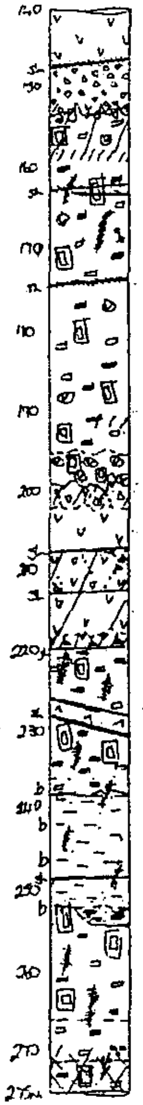

147.8 - 153.3m — Volcanics, continuous to 146.6 then shear to 147.6. Moderate Kfs alt^n throughout (patchy, diffuse 2-3mm). Above shear qz veining, straight, 2-3mm, <1%.
Below the shear - begin aplite intrusive bx zone, <10% which intensifies with depth. Mainly brxd 1-2cm, planar ... qz veining 150-152 BUT NOT olive green - may be alt^n ...
Min generally in aplite veins & lesser qz veins

153.3 - 195.5m — Wobbly, wispy contact over 5cm c aplite. Dark red orange MMF, Similar to E22/229 below ... Min^n generally confined to alt^n. Quite uniform to 195.5, rare ... veinlets (1-2cm, ...)

Ser zones 162.8 - 163.3, 163.7 - 164.0, 173.9 - 174.3

Overall: Veining: Qz, Qz + Kfs, ... + Kfs + ... & Sulp, straight ... - ±1% to 188 then ... 2-3% 158-159. Fracture <1%.
Bi selvedged more dominant than qz. Often Kfs or ... centred. Sum overall width ±1m from 0 ... - 169

V little veining after 169.

191.6 - 192 Veining (Qz) ... stopping

195.5 - 199.3m — Either alt^n boundary of diff porph. ... clasts angular, ≤5% 2-8cm. Porph may be ... Bx contact ... 5cm ...

199.3 - 219.0m — Variably altered, variably brxd Volcanics
199.3 - 202.6 Not too brxd (<5%). Qz veining & aplite. Black
202.6 - 207.7 Kfs ... - intense ... aplite & qz ...
... shear 207.4 - 207.7 (tectonic bx 208.1 - 208.2)
207.7 - 212.8 Kfs altered ... aplite, qz, bx ... 5% from
210 - shear (212.7 - 212.8)
212.8 - 217.5 Kfs alt^n c qz + aplite <2%
217.5 - 219.0 Qz ... 5% - OLIVE GREEN, altered, sheared contact

219.0 - 221.0m — Different porph - possibly QNP-C? Red colour, no veins, Kfs present, bleaching, more crowded (50-60%) Plag laths 60 blebs 30 Kfs 20-30 Qz v finely gran. No eyes

221.0 - 230.1m — BASIC DYKE - sheared lower contact

230.1 - 291.7m — Red porphyry gradually bleached to 288 - 294
230 - 236 ... selvedged veins (Qz + Kfs centres) ... Qz <1%
Bi + Qz overall 1-2%, rare qz veins, 2mm, straight c v thin Kfs centres
Not mineralised.
Bleached zone ... sparse aplite-like alt^n around ... Ser^n 249.4 - 251.3 ... ser/bi alt^n. ... contacts (238 - 258)

25 ... — Back to red porph, Kfs very pronounced. Mag ... NOTE ...

Poles from 264 - 271 ... evidence ... first qz (<<1%) ...

271.5 - 275.5 Very bi/ser ..., sheared, rare thin qz ... buddy centres. => ... 1-2% 269 - 279

E22/6 (2 of 2)

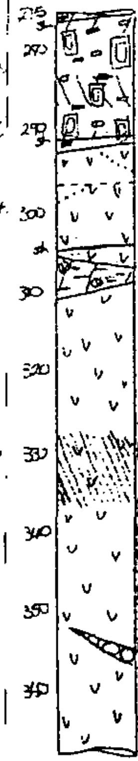

283 - 287 Sericitised
Rare qz veins to 290.7 - 291.2 ... contact. Shear 291.2

... Kfs + olive green alt^n c 296.5 ... Rare aplite 295.1 (10cm), 299.6
296.5 - 304 ORANGE altered volcanics. Overall, alt^n just ... intensity over 291 - 304. Shear 304 - 304.7
BROWN murky ...

Sharp U+L contacts ... <1%. Sparse ... veins - 2%. ... in veins ... possibly NMP?

Volcanics. Overall - variably altered, veined through v little bx ..., ...
307.5 - 326.0 Black ...

326 - 337 Pale olive green ..., shear 328 - 337

337 - 341 Orange alt^n (Kfs?)

341 - 345 Browny, greeny murky ...
345 - 349 Orange

349 - 354 Browny, murky ...

354.6 - 356.4 Possible pebble dyke c ... rounded clasts, aplite clasts, qz ..., ...
355 - 363 Grey

363 - 367 Orange

Age Relationships:

- Min seems to come c alt^n ... flooding of various qu'es
- Can't really comment on rest

E26/46 (1 of 5)

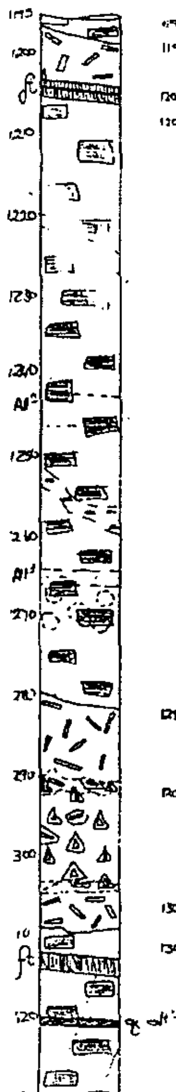

1194.8 - 1199.0m — Fine-grained BOM (FBOM) - described below. Sharp lower

1199.0 - 1203.9m — Trachyandesite, dark grey-brown, [illegible] (10-20%) probably lava. Plag laths [illegible]. Epi alt'd [illegible]. Not flow banded, random [illegible] of plag. [illegible] Sheared lower

1203.9 - 1206.2m — Fault zone c Py + Qz + [illegible] [illegible]. See 1204.4 - 1206.6

1206.2 - 1291.7m — Fine-grained BOM. Comparison photo 1211.0, 1226.9, 1249.4, 1268.2, 1265.9, 1279.7.
General description: Browny red to pale orangy pink (Bi alt or alt of gm), [illegible] rounded xenoliths. The finer variety is generally darker coloured (Kfs flood of gm) & the coarser (almost [illegible] gm) is paler. The finer varieties appear almost [illegible] in places. Kfs [illegible] a packed (>70%) porphyry with ±70% plag (laths [illegible] 2-3:1), mafics 10-15% dominantly Bi (+ Hbl?). Noticeable Kfs phenos (Small No [illegible]) 10-15%. Min? is variable, with the finer grained variety has [illegible] [illegible] alt [illegible] mafics. The paler [illegible] has [illegible] min? to [illegible] [illegible] of all Bi. Groundmass can be v.f.g. to microcrystalline (although not [illegible]). Cut by numerous 2-3, up to 10cm wide qz + ser [illegible] veins, 1 to 2/m (overall <1%). Cut [illegible] qz veins ([illegible] Kfs selvedges), straight-edged c [illegible] [illegible]. Alt? is variable, can be patchy Bi, which is [illegible] [illegible]. Alt? zones 1242.5 - 1244.5 with [illegible] of vein, sericite & possible Moly 1242.3. Another alt zone 1244 - 1246

1258.7 → Mafic porphyry, unknown contact, [illegible] from [illegible]

Spotty Bi alt? in restricted zone from 1265 - 1272.5

Sharp, intrusive lower contact

1291.7 - 1299.7m — Trachyandesite - chilled [illegible]. Epi alt? veins & spotty (patchy [illegible]). Vague Kfs [illegible] in places in [illegible] veins. Slight [illegible] alt?. No min? in veining. [illegible] to 1199 - 1203.9 unit. Possible transitional contact c [illegible] - [illegible]

1299.7 - 1304.2m — With transition zone to 1291.2 & again 1303.6 - 1304.2.
Zero porphyry: Not veined, no min? Colour is pinky brown with epi alt? of Bi phenos, ±40% Kfs (maybe higher), [illegible] [illegible], plag ±40 - [illegible]. Typically unzoned - 40-50%, [illegible], mafics Bi [illegible]. Kfs 40-50% Plag mainly laths ([illegible]). [illegible] [illegible] Trans zone - conspicuous Kfs phenos in TA, [illegible]?

1304.2 - 1308.9m — Trachyandesite - as above. Sharp lower contact. Not convinced that TA is "chill margin" of zero porphyry!

1309.9 - 1375.5m — Fine-grained BOM (as above). Major shear/fault 1312 - 1314.0
Exactly the same as unit above. Varies in colour - pale to brick red. Rare qz + ser + carb veins

1320.1 - 1321.2 Qz alt? zone - pervasive over whole [illegible]

Qz veining 2-3mm Kfs selvedged (possibly same c Bi [illegible]) [illegible], can be dilational - [illegible] 1340 to 1343 then decrease.

E26/46 (2 of 5)

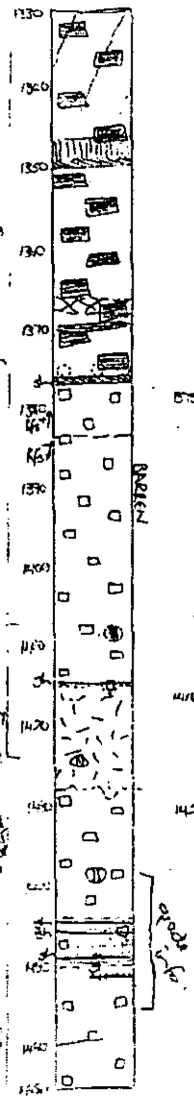

1346.8 - 1349.9 Alt? zone. Initially Bi overprint (to 1345.5) then qz + ser + bi + [illegible] fault zone

* Basically all MAFIC ONP 875.5 - 576.6 the 6B of PC in 11 [illegible]

1364.2 - 1366.5 & 1367 - 1367.3 Possible [illegible] bx/vein zone, dilational with cpy in [illegible] - [illegible] 30-40°
Alt? zone - 1368.2 - 1369
Bi alt? ↑ from 1371 so that unit becomes darker & also get Bi spots 1374.5 - 1375.6. Qz + ser + carb zones
Shear contact ↑ 1375 - 1376.5

1375.5 - [illegible] — Alt? zone upper contact with square porphyry. Brick red to brown orange, crowded (50%). The groundmass is granular and contains no quartz eyes. Mafic 5-10% Bi [illegible] (NMP of CC2 & CC7). Plag (60-70) [illegible] (laths 1 × 2:1) - Kfs, typically square to rectangular 5-7mm × 5×10mm, typically zoned, [illegible] [illegible] "black" centres. Qz alt? variable, can be [illegible] (to 1383). The unit gets paler with depth, but Kfs alt? [illegible] colour [illegible] from brick red, pale orange → red → brick red → pale. Veining, [illegible] irregular 1-3cm throughout (<1%). Min? - typically [illegible] as [illegible] Cpy ([illegible] in contact with Mafics.) Other qz veining - [illegible] 2-3mm straight edged, [illegible] insignificant

NOT ALL THE SAME UNIT * FROM 1375.5 - 1576.6 → Alternating [illegible] PC and mixed zones, especially with zones of BOM, MD or other

1416.6 - 1427.5m — Gradual indistinct contact - though noticeable Δ over 0.5m. - to PC porph (Ark Crowded). Gradual ↑ in phenos NB xenoliths (BOM ?) [illegible] clusters common. Higher [illegible], lower Kfs than above, mafics 0-5% Plag range in size from small to [illegible] [illegible] [illegible] 1:2. Min? is low, [illegible] (not in contact c Bi). Veining less than above. Colour [illegible], Pinky-grey. Alt? - insignificant, lower contact sharper than above [illegible] ±10cm

1427.5 - 1479.5m — Square porphyry - v similar to unit above. Bleached in places, qz veining similar to above (a) <1%, [illegible] Bi selvedged veins [illegible] Min? possibly slightly higher (Cpy - Bn) initially, then ↓ to ±0 [illegible] [illegible]

1443.5 - [illegible], 1445.3 - 1446.2 and [illegible] to 1449.7 [illegible] alt zones, each ending c qz - ser [illegible] vein [illegible]

Single Bi selvedged vein 1451 - 1451.3

Single qz [illegible] 1459.3 - 1459.3?
Occasional [illegible] xenolith of BOM.

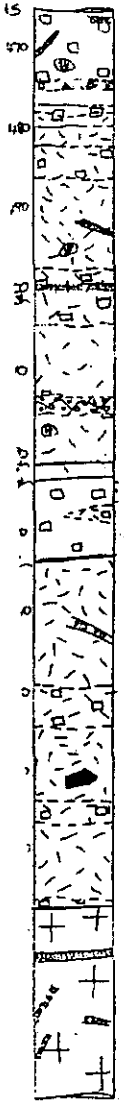

E26/4b (3 of 5)

Lots of eyes in core from 1465.
Small Bi alt^n zone 1467.7 - 1467.9 c aplite, bubbly, rim^n
Single bubble in vein c rim^n + aplite, crossing 1470.7

Small alt'd Bi zone 1473 - 1475
Broken core from 1477.2 - 1479.0
Transitional contact from 1478.0

1477.5 - 1497.2m: PC porph. Contact indistinct over ±5cm (clasts similar to E6.7 Spinifex bank)
Mixed □ / ∴ zone 1482 - 1486.2 - possible xenoliths of different phase c equi gm
PC unit as above.
Speckled Bi dyke with very sharp contacts 1493.7 - 1493.9

1497.2 - 1504.0m: Mixed zone of PC and □ porphs where boundary is difficult to distinguish but the different porphs are distinctive over 2-5cm. Shear/alt^n 1499 - 1500

1504.0 - 1519.9m: PC porph. Rare straight-edged, Bi selv'd veins 2-3mm

1513.5 - 1513.2 Sheared, bi'd, alt^n possibly c aplite matrix, bubbly
Hb + Qz veining - diffuse contacts
Quite a distinct lower contact

1519.9 - 1532.9m: Square porphyry (as described above).
Fault zone 1520.9 - 1521.2, 1522.9 - 1523.2
Rare sulphide Qz veins @ 1521.7 (flow veins?)
Possible mixed zone 1527.6 - 1527.8

Sheared contact at base

1532.9 - 1549.0m: PC porph.
Bi alt^n of gm (grey colour) 1538 - 1541
This example distinctly smaller phenos, plag up to 10% and Kfs + . Rare disseminated min^n
Little pebble dyke 1543.2 - 2cm

1549.0 - 1554.1m: Mixed zone.

1554.1 - 1563.7m: PC porph. Also finer (more crowded?) variety as for 1532.9 - 1549.0m unit.
Singular block, angular xenolith of unknown derivat^n 1562.1 - 1562.5

1563.7 - 1566.2m: Mixed zone, much broken core.

1566.2 - 1576.6m: PC porphyry

3-4cm □ porph just above shear
Sheared lower contact

1576.6 - 1644.9m: Monzodiorite - equigranular, light grey - greenish to pale pinkish - speckled. Quite coarse grained (3-5mm Xals)
Not porphyritic. Varies in alt^n. Scoriae from fine-grained BOM + BOM. Alt^n - variable Kfs flooding of pervasive (can be moderate to extreme) Bi alt^n of plag - alt^n causes colour variability.
Quite uniform, though grain size longer, can be as fine as normal BOM. Rare aplite dykes. Qz-Hb veins ±1 2-10cm (sheep). Bi selvages are common, up to 2cm
Massive ?? c Kfs flood of gm 1518.3 - 1518.9, 1617.1 - 1617.7
No min^n! No Qz. Overall comp: Bi 30 : 10 plag 60 Kfs (gm) 10
Bi-hedral

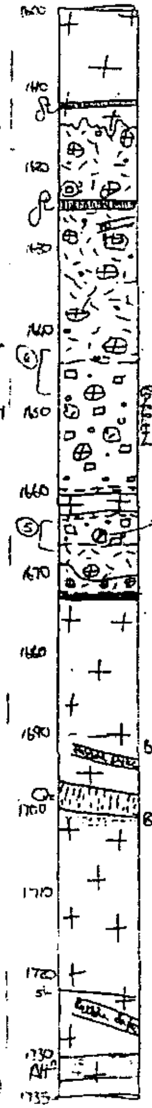

E26/4b (4 of 5)

Overall: Moderate to intense Bi alt^n

Keep distinctions □° & ∴, just both magic

distinct intrusive contact 1644.9 - 1643.7m: Sharp, wiggly, intrusive lower contact
PC porph. Abundant MD clasts/xenoliths, subrounded 3-8cm.

* This zone has Qz eyes in gm and ±1% dissem min^n - NOT in any of the PC units above
Fault 1624 - 1625 and pebble dyke 1646 - 2cm
Alt^n fluid pathway 1627.9 - 1628.4
Alt^n zone 1632 - 1633 — Possible core ... are before ...
Not really veined or alt^n. Phenocrysts smaller (finer) (as for 1st 3 PC units above) Plag 70-90 Kf 10-20 Mafics 5-10

Gradual lower contact over ±10cm

1643.7 - 1659.5m: Square porphyry. Distinct Qz eyes in gm, which is variably Kfs flooded. Min^n ±1%, disseminated, some with Qz, some c mafics - Gradual U + L contacts. Abundant MD xenoliths. Noticeable higher Kfs; lower plag. Veining as usual, with Qz

1659.5 - 1663.4m: Monzodiorite finger through 30cm upper and 80cm lower, zones of PC porph + sharp contacts c MD
Monzodiorite clasts: 1662.4 - 1666.4m: Square porphyry with MD xenos (c Qz ?)
1666.4 - 1670.1m: PC porphyry - quite grey towards base
1670.1 - 1673.4m: As above c higher frequency of MD xenoliths
Grey porph at base 1.5m, fairly indistinct contact with PC porph, thought to be late.

1673.4 - 1737.6m: Monzodiorite - pretty much all the same, though some grain size and colour variations.
Numerous pebble dykes that contain rounded (milled?) clasts in dark grey to black aph gm (phenocrysts ??). Clasts are MD AND PC porph - maybe others too.
Pervasive Bi alt^n 1690 - 1693. Pebble dyke 1693.4 - 1694.1

Massive Qz zone (FT ?) 1697.4 - 1700

The zone above 1700 is variably Kfs alt'd, the relatively below

Hb + Qz fault zone 1724.1 - 1726.3

Pebble dyke 1726.6 - 1726.9

Alt^n zone 1729.9 - 1732.5

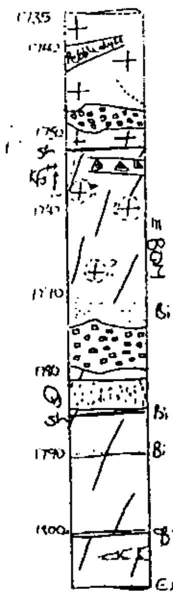

1747.6–1749.6m
1749.6–1751.8m
1751.8–1773.0m
1773.0–1779.2m
1779.2–1806.6m

Pebble dyke 1739.3 – 1740.0 – with veining AFTER dyke

Aplite dyke 1746.8 – 1747.1

Zero porphyry – possibly ≠ others, grey, fine, sharp U & L contacts

Monzodiorite. Very Ser/Bi alt'd, sheared lower contact
Monzosyenite – looks like Kfs flooded Monzodiorite (problem that it is significantly different enough to deserve separate status) Possible clasts of MD
Kfs flooded for upper 5m. Big bioggregates of plag's !!!

Dyke of zero porph c MS clasts 1753.4 – 1753.5

Bi alt= extreme in places 1770.5 – 1773.0

Zero (grey) porph. Sharp U & L, NO veining or ...

Monzosyenite Bi alt= 1784.8 – 1785.3, 1789.4 – 1790.3
Massive Qz 1780.5 – 1783.7m Shear (with Bi 1775)
Variably Kfs flooded (though dif to tell ∵ Kfs rich inherently)

1778.8 – 1779 Qz!

Kfs Flood 1802.2 – 1802.5

Age relationships:

Zero porphs

Trachyandesite

Pebble dykes ??? Variable clast types

Clasts of ... cm @ 4

Monzosyenite

Monzodiorite

E26/189 (1 of 2)

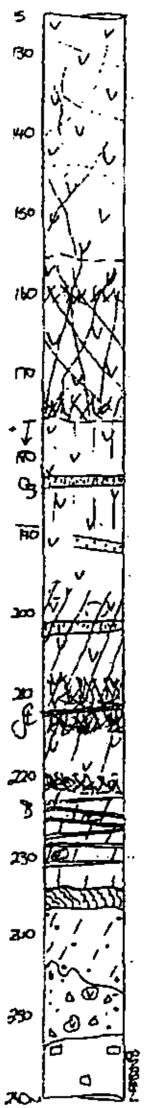

126.3 - 153.6m — Volcanics, brownish but, Kfs overprinting in veins + pervasive (bq suggests flow banding present?? - not sure?) Colour variation makes it dustified in places. Qz veins present <1%, thin c min; this veining is AFTER Kfs alt. Small zones of "bx", though think this is alt feature.
Kfs alt can be quite intense. Qz veins straight + continuous

Unclear/diffuse lower contact

153.6 - 176.6m — Volcanics, brecciated by alt ⇒ pseudo bx, not aplite or porphyry, mainly by Qz veins → stockwork bx maybe? Veins carry bn-cpy. Colour - pale cream to rusty red to black c spotty B. Qz veins 2-5%, generally 2-3mm, up to 10mm. 160-162m >5% and 173.7-176.6m >5%.
Min related to veins; + ∴ quite a lot of bb of veins

176.6 - 221.9m — Volcanics, alt'd, orangey - looks bx'd in places. Alt is varied (Kfs, Bi blotchy, etc)
Bi clotting AFTER Kfs alt. Bi continues to 189
Massive (>50%) Qz 182.7-183.3

Aplite / qz bx zone 190.7-190.9 + then intense Kfs to 196.

Bi blotches from 196, >5% Qz from 196.

± Massive Qz 200.9-201.6 ⇒ with min !!
NB Overall colour - PALE ORANGE, qz ↑ c depth + cause almost bx ⇒ STOCKWORK probably, up to 20%
Qz quite thick 10-20mm, with min, straight edges AFTER ALL ALTN. Fault 210.9-211.9

219.5 - 221.9 ±40% qz. Not sheeted. Indistinct lower contact

221.9 - 234.1m — Magenta porphyry (QMI) have angular Vv clasts. V few Kfs phenos. Straight-edged qz veins. Massive qz zones 222.3 - 222.5, 224.1 - 224.5, 224.7 - 224.8, 226.9 - 227.0, 228.4 - 229.7, 231.0 - 231.5. Overall qz >40%. Stockwork. Sparse, pale galena. Min along vein. Plag 10, Vfg qm <5% mafic <10% Kfs. Veins slightly curved, no Kfs

234.1 - 236.6m — Brown rock, overall >90% qz - aplite/porphyry <10%

236.6 - 246.9m — Sheeting QMP - Kfs, mega ▭ phenos, qz xtals, rare veining. Pale orange - cream. Towards base ↑ veins + clumps (Qz) Dafter min in qz clots. Kfs 20-30%. Breccia 244.6 - 245.3, 246 - 246.1 + from 247.5 (as fingers above)

246.9 - 252.1m — Intrusive bx zone with alt'd v and aplite porphyry (containing qz xtals as part of the matrix). Min in massive qz, along qz in veins (no real alt - except qz - from above)

252.1 - 296.7m — Square porphyry. Dark red to orange. Drastic ↓ in qz to cal (as crystals). Variably alt'd from pale to dark red. Vfg qm bn/cpy clots. Appears to become mafic (less alt'd??) with depth

E26/189 (2 of 2)

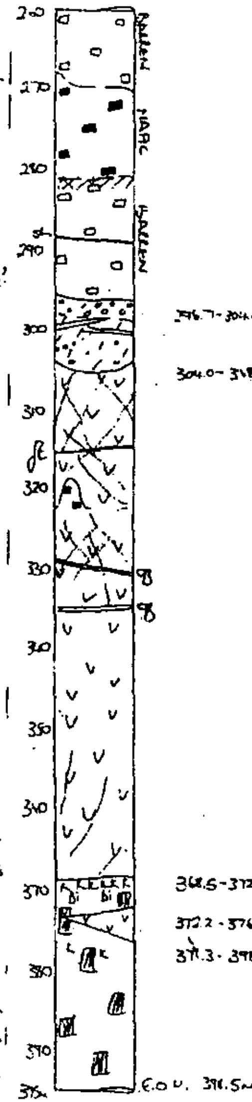

Very gradual (completely disguised) lower contact with more mafic variety - which is defined by 273 and runs to about 282. Veining and alt c = 282/148

Sheeted veins from 280.8 - 281.2
Turns around again to getting min clots, paler, less mafics, ↑ Qz blobs/clots to 2-5%

Shear @ 289

296.7 - 304.0m — Qz vein dominated "//" unit with dykelets of bubbly stuff (Xtals, matrix, min). Qz veins >5%, of "massive qz" (40-60%) to 299. Min Veins + disten, veins 6% 2-3mm

304.0 - 368.5m — Volcanics, qz veined 2-5%, straight edged, Kfs selvedges. Rare patchy Bi alt

Fault 314.8 - 315.0m
Veining ↓ to 1-2% after fault.
Kfs flooding can be quite intense in places
Finger of QMP 320 - 322 and 323

Massive qz 329.5 - 330.4, 334.1 - 335.2

Veining after massive qz <1%

Shear 352.6 - 352.7, 355.6 - 356.7

Veining ↑ again to ±1%

Brecciated lower contact with BQM + Kfs flooded!!! to

368.5 - 372.2m — Kfs to 369 then Bi overprint to 370.7. Possibly chilled BQM to 372.2.

372.2 - 376.3m — Volcanics - Kfs alt'd c bx in dykes of BQM

376.3 - 396.5m — BQM, Kfs flooded to 378
Veins <1% with minor min. Rare Kfs phenos
Rare VD's + aplites.

Timing relationships: "//" might be before ○ c / ● ■

E27/369 (1 of 1)

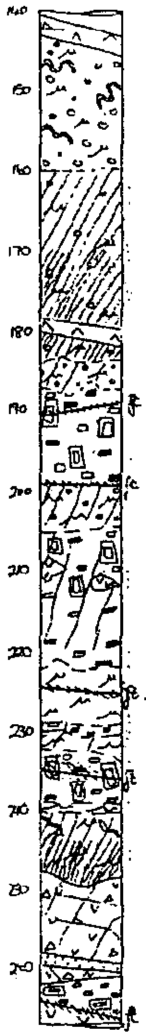

140.0 - 143.0m — QMP-μ described below
143.0 - 145.8m — Basic dyke
145.8 - 179.4m — QMP-μ/Pdark to pale greeny, salmon pink. UG (40-50%) Plag 60-70 (b-l ≈ 4:1). Kfs 20% Qz eyes 5-10% (might be 0). eyes rounded & mag blebs. Green qu. Variably alt'd & can be bleached in places. Min as dissem & veins. 154-157 - murky, smudged appearance - greyish str. veins & distinct inc in Qz ⇒ MN ≈ NT?
Overall veining to 5% ± 5% E irreg sides, wobbly & discont. Sheeted veins from 159.5 - 163.6 E veining 5-10%, up to 20% from 170-172.6 (after basic dyke)
Might be bubbly
E negative Qz

179.4 - 181.7m — Basic dyke
181.7 - 183.6m — QMP-μ/P E good grade (vein assoc) 182-184.
183.6 - 187.2m — QMP-μ/P BUT 1-5% qz eyes, veining 1-5% sheeted the [illegible] diffuse, boundaries irreg as well as str. Min dissem (20), lenses (80). Mafic <2% ... Kfs [illegible] & NIGHT BK NT?
187.2 - 222.1m — QMP-C (II) variably alt'd. Mafic ±2% 50% phenos. Plag ±70 (b-l 40:30) Kfs 30. Mega ±5%. <1% qz eyes. Total mineralisation 1-3% & veining ±2%, some str, some cut/dissem (in veining [illegible]). Kfs 189.4 - 190, 191.2-
199.0 - 205.0m — Zone of μ to P with lots of veining (15%) & dissem min

Trachyandesite ?x clasts @ 207-210 and [illegible] clast 204-201. veining + fines ± 208.

Indistinct lower contact
222.1 - 229.0m ?? — QMP-μ : main difference // this and above is green qu, slightly more coarse? Min rare, the dissem + clots
224.5 - 225.5
229.0 - 230.5m — MMP
230.5 - 232.5m — As for above MMP with veining ±2% CONTACTS??
232.5 - 241.5m — QMP-C 40-50% (typical QMP-C [illegible] a little less crowded) Min restricted to str veining. Variable alt'd, though often grey mottling. Zone of μ 239-240.
251.2 - 254m
241.5 - 245.4m shearing? — μ QMP, the first of eyes. Min ≤3% (veining in Q[illegible] veins & clots (Cordon NB). Mafic <2% b'l ≥ 1:1 [illegible] 70 Kfs ± 30%
↳ 242 alt'd vol
Veining initially ≤1%, but sheeted 10-5% from 242-244. wobbly edged veins as well as clots min "about" to veins
247.9 - 260.3m — Variably alt'd & veined volcanics with perhaps ... μ as breccia → actually INTRUSIVE BRECCIA. [illegible] of thicker porph 25, 252 + 254.6. Clasts >90%
259 - 259.9m — Aplite dyke CE Kfs flood
260.3 - 264.3m — QMP-C, sharp upper contact, [illegible] lower. Veining <1%, no mineralisation
264.3 - ..... — Volcanics

Age Relationships

°0 AFTER QMP-C ?? (based on veining ??)

E27/4 (1 of 3)

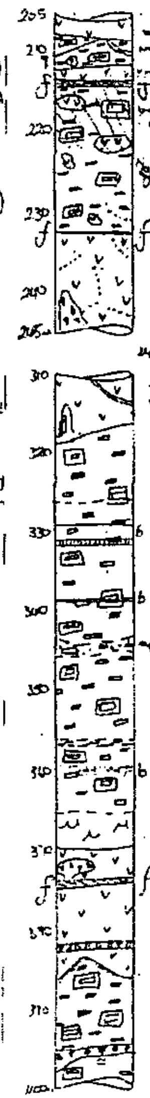

204.6 - 208.2m — Fine grained basalt volcanics, E rare Kfs vein alt. Sharp planar contact with mafic [illegible]
201.2 - 211.9m — Mafic vein with sharp planar basal contact. Single ½ vein [illegible] @ 210.3. [illegible]
209.9 - 213.2m / 211.3 - 214.2m — [illegible] cross-cut by qz vein (2cm) @ 213.3m. Timing of fault zone
214.2 - 232.6 — Faulted upper AND lower boundaries. Ser + carb alt to 222.5.
Abundant vv xenoliths - larger (5-70 vs 1-2 cm) and angular vs rounded
Minor aplite dyke - eg 231m
232.6 - 245.9m — Fine-grained black volcanics with VD/aplite dykelets (0.5-2cm) @ regular intervals of 1 06-1m, up to 20cm @ 237.6m
243.2 - 243.9m — intrusive breccia with mafic [illegible] as matrix

245 - 310m CORE NOT LOGGED

309.0 - 317.5m — Blk, fine grained volcanics with rare VD's (312.1m) & Kfs veinlets. Zone sharp contact edge of QMP @ 316.3m. Sharp contact with QMP below
315 - 343.6m — QMP & main difference between this QMP and that of 1.28 is the noticeable Kfs phenos. Bleached zones 329-331, 331.2-331.7, 331.0-331.5 → mixed zone of dyke fault?
326.0 - 331.0m — Herman's QMP contact, 317.5-324 called mafic [illegible]
Mixed [illegible]/fault? zone?

344.6 - 345.0m — Mixed zone where QMP is brecciated by aplite dykes
345.0 - 356.0m — QMP → Crowded, 50-60% phenos, Kfs (20%) - euhedral, plag - generally of subhedral laths 2mm 4 × 2 × 2H - about 1/2 and 70-80%. Qz - granular intergrowth of Kfs + Qz. Low dissem [illegible] at sites of <2%
356.0 - 356.6m — Possibly coarse-grained, with single wobbly qz vein?
356.6 - 358.0m — QMP with bleached zone @ 359.6 - 350.6
Variably sericitised mass QMP, qz veins. Uncrowded [illegible] crystalline qu. with 1-2% qz eyes. Large Kfs euhedra
358.0 - 359.7m — 10-20%, Hubby plag 30-40%, [illegible] 60% - the Kfs [illegible] (& blebs NOT!). Veining restricted to this unit
359.7 - 381.5m — Volcanics with intrusive bx @ 372.0 - 375.6m - MMP matrix. Sericitic fault zone @ 373.5 - 374.5m

Vein dykes brecciating ?x @ 381.4 - 382.4m
Sharp contact with MMP, E 5cm [illegible] at 386.9m

386.9 - 394.6m — Mafic xenolith - exactly the same as 210m. Homogeneous with [illegible] - angular, large and small/rounded @ 390-390.2 and 393 - 393.1
394.6 - 395.5m — Intrusive breccia
395.5 - 400.5m — QMP or equivalent intrusion to 350m, [illegible]

E27/4 (2 of 3)

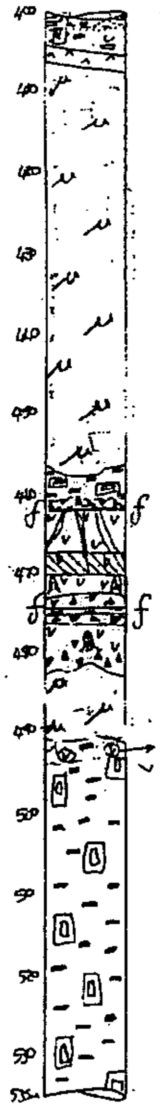

400.5 - 401.5m	Minor qtz/aplite zone, similar to 384.5m
401.5 - 401.8m	aplite
401.8 - 405.0m	Granite ... with rare qtz veins
405.0 - 407.4m	Basic dyke
407.4 - 457.0m	Qtz ... - as 367m; Qz veins only appear to be in this intrusion type. Description @ 367m
	Veining restricted to this unit & qz veins (often assoc. Kfs & sulphide). Occur for 5-10mm & ... of ... as before - apparent NMP ... block as "cut zone", both upper and lower
	lower contact indistinct ... last occurrence of ...
457.0 - 460.4m	NMP with brecciated lower contact to 461.3
460.4 - 461.3m	Brecciated contact
461.3 - 470.4m	Volcanics with Kfs veining and f 461.9m Ep/Se ?? alt? from 467.5 → Kfs seems to be after Qz?
470.4 - 472.3m	Volcanics - No alt? or veining though. NMP fingers 5 & 10cm @ 471.8 & 473.3m respectively.
472.3 - 474.2m	Breccia ... 473.0 fault
474.1 - 480.0m	Volcanics with NMP finger (10cm) @ 479.2 & bx 480-482.2
480.0 - 482.2m	Intrusive breccia
482.2 - 497.0m	Sharp upper intrusive contact, gradual lower. This ... intrusion hosts qz veining. Qtz
	altd volc xenos (possibly indicating NMP older than ...)
497.0 - 545.6m	Gradual contact (obscured by alt??). Mafic ... porphyry - exactly the same as ... from 223m CONSPICUOUS → No qz veining. Mafic

E27/4 (3 of 3)

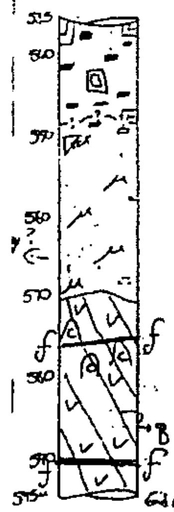

	Uncertain lower contact - possibly alt? obscured
548.8 - 570.8m	Qtz ... - more mafic variety of ..., also mineralised. Magnetic. Distinct (qz veining). Unaltered. Bubbly plag 30-40%, Kfs 10-20, mafics 25 ... plag 540. ... very fine & no qz ...
	Nonporphyritic xenolith 566.2 - 566.3
570.8 - 596.0m	Fine grained black volcanics - distinct qz veins (AFTER Kfs alt?). Qz veins ~5%, ≤ 5mm, but up to 30mm. 574.6 - 574.9 - qz vein acts as upper contact for ... finger. Other fingers @ 577.3 - 577.7, 579.3 - 579.9
	Faults @ 576m (0.5m) and 591 - 591.9m
	Min? ... after 583m
	... qz veining ... after Kfs ... veins (E Sulph and tend to be ...)

End of log. 596m

Hole continues to 629.3.

Age relationships

Very difficult to establish because no evidence of actual contacts.

Could infer

aplite - youngest

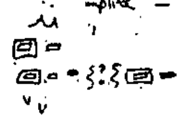

NB Veining in ... & non-veining in mafic @ 490-500 might be ∴ veining confined?

11/10/00.

E18/2 (1 of 2)

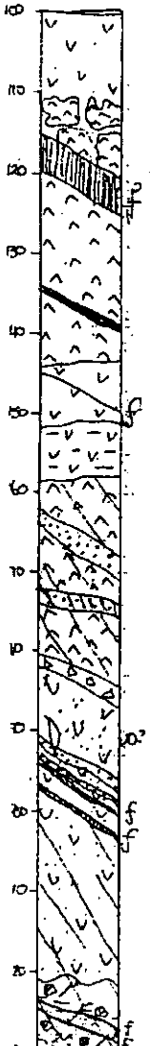

101.9 - 111.5		Volcaniclastics, brown, hm alt'd (patchy). Rare Qz veining (<1%). Weak bi/mag alt'n
111.5 - 116.6		Trachyandesite, autobrecciated
116.6 - 120.0		MAJOR FAULT zone
120 - 143.5		Trachyandesite lava
		Sample taken 137.6
143.5 - 150.9		Volcaniclastics, coarse. Fault 144.5 - 146.0. Veining ±1% c sulphides. No Kfs selvedges, mainly B
150.9 - 157.0		Volcanic siltstone, tan coloured, less veining but more sulph
157.0 - 191.0		Trachyandesite lava, Mod veining, Sulf c bn possibly also thin sulphide veinlets. Overall veining 2-3%
	165.2 - 167.2	Aplite porph, pinkish orange, v sparse KF phenos in ... ??
	172.5 - 175.0	Aplite porph, as above, contact ± ⊥, more veined than above (B sides), lower boundary diffuse over 2-3cm
191.0 - 196.5		FAULT BRECCIA
192.5 - 220.6		Volcanic sst, brown, vein dyke / alt? 190.1, veining <2% Qz+sulph
	192.8 - 194.2	Aplite porph (or KFs alt? ?) indistinct contacts, veined & dissem min, 3-5% KF phenos
	195.5 - 199.3	Aplite porph, distinct KF phenos but indistinct contacts
		Fault 196.3 - 196.9, 20°/L to CA 197.1 - 197.4
		Volcanics brown / black, distinct ↑ in veining & sulph in veins - up to 5% by 202 - 217 then 2% to contact
		Min? mainly in veins, centre + edges, patchy, assoc KF alt'n
220.6 - 224.5	*	ORE ONP, volcanic clasts, angular 2-5cm, 5-20%, pinkish clasts random. Sharp contact. KFs phenos ≤20, ust plag. Min in veins & dissem. Veining ±2%
224.5 - 229.5	*	SER ORE PORPH, probably related, same as above, the alt'd totally, rare dissem. Fault 225.5 - 226, 226.5 - 227

E18/2 (2 of 2) (40)

229.5 - 236.0	VERY SER ORE ONP almost grey/black. Major ff 230-231. Odd vole ~ still unrecognisable, rare plag leaching, qtz ... in alt'n
236.0 - 247.0	SER ORE ONP, vein selvedges & black, ser 10cm, voles, Min mainly dissem. Min clear. Veins 2-3% & have ... * cpy > bn
247.0 - 249.3	V SER ORE ONP, black/grey, bleached & v broken core
249.3 - 250.3	Volcanics - distinct veined volcanics, v ser alt'd
250.3 - 259.0	VERY SER ORE ONP, veining Mod to ±5%, bleached B
259.0 - 269.5	SER ORE ONP, v sim to 236-247, but fewer v veining 2% 2-3cm c sulphs. Min mainly dissem & in veinlets. Looks like it should be ONP-C, but isn't covered ... Fault alt? 263.2 - 264, 265.5 - 266.7, 267 - 267.6, 268.5 - ... Rare patches of ... 264.2 - 264.3
269.5 - 307.3	Brown ONP, no ... alt'n, distinct D in colour, ... Veining ±2%, c some sulphides, min? dissem & veins
	Veining ↑ after 288, & colour distinctly less alt'd
	Faults 297.4 - 298.3, 300 - 300.4, 303 - 303.2
	① Distinct dissem min & xenoliths towards base
	W defined ↑ in veining, the actual porph ???
307.3 - 327.4	ORE ONP, sheeted vein system, new ONP c fewer Kfs. Upper contact well defined by ↑ in veining, lower very uncertain - totally as ↓ in stockwork. Also patches of stockwork-like veining to 334.
	Stockwork veining up to 20%, mainly thin 2-3mm Sulph + Qz veins. Porph itself quite similar to above ① the less-douched (bottom). Fault Q... alt? features 318-320. NO VOLCANIC XENOS. Fault 323.7 - 324.1
327.4 - 334.0	MIXED 2 intrusions zone. Ser alt'd & sheeted => possible gradational contact
334.0 - 343.9	ORE ONP
	Fault 335.5 - 336, 336.5 - 337
343.9 - 345.8	Fault with ONP 344.2 - 344.5, rare Vv.
345.8 - 349.7	VERY SER ALT? ORE ONP, c voles, brown contact ?... Fault
349.7 - 350.6	Tectonic ff b>
350.1 - 352	Trachyandesite lava. Brown, ... with fault from 351, overall veining <2%

Thinking ① If this contains Vv & ... ... this ... is ... than ... P.T.O.

E48/15W1 (1 of 3)

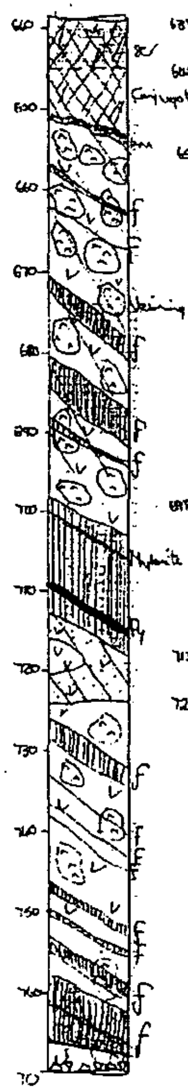

638.8 - 645.5 — ORE QNP, sericitised, gradational lower contact c less alt'd variety below, sericite alt^n destructive. Veining would be conjugate sets

645.5 - 653.6 — ORE QNP, pervasive low alt^n from 653, diss sulph 2-3%, veining 10-20% (twin in vein > diss), brecciated, uncrowded qtz, cpx to ufg, plag 40-50, Kfs 20-25%, ... intrusive lower contact c volcs

653.6 - 679.9 — Volcaniclastic, coarse with lava frags, overall veining ≈ 5%, mostly 10% qtz c sulph Kfs alteration
Light brownish-green to dark brown volcs, mostly lithic lava frags, becomes sed-rich towards base
Faults: 659.4 - 659.7, 662 - 662.5, 672.1 - 680.0, 682.1 - 686.0, 687.9 - 690

Breccias of veins, often containing sulphides

689.9 - 713.8 — MAJOR FAULT ZONE c intense ser alt^n, ±30 to CA. Mylonite zone 700; contains nearly 100% Py from 704-711
Significant truncation of c from bar

713.8 - 723.5 — Volcanic sdst, faulted upper & lower contacts, veining ≈ 5% with rafts of sdst (lava) frequent (that are less intensely veined @ 716). Brown to green, crystal rich.

723.5 - 771.4 — Volcaniclastics, coarse grained with lava fragments
Faults 727.1 - 728.8, shears (10cm) 735.8, 736.2, 737.1 (45°)
Overall veining 1-2%
Lots faults 747.1 - 747.6, 749.6 - 750.3
All faults & shears show significant
Massive shear 752.9 - 755.2, 755 - 760.4
7V - major fabric
Fault Zone 770.5 - 771.8, breccia & pervasive ser

E48/15W1 (2 of 3)

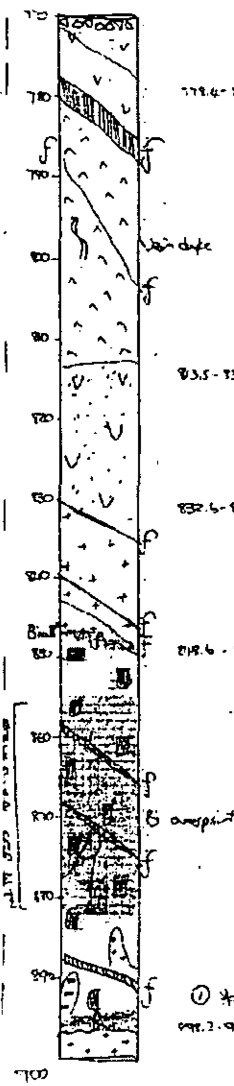

779.4 - 813.5 — Trachyandesite lava, faulted upper contact, veining 1-2%, Kfs alteration & Q sulph
Fault 790.5 - 792.4, v low ∠ to core, almost vertical
Intense ser alt^n 773.5 - 778.4
Vein dyke 797.8
NB Bi clots c magnetite alt^n
Carbonate veining related to faulting 799 - 812
Lower contact over 10cm

813.5 - 832.6 — Volcanic sdst, gradational contact. Olive green to pinkish brown, totally alt'd (ser overprint). Overall veining 2-5%, mostly Q minor sulph - Kfs alteration, 0.2-0.4 cm. Lower vein styles (NO DEPTHS.) Lower contact veined c ser alt^n

832.6 - 849.6 — Microgranite, contact 10-20 ∠ to CA, Kfs + Q equigranular (70-80%) where Q > Kfs & 20-30% plag phenos - ALBITE MANTLED, white rock, v rare Bi phenos
V subtle changes to 847.9 - 849.0 → 70cm of "black" alt^n (Q + bi ± sulph). Few patches of ser alt^n & faulting at 837.6 - 840.1. Total veining 2-5%, Usually 0.5-1cm. Fracture 842.7 - 842.9
Very distinct wiggly contact

849.6 - 890.2 — BQM, 1st occurrence of pink feldspars, BUT texturally quite similar to ser overprint.
Ser alt^n completely destroys texture 849 - 853, also F in plag phenos & Kfs in qm is more glomerated rather than large granular (as for microgranite)
Structural overprint on & off from 854 - 883.2, with faults (lots of Py) 859.7 - 860.9, 868.6 - 869.7
Major question is where microgranite is different from BQM
872.3 → onwards, BQM higher prop of phenos

871.0 - 873.0 — Microgranite, fine, sharp contacts
Fault 885.5 - 888.7
Microgranite patch 885 - 889
Not as alt'd between 887 - 891, then moderate to strong ser alt^n again, as well as bi alt^n?

① 890.2 - 890.6 — NAGL QNP with veining across contact - mixing of mafic & ser units 893 on of 894.7

898.2 - 906.5 — Microgranite ... intrusive (c possible dyke into BQM @ 895.1 → younger) Kfs + Q matrix ±70%, mainly plag, irregular graphic intergrowth. lower contact veining

E48/1521 (3 of 3)

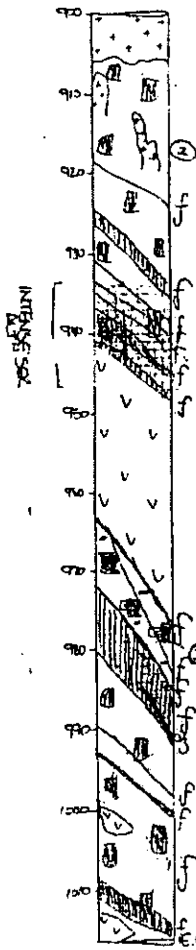

906.5 - 942.5 BQM, with small, tw distinct dykes of microgranite (this time, the with pink fs, NOT white) & intrusive contact at 912.1 (? hairline), 911.1 - 913.4 ; 918.5 - 918.9

Fault 920.3 - 920.4

Paler "BQM", more sericite altd to fault zone 926 - 927.6

Very sericitised fault zones 934 - 934.5, 935 - 936.1, 937 - 937.5 939 - 939.6 941 - 942

Faulted lower contact with volcanics

942.5 - 966.3 Volcaniclastic, coarse with large frags. Rarely <1% quartz, qz, n KFS selvedging + v fine sulphides

Prominent ff 966.3 20° of CA

that its mafic, bordering c BQM

966.3 - 972.3 MAFIC/BASALTIC or?, little Q, corroded, unusual (<1%), very few KFS phenos but fs 50-60%, fg. possibly Q, phenos or cry. Upper & lower contacts - faults, lower v sericite altd

972.3 - 982.5 MAJOR FAULT ZONE, v str altd

982.5 - 1016.7 BQM with sericitised faults @ 990, 991 - 991.4, 992

The BQM ranges in colour from buff to light orange to pink. Towards base ser. alt weaker towards base - where has alt weaker under with depth. + can begin being mafic towards the end of the hole.

Volcanic xenoliths 999 - 1001.9

1009.2 - 1010.6 fault with 1009.3 - 1009.9 v v

E.O.H. 1016.7

TIMING RELATIONSHIPS ① Evidence that Mafic older than volcanics

② Possibly microgranite is later than BQM

③ Because very little veining & fault bounded, may be barren (younger than BQM)

Appendix B

Fluid Inclusion Results

APPENDIX B1 – Microthermometric results

$T_{eut.}$= eutectic temperature

$T_{m\ ice}$= melting temperature of ice

T_hV = temperature of bubble disappearance

T_mH = temperature of halite dissolution

T_mS = temperature of sylvite dissolution

T_mO = temperature of unspecified daughter dissolution

Homog = homogenisation behaviour

T_hF = final temperature of homogenisation

APPENDIX B2 – Decrepitation results

Sample	Borehole ID	Inc No.	Type	P/S/PS	T eut.	Tm ice	ThV	TmH	TmS	TmO	Homog	ThF	NaCl± KCl wt%	wt% KCl	Na/Na+K
Early stage															
E48/26	E48/2/189.9	44	3cH	p			136.8	601		408.5	H	601	62.2		
E48/26	E48/2/189.9	51	3bD	p			106.1	479.8	273.3	343.8	D		71.3	27.8	0.67
E48/26	E48/2/189.9	52	3cH	p			416.3	482.7		359.9	H	482.7	54.4		
E48/26	E48/2/189.9	56	3cH	p			386.3	501.3		~330.0	H	501.3	56.5		
E27/87	E27/248/384.9	112	2aV	ps			540.6				V	540.6			
E27/87	E27/248/384.9	113	2aV	ps			489.4				V	489.4			
E27/87	E27/248/384.9	117	3cO	p			599.1	528.7		594.7	A	599.1	59.7		
E27/90	E27/48/224.1	161	3aH	p			-	566.5			H	566.5	63.1		
E48/27	E48/15w1/848.0	270	3aL	p			601	485.2			L	601	54.7		
E48/27	E48/15w1/848.0	271	3aL	p			601	491			L	601	55.3		
E22/25	E22/205/296.7	283	3bH	p			169.8	543.9	137.4		H	543.9	71.8	12.8	0.85
E22/25	E22/205/296.7	284	3aH	p			447.2	534.7			H		60.4		
E22/25	E22/205/296.7	285	3aH	p			474.4	550			H		62.2		
E22/25	E22/205/296.7	286	3aN	p			601	538.7			N	601	60.9		
E22/25	E22/205/296.7	287	3aN	p			601	564.9			N	601	64.1		
E22/25	E22/205/296.7	288	3aN	p			601	581			N	601	66.2		
E22/25	E22/205/296.7	289	3aN	p			601	512.5			N	601	57.7		
E22/25	E22/205/296.7	290	3aH	p			228.4	533.9			H	533.9	60.3		
E22/25	E22/205/296.7	291	3cH	p			601	570.4		367.5	H	601	64.8		
E22/25	E22/205/296.7	292	3aN	p			601	599.9			N	601	68.7		
E22/25	E22/205/296.7	293	3aN	p			601	589.7			N	601	67.3		
E22/25	E22/205/296.7	294	3aN	p			601	530.1			N	601	59.8		
E22/25	E22/205/296.7	295	3aN	p			601	570.4			N	601	64.8		
E22/25	E22/205/296.7	296	3aN	p			601	591.3			N	601	67.5		
E26/72	E26/287/122.2	335	3cH	p			137.6	567.1			H	567.1	64.4		
E26/72	E26/287/122.2	336	3aH	p			143	500.1			H	500.1	56.3		
E26/72	E26/287/122.2	338	3aH	p			77.2	589.7			H	589.7	67.3		
E26/72	E26/287/122.2	339	3bH	p			160.1	545.7	187.1	523.5	H	545.7	73.7	16.1	0.82
E26/72	E26/287/122.2	340	3aH	p			284.4	536.5			H	536.5	60.6		
E26/72	E26/287/122.2	341	3bH	p			135.6	563.7	162.5		H	563.7	74.8	13.4	0.85
E26/72	E26/287/122.2	342	3aH	p			131.9	564.5			H	564.5	64.1		
E26/72	E26/287/122.2	343	3aH	p			269.9	566.1			H	566.1	64.3		
E26/72	E26/287/122.2	344	3aH	p			145.7	570.1		465.1?	H	570.1	64.8		
E26/72	E26/287/122.2	345	3aH	p			135.1	583.2			H	583.2	67.2		
E26/72	E26/287/122.2	352	3aH	p			143.5	593			H	593	67.8		
E26/72	E26/287/122.2	353	3aH	p			271.1	550.1			H	550.1	62.3		
E26/72	E26/287/122.2	355	3aH	p			195.1	591.6			H	591.6	67.6		
E26/72	E26/287/122.2	357	1aL	ps		~-20.0	408.7				L	408.7	22.66		
E26/72	E26/287/122.2	359	3bH	p	<-37.3		287	553.5			H	553.5	62.7		
E26/72	E26/287/122.2	360	1aL	ps			350				L	351			
E26/72	E26/287/122.2	362	1aL	ps		-19.7	376.1				L	376.1	22.447		
E26/72	E26/287/122.2	371	1aL	ps	-32	-22.8	431.7				L	431.7	24.569		
E26/72	E26/287/122.2	374	2aV	ps			333				V	333			
E48/24	E48/13w2/1029.(	420	4aH	p			601	462.1			H	601	52.2		
E48/24	E48/13w2/1029.(	422	3aH	p			170.1	458.4			H	458.4	51.8		
E48/24	E48/13w2/1029.(	430	3aH	p			346.6	521.7			H	521.7	58.8		
E48/24	E48/13w2/1029.(	440	3aH	p			326.7	370.8			H		43.4		
E48/24	E48/13w2/1029.(	444	3aH	p			93.4	420.3			H		48		
E48/24	E48/13w2/1029.(	446	1aL	ps		-2.8	313.9				L	313.9	4.634		
E27/86	E27/7/67.5	543	3aH	p				490.3			H		55.2		
E27/86	E27/7/67.5	544	3cH	p			105.3	554.2			H		62.8		
E27/86	E27/7/67.5	546	3aH	p			160.6	520.3			H		58.7		
E27/86	E27/7/67.5	547	1bL	ps			450.1				L				
E27/86	E27/7/67.5	554	3aH	p				496.8			H		56		
Transitional magmatic stage															
E26/53	E26/132w2/757.(	2	3aH	p				485.3			H	485.3	54.7		
E26/53	E26/132w2/757.(	3	3bH	p			81.1	451.1			H	451.1	51		
E22/19	E22/2/306.0	11	3bH	pp			93.3	501.7	122.2		H	501.7	66.7	13.7	0.83
E22/19	E22/2/306.0	16	3bH	p			-	537.9	205.1		H	537.9	73.6	17.9	0.8
E22/19	E22/2/306.0	23	3aL	p			581.6	539.4				581.6	60.9		
E22/19	E22/2/306.0	24	3aH	p				501.1		411.1	H	501.1	56.4		
E22/19	E22/2/306.0	25	3bH	p			67.6	465.7	260		H	465.7	69.5	27.5	0.66
E22/19	E22/2/306.0	26	3aH	p			259.9	404.2			H	404.2	46.4		
E22/19	E22/2/306.0	27	3cN	p			233.7	460		>550.0		551	52		
E48/25	E48/15/453.1	71	3cH	pp			490.6	532.5	388.4		H	532.5	81.4	36	0.62
E26/78	E26/295/282.9	72	3aH	p			339.7	395.2			H	395.2	45.6		
E26/78	E26/295/282.9	73	3cH	p				419.6			H	419.6	47.9		
E26/78	E26/295/282.9	74	3aH	p			138	408.9			H	408.9	46.9		
E26/78	E26/295/282.9	78	3aH	p			189.6	467.1			H	467.1	52.7		
E26/78	E26/295/282.9	80	3aH	p			141.6	535.1			H	535.1	60.4		
E26/78	E26/295/282.9	81	3aH	p			418.9	441.7			H	441.7	50.1		
E26/78	E26/295/282.9	85	3aO	p			249.3	543.5		589.5	O	543.5	61.4		
E26/78	E26/295/282.9	87	3aH	p			119.4	299			H	299	37.8		
E26/78	E26/295/282.9	88	2aV	ps		-21.4					V	450	23.631		
E26/78	E26/295/282.9	89	1bL	ps			256.2				L	256.2			
E26/78	E26/295/282.9	90	3aH	p			394.6	595.3			H	595.3	68.1		
E26/78	E26/295/282.9	91	3aH	p			441	540.1			H	540.1	61		
E26/78	E26/295/282.9	92	3aH	p			330	582.6			H	582.6	66.4		
E27/88	E27/386/268.6	94	3aH	p				495.7			H	495.7	55.8		
E27/88	E27/386/268.6	95	3aH	p				529.4			H	529.4	59.7		
E27/88	E27/386/268.6	97	3aH	p			143.8	535.8			H	535.8	60.5		
E22/33	E22/6/248.2	103	3aH	pp			342.8	427.8			H	427.8	48.7		
E22/33	E22/6/248.2	104	3cH	p				578.2		358.9	H	578.2	65.8		
E22/33	E22/6/248.2	106	3aH	p			183.2	536			H	536	60.5		
E22/33	E22/6/248.2	107	3aH	p			-	544.4			H	544.4	61.6		
E22/33	E22/6/248.2	111	3aH	p			73.5	520.3			H	520.3	58.7		
E27/87	E27/248/384.9	125	2aV	p			519.7				V	519.7			
E27/87	E27/248/384.9	126	3aH	p			181.2	508.7			H	508.7	57.3		
E27/87	E27/248/384.9	135	2aV	p			545				V	545			
E26/74	E26/184/125.9	217	3aH	p			241.1	525.4			H	525.4	59.3		
E26/74	E26/184/125.9	218	3aH	p				509.8			H	509.8	57.4		
E26/74	E26/184/125.9	219	3aH	p				351.7		318.7	H	351.7	41.9		

Sample	Borehole ID	Inc No.	Type	P/S/PS	T eut.	Tm ice	ThV	TmH	TmS	TmO	Homog	ThF	NaCl± KCl wt%	wt% KCl	Na/Na+K
E26/74	E26/184/125.9	220	3aH	p				267			H	267	35.7		
E26/74	E26/184/125.9	221	3aL	p			581.6	545.6			L	545.6	61.7		
E26/74	E26/184/125.9	222	3aH	p				594.4			H	594.4	67.9		
E26/74	E26/184/125.9	223	1bL	p			542.1				L	542.1			
E26/74	E26/184/125.9	224	3aL	p			469.8	466.5			L	466.5	52.6		
E26/74	E26/184/125.9	225	3bH	p			453	499.6	307.9		H	499.6	74.6	29.9	0.66
E26/74	E26/184/125.9	226	3aH	p			395.6	534.7			H	534.7	60.4		
E26/74	E26/184/125.9	227	3bH	p			430.4	515.3	274.1		H	515.3	74.2	25.3	0.71
E26/74	E26/184/125.9	228	3aH	p			496	565			H	565	64.1		
E26/74	E26/184/125.9	229	3aH	p			488.2	527.1			H	527.1	59.5		
E48/27	E48/15w1/848.0	246	3aN	p			601	601			N	601	62		
E48/12	E48/15/651.1	416	2aD	ps			578.6				D				
E48/12	E48/15/651.1	417	3bN	p			601	471	229.3	546.2	N	601	68.3	24.2	0.7
E26/57	E26/189/235.8	450	2aV	ps			372.2				V	372.2			
E26/57	E26/189/235.8	451	3aH	p			68.7	582.5			H	582.5	66.3		
E26/57	E26/189/235.8	452	3bH	p			68.7	575.3	199.7		H	575.3	77.2	15.1	0.84
E26/57	E26/189/235.8	453	3aH	ps			174.7	510			H	510	57.5		
E26/57	E26/189/235.8	454	3aH	ps			68.7	492.2			H	492.2	55.4		
E26/57	E26/189/235.8	455	3aH	ps			68.7	368.7			H	368.7	43.3		
E26/57	E26/189/235.8	456	3bN	p			134.4	510.9	227.4		N		71.8	21.5	0.75
E26/57	E26/189/235.8	457	2aV	p			294.5				V	294.5			
E26/57	E26/189/235.8	458	3aH	p			96.8	481.9			H	481.9	54.3		
E26/57	E26/189/235.8	459	3aH	p			123.3	459.1			H	459.1	51.9		
E26/57	E26/189/235.8	462	3aH	p			244.6	508.7			H	508.7	57.3		
E26/57	E26/189/235.8	463	3bH	ps			68.7	470.6			H	470.6	53.1		
E26/57	E26/189/235.8	464	3aH	ps			165.9	365.9			H	365.9	43		
E26/57	E26/189/235.8	468	3aH	ps				492.2			H	492.2	55.4		
E26/57	E26/189/235.8	469	3aH	ps				519.5			H	519.5	58.6		
E26/71	E26/46/1253.7	503	3aH	p			95	486.9			H	486.9	54.9		
E26/71	E26/46/1253.7	504	3aH	p			140.7	436			H	436	49.5		
E26/71	E26/46/1253.7	508	3cH	p			176.4	473.1			H		53.3		
E26/71	E26/46/1253.7	509	3aH	p			80.2	472.2			H	472.2	53.3		
E26/71	E26/46/1253.7	510	3bH	p			176.2	543	146		H	543	72	13.4	0.85
E26/71	E26/46/1253.7	511	3aH	p			151.4	444.4			H	444.4	50.4		
E26/71	E26/46/1253.7	512	3cH	p			142.1	479.8			H		54.1		
E26/71	E26/46/1253.7	518	3aH	p				595			H	595	68		
E26/71	E26/46/1253.7	519	3aH	p			592			567.5	N		64.4		
VL S24	E26/91/136.7	520	3aH	ps			286.5	467.2			H	467.2	52.7		
VL S24	E26/91/136.7	521	3bH	ps			274.7	464			H	464	52.4		
VL S24	E26/91/136.7	523	3bH	p			264.8	549.3	179.1		H	549.3	73.8	15.3	0.83
VL S24	E26/91/136.7	525	3bH	p			361.4	497.1	192.2		H	497.1	69	19.4	0.77
VL S24	E26/91/136.7	527	3bH	ps			99.8	451.4	183.5	230	H	451.4	64.4	21.2	0.72
VL S24	E26/91/136.7	528	3bH	ps			335.9	465.5	144.8		H	465.5	63.9	17.1	0.78
VL S24	E26/91/136.7	530	2aN	p							N				
VL S24	E26/91/136.7	531	3bH	p			382.6	528.8	223.7		H	528.8	73.4	20	0.77
VL S24	E26/91/136.7	532	3aH	p			353.3	511.9			H	511.9	57.7		
VL S24	E26/91/136.7	533	3bH	p			265.1	498.7	241.5		H	498.7	71.3	23.5	0.72
VL S24	E26/91/136.7	534	3bH	p			160.3	508.8			H	508.8	57.3		
VL S24	E26/91/136.7	535	3cO	p			159.6	558.7	261.2	573	A	573	56.8	20.8	0.78
VL S24	E26/91/136.7	536	3aH	p			146.2	517.9			H	517.9	58.4		
VL S24	E26/91/136.7	537	3bH	p			219.4	494.7	229		H	494.7	70.4	22.7	0.73
VL S24	E26/91/136.7	538	3bH	p			152.1	516.4	275.6		H	516.4	74.4	25.4	0.71
VL S24	E26/91/136.7	541	3bH	p			129.1	492.8	199.7		H	492.8	69	20.3	0.75
E22/28	E22/205/454.1	556	3aH	p			366.6	591.5			H	591.5	67.6		
E22/28	E22/205/454.1	557	3bH	p				504.1	333.9		H	504.1	76.4	32.3	0.63
E22/28	E22/205/454.1	559	3cH	p			136.5	598.6		578.7	H	598.6	68.5		
E22/28	E22/205/454.1	560	3cH	p			147.3	561.2		560.3	H	561.2	63.8		
E22/28	E22/205/454.1	561	3bH	p			325.8	601			H	601	68.7		
E22/28	E22/205/454.1	562	3bH	p			265	583			H	583	66.4		
E22/28	E22/205/454.1	565	3aH	p				563.8			H	563.8	64		
Transitional hydrothermal stage															
E22/6	E22/229/639.5	608	3aH	p			525.5	540.1			H	540.1	61		
E22/6	E22/229/639.5	609	3aH	p			378.8	515.4			H	515.4	58.1		
E22/6	E22/229/639.5	611	3aH	p			312.3	518.8			H	518.8	58.5		
E22/6	E22/229/639.5	612	3aH	p			274.8	534.1			H	534.1	60.3		
E22/6	E22/229/639.5	615	3aH	p				540			H	540	61		
E22/6	E22/229/639.5	616	3aH	p			230.3	529.1			H	529.1	59.7		
E22/6	E22/229/639.5	617	3aH	p			163.7	494.9			H	464.9	52.5		
E22/6	E22/229/639.5	627	3aH	p			403.5	501.1			H	501.1	56.4		
E22/6	E22/229/639.5	630	3aH	p			129.6	410			H	410	47		
E22/6	E22/229/639.5	643	3aH	p				404.6			H	404.6	46.5		
E22/6	E22/229/639.5	645	3aH	p			98.9	380.1			H	380.1	44.3		
E22/6	E22/229/639.5	653	3aH	p			365.7	499.8			H	499.8	56.3		
E22/6	E22/229/639.5	654	3aH	p			88.2	405.7			H	405.7	46.6		
E22/6	E22/229/639.5	657	3aH	p			341.9	530.7			H	530.7	59.9		
E22/6	E22/229/639.5	659	3aH	p			91.7	501.1			H	501.1	56.4		
E22/6	E22/229/639.5	638	3aHN	p				567.4			H	601	64.4		
E22/6	E22/229/639.5	639	3aHN	p			529.1	532.2		>600.0	H	601	60.1		
E22/6	E22/229/639.5	640	3aHN	p				469		>600.0	H	601	52.9		
E22/6	E22/229/639.5	649	3aL	p			447.4	446.1			L	447.4	50.5		
E22/6	E22/229/639.5	628	3aV	p			513.7	413.3			V	513.7	47.3		
E22/6	E22/229/639.5	629	3aV	p			512.6	434.4			V	512.6	49.3		
E22/6	E22/229/639.5	631	3aV	p			554.4	411.7			V	554.4	47.1		
E22/6	E22/229/639.5	634	3aV	p			551.6	491.3			V	551.6	55.3		
E22/6	E22/229/639.5	635	3aV	p			562.4	489.6			V	562.4	55.2		
E22/6	E22/229/639.5	642	3aV	p			507.6	404.7			V	507.6	46.5		
E22/6	E22/229/639.5	610	3bH	p			357.6	506.1	106.1		H	506.1	66.5	12.3	0.85
E22/6	E22/229/639.5	613	3bH	p			286.2	527.9	140.3		H	527.9	70.2	13.8	0.84
E22/6	E22/229/639.5	614	3bH	p			461.9	505.5	166.7		H	505.5	68.8	16.9	0.8
E22/6	E22/229/639.5	619	3bH	p			377.6	499.9	184.7		H	499.9	69	18.6	0.78
E22/6	E22/229/639.5	620	3bH	p				429.3	153		H	429.5	60.9	19.5	0.73
E22/6	E22/229/639.5	623	3bH	p				496.1	162.6		H	496.1	67.7	17.1	0.79
E22/6	E22/229/639.5	624	3bH	p			116.9	204.9	142.8		H	204.9	45.4	25.6	0.5
E22/6	E22/229/639.5	625	3bH	p				405.7	170.5		H	405.7	59.8	22.2	0.68

Sample	Borehole ID	Inc No.	Type	P/S/PS	T eut.	Tm ice	ThV	TmH	TmS	TmO	Homog	ThF	NaCl± KCl wt%	wt% KCl	Na/Na+K
E22/6	E22/229/639.5	646	3bH	p			93.8	398.8	162.7		H	398.8	58.8	21.2	0.69
E22/6	E22/229/639.5	650	3bL	p			431.7	287.1	163.9		L	431.7	51	26	0.53
E22/6	E22/229/639.5	652	3cO	p			92.3	526.6		565.5	A	565.5	59.4		
E22/6	E22/229/639.5	658	3cO	p				377.2		561.7	A	561.7	44		
E22/6	E22/229/639.5	618	3cH	p			308.4	522.7	133	183.9	H	522.7	69.4	13.5	0.84
E22/6	E22/229/639.5	621	3cH	p			264.9	527.6	165.6	504.7	H	527.6	71.1	15.6	0.82
E22/6	E22/229/639.5	626	3cHN	p			307.6	511.7		545.3	H	545.3	57.7		
E22/6	E22/229/639.5	644	3cL	p			599.1	552.3		595.7	L	599.1	62.5		
E22/8	E22/229/642.3	586	1aL	p		-3.6	397.6				L	397.6	5.846		
E22/8	E22/229/642.3	588	1aL	p		-2.3	382.9				L	382.9	3.852		
E22/8	E22/229/642.3	594	1aL	p		-18.4	417.7				L	417.7	21.499		
E22/8	E22/229/642.3	607	1bV	p			593.4				V	593.4			
E22/8	E22/229/642.3	569	2aV	p			481.6				V	481.6			
E22/8	E22/229/642.3	595	2aV	p			399.6				V	399.6			
E22/8	E22/229/642.3	570	3aH	p			92.7	353.4			H	353.4	42		
E22/6	E22/229/642.3	571	3aH	p			63.2	472.8			H	472.8	53.3		
E22/8	E22/229/642.3	572	3aH	p			111.8	396.3			H	396.3	45.7		
E22/8	E22/229/642.3	574	3aH	p			121.3	473.4			H	473.4	53.4		
E22/8	E22/229/642.3	577	3aH	p			162.3	345.8			H	345.8	41.4		
E22/8	E22/229/642.3	578	3aH	p			123.3	431.7			H	431.7	49.1		
E22/8	E22/229/642.3	587	3aH	p			315	454.9			H	454.9	51.4		
E22/8	E22/229/642.3	590	3aH	p			140.2	394.3			H	394.3	45.5		
E22/8	E22/229/642.3	593	3aH	p			289.9	471.4			H	471.4	53.2		
E22/8	E22/229/642.3	598	3aH	p			273.7	499.6			H	499.6	56.3		
E22/8	E22/229/642.3	602	3aH	p			295.3	438.6			H	438.6	49.8		
E22/8	E22/229/642.3	604	3aH	p			279.3	471.9			H	471.9	53.2		
E22/8	E22/229/642.3	605	3aH	p				430.6			H	430.6	49		
E22/8	E22/229/642.3	576	3bH	p			94.6	528.3	327.8		H	528.3	77.8	29.5	0.68
E22/8	E22/229/642.3	601	3bH	p			304.2	469.5			H	469.5	53		
E22/8	E22/229/642.3	603	3bH	p			300.4	487.2			H	487.2	54.9		
E22/8	E22/229/642.3	591	3cO	p			212.7	501.1	182.7	522	A		69	18.4	0.78
E22/6	E22/229/642.3	579	3cH	p			100.5	471.9			H	471.9	53.2		
E22/8	E22/229/642.3	580	3cH	p			201.9	400.1		280.9	H	400.1	46.1		
E22/8	E22/229/642.3	599	3cH	p			302.6	490.4	155.8		H	490.4	66.9	16.8	0.79
E22/8	E22/229/642.3	596	3cHN	p			320.8	477.4	142.7		H		65	16.4	0.79
E22/8	E22/229/642.3	600	3cHN	p			256.9	492.1		>600.0	H	492.1	55.4		
E26/57	E26/189/235.8	480	1aL	ps			440.1				L	440.1			
E26/57	E26/189/235.8	478	1bL	ps			441.7				L	441.7			
E26/57	E26/189/235.8	484	3aH	ps			161.7	176.8			H	176.8	30.8		
E26/57	E26/189/235.8	485	3aH	ps			148.4	163.5			H	163.5	30.2		
E26/57	E26/189/235.8	494	3aH	p			378.8	548.6			H	548.6	62.1		
E26/57	E26/189/235.8	495	3aH	p			394.1	503.8			H	503.8	56.7		
E26/57	E26/189/235.8	498	3aHN	p				527.7			H	601	59.5		
E26/57	E26/189/235.8	499	3aHN	p				510			H	601	57.5		
E26/57	E26/189/235.8	500	3aHN	p				572.6			H	601	65.1		
E26/57	E26/189/235.8	497	3aN	p							N	601	68.7		
E26/57	E26/189/235.8	482	3bH	ps			137.8	185.7	124.3		H	185.7	43.3	23.7	0.51
E26/57	E26/189/235.8	483	3bH	p			214.2	354.2	133.1	196.9	H	354.2	53.6	20.5	0.67
E26/57	E26/189/235.8	486	3cO	ps			160.9	167.1		184.7	O	167.1	30.4		
E26/57	E26/189/235.8	487	3bH	p?				428.8	122.1		H	428.8	59.3	16.7	0.76
E26/57	E26/189/235.8	488	3bH	ps			148	213	127.6		H	213	44.7	23.6	0.53
E26/57	E26/189/235.8	489	3bH	ps			147.5	216.3	128.4		H	216.3	44.9	23.6	0.54
E26/57	E26/189/235.8	490	3bH	ps			141.6	197.5	129.7		H	197.5	44.2	24.1	0.51
E26/57	E26/189/235.8	492	3bH	p			459	554.6	240.6		H	554.6	76.5	19.5	0.79
E26/57	E26/189/235.8	493	3bSN	p							N	601	68.7		
E27/87	E27/248/384.9	129	3aH	pp			248.7	506.5			H	506.5	57.1		
E27/87	E27/248/384.9	130	3aH	pp			269.6	488.2			H	488.2	55		
E27/87	E27/248/384.9	131	3aH	pp				487.9			H	487.9	55		

Main stage

Sample	Borehole ID	Inc No.	Type	P/S/PS	T eut.	Tm ice	ThV	TmH	TmS	TmO	Homog	ThF	NaCl± KCl wt%	wt% KCl	Na/Na+K
E27/89	E27/4/490.9	30	3aH	p			109.4	532		405.2	H	532	60		
E27/89	E27/4/490.9	34	3aH	p			108.6	540.2			H	540.2	61		
E48/26	E48/2/189.9	45	3aH	ps			396.9	404.8			H	404.8	46.5		
E48/26	E48/2/189.9	47	3aL	ps			440.3				L	440.3			
E48/26	E48/2/189.9	53	3aH	ps			173.7	386.8			H	386.8	44.9		
E48/26	E48/2/189.9	54	3aH	ps			157.1	438.7			H	438.7	49.8		
E48/26	E48/2/189.9	55	3cH	ps			180.8	428.7			H	428.7	48.8		
E27/87	E27/248/384.9	122	3aH	pp			327.2	461.6			H	461.6	52.1		
E27/87	E27/248/384.9	123	3aH	pp			326.9	451.7			H	451.7	51.1		
E27/90	E27/48/224.1	155	1aL	ps				403.7			L	403.7			
E27/90	E27/48/224.1	157	3bH	p			120.8	539.4	214.5		H	539.4	74	18.5	0.79
E27/90	E27/48/224.1	159	3aN	p			601	533.4			N	601	60.2		
E27/90	E27/48/224.1	162	3aH	p				472.6			H	472.6	53.3		
E27/90	E27/48/224.1	163	3aH	p				465.8			H	465.8	56.3		
E27/90	E27/48/224.1	167	3aHN	p			298	601			H	601	68.7		
E27/90	E27/48/224.1	168	3aH	p			495.8	480.5			H	495.8	54.2		
E27/90	E27/48/224.1	169	3aD	p			440.6	572.3			D		65.1		
E27/90	E27/48/224.1	170	3aH	p				559.2			H	559.2	63.4		
E27/90	E27/48/224.1	171	3aH	p			328.9	537.2			H	537.2	60.7		
E27/90	E27/48/224.1	172	3aH	p			302.8	534.9			H	534.9	60.4		
E26/80	E26/272/178.5	191	3aH	p			254.8	381.6			H	381.6	44.4		
E26/80	E26/272/178.5	192	3aH	p			268.2	357			H	357	42.3		
E26/80	E26/272/178.5	193	3aH	p			331.7	571.2			H	571.2	64.9		
E26/80	E26/272/178.5	194	3aH	p			384.1	536.2			H	536.2	60.6		
E26/80	E26/272/178.5	195	3aL	p			355.2	501.8		–	L	355.2	57.2		
E26/80	E26/272/178.5	196	3cHN	p			599.9	487.2			H	599.9	54.9		
E26/80	E26/272/178.5	197	3aH	p			271.5	544.4			H	544.4	61.6		
E26/80	E26/272/178.5	199	3aH	p			110.4	498.7			H	498.7	61.1		
E26/80	E26/272/178.5	200	3aHD	p			539.6				H				
E26/80	E26/272/178.5	201	3cHD	p			376.5	460.2		>539.6	H		55.5		
E26/80	E26/272/178.5	202	3aH	p			240.2	461.6			H	461.6	55.7		
E26/80	E26/272/178.5	203	3aHN	p							H	601	68.7		
E26/80	E26/272/178.5	204	3cH	p			410	567.8			H	567.8	64.5		
E26/80	E26/272/178.5	205	3aL	p			503.5				L				
E26/80	E26/272/178.5	206	3aH	p			182.9	499.9			H	499.9	56.3		

Sample	Borehole ID	Inc No.	Type	P/S/PS	T eut.	Tm ice	ThV	TmH	TmS	TmO	Homog	ThF	NaCl± KCl wt%	wt% KCl	Na/Na+K
E26/80	E26/272/178.5	207	3aH	p			272.5	500.8			H	500.8	56.4		
E26/80	E26/272/178.5	208	3aH	p			264.5	474.6			H	474.6	53.5		
E26/80	E26/272/178.5	210	3aH	p				522			H	522	48.1		
E26/80	E26/272/178.5	211	3aH	p				511.5			H	511.5	57.6		
E26/80	E26/272/178.5	215	3aL	p			516.9	469.6			L	469.6	53		
E26/80	E26/272/178.5	216	3cHN	p			493.9	508.3		>600.0	H	601	62.5		
E22/25	E22/205/296.7	316	3bH	ps			156.2	576.7	239.8		H	576.7	78.6	17.8	0.81
E22/25	E22/205/296.7	317	3bN	ps			601	595.7	228.1		N	601	80.1	15.6	0.84
E22/25	E22/205/296.7	318	2aV	ps			601				V	601			
E22/25	E22/205/296.7	320	3bN	ps			601	596.9	224.8		N	601	80.2	15.3	0.84
E22/25	E22/205/296.7	322	3cH	ps			103.4	369.9		314.7(14	H	369.9	43.4		
E22/25	E22/205/296.7	323	3aH	ps			100.1	348.2			H	348.2	41.6		
E22/25	E22/205/296.7	324	3aH	ps			122.1	426.4			H	426.4	48.4		
E22/25	E22/205/296.7	325	3bH	ps			168	326.6	209.7		H	326.6	56.5	39.6	0.54
E22/25	E22/205/296.7	326	3aH	ps			215.9	489.5			H	489.5	55.1		
E22/25	E22/205/296.7	327	3aN	ps			601	601		564.4	N	601	68.7		
E22/25	E22/205/296.7	328	3cN	ps			429.7	456.3		489.9	N	489.9	51.6		
E22/25	E22/205/296.7	330	3aH	ps			233.6	485.1			H	485.1	59.1		
E22/25	E22/205/296.7	331	3cH	ps			356.4	545.4		314.4 (3:	H	545.4	67.9		
E26/72	E26/287/122.2	348	2aV	ps		~-26.3	480.7				V	480.7	26.824		
E26/72	E26/287/122.2	350	1aL	p		~-20.0	485.2				L	485.2	22.66		
E48/12	E48/15/651.1	388	3bH	p			189.7	486.8	121.4		H	486.8	65.1	14.3	0.82
E48/12	E48/15/651.1	390	3aH	p			249.6	467.2			H	467.2	52.7		
E48/12	E48/15/651.1	391	3bH	p			247.5	494.9	125.3		H	494.9	66.1	14.2	0.82
E48/12	E48/15/651.1	392	3aH	p			220.6	499.3			H	499.3	56.2		
E48/12	E48/15/651.1	393	3cH	p			199.3	491.9			H	491.9	55.4		
E48/12	E48/15/651.1	.394	3bH	p			415.9	464.2	155.9		H	464.2	64.3	18.1	0.76
E48/12	E48/15/651.1	397	3bH	p			231	499.9	136.5		H	499.9	67.1	14.9	0.82
E48/12	E48/15/651.1	398	3aH	p			161.4	497.6			H	497.6	56		
E48/12	E48/15/651.1	402	3aH	p			127.8	539.5			H	539.5	61		
E48/12	E48/15/651.1	403	3aH	p			138.6	544.3			H	544.3	61.5		
E48/12	E48/15/651.1	405	3aH	p			106.1	542.7			H	542.7	61.3		
E48/12	E48/15/651.1	406	2aV	ps			461				V	461			
E48/12	E48/15/651.1	407	2aV	ps			451				V	451			
E48/12	E48/15/651.1	410	3aH	p				482.3			H	482.3	54.3		
E48/12	E48/15/651.1	412	3aH	p				437.3			H	437.3	49.6		
Late stage															
E48/25	E48/15/453.1	62	2aV	p			420.5				V	420.5			
E48/25	E48/15/453.1	63	2aV	p			425.8				V	425.8			
E48/25	E48/15/453.1	64	1aL	p	-32.1	-16.7	378.2				L	378.2	20.19		
E48/25	E48/15/453.1	65	2aV	p			387.9				V	387.9			
E48/25	E48/15/453.1	67	1aL	ps			272.1				L	272.1			
E48/25	E48/15/453.1	68	3aH	p			387.5	474.9			H	474.9	53.5		
E48/25	E48/15/453.1	69	3aH	p			327.1	370.5			H	370.5	43.3		
E48/25	E48/15/453.1	70	3aH	p			326.3	478.2			H	478.2	53.9		
E26/76	E26/286/123.6	137	3aH	p				285			H	285	36.9		
E26/76	E26/286/123.6	138	3aH	p				300.7			H	300.7	38		
E26/76	E26/286/123.6	139	2aV	ps			262.5				V	262.5			
E26/76	E26/286/123.6	140	1aL	ps	-12	-18.6	391.6				L	391.6	21.647		
E26/76	E26/286/123.6	141	1aL	ps		-16.9	381				L	381	20.348		
E26/76	E26/286/123.6	149	3aH	p				307			H	307	38.4		
E26/76	E26/286/123.6	152	3aH	p				275.3			H	275.3	36.2		
E26/76	E26/286/123.6	153	1aL	ps	-12.1	-5.3	185.5				L	185.5	8.267		
E26/76	E26/286/123.6	154	3aH	p				354.9			H	354.9	42.1		
E27/90	E27/48/224.1	174	3aH	p			267.3	322.4			H	322.4	39.6		
E27/90	E27/48/224.1	175	3aH	p			338.4	358.4			H	358.4	42.4		
E27/90	E27/48/224.1	176	3aL	p			395.1	370.2			L	395.1	42.9		
E27/90	E27/48/224.1	177	3aH	p			316	403.6			H	403.6	46.4		
E27/90	E27/48/224.1	178	3aL	p			373.7	347			L	373.7	41.5		
E27/90	E27/48/224.1	179	3aH	p				327.1			H	327.1	39.9		
E27/90	E27/48/224.1	180	3aH	p			365.1	377			H	377	44		
E27/90	E27/48/224.1	182	3aH	p			351.2	364.9			H	364.9	42.3		
E27/90	E27/48/224.1	183	3aH	p			380.4	383.4			H	383.4	44.6		
E27/90	E27/48/224.1	188	3aL	p			389.1	374.2			L	389.1	43.8		
E26/80	E26/272/178.5	189	2aV	ps			380				V	380			
E26/80	E26/272/178.5	190	1aL	ps	-5.1	-1.8	350.2				L	350.2	3.051		
E48/27	E48/15w1/848.0	234	1aM	p		-12.5	375.4				M	375.4	16.528		
E48/27	E48/15w1/848.0	241	1aL	p		-11.3	351.6				L	351.6	15.346		
E48/27	E48/15w1/848.0	244	3aH	p			265.5	396.1			H	396.1	45.7		
E48/27	E48/15w1/848.0	245	3aH	p			327.4	400.4			H	400.4	46.1		
E48/27	E48/15w1/848.0	247	3bH	p			352.3	461.5	306.5		H	461.5	71.8	32.7	0.6
E48/27	E48/15w1/848.0	248	3aL	p			464.5	376			L	464.5	43.9		
E48/27	E48/15w1/848.0	262	3aH	p			130	324.5			H	324.5	39.7		
E48/27	E48/15w1/848.0	263	3aH	p			230.3	375.1			H	375.1	43.8		
E48/27	E48/15w1/848.0	264	3aH	p			234.9	357.6			H	357.6	42.3		
E48/27	E48/15w1/848.0	265	3aH	p			501	423			H	501	48.2		
E48/27	E48/15w1/848.0	266	1aL	p		-24.3	413.5				L	413.5	25.547		
E48/27	E48/15w1/848.0	267	2aV	p			404.2				V	404.2			
E48/27	E48/15w1/848.0	268	3aH	p			465.6	471.8			H	471.8	57.1		
E48/27	E48/15w1/848.0	269	3aL	p			473.3	442.3			L	473.3	50.1		
E48/27	E48/15w1/848.0	273	1aL	p		-13.9	380.3				L	370.3	17.826		
E48/27	E48/15w1/848.0	277	2aV	p			388.2				V	388.2			

Thin section	Stage	Label	A%(O)	A%(Na)	A%(Mg)	A%(K)	A%(Ca)	A%(Mn)	A%(Fe)	A%(Al)	A%(Si)	A%(P)	A%(S)	A%(Cl)	A%(F)	A%(Ti)	A%(Cu)	A%(Se)
E26/72/18	EQ	chip2/1	64.11	0.32	0.02	0.61	0.13	1.06	4.25	0.95	27.74	0.00	0.27	0.04	0.00	0.00	0.49	0.01
E26/72/18	EQ	chip2/2	64.15	0.35	0.03	0.54	0.12	1.04	4.12	1.08	27.64	0.00	0.28	0.04	0.00	0.07	0.53	0.00
E22/19/20	TMQ	chip5/1	66.49	0.10	0.00	0.10	0.11	0.00	0.12	0.03	33.04	0.00	0.00	0.00	0.00	0.01	0.00	0.00
E22/19/20	TMQ	chip5/4	65.49	0.32	0.00	0.47	0.53	0.20	1.16	0.04	31.46	0.02	0.00	0.09	0.00	0.00	0.21	0.00
E22/19/20	TMQ	chip5/6	66.45	0.11	0.00	0.04	0.09	0.02	0.18	0.01	32.93	0.04	0.00	0.02	0.00	0.00	0.10	0.00
E26/57/15	TMQ	chip6/1	64.99	0.36	0.03	0.79	0.49	0.29	1.27	0.07	30.44	0.01	0.03	0.00	0.00	0.01	1.22	0.00
E26/57/15	TMQ	chip6/1b	64.49	0.27	0.02	0.58	0.35	0.73	2.48	0.07	29.25	0.05	0.03	0.00	0.00	0.00	1.67	0.01
E26/57/15	TMQ	chip6/2	64.26	0.62	0.05	1.29	0.66	0.56	1.77	0.07	29.42	0.00	0.03	0.02	0.00	0.00	1.25	0.00
E26/78/23	TMQ	chip7/1	65.66	0.36	0.00	0.41	0.22	0.05	0.60	1.57	30.90	0.00	0.02	0.01	0.00	0.00	0.20	0.00
E26/78/24	TMQ	chip7/2	66.50	0.04	0.01	0.05	0.06	0.01	0.08	0.05	33.00	0.02	0.01	0.02	0.00	0.01	0.13	0.00
E22/19/21	TMQ	chip8/1	65.58	0.75	0.01	0.55	0.12	0.06	0.97	0.02	31.78	0.02	0.00	0.01	0.00	0.00	0.13	0.00
E22/19/21	TMQ	chip8/2	65.41	0.59	0.04	0.68	0.31	0.30	1.04	0.02	31.45	0.00	0.00	0.03	0.00	0.04	0.07	0.00
E22/8/38	THQ	chip9/1	65.81	0.07	0.01	0.04	0.12	0.60	1.63	0.07	31.65	0.00	0.00	0.00	0.00	0.00	0.01	0.01
E22/8/38	THQ	chip9/10	64.89	0.38	0.01	0.26	0.45	0.83	2.81	0.04	30.10	0.00	0.00	0.00	0.00	0.00	0.19	0.02
E22/8/38	THQ	chip9/11	65.10	0.20	0.03	0.09	0.27	0.57	3.13	0.06	30.36	0.00	0.00	0.04	0.00	0.03	0.10	0.02
E22/8/38	THQ	chip9/13	66.41	0.04	0.01	0.05	0.04	0.02	0.52	0.04	32.80	0.00	0.00	0.00	0.00	0.04	0.01	0.00
E22/8/38	THQ	chip9/14	66.06	0.07	0.01	0.04	0.24	0.26	1.12	0.02	32.16	0.00	0.00	0.00	0.00	0.01	0.00	0.00
E22/8/38	THQ	chip9/2	65.56	0.05	0.02	0.04	0.12	0.63	2.27	0.05	31.12	0.00	0.03	0.05	0.00	0.02	0.03	0.00
E22/8/38	THQ	chip9/3	66.46	0.06	0.00	0.02	0.05	0.01	0.39	0.05	32.89	0.00	0.02	0.00	0.00	0.02	0.03	0.00
E22/8/38	THQ	chip9/4	66.42	0.05	0.00	0.01	0.09	0.01	0.30	0.03	32.95	0.01	0.00	0.01	0.07	0.00	0.05	0.01
E22/6/40	THQ	chip10/10	66.06	0.02	0.02	0.02	0.29	0.62	0.81	0.03	32.07	0.00	0.03	0.00	0.00	0.00	0.02	0.00
E22/6/40	THQ	chip10/11	64.89	0.11	0.03	0.31	0.34	1.42	2.85	0.14	29.87	0.00	0.00	0.00	0.00	0.04	0.00	0.00
E22/6/40	THQ	chip10/13	66.17	0.06	0.03	0.14	0.07	0.04	0.49	1.18	31.76	0.01	0.04	0.00	0.00	0.00	0.00	0.01
E22/6/40	THQ	chip10/14	66.09	0.06	0.00	0.06	0.06	0.17	1.20	0.04	32.19	0.02	0.00	0.01	0.00	0.03	0.09	0.00
E22/6/40	THQ	chip10/2	66.40	0.01	0.00	0.02	0.03	0.15	0.52	0.03	32.82	0.00	0.00	0.01	0.00	0.00	0.00	0.00
E22/6/40	THQ	chip10/7	63.34	0.50	0.10	2.04	0.68	0.85	3.48	2.13	26.75	0.02	0.05	0.01	0.00	0.04	0.03	0.00
E22/6/40	THQ	chip10/8	64.14	0.27	0.00	0.80	0.29	0.88	4.80	0.02	28.75	0.00	0.00	0.00	0.00	0.05	0.00	0.00
E22/6/40	THQ	chip10/9	61.95	0.11	0.05	0.03	2.03	3.54	8.09	0.27	23.81	0.00	0.00	0.03	0.00	0.08	0.00	0.00
E26/57/27	THQ	chip11/3	66.47	0.02	0.00	0.02	0.01	0.09	0.32	0.04	32.98	0.00	0.00	0.00	0.03	0.03	0.00	0.00
E26/57/27	THQ	chip11/4	66.42	0.02	0.04	0.00	0.23	0.10	0.33	0.04	32.81	0.01	0.00	0.00	0.00	0.00	0.00	0.00
E26/57/30	THQ	chip12/1	65.26	0.04	0.06	0.03	0.26	0.37	3.35	0.04	30.44	0.04	0.02	0.01	0.00	0.00	0.07	0.00
E26/57/30	THQ	chip12/10	64.47	0.06	0.17	0.04	0.28	2.03	3.41	0.06	28.92	0.00	0.02	0.00	0.00	0.01	0.52	0.00
E26/57/30	THQ	chip12/11	65.99	0.06	0.00	0.51	0.12	0.19	0.83	0.08	32.15	0.03	0.02	0.00	0.00	0.00	0.00	0.00
E26/57/30	THQ	chip12/1b	65.99	0.01	0.02	0.01	0.03	0.18	1.70	0.03	31.91	0.01	0.00	0.01	0.00	0.07	0.03	0.00
E26/57/30	THQ	chip12/3	64.86	0.02	0.00	0.20	0.23	2.67	2.06	0.29	29.57	0.00	0.05	0.00	0.00	0.04	0.00	0.01
E26/57/30	THQ	chip12/4	64.54	0.06	0.01	0.02	0.22	2.97	3.00	0.09	29.02	0.00	0.00	0.00	0.00	0.06	0.00	0.00
E26/80/44	MQ	chip13/1	66.52	0.04	0.02	0.01	0.03	0.00	0.19	0.08	33.04	0.00	0.03	0.02	0.01	0.00	0.00	0.01
E27/91/49	MQ	chip14/2	64.23	0.02	0.03	0.01	0.34	1.88	4.93	0.10	28.35	0.00	0.01	0.01	0.00	0.06	0.02	0.00
E48/12/47	MQ	chip15/2	66.53	0.01	0.03	0.01	0.01	0.00	0.22	0.16	33.00	0.00	0.01	0.01	0.00	0.00	0.01	0.00
E48/12/47	MQ	chip16/4	65.25	0.07	0.00	0.04	0.05	0.62	3.12	0.00	30.69	0.00	0.00	0.10	0.00	0.00	0.05	0.00
E48/12/47	MQ	chip16/3	66.19	0.01	0.02	0.04	0.01	0.24	1.09	0.01	32.34	0.03	0.00	0.01	0.00	0.02	0.00	0.00
E26/76/57	LQ	chip17/3	66.34	0.02	0.01	0.01	0.27	0.04	0.59	0.11	32.46	0.05	0.02	0.01	0.00	0.06	0.01	0.00
E26/76/53	LQ	chip17/7	66.60	0.00	0.00	0.02	0.01	0.00	0.02	0.15	33.15	0.00	0.00	0.02	0.00	0.02	0.00	0.00
E48/27/58	LQ	chip19/4	66.51	0.01	0.01	0.03	0.02	0.04	0.32	0.01	32.97	0.04	0.01	0.01	0.00	0.00	0.02	0.00

Appendix C

Sulphur Isotopes

APPENDIX C1 – Sulphide and sulphate $\delta^{34}S$ values

APPENDIX C2 – Empirical correction for bornite

BH-ID	Sample	Mineral	Stage	δ34S	Method	Source
E22/2/360.2	VL S47A	bor	E22 E	-6.06	laser	VL
E22/2/360.2	VL S47B	bor	E22 T	-6.03	laser	VL
E22/229/631.9	VL S45	bor	E22 T	-17.45	laser	VL
E22/229/642.0	VL S50	bor	E22 T	-7.12	conv	VL
E22/2/286.8	VL S48	bor	E22 M	-3.98	conv	VL
E22/205/454.1	VL S46	bor	E22 M	-4.79	conv	VL
E22/205/342.6	VL S49	bor	E22 L	-3.64	conv	VL
E26	PH2	clot	E26 clot	-4.70	conv	PH
E26/264/213.7	VL S10	clot	E26 clot	-3.79	conv	VL
E26/284/288.0	VL S 6	clot	E26 clot	-4.02	conv	VL
E26/295/282.9	VL S 5A	clot	E26 clot	-4.53	conv	VL
E26/282/122.2	VL S16	bor	E26 E	-1.14	conv	VL
E26/287/245.5	VL S18	bor	E26 E	-2.70	conv	VL
E26/39/452.0	PH39/452A	bor	E26 E	-2.90	conv	PH
E26/39/452.0	PH39/452B	cpy	E26 E	-3.50	conv	PH
E26/132w2/757.6	VL S15	bor	E26 T	-4.40	conv	VL
E26/184/125.9	VL S22	bor	E26 T	-5.47	laser	VL
E26/184/128.8	VL S21	bor	E26 T	-5.78	laser	VL
E26/189/297.5	VL S19	bor	E26 T	-1.19	conv	VL
E26/272/197.2	VL S55	anh	E26 T	4.84	conv	VL
E26/272/197.2	BN STD	bor	E26 T	-1.85	both	VL
E26/274/184.1	VL S14	bor	E26 T	-5.05	conv	VL
E26/284/137.5	VL S53	anh	E26 T	4.37	conv	VL
E26/287/153.6	VL S17B	bor	E26 T	-6.99	laser	VL
E26/295/282.9	VL S5B	bor	E26 T	-5.17	laser	VL
E26/42/614.0	PH42/614	bor	E26 T	-2.90	conv	PH
E26/46/1253.7	VL S2A	bor	E26 T	-15.36	laser	VL
E26/46/1470.6	VL S1	bor	E26 T	-5.62	laser	VL
E26/91/136.7	VL S24	bor	E26 T	-4.66	laser	VL
E28/189/235.8	VL S20	bor	E26 T	-4.57	laser	VL
E26/26/135.0	PH26/135	bor	E26 M	-8.00	conv	PH
E26/26/214.0	PH26/214	bor	E26 M	-5.00	conv	PH
E26/272/178.5	VL S11	bor	E26 M	-3.75	conv	VL
E26/274/140.1	VL S56	anh	E26 M	7.24	conv	VL
E26/282/387.5	VL S 4	bor	E26 M	-4.37	conv	VL
E26/284/203.9	VL S 7	bor	E26 M	-4.71	conv	VL
E26/286/123.6	VL S54	anh	E26 M	7.35	conv	VL
E26/286/123.6	VL S13	bor	E26 M	-3.81	conv	VL
E26/286/150.1	VL S12	bor	E26 M	-3.79	conv	VL
E26/287/153.6	VL S17A	bor	E26 M	-3.98	laser	VL
E26/38/313.0	PH38/313A	bor	E26 M	-3.40	conv	PH
E26/38/313.0	PH38/313B	cpy	E26 M	-4.50	conv	PH
E26/38/443.0	PH38/443	bor	E26 M	-4.40	conv	PH
E26/42/625.0	PH42/625B	anh	E26 M	14.10	conv	PH
E26/42/625.0	PH42/625A	bor	E26 M	-5.00	conv	PH
E26/66/1069.0	PH66/1069B	anh	E26 M	7.30	conv	PH
E26/66/1069.0	PH66/1069A	cpy	E26 M	-4.20	conv	PH
E26/75/173.0	PH75/173	cpy	E26 M	-7.20	conv	PH
E26/75/174.0	PH75/174	bor	E26 M	-6.50	conv	PH
E26/91/134.1	VL S23	bor	E26 M	-5.19	conv	VL
E26/10300	AH961	gyp	E26 L	6.90	conv	AH
E26/10300	AH962	gyp	E26 L	7.30	conv	AH
E26/106/340.0	PH106/340	py	E26 L	-7.50	conv	PH
E26/132w2/969.3	VL S 9	bor	E26 L	-1.87	conv	VL
E26/282/427.7	VL S3	bor	E26 L	-7.89	laser	VL
E26/284/99/5	VL S 8	bor	E26 L	-4.71	conv	VL
E26/286/244.0	VL S57	anh	E26 L	7.11	conv	VL
E26/40/129.0	PH40/129	py	E26 L	-7.10	conv	PH
E26/46/253.0	DR46/253	py	E26 L	-3.80	laser	DR
E26/46/258.0	DR46/258	gyp	E26 L	8.90	conv	DR
E26/46/279.0	DR46/279A	py	E26 L	-7.40	laser	DR
E26/46/279.0	DR46/279B	py	E26 L	-7.60	laser	DR
E26/46/437.0	PH46/437	anh	E26 L	11.60	conv	PH
E26/46/847.0	PH46/847B	anh	E26 L	16.60	conv	PH
E26/46/847.0	PH46/847A	py	E26 L	-7.70	conv	PH
E26/68/380.0	PH68/380B	gyp	E26 L	21.80	conv	PH
E26/68/380.0	PH68/380A	py	E26 L	-6.80	conv	PH
E26/9700	AH9700B	anh	E26 L	7.50	conv	AH
E26/9700	AH9700A	py	E26 L	-5.90	conv	AH
E26/9800	AH661	anh	E26 L	8.40	conv	AH
E26/9800	AH662	anh	E26 L	8.20	conv	AH
E26/9800	AH663	py	E26 L	-5.00	conv	AH
EX425A	EX425A	py	E26 L	-3.20	laser	DR
G183-107	G183-107	gyp	E26 L	8.80	conv	DR
GAD3	GAD3	gyp	E26 L	8.70	conv	DR
GEX450	GEX450	gyp	E26 L	7.50	conv	DR
RAE0S	RAE0S	py	E26 L	-3.50	laser	DR
SAD3	SAD3	py	E26 L	-4.90	laser	DR
E27/386/191.9	VL S40	clot	E27clot	-4.75	conv	VL
E27/W/29	VL S41	clot	E27 clot	-4.63	conv	VL
E27/248/384.9	VL S38A	bor	E27 E	-5.58	conv	VL
E27/7/67.1	VL S42	bor	E27 E	-5.64	conv	VL
E27/248/384.9	VL S38B	bor	E27 T	-5.43	conv	VL
E27/386/199.6	VL S44A	bor	E27 T	-4.96	conv	VL
E27/4/490.9	VL S36	bor	E27 T	-19.71	laser	VL
E27/369/171.1	VL S43	bor	E27 M	-5.10	conv	VL
E27/386/199.6	VL S44B	bor	E27 M	-4.99	conv	VL
E27/48/224.1	VL S37	bor	E27 M	-5.59	conv	VL
E48/19w3/480.0	JH19/480B	bor	E48 E	-5.60	conv	JHR
E48/19w3/480.0	JH19/480A	cpy	E48 E	-4.30	conv	JHR
E48/19w3/536.0	JH19/536	cpy	E48 E	-5.00	conv	JHR
E48/19w3/734.0	JH19/734	cpy	E48 E	-3.00	conv	JHR
E48/19w3/788.0	JH19/788B	bor	E48 E	-5.80	conv	JHR
E48/19w3/788.0	JH19/788A	cpy	E48 E	-5.00	conv	JHR
E48/2/189.9	VL S35	bor	E48 E	-5.25	conv	VL
E48/20/700.0	JH20/700	bor	E48 E	-5.50	conv	JHR
E48/20/712.0	JH20/712	bor	E48 E	-5.10	conv	JHR
E48/21/478.0	JH21/478	bor	E48 E	-5.20	conv	JHR
E48/11/503.1	VL S30	bor	E48 T	-4.44	laser	VL
E48/13w1/708.4	VL S28A	bor	E48 T	-4.80	conv	VL
E48/15/453.1	VL S32	bor	E48 T	-5.83	conv	VL
E48/11/466.6	VL S31B	bor	E48 M	-4.71	conv	VL
E48/13w2/834.3	VL S27A	bor	E48 M	-4.80	conv	VL
E48/15/651.1	VL S29	bor	E48 M	-4.16	laser	VL
E48/19w3/678.0	JH19/678	bor	E48 M	-6.00	conv	JHR
E48/19w3/849.0	JH19/849	bor	E48 M	-6.00	conv	JHR
E48/20w1/554.0	JH20/554	bor	E48 M	-4.40	conv	JHR
E48/20w1/643.0	JH20/643	cpy	E48 M	-4.10	conv	JHR
E48/20w1/833.0	JH20/833	bor	E48 M	-4.20	conv	JHR
E48/21/259.0	JH21/259	bor	E48 M	-4.20	conv	JHR
E48/21/433.0	JH21/433	cpy	E48 M	-3.80	conv	JHR
E48/21/433.0	JH21/433	cpy	E48 M	-4.70	conv	JHR
E48/21/438.0	JH21/438	bor	E48 M	-4.20	conv	JHR
E48/7/285.0	VL S34	bor	E48 M	-4.96	conv	VL
E48/13w1/708.4	VL S28B	bor	E48 L	-3.24	conv	VL
E48/15w1/848.0	VL S33	bor	E48 L	0.70	laser	VL
E48/20w1/320.0	JH20/320	py	E48 L	-3.50	conv	JHR
E48/21/346.0	JH21/346	py	E48 L	-3.50	conv	JHR

Standard deviation od bornite analyses: Laser ablation method (all samples): 5.27
excluding 3 very negative samples: 2.07
Conventional method: 1.36

Appendix C2

Empirical Correction factor for Bornite

The determination of the empirical correction factor for $\delta^{34}S$ with respect to CDT of bornite, based on SO_2 formed by laser ablation at 25 torr oxygen pressure, April 2001, Central Science Laboratory, University of Tasmania, Keith Harris.

Laser ablation of 4 small polished chips (2 spots per grain, integrated gas yield) of a specimen of bornite gave the following results:

Chip	$\delta^{34}S$	Precision
1	-6.139	0.045
2	-6.227	0.033
3	-6.123	0.027
4	-6.416	0.028

Average $\delta^{34}S$ = -6.226

These 4 chips were then crushed with Cu_2O and oxidised to SO_2 on the conventional line; the measured $\delta^{34}S$ was –2.23‰ (average of 5 ratio traces); when normalised to the results for Broken Hill galena (+3.40‰) and Roseberry galena (+12.40‰), this is -2.405‰ with respect to CDT.

The empirical correction offset for bornite is the difference between the two series of measurements; i.e. the correct value with respect to CDT – the value from the laser technique, or -2.405 – -6.226‰ = +3.821‰. To correct the laser data, add 3.821‰.

Because conventional and laser techniques samples similar bornite populations, the distributions of $\delta^{34}S$ values were expected to be similar for the two populations. However, using the correction factor of +3.821‰, the $\delta^{34}S$ distribution for laser results was skewed towards lighter $\delta^{34}S$ values by ~0.75‰ when compared with the conventional population. The difference is probably due to minor fluctuations in homogeneity of the bornite used for the standard. Changing the empirical correction factor to +4.571‰ (+3.821 + 0.75) corrects the skewness and is within analytical error and technique accuracy.

Appendix D

Biotite and Apatite Electron Microprobe Analyses

All elemental analyses were obtained from polished thin sections using a Cameca SX50 electron microprobe at the University of Tasmania's Central Science Laboratory.

APPENDIX D1 – Biotite

- Beam current = 25nA
- Acceleration voltage = 15kV
- Spot size ~5μm
- Counting time = 30 seconds.
- F, Cl and Na were analysed first to minimise halogen loss and alkali migration respectively.
- Atomic percentages calculated on 22 oxygen and 4 OH, F, Cl.

APPENDIX D2 – Apatite

- Analyses were restricted to apatite crystals oriented in thin section parallel to the c-axis;
- Counting time = 30 seconds
- F, Na, Cl, Ca and Mn were analysed using a 15nA beam current, a 20kV acceleration voltage and a ~10μm nominal spot size; all remaining elements were analysed using a 60nA beam current, a 25kV acceleration voltage and a ~5μm nominal spot size; and
- F, Cl and Na were analysed first to minimise halogen loss and alkali migration respectively. Atomic percentages calculated on 25 oxygen and 2 OH, F, Cl.

Label	*E22_31_1_2ndBi_-1-1*	*E22_31_1_2ndBi_-3-1*	*E22_31_2_2ndBi_-4-1*	*E22_31_2_2ndBi_-6-1*	*E22_32_3_2ndBi_-5-1*	*E26_14_2_2ndBi_-16-1*	*E26_14_2_2ndBi_-17-1*	*E26_14_3_2ndBi_-24-1*	*E26_18_1_2ndBi_-1-1*	*E26_18_5_2ndBi_-4-1*	*E26_18_5_2ndBi_-5-1*	*E26_18_7_Prim Bi?_-1*	*E26_18_7_Prim Bi?_-2*	*E26_18_7_Prim Bi?_-3*
P/A/V/I *	a	a	a	a	a	a	a	a	a	a	a	a	a	a
SiO2%	36.51	37.40	38.33	37.31	37.36	38.81	36.77	37.75	39.13	38.93	38.73	38.16	38.96	38.95
TiO2%	3.85	3.66	3.62	3.59	3.09	2.83	2.61	2.92	3.24	3.64	3.23	3.67	3.30	3.40
Al2O3%	14.84	14.79	13.81	15.49	14.57	14.93	15.46	15.07	13.31	14.01	13.92	14.00	13.65	13.72
Cr2O3%	0.00	0.05	0.00	0.00	0.00	0.06	0.00	0.00	0.02	0.00	0.00	0.05	0.00	0.01
FeO%total	13.57	13.05	11.96	13.52	12.64	12.36	13.04	12.94	11.67	11.87	11.62	11.43	10.68	10.91
V2O3%	0.04	0.04	0.03	0.06	0.06	0.09	0.10	0.05	0.00	0.08	0.10	0.12	0.11	0.17
ZnO%	0.00	0.10	0.00	0.00	0.06	0.00	0.00	0.04	0.01	0.00	0.02	0.05	0.00	0.00
MnO%	0.29	0.22	0.25	0.24	0.35	0.08	0.24	0.17	0.03	0.13	0.12	0.09	0.18	0.16
MgO%	16.36	16.18	17.60	15.72	18.00	16.23	17.81	15.53	18.29	17.50	18.03	17.52	18.45	18.37
Ca%O	0.02	0.12	0.00	0.01	0.07	0.00	0.02	0.00	0.02	0.00	0.31	0.03	0.06	0.07
Na2O%	0.27	0.30	0.30	0.26	0.16	0.16	0.13	0.18	0.21	0.27	0.19	0.33	0.30	0.30
K2O%	9.25	9.59	9.65	9.06	6.99	9.34	6.99	9.64	9.48	10.03	9.04	9.91	9.88	9.99
BaO%	0.00	0.00	0.00	0.00	0.00	0.00	0.00	0.00	0.00	0.00	0.00	0.00	0.09	0.00
NiO%	0.04	0.00	0.02	0.00	0.02	0.02	0.04	0.00	0.05	0.00	0.02	0.04	0.00	0.01
F%	1.91	1.98	2.18	1.92	1.66	1.95	1.98	1.93	2.70	2.81	2.55	2.90	3.14	3.17
Cl %	0.11	0.10	0.12	0.10	0.09	0.15	0.13	0.16	0.10	0.12	0.09	0.09	0.09	0.08
H2O(c)	3.08	3.08	3.01	3.11	3.21	3.10	3.04	3.05	2.78	2.75	2.86	2.67	2.59	2.59
O=F	0.80	0.83	0.92	0.81	0.70	0.82	0.84	0.81	1.14	1.19	1.07	1.22	1.32	1.33
O=Cl	0.03	0.02	0.03	0.02	0.02	0.03	0.03	0.04	0.02	0.03	0.02	0.02	0.02	0.02
Sum Ox%	99.30	99.82	99.92	99.54	97.60	99.27	97.50	98.57	99.89	100.93	99.74	99.82	100.12	100.55
Cations														
Si	5.45	5.54	5.64	5.53	5.57	5.72	5.50	5.65	5.74	5.67	5.68	5.62	5.70	5.68
Ti	0.43	0.41	0.40	0.40	0.35	0.31	0.29	0.33	0.36	0.40	0.36	0.41	0.36	0.37
Al as AlIV	2.55	2.46	2.36	2.47	2.43	2.28	2.51	2.35	2.26	2.33	2.32	2.38	2.30	2.32
AlVI	0.07	0.13	0.04	0.24	0.13	0.32	0.22	0.30	0.04	0.08	0.08	0.06	0.05	0.04
Cr	0.00	0.01	0.00	0.00	0.00	0.01	0.00	0.00	0.00	0.00	0.00	0.01	0.00	0.00
Fe2+	1.70	1.62	1.47	1.68	1.58	1.52	1.63	1.62	1.43	1.45	1.42	1.41	1.31	1.33
V	0.01	0.01	0.00	0.01	0.01	0.01	0.01	0.01	0.00	0.01	0.01	0.01	0.01	0.02
Zn	0.00	0.01	0.00	0.00	0.01	0.00	0.00	0.00	0.00	0.00	0.00	0.01	0.00	0.00
Mn2+	0.04	0.03	0.03	0.03	0.04	0.01	0.03	0.02	0.00	0.02	0.02	0.01	0.02	0.02
Mg	3.64	3.58	3.86	3.47	4.00	3.57	3.97	3.46	4.00	3.80	3.94	3.85	4.02	3.99
Ca	0.00	0.02	0.00	0.00	0.01	0.00	0.00	0.00	0.00	0.00	0.05	0.00	0.01	0.01
Na	0.08	0.09	0.09	0.07	0.05	0.05	0.04	0.05	0.06	0.08	0.05	0.09	0.09	0.09
K	1.76	1.82	1.81	1.71	1.33	1.76	1.33	1.84	1.77	1.86	1.69	1.86	1.84	1.86
Ba	0.00	0.00	0.00	0.00	0.00	0.00	0.00	0.00	0.00	0.00	0.00	0.00	0.01	0.00
Ni	0.00	0.00	0.00	0.00	0.00	0.00	0.01	0.00	0.01	0.00	0.00	0.01	0.00	0.00
F	0.90	0.93	1.01	0.90	0.78	0.91	0.94	0.91	1.25	1.30	1.18	1.35	1.45	1.46
Cl	0.03	0.03	0.03	0.03	0.02	0.04	0.03	0.04	0.03	0.03	0.02	0.02	0.02	0.02
OH	3.07	3.05	2.96	3.08	3.19	3.05	3.03	3.05	2.72	2.67	2.80	2.63	2.53	2.52
Sum Cations	19.73	19.70	19.71	19.61	19.49	19.56	19.53	19.64	19.67	19.69	19.63	19.72	19.72	19.73
XMg	0.68	0.69	0.72	0.68	0.72	0.70	0.71	0.68	0.74	0.72	0.73	0.73	0.76	0.75
Oct	5.88	5.78	5.81	5.81	6.10	5.74	6.14	5.74	5.84	5.74	5.82	5.75	5.77	5.76
Int	1.84	1.92	1.90	1.79	1.39	1.80	1.37	1.89	1.84	1.94	1.79	1.96	1.94	1.96
F/Cl	31.07	35.65	33.80	35.92	32.63	23.97	28.39	22.80	48.15	44.72	56.33	64.43	66.05	76.95
Mg#	68.24	68.85	72.40	67.46	71.74	70.06	70.89	68.15	73.63	72.43	73.45	73.20	75.49	75.01
F/F+Cl	0.97	0.97	0.97	0.97	0.97	0.96	0.97	0.96	0.98	0.98	0.98	0.98	0.99	0.99
X[phlog]	0.62	0.62	0.67	0.60	0.66	0.62	0.65	0.60	0.68	0.66	0.68	0.67	0.70	0.69
X[sid]	0.19	0.16	0.12	0.18	0.14	0.11	0.16	0.14	0.08	0.11	0.10	0.12	0.09	0.10
X[ann]	0.19	0.22	0.22	0.23	0.20	0.27	0.19	0.26	0.23	0.23	0.22	0.21	0.21	0.21
Calculations														
IV(F)	1.59	1.58	1.59	1.57	1.72	1.60	1.60	1.58	1.49	1.44	1.51	1.42	1.41	1.40
IV(Cl)	-4.18	-4.14	-4.30	-4.07	-4.15	-4.30	-4.29	-4.29	-4.31	-4.32	-4.19	-4.21	-4.30	-4.23
IV(F/Cl)	5.77	5.72	5.89	5.65	5.87	5.91	5.90	5.87	5.80	5.76	5.71	5.62	5.70	5.62
log(XF/XOH)	-0.53	-0.52	-0.46	-0.53	-0.61	-0.52	-0.51	-0.52	-0.34	-0.31	-0.37	-0.29	-0.24	-0.24
log(XCl/XOH)	-2.02	-2.07	-1.99	-2.09	-2.12	-1.90	-1.96	-1.88	-2.02	-1.96	-2.12	-2.10	-2.06	-2.12
log(XF/XCl)	1.49	1.55	1.53	1.56	1.51	1.38	1.45	1.36	1.68	1.65	1.75	1.81	1.82	1.89
log(fH2O/fHF)	5.28	5.27	5.27	5.27	5.41	5.30	5.30	5.27	5.17	5.12	5.20	5.11	5.10	5.09
log(fH2O/FHCl)	4.81	4.86	4.81	4.87	4.94	4.71	4.77	4.67	4.85	4.79	4.95	4.92	4.90	4.96
log(fHF/FHCl)	-1.50	-1.46	-1.56	-1.42	-1.56	-1.66	-1.60	-1.64	-1.43	-1.44	-1.36	-1.30	-1.34	-1.26

* p - primary; a - secondary/alteration; v - vein; i - inclusion

Label	*E26_18_7_Prim Bi?_-4*	*E26_18_7_Prim Bi?_-5*	*E26_67_1_2ndBi in volcs-1-1*	*E26_67_1_2ndBi in volcs-2-1*	*E26_67_1_2ndBi in volcs-4-1*	*E26_67_1_2ndBi_-1*	*E26_67_1_2ndBi_-2*	*E27/26/4/bi-a1*	*E27/26/4/bi-a2*	*E27/26/4/bi-a3*	*E27/26/4/bi-a4*	*27_68_4_1*	*27_68_4_2*
P/A/V/I *	a	a	a	a	a	a	a	a	a	a	a	i	i
SiO2%	38.90	39.25	38.86	39.18	38.80	38.78	38.88	36.63	36.97	37.73	37.01	39.91	39.93
TiO2%	3.46	3.35	2.67	2.92	3.16	3.27	3.33	2.97	2.89	2.98	3.12	2.63	2.64
Al2O3%	13.68	13.60	13.76	13.76	14.13	13.25	13.18	14.24	14.00	14.90	14.21	12.35	12.02
Cr2O3%	0.00	0.00	0.00	0.00	0.00	0.01	0.00	0.04	0.03	0.00	0.03	0.01	0.00
FeO%total	10.94	10.68	11.78	11.89	12.16	12.50	12.56	13.07	12.58	12.82	13.05	9.93	9.87
V2O3%	0.10	0.11	0.04	0.05	0.07	0.15	0.15	0.00	0.00	0.00	0.00	0.17	0.12
ZnO%	0.00	0.00	0.06	0.00	0.06	0.08	0.00	0.03	0.00	0.00	0.04	0.02	0.20
MnO%	0.22	0.16	0.13	0.18	0.14	0.08	0.10	0.40	0.43	0.30	0.28	0.19	0.18
MgO%	18.53	18.47	17.47	17.42	17.01	17.35	17.38	16.16	16.49	15.22	15.89	19.20	19.25
Ca%O	0.05	0.06	0.07	0.06	0.00	0.03	0.06	0.10	0.09	0.08	0.08	0.04	0.07
Na2O%	0.29	0.28	0.15	0.30	0.21	0.21	0.20	0.14	0.14	0.12	0.14	0.09	0.11
K2O%	10.00	10.01	9.09	9.26	9.78	9.64	9.52	9.06	9.52	9.51	9.34	9.04	8.85
BaO%	0.00	0.00	0.00	0.00	0.00	0.00	0.00	0.00	0.02	0.00	0.00	0.02	0.00
NiO%	0.00	0.03	0.00	0.04	0.05	0.05	0.12	0.00	0.04	0.00	0.00	0.00	0.01
F%	3.16	3.04	2.38	2.42	2.41	2.59	2.45	1.44	1.59	1.68	1.45	2.19	2.21
Cl %	0.09	0.09	0.13	0.13	0.12	0.12	0.11	0.16	0.15	0.14	0.14	0.14	0.10
H2O(c)	2.59	2.65	2.88	2.90	2.90	2.80	2.87	3.21	3.16	3.15	3.23	2.98	2.97
O=F	1.33	1.28	1.00	1.02	1.02	1.09	1.03	0.61	0.67	0.71	0.61	0.92	0.93
O=Cl	0.02	0.02	0.03	0.03	0.03	0.03	0.03	0.04	0.03	0.03	0.03	0.03	0.02
Sum Ox%	100.65	100.48	98.44	99.46	99.97	99.80	99.87	97.03	97.39	97.90	97.37	97.93	97.57
Cations													
Si	5.67	5.72	5.77	5.77	5.71	5.73	5.73	5.58	5.61	5.68	5.62	5.90	5.92
Ti	0.38	0.37	0.30	0.32	0.35	0.36	0.37	0.34	0.33	0.34	0.36	0.29	0.30
Al as AlIV	2.33	2.28	2.23	2.23	2.29	2.27	2.27	2.42	2.39	2.32	2.38	2.10	2.08
AlVI	0.02	0.05	0.18	0.15	0.16	0.03	0.02	0.14	0.12	0.32	0.16	0.05	0.03
Cr	0.00	0.00	0.00	0.00	0.00	0.00	0.00	0.01	0.00	0.00	0.00	0.00	0.00
Fe2+	1.33	1.30	1.46	1.46	1.50	1.54	1.55	1.67	1.60	1.61	1.66	1.23	1.22
V	0.01	0.01	0.01	0.01	0.01	0.02	0.02	0.00	0.00	0.00	0.00	0.02	0.01
Zn	0.00	0.00	0.01	0.00	0.01	0.01	0.00	0.00	0.00	0.00	0.00	0.00	0.02
Mn2+	0.03	0.02	0.02	0.02	0.02	0.01	0.01	0.05	0.06	0.04	0.04	0.02	0.02
Mg	4.03	4.01	3.87	3.82	3.73	3.82	3.82	3.67	3.73	3.41	3.60	4.23	4.26
Ca	0.01	0.01	0.01	0.01	0.00	0.00	0.01	0.02	0.01	0.01	0.01	0.01	0.01
Na	0.08	0.08	0.04	0.09	0.06	0.06	0.06	0.04	0.04	0.03	0.04	0.03	0.03
K	1.86	1.86	1.72	1.74	1.84	1.82	1.79	1.76	1.85	1.83	1.81	1.71	1.67
Ba	0.00	0.00	0.00	0.00	0.00	0.00	0.00	0.00	0.00	0.00	0.00	0.00	0.00
Ni	0.00	0.00	0.00	0.00	0.01	0.01	0.01	0.00	0.00	0.00	0.00	0.00	0.00
F	1.46	1.40	1.12	1.13	1.12	1.21	1.14	0.70	0.77	0.80	0.70	1.02	1.04
Cl	0.02	0.02	0.03	0.03	0.03	0.03	0.03	0.04	0.04	0.04	0.04	0.03	0.03
OH	2.52	2.58	2.85	2.84	2.85	2.76	2.83	3.27	3.20	3.16	3.27	2.94	2.94
Sum Cations	19.74	19.71	19.61	19.63	19.66	19.69	19.67	19.70	19.75	19.59	19.68	19.59	19.58
XMg	0.75	0.76	0.73	0.72	0.71	0.71	0.71	0.69	0.70	0.68	0.69	0.78	0.78
Oct	5.78	5.75	5.83	5.79	5.76	5.79	5.79	5.88	5.84	5.72	5.81	5.83	5.85
Int	1.95	1.95	1.78	1.84	1.89	1.88	1.86	1.82	1.90	1.87	1.86	1.74	1.72
F/Cl	66.18	63.64	34.88	35.19	37.43	40.30	40.86	17.38	20.16	22.22	19.36	30.12	41.48
Mg#	75.12	75.52	72.54	72.30	71.37	71.21	71.15	68.78	70.02	67.91	68.47	77.52	77.66
F/F+Cl	0.99	0.98	0.97	0.97	0.97	0.98	0.98	0.95	0.95	0.96	0.95	0.97	0.98
X[phlog]	0.70	0.70	0.66	0.66	0.65	0.66	0.66	0.62	0.64	0.60	0.62	0.73	0.73
X[sid]	0.10	0.09	0.08	0.08	0.10	0.09	0.09	0.15	0.13	0.13	0.14	0.03	0.02
X[ann]	0.21	0.22	0.26	0.26	0.25	0.25	0.25	0.23	0.23	0.28	0.24	0.24	0.25
Calculations													
IV(F)	1.40	1.43	1.54	1.53	1.51	1.48	1.52	1.75	1.71	1.65	1.74	1.67	1.67
IV(Cl)	-4.29	-4.29	-4.34	-4.34	-4.28	-4.32	-4.28	-4.30	-4.32	-4.22	-4.25	-4.47	-4.34
IV(F/Cl)	5.70	5.72	5.88	5.87	5.80	5.80	5.80	6.05	6.03	5.86	5.99	6.14	6.01
log(XF/XOH)	-0.24	-0.26	-0.41	-0.40	-0.40	-0.36	-0.39	-0.67	-0.62	-0.60	-0.67	-0.46	-0.45
log(XCl/XOH)	-2.06	-2.07	-1.95	-1.95	-1.98	-1.96	-2.00	-1.91	-1.92	-1.94	-1.96	-1.94	-2.07
log(XF/XCl)	1.82	1.80	1.54	1.55	1.57	1.61	1.61	1.24	1.30	1.35	1.29	1.48	1.62
log(fH2O/fHF)	5.09	5.12	5.22	5.21	5.20	5.15	5.18	5.43	5.39	5.34	5.42	4.80	4.80
log(fH2O/FHCl)	4.90	4.91	4.77	4.77	4.79	4.78	4.82	4.71	4.73	4.73	4.75	4.53	4.67
log(fHF/FHCl)	-1.33	-1.36	-1.55	-1.54	-1.49	-1.46	-1.45	-1.77	-1.73	-1.64	-1.71	-1.31	-1.17

* p - primary; a - s* p - primary; a - secondary/alteration; v - vein; i - inclusion

Label	*48_12 _5_1*	*48_12 _5_2*	*48_12 _5_3*	*48_24 _2_1*	*48_24 _2_2*	*E26/55/2/i nclu-maghtQz3*	*E27/68/ 7/_inclu _htQz*	*s6/bi*	*E22_31_ 4_PrimBi in dyke_- 11-1*	*E22_31_ 4_PrimBi in dyke_- 8-1*	*E26_14_ 2_Bi pheno_- 12-1*	*E26_14_ 3_Bi pheno_- 18-1*
P/A/V/I *	i	i	i	i	i	i	i	i	p	p	p	p
SiO2%	40.48	40.68	40.90	39.24	40.11	40.75	40.50	40.58	36.41	36.05	37.16	36.15
TiO2%	2.69	2.72	2.73	2.41	2.77	3.04	2.73	2.31	3.86	3.45	3.66	4.41
Al2O3%	11.60	11.77	11.95	12.22	11.93	13.13	11.47	11.50	14.19	15.04	15.57	14.78
Cr2O3%	0.04	0.00	0.01	0.01	0.00	0.04	0.02	0.01	0.00	0.00	0.00	0.00
FeO%total	7.63	8.25	8.03	9.88	9.73	9.57	10.42	8.61	13.40	16.46	13.83	14.55
V2O3%	0.07	0.07	0.04	0.06	0.08	0.06	0.00	0.12	0.00	0.04	0.08	0.04
ZnO%	0.04	0.03	0.07	0.00	0.05	0.08	0.00	0.04	0.12	0.09	0.07	0.01
MnO%	0.13	0.20	0.17	0.36	0.38	0.15	0.25	0.16	0.50	0.47	0.14	0.12
MgO%	21.03	20.88	21.39	19.41	19.11	19.49	18.94	20.45	16.37	15.01	15.30	15.57
Ca%O	0.00	0.00	0.00	0.00	0.01	0.01	0.01	0.07	0.01	0.04	0.00	0.00
Na2O%	0.17	0.17	0.18	0.13	0.16	0.27	0.22	0.23	0.31	0.34	0.22	0.22
K2O%	9.85	10.03	9.88	9.13	9.63	9.82	9.51	9.52	8.73	8.03	8.45	8.46
BaO%	0.00	0.00	0.00	0.00	0.00	0.00	0.00	0.00	0.02	0.15	0.20	0.23
NiO%	0.00	0.00	0.03	0.00	0.04	0.02	0.02	0.04	0.00	0.07	0.04	0.00
F%	3.60	3.49	3.46	2.82	2.64	3.03	2.53	2.72	1.86	1.57	1.55	1.62
Cl %	0.08	0.04	0.06	0.10	0.10	0.10	0.10	0.08	0.09	0.08	0.10	0.12
H2O(c)	2.36	2.45	2.50	2.65	2.78	2.72	2.83	2.76	3.07	3.22	3.27	3.19
O=F	1.51	1.47	1.46	1.19	1.11	1.27	1.06	1.15	0.78	0.66	0.65	0.68
O=Cl	0.02	0.01	0.01	0.02	0.02	0.02	0.02	0.02	0.02	0.02	0.02	0.03
Sum Ox%	98.24	99.31	99.93	97.21	98.40	100.97	98.47	98.02	98.16	99.43	98.95	98.75
Cations												
Si	5.94	5.92	5.91	5.86	5.93	5.85	5.99	5.98	5.50	5.43	5.54	5.44
Ti	0.30	0.30	0.30	0.27	0.31	0.33	0.30	0.26	0.44	0.39	0.41	0.50
Al as AlIV	2.01	2.02	2.03	2.14	2.07	2.15	2.00	2.00	2.50	2.57	2.46	2.56
AlVI	0.00	0.00	0.00	0.02	0.00	0.07	0.00	0.00	0.02	0.10	0.27	0.06
Cr	0.01	0.00	0.00	0.00	0.00	0.00	0.00	0.00	0.00	0.00	0.00	0.00
Fe2+	0.94	1.00	0.97	1.23	1.20	1.15	1.29	1.06	1.69	2.07	1.72	1.83
V	0.01	0.01	0.01	0.01	0.01	0.01	0.00	0.01	0.00	0.00	0.01	0.01
Zn	0.00	0.00	0.01	0.00	0.01	0.01	0.00	0.00	0.01	0.01	0.01	0.00
Mn2+	0.02	0.03	0.02	0.05	0.05	0.02	0.03	0.02	0.07	0.06	0.02	0.02
Mg	4.60	4.53	4.60	4.32	4.21	4.17	4.17	4.49	3.68	3.37	3.40	3.49
Ca	0.00	0.00	0.00	0.00	0.00	0.00	0.00	0.01	0.00	0.01	0.00	0.00
Na	0.05	0.05	0.05	0.04	0.05	0.07	0.06	0.06	0.09	0.10	0.06	0.06
K	1.84	1.86	1.82	1.74	1.82	1.80	1.79	1.79	1.68	1.54	1.61	1.62
Ba	0.00	0.00	0.00	0.00	0.00	0.00	0.00	0.00	0.00	0.01	0.01	0.01
Ni	0.00	0.00	0.00	0.00	0.01	0.00	0.00	0.01	0.00	0.01	0.01	0.00
F	1.67	1.61	1.58	1.33	1.23	1.37	1.18	1.27	0.89	0.75	0.73	0.77
Cl	0.02	0.01	0.02	0.03	0.02	0.02	0.03	0.02	0.02	0.02	0.03	0.03
OH	2.31	2.38	2.40	2.64	2.74	2.60	2.79	2.71	3.09	3.23	3.25	3.20
Sum Cations	19.70	19.72	19.71	19.67	19.65	19.64	19.64	19.69	19.69	19.67	19.52	19.60
XMg	0.83	0.82	0.83	0.78	0.78	0.78	0.76	0.81	0.69	0.62	0.66	0.66
Oct	5.86	5.86	5.90	5.89	5.78	5.76	5.80	5.84	5.91	6.01	5.83	5.89
Int	1.89	1.91	1.87	1.78	1.86	1.88	1.86	1.86	1.78	1.66	1.68	1.70
F/Cl	79.43	160.80	105.40	49.30	51.33	59.74	47.24	60.43	38.65	39.32	29.16	24.84
Mg#	83.09	81.86	82.59	77.80	77.79	78.41	76.41	80.90	68.53	61.91	66.35	65.60
F/F+Cl	0.99	0.99	0.99	0.98	0.98	0.98	0.98	0.98	0.97	0.98	0.97	0.96
X[phlog]	0.79	0.77	0.78	0.73	0.73	0.72	0.72	0.77	0.62	0.56	0.58	0.59
X[sid]	0.00	0.01	0.01	0.04	0.02	0.04	0.00	0.00	0.17	0.22	0.18	0.20
X[ann]	0.21	0.22	0.21	0.23	0.25	0.23	0.28	0.23	0.20	0.22	0.24	0.20
Calculations												
IV(F)	1.42	1.44	1.46	1.52	1.56	1.48	1.58	1.60	1.61	1.62	1.67	1.65
IV(Cl)	-4.48	-4.13	-4.31	-4.44	-4.36	-4.36	-4.35	-4.38	-4.08	-3.86	-4.02	-4.14
IV(F/Cl)	5.91	5.56	5.77	5.95	5.92	5.84	5.93	5.98	5.69	5.49	5.69	5.78
log(XF/XOH)	-0.14	-0.17	-0.18	-0.30	-0.35	-0.28	-0.37	-0.33	-0.54	-0.64	-0.65	-0.62
log(XCl/XOH)	-2.04	-2.38	-2.20	-1.99	-2.06	-2.05	-2.05	-2.11	-2.13	-2.23	-2.11	-2.01
log(XF/XCl)	1.90	2.21	2.02	1.69	1.71	1.78	1.67	1.78	1.59	1.59	1.46	1.40
log(fH2O/fHF)	4.56	4.58	4.60	4.65	4.70	4.63	4.70	4.72	4.18	4.20	4.26	4.23
log(fH2O/FHCl)	4.67	5.00	4.83	4.59	4.66	4.65	4.64	4.73	4.38	4.44	4.35	4.25
log(fHF/FHCl)	-1.00	-0.67	-0.87	-1.10	-1.08	-1.03	-1.09	-1.07	-0.58	-0.46	-0.66	-0.72

* p - primary; a - s* p - primary; a - secondary/alteration; v - vein; i - inclusion

Label	E26_14_ 3_Bi pheno_- 20-1	E26_14_ 3_Bi pheno_- 21-1	E26_14 _3_Bi pheno_- 23-1	E26_14 _4_bi pheno_- 25-1	E26_14 _4_bi pheno2 _-33-1	E26_14 _4_bi pheno2 _-34-1	E26_1 4_1_bi in Kfs_- 2-1	E26_14 _1a_bi in Kfs_- 3-1	E27/2 6/1/bi- p1	E27/26 /1/bi- p2	E27_76 _a_bi_- 1-1	E27_7 6_b_bi _-10-1
P/A/V/I *	p	p	p	p	p	p	pk	pk	p	p	p	p
SiO2%	36.70	36.14	36.55	36.51	34.56	36.48	36.53	36.30	36.69	36.46	35.65	37.77
TiO2%	4.47	4.68	4.48	4.35	4.76	4.47	3.48	4.61	4.43	3.96	3.73	3.96
Al2O3%	14.59	14.25	14.44	15.17	15.65	15.37	15.39	15.17	13.93	13.92	15.64	13.42
Cr2O3%	0.01	0.01	0.00	0.06	0.00	0.04	0.00	0.00	0.00	0.00	0.05	0.00
FeO%total	13.88	13.82	13.86	14.42	14.07	14.05	14.14	14.17	15.02	14.88	13.88	13.69
V2O3%	0.02	0.00	0.00	0.01	0.10	0.04	0.00	0.01	0.00	0.00	0.04	0.05
ZnO%	0.00	0.01	0.03	0.00	0.00	0.03	0.00	0.03	0.08	0.10	0.05	0.02
MnO%	0.14	0.14	0.17	0.12	0.22	0.09	0.17	0.23	0.58	0.61	0.33	0.28
MgO%	15.32	14.89	15.59	15.35	16.37	15.30	16.27	15.24	14.69	15.05	16.42	16.46
Ca%O	0.00	0.00	0.00	0.05	0.03	0.05	0.04	0.03	0.05	0.00	0.05	0.01
Na2O%	0.29	0.24	0.25	0.25	0.19	0.18	0.20	0.24	0.33	0.23	0.18	0.32
K2O%	9.52	9.17	9.43	8.26	6.94	7.72	7.87	8.52	9.64	9.50	6.75	9.45
BaO%	0.37	1.29	0.30	0.27	0.15	0.12	0.03	0.34	0.19	0.09	0.10	0.00
NiO%	0.02	0.00	0.00	0.01	0.00	0.00	0.01	0.02	0.00	0.04	0.00	0.01
F%	1.71	1.69	1.75	1.70	1.73	1.79	1.56	1.59	1.47	1.44	1.69	2.01
Cl %	0.13	0.16	0.15	0.14	0.12	0.12	0.11	0.13	0.11	0.13	0.08	0.10
H2O(c)	3.16	3.11	3.13	3.17	3.10	3.12	3.24	3.22	3.26	3.24	3.15	3.05
O=F	0.72	0.71	0.74	0.72	0.73	0.75	0.66	0.67	0.62	0.61	0.71	0.85
O=Cl	0.03	0.04	0.03	0.03	0.03	0.03	0.02	0.03	0.02	0.03	0.02	0.02
Sum Ox%	99.59	98.85	99.38	99.08	97.25	98.19	98.37	99.13	99.83	99.02	97.05	99.74
Cations												
Si	5.49	5.48	5.48	5.46	5.24	5.47	5.47	5.43	5.52	5.52	5.39	5.62
Ti	0.50	0.53	0.51	0.49	0.54	0.50	0.39	0.52	0.50	0.45	0.42	0.44
Al as AlIV	2.51	2.52	2.52	2.54	2.76	2.53	2.53	2.57	2.47	2.48	2.61	2.35
AlVI	0.06	0.03	0.03	0.13	0.04	0.18	0.18	0.11	0.00	0.01	0.17	0.00
Cr	0.00	0.00	0.00	0.01	0.00	0.00	0.00	0.00	0.00	0.00	0.01	0.00
Fe2+	1.74	1.75	1.74	1.80	1.78	1.76	1.77	1.77	1.89	1.88	1.75	1.70
V	0.00	0.00	0.00	0.00	0.01	0.01	0.00	0.00	0.00	0.00	0.01	0.01
Zn	0.00	0.00	0.00	0.00	0.00	0.00	0.00	0.00	0.01	0.01	0.01	0.00
Mn2+	0.02	0.02	0.02	0.02	0.03	0.01	0.02	0.03	0.07	0.08	0.04	0.04
Mg	3.42	3.37	3.48	3.42	3.70	3.42	3.63	3.40	3.29	3.40	3.70	3.65
Ca	0.00	0.00	0.00	0.01	0.01	0.01	0.01	0.00	0.01	0.00	0.01	0.00
Na	0.08	0.07	0.07	0.07	0.06	0.05	0.06	0.07	0.10	0.07	0.05	0.09
K	1.82	1.78	1.80	1.58	1.34	1.48	1.50	1.63	1.85	1.84	1.30	1.79
Ba	0.02	0.08	0.02	0.02	0.01	0.01	0.00	0.02	0.01	0.01	0.01	0.00
Ni	0.00	0.00	0.00	0.00	0.00	0.00	0.00	0.00	0.00	0.00	0.00	0.00
F	0.81	0.81	0.83	0.80	0.83	0.85	0.74	0.75	0.70	0.69	0.81	0.95
Cl	0.03	0.04	0.04	0.03	0.03	0.03	0.03	0.03	0.03	0.03	0.02	0.02
OH	3.16	3.15	3.13	3.16	3.14	3.12	3.23	3.21	3.27	3.28	3.17	3.03
Sum Cations	19.67	19.63	19.68	19.54	19.51	19.43	19.57	19.56	19.72	19.74	19.47	19.70
XMg	0.66	0.66	0.67	0.66	0.68	0.66	0.67	0.66	0.64	0.64	0.68	0.68
Oct	5.74	5.71	5.78	5.86	6.09	5.88	6.00	5.84	5.77	5.83	6.10	5.84
Int	1.92	1.92	1.90	1.67	1.41	1.54	1.57	1.72	1.97	1.91	1.37	1.89
F/Cl	23.79	19.76	22.41	23.62	26.81	29.21	27.41	23.56	24.93	20.32	36.73	39.42
Mg#	66.30	65.78	66.72	65.49	67.46	65.99	67.22	65.71	63.55	64.31	67.82	68.19
F/F+Cl	0.96	0.95	0.96	0.96	0.96	0.97	0.96	0.96	0.96	0.95	0.97	0.98
X[phlog]	0.59	0.59	0.60	0.58	0.61	0.58	0.61	0.58	0.57	0.58	0.61	0.63
X[sid]	0.19	0.19	0.19	0.20	0.25	0.20	0.19	0.21	0.19	0.18	0.21	0.13
X[ann]	0.22	0.22	0.21	0.21	0.15	0.22	0.20	0.21	0.24	0.23	0.18	0.24
Calculations												
IV(F)	1.62	1.62	1.62	1.61	1.61	1.58	1.68	1.64	1.68	1.70	1.63	1.58
IV(Cl)	-4.19	-4.26	-4.24	-4.17	-4.18	-4.10	-4.10	-4.13	-4.04	-4.15	-4.02	-4.12
IV(F/Cl)	5.82	5.88	5.86	5.78	5.79	5.68	5.78	5.78	5.72	5.85	5.66	5.70
log(XF/XOH)	-0.59	-0.59	-0.58	-0.60	-0.58	-0.57	-0.64	-0.63	-0.67	-0.68	-0.59	-0.51
log(XCl/XOH)	-1.97	-1.89	-1.93	-1.97	-2.01	-2.03	-2.08	-2.00	-2.07	-1.98	-2.16	-2.10
log(XF/XCl)	1.38	1.30	1.35	1.37	1.43	1.47	1.44	1.37	1.40	1.31	1.56	1.60
log(fH2O/fHF)	4.21	4.20	4.20	4.20	4.21	4.18	4.27	4.24	4.25	4.27	4.23	4.14
log(fH2O/FHCl)	4.20	4.12	4.17	4.20	4.25	4.27	4.32	4.24	4.29	4.21	4.40	4.35
log(fHF/FHCl)	-0.75	-0.82	-0.78	-0.74	-0.72	-0.66	-0.71	-0.75	-0.68	-0.79	-0.59	-0.56

* p - primary; a - s* p - primary; a - secondary/alteration; v - vein; i - inclusion

Label	E27_76_b_bi_-11-1	E27_76_b_bi_-12-1	E27_76_b_bi_-13-1	E27_76_b_bi_-14-1	E27_76_b_bi_-15-1	E27_76_b_bi_-6-1	E27_76_b_bi_-7-1	E27_76_b_bi_-9-1	E22/12/3/Bi-pheno-Kfs	E22/12/3/Bi-pheno-Kfs1	E22/12/4/Bi-pheno-Kfs	E22/12/4/Bi-pheno-Kfs1	E22/12/4/Bi-pheno-Kfs2
P/A/V/I *	p	p	p	p	p	p	p	p	pk	pk	pk	pk	pk
SiO2%	36.67	37.56	37.42	37.37	37.89	36.78	37.63	36.06	37.27	37.06	36.61	36.80	36.62
TiO2%	3.98	4.41	4.57	4.33	4.23	4.19	4.12	4.01	4.14	3.98	4.05	4.11	3.81
Al2O3%	14.54	13.70	13.71	13.76	13.55	13.69	13.68	14.24	14.05	14.62	14.17	14.18	14.16
Cr2O3%	0.04	0.00	0.00	0.02	0.00	0.02	0.00	0.00	0.05	0.01	0.00	0.00	0.00
FeO%total	14.00	13.69	14.11	14.06	13.92	14.67	13.87	14.84	14.12	14.34	14.78	14.38	14.28
V2O3%	0.06	0.00	0.02	0.06	0.06	0.06	0.02	0.08	0.00	0.00	0.00	0.00	0.00
ZnO%	0.00	0.00	0.00	0.02	0.00	0.00	0.07	0.14	0.00	0.06	0.02	0.29	0.05
MnO%	0.44	0.35	0.31	0.34	0.36	0.33	0.28	0.29	0.23	0.27	0.55	0.59	0.52
MgO%	16.20	16.23	15.93	16.22	16.38	15.95	16.22	16.11	15.70	15.25	15.10	15.27	15.27
Ca%O	0.02	0.10	0.02	0.00	0.00	0.04	0.01	0.04	0.00	0.00	0.00	0.00	0.01
Na2O%	0.22	0.38	0.39	0.35	0.35	0.29	0.36	0.30	0.34	0.35	0.34	0.38	0.35
K2O%	7.99	9.30	9.42	8.93	9.52	8.92	9.08	7.96	9.75	9.29	9.60	9.71	9.41
BaO%	0.00	0.00	0.00	0.00	0.00	0.28	0.00	0.00	0.09	0.00	0.05	0.00	0.00
NiO%	0.03	0.01	0.00	0.00	0.00	0.00	0.00	0.05	0.06	0.03	0.00	0.00	0.00
F%	1.84	1.84	1.86	1.84	1.86	1.80	1.94	1.85	1.74	1.60	1.62	1.64	1.65
Cl %	0.08	0.08	0.10	0.12	0.10	0.10	0.11	0.11	0.11	0.09	0.11	0.10	0.07
H2O(c)	3.11	3.15	3.13	3.13	3.15	3.12	3.08	3.07	3.17	3.23	3.19	3.20	3.17
O=F	0.77	0.78	0.78	0.77	0.78	0.76	0.82	0.78	0.73	0.67	0.68	0.69	0.70
O=Cl	0.02	0.02	0.02	0.03	0.02	0.02	0.03	0.02	0.03	0.02	0.03	0.02	0.02
Sum Ox%	98.43	100.02	100.18	99.73	100.56	99.45	99.65	98.34	100.08	99.50	99.49	99.96	98.66
Cations													
Si	5.50	5.57	5.56	5.56	5.60	5.52	5.60	5.45	5.55	5.54	5.51	5.51	5.54
Ti	0.45	0.49	0.51	0.48	0.47	0.47	0.46	0.46	0.46	0.45	0.46	0.46	0.43
Al as AlIV	2.50	2.40	2.40	2.41	2.36	2.42	2.40	2.53	2.45	2.46	2.49	2.49	2.46
AlVI	0.07	0.00	0.00	0.00	0.00	0.00	0.00	0.00	0.02	0.11	0.02	0.01	0.06
Cr	0.01	0.00	0.00	0.00	0.00	0.00	0.00	0.00	0.01	0.00	0.00	0.00	0.00
Fe2+	1.76	1.70	1.75	1.75	1.72	1.84	1.73	1.88	1.76	1.79	1.86	1.80	1.81
V	0.01	0.00	0.00	0.01	0.01	0.01	0.00	0.01	0.00	0.00	0.00	0.00	0.00
Zn	0.00	0.00	0.00	0.00	0.00	0.00	0.01	0.02	0.00	0.01	0.00	0.03	0.01
Mn2+	0.06	0.04	0.04	0.04	0.05	0.04	0.04	0.04	0.03	0.04	0.07	0.08	0.07
Mg	3.62	3.59	3.53	3.60	3.61	3.57	3.60	3.63	3.49	3.40	3.39	3.41	3.44
Ca	0.00	0.02	0.00	0.00	0.00	0.01	0.00	0.01	0.00	0.00	0.00	0.00	0.00
Na	0.06	0.11	0.11	0.10	0.10	0.08	0.10	0.09	0.10	0.10	0.10	0.11	0.10
K	1.53	1.76	1.78	1.69	1.80	1.71	1.72	1.53	1.85	1.77	1.84	1.86	1.81
Ba	0.00	0.00	0.00	0.00	0.00	0.02	0.00	0.00	0.01	0.00	0.00	0.00	0.00
Ni	0.00	0.00	0.00	0.00	0.00	0.00	0.00	0.01	0.01	0.00	0.00	0.00	0.00
F	0.87	0.86	0.87	0.86	0.87	0.85	0.91	0.88	0.82	0.76	0.77	0.78	0.79
Cl	0.02	0.02	0.03	0.03	0.02	0.02	0.03	0.03	0.03	0.02	0.03	0.03	0.02
OH	3.11	3.12	3.10	3.11	3.11	3.12	3.06	3.09	3.15	3.22	3.20	3.20	3.19
Sum Cations	19.56	19.68	19.68	19.65	19.70	19.69	19.66	19.64	19.72	19.66	19.75	19.76	19.73
XMg	0.67	0.68	0.67	0.67	0.68	0.66	0.68	0.66	0.67	0.66	0.65	0.65	0.66
Oct	5.96	5.82	5.83	5.88	5.84	5.93	5.83	6.02	5.77	5.79	5.80	5.79	5.81
Int	1.60	1.89	1.90	1.80	1.90	1.81	1.83	1.63	1.96	1.87	1.94	1.97	1.92
F/Cl	41.52	43.20	34.96	27.87	36.21	35.58	31.45	32.74	28.31	32.91	26.62	29.88	46.41
Mg#	67.34	67.86	66.82	67.27	67.72	65.95	67.59	65.93	66.46	65.46	64.56	65.43	65.59
F/F+Cl	0.98	0.98	0.97	0.97	0.97	0.97	0.97	0.97	0.97	0.97	0.96	0.97	0.98
X[phlog]	0.61	0.62	0.61	0.61	0.62	0.60	0.62	0.60	0.60	0.59	0.58	0.59	0.59
X[sid]	0.18	0.15	0.15	0.15	0.14	0.16	0.15	0.19	0.17	0.18	0.19	0.19	0.18
X[ann]	0.21	0.24	0.24	0.23	0.25	0.23	0.24	0.20	0.23	0.24	0.23	0.23	0.23
Calculations													
IV(F)	1.60	1.62	1.60	1.61	1.62	1.61	1.59	1.58	1.63	1.65	1.64	1.64	1.64
IV(Cl)	-4.01	-4.01	-4.08	-4.19	-4.09	-4.06	-4.18	-4.12	-4.14	-4.00	-4.09	-4.06	-3.88
IV(F/Cl)	5.61	5.63	5.69	5.80	5.71	5.67	5.77	5.70	5.77	5.65	5.73	5.70	5.52
log(XF/XOH)	-0.55	-0.56	-0.55	-0.56	-0.55	-0.56	-0.53	-0.54	-0.58	-0.63	-0.62	-0.61	-0.61
log(XCl/XOH)	-2.17	-2.19	-2.09	-2.00	-2.11	-2.11	-2.02	-2.06	-2.04	-2.15	-2.04	-2.09	-2.27
log(XF/XCl)	1.62	1.64	1.54	1.45	1.56	1.55	1.50	1.52	1.45	1.52	1.43	1.48	1.67
log(fH2O/fHF)	4.18	4.19	4.17	4.18	4.18	4.17	4.16	4.15	4.20	4.24	4.21	4.22	4.21
log(fH2O/FHCl)	4.41	4.44	4.33	4.24	4.36	4.35	4.27	4.29	4.27	4.38	4.27	4.32	4.51
log(fHF/FHCl)	-0.53	-0.52	-0.59	-0.70	-0.59	-0.57	-0.65	-0.61	-0.68	-0.60	-0.67	-0.64	-0.45

* p - primary; a - s* p - primary; a - secondary/alteration; v - vein; i - inclusion

Label	E22/12/4/Bi-pheno-Kfs3	E22/12/4/Bi-pheno-Kfs4	E27/68/5/biotite_p_pheno	E27/68/5/biotite_p_pheno2	E26_55_primBi-1	E26_55_primBi-2	E26_55_primBi-3	E26_55_primBi-4	E26_55_primBi-5	E26_55_primBi-7
P/A/V/I *	pk	pk	po	po	po	po	po	po	po	po
SiO2%	36.53	36.67	37.31	37.16	37.98	37.87	37.97	38.01	37.91	37.88
TiO2%	4.02	4.03	4.01	4.05	4.20	4.37	4.24	4.11	4.31	4.24
Al2O3%	14.28	13.88	13.98	13.64	13.90	13.64	13.71	13.73	13.68	13.88
Cr2O3%	0.00	0.03	0.05	0.00	0.00	0.00	0.01	0.00	0.02	0.04
FeO%total	14.59	14.02	13.06	13.19	11.62	11.74	11.54	10.98	10.91	11.64
V2O3%	0.00	0.00	0.00	0.00	0.01	0.02	0.06	0.09	0.08	0.09
ZnO%	0.02	0.10	0.03	0.12	0.00	0.05	0.05	0.08	0.05	0.05
MnO%	0.52	0.55	0.30	0.31	0.14	0.20	0.22	0.17	0.19	0.20
MgO%	15.09	15.36	15.84	15.79	17.60	17.31	17.48	18.06	17.75	17.21
Ca%O	0.00	0.00	0.02	0.01	0.01	0.00	0.05	0.00	0.00	0.00
Na2O%	0.32	0.32	0.37	0.30	0.36	0.36	0.39	0.36	0.39	0.36
K2O%	9.53	9.75	9.56	9.42	9.76	9.59	9.63	9.71	9.59	9.62
BaO%	0.15	0.00	0.04	0.11	0.00	0.00	0.00	0.00	0.00	0.00
NiO%	0.05	0.00	0.00	0.00	0.00	0.04	0.00	0.06	0.00	0.06
F%	1.67	1.72	1.93	1.91	2.40	2.52	2.49	2.57	2.47	2.53
Cl %	0.09	0.11	0.09	0.15	0.11	0.09	0.09	0.08	0.09	0.10
H2O(c)	3.16	3.13	3.06	3.03	2.91	2.84	2.86	2.83	2.87	2.84
O=F	0.70	0.72	0.81	0.80	1.01	1.06	1.05	1.08	1.04	1.06
O=Cl	0.02	0.02	0.02	0.03	0.03	0.02	0.02	0.02	0.02	0.02
Sum Ox%	99.29	98.93	98.83	98.34	99.97	99.56	99.73	99.74	99.25	99.65
Cations										
Si	5.51	5.54	5.59	5.61	5.59	5.60	5.60	5.59	5.60	5.60
Ti	0.46	0.46	0.45	0.46	0.47	0.49	0.47	0.46	0.48	0.47
Al as AlIV	2.49	2.46	2.41	2.39	2.41	2.38	2.38	2.38	2.38	2.41
AlVI	0.04	0.01	0.07	0.03	0.00	0.00	0.00	0.00	0.00	0.01
Cr	0.00	0.00	0.01	0.00	0.00	0.00	0.00	0.00	0.00	0.01
Fe2+	1.84	1.77	1.64	1.67	1.43	1.45	1.42	1.35	1.35	1.44
V	0.00	0.00	0.00	0.00	0.00	0.00	0.01	0.01	0.01	0.01
Zn	0.00	0.01	0.00	0.01	0.00	0.01	0.01	0.01	0.01	0.01
Mn2+	0.07	0.07	0.04	0.04	0.02	0.03	0.03	0.02	0.02	0.03
Mg	3.39	3.46	3.54	3.55	3.86	3.82	3.84	3.96	3.91	3.79
Ca	0.00	0.00	0.00	0.00	0.00	0.00	0.01	0.00	0.00	0.00
Na	0.09	0.10	0.11	0.09	0.10	0.10	0.11	0.10	0.11	0.10
K	1.83	1.88	1.83	1.81	1.83	1.81	1.81	1.82	1.81	1.81
Ba	0.01	0.00	0.00	0.01	0.00	0.00	0.00	0.00	0.00	0.00
Ni	0.01	0.00	0.00	0.00	0.00	0.00	0.00	0.01	0.00	0.01
F	0.80	0.82	0.92	0.91	1.12	1.18	1.16	1.20	1.15	1.18
Cl	0.02	0.03	0.02	0.04	0.03	0.02	0.02	0.02	0.02	0.03
OH	3.18	3.15	3.06	3.05	2.85	2.80	2.82	2.78	2.82	2.79
Sum Cations	19.73	19.75	19.68	19.67	19.71	19.68	19.69	19.72	19.68	19.68
XMg	0.65	0.66	0.68	0.68	0.73	0.72	0.73	0.75	0.74	0.73
Oct	5.80	5.78	5.74	5.76	5.77	5.79	5.77	5.80	5.77	5.75
Int	1.93	1.97	1.94	1.91	1.94	1.91	1.93	1.93	1.92	1.92
F/Cl	34.61	30.41	38.13	24.65	39.93	53.50	50.43	59.85	52.45	47.24
Mg#	64.84	66.13	68.36	68.09	72.98	72.44	72.98	74.57	74.36	72.48
F/F+Cl	0.97	0.97	0.97	0.96	0.98	0.98	0.98	0.98	0.98	0.98
X[phlog]	0.58	0.60	0.62	0.62	0.67	0.66	0.67	0.68	0.68	0.66
X[sid]	0.19	0.17	0.15	0.14	0.13	0.13	0.12	0.12	0.12	0.13
X[ann]	0.23	0.23	0.24	0.24	0.20	0.22	0.21	0.20	0.20	0.21
Calculations										
IV(F)	1.62	1.62	1.59	1.59	1.53	1.49	1.51	1.51	1.53	1.49
IV(Cl)	-4.00	-4.10	-4.09	-4.28	-4.29	-4.18	-4.21	-4.18	-4.21	-4.23
IV(F/Cl)	5.62	5.72	5.68	5.87	5.83	5.67	5.72	5.69	5.74	5.72
log(XF/XOH)	-0.60	-0.58	-0.52	-0.52	-0.41	-0.38	-0.39	-0.37	-0.39	-0.37
log(XCl/XOH)	-2.14	-2.07	-2.11	-1.92	-2.01	-2.10	-2.09	-2.14	-2.11	-2.05
log(XF/XCl)	1.54	1.48	1.58	1.39	1.60	1.73	1.70	1.78	1.72	1.67
log(fH2O/fHF)	4.20	4.20	4.16	4.16	4.10	4.06	4.08	4.08	4.10	4.06
log(fH2O/FHCl)	4.37	4.30	4.35	4.16	4.28	4.38	4.36	4.43	4.39	4.32
log(fHF/FHCl)	-0.56	-0.64	-0.58	-0.77	-0.64	-0.50	-0.54	-0.49	-0.55	-0.56

* p - primary; a - s* p - primary; a - secondary/alteration; v - vein; i - inclusion

Label	CS16 2/1/ap a1_ri m1	CS162 /1/apa 1_core 1-1-1	CS16 2/1/ap a1_ri m2	CS16 2/1/ap a1i_co re1	CS16 2/2/ap a1_tra v-2	CS16 2/2/ap a1_tra v-3	CS16 2/2/ap a2_tra v-1	CS16 2/2/ap a2_tra v-2	CS16 2/2/ap a2_tra v-3	CS16 2/3/ap a_trav- 1	CS16 2/3/ap a_trav- 2	CS16 2/3/ap a_trav- 3	CS16 2/3/ap a_trav- 4	CS16 2/3/ap a_trav- 5
SiO2%	0.23	0.2	0.27	0.2	0.37	0.32	0.86	0.18	0.25	0.26	0.21	0.2	0.21	0.31
Fe2O3%	0.57	0.57	0.29	0.57	0.37	0.43	0.35	0.6	0.3	0.32	0.52	0.57	0.64	0.54
MnO%	0.09	0.09	0.06	0.11	0.1	0.06	0.11	0.08	0.08	0.11	0.08	0.13	0.14	0.12
MgO%	0.05	0.19	0.02	0.19	0.03	0.04	0.03	0.22	0.03	0.04	0.13	0.18	0.18	0.03
CaO%	53.77	53.72	53.56	54.07	53.41	53.65	53.63	53.59	53.73	53.4	54.08	53.66	54.39	54.11
Na2O%	0.06	0.04	0.12	0.06	0.13	0.11	0.13	0.03	0.09	0.09	0.04	0.02	0.02	0.1
P2O5%	41.84	42.01	41.68	42.06	41.32	42.11	41.36	41.89	42.02	41.61	41.46	42.06	41.61	41.98
SO3%	0	0	0	0	0.01	0.02	0.01	0	0.01	0	0.01	0	0.01	0.01
La2O3%	0.12	0.08	0.18	0.06	0.22	0.16	0.18	0.08	0.16	0.15	0.1	0.07	0.08	0.17
Ce2O3%	0.32	0.16	0.46	0.16	0.48	0.35	0.41	0.15	0.36	0.36	0.23	0.17	0.18	0.38
Pr2O3%	0.06	0	0.07	0.03	0.06	0.04	0.11	0	0	0.1	0	0	0	0
Nd2O3%	0.21	0.15	0.28	0.13	0.3	0.31	0.26	0.19	0.24	0.3	0.15	0.17	0.17	0.25
Sm2O3%	0.06	0	0	0.01	0.08	0.02	0.05	0.07	0.05	0.01	0.05	0.05	0.06	0.07
Y2O3%	0.1	0.04	0.1	0.04	0.16	0.14	0.09	0.05	0.1	0.13	0.09	0.09	0.06	0.14
SrO%	0.06	0.11	0	0.13	0	0.02	0.01	0.13	0.02	0.01	0.11	0.13	0.12	0.01
BaO%	0.01	0	0	0	0	0	0	0	0.01	0.01	0	0	0	0
As2O3%	0.01	0	0	0	0.02	0	0.01	0	0	0	0	0	0	0
F%	3.05	2.83	3.26	3.27	3.3	3.45	3.58	3.22	3.63	3.46	3.17	2.85	2.95	3.28
Cl%	0.61	0.65	0.59	0.64	0.55	0.56	0.49	0.62	0.55	0.54	0.57	0.63	0.55	0.7
H2O(c)	0.17	0.27	0.07	0.07	0.06	0.01	0	0.09	0	0	0.12	0.27	0.24	0.05
O=F	1.28	1.19	1.37	1.38	1.39	1.45	1.51	1.36	1.53	1.46	1.34	1.2	1.24	1.38
O=Cl	0.14	0.15	0.13	0.14	0.12	0.13	0.11	0.14	0.12	0.12	0.13	0.14	0.12	0.16
Sum Ox%	99.95	99.78	99.51	100.3	99.46	100.2	100	99.71	99.98	99.34	99.65	99.9	100.2	100.7
Cations														
Si	0.038	0.034	0.046	0.033	0.063	0.054	0.145	0.031	0.042	0.044	0.035	0.033	0.036	0.052
Fe3+	0.072	0.072	0.038	0.072	0.047	0.055	0.044	0.077	0.039	0.041	0.066	0.072	0.081	0.068
Mn2+	0.013	0.013	0.009	0.016	0.015	0.008	0.015	0.012	0.012	0.016	0.012	0.018	0.019	0.016
Mg	0.012	0.047	0.006	0.047	0.008	0.009	0.008	0.056	0.008	0.01	0.033	0.046	0.046	0.006
Ca	9.731	9.708	9.739	9.737	9.741	9.672	9.706	9.703	9.718	9.729	9.825	9.689	9.824	9.735
Na	0.019	0.014	0.039	0.019	0.042	0.035	0.043	0.01	0.028	0.028	0.014	0.008	0.006	0.032
P	5.984	5.999	5.989	5.984	5.954	5.999	5.914	5.993	6.005	5.99	5.952	6.001	5.938	5.967
S	0	0	0	0.001	0.001	0.002	0.001	0	0.001	0	0.001	0	0.002	0.001
La	0.008	0.005	0.011	0.004	0.014	0.01	0.012	0.005	0.01	0.009	0.006	0.004	0.005	0.011
Ce	0.02	0.01	0.028	0.01	0.03	0.022	0.025	0.009	0.023	0.023	0.014	0.01	0.011	0.024
Pr	0.003	0	0.005	0.002	0.004	0.003	0.007	0	0	0.006	0	0	0	0
Nd	0.013	0.009	0.017	0.008	0.018	0.019	0.016	0.012	0.014	0.018	0.009	0.01	0.01	0.015
Sm	0.003	0	0	0.001	0.004	0.001	0.003	0.004	0.003	0.001	0.003	0.003	0.003	0.004
Y	0.009	0.004	0.009	0.004	0.015	0.013	0.008	0.005	0.009	0.012	0.008	0.008	0.006	0.013
Sr	0.005	0.01	0	0.013	0	0.002	0.001	0.013	0.002	0.001	0.011	0.012	0.012	0.001
Ba	0	0	0	0	0	0	0	0	0.001	0	0	0	0	0
As	0.001	0	0	0	0.002	0	0.001	0	0	0	0	0	0	0
F	1.629	1.508	1.753	1.736	1.778	1.834	1.911	1.722	1.941	1.859	1.702	1.518	1.571	1.74
Cl	0.174	0.186	0.169	0.183	0.158	0.159	0.141	0.178	0.158	0.157	0.165	0.18	0.157	0.2
OH	0.197	0.306	0.078	0.081	0.064	0.007	0.001	0.1	0.001	0.001	0.134	0.302	0.272	0.06
Sum Cat#	17.93	17.925	17.94	17.95	17.96	17.9	18	17.93	18.01	17.95	17.99	17.92	18	17.94

Label	E22_3 1_2_2 ndapa ?_-7-1	E22_3 1_2_2 ndapa ?_-7-2	E22_3 1_2_2 ndapa ?_-7-3	E22_3 2_3_a pa2nd ?_-1	E22_3 2_3_a pa2nd ?_-2	E22_3 2_3_a pa2nd ?_-3	E22_3 2_3_a pa2nd ?_-4	E22_3 2_3_a pa2nd ?_-5	E22_3 2_3_a pa2nd ?2_-1	E22_3 2_3_a pa2nd ?2_-2	E26_7 0_apa ?-15-1	E26_7 0_apa ?-16-1	E26_7 0_apa ?-18-1	E26_7 0_2nd ?apa- 22-1
SiO2%	0.15	0.11	0.13	0.13	0.13	0.13	0.14	0.21	0.19	0.18	0.55	0.29	0.36	0.34
Fe2O3%	0.17	0.16	0.15	0.27	0.34	0.3	0.39	0.19	0.18	0.09	0.21	0.26	0.29	0.18
MnO%	0.09	0.15	0.13	0.13	0.1	0.13	0.14	0.1	0.11	0.12	0.38	0.46	0.52	0.2
MgO%	0.04	0.04	0.04	0.03	0.01	0.02	0.03	0.03	0.03	0.03	0.08	0.09	0.09	0.04
CaO%	55.29	54.98	54.89	54.5	54.4	53.39	54.57	54.35	54.18	53.88	53.89	53.36	53.46	54.59
Na2O%	0.14	0.15	0.18	0.02	0.05	0.02	0.04	0.05	0.06	0.07	0.17	0.19	0.27	0.12
P2O5%	40.84	40.52	40.53	40.8	40.32	40.82	40.55	40.31	40.27	40.65	41.37	40.97	40.6	40.96
SO3%	0.29	0.24	0.3	0.05	0.09	0.06	0.06	0.14	0.09	0.07	0.16	0.34	0.52	0.21
La2O3%	0.06	0.04	0.06	0.06	0.05	0.04	0.04	0.06	0.06	0.07	0.09	0.14	0.11	0.14
Ce2O3%	0.12	0.13	0.13	0.11	0.13	0.1	0.11	0.12	0.17	0.16	0.19	0.24	0.24	0.29
Pr2O3%	0	0	0.01	0	0.02	0	0	0.04	0	0.02	0.03	0	0	0.03
Nd2O3%	0.08	0.09	0.15	0.08	0.12	0.13	0.1	0.07	0.05	0.08	0.09	0.13	0.15	0.11
Sm2O3%	0.05	0.07	0.05	0	0	0.05	0	0.02	0.03	0.04	0.04	0.09	0.02	0.03
Y2O3%	0.15	0.13	0.12	0.04	0.05	0.07	0.04	0.07	0.09	0.07	0.2	0.2	0.28	0.16
SrO%	0.04	0.03	0.03	0.08	0.1	0.13	0.12	0.09	0.12	0.13	0.08	0.06	0.07	0.07
BaO%	0	0	0	0	0	0	0	0	0	0.02	0.01	0	0	0
As2O3%	0.01	0	0.02	0.01	0.01	0	0.01	0	0	0	0	0	0	0.01
F%	3.3	3.49	3.45	3.2	3.18	3.24	3.28	3.09	3.3	3.29	4.07	3.81	3.59	3.41
Cl%	0.39	0.34	0.41	0.32	0.32	0.33	0.34	0.33	0.33	0.34	0.36	0.44	0.41	0.39
H2O(c)	0.11	0.01	0.02	0.15	0.15	0.12	0.1	0.19	0.09	0.09	0	0	0	0.05
O=F	1.39	1.47	1.45	1.35	1.34	1.36	1.38	1.3	1.39	1.39	1.71	1.6	1.51	1.44
O=Cl	0.09	0.08	0.09	0.07	0.07	0.07	0.08	0.07	0.07	0.08	0.08	0.1	0.09	0.09
Sum Ox%	99.83	99.14	99.26	98.55	98.17	97.64	98.6	98.08	97.89	97.93	100.2	99.37	99.36	99.8
Cations														
Si	0.026	0.019	0.022	0.02	0.02	0.02	0.03	0.04	0.03	0.03	0.093	0.049	0.062	0.057
Fe3+	0.022	0.02	0.02	0.04	0.04	0.04	0.05	0.03	0.02	0.01	0.026	0.034	0.038	0.023
Mn2+	0.013	0.022	0.019	0.02	0.02	0.02	0.02	0.01	0.02	0.02	0.054	0.067	0.075	0.028
Mg	0.01	0.011	0.01	0.01	0	0	0.01	0.01	0.01	0.01	0.02	0.022	0.022	0.011
Ca	10.047	10.07	10.044	10.01	10.06	9.88	10.04	10.04	10.04	9.96	9.75	9.739	9.755	9.922
Na	0.045	0.049	0.06	0.007	0.016	0.006	0.013	0.016	0.019	0.023	0.055	0.063	0.088	0.04
P	5.863	5.864	5.86	5.922	5.889	5.967	5.894	5.886	5.895	5.937	5.915	5.909	5.854	5.883
S	0.037	0.031	0.038	0.006	0.011	0.008	0.008	0.018	0.011	0.009	0.02	0.043	0.066	0.026
La	0.004	0.002	0.004	0.004	0.003	0.002	0.003	0.004	0.004	0.004	0.006	0.009	0.007	0.009
Ce	0.008	0.008	0.008	0.007	0.008	0.007	0.007	0.007	0.011	0.01	0.012	0.015	0.015	0.018
Pr	0	0	0.001	0	0.001	0	0	0.002	0	0.002	0.002	0	0	0.002
Nd	0.005	0.006	0.009	0.005	0.007	0.008	0.006	0.004	0.003	0.005	0.006	0.008	0.009	0.006
Sm	0.003	0.004	0.003	0	0	0.003	0	0.001	0.002	0.002	0.002	0.006	0.001	0.002
Y	0.013	0.012	0.011	0.004	0.005	0.006	0.003	0.006	0.008	0.007	0.018	0.018	0.026	0.014
Sr	0.004	0.003	0.003	0.008	0.01	0.013	0.011	0.009	0.012	0.013	0.007	0.006	0.006	0.006
Ba	0	0	0	0	0	0	0	0	0	0.001	0.001	0	0	0
As	0.001	0	0.002	0.001	0.001	0	0.001	0	0.001	0	0	0	0	0.001
F	1.768	1.887	1.862	1.735	1.733	1.767	1.78	1.687	1.806	1.796	2.173	2.052	1.936	1.83
Cl	0.111	0.1	0.119	0.092	0.094	0.097	0.1	0.096	0.095	0.1	0.102	0.127	0.117	0.113
OH	0.121	0.013	0.019	0.173	0.172	0.136	0.12	0.217	0.099	0.103	0.001	0.001	0.001	0.057
Sum Cat#	18.1	18.121	18.114	18.059	18.094	17.982	18.09	18.082	18.085	18.037	18.26	18.17	18.08	18.05

Label	E26_67_1_2ndApa2-2	E26_18_3_apa2nd?_-1	E26_18_3_apa2nd?_-2	E26_18_3_apa2nd?_-3	E27/68/1/apa_inclu_htQz	E22/12/2/apa-mag/htQz	E27/85/6/apa-inclu1	E27/85/6/apa-inclu2	E27/85/7/apa-inclu	E27/85/7/apa-inclu1	E27/85/10/apa-incarb	E27_85_a_inclu_apa_r	E27_85_a_inclu_a_c	E27_85_a_inclu_apa_r	E27_85_b_inclu_apa_c	E27_85_c_inclu_apa	E27_85_e_inclu_apa	E26_71_6_1	E27_87_14_1	E27_87_14_2	E27_87_14_3	E22_31_5_apa_-1	E22_31_5_apa_-2	E22_31_5_apa_-3	E22_31_5_apa2_-12-1	E22_31_5_apa2_-12-2	E22_32_1_apa_-1	E22_32_1_apa_-2	E22_32_2_apa_-1
SiO2%	0.46	0.1	0.01	0.04	0.25	0.49	0.31	0.3	0.25	0.36	0.22	0.39	0.39	0.37	0.44	0.33	0.96	0.29	0.33	0.12	0.22	0.11	0.15	0.21	0.21	0.21	0.21	0.15	0.15
Fe2O3%	0.27	0.29	0.23	0.36	0.06	0.54	0.17	0.15	0.26	0.19	0.15	0.25	0.35	0.08	0.14	0.15	0.02	0.46	0.15	0.05	0.13	0.11	0.12	0.17	0.13	0.12	0.16	0.14	0.17
MnO%	0.17	0.33	0.35	0.39	0.11	0.11	0.18	0.14	0.09	0.16	0.14	0.14	0.13	0.14	0.19	0.22	0.13	0.7	0.16	0.17	0.09	0.1	0.16	0.14	0.16	0.12	0.12	0.11	0.09
MgO%	0.12	0.12	0.11	0.14	0.02	0.01	0	0.01	0	0.01	0.03	0.02	0.02	0.03	0	0	0	0.17	0.03	0.02	0.02	0.03	0.03	0.03	0.03	0.03	0.02	0.01	0.01
CaO%	53.53	54.32	54.4	54.34	55.74	55.73	55.16	55.2	54.84	54.45	55.2	55.04	44.77	55.2	54.65	54.27	55.14	53.54	53.51	54.31	53.7	54.59	54.98	55.05	54.03	55.1	54.85	54.5	54.85
Na2O%	0.11	0.19	0.11	0.16	0.24	0.26	0.11	0.09	0.1	0.11	0.12	0.11	0.13	0.09	0.06	0.19	0.07	0.23	0.1	0.08	0.07	0.2	0.11	0.15	0.14	0.15	0.09	0.1	0.06
P2O5%	40.84	41.3	41.43	41.31	41.42	40.96	41.72	40.97	41.59	41.16	41.82	40.94	34.01	40.77	40.77	41.31	39.81	41.45	40.66	41.07	41.3	40.63	40.71	40.12	40.61	40.44	40.95	40.81	40.82
SO3%	0.14	0.25	0.11	0.13	0.58	0.92	0.35	0.27	0.46	0.32	0.35	0.34	0.33	0.26	0.14	0.1	0.25	0.12	0.18	0.11	0.1	0.35	0.15	0.3	0.16	0.11	0.25	0.2	0.07
La2O3%	0.08	0.05	0.05	0.06	0.04	0.03	0.03	0	0.03	0.05	0.06	0.12	0.1	0.06	0.17	0.12	0.04	0.03	0.11	0.04	0.11	0.04	0.07	0.07	0.07	0.05	0.07	0.07	0.1
Ce2O3%	0.16	0.12	0.14	0.13	0	0.01	0.05	0.07	0.06	0.04	0.05	0.05	0.01	0	0.12	0.14	0.05	0.06	0.07	0.07	0.02	0.11	0.16	0.1	0.14	0.13	0.16	0.15	0.18
Pr2O3%	0.03	0.04	0	0.03	-	-	-	-	-	-	-	-	-	-	-	-	-	-	-	-	-	0	0.01	0	0	0.02	0.01	0	0.03
Nd2O3%	0.14	0.1	0.14	0.15	-	-	-	-	-	-	-	-	-	-	-	-	-	-	-	-	-	0.05	0.15	0.13	0.1	0.08	0.08	0.04	0.11
Sm2O3%	0.07	0.08	0	0	-	-	-	-	-	-	-	-	-	-	-	-	-	-	-	-	-	0.06	0.02	0	0.03	0.01	0	0.01	0
Y2O3%	0.17	0.19	0.15	0.16	0	0.13	0	0.03	0	0.03	0	0.03	0.07	0.06	0.06	0.2	0	0.29	0.15	0.14	0.11	0.1	0.18	0.16	0.15	0.12	0.12	0.07	0.07
SrO%	0.09	0.02	0.05	0.05	0.01	0.11	0.05	0.06	0.04	0.04	0.13	0.02	0.03	0	0.02	0	0	0.14	0.06	0.01	0.1	0.03	0.01	0.02	0.02	0.04	0.09	0.11	0.1
BaO%	0	0.01	0	0.01	0.26	0.31	0.19	0.17	0.22	0.14	0.14	0.14	0.09	0.19	0.27	0.37	0.13	0.12	0.32	0.25	0.12	0.01	0.01	0	0.01	0	0	0	0
As2O3%	0	0	0	0	-	-	-	-	-	-	-	-	-	-	-	-	-	-	-	-	-	0	0	0.01	0.01	0	0.01	0.01	0
F%	3.53	4.09	4.05	4.18	3.57	3.36	3.33	3.22	3.26	3.2	2.65	2.95	2.93	2.93	2.75	3.02	2.9	3.44	3.2	3.37	3.29	3.56	3.42	3.5	3.64	3.22	3.21	3.32	3.44
Cl%	0.27	0.31	0.32	0.33	0.28	0.35	0.51	0.45	0.41	0.47	0.37	0.4	0.39	0.24	0.47	0.41	0.38	0.4	0.29	0.28	0.31	0.41	0.32	0.37	0.38	0.32	0.35	0.35	0.34
H2O(c)	0.01	0	0	0	0.03	0.12	0.08	0.13	0.13	0.13	0.44	0.27	0	0.32	0.34	0.23	0.28	0.04	0.15	0.08	0.12	0	0.06	0	0	0.14	0.15	0.09	0.04
O=F	1.49	1.72	1.71	1.76	1.5	1.42	1.4	1.36	1.37	1.35	1.12	1.24	1.23	1.23	1.16	1.27	1.22	1.45	1.35	1.42	1.38	1.5	1.44	1.48	1.53	1.36	1.35	1.4	1.45
O=Cl	0.06	0.07	0.07	0.07	0.06	0.08	0.11	0.1	0.09	0.11	0.08	0.09	0.09	0.05	0.11	0.09	0.08	0.09	0.06	0.06	0.07	0.09	0.07	0.08	0.09	0.07	0.08	0.08	0.08
Sum Ox%	98.66	100.1	99.88	100.1	101.06	101.94	100.7	99.81	100.3	99.43	100.7	99.89	82.43	99.45	99.33	99.7	98.85	99.94	98.04	98.68	98.34	98.91	99.33	98.99	98.41	98.99	99.47	98.78	99.12
Cations																													
Si	0.078	0.02	0	0.01	0.041	0.081	0.052	0.05	0.041	0.061	0.037	0.07	0.08	0.06	0.08	0.06	0.16	0.05	0.06	0.02	0.04	0.018	0.026	0.036	0.036	0.035	0.04	0.03	0.03
Fe3+	0.034	0.04	0.03	0.05	0.008	0.067	0.021	0.019	0.033	0.024	0.019	0.03	0.05	0.01	0.02	0.02	0	0.06	0.02	0.01	0.02	0.015	0.016	0.022	0.017	0.015	0.02	0.02	0.02
Mn2+	0.025	0.05	0.05	0.06	0.015	0.015	0.026	0.02	0.012	0.023	0.02	0.02	0.02	0.02	0.03	0.03	0.02	0.1	0.02	0.03	0.01	0.015	0.023	0.02	0.024	0.017	0.02	0.02	0.01
Mg	0.031	0.03	0.03	0.04	0.006	0.002	0	0.004	0	0.001	0.008	0.01	0.01	0.01	0	0	0	0.04	0.01	0	0	0.008	0.009	0.008	0.008	0.008	0.01	0	0
Ca	9.806	9.85	9.89	9.87	9.97	9.904	9.889	10.02	9.865	9.886	9.888	9.967	9.805	10.04	9.974	9.858	10.11	9.7	9.87	9.95	9.84	10	10.05	10.11	9.952	10.11	9.99	9.99	10.04
Na	0.036	0.061	0.037	0.053	0.078	0.082	0.036	0.03	0.032	0.036	0.04	0.035	0.053	0.03	0.021	0.062	0.023	0.074	0.033	0.026	0.023	0.068	0.038	0.051	0.047	0.05	0.029	0.033	0.021
P	5.912	5.917	5.949	5.929	5.854	5.752	5.91	5.874	5.91	5.905	5.919	5.859	5.886	5.86	5.88	5.929	5.766	5.93	5.924	5.947	5.98	5.883	5.88	5.824	5.911	5.862	5.89	5.909	5.905
S	0.018	0.032	0.014	0.016	0.072	0.114	0.044	0.035	0.058	0.041	0.044	0.044	0.051	0.033	0.018	0.013	0.032	0.016	0.024	0.014	0.012	0.045	0.02	0.039	0.02	0.014	0.031	0.026	0.008
La	0.005	0.003	0.003	0.004	0.002	0.002	0.002	0	0.002	0.003	0.004	0.007	0.008	0.004	0.01	0.007	0.003	0.002	0.007	0.002	0.007	0.003	0.004	0.004	0.005	0.003	0.004	0.005	0.006
Ce	0.01	0.008	0.009	0.008	0	0	0.003	0.004	0.003	0.003	0.003	0.003	0.001	0	0.007	0.009	0.003	0.004	0.004	0.005	0.001	0.007	0.01	0.006	0.009	0.008	0.01	0.009	0.011
Pr	0.002	0.002	0	0.002	-	-	-	-	-	-	-	-	-	-	-	-	-	-	-	-	-	0	0.001	0	0	0.001	0	0	0.002
Nd	0.009	0.006	0.008	0.009	-	-	-	-	-	-	-	-	-	-	-	-	-	-	-	-	-	0.003	0.009	0.008	0.006	0.005	0.005	0.003	0.007
Sm	0.004	0.004	0	0	-	-	-	-	-	-	-	-	-	-	-	-	-	-	-	-	-	0.003	0.001	0	0.002	0.001	0	0.001	0
Y	0.015	0.017	0.014	0.014	0	0.012	0	0.003	0	0.003	0	0.002	0.008	0.006	0.006	0.018	0	0.026	0.013	0.013	0.01	0.009	0.017	0.015	0.014	0.011	0.011	0.006	0.006
Sr	0.009	0.002	0.005	0.005	0.001	0.01	0.005	0.006	0.004	0.004	0.012	0.002	0.003	0	0.002	0	0	0.013	0.006	0.001	0.01	0.003	0.001	0.002	0.002	0.004	0.009	0.011	0.01
Ba	0	0	0	0.001	0.017	0.02	0.013	0.011	0.014	0.009	0.009	0.01	0.007	0.013	0.018	0.025	0.009	0.008	0.022	0.017	0.008	0.001	0	0	0	0	0	0	0
As	0	0	0	0	-	-	-	-	-	-	-	-	-	-	-	-	-	-	-	-	-	0	0	0.001	0.001	0	0.001	0.001	0
F	1.91	2.191	2.174	2.239	1.886	1.765	1.764	1.726	1.733	1.712	1.401	1.578	1.896	1.573	1.483	1.618	1.57	1.84	1.743	1.821	1.778	1.927	1.843	1.9	1.979	1.745	1.723	1.794	1.861
Cl	0.077	0.088	0.093	0.094	0.08	0.098	0.144	0.13	0.116	0.136	0.104	0.114	0.136	0.069	0.135	0.118	0.109	0.115	0.083	0.082	0.089	0.117	0.092	0.107	0.112	0.092	0.102	0.1	0.098
OH	0.013	0.001	0.001	0.001	0.033	0.137	0.091	0.144	0.15	0.151	0.495	0.308	0.001	0.358	0.382	0.264	0.321	0.045	0.173	0.096	0.133	0.001	0.065	0.001	0.001	0.162	0.175	0.105	0.041
Sum Cat#	18	18.31	18.3	18.39	18.066	18.064	18	18.07	17.98	18	18	18.05	18.01	18.09	18.06	18.03	18.13	18.02	18.01	18.03	17.96	18.13	18.1	18.16	18.15	18.15	18.06	18.05	18.08

Label	E22_3 2_2_a pa_-2	E22_3 2_2_a pa_-3	E22_3 2_2_a pa_-4	E22_3 2_2_a pa_-5	E22_3 2_5_a pa_-1	E22_3 2_5_a pa_-2	E22_3 2_5_a pa_-3	E22_3 2_5_a pa_-4	E22_3 2_5_a pa_-5	E22_3 2_6_a pa_-1	E22_3 2_6_a pa_-2	E22_3 2_6_a pa_-3	E22_3 2_1_a pa2_-1	E22_3 2_1_a pa2_-2	E26_6 9_1_a pa_-1
SiO2%	0.16	0.19	0.15	0.16	0.26	0.18	0.16	0.13	0.69	0.25	0.18	0.28	0.3	0.22	0.17
Fe2O3%	0.16	0.18	0.1	0.09	0.09	0.1	0.08	0.12	0.19	0.16	0.15	0.17	0.17	0.16	0.37
MnO%	0.08	0.12	0.09	0.12	0.1	0.07	0.08	0.07	0.09	0.09	0.12	0.12	0.1	0.09	0.35
MgO%	0.02	0.02	0.01	0.02	0.02	0.02	0.01	0.01	0.01	0.02	0.02	0.02	0.02	0.02	0.11
CaO%	54.92	54.82	54.92	54.42	54.34	53.57	53.65	54.18	53.52	53.61	54.24	54.1	54.28	53.92	51.87
Na2O%	0.04	0.06	0.07	0.04	0.1	0.06	0.07	0.07	0.16	0.18	0.16	0.13	0.17	0.15	0.22
P2O5%	40.64	40.74	41.16	40.54	40.56	40.46	40.78	40.97	40.12	40.39	40.09	40.14	40.06	40.3	40.5
SO3%	0.09	0.15	0.12	0.1	0.12	0.08	0.11	0.1	0.22	0.25	0.31	0.23	0.22	0.23	0.08
La2O3%	0.11	0.1	0.08	0.1	0.1	0.11	0.09	0.1	0.09	0.05	0.04	0.06	0.09	0.05	0.09
Ce2O3%	0.18	0.16	0.13	0.19	0.19	0.19	0.16	0.19	0.15	0.12	0.14	0.14	0.16	0.11	0.18
Pr2O3%	0.04	0	0	0	0	0	0	0	0	0.02	0	0.01	0	0.03	0.01
Nd2O3%	0.07	0.1	0.12	0.07	0.09	0.13	0.08	0.09	0.1	0.17	0.1	0.12	0.14	0.04	0.16
Sm2O3%	0	0	0	0.01	0.07	0.05	0.03	0.02	0.02	0.06	0.01	0.02	0.02	0.03	0.07
Y2O3%	0.05	0.05	0.04	0.05	0.1	0.09	0.1	0.05	0.07	0.13	0.13	0.1	0.16	0.04	0.47
SrO%	0.1	0.1	0.09	0.09	0.1	0.1	0.09	0.1	0.09	0.1	0.1	0.1	0.1	0.1	0.07
BaO%	0.01	0	0.01	0	0.01	0	0	0.01	0	0	0	0	0	0	0
As2O3%	0.01	0.01	0.01	0.01	0.01	0.02	0.03	0.04	0.01	0.01	0.01	0.01	0	0.01	0
F%	3.32	3.26	3.33	3.22	3.14	3.08	2.95	3.14	3.41	3.12	3.13	3.13	3.33	3.28	3.51
Cl%	0.36	0.33	0.35	0.35	0.34	0.34	0.35	0.34	0.34	0.37	0.38	0.39	0.31	0.31	0.56
H2O(c)	0.09	0.13	0.1	0.13	0.17	0.18	0.25	0.17	0.03	0.16	0.15	0.16	0.08	0.1	0
O=F	1.4	1.37	1.4	1.36	1.32	1.3	1.24	1.32	1.44	1.32	1.32	1.32	1.4	1.38	1.48
O=Cl	0.08	0.07	0.08	0.08	0.08	0.08	0.08	0.08	0.08	0.08	0.08	0.09	0.07	0.07	0.13
Sum Ox%	98.97	99.07	99.39	98.27	98.5	97.44	97.76	98.49	97.82	97.86	98.05	98.03	98.24	97.73	97.19
Cations															
Si	0.03	0.03	0.03	0.03	0.04	0.03	0.03	0.02	0.12	0.04	0.03	0.05	0.05	0.04	0.03
Fe3+	0.02	0.02	0.01	0.01	0.01	0.01	0.01	0.02	0.03	0.02	0.02	0.02	0.02	0.02	0.05
Mn2+	0.01	0.02	0.01	0.02	0.01	0.01	0.01	0.01	0.01	0.01	0.02	0.02	0.02	0.01	0.05
Mg	0.01	0	0	0	0	0.01	0	0	0	0	0.01	0.01	0.01	0.01	0.03
Ca	10.07	10.03	10	10.04	10	9.95	9.91	9.95	9.89	9.91	10.03	10.01	10.03	9.98	9.67
Na	0.015	0.021	0.023	0.014	0.032	0.019	0.025	0.024	0.054	0.059	0.053	0.042	0.058	0.049	0.073
P	5.89	5.891	5.924	5.908	5.898	5.938	5.955	5.945	5.859	5.902	5.859	5.868	5.851	5.896	5.97
S	0.012	0.019	0.015	0.012	0.015	0.011	0.014	0.013	0.029	0.032	0.04	0.03	0.028	0.03	0.011
La	0.007	0.007	0.005	0.006	0.007	0.007	0.006	0.006	0.006	0.003	0.002	0.004	0.006	0.003	0.006
Ce	0.011	0.01	0.008	0.012	0.012	0.012	0.01	0.012	0.009	0.007	0.009	0.009	0.01	0.007	0.011
Pr	0.002	0	0	0	0	0	0	0	0	0.002	0	0.001	0	0.002	0.001
Nd	0.004	0.006	0.007	0.004	0.006	0.008	0.005	0.006	0.006	0.01	0.006	0.008	0.009	0.002	0.01
Sm	0	0	0	0.001	0.004	0.003	0.002	0.001	0.001	0.004	0.001	0.001	0.001	0.002	0.004
Y	0.005	0.005	0.003	0.004	0.009	0.008	0.009	0.004	0.007	0.012	0.012	0.01	0.015	0.004	0.044
Sr	0.01	0.01	0.009	0.009	0.01	0.01	0.009	0.01	0.009	0.01	0.01	0.01	0.01	0.01	0.007
Ba	0	0	0.001	0	0.001	0	0	0.001	0	0	0	0	0	0	0
As	0.001	0.001	0.001	0.001	0.001	0.002	0.003	0.004	0.001	0.001	0.001	0.002	0	0.001	0
F	1.797	1.76	1.79	1.753	1.708	1.689	1.611	1.702	1.863	1.705	1.712	1.707	1.815	1.791	1.931
Cl	0.105	0.095	0.1	0.103	0.098	0.101	0.102	0.098	0.099	0.108	0.11	0.113	0.092	0.091	0.165
OH	0.098	0.145	0.11	0.144	0.195	0.21	0.287	0.2	0.038	0.187	0.178	0.18	0.093	0.118	0.001
Sum Cat#	18.1	18.08	18.05	18.07	18.07	18.02	18	18.02	18.04	18.04	18.1	18.08	18.11	18.06	18.07

Label	E26_6 9_1_a pa_-2	E26_6 9_1_a pa_-4	E26_6 9_1_a pa2_-1	E26_6 9_1_a pa2_-2	E26_6 9_1_a pa2_-3	E26_6 9_2_a pa2_-3	E26_6 9_2_a pa3_-1	E26_6 9_2_a pa3_-2	E27_3 9_1_a pa_-1	E27_3 9_1_a pa_-2	E27_3 9_1_a pa_-3	E27_3 9_1_a pa_-4	E27_3 9_1_a pa_-5	E27_3 9_2_a pa_-1
SiO2%	0.11	0.11	0.7	0.14	0.05	0.18	0.12	0.15	0.16	0.16	0.13	0.15	0.15	0.27
Fe2O3%	0.27	0.41	0.49	0.48	0.45	1.42	0.49	0.49	0.12	0.05	0.06	0.07	0.07	0.06
MnO%	0.29	0.48	0.43	0.49	0.4	0.6	0.57	0.63	0.12	0.13	0.09	0.16	0.11	0.13
MgO%	0.1	0.13	0.14	0.14	0.14	0.13	0.14	0.14	0.01	0.01	0.01	0.02	0.01	0.01
CaO%	53.09	52.61	51.75	51.62	52.24	51.73	51.28	51.6	54.4	55.18	54.52	55.23	55	54.94
Na2O%	0.24	0.2	0.25	0.23	0.27	0.3	0.36	0.32	0.07	0.05	0.04	0.09	0.06	0.07
P2O5%	40.88	40.72	39.84	40.61	40.68	39.87	40.11	40.18	40.5	40.54	40.28	40.58	40.43	40.96
SO3%	0.06	0.05	0.07	0.06	0.13	0.21	0.15	0.15	0.28	0.17	0.14	0.14	0.17	0.32
La2O3%	0.08	0.07	0.08	0.07	0.07	0.08	0.11	0.09	0.05	0.06	0.05	0.06	0.05	0.08
Ce2O3%	0.22	0.18	0.18	0.22	0.17	0.27	0.31	0.28	0.1	0.12	0.1	0.14	0.1	0.13
Pr2O3%	0.02	0	0.01	0	0.04	0.01	0.03	0.01	0.02	0.03	0.04	0	0.04	0.01
Nd2O3%	0.16	0.13	0.16	0.15	0.15	0.19	0.2	0.17	0.07	0.02	0.03	0.08	0.05	0.07
Sm2O3%	0.05	0.04	0.01	0.04	0.04	0.08	0.09	0.05	0	0.09	0	0.04	0	0.06
Y2O3%	0.47	0.38	0.37	0.44	0.35	0.43	0.38	0.41	0.09	0.04	0.06	0.08	0.09	0.05
SrO%	0.05	0.05	0.07	0.06	0.07	0.06	0.07	0.06	0.07	0.06	0.08	0.11	0.07	0.06
BaO%	0	0	0	0	0	0	0	0	0	0	0.01	0	0	0
As2O3%	0	0	0	0	0	0	0	0	0	0.01	0.01	0.01	0.01	0
F%	3.35	3.55	3.41	3.41	3.46	3.58	3.65	3.78	3.22	3.21	3.23	3.17	2.98	3.31
Cl%	0.55	0.54	0.61	0.57	0.57	0.61	0.62	0.62	0.52	0.59	0.5	0.48	0.56	0.64
H2O(c)	0.02	0	0	0	0	0	0	0	0.09	0.08	0.08	0.13	0.19	0.04
O=F	1.41	1.49	1.44	1.44	1.46	1.51	1.53	1.59	1.36	1.35	1.36	1.33	1.25	1.39
O=Cl	0.12	0.12	0.14	0.13	0.13	0.14	0.14	0.14	0.12	0.13	0.11	0.11	0.13	0.14
Sum Ox%	98.46	98.04	97.01	97.15	97.7	98.12	96.99	97.41	98.42	99.12	97.98	99.29	98.74	99.67
Cations														
Si	0.02	0.02	0.12	0.02	0.01	0.03	0.02	0.03	0.028	0.027	0.023	0.026	0.025	0.046
Fe3+	0.04	0.05	0.06	0.06	0.06	0.19	0.06	0.07	0.016	0.006	0.007	0.008	0.009	0.008
Mn2+	0.04	0.07	0.06	0.07	0.06	0.09	0.08	0.09	0.018	0.019	0.014	0.023	0.015	0.018
Mg	0.02	0.03	0.04	0.04	0.04	0.04	0.04	0.04	0.003	0.002	0.003	0.004	0.004	0.003
Ca	9.78	9.74	9.67	9.62	9.69	9.62	9.62	9.65	10.01	10.12	10.09	10.11	10.11	9.986
Na	0.08	0.068	0.086	0.077	0.091	0.1	0.123	0.109	0.022	0.017	0.014	0.031	0.021	0.024
P	5.952	5.955	5.885	5.981	5.964	5.861	5.947	5.936	5.891	5.873	5.893	5.87	5.874	5.884
S	0.007	0.007	0.01	0.008	0.017	0.028	0.019	0.02	0.035	0.022	0.018	0.018	0.022	0.041
La	0.005	0.004	0.005	0.004	0.004	0.005	0.007	0.006	0.003	0.004	0.003	0.004	0.003	0.005
Ce	0.014	0.011	0.011	0.014	0.011	0.017	0.02	0.018	0.006	0.007	0.006	0.009	0.006	0.008
Pr	0.001	0	0.001	0	0.002	0.001	0.002	0.001	0.002	0.002	0.002	0	0.002	0
Nd	0.01	0.008	0.01	0.01	0.009	0.012	0.012	0.011	0.004	0.001	0.002	0.005	0.003	0.004
Sm	0.003	0.003	0	0.002	0.002	0.005	0.005	0.003	0	0.005	0	0.003	0	0.003
Y	0.043	0.035	0.034	0.041	0.033	0.04	0.035	0.038	0.008	0.004	0.006	0.007	0.008	0.005
Sr	0.005	0.005	0.007	0.006	0.007	0.006	0.007	0.006	0.007	0.006	0.008	0.011	0.007	0.006
Ba	0	0	0	0	0	0	0	0	0	0	0	0	0	0
As	0	0	0	0	0	0	0	0	0	0.002	0.001	0.001	0.001	0
F	1.823	1.938	1.883	1.877	1.898	1.964	2.019	2.087	1.75	1.736	1.765	1.711	1.616	1.776
Cl	0.159	0.157	0.179	0.167	0.167	0.18	0.184	0.183	0.15	0.172	0.145	0.139	0.162	0.183
OH	0.018	0.001	0.001	0.001	0.001	0.001	0.001	0.001	0.099	0.091	0.09	0.15	0.221	0.041
Sum Cat#	18.02	18.11	18.07	18.01	18.06	18.18	18.21	18.28	18.06	18.11	18.09	18.13	18.12	18.04

Label	E27_39_2_apa_-2	E27_39_2_apa_-3	E27_39_3_apa_-1	E27_39_3_apa_-2	E27_39_3_apa_-3	E27_39_4_apa_-2	E48_18_168_2_apa-1	E48_18_168_3_apa-1	E48_18_168_3_apa-2	E48_18_168_3_apa-3	E48_18_168_3_apa-4	E48_18_168_3_apa-5	E48_18_168_4_apa-1	E48_18_168_4_apa-2
SiO2%	0.22	0.25	0.13	0.3	0.26	0.12	0.18	0.15	0.17	0.18	0.17	0.18	0.15	0.13
Fe2O3%	0.06	0.16	0.07	0.08	0.08	0.06	0.33	0.27	0.31	0.31	0.3	0.28	0.37	0.28
MnO%	0.14	0.14	0.07	0.12	0.13	0.11	0.1	0.14	0.13	0.11	0.11	0.12	0.12	0.1
MgO%	0.02	0.03	0	0.02	0.02	0	0.25	0.24	0.26	0.25	0.23	0.24	0.24	0.31
CaO%	55.04	54.46	53.85	54.43	54.55	54.91	53.77	53.92	53.23	53.46	54.19	53.92	54.62	54.39
Na2O%	0.12	0.09	0.04	0.12	0.1	0.04	0.05	0.04	0.01	0.02	0.03	0.04	0.04	0
P2O5%	40.23	40.7	41.07	40.63	40.45	40.42	41.13	41.17	40.91	41.14	41.11	40.63	41.26	41.13
SO3%	0.33	0.26	0.1	0.41	0.33	0.09	0.02	0.06	0.02	0.04	0.02	0.02	0.02	0.01
La2O3%	0.07	0.07	0.02	0.07	0.05	0.06	0.06	0.05	0.06	0.05	0.06	0.05	0.06	0.05
Ce2O3%	0.15	0.15	0.02	0.15	0.13	0.09	0.16	0.12	0.13	0.11	0.12	0.11	0.16	0.11
Pr2O3%	0	0	0	0.01	0.03	0.01	0	0	0	0	0	0	0.01	0
Nd2O3%	0.15	0.12	0.03	0.12	0.13	0.09	0.12	0.1	0.11	0.1	0.09	0.11	0.09	0.11
Sm2O3%	0	0.02	0.03	0.01	0.01	0.01	0.03	0.03	0.06	0	0.03	0	0.07	0
Y2O3%	0.09	0.07	0	0.04	0.05	0.06	0.08	0.04	0.05	0.03	0.07	0.06	0.07	0.07
SrO%	0.07	0.08	0.06	0.06	0.06	0.05	0.18	0.2	0.19	0.18	0.17	0.18	0.17	0.17
BaO%	0	0	0	0.01	0.01	0	0	0.02	0.01	0	0	0.01	0	0.01
As2O3%	0	0.01	0.01	0	0.02	0.01	0	0	0	0	0	0	0	0
F%	3.21	3.21	3.61	3.08	3.25	3.56	3.74	3.15	2.55	2.52	2.76	2.85	3.26	2.86
Cl%	0.54	0.63	0.41	0.49	0.5	0.34	0.32	0.3	0.4	0.39	0.38	0.27	0.3	0.41
H2O(c)	0.09	0.07	0	0.17	0.08	0	0	0.19	0.43	0.45	0.35	0.32	0.15	0.3
O=F	1.35	1.35	1.52	1.3	1.37	1.5	1.58	1.33	1.07	1.06	1.16	1.2	1.37	1.2
O=Cl	0.12	0.14	0.09	0.11	0.11	0.08	0.07	0.07	0.09	0.09	0.09	0.06	0.07	0.09
Sum Ox%	99.05	99.03	97.92	98.91	98.78	98.47	98.88	98.8	97.88	98.19	98.96	98.13	99.7	99.14
Cations														
Si	0.038	0.043	0.023	0.051	0.044	0.021	0.031	0.026	0.029	0.031	0.03	0.031	0.025	0.021
Fe3+	0.008	0.02	0.009	0.011	0.011	0.008	0.043	0.035	0.04	0.04	0.039	0.036	0.047	0.036
Mn2+	0.02	0.02	0.01	0.017	0.019	0.016	0.015	0.02	0.019	0.016	0.017	0.017	0.017	0.015
Mg	0.005	0.007	0.001	0.005	0.006	0	0.064	0.061	0.067	0.064	0.059	0.061	0.061	0.078
Ca	10.1	9.97	9.92	9.956	10.01	10.13	9.843	9.86	9.819	9.815	9.902	9.941	9.922	9.926
Na	0.041	0.031	0.013	0.04	0.034	0.013	0.017	0.014	0.003	0.007	0.01	0.015	0.013	0
P	5.833	5.887	5.978	5.873	5.866	5.888	5.949	5.949	5.962	5.968	5.935	5.919	5.922	5.931
S	0.043	0.033	0.014	0.052	0.043	0.012	0.002	0.007	0.003	0.005	0.003	0.003	0.003	0.001
La	0.004	0.005	0.001	0.004	0.003	0.004	0.004	0.003	0.004	0.003	0.004	0.003	0.004	0.003
Ce	0.009	0.009	0.002	0.01	0.008	0.006	0.01	0.007	0.008	0.007	0.008	0.007	0.01	0.007
Pr	0	0	0	0	0.002	0.001	0	0	0	0	0	0	0.001	0
Nd	0.009	0.008	0.002	0.007	0.008	0.005	0.008	0.006	0.007	0.006	0.005	0.007	0.005	0.007
Sm	0	0.001	0.002	0.001	0	0.001	0.002	0.002	0.004	0	0.002	0	0.004	0
Y	0.008	0.006	0	0.003	0.004	0.006	0.007	0.004	0.004	0.003	0.006	0.005	0.007	0.006
Sr	0.006	0.008	0.006	0.006	0.006	0.005	0.018	0.02	0.019	0.018	0.017	0.018	0.016	0.017
Ba	0	0	0	0.001	0.001	0	0	0.001	0.001	0	0	0.001	0	0.001
As	0	0.001	0.001	0	0.002	0.001	0	0	0	0	0	0	0	0
F	1.737	1.735	1.963	1.663	1.761	1.937	2.022	1.699	1.389	1.367	1.49	1.553	1.746	1.541
Cl	0.156	0.182	0.119	0.143	0.146	0.098	0.092	0.086	0.118	0.114	0.11	0.08	0.086	0.12
OH	0.107	0.083	0.001	0.193	0.093	0.001	0.001	0.215	0.493	0.519	0.4	0.367	0.169	0.34
Sum Cat#	18.13	18.05	18.06	18.04	18.07	18.15	18.127	18.016	17.99	17.982	18.036	18.064	18.055	18.05

Label	E48_18_168_4_apa-3	E48_18_168_4_apa-4	E48_18_168_4_apatrav_-1	E48_18_168_4_apatrav_-2	E48_18_168_4_apatrav_-3	E48_18_168_4_apatrav_-4	E48_18_168_6_apa_-2	E48_8_182_5_apa_-1	E48_8_182_5_apa_-2	E48_8_182_3_apa1_-3	E48_8_182_3_apa2_-1	E48_8_182_3_apa2_-2	E48_8_182_3_apa2_-3
SiO2%	0.15	0.12	0.17	0.12	0.14	0.16	0.18	0.16	0.13	0.15	0.22	0.48	0.12
Fe2O3%	0.34	0.27	0.34	0.31	0.32	0.34	0.18	0.22	0.15	0.15	0.22	0.21	0.26
MnO%	0.07	0.11	0.13	0.1	0.07	0.12	0.09	0.23	0.18	0.15	0.13	0.17	0.19
MgO%	0.3	0.24	0.22	0.31	0.32	0.25	0.32	0.03	0.03	0.02	0.02	0.03	0.03
CaO%	54.67	54.25	54.36	54.31	54.26	54.18	53.4	54.96	55.01	54.71	54.88	54.19	55.55
Na2O%	0.01	0.02	0.03	0.04	0.02	0.02	0.07	0.08	0.08	0.08	0.17	0.11	0.14
P2O5%	40.91	41.25	41.34	41.33	41.1	41.16	41.5	40.6	40.58	41.12	40.35	40.67	40.52
SO3%	0.02	0.03	0.02	0.02	0.01	0.02	0.11	0.12	0.1	0.12	0.15	0.11	0.13
La2O3%	0.05	0.04	0.07	0.05	0.04	0.06	0.06	0.08	0.06	0.07	0.05	0.07	0.08
Ce2O3%	0.12	0.08	0.15	0.12	0.1	0.14	0.1	0.14	0.14	0.16	0.13	0.14	0.15
Pr2O3%	0	0	0	0.03	0	0.01	0.02	0.01	0	0.01	0	0	0.03
Nd2O3%	0.08	0.08	0.09	0.13	0.07	0.1	0.09	0.08	0.12	0.12	0.09	0.12	0.1
Sm2O3%	0.01	0.03	0	0.07	0	0	0	0	0	0.04	0.02	0.01	0.01
Y2O3%	0.05	0.07	0.05	0.06	0.06	0.07	0.04	0.14	0.12	0.16	0.12	0.12	0.12
SrO%	0.18	0.18	0.16	0.18	0.18	0.17	0.21	0.07	0.05	0.06	0.04	0.04	0.04
BaO%	0	0	0	0	0	0	0	0.01	0	0	0	0	0.01
As2O3%	0	0	0	0	0	0	0	0	0	0	0.01	0.01	0.01
F%	2.75	2.62	3.59	2.66	2.76	3.09	3.77	3.76	3.53	3.85	3.72	3.75	3.64
Cl%	0.44	0.44	0.31	0.43	0.45	0.39	0.26	0.27	0.31	0.24	0.2	0.23	0.22
H2O(c)	0.34	0.41	0	0.4	0.33	0.2	0	0	0	0	0	0	0
O=F	1.16	1.1	1.51	1.12	1.16	1.3	1.59	1.58	1.49	1.62	1.57	1.58	1.53
O=Cl	0.1	0.1	0.07	0.1	0.1	0.09	0.06	0.06	0.07	0.05	0.05	0.05	0.05
Sum Ox%	99.23	99.02	99.45	99.45	98.97	99.09	98.75	99.31	99.02	99.53	98.9	98.83	99.75
Cations													
Si	0.025	0.02	0.029	0.021	0.023	0.028	0.031	0.03	0.02	0.03	0.04	0.08	0.02
Fe3+	0.044	0.035	0.044	0.04	0.041	0.043	0.024	0.03	0.02	0.02	0.03	0.03	0.03
Mn2+	0.011	0.015	0.018	0.014	0.01	0.017	0.013	0.03	0.03	0.02	0.02	0.02	0.03
Mg	0.075	0.06	0.055	0.078	0.082	0.062	0.08	0.01	0.01	0	0.01	0.01	0.01
Ca	9.984	9.9	9.886	9.879	9.914	9.891	9.745	10.06	10.09	9.97	10.08	9.93	10.14
Na	0.003	0.008	0.009	0.012	0.008	0.008	0.024	0.026	0.028	0.026	0.056	0.037	0.045
P	5.903	5.948	5.941	5.94	5.933	5.937	5.984	5.874	5.881	5.921	5.858	5.888	5.843
S	0.002	0.003	0.003	0.002	0.002	0.003	0.014	0.015	0.012	0.015	0.019	0.014	0.017
La	0.003	0.002	0.005	0.003	0.003	0.004	0.003	0.005	0.004	0.005	0.003	0.005	0.005
Ce	0.007	0.005	0.009	0.008	0.006	0.009	0.006	0.008	0.008	0.01	0.008	0.009	0.01
Pr	0	0	0	0.002	0	0.001	0.001	0.001	0	0	0	0	0.002
Nd	0.005	0.005	0.005	0.008	0.004	0.006	0.005	0.005	0.007	0.008	0.006	0.007	0.006
Sm	0.001	0.002	0	0.004	0	0	0	0	0	0.003	0.001	0	0.001
Y	0.005	0.006	0.005	0.005	0.006	0.007	0.004	0.012	0.011	0.014	0.011	0.011	0.011
Sr	0.018	0.018	0.015	0.018	0.017	0.017	0.021	0.007	0.005	0.006	0.004	0.004	0.004
Ba	0	0	0	0	0	0	0	0.001	0	0	0	0	0.001
As	0	0	0	0	0	0	0	0	0	0	0.001	0.001	0.001
F	1.485	1.411	1.926	1.427	1.49	1.663	2.032	2.032	1.913	2.072	2.02	2.029	1.963
Cl	0.128	0.126	0.089	0.125	0.13	0.114	0.075	0.077	0.091	0.069	0.059	0.068	0.064
OH	0.387	0.463	0.001	0.448	0.381	0.223	0.001	0.001	0.001	0.001	0.001	0.001	0.001
Sum Cat#	18.086	18.028	18.04	18.035	18.048	18.031	18.06	18.22	18.12	18.19	18.22	18.14	18.2

Label	CS10 9/1/apa1_trav-1	CS10 9/1/apa1_trav-2	CS10 9/1/apa1_trav-3	CS10 9/1/apa2_trav-1	CS10 9/1/apa2_trav-2	CS10 9/1/apa2_trav-3	CS10 9/2/apa1_trav-1	CS10 9/2/apa1_trav-2	CS10 9/2/apa1_trav-3	CS10 9/2/apa2_trav-2	CS10 9/2/apa2_trav-3	CS10 9/3/apa1_trav-1	CS10 9/3/apa1_trav-2	CS10 9/3/apa1_trav-3	CS10 9/3/apa1_trav-4
SiO2%	0.29	0.2	0.27	0.21	0.2	0.23	0.22	0.22	0.51	0.21	0.28	0.29	0.28	0.23	0.25
Fe2O3%	0.38	0.31	0.35	0.35	0.28	0.35	0.39	0.63	0.76	0.34	0.42	0.36	0.31	0.34	0.34
MnO%	0.13	0.13	0.14	0.14	0.12	0.11	0.12	0.11	0.15	0.12	0.14	0.13	0.1	0.11	0.12
MgO%	0.27	0.27	0.25	0.27	0.27	0.28	0.27	0.26	0.41	0.28	0.26	0.27	0.29	0.28	0.28
CaO%	53.97	53.69	54.03	54.41	54.09	53.22	54.16	53.9	53.74	54.42	53.77	54.43	54.46	54.4	53.64
Na2O%	0.14	0.12	0.17	0.11	0.09	0.08	0.09	0.12	0.11	0.06	0.12	0.14	0.08	0.13	0.11
P2O5%	41.54	41.87	41.63	42.06	41.87	42.18	41.62	41.49	40.96	42	41.64	41.46	41.35	41.85	41.99
SO3%	0.55	0.43	0.49	0.36	0.29	0.29	0.36	0.4	0.4	0.32	0.46	0.5	0.55	0.45	0.48
La2O3%	0.02	0.04	0.04	0.04	0.03	0.02	0.03	0.04	0.03	0.04	0.06	0.04	0.03	0.03	0.02
Ce2O3%	0.06	0.04	0.08	0.07	0.06	0.09	0.07	0.08	0.09	0.06	0.11	0.07	0.07	0.08	0.06
Pr2O3%	0	0	0.01	0	0	0	0	0	0	0	0	0	0.05	0	0
Nd2O3%	0.03	0.12	0.09	0.04	0.04	0.09	0.04	0.05	0.11	0.06	0.1	0.09	0.01	0.04	0.03
Sm2O3%	0	0	0	0	0	0.03	0.05	0.03	0.09	0.02	0.02	0.02	0.03	0.04	0.03
Y2O3%	0.04	0.02	0.03	0.04	0.06	0.05	0.04	0	0.05	0.05	0.04	0.03	0.02	0.01	0.04
SrO%	0.27	0.28	0.23	0.25	0.29	0.28	0.28	0.27	0.21	0.3	0.22	0.25	0.29	0.28	0.27
BaO%	0	0	0	0	0.01	0.01	0.01	0	0.01	0.01	0.01	0.01	0.01	0	0
As2O3%	0	0	0	0	0	0	0	0	0	0	0	0	0	0	0
F%	2.86	2.29	2.48	3.01	2.3	2.64	2.51	2.39	2.46	2.36	2.64	2.66	2.35	2.32	2.02
Cl%	0.47	0.38	0.39	0.45	0.36	0.46	0.47	0.39	0.43	0.42	0.47	0.46	0.49	0.42	0.38
H2O(c)	0.31	0.6	0.51	0.25	0.6	0.41	0.48	0.55	0.5	0.57	0.41	0.41	0.55	0.59	0.73
O=F	1.2	0.96	1.04	1.27	0.97	1.11	1.06	1.01	1.04	0.99	1.11	1.12	0.99	0.98	0.85
O=Cl	0.11	0.09	0.09	0.1	0.08	0.1	0.11	0.09	0.1	0.1	0.11	0.1	0.11	0.1	0.09
Sum Ox%	100	99.75	100.1	100.7	99.9	99.62	100	99.86	99.89	100.6	99.95	100.4	100.2	100.5	99.84
Cations															
Si	0.048	0.033	0.045	0.035	0.034	0.039	0.037	0.037	0.085	0.035	0.048	0.048	0.046	0.039	0.041
Fe3+	0.048	0.04	0.044	0.043	0.035	0.044	0.049	0.08	0.096	0.043	0.053	0.045	0.04	0.043	0.043
Mn2+	0.019	0.018	0.02	0.02	0.017	0.016	0.017	0.016	0.021	0.017	0.02	0.019	0.014	0.015	0.017
Mg	0.067	0.068	0.063	0.067	0.068	0.07	0.067	0.066	0.103	0.069	0.065	0.068	0.071	0.07	0.07
Ca	9.71	9.667	9.714	9.727	9.736	9.584	9.756	9.722	9.71	9.744	9.682	9.777	9.797	9.738	9.631
Na	0.045	0.04	0.055	0.035	0.029	0.027	0.029	0.04	0.035	0.02	0.04	0.047	0.027	0.041	0.034
P	5.905	5.957	5.915	5.942	5.955	6.002	5.924	5.913	5.849	5.941	5.924	5.885	5.878	5.92	5.958
S	0.069	0.054	0.062	0.045	0.036	0.037	0.046	0.051	0.051	0.04	0.058	0.063	0.069	0.056	0.06
La	0.002	0.003	0.003	0.002	0.002	0.001	0.002	0.002	0.002	0.002	0.004	0.003	0.002	0.002	0.001
Ce	0.004	0.003	0.005	0.004	0.003	0.005	0.004	0.005	0.005	0.004	0.007	0.004	0.004	0.005	0.004
Pr	0	0	0	0	0	0	0	0	0	0	0	0	0.003	0	0
Nd	0.002	0.007	0.005	0.002	0.002	0.005	0.002	0.003	0.007	0.004	0.006	0.006	0.001	0.003	0.002
Sm	0	0	0	0	0	0.002	0.003	0.002	0.006	0.001	0.001	0.001	0.002	0.002	0.002
Y	0.004	0.002	0.003	0.004	0.006	0.005	0.004	0	0.005	0.005	0.004	0.002	0.002	0.001	0.004
Sr	0.026	0.027	0.022	0.025	0.028	0.027	0.027	0.027	0.021	0.029	0.021	0.024	0.028	0.027	0.027
Ba	0	0	0	0	0	0	0.001	0	0.001	0.001	0.001	0.001	0	0	0
As	0	0	0	0	0	0	0	0	0	0	0	0	0	0	0
F	1.519	1.216	1.317	1.591	1.223	1.405	1.333	1.273	1.313	1.245	1.404	1.413	1.246	1.228	1.07
Cl	0.134	0.108	0.112	0.127	0.102	0.13	0.134	0.11	0.124	0.12	0.134	0.131	0.139	0.12	0.109
OH	0.347	0.676	0.571	0.282	0.675	0.465	0.533	0.617	0.563	0.635	0.462	0.457	0.614	0.652	0.821
Sum Cat#	17.95	17.92	17.96	17.95	17.95	17.87	17.97	17.97	18	17.95	17.93	17.99	17.99	17.96	17.89

Label	CS10 9/3/apa1_trav-5	CS10 9/4/apa1_trav-1	CS10 9/4/apa1_trav-2	CS10 9/4/apa1_trav-3	E22/1 2/B/apa_trav-2	E22/1 2/B/apa_trav-3	E22/1 2/D/apa_trav-1	E22/1 2/D/apa_trav-2	E22/1 2/D/apa_trav-3	E22/1 2/Di/apa_trav-1	E22/1 2/Di/apa_trav-2	E22/1 2/Di/apa_trav-3	E22/12 /extra/apa_trav-1	E22/12 /extra/apa_trav-2
SiO2%	0.34	0.24	0.22	0.23	0.59	0.27	0.35	0.29	0.29	0.21	0.29	0.4	0.29	0.15
Fe2O3%	0.38	0.33	0.27	0.36	0.12	0.1	0.08	0.06	0.07	0.09	0.09	0.11	0.13	0.13
MnO%	0.12	0.12	0.09	0.14	0.13	0.13	0.17	0.11	0.13	0.15	0.22	0.14	0.1	0.13
MgO%	0.26	0.27	0.27	0.27	0.01	0	0.01	0.01	0	0.01	0.02	0.01	0.01	0.01
CaO%	54.28	53.94	54.36	53.51	54.9	55.12	54.3	55.19	55.04	55.2	54.63	55.04	54.85	54.87
Na2O%	0.14	0.12	0.12	0.08	0.11	0.06	0.16	0.14	0.16	0.16	0.12	0.11	0.12	0.12
P2O5%	41.48	41.54	42.01	41.69	41.78	41.73	41.81	41.38	41.62	42	41.87	41.48	41.68	42.08
SO3%	0.57	0.38	0.39	0.4	0.23	0.17	0.5	0.48	0.4	0.4	0.38	0.38	0.24	0.24
La2O3%	0.04	0.04	0.03	0.03	0.07	0.07	0.13	0.13	0.14	0.14	0.12	0.14	0.06	0.05
Ce2O3%	0.07	0.09	0.07	0.07	0.15	0.11	0.22	0.2	0.2	0.17	0.2	0.15	0.1	0.13
Pr2O3%	0	0	0	0.04	0.02	0	0	0	0	0	0	0	0	0
Nd2O3%	0.05	0.07	0.07	0.04	0.07	0.1	0.11	0.09	0.13	0.04	0.05	0.02	0.09	0.09
Sm2O3%	0	0	0.02	0.03	0.04	0.03	0.04	0	0.01	0.04	0.03	0.03	0.01	0
Y2O3%	0.04	0	0.04	0.02	0.08	0.1	0.1	0.07	0.11	0.07	0.06	0.11	0.12	0.1
SrO%	0.25	0.29	0.27	0.25	0.06	0.03	0.06	0.06	0.02	0.06	0.1	0.03	0.02	0.02
BaO%	0.01	0.01	0	0.01	0	0.01	0	0	0	0	0.01	0	0	0
As2O3%	0	0	0	0	0.01	0	0	0	0.04	0	0.01	0.04	0.01	0
F%	2.81	2.31	2.11	2.49	2.97	3.14	2.98	2.88	3.04	3.16	2.95	2.85	3	3.11
Cl%	0.44	0.45	0.38	0.35	0.31	0.31	0.33	0.36	0.36	0.35	0.37	0.34	0.37	0.3
H2O(c)	0.34	0.57	0.7	0.51	0.31	0.22	0.29	0.33	0.26	0.21	0.3	0.35	0.27	0.24
O=F	1.18	0.97	0.89	1.05	1.25	1.32	1.26	1.21	1.28	1.33	1.24	1.2	1.26	1.31
O=Cl	0.1	0.1	0.09	0.08	0.07	0.07	0.08	0.08	0.08	0.08	0.08	0.08	0.08	0.07
Sum Ox%	100.3	99.68	100.4	99.4	100.6	100.3	100.3	100.5	100.7	101	100.5	100.5	100.12	100.39
Cations														
Si	0.056	0.041	0.037	0.039	0.098	0.046	0.058	0.049	0.049	0.035	0.048	0.067	0.049	0.024
Fe3+	0.048	0.042	0.034	0.046	0.015	0.013	0.01	0.008	0.008	0.011	0.011	0.014	0.016	0.016
Mn2+	0.016	0.017	0.012	0.02	0.018	0.019	0.023	0.015	0.019	0.022	0.031	0.02	0.014	0.018
Mg	0.065	0.068	0.067	0.067	0.003	0.001	0.003	0.003	0.001	0.004	0.006	0.004	0.003	0.003
Ca	9.743	9.741	9.728	9.67	9.829	9.919	9.743	9.92	9.875	9.853	9.797	9.887	9.878	9.843
Na	0.047	0.038	0.04	0.026	0.037	0.019	0.05	0.045	0.051	0.052	0.039	0.035	0.038	0.04
P	5.883	5.929	5.94	5.953	5.911	5.933	5.928	5.877	5.901	5.924	5.933	5.888	5.932	5.965
S	0.071	0.047	0.049	0.051	0.028	0.021	0.063	0.061	0.05	0.05	0.048	0.048	0.03	0.03
La	0.002	0.002	0.002	0.002	0.004	0.004	0.008	0.008	0.009	0.008	0.007	0.008	0.004	0.003
Ce	0.004	0.005	0.004	0.004	0.009	0.007	0.014	0.012	0.012	0.01	0.013	0.009	0.006	0.008
Pr	0	0	0	0.003	0.001	0	0	0	0	0	0	0	0	0
Nd	0.003	0.004	0.004	0.003	0.004	0.006	0.006	0.006	0.008	0.003	0.003	0.001	0.005	0.006
Sm	0	0	0.001	0.002	0.002	0.002	0.002	0	0.001	0.002	0.002	0.002	0	0
Y	0.004	0	0.003	0.002	0.007	0.009	0.009	0.006	0.01	0.006	0.006	0.01	0.011	0.009
Sr	0.024	0.028	0.026	0.025	0.006	0.003	0.006	0.006	0.002	0.006	0.009	0.003	0.002	0.002
Ba	0	0.001	0	0	0	0.001	0	0	0	0	0.001	0	0	0
As	0	0	0	0	0.001	0	0	0	0.004	0	0.001	0.004	0.001	0
F	1.491	1.231	1.112	1.329	1.57	1.668	1.581	1.529	1.611	1.666	1.561	1.512	1.594	1.648
Cl	0.124	0.128	0.107	0.1	0.088	0.089	0.095	0.103	0.102	0.098	0.106	0.098	0.104	0.085
OH	0.385	0.642	0.781	0.572	0.342	0.243	0.324	0.369	0.287	0.236	0.333	0.39	0.301	0.267
Sum Cat#	17.97	17.96	17.95	17.91	17.98	18	17.93	18.02	18	17.99	17.95	18	17.99	17.967

Label	E22/12/extra/apa_trav-3	E22/15/1/apa1_trav-1	E22/15/1/apa1_trav-2	E22/15/2/apa1_trav1-1	E22/15/2/apa1_trav1-2	E22/15/2/apa1_trav1-3	E22/15/2/apa1_trav1-4	E22/15/2/apa1_trav2-1	E22/15/2/apa1_trav2-2	E22/15/3/apa1_trav-1	E22/15/3/apa1_trav-2	E22/15/4/apa1_trav-1	E22/15/4/apa1_trav-2	E22/15/4/apa1_trav-3	E22/15/4/apa1_trav-4	E22/15/4/apa1_trav-5	E22/15/4/apa1_trav2-2	E22/15/4/apa1_trav2-3	E27/64_B_apa_trav-1	E27/64_B_apa_trav-2	E27/64_B_apa_trav-3	E27/64_B_apa_trav-4	E27/64_C1_apa_trav-1	E27/64_C1_apa_trav-2	E27/64_C1_apa_trav-3	E27/64_C1_apa_trav-4	E27/64_C1_apa_trav-5
SiO2%	0.2	0.4	0.41	0.28	0.32	0.32	0.3	0.34	0.32	0.33	0.44	0.32	0.25	0.27	0.23	0.21	0.26	0.3	0.25	0.38	0.28	0.25	0.14	0.11	0.3	0.34	0.32
Fe2O3%	0.18	0.1	0.09	0.09	0.05	0.08	0.08	0.06	0.06	0.11	0.08	0.05	0.07	0.05	0.08	0.08	0.06	0.07	0.07	0.07	0.06	0.07	0.07	0.06	0.07	0.07	0.05
MnO%	0.06	0.17	0.2	0.16	0.17	0.12	0.18	0.17	0.15	0.19	0.18	0.12	0.12	0.16	0.14	0.14	0.15	0.1	0.07	0.15	0.13	0.07	0.14	0.12	0.13	0.14	0.12
MgO%	0.01	0.03	0.02	0	0.01	0.02	0.02	0.01	0.02	0.02	0.02	0.01	0.01	0.01	0.01	0	0.02	0.02	0.01	0.01	0.01	0.02	0.01	0.01	0.02	0.02	0.01
CaO%	54.66	54.91	54.62	55.35	54.74	54.8	54.99	54.73	55.03	54.4	54.26	54.24	55.01	55.66	55.12	55.5	54.85	55.25	54.82	54.97	54.92	55.14	55.58	55.18	55.01	54.79	54.69
Na2O%	0.15	0.16	0.17	0.12	0.12	0.11	0.15	0.17	0.11	0.1	0.25	0.11	0.12	0.15	0.14	0.11	0.13	0.15	0.13	0.24	0.13	0.11	0.08	0.08	0.14	0.11	0.12
P2O5%	41.87	41.36	41.58	41.85	41.48	41	40.92	41.03	40.84	41.34	40.38	41.6	41.46	41.33	41.51	41.54	41.56	40.96	41.84	40.6	41.65	41.8	42.01	41.65	41.38	41.21	41.04
SO3%	0.19	0.58	0.7	0.35	0.47	0.43	0.41	0.53	0.43	0.44	0.81	0.3	0.41	0.47	0.42	0.26	0.41	0.48	0.3	0.72	0.38	0.33	0.31	0.19	0.43	0.42	0.4
La2O3%	0.09	0.11	0.12	0.1	0.14	0.13	0.1	0.13	0.13	0.12	0.13	0.13	0.11	0.1	0.11	0.11	0.09	0.11	0.1	0.1	0.11	0.12	0.06	0.09	0.11	0.1	0.1
Ce2O3%	0.16	0.22	0.21	0.15	0.21	0.21	0.21	0.22	0.23	0.2	0.21	0.21	0.17	0.16	0.17	0.17	0.18	0.17	0.16	0.19	0.21	0.17	0.09	0.14	0.2	0.22	0.22
Pr2O3%	0	0.02	0	0	0.02	0	0.02	0.01	0	0.04	0.04	0.02	0	0	0.03	0	0	0.02	0.04	0.03	0	0	0	0	0.04	0	0
Nd2O3%	0.12	0.04	0.11	0.09	0.11	0.12	0.1	0.15	0.11	0.15	0.1	0.15	0.1	0.08	0.06	0.09	0.08	0.11	0.12	0.1	0.07	0.08	0.04	0.02	0.12	0.12	0.1
Sm2O3%	0	0.01	0.06	0.03	0.07	0	0.03	0.01	0	0.08	0.04	0.04	0	0	0	0	0.01	0.04	0.05	0.06	0	0.02	0	0.01	0.01	0.04	0.06
Y2O3%	0.18	0.08	0.06	0	0.04	0.08	0.05	0.06	0.09	0.09	0.1	0.05	0.04	0.05	0.04	0.1	0.05	0.08	0.08	0.04	0.04	0.07	0.02	0.05	0.08	0.05	0.04
SrO%	0	0.05	0.07	0.04	0.04	0.07	0.09	0.08	0.08	0.09	0.08	0.04	0.05	0.06	0.03	0.04	0.05	0.03	0.04	0.03	0.06	0.05	0.06	0.04	0.07	0.09	0.07
BaO%	0.01	0	0	0.02	0	0	0	0	0	0.01	0.01	0	0	0.01	0	0	0	0.01	0	0.01	0	0	0	0	0	0	0.01
As2O3%	0	0.01	0.01	0.02	0.01	0	0.01	0	0.01	0.01	0	0.02	0.01	0	0	0.02	0.02	0.01	0	0.02	0.01	0	0.01	0.02	0	0.01	0
F%	3.15	3.43	3.42	2.93	3.27	3.2	3	3.05	2.94	2.93	2.97	3.1	3.06	3.3	3.36	3.19	3.25	3.19	3.29	3.35	3.35	3.19	2.95	3.16	3.13	2.93	2.96
Cl%	0.31	0.38	0.39	0.44	0.41	0.43	0.47	0.44	0.47	0.43	0.48	0.35	0.37	0.4	0.36	0.35	0.38	0.39	0.31	0.41	0.38	0.4	0.31	0.27	0.34	0.37	0.32
H2O(c)	0.21	0.07	0.07	0.29	0.13	0.14	0.23	0.22	0.26	0.28	0.24	0.22	0.24	0.13	0.1	0.19	0.15	0.17	0.15	0.08	0.1	0.18	0.32	0.21	0.22	0.29	0.29
O=F	1.33	1.45	1.44	1.23	1.38	1.35	1.26	1.28	1.24	1.23	1.25	1.3	1.29	1.39	1.42	1.34	1.37	1.34	1.38	1.41	1.41	1.34	1.24	1.33	1.32	1.23	1.25
O=Cl	0.07	0.09	0.09	0.1	0.09	0.1	0.11	0.1	0.11	0.1	0.11	0.08	0.08	0.09	0.08	0.08	0.08	0.09	0.07	0.09	0.09	0.09	0.07	0.06	0.08	0.08	0.07
Sum Ox%	100.16	100.6	100.8	101	100.4	99.83	99.98	100	99.94	100	99.47	99.7	100.2	100.9	100.4	100.7	100.23	100.21	100.37	100.07	100.4	100.63	100.89	100.02	100.41	100.03	99.6
Cations																											
Si	0.034	0.066	0.069	0.046	0.055	0.054	0.05	0.058	0.055	0.055	0.075	0.053	0.042	0.045	0.039	0.036	0.043	0.05	0.041	0.065	0.047	0.041	0.023	0.019	0.051	0.057	0.054
Fe3+	0.022	0.012	0.012	0.012	0.006	0.011	0.01	0.008	0.008	0.013	0.011	0.007	0.009	0.007	0.01	0.01	0.008	0.008	0.009	0.009	0.007	0.009	0.009	0.007	0.008	0.01	0.006
Mn2+	0.009	0.024	0.028	0.022	0.025	0.018	0.026	0.025	0.022	0.027	0.026	0.018	0.017	0.022	0.02	0.019	0.022	0.014	0.01	0.021	0.019	0.01	0.019	0.017	0.018	0.02	0.017
Mg	0.002	0.006	0.005	0	0.002	0.006	0.005	0.003	0.004	0.004	0.004	0.001	0.003	0.003	0.003	0.001	0.005	0.005	0.003	0.002	0.003	0.004	0.003	0.002	0.005	0.006	0.003
Ca	9.84	9.856	9.769	9.896	9.851	9.933	9.967	9.897	9.978	9.827	9.87	9.807	9.909	9.984	9.914	9.974	9.874	9.984	9.848	9.949	9.871	9.889	9.932	9.96	9.901	9.899	9.922
Na	0.049	0.052	0.056	0.039	0.041	0.037	0.048	0.056	0.035	0.034	0.082	0.035	0.041	0.05	0.045	0.036	0.043	0.05	0.042	0.079	0.043	0.037	0.025	0.025	0.045	0.037	0.039
P	5.956	5.866	5.875	5.912	5.898	5.871	5.859	5.862	5.851	5.901	5.804	5.944	5.902	5.858	5.899	5.9	5.912	5.849	5.94	5.806	5.915	5.923	5.931	5.94	5.886	5.882	5.884
S	0.024	0.073	0.088	0.044	0.06	0.055	0.052	0.067	0.054	0.055	0.104	0.038	0.051	0.058	0.052	0.033	0.051	0.06	0.038	0.092	0.048	0.041	0.039	0.024	0.054	0.054	0.051
La	0.006	0.007	0.007	0.006	0.009	0.008	0.007	0.008	0.008	0.008	0.008	0.008	0.007	0.006	0.007	0.007	0.005	0.007	0.006	0.006	0.007	0.008	0.004	0.006	0.007	0.006	0.006
Ce	0.01	0.013	0.013	0.009	0.013	0.013	0.013	0.013	0.014	0.012	0.013	0.013	0.011	0.01	0.011	0.01	0.011	0.01	0.01	0.012	0.013	0.01	0.005	0.009	0.013	0.014	0.013
Pr	0	0.001	0	0	0.001	0	0.001	0	0	0.002	0.003	0.001	0	0	0.002	0	0	0.001	0.002	0.002	0	0	0	0	0.002	0	0
Nd	0.007	0.002	0.006	0.005	0.007	0.007	0.006	0.009	0.007	0.009	0.006	0.009	0.006	0.005	0.003	0.005	0.005	0.007	0.007	0.006	0.004	0.005	0.002	0.001	0.007	0.007	0.006
Sm	0	0	0.004	0.002	0.004	0	0.002	0.001	0	0.004	0.002	0.002	0	0	0	0	0.001	0.003	0.003	0.003	0	0.001	0	0.001	0.001	0.003	0.004
Y	0.017	0.007	0.005	0	0.003	0.007	0.004	0.005	0.008	0.008	0.009	0.004	0.004	0.005	0.004	0.009	0.004	0.008	0.007	0.003	0.003	0.006	0.002	0.004	0.008	0.004	0.004
Sr	0	0.005	0.007	0.004	0.004	0.007	0.009	0.008	0.008	0.008	0.008	0.004	0.005	0.006	0.003	0.004	0.005	0.003	0.004	0.003	0.005	0.005	0.006	0.004	0.007	0.009	0.007
Ba	0	0	0	0.001	0	0	0	0	0	0	0	0	0	0.001	0	0	0	0.001	0	0.001	0	0	0	0	0	0	0.001
As	0	0.001	0.001	0.002	0.001	0	0.001	0	0.001	0.001	0	0.002	0.001	0	0	0.002	0.002	0.001	0	0.002	0.001	0	0.001	0.002	0	0.001	0
F	1.673	1.819	1.806	1.547	1.736	1.715	1.602	1.629	1.573	1.56	1.594	1.652	1.627	1.746	1.786	1.691	1.726	1.7	1.743	1.788	1.78	1.687	1.557	1.685	1.66	1.564	1.585
Cl	0.089	0.108	0.112	0.125	0.115	0.122	0.135	0.125	0.134	0.123	0.138	0.1	0.106	0.112	0.101	0.1	0.107	0.11	0.088	0.119	0.109	0.113	0.088	0.078	0.096	0.106	0.091
OH	0.237	0.073	0.082	0.328	0.149	0.163	0.263	0.247	0.293	0.317	0.268	0.247	0.267	0.142	0.113	0.209	0.166	0.189	0.169	0.093	0.111	0.2	0.355	0.236	0.243	0.33	0.324
Sum Cat#	17.977	17.99	17.95	18	17.98	18.03	18.06	18.02	18.05	17.97	18.03	17.95	18.01	18.06	18.01	18.05	17.99	18.06	17.971	18.061	17.988	17.99	18.002	18.021	18.012	18.009	18.017

Label	E27/64_C2_apa_trav-1	E27/64_C2_apa_trav-2	E27/64_C2_apa_trav-3	E27/64_D_apa_trav-1	E27/64_D_apa_trav-2	E27/64_D_apa_trav-3	E27/64_D_apa_trav-4	E27/64_D_apa_trav-5	E27/85/A/apa_trav-1	E27/85/A/apa_trav-2	E27/85/A/apa_trav-3	E27/85/A/apa_trav-4	E27/85/A/apa_trav-5	E27/85/A/apa_trav-6	E27/85/A/apa_trav-7	E27/85/extra/apa_trav-1	E27/85/extra/apa_trav-2	E27/85/extra/apa_trav-3	E27/85/extra/apa_trav-4	E27/85/extra/apa_trav-5	E27/26/1a/apa_trav-1	E27/26/1a/apa_trav-2	E27/26/2/apa_trav-1	E27/26/2/apa_trav-2	E27/26/2/apa_trav-3	E27/26/A/apa_trav-1	E27/26/A/apa_trav-2
SiO2%	0.17	0.28	0.18	0.17	0.12	0.19	0.12	0.22	0.16	0.28	0.3	0.3	0.28	0.29	0.55	0.25	0.18	0.29	0.19	0.45	0.46	0.42	0.23	0.17	0.25	0.22	0.27
Fe2O3%	0.04	0.04	0.05	0.05	0.06	0.04	0.04	0.06	0.09	0.09	0.07	0.09	0.1	0.07	0.14	0.19	0.08	0.1	0.09	0.04	0.26	0.18	0.38	0.28	0.34	0.62	0.14
MnO%	0.11	0.1	0.14	0.13	0.1	0.12	0.06	0.1	0.14	0.12	0.12	0.15	0.11	0.15	0.16	0.15	0.17	0.14	0.14	0.12	0.19	0.2	0.11	0.15	0.1	0.08	0.09
MgO%	0.02	0.02	0.01	0.01	0	0	0	0	0.02	0.02	0.01	0.02	0.02	0.02	0.09	0.02	0.02	0.03	0.03	0.01	0.01	0.01	0.01	0.02	0.01	0	0.01
CaO%	55.24	55.16	55.08	55.28	55.53	55.16	55.3	55.12	55.6	55.26	54.86	55.05	55.22	55.62	54.8	54.87	54.98	54.8	54.74	55.48	54.7	54.8	54.99	54.65	54.81	55.21	55.33
Na2O%	0.1	0.12	0.11	0.12	0.09	0.1	0.11	0.11	0.09	0.11	0.11	0.12	0.14	0.12	0.07	0.12	0.14	0.09	0.13	0.06	0.27	0.27	0.09	0.08	0.09	0.09	0.14
P2O5%	41.79	41.31	42.01	41.86	42.13	41.58	42.03	41.88	41.78	41.23	41.15	41.58	40.79	41.38	41.68	41.36	41.7	41.06	41.63	41.58	40.73	41.24	41.88	42.04	42.12	41.99	41.41
SO3%	0.3	0.39	0.28	0.32	0.26	0.34	0.29	0.28	0.32	0.39	0.35	0.37	0.38	0.4	0.24	0.38	0.39	0.39	0.38	0.18	0.99	0.88	0.26	0.17	0.23	0.27	0.46
La2O3%	0.11	0.15	0.08	0.06	0.07	0.07	0.07	0.08	0.13	0.11	0.1	0.12	0.13	0.13	0.1	0.17	0.13	0.11	0.13	0.06	0.12	0.11	0.11	0.08	0.14	0.09	0.11
Ce2O3%	0.13	0.2	0.15	0.1	0.1	0.12	0.11	0.13	0.12	0.18	0.19	0.22	0.21	0.21	0.1	0.2	0.16	0.21	0.17	0.09	0.2	0.22	0.14	0.17	0.18	0.13	0.19
Pr2O3%	0.03	0	0	0	0	0	0	0	0	0.05	0	0.05	0	0	0.05	0.01	0	0	0	0	0	0.05	0	0	0	0	0
Nd2O3%	0.05	0.12	0.07	0.06	0.02	0.03	0.07	0.06	0.02	0.11	0.12	0.13	0.1	0.07	0.04	0.04	0.05	0.13	0.02	0	0.08	0.08	0.09	0.09	0.12	0.12	0.04
Sm2O3%	0	0	0.01	0.03	0	0	0.05	0.02	0.02	0	0.01	0.03	0.04	0.02	0.02	0.01	0	0	0	0	0.07	0.04	0	0	0	0	0
Y2O3%	0.03	0.04	0.06	0.05	0.02	0.05	0.02	0.01	0.05	0.07	0.08	0.06	0.04	0.03	0.01	0.05	0.02	0.07	0.02	0.02	0.11	0.09	0.06	0.07	0.02	0.07	0.04
SrO%	0.06	0.07	0.07	0.06	0.06	0.05	0.05	0.08	0.03	0.08	0.06	0.08	0.08	0.02	0.02	0	0.03	0.07	0.03	0.04	0.07	0.08	0.06	0.1	0.05	0.04	0.04
BaO%	0	0	0	0	0	0	0	0	0	0	0	0	0	0.01	0.01	0.01	0	0	0	0	0	0	0.02	0.01	0.01	0	0
As2O3%	0.01	0.01	0.02	0.01	0.01	0.01	0	0.01	0.01	0	0	0	0	0.01	0	0	0.01	0.01	0.01	0.02	0.01	0.01	0	0	0.01	0.01	0.01
F%	3.12	3.21	2.95	3.34	3.32	3.27	3.34	3.2	2.83	2.8	2.86	2.72	2.71	2.67	3.1	2.75	2.92	2.91	2.84	2.95	3.09	2.98	3.34	3.05	3.21	3.53	3.27
Cl%	0.33	0.35	0.33	0.32	0.24	0.39	0.4	0.3	0.42	0.43	0.46	0.46	0.43	0.4	0.44	0.36	0.38	0.4	0.36	0.32	0.45	0.45	0.39	0.41	0.38	0.27	0.37
H2O(c)	0.22	0.17	0.31	0.13	0.16	0.14	0.11	0.2	0.35	0.35	0.3	0.38	0.38	0.42	0.21	0.39	0.31	0.29	0.35	0.31	0.21	0.27	0.11	0.24	0.18	0.06	0.15
O=F	1.32	1.35	1.24	1.41	1.4	1.37	1.41	1.35	1.19	1.18	1.21	1.15	1.14	1.12	1.31	1.16	1.23	1.23	1.19	1.24	1.3	1.25	1.41	1.28	1.35	1.49	1.38
O=Cl	0.07	0.08	0.08	0.07	0.05	0.09	0.09	0.07	0.1	0.1	0.1	0.1	0.1	0.09	0.1	0.08	0.09	0.09	0.08	0.07	0.1	0.1	0.09	0.09	0.09	0.06	0.08
Sum Ox%	100.49	100.31	100.6	100.62	100.84	100.18	100.7	100.43	100.9	100.4	99.83	100.7	99.91	100.8	100.4	100.08	100.36	99.79	99.98	100.39	100.62	101.01	100.8	100.4	100.8	101.3	100.6
Cations																											
Si	0.029	0.048	0.03	0.029	0.02	0.032	0.021	0.037	0.027	0.047	0.05	0.05	0.048	0.048	0.092	0.042	0.031	0.049	0.031	0.075	0.077	0.071	0.039	0.029	0.042	0.037	0.045
Fe3+	0.005	0.005	0.006	0.007	0.008	0.005	0.006	0.008	0.011	0.011	0.008	0.012	0.012	0.009	0.018	0.023	0.01	0.013	0.011	0.005	0.032	0.023	0.048	0.035	0.043	0.077	0.018
Mn2+	0.016	0.014	0.02	0.019	0.014	0.017	0.009	0.014	0.02	0.017	0.017	0.021	0.015	0.021	0.023	0.021	0.025	0.02	0.02	0.017	0.027	0.028	0.016	0.022	0.014	0.012	0.012
Mg	0.005	0.004	0.003	0.002	0.001	0.001	0.001	0.001	0.005	0.006	0.004	0.006	0.006	0.004	0.023	0.006	0.005	0.007	0.007	0.002	0.002	0.002	0.003	0.006	0.003	0	0.003
Ca	9.918	9.945	9.869	9.911	9.923	9.936	9.906	9.893	9.955	9.96	9.937	9.884	10.02	9.98	9.834	9.901	9.88	9.932	9.867	9.968	9.828	9.794	9.852	9.817	9.802	9.845	9.937
Na	0.034	0.04	0.037	0.038	0.029	0.033	0.037	0.035	0.028	0.036	0.036	0.038	0.046	0.038	0.023	0.038	0.046	0.03	0.042	0.018	0.089	0.087	0.029	0.025	0.028	0.028	0.047
P	5.93	5.884	5.947	5.93	5.949	5.919	5.949	5.939	5.91	5.872	5.89	5.899	5.848	5.868	5.91	5.897	5.922	5.88	5.929	5.902	5.783	5.824	5.929	5.967	5.952	5.917	5.877
S	0.038	0.049	0.035	0.04	0.032	0.043	0.037	0.035	0.041	0.049	0.044	0.046	0.048	0.05	0.03	0.048	0.05	0.049	0.048	0.022	0.124	0.111	0.032	0.021	0.029	0.033	0.057
La	0.007	0.009	0.005	0.004	0.004	0.004	0.004	0.005	0.008	0.007	0.006	0.007	0.008	0.008	0.006	0.011	0.008	0.007	0.008	0.004	0.007	0.007	0.007	0.005	0.009	0.005	0.007
Ce	0.008	0.012	0.009	0.006	0.006	0.007	0.007	0.008	0.007	0.011	0.012	0.014	0.013	0.013	0.006	0.012	0.01	0.013	0.01	0.005	0.012	0.014	0.009	0.01	0.011	0.008	0.011
Pr	0.002	0	0	0	0	0	0	0	0	0.003	0	0.003	0	0	0.003	0	0	0	0	0	0	0.003	0	0	0	0	0
Nd	0.003	0.007	0.004	0.003	0.001	0.002	0.004	0.004	0.001	0.006	0.007	0.008	0.006	0.004	0.003	0.002	0.003	0.008	0.001	0	0.005	0.005	0.005	0.005	0.007	0.007	0.002
Sm	0	0	0	0.002	0	0	0.003	0.001	0.001	0	0.001	0.002	0.002	0.001	0.001	0.001	0	0	0	0	0.004	0.002	0	0	0	0	0
Y	0.002	0.003	0.005	0.004	0.002	0.004	0.002	0	0.005	0.006	0.007	0.005	0.004	0.003	0.001	0.005	0.001	0.007	0.002	0.002	0.01	0.008	0.005	0.007	0.002	0.006	0.004
Sr	0.006	0.007	0.007	0.006	0.006	0.004	0.005	0.007	0.003	0.008	0.005	0.008	0.008	0.002	0.002	0	0.003	0.007	0.003	0.004	0.007	0.007	0.006	0.01	0.005	0.004	0.004
Ba	0	0	0	0	0	0	0	0	0	0	0	0	0	0	0	0.001	0	0	0	0	0	0	0.001	0	0	0	0
As	0.001	0.001	0.002	0.001	0.001	0.001	0	0.001	0.001	0	0	0	0	0.001	0	0	0.001	0.001	0.001	0.002	0.001	0.001	0	0	0.001	0.001	0.002
F	1.656	1.708	1.563	1.768	1.752	1.736	1.764	1.693	1.493	1.488	1.531	1.444	1.449	1.415	1.645	1.463	1.549	1.557	1.509	1.565	1.638	1.572	1.768	1.617	1.692	1.857	1.733
Cl	0.094	0.101	0.095	0.09	0.067	0.11	0.113	0.085	0.12	0.122	0.131	0.13	0.122	0.115	0.124	0.102	0.108	0.116	0.102	0.09	0.127	0.128	0.112	0.117	0.108	0.077	0.105
OH	0.251	0.191	0.343	0.143	0.182	0.153	0.122	0.222	0.387	0.39	0.337	0.426	0.429	0.471	0.231	0.435	0.343	0.328	0.39	0.346	0.236	0.3	0.12	0.266	0.2	0.066	0.162
Sum Cat#	18.004	18.029	17.98	18.002	17.996	18.008	17.989	17.989	18.02	18.04	18.02	18	18.08	18.05	17.98	18.008	17.994	18.023	17.983	18.027	18.009	17.984	17.98	17.96	17.95	17.98	18.03

D2 7

Label	E27/2 6/A/ap a_trav-3	E27/2 6/A/ap a_trav-4	E27/2 6/A/ap a_trav-5	E22/26 /1/apa 1_trav-1	E22/26 /1/apa 1_trav-2	E22/26 /1/apa 1_trav-3	E22/26 /2/apa 1_trav-1	E22/26 /2/apa 1_trav-2	E22/26 /2/apa 1_trav-3	E22/26 /3/apa 1_trav-1	E22/26 /3/apa 1_trav-2	E22/26 /3/apa 1_trav-3	E22/26 /3/apa 1_trav-4	E22/26 /3/apa 1_trav-5
SiO2%	0.32	0.3	0.15	0.32	0.31	0.35	0.35	0.3	0.41	0.34	0.29	0.3	0.29	0.2
Fe2O3%	0.09	0.08	0.16	0.06	0.06	0.04	0.07	0.09	0.08	0.07	0.07	0.06	0.07	0.08
MnO%	0.07	0.11	0.05	0.12	0.1	0.11	0.12	0.16	0.14	0.12	0.13	0.16	0.13	0.11
MgO%	0.01	0.01	0	0.01	0	0.01	0.02	0.02	0.02	0.02	0.02	0.01	0.01	0.02
CaO%	55.01	54.99	55.6	54.89	54.62	55.05	55.06	55.1	55.28	55.21	54.97	55.37	55.11	55.61
Na2O%	0.13	0.14	0.06	0.09	0.15	0.09	0.11	0.15	0.11	0.16	0.1	0.11	0.13	0.13
P2O5%	41.06	41.7	42.38	41.96	41.33	41.74	41.75	41.1	41.42	41.87	41.63	41.5	41.38	41.86
SO3%	0.43	0.41	0.23	0.31	0.42	0.23	0.41	0.4	0.31	0.42	0.33	0.36	0.37	0.35
La2O3%	0.11	0.11	0.08	0.15	0.13	0.12	0.14	0.11	0.12	0.11	0.11	0.12	0.11	0.12
Ce2O3%	0.2	0.2	0.11	0.23	0.23	0.15	0.22	0.23	0.16	0.22	0.22	0.22	0.2	0.14
Pr2O3%	0.01	0.01	0.04	0.01	0	0.04	0.03	0.01	0	0	0	0	0.02	0
Nd2O3%	0.12	0.12	0.04	0.13	0.1	0.07	0.11	0.12	0.08	0.13	0.1	0.1	0.14	0.03
Sm2O3%	0	0.04	0.01	0	0.02	0.03	0.02	0.07	0.01	0	0	0.05	0.06	0
Y2O3%	0.08	0.07	0.04	0.07	0.04	0.05	0.05	0.05	0.05	0.08	0.1	0.07	0.08	0
SrO%	0.06	0.06	0.06	0.04	0.04	0.04	0.08	0.1	0.04	0.08	0.08	0.11	0.08	0.04
BaO%	0	0.01	0	0	0	0	0	0	0	0	0.01	0	0.01	0.01
As2O3%	0.02	0.02	0.01	0	0	0	0.01	0	0	0.02	0.01	0	0.01	0.01
F%	3.24	3.09	3.36	3.74	3.83	3.77	3.41	3.37	3.29	3.65	3.57	3.83	3.61	3.69
Cl%	0.4	0.4	0.32	0.19	0.2	0.19	0.23	0.22	0.23	0.23	0.24	0.27	0.25	0.23
H2O(c)	0.14	0.23	0.13	0	0	0	0.12	0.13	0.17	0.01	0.03	0	0.01	0
O=F	1.37	1.3	1.41	1.58	1.61	1.59	1.44	1.42	1.38	1.54	1.5	1.61	1.52	1.55
O=Cl	0.09	0.09	0.07	0.04	0.05	0.04	0.05	0.05	0.05	0.05	0.05	0.06	0.06	0.05
Sum Ox%	100	100.7	101.3	100.71	99.93	100.45	100.84	100.24	100.47	101.15	100.45	100.98	100.49	101.02
Cations														
Si	0.054	0.05	0.025	0.054	0.053	0.06	0.058	0.051	0.069	0.056	0.049	0.05	0.048	0.034
Fe3+	0.011	0.011	0.02	0.008	0.007	0.005	0.009	0.011	0.01	0.009	0.008	0.008	0.009	0.01
Mn2+	0.01	0.016	0.007	0.016	0.014	0.016	0.018	0.022	0.021	0.018	0.019	0.022	0.018	0.015
Mg	0.002	0.002	0.001	0.003	0	0.001	0.004	0.006	0.006	0.004	0.004	0.003	0.003	0.005
Ca	9.95	9.859	9.89	9.828	9.873	9.891	9.852	9.95	9.936	9.849	9.882	9.935	9.922	9.937
Na	0.041	0.045	0.019	0.028	0.047	0.028	0.036	0.048	0.036	0.052	0.031	0.037	0.042	0.042
P	5.868	5.907	5.956	5.936	5.903	5.926	5.903	5.865	5.883	5.902	5.913	5.884	5.887	5.91
S	0.054	0.052	0.028	0.039	0.054	0.03	0.051	0.051	0.039	0.053	0.042	0.045	0.047	0.043
La	0.007	0.007	0.005	0.009	0.008	0.007	0.009	0.007	0.007	0.007	0.007	0.007	0.007	0.007
Ce	0.012	0.012	0.006	0.014	0.014	0.009	0.014	0.014	0.01	0.013	0.013	0.013	0.012	0.009
Pr	0.001	0	0.002	0.001	0	0.002	0.002	0.001	0	0	0	0	0.001	0
Nd	0.007	0.007	0.002	0.008	0.006	0.004	0.007	0.007	0.005	0.008	0.006	0.006	0.008	0.002
Sm	0	0.002	0	0	0.001	0.002	0.001	0.004	0	0	0	0.003	0.003	0
Y	0.007	0.006	0.003	0.006	0.004	0.004	0.005	0.004	0.004	0.007	0.009	0.007	0.007	0
Sr	0.006	0.005	0.006	0.004	0.004	0.004	0.008	0.01	0.004	0.008	0.008	0.011	0.008	0.004
Ba	0	0	0	0	0	0	0	0	0	0	0	0	0.001	0.001
As	0.002	0.002	0.001	0	0	0	0.001	0	0	0.002	0.001	0	0.001	0.001
F	1.732	1.635	1.764	1.977	2.044	1.999	1.803	1.796	1.744	1.924	1.896	2.028	1.92	1.945
Cl	0.114	0.114	0.089	0.055	0.058	0.054	0.066	0.062	0.065	0.065	0.067	0.075	0.07	0.064
OH	0.154	0.251	0.147	0.001	0.001	0.001	0.13	0.143	0.191	0.011	0.037	0.001	0.01	0.001
Sum Cat#	18.03	17.98	17.97	17.987	18.091	18.043	17.979	18.05	18.029	17.988	17.992	18.135	18.024	18.031

Label	E27/4 6/3/ap a_trav-1	E27/4 6/3/ap a_trav-2	E27/4 6/3/ap a_trav-3	E27/4 6/4/ap a_trav-1	E27/4 6/4/ap a_trav-2	E27/4 6/4/ap a_trav-3	E27/4 6/A/ap a_trav-1	E27/4 6/A/ap a_trav-2	E27/4 6/A/ap a_trav-3	E27/7 6/B/ap a_2-1	E27/7 6/B/ap a_2-2	E27/7 6/A/ap a_2-1	E27/7 6/A/ap a_2-2	E27/7 6/A/ap a_2-3
SiO2%	0.26	0.19	0.16	0.25	0.34	0.28	0.35	0.29	0.37	0.09	0.2	0.14	0.27	0.32
Fe2O3%	0.14	0.12	0.12	0.21	0.15	0.15	0.19	0.14	0.18	0.25	0.21	0.09	0.06	0.06
MnO%	0.11	0.14	0.17	0.14	0.17	0.12	0.2	0.14	0.22	0.11	0.13	0.2	0.16	0.16
MgO%	0.02	0.02	0.03	0.02	0.02	0.01	0.03	0.03	0.04	0.02	0.01	0.03	0.02	0.03
CaO%	54.49	54.83	54.64	54.87	54.66	54.46	54.39	54.56	54.48	54.51	54.37	54.2	54.78	54.97
Na2O%	0.25	0.07	0.05	0.15	0.13	0.21	0.17	0.21	0.24	0.09	0.09	0.18	0.13	0.16
P2O5%	40.99	41.95	42.15	41.25	41.35	42.24	40.78	41.17	40.95	42	41.5	41.67	41.77	40.91
SO3%	0.55	0.14	0.1	0.15	0.33	0.28	0.62	0.65	0.72	0.19	0.37	0.22	0.36	0.39
La2O3%	0.12	0.11	0.1	0.12	0.14	0.15	0.1	0.11	0.1	0.09	0.14	0.05	0.11	0.12
Ce2O3%	0.22	0.23	0.22	0.28	0.26	0.32	0.19	0.17	0.23	0.09	0.14	0.1	0.19	0.23
Pr2O3%	0	0	0	0	0	0.03	0.01	0.01	0	0	0	0.01	0	0.01
Nd2O3%	0.1	0.1	0.1	0.08	0.15	0.17	0.12	0.1	0.08	0.04	0.04	0.11	0.15	0.08
Sm2O3%	0.02	0.02	0	0	0.03	0.01	0.07	0.01	0.05	0	0.03	0.06	0.01	0.05
Y2O3%	0.19	0.11	0.09	0.19	0.15	0.25	0.05	0.06	0.08	0.02	0.05	0.21	0.06	0.08
SrO%	0	0.08	0.11	0.02	0.04	0	0.1	0.09	0.08	0.03	0.02	0	0.1	0.09
BaO%	0	0	0.01	0	0	0	0.01	0	0	0.01	0.01	0	0	0
As2O3%	0.01	0.01	0	0.01	0.01	0	0	0	0.02	0.02	0.03	0	0	0.01
F%	3.15	3.04	2.84	2.96	2.99	3.33	2.84	2.87	2.76	3.09	3.09	3.19	3.28	3.22
Cl%	0.36	0.48	0.5	0.44	0.53	0.26	0.52	0.55	0.58	0.25	0.32	0.22	0.28	0.3
H2O(c)	0.19	0.22	0.31	0.26	0.23	0.15	0.29	0.28	0.32	0.25	0.23	0.21	0.16	0.17
O=F	1.33	1.28	1.19	1.25	1.26	1.4	1.2	1.21	1.16	1.3	1.3	1.34	1.38	1.35
O=Cl	0.08	0.11	0.11	0.1	0.12	0.06	0.12	0.12	0.13	0.06	0.07	0.05	0.06	0.07
Sum Ox%	99.76	100.5	100.4	100.1	100.3	101	99.72	100.1	100.2	99.77	99.63	99.49	100.5	99.93
Cations														
Si	0.044	0.031	0.026	0.042	0.058	0.046	0.059	0.048	0.062	0.015	0.035	0.025	0.045	0.053
Fe3+	0.017	0.015	0.015	0.027	0.019	0.018	0.024	0.018	0.022	0.031	0.027	0.012	0.008	0.008
Mn2+	0.016	0.02	0.024	0.019	0.024	0.017	0.029	0.02	0.031	0.015	0.019	0.028	0.022	0.023
Mg	0.005	0.005	0.007	0.006	0.006	0.004	0.007	0.007	0.009	0.005	0.003	0.008	0.005	0.007
Ca	9.873	9.859	9.822	9.936	9.864	9.725	9.867	9.844	9.83	9.828	9.836	9.816	9.836	9.963
Na	0.084	0.024	0.015	0.05	0.041	0.067	0.057	0.067	0.078	0.03	0.029	0.06	0.041	0.051
P	5.868	5.96	5.986	5.903	5.896	5.96	5.846	5.869	5.839	5.984	5.932	5.964	5.926	5.859
S	0.07	0.018	0.012	0.019	0.042	0.035	0.078	0.082	0.091	0.024	0.047	0.028	0.046	0.05
La	0.008	0.007	0.006	0.007	0.008	0.009	0.006	0.007	0.006	0.006	0.009	0.003	0.007	0.007
Ce	0.013	0.014	0.014	0.017	0.016	0.019	0.012	0.01	0.014	0.005	0.009	0.006	0.012	0.014
Pr	0	0	0	0	0	0.002	0	0.001	0	0	0	0	0	0
Nd	0.006	0.006	0.006	0.005	0.009	0.01	0.007	0.006	0.005	0.002	0.002	0.007	0.009	0.005
Sm	0.001	0.001	0	0	0.002	0.001	0.004	0.001	0.003	0	0.002	0.003	0.001	0.003
Y	0.017	0.01	0.008	0.017	0.013	0.022	0.005	0.005	0.007	0.002	0.004	0.019	0.005	0.007
Sr	0	0.008	0.011	0.002	0.004	0	0.01	0.009	0.008	0.003	0.002	0	0.01	0.009
Ba	0	0	0.001	0	0	0	0	0	0	0	0.001	0	0	0
As	0.001	0.001	0	0.002	0.001	0	0	0	0.002	0.002	0.004	0	0	0.002
F	1.685	1.615	1.505	1.581	1.592	1.755	1.523	1.527	1.471	1.643	1.652	1.706	1.739	1.721
Cl	0.103	0.135	0.143	0.125	0.151	0.074	0.148	0.158	0.165	0.072	0.092	0.063	0.079	0.087
OH	0.213	0.25	0.352	0.294	0.257	0.171	0.33	0.316	0.364	0.285	0.256	0.231	0.183	0.192
Sum Cat#	18.02	17.98	17.95	18.05	18	17.94	18.01	17.99	18.01	17.95	17.96	17.98	17.97	18.06

Label	E27/76/A/apa_2-4	E27/76/A/apa_2-5	E48_4_1_apa_-1	E48_4_1_apa_-2	E48_4_1_apa_-5	E48_4_2_apa_-1	E48_4_2_apa_-3	E48_4_2_apa_-4	E48_4_3_apa_-2	E48_4_3_apa_-3	E48_4_3_apa_-4	E48_4_3_apa_-5	E48_4_3_apa_-6	E48_4_3_apa_-7	E48_4_apa1_-1	E48_4_apa1_-2	E48_4_apa1_-3	E48_8_apa-1	E48_8_apa-2	E48_8_apa-3	E48_8_apa-4	E27/40/1_apa1	E27/40/1_apa2	E27/40/1_apa3	E27/40/1_apa4	E27/40/1_apa5	E27/40/1_apa6	E27/40/1_apa7	E27/68/1_apa1
SiO2%	0.35	0.07	0.32	0.31	0.63	0.28	0.33	0.28	0.3	0.2	0.38	0.29	0.04	0.28	0.29	0.28	0.23	0.06	0.36	0.21	0.22	0.23	0.25	0.16	0.28	0.31	0.29	0.12	0.25
Fe2O3%	0.07	0.12	0.05	0.08	0.06	0.06	0.08	0.07	0.08	0.05	0.05	0.05	0	0.08	0.06	0.03	0.06	0.33	0.08	0.1	0.08	0.09	0.11	0.06	0.11	0.09	0.07	0.08	0.07
MnO%	0.14	0.19	0.11	0.15	0.12	0.07	0.12	0.21	0.19	0.19	0.21	0.23	0.01	0.14	0.05	0.09	0.07	0.44	0.2	0.18	0.21	0.1	0.17	0.12	0.19	0.13	0.15	0.16	0.17
MgO%	0.03	0.05	0.02	0.02	0.02	0.01	0.01	0.02	0.03	0.01	0.03	0.02	0	0.02	0	0.01	0	0.09	0.03	0.03	0.03	0.03	0.02	0.02	0.03	0.03	0.03	0.03	0.02
CaO%	54.97	54.42	54.6	54.53	54.28	54.36	53.99	54.43	53.73	54.21	54.09	54.41	54.56	54.32	54.12	53.83	54.13	54.08	53.59	53.84	53.8	54.79	54.4	54.95	54.63	54.6	54.32	55.17	54.6
Na2O%	0.13	0.22	0.13	0.18	0.11	0.17	0.13	0.14	0.1	0.17	0.12	0.13	0.09	0.11	0.18	0.18	0.14	0.22	0.13	0.16	0.1	0.22	0.21	0.23	0.16	0.29	0.26	0.16	0.21
P2O5%	40.49	41.26	40.9	40.6	40.51	41.13	40.94	41.41	40.77	41.09	40.98	40.95	41.47	40.92	40.12	40.41	40.98	40.99	40.16	40.43	40.78	41.84	41.71	41.8	41.25	41.43	41.44	41.98	41.75
SO3%	0.43	0.3	0.23	0.41	0.36	0.37	0.42	0.42	0.37	0.45	0.39	0.38	0.14	0.33	0.39	0.42	0.23	0.11	0.44	0.32	0.21	0.53	0.37	0.33	0.37	0.67	0.45	0.26	0.39
La2O3%	0.12	0.05	0.09	0.12	0.12	0.09	0.16	0.13	0.12	0.09	0.12	0.14	0	0.1	0.1	0.08	0.1	0.04	0.16	0.14	0.1	0.1	0.13	0.07	0.16	0.15	0.12	0.06	0.08
Ce2O3%	0.21	0.11	0.27	0.23	0.25	0.2	0.24	0.2	0.21	0.14	0.19	0.21	0.02	0.19	0.24	0.19	0.23	0.12	0.27	0.21	0.22	0.18	0.26	0.18	0.27	0.27	0.24	0.12	0.2
Pr2O3%	0.05	0	0	0.01	0	0	0.01	0.02	0.04	0.04	0.05	0.02	0	0.01	0.05	0.01	0.01	0	0	0	0	0.02	0	0.05	0	0	0	0.01	0.02
Nd2O3%	0.08	0.01	0.15	0.18	0.15	0.12	0.16	0.1	0.13	0.08	0.15	0.14	0.01	0.11	0.12	0.16	0.15	0.1	0.08	0.15	0.09	0.13	0.16	0.17	0.14	0.18	0.17	0.11	0.14
Sm2O3%	0.04	0.01	0.04	0.02	0.03	0.06	0	0.03	0.04	0	0.04	0.01	0.03	0.03	0.01	0.02	0.01	0.03	0	0.07	0	0.03	0.03	0.05	0	0.06	0.01	0.01	0
Y2O3%	0.11	0.2	0.08	0.09	0.09	0.13	0.08	0.05	0.1	0.04	0.08	0.12	0.18	0.05	0.17	0.2	0.17	0.32	0.09	0.11	0.07	0.04	0.21	0.23	0.14	0.18	0.2	0.12	0.27
SrO%	0.08	0	0.12	0.11	0.11	0.03	0.06	0.09	0.09	0.08	0.08	0.1	0.17	0.08	0	0	0	0.03	0.07	0.07	0.07	0.04	0	0	0.01	0	0	0	0
BaO%	0	0	0	0	0	0.01	0	0.01	0	0	0	0	0.02	0	0	0	0	0	0.01	0.02	0	0	0	0	0	0	0	0	0
As2O3%	0	0.01	0.01	0	0	0.01	0.01	0.01	0	0	0	0	0.01	0	0.01	0.01	0.01	0	0	0	0	0	0	0	0	0	0.02	0	0
F%	3.24	3.01	3.11	3.19	3.43	3.37	3.2	3.04	3.29	3.43	3.28	3.45	3.8	3.3	3.47	3.6	3.6	3.51	3.59	3.6	3.69	3.3	3.35	3.35	3.37	3.45	3.53	3.62	3.28
Cl%	0.29	0.33	0.15	0.17	0.16	0.13	0.16	0.18	0.16	0.17	0.16	0.17	0	0.15	0.18	0.19	0.17	0.25	0.16	0.16	0.16	0.34	0.3	0.3	0.32	0.34	0.31	0.31	0.24
H2O(c)	0.15	0.26	0.25	0.2	0.09	0.14	0.2	0.29	0.15	0.09	0.17	0.09	0	0.15	0.05	0	0.01	0.03	0	0	0	0.14	0.12	0.13	0.1	0.07	0.03	0	0.17
O=F	1.36	1.27	1.31	1.34	1.44	1.42	1.35	1.28	1.38	1.44	1.38	1.45	1.6	1.39	1.46	1.51	1.52	1.48	1.51	1.52	1.55	1.39	1.41	1.41	1.42	1.45	1.49	1.52	1.38
O=Cl	0.07	0.08	0.03	0.04	0.04	0.03	0.04	0.04	0.04	0.04	0.04	0.04	0	0.03	0.04	0.04	0.04	0.06	0.04	0.04	0.04	0.08	0.07	0.07	0.07	0.08	0.07	0.07	0.06
Sum Ox%	99.54	99.28	99.28	99.23	99.05	99.29	98.91	99.81	98.48	99.07	99.15	99.42	98.96	98.96	98.1	98.15	98.74	99.2	97.87	98.23	98.24	100.7	100.3	100.7	100	100.7	100.1	100.7	100.4
Cations																													
Si	0.059	0.012	0.055	0.053	0.108	0.048	0.056	0.047	0.052	0.034	0.064	0.05	0.007	0.048	0.05	0.05	0.04	0.01	0.062	0.037	0.037	0.039	0.041	0.026	0.047	0.052	0.048	0.021	0.041
Fe3+	0.009	0.015	0.006	0.01	0.007	0.008	0.01	0.009	0.011	0.006	0.006	0.006	0	0.01	0.01	0	0.01	0.043	0.011	0.012	0.01	0.012	0.013	0.007	0.013	0.011	0.009	0.011	0.009
Mn2+	0.021	0.028	0.015	0.021	0.017	0.01	0.018	0.03	0.027	0.028	0.03	0.033	0.001	0.021	0.01	0.01	0.01	0.063	0.028	0.026	0.031	0.014	0.025	0.017	0.027	0.018	0.022	0.023	0.024
Mg	0.007	0.013	0.005	0.005	0.005	0.002	0.003	0.005	0.007	0.003	0.007	0.005	0	0.004	0	0	0	0.023	0.008	0.007	0.007	0.007	0.006	0.005	0.008	0.008	0.006	0.007	0.005
Ca	10.02	9.895	9.952	9.951	9.91	9.879	9.848	9.835	9.85	9.868	9.848	9.896	9.941	9.912	9.99	9.91	9.91	9.882	9.902	9.925	9.897	9.805	9.787	9.86	9.877	9.791	9.799	9.886	9.806
Na	0.041	0.072	0.042	0.058	0.036	0.057	0.042	0.045	0.032	0.057	0.04	0.041	0.031	0.038	0.059	0.06	0.048	0.071	0.042	0.052	0.035	0.07	0.068	0.074	0.052	0.094	0.084	0.051	0.067
P	5.829	5.928	5.89	5.855	5.844	5.907	5.901	5.912	5.906	5.911	5.896	5.886	5.97	5.9	5.853	5.881	5.925	5.918	5.864	5.889	5.929	5.916	5.929	5.926	5.893	5.871	5.908	5.944	5.925
S	0.055	0.039	0.029	0.053	0.046	0.047	0.054	0.053	0.047	0.057	0.049	0.048	0.018	0.043	0.051	0.055	0.029	0.015	0.057	0.042	0.027	0.066	0.047	0.041	0.047	0.084	0.057	0.032	0.049
La	0.008	0.003	0.006	0.007	0.008	0.006	0.01	0.008	0.007	0.006	0.007	0.009	0	0.007	0.006	0.005	0.006	0.002	0.01	0.009	0.007	0.006	0.008	0.005	0.01	0.009	0.007	0.003	0.005
Ce	0.013	0.007	0.017	0.015	0.016	0.012	0.015	0.012	0.013	0.009	0.012	0.013	0.002	0.012	0.015	0.012	0.014	0.007	0.017	0.013	0.014	0.011	0.016	0.011	0.017	0.017	0.015	0.007	0.012
Pr	0.003	0	0	0	0	0	0.001	0.001	0.003	0.003	0.003	0.001	0	0	0.003	0.001	0	0	0	0	0	0.001	0	0.003	0	0	0	0.001	0.001
Nd	0.005	0.001	0.009	0.011	0.009	0.008	0.009	0.006	0.008	0.005	0.009	0.009	0.001	0.006	0.007	0.01	0.009	0.006	0.005	0.009	0.005	0.008	0.009	0.01	0.009	0.011	0.01	0.007	0.008
Sm	0.002	0	0.002	0.001	0.002	0.004	0	0.002	0.002	0	0.003	0.001	0.002	0.002	0.001	0.001	0	0.002	0	0.004	0	0.002	0.002	0.003	0	0.004	0.001	0	0
Y	0.01	0.018	0.007	0.008	0.008	0.012	0.007	0.005	0.009	0.004	0.007	0.011	0.016	0.004	0.015	0.018	0.015	0.029	0.008	0.01	0.006	0.004	0.019	0.021	0.013	0.016	0.018	0.011	0.024
Sr	0.008	0	0.012	0.011	0.011	0.003	0.006	0.009	0.009	0.008	0.008	0.01	0.017	0.008	0	0	0	0.003	0.007	0.007	0.007	0.004	0	0	0.001	0	0	0	0
Ba	0	0	0	0	0	0.001	0	0.001	0	0	0	0	0.001	0	0	0	0	0	0.001	0.001	0	0	0	0	0	0	0	0	0
As	0	0.001	0.001	0	0	0.001	0.001	0.001	0	0	0	0	0.001	0	0.001	0.001	0.001	0	0	0	0	0	0	0	0	0	0.002	0	0
F	1.741	1.613	1.673	1.72	1.848	1.809	1.724	1.62	1.778	1.844	1.764	1.853	2.046	1.78	1.891	1.956	1.944	1.893	1.96	1.961	2.003	1.745	1.777	1.772	1.8	1.827	1.881	1.915	1.738
Cl	0.085	0.096	0.044	0.048	0.047	0.036	0.047	0.051	0.047	0.05	0.047	0.049	0	0.044	0.054	0.054	0.048	0.071	0.046	0.046	0.046	0.097	0.085	0.086	0.092	0.096	0.087	0.087	0.07
OH	0.174	0.291	0.283	0.232	0.105	0.155	0.229	0.33	0.175	0.106	0.189	0.098	0.001	0.176	0.056	0.001	0.008	0.035	0.001	0.001	0.001	0.157	0.138	0.141	0.107	0.077	0.032	0.001	0.192
Sum Cat#	18.08	18.03	18.05	18.06	18.03	18	17.98	17.98	17.98	18	17.99	18.02	18.05	18.02	18.07	18.04	18.01	18.07	18.03	18.05	18.06	17.97	17.97	18.01	18.01	17.99	17.99	18.01	17.98

Label	E27/68/1_apa2	E27/68/1_apa3	E27/68/A_apa1	E27/68/A_apa2	E27/68/A_apa3	E27/67/4_apa1	E27/67/4_apa2	E27/1/3/apa_trav-1	E27/1/3/apa_trav-2	E27/1/3/apa_trav-3	E27/1/4/apa_trav-1	E27/1/4/apa_trav-2	E27/1/4/apa_trav-3	E27/1/4/apa_trav-4	E27/1/4/apa_trav-5	E27/1/4/apa_trav-6	E27/1/4/apa_trav-7	E27/1/4i/apa_trav-2	E27/1/4i/apa_trav-3	E27/1/4i/apa_trav-4	E27/1/4i/apa_trav-5	E27/1/8/apa_trav-1	E27/1/8/apa_trav-2	E27/1/8/apa_trav-3	E48_1_1_apa_1-1	E48_1_1_apa_1-2	E48_1_1_3_apa1-2	E48_1_1_3_apa1-3	E48_1_1_apa_1-5
SiO2%	0.27	0.2	0.14	0.32	0.24	0.38	0.38	0.18	0.2	0.08	0.11	0.28	0.28	0.31	0.3	0.26	0.54	0.29	0.33	0.31	0.22	0.07	0.27	0.32	0.02	0.01	0.01	0.02	0.03
Fe2O3%	0.07	0.08	0.13	0.09	0.12	0.09	0.09	0.1	0.12	0.58	0.09	0.08	0.11	0.08	0.07	0.07	0.09	0.1	0.1	0.1	0.1	0.4	0.18	0.24	0.04	0.04	0.07	0.13	0.06
MnO%	0.13	0.17	0.13	0.14	0.15	0.18	0.15	0.19	0.17	0.16	0.14	0.15	0.19	0.16	0.18	0.19	0.18	0.16	0.18	0.16	0.19	0.14	0.13	0.18	0.1	0.11	0.09	0.18	0.17
MgO%	0.02	0.02	0.02	0.03	0.03	0.02	0.03	0.04	0.03	0.03	0.04	0.03	0.03	0.04	0.03	0.03	0.03	0.04	0.03	0.03	0.02	0.02	0.04	0.04	0.01	0	0.01	0.04	0.02
CaO%	54.58	55.18	54.71	54.38	54.43	54.8	54.71	54.6	55.31	54.69	54.56	54.32	54.89	55.14	55.07	54.53	54.13	53.69	54.52	54.34	54.77	54.3	53.99	54.08	54.5	54.4	54.79	54.52	54.38
Na2O%	0.1	0.15	0.17	0.13	0.17	0.18	0.13	0.18	0.11	0.19	0.2	0.22	0.23	0.16	0.15	0.12	0.2	0.13	0.13	0.15	0.16	0.39	0.36	0.42	0.2	0.18	0.15	0.16	0.23
P2O5%	41.63	42.01	41.97	41.11	41.72	41.17	41.37	41.55	41.33	41.55	42.07	41.02	41.15	41.34	41.29	41.34	41.69	41.55	41.49	41.22	41.48	41.34	40.18	40.12	41.1	40.35	41.36	41.48	39.96
SO3%	0.31	0.24	0.35	0.42	0.39	0.37	0.41	0.35	0.25	0.62	0.22	0.71	0.59	0.46	0.45	0.36	0.17	0.44	0.51	0.45	0.36	0.71	0.92	0.95	0.12	0.1	0.09	0.11	0.17
La2O3%	0.12	0.07	0.09	0.11	0.1	0.15	0.13	0.09	0.09	0.06	0.05	0.1	0.11	0.09	0.1	0.11	0.07	0.1	0.11	0.12	0.11	0.04	0.08	0.06	0.1	0.07	0.07	0.07	0.1
Ce2O3%	0.23	0.12	0.14	0.22	0.2	0.23	0.24	0.13	0.2	0.14	0.13	0.18	0.2	0.2	0.22	0.2	0.12	0.22	0.21	0.21	0.19	0.12	0.14	0.14	0.23	0.18	0.1	0.11	0.21
Pr2O3%	0.04	0	0.01	0.03	0	0	0	0	0	0	0	0	0	0.03	0.03	0.02	0	0.01	0.03	0.04	0.02	0	0.01	0	0.04	0	0	0	0
Nd2O3%	0.12	0.15	0.07	0.14	0.07	0.05	0.1	0.1	0.12	0.11	0.09	0.13	0.09	0.15	0.1	0.09	0.11	0.04	0.15	0.13	0.07	0.12	0.11	0.08	0.16	0.1	0.03	0.04	0.16
Sm2O3%	0.01	0	0	0.02	0	0.01	0.05	0	0	0	0.03	0.01	0.08	0.05	0	0.03	0.01	0.01	0	0	0.03	0.03	0.02	0.01	0.05	0.08	0	0.02	0.04
Y2O3%	0.19	0.18	0.11	0.08	0.13	0.08	0.09	0.13	0.16	0.25	0.21	0.1	0.11	0.06	0.06	0.08	0.21	0.08	0.06	0.08	0.11	0.17	0.21	0.17	0.19	0.17	0.11	0.21	0.25
SrO%	0	0	0.02	0.07	0.02	0.02	0.05	0	0.02	0	0	0.04	0.04	0.08	0.08	0.06	0	0.07	0.11	0.07	0.03	0	0	0	0.01	0.02	0.12	0.12	0.02
BaO%	0	0	0	0	0.01	0	0	0	0.01	0.01	0	0.01	0	0	0.01	0	0	0	0	0.02	0	0	0	0	0.01	0	0	0	0
As2O3%	0.01	0.01	0	0.01	0	0	0.01	0.01	0	0.01	0	0	0.01	0	0.01	0.01	0.01	0.01	0	0.01	0.01	0	0.01	0.01	0.01	0.02	0	0	0
F%	3.45	3.46	3.42	3.11	3.46	3.59	3.52	3.01	3.15	3.17	3.02	3.35	3.06	2.98	3.22	3.3	3.02	3.01	2.92	3.19	3.21	2.99	2.85	3.14	4.13	4.31	4.39	4.6	4.6
Cl%	0.25	0.24	0.27	0.28	0.24	0.24	0.24	0.26	0.29	0.24	0.28	0.31	0.36	0.31	0.33	0.35	0.28	0.34	0.33	0.33	0.32	0.3	0.35	0.32	0.14	0.12	0.1	0.11	0.12
H2O(c)	0.08	0.09	0.1	0.23	0.08	0.01	0.05	0.29	0.21	0.23	0.28	0.11	0.24	0.3	0.17	0.12	0.28	0.26	0.32	0.18	0.18	0.29	0.32	0.19	0	0	0	0	0
O=F	1.45	1.46	1.44	1.31	1.46	1.51	1.48	1.27	1.32	1.34	1.27	1.41	1.29	1.25	1.36	1.39	1.27	1.27	1.23	1.34	1.35	1.26	1.2	1.32	1.74	1.81	1.85	1.94	1.94
O=Cl	0.06	0.05	0.06	0.06	0.05	0.05	0.05	0.06	0.07	0.05	0.06	0.07	0.08	0.07	0.07	0.08	0.06	0.08	0.08	0.07	0.07	0.07	0.08	0.07	0.03	0.03	0.02	0.03	0.03
Sum Ox%	100.1	100.9	100.3	99.54	100.1	100	100.2	99.9	100.4	100.7	100.2	99.68	100.4	100.6	100.5	99.81	99.8	99.19	100.2	99.74	100.2	100.1	98.89	99.1	99.38	98.4	99.63	99.96	98.54
Cations																													
Si	0.045	0.033	0.024	0.053	0.04	0.063	0.065	0.03	0.033	0.014	0.018	0.047	0.047	0.052	0.051	0.044	0.091	0.049	0.055	0.053	0.037	0.012	0.045	0.054	0	0	0.002	0.003	0
Fe3+	0.009	0.01	0.016	0.012	0.015	0.011	0.012	0.013	0.015	0.072	0.012	0.011	0.013	0.01	0.009	0.009	0.011	0.012	0.012	0.013	0.013	0.05	0.023	0.031	0.01	0.01	0.008	0.017	0.01
Mn2+	0.019	0.023	0.018	0.02	0.021	0.026	0.022	0.027	0.025	0.022	0.02	0.021	0.027	0.023	0.026	0.027	0.025	0.023	0.026	0.024	0.027	0.019	0.019	0.027	0.02	0.02	0.012	0.026	0.03
Mg	0.006	0.005	0.005	0.008	0.006	0.006	0.006	0.009	0.007	0.006	0.009	0.008	0.008	0.009	0.007	0.007	0.008	0.009	0.007	0.008	0.005	0.006	0.01	0.009	0	0	0.004	0.009	0.01
Ca	9.838	9.873	9.82	9.865	9.8	9.904	9.858	9.856	9.978	9.801	9.808	9.831	9.888	9.91	9.914	9.869	9.762	9.732	9.811	9.838	9.876	9.782	9.865	9.864	9.96	10.08	9.979	9.909	10.1
Na	0.032	0.048	0.055	0.042	0.055	0.057	0.043	0.058	0.036	0.062	0.066	0.073	0.076	0.052	0.05	0.04	0.065	0.041	0.043	0.048	0.052	0.128	0.12	0.14	0.066	0.059	0.049	0.053	0.078
P	5.93	5.939	5.953	5.894	5.936	5.879	5.89	5.926	5.892	5.884	5.975	5.866	5.857	5.871	5.874	5.911	5.941	5.951	5.9	5.897	5.911	5.884	5.801	5.783	5.938	5.904	5.953	5.957	5.864
S	0.039	0.031	0.043	0.053	0.049	0.047	0.051	0.045	0.031	0.077	0.028	0.09	0.074	0.058	0.057	0.046	0.022	0.056	0.064	0.057	0.046	0.089	0.118	0.122	0.016	0.013	0.011	0.014	0.022
La	0.007	0.005	0.006	0.007	0.006	0.01	0.008	0.006	0.006	0.003	0.003	0.006	0.007	0.006	0.006	0.007	0.004	0.007	0.007	0.007	0.007	0.003	0.005	0.004	0.006	0.004	0.004	0.004	0.006
Ce	0.014	0.007	0.009	0.014	0.012	0.014	0.015	0.008	0.012	0.009	0.008	0.011	0.012	0.012	0.013	0.013	0.007	0.014	0.013	0.013	0.012	0.007	0.009	0.009	0.014	0.011	0.006	0.007	0.013
Pr	0.002	0	0.001	0.002	0	0	0	0	0	0	0	0	0	0.002	0.002	0.001	0	0	0.002	0.002	0.001	0	0.001	0	0.002	0	0	0	0
Nd	0.007	0.009	0.004	0.008	0.004	0.003	0.006	0.006	0.007	0.006	0.006	0.008	0.005	0.009	0.006	0.006	0.006	0.003	0.009	0.008	0.004	0.007	0.007	0.005	0.01	0.006	0.002	0.002	0.01
Sm	0	0	0	0.001	0	0	0.003	0	0	0	0.002	0	0.005	0.003	0	0.002	0.001	0.001	0	0	0.002	0.002	0.001	0.001	0.003	0.004	0	0.001	0.002
Y	0.017	0.016	0.009	0.007	0.012	0.007	0.008	0.011	0.014	0.022	0.019	0.009	0.01	0.005	0.006	0.007	0.019	0.007	0.006	0.008	0.009	0.015	0.019	0.016	0.017	0.016	0.01	0.019	0.023
Sr	0	0	0.002	0.007	0.002	0.002	0.005	0	0.002	0	0	0.004	0.004	0.007	0.008	0.006	0	0.007	0.01	0.007	0.003	0	0	0	0.001	0.002	0.012	0.012	0.002
Ba	0	0	0	0	0.001	0	0	0	0.001	0.001	0	0.001	0	0	0.001	0	0	0	0	0.001	0	0	0	0	0.001	0	0	0	0
As	0.001	0.001	0	0.001	0	0	0.001	0.002	0	0.001	0	0	0.001	0	0.001	0.001	0.001	0.001	0	0.001	0.001	0	0.001	0.001	0.001	0.002	0	0	0
F	1.834	1.829	1.811	1.666	1.839	1.915	1.874	1.602	1.676	1.679	1.603	1.792	1.626	1.579	1.712	1.762	1.607	1.613	1.549	1.702	1.711	1.59	1.539	1.693	2.228	2.356	2.36	2.466	2.521
Cl	0.071	0.067	0.077	0.08	0.069	0.068	0.068	0.074	0.084	0.067	0.08	0.089	0.101	0.089	0.093	0.1	0.081	0.096	0.095	0.095	0.09	0.086	0.101	0.091	0.042	0.034	0.029	0.033	0.036
OH	0.095	0.103	0.113	0.254	0.091	0.017	0.058	0.324	0.24	0.254	0.317	0.118	0.272	0.331	0.196	0.138	0.312	0.291	0.356	0.203	0.199	0.325	0.36	0.216	0.001	0.001	0.001	0.001	0.001
Sum Cat#	17.97	18	17.97	17.99	17.96	18.03	17.99	18	18.06	17.98	17.97	17.99	18.03	18.03	18.03	18	17.96	17.91	17.96	17.99	18.01	18.01	18.04	18.07	18.33	18.51	18.44	18.53	18.72

Label	E48_1 1_3_a pa2-2	E48_1 1_5_a pa-1	E48_1 1_5_a pa-2	E48_1 1_5_a pa-3	E48_1 1_5_a pa-4	E48_1 1_5_a pa-5	E27_3 9_4_a pl_ap a3_-1	E27_3 9_4_a pl_ap a3_-2	E27_3 9_4_a pl_ap a3_-3	E27_8 7_14_ 1	E27_8 7_14_ 2	E27_8 7_14_ 3	E48_5 _apa_- 1	E48_5 _apa_- 2	E48_5 _apa_- 3	E48_5 _apa_- 4	E48_6 _apa_ _in_kf s-1	E48_6 _apa_ _in_kf s-2	E48_6 _apa_ _in_kf s-3	E48_6 _apa_ _in_kf s-4	E26/5 0/1- apa1_ trav-1	E26/5 0/1- apa1_ trav-2	E26/5 0/1- apa1_ trav-3	E26/5 0/1- apa2_ trav-2	E26/5 0/2/ap a1_tra v-1	E26/5 0/2/ap a1_tra v-2	E26/5 0/2/ap a1_tra v-3	E26/5 0/3/ap a2_tra v-2	E26/5 0/3/ap a2_tra v-3
SiO2%	0.12	0.02	0.02	0.02	0.03	0.02	0.18	0.18	0.22	0.33	0.12	0.22	0.29	0.24	0.36	0.19	0.44	0.19	0.15	0.26	0.12	0.16	0.3	0.15	0.21	0.2	0.21	0.22	0.19
Fe2O3%	0.04	0.1	0.06	0.04	0.01	0.03	0.16	0.12	0.23	0.15	0.05	0.13	0.08	0.04	0.08	0.03	0.08	0.04	0.05	0.04	0.07	0.05	0.01	0.18	0.2	0.12	0.05	0.11	0.1
MnO%	3	0.2	0.15	0.14	0.11	0.12	0.12	0.09	0.13	0.16	0.17	0.09	0.09	0.05	0.04	0.06	0.07	0.01	0.04	0.05	0.12	0.08	0.07	0.08	0.12	0.12	0.13	0.17	0.11
MgO%	0	0.02	0.05	0	0	0	0.01	0	0.02	0.03	0.02	0.02	0.01	0	0.01	0	0	0.01	0	0.01	0	0	0	0.01	0.01	0	0	0.01	0.01
CaO%	51.17	54.14	54.52	54.64	54.32	54.33	54.88	54.79	54.77	53.51	54.31	53.7	54.24	53.4	53.87	53.39	52.89	53.36	54.22	53.59	54.51	55.24	55.05	54.76	55.06	55	54.7	54.89	54.56
Na2O%	0.41	0.2	0.22	0.21	0.32	0.24	0.09	0.12	0.11	0.1	0.08	0.07	0.14	0.15	0.14	0.1	0.1	0.11	0.12	0.07	0.04	0	0.01	0.03	0.07	0.04	0.05	0.07	0.07
P2O5%	40.36	41.34	41.69	41.56	41.35	41.73	40.55	40.15	40.85	40.66	41.07	41.3	35.85	36.09	35.9	37.2	41.2	41.27	41.23	41.56	41.98	42.33	42.48	42.02	42.07	42.12	41.74	42.12	42.11
SO3%	1.15	0.16	0.17	0.12	0.25	0.1	0.29	0.36	0.35	0.18	0.11	0.1	0.11	0.08	0.09	0.03	0.02	0.25	0.16	0.09	0.05	0.04	0.02	0.09	0.18	0.13	0.16	0.17	0.13
La2O3%	0	0.07	0.18	0.12	0.1	0.08	0.05	0.05	0.07	0.11	0.04	0.11	0.16	0.16	0.15	0.12	0.21	0.1	0.13	0.12	0.05	0.08	0.05	0.05	0.09	0.06	0.06	0.09	0.08
Ce2O3%	0.01	0.18	0.36	0.24	0.24	0.23	0.08	0.09	0.11	0.07	0.07	0.02	0.33	0.29	0.3	0.26	0.44	0.2	0.2	0.25	0.09	0.15	0.06	0.12	0.18	0.17	0.12	0.18	0.14
Pr2O3%	0	0.04	0.03	0	0.01	0	0	0.01	0	-	-	-	0.05	0.02	0	0.09	0.01	0.04	0	0	0.02	0	0.01	0	0	0	0.02	0.03	0.03
Nd2O3%	0	0.09	0.16	0.12	0.2	0.17	0.06	0.05	0.06	-	-	-	0.23	0.16	0.14	0.17	0.22	0.14	0.12	0.15	0.06	0.09	0.07	0.05	0.17	0.06	0.16	0.14	0.1
Sm2O3%	0.02	0.04	0.01	0.08	0.04	0.01	0.03	0	0	-	-	-	0.02	0.05	0.05	0.03	0	0.05	0.04	0	0.05	0	0	0.04	0.07	0	0	0.11	0
Y2O3%	0	0.18	0.21	0.24	0.25	0.26	0.05	0.04	0.03	0.15	0.14	0.11	0.15	0.14	0.12	0.09	0.15	0.12	0.07	0.09	0.03	0.08	0.04	0.07	0.08	0.08	0.04	0.12	0.09
SrO%	0.46	0.13	0.11	0.13	0.12	0.1	0.06	0.06	0.07	0.06	0.01	0.1	0	0	0	0	0	0	0.02	0.02	0.05	0.04	0.04	0.03	0.04	0.03	0.05	0.04	0.05
BaO%	0	0.02	0	0.01	0.02	0	0.01	0	0	0.32	0.25	0.12	0.01	0.04	0.04	0.02	0.01	0	0	0	0	0	0	0	0	0.01	0	0	0
As2O3%	0	0	0.01	0.02	0	0.02	0.01	0	0.01	-	-	-	0.02	0.05	0.02	0.04	0.03	0.01	0.02	0	0.03	0.04	0.04	0.08	0.01	0.01	0.01	0.01	0.01
F%	4.52	4.18	4.17	4.05	4.15	4.19	3.4	3.33	3.29	3.2	3.37	3.29	4.01	3.73	4.14	3.96	3.24	3.48	3.54	3.42	2.98	2.81	3.1	2.81	2.88	2.7	3.09	3.02	2.71
Cl%	0.03	0.12	0.12	0.12	0.12	0.13	0.54	0.49	0.59	0.29	0.28	0.31	0.21	0.22	0.14	0.2	0.23	0.23	0.2	0.23	0.42	0.45	0.23	0.62	0.38	0.35	0.33	0.34	0.41
H2O(c)	0	0	0	0	0	0	0	0.04	0.05	0.15	0.08	0.12	0	0	0	0	0.16	0.04	0.03	0.08	0.25	0.35	0.27	0.29	0.33	0.42	0.23	0.28	0.39
O=F	1.9	1.76	1.75	1.7	1.75	1.76	1.43	1.4	1.39	1.35	1.42	1.38	1.69	1.57	1.74	1.67	1.36	1.46	1.49	1.44	1.26	1.18	1.3	1.18	1.21	1.14	1.3	1.27	1.14
O=Cl	0.01	0.03	0.03	0.03	0.03	0.03	0.12	0.11	0.13	0.06	0.06	0.07	0.05	0.05	0.03	0.04	0.05	0.05	0.05	0.05	0.09	0.1	0.05	0.14	0.08	0.08	0.07	0.08	0.09
Sum Ox%	99.39	99.45	100.4	100.1	99.87	99.98	99.03	98.47	99.43	98.04	98.68	98.34	94.26	93.29	93.82	94.28	98.07	98.13	98.81	98.54	99.57	100.7	100.5	100.2	100.9	100.4	99.79	100.8	100.1
Cations																													
Si	0.02	0.003	0.004	0.003	0.005	0.004	0.031	0.031	0.037	0.056	0.02	0.037	0.05	0.05	0.07	0.04	0.08	0.03	0.03	0.04	0.021	0.026	0.05	0.025	0.035	0.033	0.036	0.037	0.032
Fe3+	0.005	0.012	0.007	0.005	0.002	0.004	0.021	0.016	0.03	0.02	0.006	0.017	0.01	0.01	0.01	0	0.01	0.01	0.01	0.01	0.009	0.006	0.001	0.023	0.025	0.015	0.006	0.014	0.013
Mn2+	0.435	0.029	0.021	0.02	0.016	0.017	0.017	0.012	0.019	0.023	0.025	0.013	0.01	0.01	0.01	0.01	0.01	0	0.01	0.01	0.018	0.012	0.009	0.011	0.017	0.017	0.018	0.024	0.016
Mg	0	0.006	0.012	0.001	0.001	0.001	0.002	0.001	0.005	0.007	0.004	0.004	0	0	0	0	0	0	0	0	0	0	0	0.002	0.003	0	0.001	0.001	0.002
Ca	9.366	9.874	9.855	9.905	9.874	9.851	10.05	10.1	9.976	9.866	9.953	9.839	10.71	10.59	10.66	10.43	9.73	9.79	9.91	9.79	9.863	9.891	9.843	9.864	9.857	9.867	9.885	9.83	9.818
Na	0.136	0.066	0.071	0.07	0.104	0.078	0.03	0.041	0.036	0.033	0.026	0.023	0.05	0.053	0.051	0.036	0.034	0.037	0.038	0.023	0.013	0	0.002	0.009	0.022	0.012	0.017	0.022	0.023
P	5.836	5.957	5.955	5.953	5.939	5.978	5.868	5.846	5.879	5.924	5.947	5.98	5.592	5.657	5.613	5.745	5.987	5.981	5.953	5.999	6.002	5.989	6.002	5.981	5.95	5.971	5.96	5.96	5.988
S	0.148	0.02	0.021	0.015	0.031	0.013	0.038	0.046	0.045	0.024	0.014	0.012	0.015	0.011	0.012	0.004	0.003	0.032	0.021	0.012	0.006	0.005	0.002	0.012	0.023	0.016	0.02	0.021	0.017
La	0	0.005	0.011	0.008	0.007	0.005	0.003	0.003	0.004	0.007	0.002	0.007	0.011	0.011	0.01	0.008	0.014	0.006	0.008	0.008	0.003	0.005	0.003	0.003	0.005	0.004	0.004	0.005	0.005
Ce	0.001	0.011	0.022	0.015	0.015	0.014	0.005	0.006	0.007	0.004	0.005	0.001	0.022	0.02	0.02	0.017	0.028	0.013	0.012	0.015	0.005	0.009	0.004	0.007	0.011	0.01	0.007	0.011	0.008
Pr	0	0.002	0.002	0	0.001	0	0	0	0	-	-	-	0.003	0.001	0	0.006	0	0.002	0	0	0.001	0	0.001	0	0	0	0.001	0.002	0.002
Nd	0	0.006	0.01	0.007	0.012	0.01	0.004	0.003	0.004	-	-	-	0.015	0.011	0.009	0.011	0.013	0.008	0.007	0.009	0.004	0.006	0.004	0.003	0.01	0.004	0.01	0.008	0.006
Sm	0.001	0.003	0.001	0.005	0.003	0.001	0.002	0	0	-	-	-	0.002	0.003	0.003	0.002	0	0.003	0.002	0	0.003	0	0	0.002	0.004	0	0	0.007	0
Y	0	0.016	0.019	0.022	0.023	0.024	0.005	0.003	0.002	0.013	0.013	0.01	0.015	0.014	0.012	0.009	0.014	0.01	0.007	0.008	0.003	0.007	0.003	0.006	0.007	0.008	0.004	0.011	0.008
Sr	0.046	0.013	0.011	0.012	0.011	0.01	0.006	0.006	0.007	0.006	0.001	0.01	0	0	0	0	0	0	0.002	0.002	0.005	0.003	0.004	0.003	0.004	0.003	0.005	0.004	0.005
Ba	0	0.001	0	0.001	0.001	0	0.001	0	0	0.022	0.017	0.008	0.001	0.003	0.003	0.002	0.001	0	0	0	0	0	0	0	0	0.001	0	0	0
As	0	0	0.001	0.002	0	0.002	0.001	0	0.001	-	-	-	0.002	0.005	0.002	0.004	0.003	0.001	0.002	0	0.003	0.004	0.004	0.008	0.001	0.001	0.001	0.001	0.001
F	2.44	2.253	2.223	2.166	2.228	2.243	1.838	1.813	1.77	1.743	1.821	1.778	2.338	2.182	2.418	2.282	1.756	1.882	1.908	1.843	1.594	1.486	1.635	1.493	1.522	1.43	1.646	1.596	1.442
Cl	0.008	0.035	0.035	0.034	0.034	0.036	0.157	0.143	0.17	0.083	0.082	0.089	0.065	0.07	0.044	0.06	0.066	0.067	0.058	0.066	0.12	0.126	0.066	0.176	0.107	0.099	0.095	0.095	0.117
OH	0.001	0.001	0.001	0.001	0.001	0.001	0.005	0.044	0.061	0.173	0.096	0.133	0.001	0.001	0.001	0.001	0.178	0.051	0.034	0.091	0.286	0.388	0.299	0.331	0.371	0.471	0.26	0.309	0.441
Sum Cat#	18.44	18.31	18.28	18.24	18.31	18.29	18.09	18.11	18.05	18.01	18.03	17.96	18.92	18.69	18.94	18.67	17.92	17.93	18	17.92	17.96	17.96	17.93	17.96	17.97	17.96	17.98	17.96	17.94

Label	E26/50/4apa1_trav-1	E26/50/4apa1_trav-2	E26/50/4apa1_trav-3	E26_50_inclu_apa	E26/46_11_apat_trav-1	E26/46_11_apat_trav-2	E26/46_11_apat_trav-3	E26/46_11_apat_trav-4	E26/46_11_apat_trav-5	E26/46_10_apat_trav-1	E26/46_10_apat_trav-2	E26/46_10_apat_trav-3	E26/46_10_apat_trav-4	E26/46_10_apat_trav-5	E26/46_10_apat_trav-6
SiO2%	0.16	0.2	0.12	0.21	0.29	0.32	0.37	0.17	0.33	0.28	0.28	0.32	0.27	0.24	0.35
Fe2O3%	0.33	0.14	0.2	0.11	0.05	0.06	0.06	0.08	0.09	0.1	0.07	0.06	0.06	0.07	0.08
MnO%	0.11	0.14	0.12	0.09	0.22	0.22	0.18	0.21	0.19	0.23	0.2	0.22	0.23	0.18	0.22
MgO%	0.01	0	0	0.01	0.03	0.02	0.02	0.02	0.02	0.03	0.03	0.02	0.03	0.02	0.02
CaO%	54.65	55.02	53.9	55.54	55.18	55.36	55.05	54.87	55	55.3	55.23	55.02	54.47	54.98	54.94
Na2O%	0.07	0.03	0.04	0.08	0.1	0.11	0.12	0.12	0.12	0.15	0.12	0.11	0.12	0.11	0.12
P2O5%	42.04	41.89	41.97	41.19	42.03	41.8	41.25	41.62	41.16	41.45	41.3	41.37	41.79	41.34	40.73
SO3%	0.09	0.07	0.07	0.17	0.48	0.5	0.44	0.27	0.47	0.41	0.41	0.45	0.45	0.33	0.44
La2O3%	0.04	0.09	0.06	0.15	0.1	0.12	0.1	0.09	0.11	0.13	0.14	0.14	0.12	0.11	0.15
Ce2O3%	0.09	0.15	0.08	0.09	0.21	0.19	0.24	0.12	0.21	0.19	0.23	0.23	0.2	0.18	0.27
Pr2O3%	0	0.05	0	-	0	0.05	0.04	0	0.04	0	0.02	0.06	0.02	0	0
Nd2O3%	0.09	0.09	0.06	-	0.08	0.06	0.16	0.08	0.17	0.05	0.06	0.17	0.11	0.07	0.16
Sm2O3%	0.03	0	0	-	0.05	0.01	0.04	0.02	0.02	0.06	0.01	0.09	0.03	0	0.05
Y2O3%	0.04	0.11	0.03	0.03	0.06	0.06	0.09	0.06	0.08	0.03	0.09	0.07	0.05	0.06	0.08
SrO%	0.03	0.02	0.05	0.08	0.1	0.11	0.15	0.13	0.13	0.08	0.09	0.09	0.1	0.11	0.09
BaO%	0	0	0.01	0.24	0	0.01	0	0	0	0	0.01	0.01	0	0	0
As2O3%	0.04	0.05	0.05	-	0	0.01	0.01	0.03	0.01	0	0	0.01	0	0.01	0.01
F%	2.88	2.96	3.08	2.99	2.94	2.65	2.62	2.69	2.71	2.85	2.54	2.71	2.51	3.32	2.67
Cl%	0.45	0.46	0.41	0.39	0.22	0.25	0.24	0.23	0.25	0.19	0.26	0.24	0.25	0.13	0.24
H2O(c)	0.31	0.27	0.21	0.26	0.35	0.48	0.48	0.45	0.44	0.39	0.52	0.44	0.54	0.17	0.45
O=F	1.21	1.25	1.3	1.26	1.24	1.11	1.1	1.13	1.14	1.2	1.07	1.14	1.06	1.4	1.12
O=Cl	0.1	0.1	0.09	0.09	0.05	0.06	0.05	0.05	0.06	0.04	0.06	0.05	0.06	0.03	0.05
Sum Ox%	100.2	100.4	99.05	100.3	101.2	101.2	100.5	100.1	100.4	100.7	100.5	100.6	100.2	100	99.87
Cations															
Si	0.027	0.033	0.02	0.04	0.049	0.053	0.062	0.029	0.056	0.047	0.046	0.053	0.046	0.041	0.06
Fe3+	0.042	0.018	0.025	0.01	0.006	0.007	0.008	0.01	0.011	0.013	0.008	0.008	0.007	0.009	0.01
Mn2+	0.016	0.02	0.017	0.01	0.031	0.031	0.026	0.029	0.027	0.032	0.028	0.031	0.032	0.026	0.031
Mg	0.004	0.001	0	0	0.006	0.005	0.006	0.005	0.006	0.006	0.008	0.004	0.007	0.005	0.006
Ca	9.836	9.901	9.784	10.05	9.823	9.866	9.904	9.893	9.913	9.923	9.939	9.888	9.783	9.928	9.967
Na	0.022	0.011	0.012	0.025	0.032	0.036	0.038	0.04	0.039	0.05	0.039	0.036	0.04	0.037	0.04
P	5.978	5.958	6.021	5.887	5.912	5.886	5.864	5.929	5.862	5.877	5.872	5.875	5.931	5.899	5.839
S	0.011	0.008	0.01	0.022	0.06	0.063	0.056	0.034	0.059	0.052	0.052	0.057	0.056	0.042	0.056
La	0.003	0.006	0.003	0.009	0.006	0.007	0.006	0.005	0.007	0.008	0.009	0.009	0.007	0.007	0.009
Ce	0.005	0.009	0.005	0.005	0.013	0.012	0.015	0.007	0.013	0.012	0.014	0.014	0.012	0.011	0.017
Pr	0	0.003	0	-	0	0.003	0.002	0	0.002	0	0.001	0.004	0.002	0	0
Nd	0.005	0.005	0.004	-	0.005	0.004	0.01	0.005	0.01	0.003	0.004	0.01	0.006	0.004	0.01
Sm	0.002	0	0	-	0.003	0	0.003	0.001	0.001	0.003	0.001	0.005	0.002	0	0.003
Y	0.003	0.009	0.003	0.003	0.005	0.006	0.008	0.006	0.007	0.003	0.008	0.007	0.004	0.006	0.007
Sr	0.003	0.002	0.005	0.008	0.009	0.01	0.015	0.013	0.013	0.008	0.009	0.009	0.01	0.011	0.008
Ba	0	0	0	0.016	0	0.001	0	0	0	0	0.001	0.001	0	0	0
As	0.004	0.006	0.005	-	0	0.001	0.001	0.003	0.001	0	0	0.001	0	0.001	0.001
F	1.53	1.572	1.648	1.594	1.546	1.392	1.392	1.431	1.44	1.509	1.347	1.439	1.331	1.767	1.428
Cl	0.128	0.13	0.117	0.111	0.062	0.07	0.069	0.065	0.071	0.053	0.073	0.067	0.07	0.037	0.069
OH	0.342	0.299	0.235	0.294	0.392	0.537	0.539	0.504	0.489	0.438	0.58	0.494	0.599	0.196	0.503
Sum Cat#	17.96	17.99	17.91	18.09	17.96	17.99	18.02	18.01	18.03	18.04	18.04	18.01	17.95	18.03	18.06

Label	E26/46_10_apat_trav-7	E26/46_9_apat_trav-1	E26/46_9_apat_trav-2	E26/46_9_apat_trav-3	E26/46_9_apat_trav-4	E26/46_9_apat_trav-5	E26/46_9_apat_trav-6	E26/46_9_apat_trav-7	E26/46_8_apat_trav-1	E26/46_8_apat_trav-2	E26/46_8_apat_trav-3	E26/46_5_apat_trav-1	E26/46_5_apat_trav-2	E26/46_5_apat_trav-3
SiO2%	0.3	0.3	0.29	0.3	0.27	0.3	0.27	0.26	0.29	0.21	0.28	0.32	0.27	0.3
Fe2O3%	0.1	0.09	0.09	0.1	0.05	0.08	0.07	0.09	0.09	0.07	0.1	0.07	0.06	0.06
MnO%	0.23	0.22	0.22	0.26	0.24	0.22	0.22	0.22	0.22	0.22	0.23	0.19	0.23	0.2
MgO%	0.02	0.02	0.02	0.03	0.02	0.03	0.02	0.03	0.02	0.02	0.02	0.03	0.02	0.02
CaO%	54.9	55.09	55.12	55.17	55.35	54.86	55.05	55.12	55.12	55.34	54.65	54.89	55.14	55.47
Na2O%	0.11	0.12	0.12	0.13	0.14	0.12	0.13	0.1	0.09	0.1	0.12	0.12	0.15	0.09
P2O5%	41.18	41.02	41.3	41.09	41.65	41.52	41.37	41.88	41.94	41.73	41.44	41.94	42.1	41.94
SO3%	0.37	0.36	0.41	0.44	0.38	0.4	0.37	0.36	0.37	0.2	0.35	0.38	0.36	0.54
La2O3%	0.11	0.11	0.13	0.12	0.12	0.13	0.14	0.13	0.13	0.11	0.13	0.16	0.13	0.14
Ce2O3%	0.2	0.19	0.23	0.21	0.2	0.23	0.21	0.2	0.21	0.21	0.21	0.25	0.22	0.25
Pr2O3%	0.02	0	0.01	0	0.08	0	0	0.02	0.05	0	0	0.03	0	0.01
Nd2O3%	0.14	0.07	0.13	0.09	0.11	0.08	0.08	0.09	0.1	0.1	0.08	0.06	0.1	0.09
Sm2O3%	0.06	0.01	0.01	0.02	0	0	0	0	0.02	0.02	0.01	0	0	0.03
Y2O3%	0.05	0.05	0.05	0.05	0.05	0.07	0.06	0.03	0.09	0.07	0.04	0.05	0.08	0.07
SrO%	0.08	0.08	0.09	0.08	0.08	0.1	0.09	0.07	0.09	0.08	0.08	0.08	0.07	0.08
BaO%	0	0	0.01	0	0	0	0	0	0	0	0	0	0.01	0.01
As2O3%	0.01	0	0.01	0.01	0	0	0	0.01	0	0.01	0	0.02	0.01	0
F%	2.75	2.96	3.48	3.69	3.47	2.79	2.76	3.07	2.94	2.64	3.06	3.27	3.09	3.26
Cl%	0.22	0.2	0.15	0.09	0.12	0.24	0.22	0.2	0.19	0.25	0.19	0.25	0.23	0.24
H2O(c)	0.42	0.32	0.1	0.01	0.12	0.4	0.42	0.29	0.36	0.47	0.28	0.18	0.28	0.2
O=F	1.16	1.25	1.47	1.55	1.46	1.17	1.16	1.29	1.24	1.11	1.29	1.38	1.3	1.37
O=Cl	0.05	0.04	0.03	0.02	0.03	0.05	0.05	0.05	0.04	0.06	0.04	0.06	0.05	0.05
Sum Ox%	100.1	99.94	100.5	100.3	101	100.3	100.3	100.9	101	100.7	99.95	100.9	101.2	101.6
Cations														
Si	0.051	0.051	0.049	0.05	0.044	0.051	0.046	0.044	0.048	0.035	0.048	0.053	0.045	0.05
Fe3+	0.012	0.011	0.011	0.013	0.006	0.009	0.008	0.011	0.011	0.009	0.013	0.009	0.008	0.008
Mn2+	0.033	0.032	0.031	0.038	0.034	0.031	0.031	0.032	0.031	0.031	0.033	0.027	0.033	0.027
Mg	0.005	0.005	0.005	0.008	0.005	0.007	0.005	0.007	0.005	0.006	0.006	0.008	0.006	0.005
Ca	9.919	9.969	9.923	9.951	9.909	9.866	9.919	9.857	9.84	9.932	9.865	9.81	9.824	9.856
Na	0.038	0.039	0.04	0.043	0.045	0.04	0.042	0.034	0.029	0.032	0.04	0.04	0.048	0.028
P	5.879	5.866	5.875	5.856	5.892	5.9	5.889	5.918	5.916	5.918	5.911	5.923	5.927	5.888
S	0.047	0.046	0.052	0.055	0.047	0.05	0.047	0.045	0.046	0.026	0.044	0.048	0.044	0.068
La	0.007	0.007	0.008	0.007	0.007	0.008	0.009	0.008	0.008	0.007	0.008	0.01	0.008	0.009
Ce	0.012	0.012	0.014	0.013	0.012	0.014	0.013	0.012	0.013	0.013	0.013	0.015	0.013	0.015
Pr	0.001	0	0	0	0.005	0	0	0.001	0.003	0	0	0.002	0	0
Nd	0.008	0.004	0.008	0.006	0.007	0.005	0.005	0.005	0.006	0.006	0.005	0.003	0.006	0.005
Sm	0.003	0.001	0	0.001	0	0	0	0	0.001	0.001	0	0	0	0.001
Y	0.004	0.004	0.005	0.004	0.004	0.006	0.005	0.002	0.008	0.006	0.004	0.005	0.007	0.006
Sr	0.008	0.008	0.008	0.008	0.008	0.01	0.009	0.007	0.009	0.008	0.008	0.007	0.007	0.008
Ba	0	0	0.001	0	0	0	0	0	0	0	0	0	0.001	0
As	0.001	0	0.001	0.001	0	0	0	0.001	0	0.001	0	0.002	0.001	0
F	1.468	1.582	1.85	1.965	1.835	1.481	1.469	1.62	1.547	1.4	1.633	1.724	1.626	1.71
Cl	0.063	0.056	0.043	0.026	0.033	0.067	0.063	0.057	0.053	0.07	0.053	0.071	0.064	0.068
OH	0.468	0.362	0.108	0.008	0.132	0.452	0.468	0.323	0.399	0.53	0.314	0.205	0.31	0.222
Sum Cat#	18.03	18.06	18.03	18.05	18.03	18	18.03	17.99	17.98	18.03	18	17.96	17.98	17.98

Label	E26/4 6_2_a pat_tr av-1	E26/4 6_2_a pat_tr av-2	E26/4 6_2_a pat_tr av-3	E22/1 1/1/ap a1_tra v-1	E22/1 1/1/ap a1_tra v-2	E22/1 1/1/ap a1_tra v-3	E22/1 1/2/ap a1_ri m-1-1	E22/1 1/2/ap a1_co re-2-1	E22/1 1/4/ap a1_tra v-1	E22/1 1/4/ap a1_tra v-2	E22/1 1/4/ap a1_tra v-3	E22/1 1/5/ap a1_tra v-1	E22/1 1/5/ap a1_tra v-2	E26_6 7_4_a pa_-2	E26_6 7_4_a pa_-3	E26/1 4/1/ap a1_tra v-1	E26/1 4/1/ap a1_tra v-2	E26/1 4/1/ap a1_tra v-3	E26/1 4/2/ap a1_tra v-1	E26/1 4/2/ap a1_tra v-2	E26/1 4/3/ap a1_tra v-1	E26/1 4/3/ap a1_tra v-2	E26/1 4/3/ap a1_tra v-3	E26/1 4/4/ap a1_tra v-1	E26/1 4/4/ap a2_tra v-1	E26/1 4/4/ap a2_tra v-2	E26/1 4/4/ap a2_tra v-3	E26/1 4/5/ap a1_tra v-2	E26/1 4/5/ap a1_tra v-3
SiO2%	0.36	0.31	0.33	0.17	0.2	0.22	0.21	0.18	0.96	0.18	0.33	0.6	0.28	0.24	0.18	0.12	0.07	0.09	0.05	0.14	0.15	0.16	0.2	0.14	0.12	0.07	0.25	0.18	0.22
Fe2O3%	0.08	0.09	0.07	0.05	0.09	0.29	0.06	0.08	0.82	0.05	0.04	0.28	0.14	0.21	0.13	0.46	0.46	0.79	0.95	0.45	0.28	0.39	0.3	1.09	0.53	0.51	0.6	0.07	0.08
MnO%	0.2	0.2	0.21	0.07	0.08	0.12	0.06	0.09	0.06	0.1	0.04	0.07	0.07	0.18	0.2	0.27	0.29	0.33	0.23	0.18	0.22	0.29	0.23	0.21	0.39	0.37	0.43	0.06	0.1
MgO%	0.03	0.02	0.02	0	0	0.02	0	0	0.03	0	0.01	0.01	0.01	0.07	0.04	0.13	0.16	0.16	0.12	0.07	0.09	0.12	0.09	0.12	0.18	0.18	0.21	0.02	0.03
CaO%	54.92	54.45	54.54	55.16	54.79	55.22	55.04	55.81	54.52	55.73	55.14	53.96	54.67	53.3	53.65	53.42	53.93	53.2	54.04	53.99	54.21	54.03	53.59	53.75	53.21	53.79	53.52	53.75	54.21
Na2O%	0.12	0.16	0.13	0.09	0.08	0.13	0.11	0.13	0.1	0.09	0.1	0.13	0.12	0.09	0.04	0.17	0.11	0.16	0.12	0.06	0.19	0.16	0.17	0.16	0.15	0.15	0.16	0.18	0.19
P2O5%	42.04	41.46	42.05	41.46	41.75	42.31	41.57	41.2	40.68	41.61	41.28	41.55	41.73	40.55	41.23	41.63	42.09	42.01	42.39	42.41	42.02	41.27	41.82	41.84	41.6	42.06	41.79	41.82	41.39
SO3%	0.52	0.45	0.47	0.12	0.1	0.15	0.17	0.12	0.13	0.13	0.16	0.11	0.17	0.09	0.08	0.07	0.04	0.09	0.06	0.02	0.07	0.12	0.15	0.15	0.08	0.04	0.14	0.18	0.2
La2O3%	0.13	0.11	0.15	0.14	0.15	0.15	0.15	0.14	0.16	0.14	0.14	0.25	0.16	0.07	0.1	0.09	0.05	0.07	0.05	0.09	0.08	0.09	0.11	0.09	0.07	0.08	0.07	0.11	0.12
Ce2O3%	0.22	0.23	0.22	0.26	0.28	0.26	0.27	0.26	0.33	0.26	0.35	0.53	0.3	0.16	0.16	0.2	0.18	0.15	0.14	0.2	0.22	0.21	0.29	0.22	0.19	0.15	0.13	0.2	0.23
Pr2O3%	0	0	0	0.03	0.04	0	0.05	0	0.01	0.03	0.05	0.01	0.03	0	0.03	0.04	0	0.07	0.06	0	0.01	0	0	0.06	0	0.01	0.01	0.04	0
Nd2O3%	0.08	0.12	0.15	0.1	0.14	0.12	0.18	0.14	0.2	0.19	0.24	0.32	0.17	0.08	0.11	0.12	0.09	0.09	0.14	0.15	0.16	0.14	0.23	0.13	0.12	0.14	0.11	0.2	0.17
Sm2O3%	0.04	0	0.09	0.06	0.03	0.07	0.01	0	0.02	0.03	0.09	0.07	0.04	0.03	0.02	0.04	0	0.03	0.03	0.01	0.02	0	0	0.01	0.04	0.03	0.06	0	0.03
Y2O3%	0.03	0.05	0.1	0.1	0.1	0.16	0.13	0.14	0.14	0.08	0.14	0.34	0.17	0.16	0.07	0.22	0.19	0.19	0.14	0.16	0.25	0.26	0.28	0.2	0.2	0.2	0.24	0.19	0.23
SrO%	0.1	0.09	0.09	0	0	0	0	0	0	0	0	0	0	0.1	0.1	0	0	0	0.03	0.01	0	0	0	0	0	0	0.02	0	0
BaO%	0	0	0	0.01	0	0	0	0	0	0.01	0.01	0	0	0.01	0	0	0	0.01	0	0	0	0	0.01	0	0	0	0.01	0	0.01
As2O3%	0.01	0.01	0	0.01	0.01	0.02	0.03	0.06	0.01	0.02	0.01	0.01	0.04	0	0	0	0	0	0	0.01	0.06	0	0	0	0	0	0	0	0
F%	3.06	2.82	2.9	3.19	3.79	3.83	3.3	3.25	3.68	3.17	3.43	3.57	3.45	3.74	3.68	2.95	2.86	2.84	3.34	3.28	2.91	3.1	2.88	2.83	3.15	3.12	2.98	2.92	3
Cl%	0.25	0.23	0.22	0.3	0.27	0.28	0.21	0.23	0.21	0.32	0.25	0.27	0.24	0.27	0.27	0.59	0.53	0.55	0.5	0.46	0.49	0.51	0.49	0.51	0.55	0.55	0.63	0.28	0.34
H2O(c)	0.29	0.39	0.37	0.18	0	0	0.16	0.18	0	0.21	0.09	0.02	0.09	0	0	0.22	0.29	0.29	0.09	0.11	0.28	0.16	0.28	0.32	0.13	0.17	0.21	0.32	0.26
O=F	1.29	1.19	1.22	1.34	1.6	1.61	1.39	1.37	1.55	1.33	1.44	1.5	1.45	1.57	1.55	1.24	1.2	1.2	1.41	1.38	1.23	1.31	1.21	1.19	1.33	1.31	1.26	1.23	1.26
O=Cl	0.06	0.05	0.05	0.07	0.06	0.06	0.05	0.05	0.05	0.07	0.06	0.06	0.05	0.06	0.06	0.13	0.12	0.12	0.11	0.1	0.11	0.12	0.11	0.12	0.12	0.12	0.14	0.06	0.08
Sum Ox%	101.1	99.96	100.9	100.1	100.3	101.6	100.3	100.6	100.4	100.9	100.4	100.5	100.4	97.71	98.47	99.37	100	99.79	100.9	100.3	100.4	99.6	99.81	100.5	99.27	100.2	100.2	99.23	99.46
Cations																													
Si	0.06	0.052	0.056	0.029	0.035	0.036	0.035	0.031	0.161	0.03	0.055	0.101	0.048	0.041	0.031	0.021	0.011	0.016	0.009	0.023	0.025	0.027	0.033	0.024	0.021	0.012	0.041	0.031	0.038
Fe3+	0.01	0.011	0.009	0.007	0.011	0.036	0.007	0.01	0.104	0.006	0.005	0.035	0.017	0.027	0.017	0.059	0.059	0.101	0.119	0.057	0.036	0.05	0.038	0.138	0.068	0.065	0.077	0.009	0.01
Mn2+	0.028	0.029	0.029	0.01	0.012	0.017	0.008	0.012	0.009	0.014	0.006	0.01	0.009	0.027	0.029	0.039	0.041	0.048	0.032	0.026	0.032	0.041	0.033	0.029	0.056	0.052	0.062	0.008	0.015
Mg	0.006	0.006	0.005	0	0.001	0.006	0.001	0.001	0.009	0	0.002	0.004	0.002	0.018	0.011	0.033	0.039	0.039	0.03	0.017	0.022	0.03	0.023	0.03	0.046	0.044	0.053	0.006	0.007
Ca	9.776	9.819	9.735	9.978	9.89	9.826	9.931	10.07	9.846	10.01	9.961	9.725	9.846	9.877	9.84	9.714	9.726	9.614	9.666	9.696	9.757	9.825	9.694	9.667	9.681	9.699	9.652	9.751	9.846
Na	0.039	0.051	0.041	0.029	0.027	0.04	0.036	0.041	0.034	0.029	0.033	0.043	0.038	0.029	0.013	0.056	0.035	0.051	0.039	0.019	0.062	0.054	0.057	0.051	0.049	0.048	0.051	0.058	0.063
P	5.913	5.908	5.932	5.925	5.954	5.949	5.926	5.877	5.804	5.907	5.893	5.916	5.939	5.936	5.975	5.981	5.998	5.998	5.99	6.019	5.977	5.93	5.977	5.946	5.98	5.992	5.955	5.994	5.94
S	0.065	0.057	0.059	0.015	0.013	0.019	0.022	0.015	0.016	0.016	0.02	0.013	0.021	0.012	0.01	0.009	0.005	0.011	0.007	0.003	0.009	0.015	0.019	0.019	0.01	0.006	0.017	0.023	0.026
La	0.008	0.007	0.009	0.009	0.009	0.009	0.009	0.008	0.01	0.009	0.009	0.015	0.01	0.004	0.006	0.006	0.003	0.004	0.003	0.006	0.005	0.005	0.007	0.005	0.004	0.005	0.004	0.007	0.007
Ce	0.013	0.014	0.014	0.016	0.017	0.016	0.017	0.016	0.02	0.016	0.022	0.032	0.019	0.01	0.01	0.013	0.011	0.009	0.009	0.012	0.013	0.013	0.018	0.013	0.012	0.009	0.008	0.012	0.014
Pr	0	0	0	0.002	0.002	0	0.003	0	0	0.002	0.003	0.001	0.002	0	0.002	0.003	0	0.004	0.003	0	0	0	0	0.004	0	0	0.001	0.002	0
Nd	0.005	0.007	0.009	0.006	0.009	0.007	0.011	0.008	0.012	0.011	0.015	0.019	0.01	0.005	0.006	0.007	0.005	0.005	0.008	0.009	0.009	0.009	0.014	0.008	0.007	0.008	0.007	0.012	0.01
Sm	0.003	0	0.005	0.004	0.002	0.004	0	0	0.001	0.002	0.005	0.004	0.002	0.002	0.001	0.002	0	0.001	0.002	0.001	0.001	0	0	0	0.002	0.002	0.003	0	0.002
Y	0.002	0.005	0.009	0.009	0.009	0.014	0.011	0.012	0.012	0.007	0.013	0.031	0.015	0.015	0.007	0.02	0.017	0.017	0.012	0.014	0.023	0.024	0.025	0.018	0.018	0.018	0.021	0.018	0.02
Sr	0.009	0.009	0.009	0	0	0	0	0	0	0	0	0	0	0.01	0.01	0	0	0	0.003	0.001	0	0	0	0	0	0	0.002	0	0
Ba	0	0	0	0	0	0	0	0	0	0	0.001	0	0	0	0	0	0	0.001	0	0	0	0	0	0	0	0	0	0	0.001
As	0.001	0.001	0	0.001	0.001	0.002	0.003	0.006	0.001	0.003	0.002	0.001	0.004	0	0	0	0	0	0	0.001	0.006	0	0	0	0	0	0	0	0
F	1.61	1.499	1.526	1.705	2.022	2.01	1.756	1.731	1.96	1.68	1.827	1.9	1.834	2.045	1.994	1.584	1.522	1.517	1.764	1.74	1.547	1.666	1.539	1.5	1.693	1.658	1.587	1.564	1.609
Cl	0.069	0.065	0.061	0.087	0.078	0.078	0.06	0.066	0.061	0.09	0.073	0.077	0.067	0.08	0.078	0.171	0.152	0.158	0.14	0.132	0.141	0.148	0.14	0.145	0.158	0.156	0.179	0.08	0.098
OH	0.321	0.435	0.413	0.208	0.001	0.001	0.183	0.203	0.001	0.23	0.101	0.023	0.099	0.001	0.001	0.246	0.326	0.326	0.096	0.129	0.312	0.186	0.321	0.354	0.149	0.186	0.234	0.356	0.293
Sum Cat#	17.94	17.98	17.92	18.04	18.09	18.07	18.02	18.11	18.06	18.06	18.04	17.95	17.98	18.14	18.04	17.96	17.95	17.92	17.93	17.9	17.98	18.02	17.94	17.95	17.96	17.96	17.96	17.93	18

Label	E26_71_6_1	E26_71_6_3	E27/58/1/apa1_trav-1	E27/58/1/apa1_trav-2	E27/58/2/apa1_trav-1	E27/58/2/apa1_trav-2	E27/58/2/apa1_trav-3	E27/58/3/apa1_trav-1	E27/58/3/apa1_trav-2	E27/58/3/apa1_trav-3	E27/58/4/apa1_trav-1	E27/58/4/apa1_trav-2	E27/58/4/apa1_trav-3	E27/58/4/apa1_trav-4	E27/58/4/apa1_trav-5	E27/58/4/apa1_trav-6	E27/58/4/apa1_trav-7	E27/58/4/apa1_trav-8	E27/58/4/apa1_trav-9	E27_56_2_apa in Kfs_-5-1	E27_56_5_2ndApa_-1	E27_56_5_2ndApa_-2	E27_56_5_2ndApa_-3	E27_56_5_apa in Kfs_-1	E27_56_5_apa in Kfs_-2	E27_56_5_apa in Kfs_-3	E48_2_1_apa_-1	E48_2_1_apa_-2	E48_2_1_apa_-3
SiO2%	0.29	0.56	0.33	0.33	0.51	0.3	0.47	0.33	0.25	0.36	0.2	0.27	0.29	0.31	0.31	0.33	0.33	0.27	0.19	0.23	0.24	0.28	0.51	0.22	0.45	0.36	0.33	0.2	0.21
Fe2O3%	0.46	0.08	0.31	0.15	0.08	0.06	0.08	0.06	0.04	0.13	0.06	0.05	0.07	0.01	0.05	0.04	0.07	0.06	0.06	0.12	0.12	0.1	0.08	0.06	0.07	0.05	0.04	0.03	0.08
MnO%	0.7	0.27	0.14	0.14	0.18	0.16	0.19	0.17	0.15	0.16	0.13	0.16	0.12	0.09	0.09	0.12	0.08	0.11	0.09	0.13	0.11	0.14	0.17	0.14	0.11	0.14	0.08	0.06	0.05
MgO%	0.17	0.07	0.04	0.02	0.02	0.01	0.01	0.01	0.02	0.02	0.01	0.01	0.01	0	0	0.01	0.01	0	0	0.01	0.03	0.02	0.02	0	0.01	0.01	0	0	0.01
CaO%	53.54	54.3	54.55	54.7	53.86	54.84	54.64	54.5	54.84	54.3	55.24	54.7	54.48	55.29	54.74	54.31	54.85	54.56	55.28	54.77	54.63	54.23	53.84	54.88	54.46	54.19	54.13	54.45	54.32
Na2O%	0.23	0.19	0.08	0.13	0.13	0.13	0.1	0.12	0.22	0.13	0.09	0.13	0.11	0.14	0.12	0.17	0.12	0.08	0.03	0.08	0.17	0.19	0.18	0.07	0.17	0.2	0.14	0.11	0.12
P2O5%	41.45	41.34	41.62	41.74	40.59	41.99	41.23	41.34	41.31	41.33	41.69	41.61	41.05	41.3	41.27	41.12	41.34	41.68	42.03	41.03	40.64	40.62	40.32	40.99	39.96	40.36	40.22	40.67	40.9
SO3%	0.12	0.5	0.43	0.44	0.28	0.32	0.23	0.4	0.59	0.34	0.34	0.46	0.41	0.55	0.55	0.49	0.46	0.38	0.1	0.25	0.2	0.31	0.23	0.14	0.67	0.56	0.15	0.18	0.21
La2O3%	0.03	0.16	0.12	0.1	0.13	0.12	0.11	0.14	0.06	0.11	0.15	0.09	0.12	0.13	0.12	0.1	0.12	0.12	0.04	0.09	0.13	0.13	0.18	0.07	0.12	0.11	0.11	0.11	0.09
Ce2O3%	0.06	0.06	0.21	0.2	0.16	0.2	0.12	0.25	0.17	0.22	0.16	0.18	0.2	0.17	0.17	0.2	0.23	0.19	0.08	0.22	0.27	0.3	0.41	0.17	0.28	0.24	0.21	0.19	0.17
Pr2O3%	-	-	0	0.03	0	0.03	0	0.07	0	0.05	0.02	0	0	0	0	0.04	0	0	0	0.04	0.07	0.02	0	0	0.01	0.04	0	0.02	0
Nd2O3%	-	-	0.12	0.11	0.08	0.11	0.08	0.11	0.09	0.08	0.04	0.06	0.09	0.09	0.06	0.12	0.09	0.1	0.1	0.11	0.23	0.21	0.33	0.07	0.15	0.15	0.12	0.12	0.19
Sm2O3%	-	-	0	0.02	0	0	0	0	0	0.01	0.02	0.01	0.05	0.05	0	0	0.04	0.01	0	0	0.01	0.05	0.05	0.03	0.02	0.05	0	0.01	0.01
Y2O3%	0.29	0.13	0.05	0.06	0	0.09	0.01	0.07	0.05	0.08	0.02	0.09	0.09	0.05	0.04	0.05	0.08	0.08	0.06	0.09	0.23	0.24	0.39	0.06	0.13	0.1	0.12	0.12	0.16
SrO%	0.14	0.01	0.08	0.07	0.01	0.05	0.02	0.02	0.1	0.07	0.02	0.1	0.05	0.01	0.01	0.04	0.04	0.04	0.02	0.1	0	0	0	0.1	0.06	0.07	0.01	0.02	0.01
BaO%	0.12	0.31	0	0.01	0.02	0	0	0	0	0	0.01	0	0	0	0.01	0.01	0.01	0	0	0	0.01	0.01	0	0.01	0	0	0	0	0
As2O3%	-	-	0	0.01	0	0.02	0.01	0.01	0.01	0.01	0.01	0.01	0.01	0	0.01	0.01	0.01	0.01	0	0.01	0	0.01	0	0.02	0.01	0.02	0.01	0.02	0.03
F%	3.44	4.08	2.93	3	3.36	3.71	3.21	2.82	3.1	2.96	3.12	2.93	2.89	2.85	2.74	2.92	3.15	2.99	3.12	3.71	3.56	3.52	3.65	3.79	3.73	3.64	3.33	3.43	3.53
Cl%	0.4	0.22	0.44	0.43	0.29	0.32	0.3	0.38	0.37	0.38	0.39	0.39	0.38	0.39	0.4	0.39	0.38	0.38	0.36	0.17	0.27	0.28	0.23	0.15	0.22	0.25	0.2	0.2	0.23
H2O(c)	0.04	0	0.28	0.26	0.08	0	0.18	0.35	0.22	0.27	0.21	0.3	0.3	0.34	0.38	0.29	0.19	0.27	0.22	0	0	0.02	0	0	0	0	0.11	0.07	0.02
O=F	1.45	1.72	1.24	1.26	1.42	1.56	1.35	1.19	1.3	1.25	1.32	1.23	1.22	1.2	1.15	1.23	1.33	1.26	1.31	1.56	1.5	1.48	1.54	1.6	1.57	1.53	1.4	1.44	1.49
O=Cl	0.09	0.05	0.1	0.1	0.07	0.07	0.07	0.08	0.08	0.09	0.09	0.09	0.09	0.09	0.09	0.09	0.09	0.09	0.08	0.04	0.06	0.06	0.05	0.03	0.05	0.06	0.05	0.04	0.05
Sum Ox%	99.94	100.5	100.4	100.6	98.3	100.8	99.57	99.87	100.2	99.69	100.5	100.2	99.4	100.5	99.86	99.44	100.2	99.97	100.4	99.56	99.36	99.13	99.02	99.34	99.01	98.93	97.85	98.54	98.79
Cations																													
Si	0.049	0.094	0.055	0.055	0.087	0.05	0.079	0.056	0.042	0.062	0.034	0.045	0.05	0.053	0.053	0.056	0.055	0.046	0.031	0.039	0.041	0.049	0.087	0.037	0.076	0.062	0.057	0.034	0.037
Fe3+	0.059	0.01	0.039	0.019	0.01	0.007	0.01	0.007	0.005	0.017	0.008	0.007	0.008	0.002	0.007	0.005	0.009	0.008	0.008	0.015	0.016	0.013	0.01	0.008	0.009	0.006	0.005	0.004	0.01
Mn2+	0.1	0.039	0.02	0.02	0.026	0.022	0.027	0.025	0.021	0.023	0.018	0.022	0.017	0.013	0.013	0.017	0.012	0.015	0.013	0.018	0.015	0.02	0.025	0.02	0.016	0.02	0.011	0.008	0.007
Mg	0.043	0.018	0.01	0.004	0.006	0.001	0.004	0.003	0.005	0.005	0.003	0.002	0.003	0.001	0	0.003	0.001	0	0	0.003	0.007	0.005	0.004	0.001	0.003	0.002	0.001	0.001	0.002
Ca	9.695	9.768	9.8	9.807	9.89	9.816	9.902	9.851	9.877	9.829	9.922	9.84	9.9	9.938	9.882	9.852	9.887	9.833	9.926	9.961	9.99	9.924	9.887	10.01	9.98	9.921	10.02	10	9.943
Na	0.074	0.062	0.028	0.044	0.044	0.041	0.032	0.038	0.071	0.042	0.028	0.043	0.037	0.045	0.04	0.055	0.04	0.026	0.011	0.027	0.056	0.062	0.061	0.022	0.057	0.066	0.046	0.038	0.041
P	5.93	5.877	5.907	5.914	5.889	5.939	5.903	5.904	5.88	5.912	5.916	5.915	5.893	5.865	5.887	5.895	5.889	5.935	5.964	5.896	5.872	5.873	5.851	5.906	5.787	5.839	5.882	5.904	5.916
S	0.016	0.063	0.054	0.055	0.036	0.04	0.029	0.051	0.075	0.044	0.043	0.058	0.053	0.069	0.069	0.063	0.058	0.047	0.013	0.032	0.026	0.04	0.03	0.018	0.086	0.072	0.019	0.024	0.027
La	0.002	0.01	0.008	0.006	0.008	0.007	0.007	0.009	0.004	0.007	0.01	0.006	0.007	0.008	0.007	0.006	0.008	0.007	0.003	0.006	0.008	0.008	0.012	0.004	0.008	0.007	0.007	0.007	0.005
Ce	0.004	0.004	0.013	0.012	0.01	0.012	0.008	0.015	0.01	0.014	0.01	0.011	0.012	0.01	0.01	0.012	0.014	0.012	0.005	0.013	0.017	0.019	0.026	0.01	0.017	0.015	0.013	0.012	0.01
Pr	-	-	0	0.002	0	0.002	0	0.005	0	0.003	0.001	0	0	0	0	0.002	0	0	0	0.002	0.004	0.001	0	0	0	0.002	0	0.001	0
Nd	-	-	0.007	0.007	0.005	0.007	0.005	0.007	0.006	0.005	0.002	0.003	0.005	0.005	0.004	0.007	0.005	0.006	0.006	0.007	0.014	0.013	0.02	0.004	0.009	0.009	0.007	0.008	0.012
Sm	-	-	0	0.001	0	0	0	0	0	0	0.001	0	0.003	0.003	0	0	0.002	0	0	0	0.001	0.003	0.003	0.002	0.001	0.003	0	0.001	0
Y	0.026	0.012	0.005	0.006	0	0.008	0.001	0.006	0.004	0.007	0.002	0.008	0.008	0.004	0.004	0.005	0.007	0.007	0.005	0.008	0.021	0.022	0.035	0.006	0.012	0.009	0.011	0.011	0.014
Sr	0.013	0.001	0.008	0.007	0.001	0.005	0.002	0.002	0.01	0.007	0.002	0.009	0.005	0.001	0.001	0.004	0.004	0.004	0.002	0.01	0	0	0	0.01	0.006	0.007	0.001	0.002	0.001
Ba	0.008	0.02	0	0	0.001	0	0	0	0	0	0	0	0	0	0.001	0	0.001	0	0	0	0	0.001	0	0	0	0	0	0	0
As	-	-	0	0.001	0	0.002	0.001	0.001	0.001	0.001	0.001	0.001	0.001	0	0.001	0.001	0.001	0.001	0	0.001	0	0.001	0	0.002	0.001	0.002	0.001	0.003	0.003
F	1.84	2.169	1.556	1.589	1.822	1.96	1.717	1.502	1.647	1.584	1.656	1.556	1.553	1.511	1.459	1.562	1.677	1.589	1.653	1.993	1.922	1.9	1.981	2.039	2.018	1.968	1.819	1.86	1.909
Cl	0.115	0.063	0.126	0.121	0.084	0.09	0.085	0.108	0.104	0.109	0.109	0.111	0.11	0.112	0.116	0.113	0.108	0.109	0.103	0.05	0.079	0.081	0.067	0.044	0.065	0.073	0.059	0.058	0.066
OH	0.045	0.001	0.318	0.29	0.094	0.001	0.198	0.39	0.249	0.307	0.235	0.333	0.337	0.377	0.425	0.326	0.215	0.303	0.245	0.001	0.001	0.02	0.001	0.001	0.001	0.001	0.121	0.083	0.026
Sum Cat#	18.02	18.21	17.95	17.96	18.01	18.01	18.01	17.98	18.01	17.98	18	17.97	18	18.02	17.98	17.98	17.99	17.95	17.99	18.08	18.09	18.05	18.1	18.14	18.15	18.08	18.08	18.06	18.03

Label	E48_2_2_apa-1	E48_2_2_apa-2	E48_2_2_apa-3	E48_2_2_apa-4	E48_2_2_apa-5	E48_2_4_apa1_-1	E48_2_4_apa1_-2	E48_2_4_apa1_-3	E48_2_6_apa__in_kfs-1	E48_2_6_apa__in_kfs-2	E48_2_6_apa__in_kfs-3	E48_2_6_apa__in_kfs-4	E48_17_apa in Kfs_-3	E48_17_3_apa_-1	E48_17_3_apa_-2	E48_17_3_apa_-3	E48_17_3_apa_-4	E48_17_3_apa_-5	E48_17_4_apa_-1	E48_17_4_apa_-2	E48_17_4_apa_-3	E48_17_5_apa_-1	E48_17_5_apa_-2	E48_17_5_apa_-3	E48_17_5_apa_-4	E48_17_5_apa_-5	CS18 9/1/apa1_trav-1	CS18 9/1/apa1_trav-2	CS18 9/3/apa1_trav-1
SiO2%	0.21	0.17	0.17	0.18	0.16	0.29	0.28	0.23	0.44	0.19	0.15	0.26	0.42	0.18	0.37	0.25	0.26	0.18	0.37	0.35	0.3	0.23	0.3	0.2	0.21	0.18	0.26	0.23	0.22
Fe2O3%	0.1	0.08	0.09	0.08	0.12	0.06	0.03	0.06	0.08	0.04	0.05	0.04	0.12	0.07	0.1	0.08	0.1	0.11	0.11	0.11	0.1	0.06	0.09	0.07	0.07	0.08	1.29	0.47	0.34
MnO%	0.06	0.05	0.09	0.1	0.09	0.05	0.09	0.07	0.07	0.01	0.04	0.05	0.22	0.12	0.15	0.1	0.13	0.1	0.13	0.14	0.12	0.09	0.14	0.15	0.11	0.1	0.28	0.28	0.12
MgO%	0.01	0.02	0.01	0.02	0.01	0	0.01	0	0	0.01	0	0.01	0.04	0.03	0.03	0.04	0.03	0.02	0.03	0.03	0.03	0.02	0.03	0.03	0.03	0.03	0.04	0.04	0.26
CaO%	54.55	54.8	54.42	54.29	54.65	54.12	53.83	54.13	52.89	53.36	54.22	53.59	54.04	53.69	54.36	54.22	54.37	53.66	53.98	53.37	53.5	54.45	53.38	54.72	54.57	54.84	52.66	52.89	53.81
Na2O%	0.07	0.09	0.14	0.12	0.1	0.18	0.18	0.14	0.1	0.11	0.12	0.07	0.18	0.13	0.15	0.08	0.12	0.13	0.16	0.17	0.14	0.18	0.08	0.09	0.11	0.14	0.16	0.25	0.1
P2O5%	41.12	40.5	40.65	40.72	40.44	40.12	40.41	40.98	41.2	41.27	41.23	41.56	40.2	40.69	40.26	41.03	40.64	41.12	39.95	40.26	41	40.22	40.47	40.71	40.45	40.49	40.26	41.44	41.75
SO3%	0.08	0.1	0.15	0.17	0.11	0.39	0.42	0.23	0.02	0.25	0.16	0.09	0.38	0.22	0.47	0.25	0.29	0.18	0.47	0.48	0.45	0.13	0.26	0.2	0.2	0.17	0.17	0.5	0.36
La2O3%	0.13	0.13	0.14	0.13	0.14	0.1	0.08	0.1	0.21	0.1	0.13	0.12	0.2	0.1	0.17	0.15	0.13	0.11	0.11	0.12	0.12	0.11	0.15	0.1	0.13	0.08	0.19	0.14	0.04
Ce2O3%	0.22	0.24	0.23	0.22	0.23	0.24	0.19	0.23	0.44	0.2	0.2	0.25	0.31	0.16	0.29	0.23	0.24	0.18	0.2	0.25	0.22	0.23	0.22	0.24	0.24	0.21	0.36	0.32	0.06
Pr2O3%	0	0	0	0.02	0.02	0.05	0.01	0.01	0.01	0.04	0	0	0.04	0	0	0.05	0.01	0	0	0	0.01	0.01	0	0	0.05	0.02	0	0	0.05
Nd2O3%	0.14	0.19	0.12	0.14	0.15	0.12	0.16	0.15	0.22	0.14	0.12	0.15	0.12	0.15	0.1	0.13	0.13	0.1	0.1	0.17	0.1	0.16	0.18	0.11	0.15	0.11	0.21	0.15	0.03
Sm2O3%	0.06	0	0.01	0.03	0.09	0.01	0.02	0.01	0	0.05	0.04	0	0	0	0	0.1	0.04	0	0.01	0.03	0	0.02	0	0	0.01	0.06	0.02	0.01	0.03
Y2O3%	0.11	0.13	0.19	0.16	0.12	0.17	0.2	0.17	0.15	0.12	0.07	0.09	0.08	0.08	0.12	0.08	0.04	0.16	0.12	0.16	0.1	0.28	0.06	0.06	0.11	0.23	0.12	0.11	0.07
SrO%	0	0	0	0	0	0	0	0	0	0	0.02	0.02	0.04	0.04	0.06	0.07	0.07	0.01	0.04	0.08	0.05	0	0.1	0.08	0.04	0	0	0.01	0.27
BaO%	0	0.01	0	0	0.02	0	0	0	0.01	0	0	0	0	0	0	0	0	0	0	0	0	0.01	0.01	0	0.01	0	0	0.01	0.01
As2O3%	0.01	0	0.01	0.01	0	0.01	0.01	0.01	0.03	0.01	0.02	0	0	0.04	0.01	0	0	0.03	0	0.02	0.01	0	0	0	0.01	0	0	0	0
F%	3.36	3.33	3.24	3.42	3.49	3.47	3.6	3.6	3.24	3.48	3.54	3.42	3.31	2.79	2.99	3.11	3.1	3.04	2.87	2.98	2.86	3.13	2.98	2.95	3.03	3.06	2.02	1.8	2.35
Cl%	0.26	0.27	0.28	0.29	0.27	0.18	0.19	0.17	0.23	0.23	0.2	0.23	0.59	0.83	0.61	0.6	0.55	0.79	0.82	0.77	0.84	0.72	0.64	0.66	0.66	0.79	1.79	1.75	0.29
H2O(c)	0.1	0.1	0.14	0.05	0.02	0.05	0	0.01	0.16	0.04	0.03	0.08	0.03	0.21	0.18	0.13	0.14	0.11	0.17	0.13	0.19	0.07	0.16	0.19	0.14	0.1	0.32	0.47	0.6
O=F	1.41	1.4	1.37	1.44	1.47	1.46	1.51	1.52	1.36	1.46	1.49	1.44	1.39	1.18	1.26	1.31	1.31	1.28	1.21	1.25	1.2	1.32	1.26	1.24	1.27	1.29	0.85	0.76	0.99
O=Cl	0.06	0.06	0.06	0.07	0.06	0.04	0.04	0.04	0.05	0.05	0.05	0.05	0.13	0.19	0.14	0.14	0.13	0.18	0.19	0.17	0.19	0.16	0.14	0.15	0.15	0.18	0.4	0.39	0.07
Sum Ox%	99.13	98.73	98.64	98.65	98.7	98.1	98.15	98.74	98.07	98.13	98.81	98.54	98.8	98.16	99.04	99.27	98.98	98.56	98.25	98.19	98.76	98.66	97.85	99.18	98.91	99.22	98.9	99.71	99.7
Cations																													
Si	0.036	0.029	0.029	0.032	0.027	0.049	0.048	0.04	0.075	0.032	0.026	0.044	0.072	0.031	0.064	0.043	0.044	0.031	0.063	0.06	0.051	0.04	0.052	0.035	0.036	0.031	0.044	0.039	0.037
Fe3+	0.013	0.01	0.012	0.011	0.016	0.008	0.004	0.008	0.01	0.006	0.006	0.006	0.016	0.009	0.013	0.011	0.012	0.014	0.014	0.014	0.013	0.008	0.012	0.009	0.01	0.011	0.167	0.059	0.043
Mn2+	0.008	0.007	0.013	0.014	0.013	0.007	0.013	0.011	0.01	0.001	0.005	0.007	0.031	0.018	0.021	0.014	0.019	0.014	0.02	0.021	0.018	0.013	0.021	0.022	0.016	0.014	0.041	0.041	0.018
Mg	0.002	0.004	0.001	0.005	0.003	0	0.001	0	0	0.003	0	0.001	0.01	0.008	0.007	0.009	0.008	0.004	0.006	0.009	0.008	0.006	0.007	0.008	0.007	0.007	0.01	0.01	0.066
Ca	9.957	10.08	10	9.971	10.06	9.993	9.913	9.905	9.725	9.788	9.909	9.789	9.935	9.904	9.964	9.895	9.961	9.844	9.974	9.852	9.783	10.05	9.876	10.02	10.03	10.06	9.731	9.607	9.7
Na	0.024	0.03	0.046	0.039	0.035	0.059	0.06	0.048	0.034	0.037	0.038	0.023	0.059	0.043	0.051	0.025	0.041	0.044	0.053	0.055	0.048	0.062	0.025	0.031	0.036	0.047	0.055	0.083	0.033
P	5.932	5.886	5.903	5.909	5.883	5.853	5.881	5.925	5.987	5.981	5.953	5.999	5.84	5.932	5.831	5.916	5.884	5.96	5.833	5.872	5.923	5.867	5.916	5.888	5.875	5.87	5.879	5.948	5.948
S	0.01	0.012	0.019	0.022	0.014	0.051	0.055	0.029	0.003	0.032	0.021	0.012	0.049	0.028	0.06	0.032	0.037	0.023	0.061	0.062	0.058	0.017	0.033	0.026	0.026	0.021	0.022	0.063	0.045
La	0.008	0.008	0.009	0.008	0.009	0.006	0.005	0.006	0.014	0.006	0.008	0.008	0.012	0.006	0.011	0.01	0.008	0.007	0.007	0.008	0.008	0.007	0.01	0.006	0.008	0.005	0.012	0.009	0.003
Ce	0.014	0.015	0.015	0.014	0.015	0.015	0.012	0.014	0.028	0.013	0.012	0.015	0.02	0.01	0.018	0.015	0.015	0.011	0.013	0.016	0.014	0.015	0.014	0.015	0.015	0.013	0.023	0.02	0.004
Pr	0	0	0	0.001	0.001	0.003	0.001	0	0	0.002	0	0	0.002	0	0	0.003	0.001	0	0	0	0.001	0.001	0	0	0.003	0.001	0	0	0.003
Nd	0.008	0.012	0.007	0.009	0.009	0.007	0.01	0.009	0.013	0.008	0.007	0.009	0.007	0.009	0.006	0.008	0.008	0.006	0.006	0.01	0.006	0.01	0.011	0.007	0.009	0.007	0.013	0.009	0.002
Sm	0.004	0	0	0.002	0.006	0.001	0.001	0	0	0.003	0.002	0	0	0	0	0.006	0.002	0	0.001	0.002	0	0.001	0	0	0	0.003	0.001	0.001	0.002
Y	0.01	0.012	0.017	0.014	0.011	0.015	0.018	0.015	0.014	0.01	0.007	0.008	0.007	0.007	0.011	0.008	0.003	0.014	0.011	0.014	0.009	0.026	0.006	0.006	0.01	0.021	0.011	0.01	0.006
Sr	0	0	0	0	0	0	0	0	0	0	0.002	0.002	0.004	0.004	0.006	0.007	0.007	0.001	0.004	0.008	0.005	0	0.01	0.008	0.004	0	0	0.001	0.026
Ba	0	0	0	0	0.001	0	0	0	0.001	0	0	0	0	0	0	0	0	0	0	0	0	0	0.001	0	0	0	0	0	0.001
As	0.001	0	0.001	0.001	0	0.001	0.001	0.001	0.003	0.001	0.002	0	0	0.005	0.001	0	0	0.003	0	0.002	0.001	0	0	0	0.001	0	0	0	0
F	1.809	1.805	1.76	1.853	1.899	1.891	1.956	1.944	1.756	1.882	1.908	1.843	1.796	1.522	1.62	1.677	1.678	1.649	1.564	1.622	1.544	1.706	1.629	1.593	1.643	1.657	1.104	0.966	1.248
Cl	0.076	0.078	0.081	0.084	0.079	0.054	0.054	0.048	0.066	0.067	0.058	0.066	0.173	0.242	0.176	0.173	0.161	0.229	0.24	0.226	0.244	0.21	0.188	0.19	0.192	0.229	0.524	0.503	0.084
OH	0.116	0.117	0.159	0.063	0.022	0.056	0.001	0.008	0.178	0.051	0.034	0.091	0.031	0.236	0.204	0.15	0.161	0.122	0.195	0.153	0.212	0.084	0.183	0.217	0.165	0.114	0.372	0.531	0.668
Sum Cat#	18.03	18.11	18.07	18.05	18.1	18.07	18.04	18.01	17.92	17.93	18	17.92	18.07	18.01	18.06	18	18.05	17.98	18.07	18	17.95	18.12	17.99	18.08	18.09	18.11	18.01	17.9	17.94

Label	CS18 9/3/apa1_trav-2	CS18 9/3/apa1_trav-3	CS18 9/4/apa1_trav-1	CS18 9/4/apa1_trav-2	CS18 9/4/apa1_trav-3	CS18 9/4/apa1_trav-4	CS19 9/2/apa1_trav-1	CS19 9/2/apa1_trav-2	CS19 9/3/apa1_trav-1	CS19 9/3/apa1_trav-3	CS19 9/4/apa1_trav-1	CS19 9/4/apa1_trav-2	CS19 9/5/apa1_trav-2	CS19 9/5/apa1_trav-3	CS19 9/5/apa1_trav-4	CS19 9/5/apa1_trav-5	VL10-3_2_apa in hbl_-1	VL10-3_2_apa in hbl_-2	VL10-3_2_apa in hbl_-3	VL10-3_3_apa in sphn_-2	VL10-3_3_apa in sphn_-3	VL9-2_5_apa_-1	VL9-2_5_apa_-2	VL9-2_5_apa_-3	VL9-2_1_apa2
SiO2%	0.25	0.21	0.57	0.3	0.34	0.29	0.28	0.38	0.27	0.51	0.36	0.25	0.25	0.32	0.27	0.25	0.45	0.38	0.41	0.39	0.42	0.34	0.38	0.66	0.64
Fe2O3%	0.31	0.33	0.42	0.33	0.38	0.59	0.2	0.63	0.3	0.33	0.18	0.27	0.2	0.19	0.27	0.21	0.32	0.31	0.31	0.15	0.1	0.18	0.15	0.21	0.29
MnO%	0.09	0.1	0.14	0.09	0.09	0.06	0.1	0.17	0.15	0.18	0.12	0.16	0.23	0.16	0.13	0.2	0.2	0.2	0.18	0.19	0.2	0.17	0.19	0.18	0.3
MgO%	0.27	0.27	0.32	0.29	0.3	0.27	0.14	0.03	0.23	0.05	0.02	0.1	0.04	0.1	0.21	0.12	0.06	0.06	0.07	0.06	0.03	0.09	0.08	0.1	0.05
CaO%	53.8	54.14	52.94	53.83	53.74	53.8	54.1	53.95	53.66	53.92	54.35	53.72	53.8	53.83	54	54.02	54.52	54.38	54.18	54.7	54.33	53.83	53.53	53.55	53.31
Na2O%	0.09	0.11	0.17	0.14	0.15	0.09	0.1	0.08	0.09	0.04	0.08	0.08	0.1	0.1	0.13	0.09	0.17	0.23	0.25	0.2	0.16	0.18	0.19	0.16	0.2
P2O5%	41.48	41.9	41.33	41.26	41.27	41.41	41.73	41.98	41.52	41.3	41.97	42.12	41.62	41.42	41.54	41.41	40.22	39.98	39.65	39.99	39.85	40.65	40.11	39.46	39.77
SO3%	0.36	0.35	0.64	0.62	0.69	0.56	0.13	0.08	0.21	0.11	0.05	0.14	0.33	0.24	0.46	0.32	0.58	0.8	0.89	0.53	0.57	0.53	0.59	0.53	0.43
La2O3%	0.03	0.06	0.03	0.01	0.04	0.03	0.04	0.05	0.07	0.06	0.1	0.1	0.09	0.07	0.06	0.08	0.09	0.08	0.09	0.1	0.07	0.07	0.06	0.07	0.17
Ce2O3%	0.07	0.06	0.05	0.05	0.05	0.05	0.11	0.11	0.13	0.11	0.16	0.19	0.14	0.13	0.12	0.17	0.13	0.13	0.13	0.2	0.2	0.14	0.14	0.13	0.31
Pr2O3%	0	0	0.01	0	0	0	0.02	0	0.01	0	0.02	0	0	0.03	0.09	0.01	0.01	0.04	0	0.06	0	0	0.03	0	0.05
Nd2O3%	0.1	0.08	0.08	0.05	0.06	0.04	0.1	0.08	0.12	0.08	0.11	0.11	0.06	0.17	0.03	0.09	0.1	0.08	0.1	0.07	0.17	0.11	0.11	0.11	0.17
Sm2O3%	0.04	0	0.06	0	0.01	0.03	0	0.04	0.02	0.05	0	0.04	0.01	0	0.01	0.03	0	0.05	0.04	0.01	0.01	0.01	0.02	0.03	0
Y2O3%	0.03	0.02	0.01	0.02	0.03	0.04	0.06	0.05	0.08	0.02	0.07	0.02	0.06	0.05	0.06	0.08	0.05	0.02	0.05	0.13	0.12	0.09	0.11	0.09	0.14
SrO%	0.28	0.27	0.26	0.28	0.28	0.27	0.17	0.09	0.22	0.12	0.01	0.16	0.15	0.16	0.24	0.19	0.06	0.08	0.08	0.1	0.09	0.14	0.14	0.14	0.05
BaO%	0	0	0	0	0	0	0	0	0.02	0.01	0	0	0	0	0.01	0	0	0	0	0.01	0	0.01	0	0	0
As2O3%	0	0	0	0	0	0	0	0.03	0	0	0.03	0	0	0	0	0	0	0	0	0	0	0	0	0	0.02
F%	2.23	2.58	2.72	2.39	2.43	2.38	3.98	3.87	2.49	2.79	2.6	2.49	2.57	2.39	2.08	2.35	2.74	2.69	2.7	2.74	2.89	3.43	3.51	3.4	3.44
Cl%	0.34	0.49	0.49	0.41	0.37	0.34	0.25	0.31	0.43	1.02	1.01	0.92	1.01	0.92	0.7	0.84	0.7	0.72	0.74	0.56	0.54	0.74	0.69	0.71	0.84
H2O(c)	0.63	0.44	0.36	0.54	0.54	0.57	0	0	0.48	0.19	0.29	0.37	0.3	0.4	0.62	0.45	0.29	0.3	0.28	0.31	0.24	0	0	0	0
O=F	0.94	1.09	1.14	1.01	1.02	1	1.68	1.63	1.05	1.17	1.1	1.05	1.08	1.01	0.88	0.99	1.15	1.13	1.14	1.16	1.22	1.44	1.48	1.43	1.45
O=Cl	0.08	0.11	0.11	0.09	0.08	0.08	0.06	0.07	0.1	0.23	0.23	0.21	0.23	0.21	0.16	0.19	0.16	0.16	0.17	0.13	0.12	0.17	0.15	0.16	0.19
Sum Ox%	99.41	100.2	99.33	99.5	99.66	99.76	99.76	100.2	99.38	99.49	100.2	100	99.65	99.48	100	99.74	99.38	99.25	98.83	99.23	98.67	99.09	98.4	97.94	98.55
Cations																									
Si	0.042	0.035	0.096	0.051	0.057	0.049	0.047	0.064	0.046	0.086	0.061	0.042	0.042	0.054	0.045	0.043	0.076	0.065	0.07	0.066	0.072	0.06	0.07	0.11	0.11
Fe3+	0.039	0.042	0.053	0.042	0.048	0.075	0.025	0.079	0.039	0.042	0.023	0.035	0.025	0.025	0.035	0.027	0.041	0.04	0.04	0.019	0.013	0.02	0.02	0.03	0.04
Mn2+	0.013	0.014	0.02	0.013	0.012	0.009	0.014	0.024	0.022	0.026	0.017	0.023	0.033	0.023	0.019	0.029	0.029	0.029	0.026	0.027	0.03	0.02	0.03	0.03	0.04
Mg	0.069	0.068	0.079	0.072	0.074	0.067	0.036	0.008	0.059	0.014	0.004	0.026	0.009	0.026	0.053	0.029	0.015	0.015	0.018	0.017	0.008	0.02	0.02	0.03	0.01
Ca	9.737	9.723	9.563	9.726	9.691	9.695	9.79	9.71	9.733	9.803	9.795	9.685	9.747	9.776	9.736	9.789	9.948	9.939	9.947	10.02	9.997	9.84	9.87	9.93	9.85
Na	0.031	0.037	0.055	0.046	0.049	0.03	0.032	0.026	0.028	0.014	0.027	0.026	0.033	0.034	0.043	0.03	0.057	0.077	0.084	0.065	0.055	0.058	0.063	0.055	0.068
P	5.932	5.946	5.899	5.891	5.881	5.897	5.966	5.97	5.951	5.932	5.977	6.001	5.958	5.944	5.918	5.93	5.799	5.773	5.752	5.787	5.794	5.869	5.84	5.783	5.807
S	0.046	0.044	0.081	0.078	0.088	0.071	0.016	0.01	0.026	0.013	0.007	0.018	0.042	0.031	0.058	0.041	0.075	0.103	0.114	0.069	0.073	0.068	0.077	0.068	0.056
La	0.002	0.003	0.002	0.001	0.003	0.002	0.002	0.003	0.005	0.004	0.006	0.007	0.006	0.005	0.004	0.005	0.006	0.005	0.005	0.006	0.005	0.004	0.004	0.004	0.011
Ce	0.004	0.004	0.003	0.003	0.003	0.003	0.007	0.007	0.008	0.007	0.01	0.012	0.008	0.008	0.007	0.011	0.008	0.008	0.008	0.012	0.012	0.009	0.009	0.009	0.02
Pr	0	0	0	0	0	0	0.001	0	0.001	0	0.001	0	0	0.002	0.006	0	0.001	0.003	0	0.003	0	0	0.002	0	0.003
Nd	0.006	0.005	0.005	0.003	0.004	0.002	0.006	0.005	0.008	0.005	0.007	0.007	0.004	0.01	0.002	0.005	0.006	0.005	0.006	0.005	0.011	0.007	0.007	0.007	0.01
Sm	0.003	0	0.003	0	0	0.002	0	0.002	0.001	0.003	0	0.002	0.001	0	0	0.002	0	0.003	0.002	0.001	0.001	0	0.001	0.002	0
Y	0.003	0.002	0.001	0.001	0.003	0.004	0.006	0.004	0.007	0.002	0.007	0.002	0.006	0.004	0.005	0.007	0.005	0.002	0.004	0.012	0.011	0.008	0.01	0.008	0.013
Sr	0.027	0.026	0.025	0.027	0.028	0.026	0.017	0.009	0.022	0.012	0.001	0.016	0.014	0.016	0.024	0.018	0.006	0.008	0.008	0.01	0.009	0.014	0.014	0.014	0.005
Ba	0	0	0	0	0	0	0	0	0.001	0.001	0	0	0	0	0	0	0	0	0	0.001	0	0.001	0	0	0
As	0	0	0	0	0	0	0	0.003	0	0	0.003	0	0	0	0	0	0	0	0	0	0	0	0	0	0.002
F	1.189	1.367	1.449	1.275	1.292	1.268	2.129	2.055	1.331	1.496	1.386	1.325	1.377	1.281	1.107	1.256	1.475	1.451	1.463	1.484	1.569	1.848	1.908	1.859	1.876
Cl	0.097	0.14	0.141	0.117	0.107	0.097	0.072	0.089	0.124	0.292	0.287	0.262	0.289	0.265	0.198	0.241	0.201	0.208	0.215	0.161	0.158	0.212	0.2	0.207	0.247
OH	0.715	0.493	0.41	0.608	0.601	0.635	0.001	0.001	0.545	0.212	0.327	0.413	0.334	0.455	0.694	0.503	0.324	0.341	0.322	0.355	0.274	0.001	0.001	0.001	0.001
Sum Cat#	17.96	17.95	17.89	17.96	17.94	17.93	18.16	18.07	17.96	17.96	17.95	17.9	17.93	17.96	17.96	17.97	18.07	18.08	18.08	18.12	18.09	18.07	18.13	18.14	18.18

Appendix E

Geochemical Analyses

APPENDIX E1 – Whole rock XRD and XRF analyses

APPENDIX E2 – Whole rock REE ICP-MS analyses

APPENDIX E3 – Radiogenic isotope data

APPENDIX E4 – $^{40}Ar/^{39}Ar$ dating results

Appendix E1

Whole rock Major and Trace Element Analyses

DATA SOURCES

- Blevin, P. L. and Morrison, G. W., 1997. Magmatic and hydrothermal evolution of major intrusive related gold deposits: AMIRA, P425, final report, p. Parts 11 and 14.
- Clarke, I., 1990. Igneous petrology, *in* Clarke, I., and Sherwin, L., eds., Geological setting of gold and copper deposits in the Parkes area, New South Wales, 23. Records of the Geological Survey of N.S.W., New South Wales Geological Survey, p. 95-136.
- Crawford, A. J., Cooke, D. R. and Glen, R. A., 2001. NSW Ordovician SPIRT Report: Hobart, Centre for Ore Deposit Reaseach, 510 p.
- Hall, M. C., 1993. The stratigraphy and palaeovolcanology of the Late Ordovician Goonumbla Volcanics, Goonumbla, N.S.W.: Unpub. BSc Honours thesis, Monash University, 158 p.
- Harris, A. C., 1997. Vein emplacement, E26N porphyry Cu-Au deposit, Goonumbla, New South Wales: Unpub. BSc Honours thesis, University of Queensland, 102 p.
- Heithersay, P. S., 1991. The shoshonite-associated Endeavour 26 North porphyry copper-gold deposit, Goonumbla, NSW: Unpub. PhD manuscript thesis, Australian National University, 187 p.
- Howland-Rose, J. S., 1996. Fluid evolution at the Endeavour 48 porphyry Cu-Au deposit, Parkes, NSW: Unpub. BSc Honours thesis, University of Newcastle, 87 p.
- Müller, D., Heithersay, P. S. and Groves, D. I., 1994. The shoshonite porphyry Cu-Au association in the Goonumbla district, N.S.W., Australia: Mineralogy and Petrology; v. 51, p. 299-321.
- *Northparkes Mines Limited*
- Radclyffe, D., 1995. Regional-scale propylitic alteration in the Goonumbla mineral field, Parkes, NSW: Unpub. BSc Honours thesis, University of Tasmania, 118 p.
- Simpson, C. J. and Cas, R. A. F., 1999. The stratigraphy, volcanology and palaoegeographic interpretation of the Goonumbla Volcanic Complex, Parkes region, NSW: Clayton, Monash University, 113 p.
- Squires, V. E., 1992. The mineralisation and alteration of the Endeavour 27 porphyry copper-gold deposit, Goonumbla, New South Wales: Unpub. BSc Honours thesis, University of Sydney, 123 p.
- Wolfe, R. C., 1994. The geology, paragenesis and alteration geochemistry of the Endeavour 48 Cu-Au porphyry, Goonumbla N.S.W.: Unpub. BSc Honours thesis, University of Tasmania, 102 p.

Sample	*Aplite 22vl*	*Aplite 22vl*	*Aplite 26vl*	*Aplite 26vl*	*Aplite 27vl*	*Aplite 27vl*	*Aplite 48*	*Aplite 48vl*	*BQM 22vl, ICP1*	*BQM 26*	*BQM 26*	*BQM 26*	*BQM 26vl*	*BQM 26vl*	*BQM 26vl, ICP14*	*BQM 27, GOO37*	*BQM 27, GOO38*	*BQM 27vl, ICP5*	*BQM 48*
Source	Lickfold	Lickfold	Lickfold	Lickfold	Lickfold	Lickfold	Wolfe 1994	Lickfold	Lickfold	Heithersay 1991	Heithersay 1991	Heithersay 1991	Lickfold	Lickfold	Lickfold	AMIRA 425	AMIRA 425	Lickfold	Wolfe 1994
Deposit/Sample No	E22/2/271.1	E22/228/636.4	E26/284/340.8	E26/295/385.3	E27/248/382.7	E27/E/14	E48/13W2/980.0	E48/15/449.0	E22/229/728.6, VL-1 ICP	ACH119-3	E26/46/669.0 - 671.0	E26/46/389.0	E26/46/1759.6	E26/189/390.8	E26/287/220.3, VL-14 ICP	E27/28/608.9, GOO37	E27/28/668.7, GOO38	E27/28/709.0, VL-5 ICP	E48/15W1/1015.0
SiO[2]	63.79	66.37	73.71	63.16	76.47	69.20	61.95	82.58	68.02	57.57	59.32	60.40	65.00	64.31	61.54	68.04	67.90	64.52	60.33
TiO[2]	0.42	0.42	0.17	0.27	0.17	0.21	0.60	0.09	0.27	0.44	0.37	0.37	0.31	0.44	0.44	0.23	0.26	0.35	0.38
Al[2]O[3]	17.58	16.82	13.36	15.74	11.94	15.74	18.38	7.73	16.61	17.35	16.83	17.22	17.30	17.17	18.00	15.62	15.57	17.49	17.47
Fe[2]O[3]	1.73	2.32	0.85	0.90	0.79	0.85	3.80	1.04	2.18	5.04	4.46	4.04	2.53	1.81	2.94	1.35	2.16	3.48	3.31
MnO	0.09	0.07	0.01	0.03	0.02	0.03	0.04	0.03	0.07	0.11	0.11	0.11	0.04	0.03	0.02	0.03	0.03	0.07	0.03
MgO	2.05	1.64	0.25	0.61	0.20	0.43	1.29	1.04	0.68	0.93	1.64	1.41	1.21	1.83	1.88	0.45	0.85	1.24	1.57
CaO	1.81	2.14	1.71	7.43	0.63	1.03	1.76	1.31	1.83	4.59	3.34	2.40	2.86	3.08	4.39	0.99	0.79	2.16	1.12
Na[2]O	3.59	4.08	3.06	3.34	2.12	2.18	5.95	1.48	3.86	4.68	5.05	6.63	4.90	4.14	5.21	4.55	4.86	4.95	4.38
K[2]O	8.45	5.26	6.26	7.15	6.91	10.21	5.57	2.80	6.26	3.86	4.12	4.39	5.48	5.56	4.63	6.27	5.61	5.44	5.04
P[2]O[5]	0.26	0.24	0.03	0.37	0.03	0.04	0.35	0.03	0.11	0.30	0.20	0.20	0.17	0.26	0.27	0.07	0.09	0.20	0.21
Total %	99.39	99.76	99.94	99.39	100.11	99.76	99.78	100.09	99.60				99.77	99.86	99.14			99.48	99.69
LOI %	2.30	3.02	3.10	8.99	1.12	1.39	4.35	2.78	2.57				3.89	4.54	4.90			2.59	
Ba	1123	453	697	784	758	1460	903	689	382	1050	680	850	746	780	712	405	565	655	674
Rb	98.0	76.8	83.3	75.4	77.1	103.7	65	34.5	95	67	72	58	71	77.7	70	88	84	79	91
Sr	385	478	457	938	142	462	505	208	338	805	800	1060	550	675	1211	281	459	543	749
Pb	10	5	8	6	2	5	2	3	7	18	9	11	7	8	7	6	6	6	6
Zr	127	125	68	68	68	106	142	27	195	93	112	110	174	94	103	215	181	147	120
Nb	6	7	3	4	2	4	8.4	1	10.5	4		3	8.7	6	5.4	10	8	7.7	5
Y	18	13	14	20	3	10	21	3	19	2		2	22	14	15	16	18	18	17
La	9	10	<2	12	<2	4		2	18	10.4		11.7	16	10	11	14	18	17	
Ce	23	20	4	30	5	15		8	35	32	32	34	38	24	33	28	34	38	
Nd	12	9	2	18	2	6		4	17	10.7		11	19	13	15			18	
Sc	10	8	2	4	3	2		3	4	32	32	34	4	9	9	4	4	6	
Cr	2	2	8	3	1	<1	2	2	2	10		5	3	6	5	1	1*	3	5
Ni	4	2	1	1	<1	<1		<1	1	5*		5*	2	4	4	1*	1*	1	
Cu	3300	4900	4700	7300	5700	684	2000	14600	744				1500	10300	5200	2310	2000	778	641
Zn	94	112	10	37	8	13	48	11	36	182	4220	1410	39	45	48	24	31	50	48
V	83	93	47	99	29	28		23	56				72	194	148	41	51	87	

Sample	*BQM 48*	*BQM 48, GOO76*	*BQM 48vl*	*BQM 48vl, ICP9*	*BQM eq. Hall*	*BQM eq. Rad*	*BQM eq. Rad*	*BQM eq. Rad*	*BQM eq. Rad*	*BQM eq. Rad*	*B-QMP 22vl - early*	*B-QMP 22vl - early*	*B-QMP 22vl, ICP2 - early*	*B-QMP 26vl*	*B-QMP 26vl - late*	*B-QMP 26vl - ealry*	*B-QMP 26vl - early*	*B-QMP 26vl, ICP15 - post*	*B-QMP 27*	*B-QMP 27, GOO30*
Source	Lickfold	AMIRA 425	Lickfold	Lickfold	Hall 1993	Radclyffe 1995	Radclyffe 1995	Radclyffe 1995	Radclyffe 1995	Radclyffe 1995	Lickfold	Lickfold	Lickfold	AMIRA 425	Lickfold	Lickfold	Lickfold	Lickfold	Squires 1992	AMIRA 425
Deposit/Sample No	E48/15W 1/890.3	E48/15W 1/986.0-986.4, GOO76	E48/7/76.1	E48/13w2/970.7, VL-9 ICP	15941	RA100	RA0	EX425	EX525	EX550	E22/39/58 1.0	E22/229/6 85.2	E22/229/6 35.1, VL-2 ICP	E26/132/6 64.0	E26/46/16 38.6	E26/284/2 49.0	E26/132 W2/765.6	E26/264/2 35.3, VL-15 ICP	E274/22 3.0	E27/10/41 8.1, GOO30
SiO[2]	64.02	63.51	60.48	63.07	54.79	60.83	61.33	67.05	54.25	65.73	64.44	66.59	65.33	61.65	63.37	65.55	64.29	65.10	65.24	64.06
TiO[2]	0.40	0.34	0.50	0.43	0.79	0.48	0.46	0.27	0.73	0.27	0.33	0.29	0.29	0.29	0.30	0.26	0.27	0.29	0.45	0.27
Al[2]O[3]	17.62	16.39	18.55	18.18	18.74	18.32	18.23	17.58	18.93	18.17	18.04	17.48	18.19	17.56	18.33	17.30	18.56	17.68	18.44	17.54
Fe[2]O[3]	3.71	3.11	5.29	5.06	7.26	4.35	5.52	2.09	8.75	2.42	2.76	1.76	1.90	3.09	2.68	2.26	2.89	1.87	1.61	2.26
MnO	0.03	0.03	0.08	0.05	0.18	0.05	0.08	0.07	0.22	0.05	0.08	0.08	0.04	0.07	0.01	0.02	0.06	0.04	0.04	0.05
MgO	2.06	1.18	2.51	1.88	2.89	2.25	2.08	0.87	3.62	0.65	0.89	0.90	0.91	0.82	1.06	0.86	1.04	0.92	0.64	0.75
CaO	2.04	1.10	2.65	1.73	6.89	4.51	3.33	0.82	4.60	0.91	2.69	2.75	2.75	2.52	3.61	2.04	1.90	2.71	3.99	1.72
Na[2]O	4.13	4.87	5.06	5.01	4.09	4.48	4.60	4.43	4.64	4.88	5.26	3.83	4.61	6.17	6.18	5.33	6.31	5.48	4.43	6.27
K[2]O	5.16	5.14	4.41	4.25	3.94	4.38	4.04	5.53	3.69	5.76	5.26	5.68	5.14	4.19	4.25	5.60	4.51	5.38	3.84	4.58
P[2]O[5]	0.26	0.18	0.31	0.27	0.43	0.32	0.29	0.07	0.45	0.07	0.14	0.14	0.15	0.10	0.14	0.08	0.11	0.09	0.11	0.08
Total %	99.67		99.60	99.63	99.72	99.81	101.06	99.40	100.21	100.23	99.49	99.45	99.49		99.42	99.59	99.53	99.56	99.66	
LOI %	5.28		3.27	5.59	1.76	5.99	4.54	1.87	4.27	1.69	3.23	4.34	4.22		3.74	3.18	2.03	3.61	4.69	
Ba	683	740	798	728	827	731	653	593	812	423	1470	1342	1102	1210	1097	960	1263	1113	514	1160
Rb	80.4	76	59.7	69.7	57	85	75	89	54	99	62	71.4	68	55	51	53	51	48	64	45.5
Sr	404	419	625	525	1290	942	731	288	915	567	1058	1373	731	1160	1362	777	1302	960	361	695
Pb	4	6	5	5	8	6	6	45	10	20	7	14	4	16	5	5	5	7	6	4
Zr	106	138	128	126	115	116	113	291	66	298	74	91	73	68	85	81	74	79	82	76
Nb	6	8	7	8	7	5	6	15	3	17	4.5	4	3.8	3	4.7	3.7	3.2	4.1	6	3
Y	17	17	18	16	22	14	17	28	20	31	13	12	10	11	11	9	11	12	12	11
La	16	19	18	23	35						11	11	9	14	10	7	11	11	14	14
Ce	34	38	36	37	32						32	25	23	28	25	21	25	26	21	26
Nd	16		19	19	20						16	12	12		11	11	12	12	12	
Sc	7	6	10	7	7	9	9	4	17	3	4	5	4	4	5	5	4	4	5	3
Cr	3	1*	4	3	5*	2	5	2	1	2	3	3	2	1	4	3	2	2	5	1*
Ni	2	1*	3	2	4						1	2	1	1	4	3	2	1	7	1*
Cu	4300	2980	1102	442	164	207	261	597	206	239	786	3800	5200	590	595	5300	541	3400	660	2310
Zn	82	52	56	60	90	32	27	104	121	32	48	59	40	64	16	52	40	28	31	27
V	115	91	159	125	230	136	135	21	249	14	88	113	78	76	92	100	76	72	514	69

Sample	*B-QMP 27, GOO31*	*B-QMP 27, GOO32*	*B-QMP 27, GOO48*	*B-QMP 27vl - late*	*B-QMP 27vl, ICP6 - pre*	*B-QMP 48vl - early*	*Basaltic trachyandesite 26*	*BTA 26, GOO64*	*BTA 26, GOO70*	*Basaltic trachyandesite 26vl*	*KA-QMP 22vl*	*KA-QMP 22vl*	*KA-QMP 22vl, ICP3*	*KA-QMP 26*	*KA-QMP 26*	*KA-QMP 26*	*KA-QMP 26*	*KA-QMP 26*	*KA-QMP 26vl*	*KA-QMP 26vl, ICP16*
Source	AMIRA 425	AMIRA 425	AMIRA 425	Lickfold	Lickfold	Lickfold	Heithersay 1991	AMIRA 425	AMIRA 425	Lickfold	Lickfold	Lickfold	Lickfold	Heithersay 1991	Heithersay 1991	Heithersay 1991	Heithersay 1991	Wolfe 1994	Lickfold	Lickfold
Deposit/Sample No	E27/10/433.8, GOO31	E27/10/442.0, GOO32	E27/248/347.2, GOO48	E27/S/1	E27/4/225.9, VL-6 ICP	E48/13/69.5	E26/40/565.0	E26/46/1284.6, GOO65	E26/46/1202.3, GOO70	E26/46/1284.8	E22/6/153.8	E22/205/325.8	E22/2/345.7, VL-3 ICP	E26 DDH 26	E26/64/609.0	E26/39/576.0	E26/42/1112.0	E26/31/150.0	E26/286/173.2	E26/286/184.0, VL-16 ICP
SiO[2]	63.73	64.01	64.95	64.77	64.54	67.23	51.99	50.80	51.64	54.14	66.12	65.99	72.49	62.56	63.77	62.75	61.79	64.83	64.30	65.13
TiO[2]	0.28	0.27	0.25	0.28	0.29	0.29	0.58	0.57	0.56	0.59	0.27	0.29	0.15	0.28	0.24	0.27	0.28	0.29	0.28	0.28
Al[2]O[3]	17.79	17.92	17.03	18.39	18.33	17.27	18.85	17.45	17.41	18.44	17.17	17.92	15.12	16.87	16.41	17.43	17.40	18.25	17.51	17.73
Fe[2]O[3]	2.75	2.67	2.42	3.11	2.87	2.48	6.93	7.33	8.65	8.58	2.28	2.05	1.19	2.91	0.89	2.47	3.57	3.06	3.07	1.50
MnO	0.05	0.06	0.07	0.04	0.03	0.03	0.50	0.24	0.20	0.24	0.03	0.04	0.03	0.09	0.02	0.07	0.07	0.02	0.02	0.03
MgO	1.01	0.89	0.57	0.74	1.00	0.97	6.30	3.60	3.39	3.53	0.96	0.75	0.36	0.64	0.90	1.00	1.24	0.84	0.98	0.94
CaO	1.64	1.75	2.03	2.65	2.29	0.76	1.90	4.96	3.75	5.55	1.70	1.62	1.15	1.96	2.53	2.57	2.61	1.27	2.94	3.34
Na[2]O	6.36	6.41	5.62	5.26	5.83	5.85	3.25	1.90	1.02	2.33	4.26	5.31	3.72	6.33	6.09	5.80	5.56	6.14	5.26	5.10
K[2]O	4.50	4.45	4.75	4.57	4.63	4.85	4.47	6.02	7.00	6.10	6.05	5.55	5.65	4.67	3.46	4.16	3.90	4.96	5.12	5.41
P[2]O[5]	0.09	0.09	0.07	0.10	0.10	0.11	0.50	0.46	0.45	0.50	0.09	0.10	0.04	0.11	0.06	0.10	0.13	0.12	0.12	0.11
Total %				99.54	99.63	99.43				99.97	99.90	99.61	99.59					100.07	99.78	99.98
LOI %				3.69	2.89	1.30				6.66	3.58	2.98	2.00					2.91	4.29	5.27
Ba	1130	1410	1120	1053	1120	789	800	1310	1410	1178	2818	1034	598	980	860	1110	1000	828	1291	1573
Rb	46	45.5	68	55	57	55.3	79	130	133	123	69	53.7	77.8	47	43.5	48.5	67	53	49.9	55.3
Sr	1130	1590	835	671	560	399	705	1160	535	715	595	705	267	660	1140	1060	785	484	1030	1213
Pb	4	6	8	4	3	9	7	10	10	6	13	4	7	9	6	7	11	9	6	3
Zr	75	75	77	78	77	96	90	91	85	88	68	73	91	63	76	57	65	72	81	77
Nb	3	3	4	3.8	4.0	5		8	8	7.9	3.0	4	4			1	2	4	3	4
Y	11	11	10	11	13	9		17	17	17	9	11	6			2	2	12	11	10
La	13	13	13	10	14	8		24	35	20	7	11	8			8.6	16.3		9	9
Ce	22	24	24	24	30	17	32	50	72	42	26	25	18	23	31	25	26		25	26
Nd				11	14	9				21	17	12	6			7.5	11.6		10	11
Sc	3	3	3	3	3	3	32	17	17	14	4	3	2	23	31	25	26		4	4
Cr	2	1*	1*	2	3	2		12	12	13	3	2	1			5*	5*	3	3	6
Ni	1*	1*	1*	1	1	1		7	6	8	2	1	<1			5*	5*		2	1
Cu	1160	685	545	581	590	1156		23	525	34	8200	2900	795	3080	3870	1190	211	1300	3000	3300
Zn	24	26	41	19	20	32	1240	124	136	122	105	47	39					33	23	22
V	77	67	62	75	78	95		156	154	171	83	83	45						100	95

Sample	*KA-QMP 27*	*KA-QMP 27*	*KA-QMP 27, GOO43*	*KA-QMP 27, GOO52*	*KA-QMP 27, GOO53*	*KA-QMP 27,GOO49*	*KA-QMP 27vl*	*KA-QMP 27vl, ICP7*	*KA-QMP 48vl*	*KA-QMP 48vl*	*KA-QMP 48vl, ICP11*	*K-QMP 22vl*	*K-QMP 22vl*	*K-QMP 22vl*	*K-QMP 22vl, ICP4*	*K-QMP 26*	*K-QMP 26*	*K-QMP 26vl*	*K-QMP 26vl*	*K-QMP 26vl*
Source	Squires 1992	Squires 1992	AMIRA 425	AMIRA 425	Lickfold	AMIRA 425	Lickfold	Squires 1992	Lickfold	Lickfold	Lickfold	Lickfold	Lickfold	Lickfold	Lickfold	Müller 1994	Müller 1994	Lickfold	Lickfold	Lickfold
Deposit/Sample No	E27/4/366.1	E27/4/557.0	E27/4/354.5, GOO43	E27/11/111.0, GOO52	E27/4/329.3	E27/7/198.9, GOO49	E27/7/147.8, VL-7 ICP	E27/4/323.2	E48/11/495.4	E48/13W2/816.7	E48/11/531.5, VL-11 ICP	E22/205/353.3	E22/228/613.1	E22/6/237.7	E22/205/400.9, VL-4 ICP	E26/38/149.3 - 180.7	E26/38/149.3 - 180.7	E26/287/132.6	E26/184/134.5	E26/287/139.4
SiO[2]	69.55	66.35	62.94	62.61	65.30	62.95	68.02	64.64	68.82	68.69	69.38	72.98	70.91	70.86	69.73	65.84	65.87	67.50	70.28	67.95
TiO[2]	0.27	0.33	0.28	0.27	0.27	0.26	0.23	0.32	0.23	0.23	0.22	0.14	0.18	0.19	0.20	0.37	0.37	0.25	0.22	0.24
Al[2]O[3]	17.10	18.25	17.60	17.57	18.68	17.50	16.98	18.58	17.76	16.96	16.72	14.67	15.37	15.83	16.09	20.08	19.89	17.39	15.39	16.41
Fe[2]O[3]	0.20	1.02	2.91	2.76	2.11	2.77	2.56	1.58	0.77	1.13	0.54	0.60	1.64	0.81	0.85	1.93	2.16	0.66	0.63	0.84
MnO	0.03	0.03	0.04	0.05	0.04	0.02	0.04	0.04	0.01	0.02	0.01	0.03	0.04	0.02	0.04	0.03	0.03	0.02	0.02	0.02
MgO	0.37	0.78	0.82	0.71	0.84	0.69	0.77	0.81	0.62	0.84	0.52	0.59	0.61	0.47	0.63	1.41	1.06	0.99	0.85	0.80
CaO	1.84	1.16	1.78	1.88	1.69	1.61	1.66	1.90	0.52	1.55	0.55	1.00	1.48	1.04	1.80	0.89	1.17	2.61	0.67	1.74
Na[2]O	4.04	6.00	6.33	6.15	5.91	6.26	4.53	5.82	4.16	4.68	2.38	3.56	3.83	3.90	2.97	5.87	6.49	6.69	3.69	4.77
K[2]O	6.10	4.86	4.03	4.56	4.76	4.45	5.10	4.43	6.24	5.49	8.89	6.10	5.64	6.24	6.72	4.77	4.05	3.27	7.10	5.69
P[2]O[5]	0.07	0.09	0.09	0.09	0.09	0.09	0.08	0.11	0.08	0.08	0.07	0.03	0.06	0.05	0.06	0.18	0.15	0.05	0.02	0.08
Total %	99.52	99.75			99.40		99.63	99.69	100.08	99.63	99.72	99.87	99.87	99.73	99.65	100.12	100.35	99.31	100.28	99.75
LOI %	2.55	1.89			3.34		3.65	3.23	1.95	3.06	1.88	2.06	2.94	2.19	3.19	2.01	1.83	3.97	1.93	3.24
Ba	1167	1165	1010	975	1309	980	694	1337	1258	622	880	583	952	989	961	810	850	639	734	790
Rb	68	50	49.5	56	59	52	72	54	71.8	52.4	79.9	69	67.8	67.4	82	90	70	41	75	60
Sr	443	596	950	620	1022	615	507	721	304	303	232	357	541	343	684	680	650	819	624	772
Pb	8	5	9	3	3	2	4	7	15	<1.5	7	41	7	7	25	1*	1*	5	10	7
Zr	96	89	74	69	77	70	77	86	71	73	76	109	84	88	86	100	95	92	70	84
Nb	7	6	4	3	4.3	3	3.7	5	4	3	3	5.2	4	5	4.8	5	2	5.2	2.1	3.5
Y	7	10	13	11	11	11	9	12	8	10	8	7	5	5	6	16	12	12	2	7
La	8	12	15	14	13	13	12	14	10	10	2	10	8	6	3	14.3	13	13	2*	4
Ce	5	19	28	26	32	26	24	23	25	23	18	19	11	13	16	22	20	29	6	14
Nd	5	12			14		12	13	11	11	7	6	5	6	5	5	4	12	4	7
Sc	5	2	3	3	3	3	2	0	2	4	3	2	3	2	4			4	3	4
Cr	4	1	1	1	2	1*	1	5	2	3	1	2	5	<1	2			2	3	3
Ni	4	5	1	1*	1	1*	1	7	1	2	1	1	1	1	1			1	2	1
Cu	47	2548	1140	745	2300	835	227	623	6100	2500	5500	2200	1900	4600	7000	3560	4150	4300	8800	11300
Zn	22	30	44	25	32	48	31	27	27	16	46	51	163	59	103	77	68	36	116	25
V	44	12	78	75	83	77	55	86	88	64	42	25	76	38	44	120	110	83	53	72

Sample	*K-QMP 26vl*	*K-QMP 26vl, ICP17*	*K-QMP 27*	*K-QMP 27*	*K-QMP 27, GOO33*	*K-QMP 27vl, ICP19*	*K-QMP 27vl, ICP8*	*K-QMP 48*	*K-QMP 48*	*K-QMP 48*	*K-QMP 48*	*K-QMP 48vl*	*K-QMP 48vl, ICP12*	*K-QMP22*	*Mafic dyke, E27*	*Microgranite 48vl, ICP10*	*Monzodiorite 26*	*Monzodiorite 26vl, ICP13*	*Zero 26*	*Zero 26*
Source	Lickfold	Lickfold	Squires 1992	Squires 1992	AMIRA 425	Lickfold	Lickfold	NSW SPIRT	Lickfold	Wolfe 1994	Wolfe 1994	Lickfold	Lickfold	Heithersay 1991	Lickfold	Lickfold	Heithersay 1991	Lickfold	AMIRA 425	Heithersay 1991
Deposit/Sample No	E26/284/212.7	E26/189/229.8, VL-17 ICP	E27/4/444.3	E27/4/492.0	E27/10/471.5, GOO33	E27/11/73.6, VL-19 ICP	E27/386/189.2, VL-8 ICP	E48/2/295.1	E48/2/236.4	E48/2/290.0	E48/7/300.0	E48/13W2/703.8	E48/15W1/651.3, VL-12 ICP	E22 DDH6	E27/386/185.8	E48/13W2/951.2, VL-10 ICP	E26 DDH46	E26/46/1720.2, VL-13 ICP	E26/46/1121.5, GOO66	E26/40/569.0
SiO_2	72.34	66.02	67.91	66.23	65.93	65.80	65.49	65.99	68.68	66.01	66.69	70.64	72.78	67.80	45.42	68.91	55.21	56.28	62.58	59.79
TiO_2	0.26	0.32	0.26	0.31	0.22	0.27	0.26	0.23	0.26	0.26	0.25	0.20	0.22	0.19	0.52	0.23	0.52	0.59	0.23	0.36
Al_2O_3	13.37	17.01	17.13	17.87	16.37	17.98	17.63	16.39	17.95	18.15	17.50	16.51	16.06	15.59	12.93	17.00	17.65	18.90	17.30	17.21
Fe_2O_3	0.69	0.79	0.49	0.75	2.08	1.72	2.50	1.78	0.86	1.89	1.30	0.64	0.91	1.13	7.93	0.34	6.00	6.47	2.45	4.13
MnO	0.02	0.01	0.04	0.04	0.03	0.03	0.04	0.03	0.02	0.03	0.02	0.01	0.01	0.04	0.13	0.01	0.04	0.11	0.06	0.17
MgO	0.67	0.64	0.63	0.63	0.64	0.90	0.87	0.89	1.11	1.14	1.10	0.59	0.93	1.44	9.76	0.39	2.29	2.69	0.88	1.50
CaO	1.57	1.34	1.52	1.96	1.33	1.69	1.21	1.67	3.03	2.53	1.71	0.80	1.23	1.44	8.93	0.54	5.58	6.40	3.08	3.67
Na_2O	2.29	2.86	5.40	5.48	5.66	4.88	5.21	4.06	3.04	4.94	5.11	4.77	1.90	5.23	2	3.02	4.18	4.76	5.82	5.04
K_2O	7.06	8.23	4.63	5.08	4.77	5.80	6.38	4.32	3.22	4.63	5.18	4.94	4.31	5.41	1.04	9.35	3.27	3.31	3.71	3.67
P_2O_5	0.11	0.09	0.08	0.09	0.07	0.10	0.10	0.07	0.07	0.09	0.08	0.06	0.04	0.06	0.19	0.07	0.37	0.44	0.07	0.22
Total %	100.43	101.06	99.75	99.45		99.70	100.25	100.12	99.59	100.07	100.50	99.42	100.00		100.03	99.97		99.97		
LOI %	2.92	3.11	2.96	3.30		3.21	3.10	3.78	5.57	4.58	3.42	2.19	3.82		11.17	1.51		2.47		
Ba	916	1064	1013	1383	1090	826	905	545	1794	811	978	1311	752	1600	284	955	845	893	840	875
Rb	66.5	82.1	59	53	48.5	72	57	50.3	40.9	51	51	46.2	46.4	74	25	85.4	62	54	63	54
Sr	682	811	454	543	615	449	557	507	614	558	596	248	140	468	992	168	1530	1611	690	840
Pb	10	8	7	8	2	5	1.5*	7	4	1.5	4	7	<1.5	10	3	17	7	4	13	6
Zr	94	76	91	83	77	77	74	68	65	72	69	76	67	76	41	82	62	67	78	75
Nb	3	3	6	6	3	3.5	3.6	3	3	3.5	2.5	4	3		1.6	3		4.3	3	3
Y	3	4	11	11	9	7	11	9	7.1	12	8	7	4		10	6		17	10	4
La	2	5	12	17	10	4	5	7	7			9	4		12	7		15	14	18.8
Ce	11	13	22	21	20	16	19	18	24			23	16	20	25	16	33	32	24	32
Nd	2	8	11	15		7	12	10	9			8	5		13	4		17		14.6
Sc	5	5	3	1	3	3	2	3	4			2	2	20	26	3	33	12	2	32
Cr	2	2	4	7	1*	3	2	3	2	2	2	2	1		781	<1		4	1*	5
Ni	1	2	6	6	1*	2	2	1	2			1	2		203	<1		3	1*	5*
Cu	12700	21100	1381	2361	1840	6300	2300	6800	13200	2200	9200	6600	12300		88	1050		329	3	
Zn	35	41	31	29	19	24	17	64	51	42	30	91	1016	1680	64	22	2630	37	32	6
V	58	86	60	73	81	126	116	87	95			40	25		215	29		194	61	

Sample	*Zero 26vl*	*Zero 26vl, ICP18*	*Nelungaloo Vol, Hi Ti bas*	*Nelungaloo Vol, Hi Ti bas*	*Nelungaloo Vol, Hi Ti bas*	*Nelungaloo Vol, north*	*Nelungaloo Vol, north*	*Nelungaloo Vol, north*	*Nelungaloo Vol, north*	*Nelungaloo Vol, north*	*Nelungaloo Vol, north*	*Nelungaloo Vol, north*	*Nelungaloo Vol, north*	*Nelungaloo Vol, north*	*Nelungaloo Vol, north*	*Nelungaloo Vol, north*	*Nelungaloo Vol, north*
Source	Lickfold	Lickfold	NSW SPIRT	NSW SPIRT	NSW SPIRT	Clarke 1990	NSW SPIRT	NSW SPIRT	NSW SPIRT	NSW SPIRT	NSW SPIRT	NSW SPIRT	NSW SPIRT	NSW SPIRT	NSW SPIRT	NSW SPIRT	NSW SPIRT
Deposit/Sample No	E26/46/1777.5	E26/264/263.0, VL-18 ICP	N40	N42	N43	M33/086	N1	N12	N13	N18	N2	N22	N3	N5	N6	N7	N8
SiO[2]	64.95	65.41	52.59	53.12	49.79	56.05	56.12	55.07	62.55	56.82	57.38	57.77	58.29	56.68	62.38	58.50	55.14
TiO[2]	0.29	0.27	1.04	1.04	1.04	0.67	0.58	0.56	0.45	0.62	0.56	0.53	0.51	0.61	0.62	0.59	0.58
Al[2]O[3]	16.68	18.22	16.83	16.85	16.64	16.85	17.87	17.62	13.99	15.50	16.74	15.11	14.72	17.27	16.92	16.41	17.01
Fe[2]O[3]	3.02	2.77	8.94	10.51	9.67	7.85	8.87	9.00	7.22	7.54	8.15	9.69	9.84	8.22	6.44	8.16	8.59
MnO	0.10	0.08	0.28	0.16	0.34	0.15	0.18	0.10	0.10	0.16	0.12	0.12	0.11	0.12	0.05	0.14	0.14
MgO	1.28	1.26	2.96	3.64	3.37	3.25	3.87	2.06	2.22	3.29	2.52	3.79	3.39	3.52	1.18	3.86	4.65
CaO	4.81	2.03	12.00	10.98	14.29	6.44	6.18	9.19	9.09	8.89	9.68	7.17	8.73	7.61	3.81	6.37	7.52
Na[2]O	4.33	4.49	4.39	3.01	3.96	4.37	4.37	5.41	4.08	5.95	4.50	4.98	4.08	2.85	4.96	2.97	3.85
K[2]O	4.42	5.39	0.62	0.33	0.56	2.51	1.67	0.05	0.10	0.88	0.09	0.57	0.10	2.83	3.24	2.68	2.26
P[2]O[5]	0.10	0.08	0.35	0.35	0.35	0.38	0.28	0.94	0.19	0.34	0.25	0.27	0.21	0.30	0.39	0.30	0.25
Total %	100.11	99.91															
LOI %	4.78	3.02	8.69	6.95	11.12	3.50	2.33	2.90	2.36	4.51	2.80	2.21	2.60	1.57	1.57	1.75	1.38
Ba	1064	1527	183	160	305	552	417	171	76	893	118	214	58	531	923	571	634
Rb	77.9	83	3	1	4	35	21		3	11		11	1	39	49	38	22
Sr	519	855	753	817	742	1034	1088	262	174	1635	1	784	354	1114	814	1087	1108
Pb	17	8	4	4	2	4	3	4	5	2	6	4	4	4	3	4	3
Zr	97	80	141	136	142	130	86	84	75	123	92	66	62	109	143	106	96
Nb	7	3.7	10.6	8.7	9.5	6.1	5.3	5.0	4.1	5.7	5.8	4.2	2.9	5.7	7.8	5.9	4.7
Y	14	12	25	22	24	21	15	18	12	16	14	13	13	16	16	16	15
La	19	13	14.6	18.0	16.3	19.3	16.6	20.4	15.2	21.8	16.5	14.2	17.4	21.7	29.8	18.3	15.0
Ce	35	30	37.5	41.8	45.4	40.6	38.4	47.7	32.8	53.2	38.7	34.0	34.7	49.1	62.0	48.5	42.7
Nd	13	15	25.2	22.6	28.3	23.4	22.4	22.7	19.3	30.5	22.1	21.2	19.6	27.2	34.4	26.3	24.0
Sc	7	2	40	38	41	15	24	24	23	26	31	31	28	24	16	23	26
Cr	4	2	72	65	76	2	19	20	55	241	72	87	48	38	20	35	79
Ni	2	1	21	22	22	3	13	11	18	46	18	22	19	15	8	17	33
Cu	10	9	26	44	58	10	64	99	27	157	22	53	260	99	221	41	27
Zn	72	38	97	96	88	61	98	65	54	78	55	74	63	68	61	79	80
V	66	71	363	363	363		227	227	150	235	246	222	258	230	186	226	242

Sample	Nelungaloo Vol, north	Nelungaloo Vol, north	Nelungaloo Vol, north	Nelungaloo Vol, north	Nelungaloo Vol, north	Nelungaloo Vol, south	Nelungaloo Vol, south	Nelungaloo Vol, south	Nelungaloo Vol, south	Nelungaloo Vol, south	Nelungaloo Vol, south	Nelungaloo Vol, south	Nelungaloo Vol, south	Nelungaloo Vol, south	Nelungaloo Vol, Trachy's	Nelungaloo Vol, Trachy's
Source	NSW SPIRT	Hall 1993	North	North	North	Clarke 1990	NSW SPIRT	NSW SPIRT	NSW SPIRT	NSW SPIRT	NSW SPIRT	NSW SPIRT	NSW SPIRT	NSW SPIRT	Clarke 1990	NSW SPIRT
Deposit/Sample No	N9	15939	1503-42/61.0	1503-42/63.0	1503-49/91.5	M33/142	N24	N26	N27	N31	N33(to be repeated)	N36	N39	N45	M33/093	N29
SiO[2]	60.77	54.78	51.27	53.05	55.85	53.19	52.83	50.17	52.59	50.13	52.09	51.75	53.87	51.70	60.10	60.63
TiO[2]	0.51	0.73	0.79	0.69	0.61	0.78	0.68	0.85	0.84	0.85	1.61	0.83	0.89	0.83	0.80	.0.91
Al[2]O[3]	14.62	17.09	20.46	19.27	15.81	16.84	16.11	17.65	17.17	17.49	16.24	16.96	18.67	17.07	15.75	15.88
Fe[2]O[3]	8.39	8.45	10.97	10.24	8.93	6.24	9.45	11.60	9.95	10.52	10.60	11.03	8.21	11.18	7.65	8.64
MnO	0.12	0.15	0.16	0.23	0.13	0.17	0.14	0.17	0.15	0.17	0.17	0.20	0.11	0.19	0.15	0.08
MgO	3.47	4.20	4.29	4.47	6.22	1.55	5.47	4.83	3.98	4.13	4.64	5.11	2.82	5.37	2.31	4.18
CaO	7.14	7.17	5.67	5.21	8.25	12.37	9.20	10.10	9.71	10.80	8.47	9.68	7.95	8.32	4.05	3.28
Na[2]O	4.28	5.63	3.78	6.14	3.02	7.04	4.70	3.06	3.25	5.50	4.55	2.68	6.28	3.54	3.91	5.45
K[2]O	0.46	1.46	2.29	0.40	0.93	0.25	1.10	1.25	2.01	0.06	1.28	1.43	0.78	1.49	3.52	0.41
P[2]O[5]	0.24	0.34	0.29	0.30	0.23	0.36	0.31	0.31	0.33	0.34	0.35	0.33	0.43	0.32	0.56	0.54
Total %																
LOI %	2.52	2.01	3.91	3.64	4.10	7.30	3.05	2.85	3.27	5.33	2.55	2.14	6.13	2.00	2.20	4.17
Ba	197	296	365	68	203	70	795	518	806	38	670	571	191	329	673	142
Rb	6	18	45	5	14	1	12	10	17		12	14	7	16	53	3
Sr	540	1081	905	610	770	383	1072	1377	1336	252	1217	892	911	1092	858	1055
Pb	4	6	3	2	4	3	7	3	3	3		4	6		7	5
Zr	86	96	103	87	77	79	117	84	94	94	147	99	209	84	228	148
Nb	4.4	6.0	5.5	4.5	2.8	4.3	6.7	4.2	4.4	3.9	8.1	4.6	14.3	3.8	8.0	6.5
Y	13	18	22	14	13	21	18	21	20	20	31	21	19	19	24	27
La	18.4	20.4				21.3	19.5	21.4	21.3	17.7	17.7	22.7	35.3	15.8	47.2	25.2
Ce	36.1	27.5				40.5	54.4	43.2	47.2	40.2	43.2	45.8	76.8	45.8	106.4	70.8
Nd	22.7	11.2				27.7	29.9	28.2	29.3	26.6	28.5	28.5	41.0	24.5	62.2	37.4
Sc	22	19	35	26	35	33	28	31	34	32	35	28	30	28	19	27
Cr	42	117	27	12	258	42	171	41	42	44	46	39	40	38	7	3
Ni	18	41	18	12	72	7	55	25	20	18	15	20	17	21	-3	5
Cu	33	170	29	33	104	197	58	210	214	208	62	218	221	202	176	222
Zn	68	80	106	132	82	80	81	97	90	99	89	78	110	94	75	108
V	241	224	269	242	277		240	369	368	370	335	338	250	336		275

Sample	*Nelungaloo Vol, Trachy's*	*Nelungaloo Vol, Trachy's*	*Nelungaloo MD, 484Ma*	*Nelungaloo MD, 484Ma*	*Nelungaloo Intrusion*	*Nelungaloo Intrusion*	*Nelungaloo Intrusion*	*Nelungaloo Intrusion*	*Nelungaloo Intrusion*	*Nelungaloo Intrusion*	*Nelungaloo Intrusion*	*Nelungaloo Intrusion*	*Nelungaloo Intrusion*	*Nelungaloo Intrusion*	*Nelungaloo Intrusion*	*Condobolin Rd Monzodiorite*	*Condobolin Rd Monzodiorite*
Source	North	North	AMIRA 425	AMIRA 425	AMIRA 425	AMIRA 425	NSW SPIRT	NSW SPIRT	NSW SPIRT	NSW SPIRT	NSW SPIRT	NSW SPIRT	NSW SPIRT	NSW SPIRT	Lickfold	AMIRA 425	Clarke 1990
Deposit/Sample No	GPR9724	1503-25/39.6	GOO102	GOO103	GOO98	GOO99	M33/098	M33/217 - C134	M33/094	M33/141	1503-22/43.3, t21i	1503-23/39.4, t22	1503-54/40.6, t23	1503-22/43.1, t21ii	VL8-1	GOO58	M33/100 - C162
SiO[2]	58.88	60.37	54.44	60.42	54.24	56.01	57.57	55.89	52.39	51.11	55.07	54.76	54.03	59.07	51.63	54.08	55.13
TiO[2]	0.68	0.84	0.65	0.69	0.61	0.59	0.58	0.57	0.82	0.80	0.68	0.63	0.62	0.96	0.83	0.60	0.60
Al[2]O[3]	17.34	16.12	18.09	15.13	18.89	17.51	18.16	19.38	16.94	17.07	18.73	20.02	19.59	14.85	16.91	18.97	19.37
Fe[2]O[3]	6.11	7.85	4.03	4.29	2.90	2.89	6.41	7.85	11.15	11.31	8.93	7.85	8.86	9.41	11.31	3.71	2.99
MnO	0.08	0.09	0.13	0.17	0.13	0.17	0.15	0.14	0.19	0.21	0.16	0.12	0.13	0.19	0.20	0.14	0.13
MgO	0.98	1.99	2.82	2.18	2.27	2.62	2.42	2.36	5.25	5.38	3.55	3.39	3.19	2.26	5.76	2.63	2.68
CaO	4.93	5.07	6.10	2.65	7.24	5.77	6.07	7.57	8.49	10.45	5.52	5.11	7.99	5.41	7.85	7.65	7.88
Na[2]O	6.44	3.47	4.14	4.72	3.83	5.00	4.85	3.79	3.64	2.59	4.23	6.81	4.25	3.89	3.89	3.32	3.92
K[2]O	2.26	3.52	2.64	3.82	2.50	3.70	3.85	2.52	1.48	1.20	2.65	0.88	0.93	3.16	1.27	2.05	2.14
P[2]O[5]	0.42	0.60	0.40	0.47	0.36	0.27	0.26	0.39	0.31	0.33	0.39	0.38	0.35	0.71	0.34	0.33	0.31
Total %							98.92								100.55		99.04
LOI %	2.05	.3.43					2.00	2.80	2.50	2.20	2.23	4.81	4.71	2.26	3.22		2.06
Ba	543	735	545	725	525	900	941	552	323	273	719	298	204	719	818	545	431
Rb	20	44	37.5	42	32	54	64	33	11	5	37	28	11	34	17	21.5	22
Sr	289	621	815	282	1230	1170	1321	1235	1010	814	406	831	892	406	1174	1070	968
Pb	268	9	4	7	5	6	4	7	2*	2*	4	3	6	2	2	5	5
Zr	180	213	110	212	108	96	104	119	88	69	182	118	100	182	109	102	104
Nb	10	10.9	5	11	6	6	6.2	5.1	4.2	3.1	12.0	6.7	5.4	12.0	6	5	5
Y	22	24	21	32	19	18	24	22	24	21	20	13	17	33	20	18	21
La	27		25	39	24	16	14.4	24.6	19.7	17.6	0.0	0.0	0.0	0.0	10	21	18
Ce	70		60	98	58	30	27.9	57.4	52.0	56.9	0.0	0.0	0.0	0.0	31	52	50
Nd	36						15.5	35.9	33.3	34.1	0.0	0.0	0.0	0.0	14		31
Sc	13	19	25	26	21	14	12	21	29	34	20	21	25	20	6	23	15
Cr	15	4	6	3	6	2	0	10	46	48	2	6	13	2	3	7	12
Ni	7	2	5	1	3	4	0	41	14	22	7	27	7	3	22	5	3*
Cu	64	173	156	174	191	150	0	210	239	207	211	22	226	160	198	284	170
Zn	12	94	73	99	85	79	0	169	130	103	87	90	78	137	88	87	100
V	178	251	161	98	166	182	0	0	0	0	134	188	204	134	89	160	

Sample	*Condobolin Rd Monzodiorite*	*Condobolin Rd Monzodiorite*	*Condobolin Rd Monzodiorite*	*Goonumbla, basal*	*Goonumbla, basal*	*Goonumbla, basal*	*Goonumbla, basal*	*Goonumbla, basal*	*Goonumbla, basal*	*Goonumbla, basal*	*Goonumbla, basal*	*Goonumbla, basal*	*Goonumbla, basal*	*Goonumbla, basal*	*Goonumbla, east*	*Goonumbla, east*
Source	NSW SPIRT	Lickfold	Radclyffe 1995	North	North	Simpson/NSW SPIRT	Simpson/NSW SPIRT	Simpson/NSW SPIRT	Simpson/NSW SPIRT	Simpson/NSW SPIRT	Simpson/NSW SPIRT	Simpson/NSW SPIRT	Simpson/NSW SPIRT	Simpson/NSW SPIRT	Clarke 1990	Clarke 1990
Deposit/Sample No	CSG162, t17 VL 7	VL7-2	Monz3	1503-16/68.2	E33H1-83.8	CSG111	CSG112	CSG154	CSG17	CSG172	CSG23	CSG40	CSG51	CSG88	M33/102	M33/185
SiO[2]	54.74	55.40	54.89	54.07	53.35	53.85	51.81	52.21	53.60	54.60	54.75	55.60	55.31	56.87	55.76	57.86
TiO[2]	0.66	0.52	0.61	0.74	0.65	0.62	0.53	0.52	0.84	0.69	0.66	0.66	0.76	0.62	0.61	0.59
Al[2]O[3]	18.46	20.55	18.04	17.08	15.69	16.49	14.59	14.69	17.14	16.44	16.90	17.28	18.24	15.82	19.43	18.28
Fe[2]O[3]	9.07	6.86	8.73	9.48	10.38	8.16	9.68	10.42	8.91	9.08	8.69	8.51	8.12	8.37	6.76	6.25
MnO	0.18	0.12	0.14	0.11	0.17	0.14	0.17	0.15	0.17	0.19	0.16	0.17	0.17	0.14	0.15	0.15
MgO	3.11	2.43	2.88	4.69	5.38	4.87	6.07	6.78	4.39	5.08	4.93	3.71	3.10	3.93	2.52	2.31
CaO	8.03	7.22	7.11	8.06	7.12	8.49	11.43	9.23	7.24	6.72	7.76	6.82	7.12	6.96	7.42	1.60
Na[2]O	3.31	4.18	3.67	3.08	4.95	3.18	2.38	2.28	3.39	3.06	3.22	4.95	3.98	4.06	4.33	5.63
K[2]O	2.05	2.37	2.51	2.15	1.84	3.74	2.87	3.22	3.81	3.76	2.51	1.92	2.76	2.76	2.51	5.10
P[2]O[5]	0.37	0.34	0.38	0.46	0.38	0.39	0.40	0.40	0.47	0.31	0.35	0.32	0.37	0.39	0.33	0.44
Total %		99.95	100.25													
LOI %	1.52	2.06	1.89	3.42	1.85	2.72	3.96	4.58	1.69	2.02	1.47	1.28	1.05	1.97	0.90	2.80
Ba	494	561	601	485	460	646	611	560	561	842	549	580	594	653	579	1691
Rb	23	32	33	22	22	60	37	46	69		21	32	45	36	35	63
Sr	962	1090	952	1155	671	889	949	862	1095	1085	1083	1275	1129	1093	1368	857
Pb	7	4	5	8	4	10	5	3	9	0	5	5	5	7	5	7
Zr	114	95	105	82	67	118	36	37	115	97	93	85	116	101	104	120
Nb	6.3	6	6	5.5	6.2	8.8	3.7	4.2	7.4	7.2	6.6	5.2	8.2	6.6	5.0	5.0
Y	20	17	21	18	16	16	12	12	21	0	17	16	20	17	17	21
La		20													12.1	26.1
Ce		48													27.2	49.2
Nd		26													14.1	24.1
Sc	21	17	21	28	27	16	28	31	19	22	17	18	13	20	9	15
Cr	10	7	8	54	146	230	228	247	32	156	125	44	9	219	7	
Ni	8	4		16	40	84	54	55	22		47	21	9	80	3	3
Cu	200	163	240	155	144	169	157	142	159		172	87	144	156	131	65
Zn	118	76	64	98	85	74	79	73	87		86	82	89	75	96	75
V	194	142	204	256	269	201	282	290	241	248	217	238	172	193		

Sample	*Goonumbla, east*	*Goonumbla, east*	*Goonumbla, east*	*Goonumbla, east*	*Goonumbla, east*	*Goonumbla, east*	*Goonumbla, east*	*Goonumbla, east*	*Goonumbla, east*	*Goonumbla, east*	*Goonumbla, east*	*Goonumbla, west*	*Goonumbla, west*	*Goonumbla, west*	*Goonumbla, west*	*Goonumbla, west*
Source	Clarke 1990	Clarke 1990	NSW SPIRT	NSW SPIRT	North	North	North	North	Simpson/NSW SPIRT	Simpson/NSW SPIRT	Simpson/NSW SPIRT	Clarke 1990	Clarke 1990	Clarke 1990	Clarke 1990	North
Deposit/Sample No	M33/186	M33/228	N46	N47(to be repeated)	10-22-1	10-22-13	10-22-2	10-22-5	CSG114	CSG50	CSG98	M33/147	M33/148	M33/149	M33/150	GPR9530
SiO[2]	55.74	56.68	58.01	57.17	55.33	55.41	54.39	55.06	55.17	54.52	55.24	60.16	60.58	56.20	60.62	61.41
TiO[2]	0.60	0.54	0.55	0.55	0.68	0.67	0.68	0.67	0.66	0.72	0.67	0.65	0.65	0.59	0.74	0.47
Al[2]O[3]	18.41	19.03	19.74	19.44	18.96	19.02	18.97	19.52	19.59	17.51	19.50	18.97	18.91	14.92	18.53	18.48
Fe[2]O[3]	6.02	5.78	5.89	5.87	6.34	6.58	6.70	6.62	7.08	7.65	7.11	6.15	6.13	6.74	5.59	3.99
MnO	0.18	0.20	0.10	0.08	0.16	0.16	0.14	0.15	0.18	0.13	0.18	0.14	0.14	0.10	0.12	0.16
MgO	2.41	1.96	1.98	2.02	2.67	3.15	2.97	3.00	2.68	3.25	2.59	1.38	1.37	3.37	1.02	1.14
CaO	5.88	6.04	5.19	5.09	5.98	4.79	5.23	5.36	7.66	4.41	7.64	1.76	1.76	9.89	5.17	1.64
Na[2]O	5.43	5.24	5.74	4.45	5.27	3.62	5.33	4.28	4.39	5.99	4.48	9.08	9.05	5.82	6.45	5.95
K[2]O	3.58	3.71	3.84	4.43	3.24	5.98	3.62	4.82	2.17	1.65	2.20	0.57	0.57	0.13	0.84	5.77
P[2]O[5]	0.41	0.35	0.50	0.50	0.42	0.41	0.45	0.41	0.34	0.36	0.35	0.25	0.25	0.39	0.36	0.22
Total %																
LOI %	2.00	0.90	1.56	1.95	1.68	2.06	3.05	2.02	1.21	5.67	1.07	1.90	1.90	2.70	2.20	1.43
Ba	773	823	677	839	865	1233	818	966	569	534	543	163	448	130	384	1137
Rb	63	58	51	57	53	88	59	77	29	27	29	1	14	1	6	95
Sr	1157	1637	1342	1828	1355	3069	1840	1258	1341	815	1274	1231	1090	215	1176	697
Pb	5	6	8	8	6	7	7	9	3	6	4	4	4	10	7	14
Zr	136	112	90	92	122	127	122	112	71	126	69	126	63	64	116	156
Nb	6.0	5.0	6.3	6.0	8.3	7.4	8.5	7.3	5.6	9.7	4.0	8.2	1.0	4.1	7.2	10.1
Y	24	24	14	14	21	20	22	19	17	20	17	29	15	16	24	24
La	22.1	17.1	14.0	13.5								12.2	13.2	13.3	15.4	23.3
Ce	33.2	36.2	33.0	35.6								28.6	16.3	28.6	44.0	53.6
Nd	21.1	22.1	18.9	19.8								17.3	17.3	12.3	23.6	23.3
Sc	13	4	11	9	8	9	8	14	9	16	8	11	27	26	15	8
Cr		6	17	15	4	3	4	4	3	7	3	8	43	50	10	14
Ni	3	35	8	8	4	4	5	6	3	7	2	3	11	11	3	3
Cu	433	96	211	198	181	156	166	124	134	119	49	66	117	148	169	43
Zn	75	101	69	72	90	92	86	86	70	91	68	82	86	66	82	90
V			143	146	209	201	208	194	165	189	166					70

Sample	*Goonumbla, west*	*Goonumbla, west*	*Goonumbla, west*	*Goonumbla, west*	*Goonumbla, west*	*Goonumbla, west*	*Goonumbla, west*	*Goonumbla, west*	*Goonumbla, west*	*Goonumbla, west*	*Goonumbla, west*	*Goonumbla, west*	*Goonumbla, west*	*Cardiff Monzodiorite*	*Cardiff Monzodiorite*	*Cardiff Monzodiorite*
Source	North	Simpson/NSW SPIRT	Simpson/NSW SPIRT	Simpson/NSW SPIRT	Simpson/NSW SPIRT	Simpson/NSW SPIRT	Simpson/NSW SPIRT	Simpson/NSW SPIRT	Simpson/NSW SPIRT	Simpson/NSW SPIRT	Simpson/NSW SPIRT	Simpson/NSW SPIRT	Simpson/NSW SPIRT	AMIRA 425	NSW SPIRT	NSW SPIRT
Deposit/Sample No	GPR9547	CSG101	CSG141B	CSG158	CSG163	CSG194	CSG219	CSG252	CSG44	CSG53	CSG85	CSG89	CSG93	GOO90	CSG72, t4, VL 6	M33/219
SiO[2]	56.06	57.57	56.02	62.39	62.59	55.43	53.96	56.18	56.30	58.25	57.95	53.00	56.86	53.77	55.36	56.23
TiO[2]	0.71	0.74	0.81	0.59	0.66	0.81	0.73	0.70	0.72	0.76	0.73	0.76	0.71	0.78	0.74	0.73
Al[2]O[3]	18.62	18.40	18.00	17.92	16.50	18.35	18.82	19.54	18.78	18.55	18.91	18.53	18.64	17.78	18.41	18.09
Fe[2]O[3]	6.31	7.14	8.28	6.08	6.71	7.73	6.92	6.80	7.02	8.55	7.11	8.74	6.95	3.73	8.23	8.18
MnO	0.21	0.16	0.22	0.15	0.17	0.18	0.18	0.20	0.19	0.16	0.18	0.15	0.17	0.21	0.16	0.21
MgO	2.19	2.63	3.71	2.36	1.79	2.91	2.66	2.37	2.41	3.45	2.53	3.44	2.24	3.20	3.13	3.10
CaO	5.33	6.45	2.91	4.37	4.06	6.87	6.66	7.39	6.58	5.50	6.47	6.20	5.85	6.79	5.91	5.46
Na[2]O	5.18	3.98	6.28	4.80	5.00	4.20	5.02	4.61	4.71	3.93	4.79	5.08	4.56	4.23	4.37	4.55
K[2]O	3.91	3.42	0.74	3.62	2.12	3.07	3.14	3.71	2.89	3.76	2.80	2.22	3.61	2.69	3.26	3.48
P[2]O[5]	0.34	0.36	0.22	0.25	0.29	0.35	0.47	0.46	0.36	0.38	0.35	0.37	0.34	0.37	0.36	0.39
Total %																99.84
LOI %	1.78	1.18	3.92	1.45	2.04	0.91	2.79	0.86	1.14	2.50	0.67	2.02	0.99		2.07	3.10
Ba	836	644	150	495	1100	537	911	726	662	1007	943	883	770	590	616	687
Rb	66	54	8	68	18	46	46	64	42	59	43	36	60	41.5	60	62
Sr	1658	1250	955	780	1264	1124	1634	1640	1346	1249	1311	1043	1320	1070	1134	958
Pb	10	5	2	5	5	4	3	9	3	6	3	4	6	6	6	8
Zr	118	133	127	159	219	114	78	117	94	121	104	124	114	79	106	111
Nb	9.1	7.8	8.8	10.3	9.1	7.6	5.3	8.2	6.9	8.5	7.5	8.7	7.0	5	6.8	6.2
Y	22	21	23	18	28	21	20	24	20	20	20	21	21	17	19	24
La	17.1													13	0.0	9.3
Ce	33.2													28	0.0	41.3
Nd	19.1														0.0	25.8
Sc	7	11	21	11	18	13	10	10	12	12	10	14	9	16	14	12
Cr	8	4	13	8	15	4	4	2	3	6	4	9	3	7	7	9
Ni	4	4	9	6	7	4	2	2	2	6	2	7	2	5	6	41
Cu	233	140	149	134	61	116	93	119	20	154	227	152	105	156	147	165
Zn	78	74	86	81	101	70	74	76	71	95	69	100	86	124	92	176
V	169	161	191	145	104	195	254	184	174	179	172	139	159	167	170	0

Sample	*Goonumbla dyke*	*Goonumbla dyke*	*Goonumbla Hill MD*	*Goonumbla Hill MD*	*Goonumbla Intrusion*	*Goonumbla Intrusion*	*Goonumbla Intrusion*	*Goonumbla Intrusion*	*Goonumbla Siding*	*Goonumbla Siding*	*Goonumbla Siding*	*Goonumbla Siding*	*Goonumbla Siding*	*Goonumbla Siding, 451Ma*	*Wombin Volcanics*	*Wombin Volcanics*	*Wombin Volcanics*
Source	AMIRA 425	Heithersay 1991	NSW SPIRT	NSW SPIRT	AMIRA 425	NSW SPIRT	NSW SPIRT	NSW SPIRT	Clarke 1990	NSW SPIRT	Heithersay 1991	Lickfold	Radclyffe 1995	AMIRA 425	AMIRA 425	AMIRA 425	AMIRA 425
Deposit/Sample No	GOO87	Goonumbla Hill - dyke	CGS11, t1	CSG15, t2	GOO93	CSG94, t5	CSG113, t7	CSG146, t8	M33/087 - C11	CSG59B, t3	Goonumbla Siding	VL5-1	Monz21	GOO88	E26/66/124.1	E26/66/168.5	E27/4/127.5
SiO[2]	55.69	54.38	52.40	53.42	53.31	53.95	55.14	55.33	54.11	52.34	51.48	52.73	52.68	51.89	54.63	58.04	51.42
TiO[2]	0.61	0.60	0.82	0.86	0.72	0.74	0.70	0.80	0.64	0.80	0.69	0.68	0.72	0.69	0.71	0.60	0.75
Al[2]O[3]	18.58	18.18	19.66	16.77	17.82	18.28	18.94	18.89	19.69	17.57	17.96	19.45	19.68	19.31	18.92	18.23	18.04
Fe[2]O[3]	3.49	5.75	8.13	9.40	3.63	8.14	7.10	8.38	4.12	9.29	8.33	7.84	7.92	4.52	6.75	4.45	8.56
MnO	0.20	0.17	0.21	0.20	0.18	0.18	0.18	0.21	0.21	0.19	0.21	0.22	0.19	0.17	0.16	0.14	0.15
MgO	2.16	1.83	3.36	4.55	3.26	3.52	3.05	3.27	2.58	4.32	3.18	2.96	2.77	2.39	2.70	1.38	4.41
CaO	5.70	6.04	7.27	6.83	6.65	6.75	6.48	7.63	7.23	7.60	7.34	8.54	8.67	8.23	3.42	3.28	6.68
Na[2]O	5.41	6.74	4.26	3.89	4.14	4.00	5.04	4.70	5.36	3.33	5.45	4.67	5.21	5.07	5.80	5.69	3.47
K[2]O	3.49	3.43	3.19	3.57	3.75	3.89	2.88	0.46	2.53	4.04	2.10	2.40	1.68	2.10	3.51	5.50	3.72
P[2]O[5]	0.36	0.37	0.57	0.47	0.44	0.45	0.40	0.33	0.45	0.42	0.51	0.50	0.47	0.42	0.41	0.34	0.46
Total %									99.62			100.04	100.19				
LOI %			2.64	1.64		1.86	1.35	2.20	2.68	1.88		2.78	2.47				
Ba	760	705	1124	541	895	931	780	264	823	949	730	677	530	570	1280	1220	1070
Rb	50	50	53	64	59	64	40	4	30	54	23	30	14	21.5	62	78	52
Sr	950	895	1731	1013	1400	1408	1366	1052	1739	1538	1010	1492	977	1220	1430	785	1680
Pb	8	7	4	6	9	7	8	2	5	4	3	4	3	2	8	10	3
Zr	97	94	67	109	85	98	107	92	78	85	31	43	47	44	94	115	57
Nb	6		4.5	7.3	5	6.2	6.4	6.6	2	5.0		3	3	3	6	7	3
Y	21		20	21	19	20	20	22	19	20		18	20	18	21	23	18
La	16		0.0		16	0.0	0.0		10	0.0		16		12	18	24	13
Ce	34	30	0.0		34	0.0	0.0		22	0.0	15	28		26	36	44	26
Nd			0.0			0.0	0.0		21	0.0		16			17	18	24
Sc	8	30	14	19	17	16	12	16	14	20	15	14	13	12			
Cr	1		6	41	6	6	7	5	6	21		8	5	3	3	2	4
Ni	<1		5	24	9	8	5	3	3*	13		4		2	2	1	7
Cu	136		104	36	194	167	146	59	155	190		180	83	59	234	202	153
Zn	76	139	86	70	84	85	85	94	90	95	182	76	59	71	80	58	49
V	152		221	250	200	230	214	197		271		235	239	201	176	101	254

Sample	Wombin Volcanics	Wombin Volcanics	Wombin Volcanics	Wombin Volcanics	Wombin Volcanics	Wombin Volcanics	Wombin Volcanics	Wombin Volcanics	Wombin Volcanics	Wombin Volcanics	Wombin Volcanics	Wombin Volcanics	Wombin Volcanics	Wombin Volcanics	Wombin Volcanics	Wombin Volcanics	Wombin Volcanics	Wombin Volcanics	Wombin Volcanics
Source	AMIRA 425	Clarke 1990	Clarke 1990	Clarke 1990	Clarke 1990	Clarke 1990	Clarke 1990	Clarke 1990	Clarke 1990	Clarke 1990	Heithersay 1991	Heithersay 1991	Heithersay 1991	Heithersay 1991	Heithersay 1991	Heithersay 1991	Heithersay 1991	Heithersay 1991	North
Deposit/Sample No	E27/4/154.6	M33/089	M33/097	M33/158	M33/161	M33/163	M33/172	M33/173	M33/175	M33/190	E26/26/227.6	E26/29/321.8	E26/29/325.7	E26/44/329.5	E26/44/393.0	E26/44/548.0	E26/48/392.0	E26/68/416.3	10-22-12
SiO[2]	52.03	56.40	57.87	65.53	62.51	56.43	54.72	61.33	59.63	60.44	62.86	52.28	59.28	59.87	61.95	61.40	61.88	59.04	61.76
TiO[2]	0.76	0.65	0.62	0.23	0.43	0.69	0.78	0.43	0.49	0.55	0.26	0.53	0.55	0.50	0.36	0.42	0.47	0.45	0.41
Al[2]O[3]	17.90	19.38	18.81	17.45	17.88	19.36	18.00	18.47	18.75	18.63	16.68	17.57	17.70	17.94	17.01	17.25	17.86	17.13	18.64
Fe[2]O[3]	8.37	3.51	6.09	1.57	0.96	3.54	4.83	4.14	5.27	2.69	1.36	8.17	5.49	2.46	3.08	4.31	2.47	3.32	3.89
MnO	0.17	0.21	0.17	0.13	0.07	0.23	0.20	0.18	0.15	0.14	0.03	0.05	0.05	0.03	0.02	0.04	0.04	0.06	0.09
MgO	3.96	2.06	1.55	1.25	1.34	2.55	4.11	1.28	1.90	1.55	0.52	2.71	1.30	2.13	0.57	1.08	1.00	1.02	0.82
CaO	7.02	5.90	4.57	2.85	2.93	5.14	4.91	1.67	4.84	2.55	0.88	2.64	1.86	1.98	0.75	1.63	2.04	2.60	2.30
Na[2]O	3.80	5.46	5.99	4.81	4.92	5.31	4.63	6.02	4.61	5.17	4.48	5.94	5.28	4.51	5.07	5.36	5.41	5.53	6.50
K[2]O	3.60	3.57	4.20	4.69	5.99	3.60	3.76	6.41	4.32	6.19	6.34	4.20	5.69	6.86	7.47	5.87	6.22	6.12	5.28
P[2]O[5]	0.44	0.39	0.33	0.13	0.28	0.44	0.35	0.24	0.30	0.33	0.11	0.37	0.29	0.19	0.17	0.19	0.22	0.22	0.22
Total %		99.39		99.58	98.12	99.45	99.62			99.73									
LOI %		2.40	2.10	3.90	4.70	3.40	2.40	1.60	2.00	3.10									3.17
Ba	925	831	687	903	778	790	1068	1385	1425	1362	15140	385	900	795	440	740	675	925	832
Rb	53	54	74	87	74	55	79	109	67	102	57	105	78	108	77	72	75	84	77
Sr	1770	1234	612	549	753	1395	1131	714	1295	710	1420	805	730	750	580	535	535	885	526
Pb	4	4	13	4	11	7	4	15	8	14	9	14	17	16	13	9	8	22	12
Zr	58	84	155	73	119	120	102	152	123	146	1	60	142	152	230	197	193	177	151
Nb	3	6	9.3	4	5	5	4	3.1	5.1	4	1		7			8			8.5
Y	18	20	24	11	10	22	24	23	20	25	2		8			14			22
La	14	17	17.6	12	21	17	17	28.6	16.4	25	6.3		16.6			18.2			
Ce	30	32	46.5	17	32	34	23	58.2	36.9	56	24	25	34	51	54	43	43	80	
Nd	23	17	25.8	12	20	19	23	29.6	14.3	33	7.5		17.5			17.4			
Sc		10	10	3	5	9	18	8	11	10	24		34	51	54	43	43	80	6
Cr	4	7	10			10					15		5			15			2
Ni	7	3	3	3	3	3	5	3	3	3	5		5			5			2
Cu	183	30	196	35	6300	440	125	41	164	35		2600							14
Zn	60	85	98	50	30	105	135	77	72	75	705	52	1530	2270	1730	481	3160	3030	81
V	252																		72

Sample	*Wombin Volcanics*	*Wombin Volcanics*	*Wombin Volcanics*	*Wombin Volcanics*	*Wombin Volcanics*	*Wombin Volcanics*	*Wombin Volcanics*	*Wombin Volcanics*	*Wombin Volcanics*	*Wombin Volcanics*	*Wombin Volcanics*	*Wombin Volcanics*	*Wombin Volcanics*	*Wombin Volcanics*	*Wombin Volcanics*	*Wombin Intrusion*	*Wombin Intrusion*	*Wombin Intrusion*	*Wombin Intrusion /ring dyke*	*Wombin Intrusion /ring dyke*
Source	North	North	Simpson/ NSW SPIRT	Simpson/ NSW SPIRT	Simpson/ NSW SPIRT	Simpson/ NSW SPIRT	Simpson/ NSW SPIRT	Simpson/ NSW SPIRT	Simpson/ NSW SPIRT	Simpson/ NSW SPIRT	Simpson/ NSW SPIRT	Simpson/ NSW SPIRT	Simpson/ NSW SPIRT	Simpson/ NSW SPIRT	Simpson/ NSW SPIRT	AMIRA 425	NSW SPIRT	NSW SPIRT	AMIRA 425	Clarke 1990
Deposit/Sample No	10-22-6	E26D153-120.5	CSG100	CSG107	CSG12	CSG177	CSG195	CSG204	CSG216	CSG224	CSG245	CSG263	CSG281	CSG291?	CSG67	GOO95	CSG199, t10	CSG109, t6	GOO104	M33/167 C8
SiO_2	62.02	63.86	59.92	57.26	53.77	55.44	55.63	60.67	58.03	60.83	62.38	59.72	56.55	61.08	65.89	53.40	61.07	50.79	56.26	62.65
TiO_2	0.44	0.42	0.49	0.56	0.76	0.69	0.64	0.58	0.62	0.48	0.39	0.50	0.66	0.44	0.35	0.75	0.57	0.80	0.55	0.39
Al_2O_3	18.67	18.49	17.99	19.14	19.57	17.05	19.03	19.30	19.22	18.23	18.46	18.85	19.04	18.61	18.78	17.51	18.65	19.79	18.80	17.79
Fe_2O_3	3.62	2.67	5.84	5.66	7.41	8.50	6.49	4.21	5.43	4.67	3.73	4.84	6.45	4.35	3.09	3.85	4.48	8.72	2.67	1.92
MnO	0.06	0.22	0.14	0.24	0.17	0.08	0.20	0.13	0.13	0.14	0.15	0.16	0.18	0.16	0.00	0.19	0.11	0.19	0.13	0.11
MgO	0.51	0.97	2.26	1.76	2.94	4.17	2.33	1.24	1.85	1.61	1.14	1.70	2.43	1.48	0.12	3.28	1.32	3.79	1.55	1.65
CaO	1.72	1.53	4.89	4.85	6.87	6.12	6.81	1.78	3.84	3.38	1.67	3.65	3.75	1.99	0.00	6.59	1.69	8.61	4.43	3.39
Na_2O	5.40	5.38	4.32	6.52	4.19	5.05	4.87	5.29	4.92	5.40	5.74	5.03	3.42	5.72	7.57	4.06	5.08	3.72	4.79	4.79
K_2O	7.21	6.28	3.81	3.62	3.66	2.47	3.52	6.37	5.42	4.89	6.07	5.14	6.96	5.82	3.90	4.02	6.61	2.85	5.36	4.51
P_2O_5	0.23	0.17	0.29	0.30	0.54	0.36	0.41	0.31	0.41	0.26	0.20	0.29	0.38	0.24	0.27	0.42	0.29	0.60	0.32	0.25
Total %																				99.26
LOI %	1.57	3.45	2.37	4.70	0.59	4.45	1.01	2.90	1.09	2.96	0.84	1.17	1.75	0.83	3.00		1.58	2.63		5.75
Ba	1242	542	931	818	971	619	933	1279	1230	1085	1091	949	1754	985	128	1120	1488	1184	885	784
Rb	100	104	58	42	60	30	57	94	84	73	98	86	150	92	41	65	85	46	93	73
Sr	624	542	1408	648	1587	951	1493	791	1123	671	752	963	1856	845	18	1210	770	1652	990	875
Pb	12	25	11	6	9	2	5	13	13	10	14	8	12	11	7	9	7	1*	9	12
Zr	146	241	98	130	86	104	94	133	126	132	157	133	150	146	135	68	154	64	119	111
Nb	8.2	13.9	6.2	8.7	5.7	6.2	5.9	9.0	8.6	7.7	9.0	7.7	9.1	8.8	7.2	5	9.2	4.3	8	4
Y	23	26	17	21	21	17	23	22	20	18	22	21	22	22	19	17	23	18	18	16
La																16	0.0		17	19
Ce																34	0.0		36	19
Nd																	0.0			19
Sc	7	5	16	8	13	23	9	9	9	7	5	5	11	7	5	18	6	15	11	4
Cr	3	2	6	3	4	157	3	2	2	5	2	3	5	5	3	9	2	3	2	
Ni	2	1	9	2	4	59	3	2	3	2	3	2	4	3	2	10	1	7	3	3
Cu	26	16	34	102	101	13	95	23	43	120	24	45	107	37	18	143	14	135	76	1400
Zn	94	83	61	62	77	23	78	84	79	75	85	75	81	78	8	78	61	106	57	35
V	66	43	230	155	195	226	182	81	123	114	59	100	181	82	3	194	74	246	102	

Sample	Wombin Intrusion/r ing dyke	Wombin Intrusion/r ing dyke	Wombin Intrusion/r ing dyke	Wombin Intrusion/r ing dyke	Wombin Intrusion/r ing dyke	Wombin Intrusion/r ing dyke	Wombin Intrusion/r ing dyke	Wombin Intrusion/r ing dyke	Wombin Intrusion/r ing dyke	Wombin Intrusion/r ing dyke	Wombin Intrusion/r ing dyke	Wombin Intrusion/r ing dyke	Wombin Intrusion/r ing dyke	Wombin Intrusion/r ing dyke	Wombin Intrusion/r ing dyke	Wombin Intrusion/r ing dyke	Cooks Myalls monzonite	Cooks Myalls monzonite	Cooks Myalls monzonite
Source	Clarke 1990	Clarke 1990	Clarke 1990	Clarke 1990	Clarke 1990	Clarke 1990	Clarke 1990	Clarke 1990	Clarke 1990	NSW SPIRT	Heithersa y 1991	Heithersa y 1991	Heithersa y 1991	Heithersa y 1991	Heithersa y 1991	Lickfold	NSW SPIRT	NSW SPIRT	Lickfold
Deposit/S ample No	M33/169 - C10	M33/020 - C1	M33/088 - C2	M33/090 - C3	M33/157 - C4	M33/159 - C5	M33/160 - C6	M33/166 - C7	M33/168 - C9	M33/162, PH mineralise d suite	Wombin Gossan	Ring Dyke	E31 Outcrop	E26 South	ACH 967-106, Ring Dyke	VLM-1	CSG189, t9	CSG220, t11	VL 11-1
SiO[2]	59.43	55.80	61.08	50.41	61.27	65.13	68.80	63.94	64.64	54.54	53.26	58.31	61.74	62.75	58.49	58.21	59.76	54.01	60.57
TiO[2]	0.51	0.62	0.42	0.79	0.39	0.27	0.23	0.33	0.25	0.74	0.66	0.53	0.38	0.35	0.49	0.60	0.47	0.66	0.49
Al[2]O[3]	18.55	20.01	18.76	20.29	18.76	18.31	16.41	18.08	18.05	18.65	19.92	18.25	17.73	17.31	17.87	18.44	18.17	19.91	18.78
Fe[2]O[3]	3.14	0.31	2.14	4.81	2.65	1.56	0.21	1.84	1.47	8.21	6.27	4.88	3.75	3.89	4.77	5.96	5.51	7.51	4.59
MnO	0.07	0.15	0.14	0.16	0.11	0.06	0.04	0.13	0.09	0.12	0.15	0.10	0.07	0.16	0.08	0.18	0.17	0.18	0.16
MgO	2.15	2.25	1.22	3.76	1.33	0.83	0.68	1.07	0.94	3.42	2.42	1.80	1.44	1.25	1.61	2.44	2.05	2.17	1.69
CaO	4.93	6.19	3.14	8.99	3.96	1.23	2.06	2.78	2.64	7.09	6.80	3.33	1.81	1.62	2.55	3.88	4.77	7.05	3.33
Na[2]O	4.61	4.44	5.91	3.97	5.51	5.83	4.94	5.72	5.88	3.90	5.10	4.81	5.83	5.70	5.39	5.08	4.68	4.58	5.11
K[2]O	3.19	4.42	5.29	2.57	4.18	5.18	5.67	4.51	4.03	3.29	3.57	4.96	4.01	4.82	5.24	4.84	4.04	3.37	4.99
P[2]O[5]	0.38	0.44	0.25	0.58	0.22	0.14	0.11	0.16	0.10	0.46	0.53	0.35	0.20	0.18	0.32	0.37	0.29	0.46	0.30
Total %	97.71	99.55	99.27	98.82	99.19	99.41	98.76	99.60	99.29							99.92			99.86
LOI %	2.41	2.68	1.22	3.35	1.12	3.43	3.89	1.74	4.20	6.10						1.35	0.81	2.22	1.56
Ba	784	920	983	848	1196	755	781	1107	1107	789	905	1010	1050	1050	875	830	842	945	1036
Rb	56	76	66	38	58	54	57	74	63	60	45	87	55	63	77	80	58	49	86.6
Sr	1477	1382	717	2190	1325	502	832	1008	743	1588	1560	895	1240	550	670	952	1016	1930	1013
Pb	8	14	7	6	11	6	8	12	12	3	9	10	10	19	10	8	9	3	10
Zr	98	138	112	87	84	66	76	97	69	56	49	112	82	117	117	215	112	57	124
Nb	4	8	6	3	3	2	3	4	3	1.1	5	9				12	6.1	4.0	7
Y	18	18	25	17	17	12	8	16	12	22	2	6				24	18	21	20
La	15	20	25	13	19	14	6	15	20	16.3	11.8	20.2				21	0.0	0.0	19
Ce	25	44	52	32	26	17	14	20	18	24.9	26	40	27	34	32	47	0.0	0.0	41
Nd	18	17	28	21	16	12	11	11	12	22.8	10.3	18.7				24	0.0	0.0	19
Sc	7	17	7	24	5	2	2	4	2	17	26	40	27	34	32	12	10	6	7
Cr	9	8		9	8	3		4		0	10	5				6	9	3	4
Ni	3*	3		3	3	3*	3*	3*	3	5	5	5*				5	6	1	2
Cu	460	105		145	560	1550	6900	350	55	2982						122	62	88	42
Zn	55	70		80	40	45	40	65	35	27	212	104	595	336	109	67	92	98	68
V										0						128	128	155	89

Sample	*Gunningbland Forest 10-1vl*	*Gunningbland Forest 10-3vl*	*Gunningbland Forest 9, ajc*	*Gunningbland Forest 9-1vl*	*Gunningbland Forest 9-3vl*	*Woods Monzonite, 439Ma*	*Woods Monzonite, 439Ma*	*Wombin dyke, 439Ma*	*Zero 37, 437Ma*
Source	Lickfold	Lickfold	NSW SPIRT	Lickfold	Lickfold	AMIRA 425	AMIRA 425	AMIRA 425	NSW SPIRT
Deposit/Sample No	VL10-1	VL 10-3, VL-20 ICP	M33/101	VL9-1	VL 9-3	GOO96	GOO97	GOO92	E37H3-245.2
SiO_2	65.95	63.75	62.11	61.90	62.09	61.28	60.03	59.36	66.68
TiO_2	0.38	0.38	0.40	0.42	0.43	0.40	0.44	0.49	0.29
Al_2O_3	19.25	17.98	18.30	18.27	18.22	17.45	17.68	18.19	16.66
Fe_2O_3	2.86	4.03	4.30	4.41	4.50	2.96	3.12	2.43	2.92
MnO	0.02	0.23	0.16	0.17	0.16	0.14	0.11	0.13	0.05
MgO	0.23	1.18	1.23	1.43	1.53	1.57	1.81	1.64	1.60
CaO	0.34	2.88	3.21	3.60	3.19	2.93	3.58	2.77	1.96
Na_2O	6.28	5.31	6.58	5.78	6.06	5.77	5.28	7.29	4.15
K_2O	4.54	4.11	3.72	3.84	3.63	4.65	4.23	3.70	5.51
P_2O_5	0.14	0.15	0.16	0.18	0.18	0.24	0.28	0.23	0.10
Total %	99.17	99.60		99.35	99.65				
LOI %	2.27	1.87	1.80	1.58	1.61				3.18
Ba	1428	852	800	263	815	860	840	635	988
Rb	71	80.1	64	67	63.1	69	60	47.5	83
Sr	858	1031	861	984	858	615	1110	585	171
Pb	25	10	8	7	7	11	8	7	2
Zr	138	131	108	83	106	134	124	188	98
Nb	9	8	6.2	4	7	6	6	11	6.1
Y	30	18	20	17	18	17	17	19	12
La	146	14	12.3	19	15	17	17	17	
Ce	258	32	27.8	42	31	34	36	36	
Nd	112	13	12.3	25	15				
Sc	5	5	6	28	6	7	11	7	4
Cr	2	3	4	38	3	2	3	2	5
Ni	2	2	-3	1	2	2	2	1	2
Cu	57	49	72	48	54	50	10	62	8
Zn	35	66	67	61	57	59	42	55	48
V	75	83	0	325	97	84	101	120	68

Sample	BQM 22	B-QMP 22 pre	KA-QMP 22	K-QMP 22	BQM 27	B-QMP 27 pre	KA-QMP 27	K-QMP 27b	BQM 48	Microgranite 48	KA-QMP 48	K-QMP 48	Monzodiolite 26	BQM 26	B-QMP 26 post	KA-QMP 26	K-QMP 26	Zero 26	Goonumbla Hill monzodiorite	Goonumbla Siding monzodiorite	Condobolin Road monzodiorite	Cooks Myalls monzonite porphyry
Source	Lickfold	Lickfold	Lickfold	Lickfold	Lickfold	Lickfold	Lickfold	Lickfold	Lickfold	Lickfold	Lickfold	Lickfold	Lickfold	Lickfold	Lickfold	Lickfold	Lickfold	Lickfold	Lickfold	Lickfold	Lickfold	Lickfold
Deposit/Sample No	E22/229/728.6	E22/229/685.2	E22/2/345.7	E22/205/400.9	E27/28/709.0	E27/4/225.9	E27/7/147.8	E27/11/73.6	E48/13w2/970.7	E48/13w2/951.2	E48/11/531.5	E48/15w1/651.3	E26/46/1720.2	E26/287/220.3	E26/264/235.3	E26/286/184.0	E26/189/229.8	E26/264/263.0	CSG11	CSG59B/VL5	CSG162/VL7	CSG189/VL11
Sc	3.04	3.35	1.47	1.79	4.84	2.70	1.78	2.45	6.32	1.45	1.51	1.29	9.90	6.46	2.64	2.42	2.63	2.00	12.50	20.40	20.00	8.50
Rb	98.31	80.09	84.32	87.46	84.32	59.10	73.82	72.00	71.90	90.14	85.80	48.54	56.07	73.49	51.14	57.39	82.38	85.16	50.00	50.00	22.00	55.00
Sr	355.00	1478.00	287.00	736.00	566.00	516.00	496.00	416.00	496.00	183.00	261.00	161.00	1671.00	1291.00	991.00	1209.00	796.00	856.00	1633.00	1437.00	908.00	972.00
Y	21.01	12.54	6.50	6.51	21.99	13.84	9.55	6.62	17.22	6.68	8.40	4.43	19.02	17.36	13.78	10.50	4.91	12.47	19.00	19.00	20.00	17.00
Zr	216.00	105.00	101.00	92.50	170.00	81.40	75.20	71.00	137.96	85.48	83.84	73.49	82.49	123.65	84.65	78.83	110.30	75.38	66.00	82.00	107.00	115.00
Nb	11.34	5.61	5.32	4.99	9.48	4.56	4.89	3.20	7.82	3.91	3.86	3.32	5.00	6.72	4.89	4.19	4.43	4.14	4.66	5.19	6.30	5.51
Mo	1.19	13.16	1.13	1.28	4.64	0.91	0.80	2.55	2.03	4.17	5.41	0.71	2.34	1.75	1.73	3.64	1.23	0.62	1.04	1.34	1.89	3.29
Sn	2.34	1.43	1.15	1.48	2.55	1.60	1.55	0.13	2.15	1.61	1.87	2.24	3.99	0.75	0.19	0.35	0.27	0.38	1.89	2.14	2.19	1.76
Sb	0.43	0.36	0.19	72.22	0.19	0.15	0.19	0.37	0.31	0.24	2.67	0.73	0.12	0.05	0.20	0.07	0.08	0.67	0.21	0.30	0.26	0.03
Cs	0.46	0.70	0.44	0.69	0.42	0.59	0.53	0.70	1.08	0.18	0.19	0.30	0.18	0.22	0.20	0.69	0.20	0.45	0.48	0.37	0.16	0.40
Ba	374.00	739.00	458.00	791.00	314.00	303.00	314.00	817.00	587.00	810.00	776.00	655.00	867.00	742.00	1204.00	1542.00	851.00	1582.00	971.00	923.00	518.00	823.00
La	19.30	12.92	9.12	6.11	18.75	12.57	14.73	8.43	21.11	8.49	5.87	4.76	18.01	15.27	14.95	12.50	4.10	16.95	18.20	15.70	27.90	18.40
Ce	36.03	22.56	14.55	10.12	35.54	24.01	25.16	13.40	37.22	12.46	11.19	8.25	34.53	29.13	26.36	21.70	6.76	29.17	34.70	30.10	57.80	33.80
Pr	4.22	2.62	1.49	1.17	4.27	2.88	2.78	1.48	4.45	1.28	1.35	0.90	4.36	3.59	3.07	2.51	0.81	3.25	4.70	4.06	8.05	4.32
Nd	15.48	10.21	5.05	4.53	16.55	11.27	9.90	5.79	17.16	4.61	5.31	3.40	18.09	14.60	11.75	9.80	3.30	11.53	20.50	17.50	34.10	17.70
Sm	3.20	1.95	0.87	0.91	3.34	2.22	1.84	1.22	3.67	0.92	1.13	0.68	4.01	3.05	2.30	1.92	0.73	2.23	4.74	4.15	7.05	3.77
Eu	0.62	0.70	0.30	0.37	0.82	0.76	0.58	0.53	0.99	0.30	0.41	0.36	1.26	0.87	0.72	0.63	0.33	0.75	1.50	1.23	1.79	1.14
Gd	2.80	1.83	0.80	0.89	3.00	2.02	1.60	1.15	3.15	0.90	1.10	0.62	3.69	2.80	2.10	1.77	0.77	1.93	4.53	4.09	5.52	3.50
Tb	0.49	0.28	0.13	0.14	0.48	0.32	0.25	0.19	0.50	0.14	0.19	0.11	0.56	0.43	0.33	0.27	0.12	0.32	0.70	0.67	0.78	0.55
Dy	3.10	1.74	0.86	0.88	3.03	1.98	1.48	1.10	3.00	0.95	1.22	0.64	3.27	2.63	2.01	1.63	0.74	1.93	3.80	3.73	4.00	3.14
Ho	0.68	0.37	0.20	0.19	0.64	0.44	0.33	0.24	0.61	0.20	0.26	0.14	0.65	0.55	0.43	0.34	0.15	0.42	0.75	0.75	0.79	0.64
Er	2.14	1.18	0.65	0.61	2.09	1.34	1.01	0.74	1.91	0.65	0.85	0.50	1.91	1.65	1.30	1.05	0.52	1.30	2.21	2.27	2.26	2.04
Yb	2.58	1.30	0.92	0.75	2.29	1.46	1.26	0.88	2.06	0.76	1.00	0.59	1.79	1.68	1.41	1.08	0.63	1.48	1.97	2.13	2.13	2.08
Lu	0.42	0.21	0.17	0.15	0.36	0.24	0.21	0.15	0.33	0.13	0.17	0.11	0.27	0.26	0.23	0.17	0.12	0.23	0.31	0.34	0.34	0.34
Hf	5.35	2.55	2.89	2.49	3.90	1.90	2.24	2.09	3.49	2.17	2.03	1.90	2.09	3.14	2.05	2.00	2.78	2.01	2.01	2.45	3.09	3.24
Ta	1.14	0.68	0.91	0.70	0.88	0.51	0.57	0.48	0.77	0.76	0.75	0.59	0.52	0.62	0.57	0.58	0.92	0.45	0.39	0.44	0.48	0.53
Tl	0.30	0.22	0.18	0.31	0.16	0.16	0.22	0.22	0.18	0.20	0.31	0.14	0.18	0.19	0.12	0.17	0.33	0.30	0.10	0.15	0.05	0.11
Pb	8.01	15.51	7.64	26.87	5.10	4.05	3.77	4.74	5.11	19.10	8.46	3.17	5.71	8.02	7.71	5.68	9.39	9.61	6.30	7.01	8.05	9.83
Th	7.09	2.72	5.33	3.19	5.29	1.46	3.09	1.40	4.36	1.38	1.80	1.23	2.14	4.45	1.98	1.73	2.07	1.76	2.10	2.54	3.41	3.54
U	3.06	0.97	2.33	0.98	2.41	0.68	1.24	0.46	1.30	0.48	0.47	0.33	1.29	1.12	0.77	0.53	0.64	0.98	1.02	1.29	2.59	2.07
139 La[N]	61.26	41.02	28.96	19.39	59.51	39.91	46.77	26.77	67.01	26.94	18.65	15.10	57.18	48.48	47.45	39.67	13.02	53.81	57.84	49.99	88.63	58.55
140 Ce[N]	44.32	27.75	17.90	12.45	43.72	29.54	30.94	16.45	45.78	15.33	13.77	10.14	42.48	35.83	32.43	26.69	8.32	35.88	42.72	36.97	71.12	41.61
141 Pr[N]	36.40	22.58	12.89	10.12	36.84	24.86	23.97	12.77	38.37	11.01	11.60	7.74	37.58	30.91	26.47	21.67	7.00	28.04	40.51	34.99	69.39	37.23
146 Nd[N]	25.92	17.11	8.45	7.58	27.72	18.88	16.57	9.69	28.75	7.72	8.90	5.69	30.31	24.46	19.68	16.41	5.53	19.31	34.28	29.37	57.17	29.69
147 Sm[N]	16.67	10.16	4.56	4.72	17.39	11.58	9.59	6.36	19.13	4.80	5.88	3.54	20.89	15.88	11.99	9.99	3.79	11.61	24.68	21.59	36.70	19.64
151 Eu[N]	8.58	9.67	4.20	5.14	11.37	10.54	8.04	7.39	13.77	4.18	5.71	4.96	17.45	12.08	9.97	8.77	4.61	10.35	20.84	17.05	24.82	15.85
157 Gd[N]	10.80	7.06	3.10	3.44	11.57	7.81	6.17	4.44	12.17	3.47	4.24	2.38	14.26	10.80	8.12	6.85	2.96	7.45	17.48	15.81	21.30	13.52
159 Tb[N]	9.91	5.79	2.65	2.90	9.89	6.50	5.04	3.84	10.12	2.90	3.87	2.17	11.35	8.72	6.79	5.58	2.44	6.57	14.21	13.59	15.85	11.24
163 Dy[N]	9.55	5.34	2.65	2.72	9.34	6.08	4.56	3.38	9.22	2.91	3.76	1.95	10.06	8.10	6.18	5.01	2.27	5.92	11.69	11.47	12.31	9.67
165 Ho[N]	9.29	5.05	2.77	2.60	8.77	6.00	4.54	3.31	8.42	2.75	3.56	1.94	8.91	7.47	5.85	4.72	2.12	5.71	10.25	10.32	10.76	8.71
167 Er[N]	10.06	5.55	3.07	2.85	9.81	6.30	4.76	3.48	8.98	3.07	4.00	2.36	8.98	7.74	6.10	4.95	2.42	6.11	10.39	10.67	10.60	9.57
172 Yb[N]	12.40	6.24	4.43	3.60	10.99	7.01	6.07	4.23	9.91	3.63	4.82	2.82	8.62	8.08	6.78	5.21	3.04	7.10	9.48	10.23	10.22	10.02
175 Lu[N]	12.87	6.61	5.22	4.53	11.14	7.32	6.62	4.65	10.09	4.17	5.21	3.47	8.33	7.97	7.27	5.19	3.80	7.26	9.58	10.59	10.47	10.43
Eu*	13.42	8.47	3.76	4.03	14.18	9.51	7.69	5.31	15.26	4.08	4.99	2.90	17.26	13.10	9.87	8.27	3.35	9.30	20.77	18.48	27.96	16.30
Eu/Eu*	0.64	1.14	1.12	1.28	0.80	1.11	1.05	1.39	0.90	1.02	1.14	1.71	1.01	0.92	1.01	1.06	1.38	1.11	1.00	0.92	0.89	0.97

E2 1

Sample	VL 10-3, G/blnd QMP	E36 zero	Goonumbla Volcanics	Goonumbla Volcanics	Goonumbla Volcanics	Goonumbla Volcanics	Goonumbla Volcanics	Goonumbla Volcanics	Goonumbla Volcanics	Goonumbla Volcanics	Goonumbla Volcanics
Source	Lickfold	NSW SPIRT	NSW SPIRT	NSW SPIRT	NSW SPIRT	NSW SPIRT	NSW SPIRT	NSW SPIRT	NSW SPIRT	NSW SPIRT	NSW SPIRT
Deposit/Sample No	VL10-3	E37/3/2 45.5	CSG112	CSG23	CSG88	10-22-1	CSG114	CSG141 B	CSG158	CSG53	CSG89
Sc	4.77	5.17	33.64	20.39	19.97	9.77	9.85	20.36	11.31	14.35	16.91
Rb	80.00	83.46	38.52	20.23	34.53	53.11	28.46	8.29	54.52	59.54	35.76
Sr	940.00	151.27	945.55	1053.29	1083.95	1273.44	1337.65	943.76	714.56	1248.79	1022.48
Y	17.20	10.18	12.55	17.16	17.06	19.56	17.26	23.61	16.78	20.51	21.43
Zr	115.00	64.88	36.92	90.75	99.25	122.49	69.55	123.71	153.52	119.89	121.04
Nb	7.50	6.41	4.31	6.22	6.88	8.36	4.97	8.82	9.89	8.96	9.04
Mo	1.86	0.61	0.97	1.28	1.44	1.04	0.80	0.97	1.49	0.78	0.90
Sn	0.50	0.75	0.69	1.20	1.17	1.05	0.78	1.12	1.19	1.19	1.25
Sb	0.16	1.18	0.38	0.28	0.38	0.81	0.13	0.29	0.44	0.43	0.20
Cs	0.30	1.03	0.30	0.10	0.16	1.10	0.16	0.69	0.24	0.39	0.53
Ba	796.00	970.45	559.50	540.95	641.02	771.03	557.68	145.66	465.89	1004.09	858.57
La	18.76	13.14	11.19	14.80	15.83	17.20	12.64	14.80	14.19	15.83	15.56
Ce	31.06	20.47	19.26	28.56	29.12	32.73	23.73	30.30	28.69	30.84	30.11
Pr	3.52	2.27	2.33	3.54	3.70	4.12	3.07	4.03	3.70	3.81	3.90
Nd	13.61	8.78	9.99	15.97	16.12	17.28	14.00	18.17	16.18	17.12	17.13
Sm	2.93	1.70	2.35	3.71	3.59	3.91	3.29	4.29	3.64	3.99	4.01
Eu	0.90	0.54	0.78	1.09	1.04	1.25	1.20	1.24	1.00	1.24	1.26
Gd	2.81	1.63	2.31	3.41	3.30	4.13	3.17	4.09	3.29	3.92	3.86
Tb	0.49	0.24	0.36	0.54	0.50	0.59	0.51	0.67	0.51	0.62	0.63
Dy	2.91	1.49	2.17	3.19	2.97	3.47	3.09	4.15	3.13	3.74	3.84
Ho	0.64	0.35	0.47	0.65	0.65	0.74	0.66	0.90	0.67	0.80	0.83
Er	1.99	1.11	1.34	1.87	1.78	2.14	1.81	2.52	1.88	2.28	2.28
Yb	2.29	1.29	1.27	1.84	1.76	2.11	1.75	2.47	1.95	2.25	2.26
Lu	0.37	0.22	0.20	0.28	0.28	0.33	0.27	0.38	0.31	0.35	0.34
Hf	3.36	2.00	1.03	2.56	2.62	3.04	1.86	3.13	4.10	3.20	3.14
Ta	0.63	0.45	0.24	0.38	0.41	0.53	0.29	0.55	0.66	0.56	0.55
Tl	0.20	0.02	0.07	0.02	0.03	0.06	0.24	0.00	0.15	0.06	0.00
Pb	12.20	3.36	4.94	7.24	7.37	8.81	4.15	2.83	5.98	6.06	5.61
Th	3.73	3.27	1.66	2.41	2.65	3.73	1.32	2.08	3.96	2.77	2.64
U	1.97	1.26	0.73	1.16	1.07	1.84	0.60	1.21	2.02	1.31	1.26
139 La[N]	59.56	41.71	35.51	46.99	50.26	54.61	40.13	46.99	45.04	50.25	49.38
140 Ce[N]	38.21	25.18	23.69	35.13	35.82	40.26	29.19	37.27	35.28	37.93	37.03
141 Pr[N]	30.35	19.57	20.12	30.56	31.94	35.48	26.46	34.78	31.94	32.81	33.59
146 Nd[N]	22.80	14.71	16.73	26.75	27.00	28.94	23.46	30.44	27.10	28.68	28.70
147 Sm[N]	15.28	8.84	12.22	19.31	18.70	20.36	17.12	22.32	18.98	20.76	20.91
151 Eu[N]	12.47	7.52	10.75	15.12	14.40	17.28	16.59	17.24	13.89	17.12	17.43
157 Gd[N]	10.85	6.28	8.90	13.16	12.72	15.95	12.26	15.77	12.70	15.13	14.91
159 Tb[N]	10.09	4.91	7.29	11.08	10.30	12.12	10.49	13.70	10.51	12.61	12.94
163 Dy[N]	8.95	4.59	6.67	9.80	9.13	10.69	9.52	12.77	9.64	11.51	11.81
165 Ho[N]	8.80	4.77	6.45	8.84	8.86	10.10	9.04	12.29	9.23	10.91	11.32
167 Er[N]	9.33	5.19	6.27	8.76	8.35	10.07	8.51	11.83	8.81	10.69	10.72
172 Yb[N]	11.02	6.20	6.12	8.87	8.47	10.16	8.42	11.89	9.36	10.80	10.87
175 Lu[N]	11.37	6.66	6.21	8.68	8.68	10.17	8.25	11.73	9.48	10.74	10.47
Eu*	12.88	7.45	10.43	15.94	15.42	18.02	14.49	18.76	15.53	17.72	17.66
Eu/Eu*	0.97	1.01	1.03	0.95	0.93	0.96	1.15	0.92	0.89	0.97	0.99

Sample	Nelungaloo Volcanics	Nelungaloo Volcanics	Nelungaloo Volcanics	Nelungaloo Volcanics	Nelungaloo Volcanics	Nelungaloo Volcanics	Nelungaloo Volcanics	Wombin Volcanics	Wombin Volcanics	Wombin Volcanics	Wombin Volcanics	Wombin Volcanics
Source	NSW SPIRT	NSW SPIRT	NSW SPIRT	NSW SPIRT	NSW SPIRT	NSW SPIRT	NSW SPIRT	NSW SPIRT	NSW SPIRT	NSW SPIRT	NSW SPIRT	NSW SPIRT
Deposit/Sample No	N40	N1	N13	N26	N33	N45	N29	10-22-12	CSG100	CSG107	CSG12	CSG67
Sc	28.46	24.34	21.16	32.28	33.35	32.84	22.36	4.90	10.46	8.99	12.52	4.37
Rb	3.27	22.16	3.25	9.90	12.39	14.89	3.10	69.78	57.35	44.82	60.39	43.38
Sr	633.84	1065.28	162.03	1301.41	1121.94	1061.10	959.49	499.59	1080.72	629.12	1554.58	20.80
Y	25.59	14.77	11.06	21.10	31.30	19.82	26.45	21.44	17.11	21.62	20.77	18.70
Zr	117.23	86.05	71.91	81.00	136.31	83.49	132.81	150.51	114.26	126.94	82.85	129.42
Nb	8.41	5.28	3.61	3.91	7.46	4.07	5.93	8.92	5.74	8.74	6.06	7.90
Mo	0.68	1.40	1.23	1.11	0.97	1.14	0.75	0.99	1.03	0.45	0.71	3.48
Sn	1.66	1.04	0.97	0.96	1.55	0.81	1.35	1.52	1.26	0.80	1.08	0.88
Sb	0.10	0.33	0.41	0.35	0.21	0.30	0.60	8.65	0.45	1.66	0.54	1.33
Cs	0.00	0.26	0.02	0.10	0.05	0.12	0.15	0.32	0.28	0.16	0.98	0.11
Ba	163.09	419.07	53.20	396.74	609.57	297.07	133.36	652.08	777.73	884.38	972.82	142.64
La	16.68	18.27	17.70	18.76	18.39	18.42	27.67	20.94	17.90	17.42	18.92	10.15
Ce	36.39	38.09	33.74	38.57	39.92	40.32	58.41	38.52	33.25	31.20	36.07	19.31
Pr	5.10	5.16	4.26	5.44	5.59	5.56	8.16	4.70	4.08	3.81	4.46	2.29
Nd	22.74	22.42	18.65	24.76	25.33	24.82	35.81	18.64	16.42	16.07	20.17	9.72
Sm	5.48	4.71	3.86	5.54	5.79	5.38	7.58	4.10	3.63	3.57	4.56	2.22
Eu	1.50	1.30	1.06	1.56	1.93	1.58	2.00	1.15	1.14	1.17	1.46	0.87
Gd	5.29	3.65	3.01	4.86	6.24	4.77	6.24	3.70	3.79	3.47	4.36	2.81
Tb	0.82	0.51	0.41	0.69	0.95	0.67	0.89	0.60	0.51	0.58	0.66	0.51
Dy	4.74	2.78	2.21	3.91	5.52	3.75	4.90	3.59	2.97	3.55	3.91	3.33
Ho	0.98	0.58	0.45	0.80	1.17	0.77	1.00	0.77	0.63	0.79	0.82	0.72
Er	2.77	1.54	1.19	2.16	3.25	2.14	2.79	2.27	1.89	2.28	2.26	2.21
Yb	2.54	1.55	1.13	2.06	2.86	1.99	2.59	2.35	1.87	2.35	2.16	2.48
Lu	0.38	0.24	0.17	0.31	0.43	0.31	0.40	0.37	0.30	0.37	0.33	0.38
Hf	3.10	2.22	1.91	2.20	3.36	2.12	3.26	3.77	2.80	3.22	2.31	3.48
Ta	0.54	0.28	0.20	0.21	0.47	0.24	0.32	0.54	0.37	0.50	0.37	0.49
Tl	0.01	0.05	0.04	0.05	0.06	0.03	0.01	0.14	0.13	0.07	0.09	0.05
Pb	3.47	4.23	4.68	4.48	3.32	2.37	5.92	14.94	11.25	5.71	11.26	7.94
Th	2.28	2.78	2.40	2.06	1.56	2.03	3.11	4.84	3.27	3.39	3.02	4.31
U	1.30	2.15	1.79	1.38	0.67	1.44	2.35	1.73	1.78	0.97	1.51	1.80
139 La[N]	52.96	58.01	56.19	59.56	58.38	58.47	87.86	66.47	56.84	55.29	60.06	32.21
140 Ce[N]	44.76	46.85	41.50	47.44	49.10	49.60	71.84	47.38	40.90	38.37	44.37	23.75
141 Pr[N]	43.96	44.45	36.70	46.86	48.23	47.96	70.36	40.54	35.17	32.82	38.42	19.77
146 Nd[N]	38.10	37.55	31.24	41.47	42.43	41.58	59.98	31.23	27.51	26.92	33.78	16.28
147 Sm[N]	28.54	24.55	20.11	28.85	30.17	28.03	39.46	21.34	18.90	18.58	23.76	11.55
151 Eu[N]	20.71	18.06	14.61	21.66	26.80	21.93	27.73	15.92	15.78	16.16	20.16	12.03
157 Gd[N]	20.42	14.08	11.61	18.75	24.09	18.42	24.10	14.30	14.63	13.38	16.82	10.83
159 Tb[N]	16.70	10.36	8.30	14.07	19.43	13.75	18.22	12.23	10.39	11.75	13.55	10.50
163 Dy[N]	14.57	8.55	6.81	12.02	16.97	11.53	15.08	11.03	9.14	10.94	12.02	10.24
165 Ho[N]	13.37	7.88	6.15	10.90	16.00	10.56	13.74	10.54	8.67	10.80	11.20	9.86
167 Er[N]	13.03	7.25	5.61	10.15	15.27	10.06	13.11	10.68	8.86	10.69	10.63	10.37
172 Yb[N]	12.19	7.44	5.44	9.89	13.77	9.54	12.47	11.31	9.00	11.30	10.37	11.93
175 Lu[N]	11.84	7.29	5.33	9.52	13.23	9.50	12.33	11.36	9.20	11.45	10.31	11.66
Eu*	24.14	18.59	15.28	23.26	26.96	22.72	30.84	17.47	16.63	15.77	19.99	11.18
Eu/Eu*	0.86	0.97	0.96	0.93	0.99	0.97	0.90	0.91	0.95	1.02	1.01	1.08

Appendix E3

Compiled Sr, Nd and Pb Isotope data

DATA SOURCES

- Carr, G. R. and Dean, J. A., 1990. Mantle and crustal lead isotope signatures of Au mineralization in the western tectonic domains of the Lachlan fold belt, NSW: *in* Compston, W., ed., Seventh international conference on Geochronology, cosmochronology and isotope geology, Canberra, 1990, 15 p.

- Carr, G. R., Dean, J. A., Suppel, D. W. and Heithersay, P. S., 1995. Precise lead isotope fingerprinting of hydrothermal activity associated with Ordovician to Carboniferous metallogenic events in the Lachlan Fold Belt of New South Wales: Economic Geology; 90, 1467-1505.

- Kolkert, R., 1998. Carbonate-base metal veins peripheral to the Goonumbla Cu-Au deposits - vectors to mineralised centres?: Unpub. BSc Honours thesis, University of Tasmania, 144 p.

- Whitford, D. J., Sun, S.-s., Carr, G. R. and Heithersay, P. S., 1992. Strontium, neodymium and lead isotope geochemistry of Ordovician igneous rock from Goonumbla: a reconnaissance, CSIRO Centre for Isotope Studies Research Report, 1991-1992: Sydney, 81-84 p.

Carr and Dean's (1990) data was also used by Heithersay (1991).

Sr, Rb and Nd isotope data from Whitford *et al.* , 1992

Sample No.	*Grid Ref*	*Lithology*	*Rb(ppm)*[1]	*Sr(ppm)*[1]	$^{87}Rb/^{86}Sr$	$^{87}Sr/^{86}Sr$[2]	$(^{87}Sr/^{86}Sr)_i$[3]
68603	H967/106m	Monzonite	75	711	0.3050	0.70606±5	0.70415
68604	H1504/2/50m	Diorite	8	1040	0.0222	0.70418±5	0.70404
68605	E26/36/377m	QMP2	53	938	0.1630	0.70518±6	0.70416
68606	H1959/2/10m	Porp. Trachyte	86	758	0.3280	0.70614±5	0.70409
68607	GR004556	Monzonite	66	1200	0.1590	0.70509±5	0.70409
68608	GR057442	Trachyand. lava	51	1530	0.0964	0.70486±5	0.70426
68609	GR000400	Lava (Nelungaloo?)	21	349	0.1740	0.70572±6	0.70464

Sample No.	*Grid Ref*	*Lithology*	*Sm(ppm)*	*Nd(ppm)*	$^{147}Sm/^{144}Nd$	$^{143}Nd/^{144}Nd$	εNd_i
68607	GR057442	Trachyand. lava	1.83	8.79	0.1272	0.1512756±9	6.0
68608	GR000400	Trachyand. lava	3.79	16.40	0.1392	0.1512807±7	6.2

1 Determined by XRF on pressed powders using method of Norrish and Chappell (1967)

2 $^{87}Sr/^{86}Sr$ ratios have been normalised to $^{86}Sr/^{88}Sr = 0.1194$ NBS 987 $^{87}Sr/^{86}Sr = 0.710289 \pm 50$ n = 41.
This external precision sets a lower limit of the precision of individual samples.
Samples have been analysed on a VG354 thermal ionisation mass spectrometer run in single collector mode.

3 Initial ratios have been calculated assuming an age of 439Ma (Perkins et al, 1990).

Pb isotope ratios of galena in carbonate - base-metal veins at E28 from Kolkert, 1998

Sample No.	$^{208}Pb/^{206}Pb$	$^{207}Pb/^{206}Pb$	$^{206}Pb/^{204}Pb$	$^{207}Pb/^{204}Pb$	$^{208}Pb/^{204}Pb$
GS 27/1	2.080	0.851	18.210	15.506	37.889
GD7; 472.3m	2.082	0.852	18.194	15.485	37.872
E28 DDH4 306.9m	2.083	0.852	19.204	15.512	37.917
E28 DDH4 402.5m	2.081	0.851	18.246	15.529	37.974

Pb isotope data from Carr and Dean, 1990 (reported in Heithersay, 1991)

Sample No.	Grid Ref	Lithology	Mineral	Pb(ppm)	U(ppm)	$^{208}Pb/^{206}Pb$	$^{207}Pb/^{206}Pb$	$^{206}Pb/^{204}Pb$	$^{207}Pb/^{204}Pb$	$^{208}Pb/^{204}Pb$
B710	E26/44/232.6	Monzonite	Magnetite	3	0.8	1.9472	0.7829	19.921	15.595	38.789
B710	E26/44/232.6	Monzonite	Magnetite	3	0.8	1.9455	0.7831	19.890	15.575	38.695
B710	E26/44/232.6	Monzonite	Magnetite	-	-	1.9457	0.7834	19.886	15.579	38.691
B711	E26/26/198.2	QMP2	Feldspar concentrate	16	0.2	2.0711	0.8427	18.472	15.567	38.257
B711	E26/26/198.2	QMP2	Mixed sulphide concentrate*	-	-	2.0768	0.8531	18.169	15.500	37.733
B712	E26/31/207.8	Trachyte/ andesite	Bornite	126	0.5	2.0690	0.8482	18.320	15.539	37.903
B713	E26/38/252.2	QMP1	Silicate/carbonate component#	2	0.01	2.0551	0.8327	18.624	15.509	38.274
B713	E26/38/252.2	QMP1	Mixed sulphide concentrate*	35	0.2	2.0700	0.8430	18.416	15.525	38.122
B713	E26/38/252.2	QMP1	Mixed sulphide concentrate*	35	0.2	2.0691	0.8427	18.404	15.509	38.079
B713	E26/38/252.2	QMP1	Mixed sulphide concentrate*	36	0.2	2.0714	0.8431	18.390	15.505	38.093
B714	E26/21/85.0	Trachyte/ andesite	Bornite	44	0.1	2.0712	0.8465	18.291	15.483	37.884
B715	E26/76/669.2	QMP1	Whole rock powder	4	0.2	2.0720	0.8408	18.444	15.507	38.216
B716	E26/76/692.6	QMP2	Bornite	58	0.1	2.0790	0.8487	18.249	15.487	37.939
B717	E26/76/667.4	Monzonite	Bornite	42	0	2.0817	0.8481	18.280	15.504	38.503
B718	E26/39/538.3	QMP1	Mixed sulphide concentrate*	14	0.1	2.0729	0.8449	18.342	15.497	38.020
B719	E26/39/568.0	QMP2	Mixed sulphide concentrate*	414	0.2	2.0734	0.8486	18.235	15.474	37.808
B720	E26/39/651.0	Trachyte?	Mixed sulphide concentrate*	10	0.1	2.0771	0.8476	18.376	15.575	38.168
B721	E26/42/635.7	QMP1	Mixed sulphide concentrate*	-	-	2.0706	0.8461	18.303	15.486	37.898
B722	E26/66/1054.0	Monzonite	Mixed sulphide concentrate*	142	0.2	2.0832	0.8518	18.206	15.508	37.927
B723	E26/46/885.0	BQM	Mixed sulphide concentrate*	40	0.5	2.0716	0.8479	18.290	15.508	37.891
C375	E26S/80/515.0	Monzonite	Whole rock powder	8	0.4	2.0475	0.8337	18.608	15.514	38.101
C376	Goonumbla Hill	Monzonite	Whole rock powder	3	0.3	2.3090	0.8207	18.945	15.549	38.476
C377	Nash's Hill	Trachyte?	Whole rock powder	6	0.5	2.0381	0.8297	18.725	15.536	38.164
C378	ACH967/100/39.0	Trachyand	Whole rock powder	2	0.3	1.9878	0.7993	19.471	15.563	38.705
C379	Goonumbla Hill	Trachyand	Whole rock powder	1	0.3	1.8520	0.7236	21.671	15.680	40.134
E22			Galena					18.204	15.487	37.831
E26			Sulphides					18.215	15.486	37.838
E27			Sulphides					18.214	15.494	37.845

* minor contamination with silicate component

\# dense media separated fraction

Appendix E4

$^{40}Ar/^{39}Ar$ Dating – Queens University, Canada

SAMPLES

B1 = E26/46/1720.2 – E26 monzodiorite, biotite and hornblende, unusable age

B2 = E27/28/708.9 – E27 BQM, unusable age

B3 = E26/286/153.9 – E26 hydrothermal biotite, chloritised, consider as a maximum age

B4 = E26/284/318.0 – E26 BQM, weakly chloritised

B5 = E26/46/1161.6 – E26 B-QMP, very weakly chloritised

B6 = E22/39/581.0 – E22 B-QMP

TU-324: AC-VL-B1 Bt 40-60

Run date: 2001/10/31 Can/Pos: 174/4 J Value: 0.007185
Printed: 2001/10/01 Mass: 1.0 mg ± 0.000096

Volume 39K: 6.19 x 1E-10 cml NTP Approx. % K
Integrated Age: 475.51 ± 4.93 Ma % Ca

Initial 40/36: 1682.73 ±1232.97 (MSWD = 0.90, isochron between 0.00 and 3.00)
Correlation Age: 446.83 ± 57.33 Ma (29.0% of 39Ar, steps marked by >)

Power	36Ar/40Ar	39Ar/40Ar	r	Ca/K	%40Atm	%39Ar	40Ar*/39K	Age
0.75	0.003503±0.000101	0.003447±0.000112	0.137	8.880	103.49	1.65	-10.159±8.364	-136.74±116.95
1.50	0.002617 0.000096	0.016111 0.000479	0.257	6.662	77.28	5.87	14.079 1.917	171.05 22.56
2.25	0.000711 0.000041	0.022471 0.000136	0.039	3.913	20.99	26.32	35.154 0.626	404.30 6.48
3.00	0.000103 0.000011	0.019713 0.000179	0.016	2.656	3.01	23.36	49.199 0.646	544.08 6.19
3.50	0.000016 0.000036	0.019103 0.000566	0.005	3.593	1.07	5.96	51.799 2.113	579.91 19.96
4.00	0.000072 0.000082	0.018616 0.000485	0.013	4.854	2.11	7.22	52.577 1.900	578.15 17.87
4.75>	0.000157 0.000088	0.018852 0.000417	0.017	13.803	4.63	5.27	50.587 1.762	559.32 16.75
5.75>	0.000075 0.000097	0.020611 0.000717	0.025	9.191	2.20	7.43	47.515 2.194	533.74 21.15
7.00>	0.000057 0.000047	0.023031 0.000249	0.014	6.628	1.67	11.21	43.695 0.756	482.69 7.50
7.50>	0.000186 0.000094	0.019584 0.003050	0.053	30.615	5.44	3.10	48.280 1.745	537.26 16.79

Power	40Ar	39Ar	38Ar	37Ar	36Ar	Blank 40Ar	Atmos 40/36
0.75	29.815±0.436	0.140±0.009	0.080±0.004	0.158±0.003	0.110±0.000	0.293	288.024
1.50	22.771 0.373	0.400 0.009	0.104 0.004	0.415 0.004	0.064 0.000	0.266	288.024
2.25	74.341 0.272	1.712 0.013	0.318 0.011	1.111 0.012	0.059 0.000	0.284	288.024
3.00	73.555 0.394	1.490 0.012	0.282 0.009	0.856 0.009	0.012 0.000	0.286	288.024
3.50	19.554 0.263	0.406 0.009	0.078 0.004	0.229 0.003	0.005 0.000	0.269	288.024
4.00	24.260 0.229	0.489 0.011	0.101 0.004	0.524 0.005	0.006 0.000	0.310	288.024
4.75>	17.630 0.035	0.356 0.007	0.084 0.003	0.765 0.006	0.007 0.000	0.286	288.024
5.75>	22.768 0.432	0.503 0.012	0.115 0.009	0.720 0.010	0.006 0.000	0.316	288.024
7.00>	30.261 0.633	0.725 0.007	0.169 0.005	0.782 0.006	0.006 0.000	0.295	288.024
7.50>	16.124 0.025	0.345 0.007	0.201 0.005	1.674 0.010	0.008 0.000	0.281	288.024

Measured volumes are x 1E-10 cml NTP. All errors are 2 x standard error. Tatrimli 10-Jul-01

TU-324: AC-VL-B1 Bt 40-60

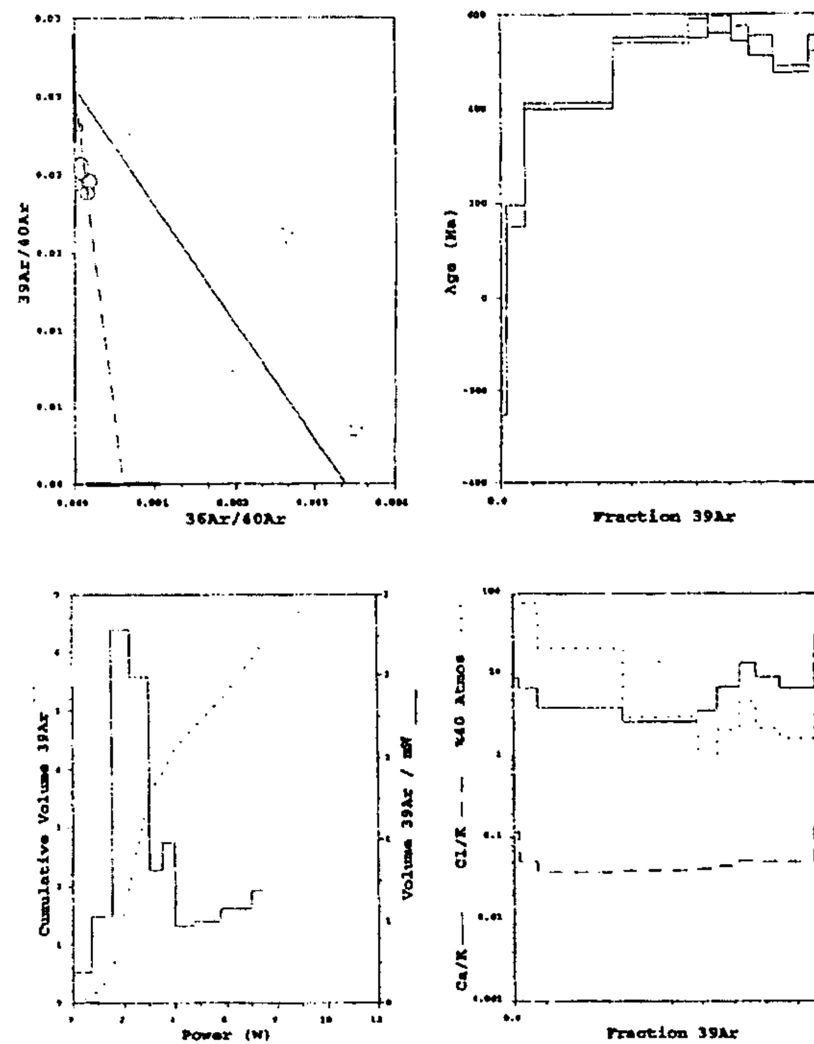

Measured volumes are x 1E-10 cml NTP. All errors are 2 x standard error. Tatrimli 10-Jul-01

TU-325: AC-VL-B1H Hb 40-60

Run date: 2001/10/02 Can/Pos: 174/3 J Value: 0.007160
Printed: 2001/10/02 Mass: 1.0 mg ± 0.000110

Volume 39K: 8.90 x 1E-10 cm3 NTP Approx. 4.86% K
Integrated Age: 673.17 ± 14.99 Ma % Ca

Initial 40/36: 332.45 ± 82.92 (MSWD = 1.02, isochron between 0.18 and 2.03)
Correlation Age: 495.55 ± 36.60 Ma (95.0% of 39Ar, steps marked by >)

Plateau Age: 519.21 ± 14.71 Ma (53.9% of 39Ar, steps marked by <)

Power	36Ar/40Ar		39Ar/40Ar		r	Ca/K	%40Atm	%39Ar		40Ar*/39K		Age
0.50			ERR									
1.25	0.001950	0.000170	0.002252	0.000476	0.210	26.299	57.60	2.02	188.275	42.219	1539.91	232.26
2.00	0.002066	0.000216	0.004141	0.000611	0.102	29.813	61.02	2.77	94.105	25.128	929.27	155.34
2.75>	0.001252	0.000213	0.008599	0.000667	0.108	55.388	36.94	5.47	73.320	6.949	761.28	75.80
3.75>	0.000988	0.000072	0.010813	0.000202	0.566	64.726	29.12	35.36	65.546	1.493	694.20	13.13
< 4.75>	0.000254	0.000104	0.020342	0.000346	0.234	62.717	7.37	29.40	45.534	1.449	509.09	16.11
< 5.75>	0.000040	0.000764	0.021055	0.000060	0.051	62.655	1.06	13.39	46.931	4.069	523.22	39.33
< 7.00>	0.000117	0.000192	0.020043	0.000598	0.136	83.462	3.27	15.13	48.261	2.799	535.46	26.87

Power	40Ar		39Ar		38Ar		37Ar		36Ar		Blank 40Ar	Atmos 40/36
0.50	19.207	±0.034	0.009	±-0.003	0.043	±0.002	0.030	±0.001	0.057	±0.000	0.121	288.024
1.25	8.133	0.015	0.032	0.003	0.033	0.003	0.082	0.002	0.018	0.003	0.117	288.024
2.00	6.080	0.020	0.339	0.003	0.021	0.002	0.126	0.002	0.015	0.003	0.116	288.024
2.75>	5.742	0.018	0.364	0.004	0.068	0.003	0.451	0.004	0.010	0.000	0.118	288.024
3.75>	29.727	0.042	0.344	0.006	0.623	0.008	3.472	0.020	0.034	0.000	0.118	288.024
< 4.75>	12.423	0.028	0.271	0.004	0.477	0.007	2.631	0.014	0.008	0.000	0.117	288.024
< 5.75>	4.467	0.013	0.108	0.004	0.147	0.004	0.961	0.007	0.003	0.000	0.116	288.024
< 7.00>	6.716	0.016	0.151	0.004	0.320	0.006	1.850	0.011	0.005	0.000	0.116	288.024

Measured volumes are x 1E-10 cm3 NTP. All errors are 2 x standard error. Intrim11 10-Jul-01

TU-325: AC-VL-B1H Hb 40-60

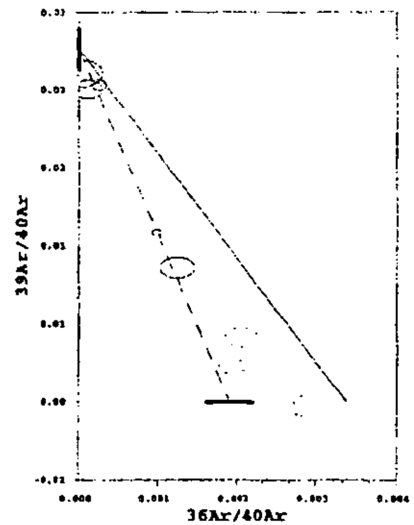

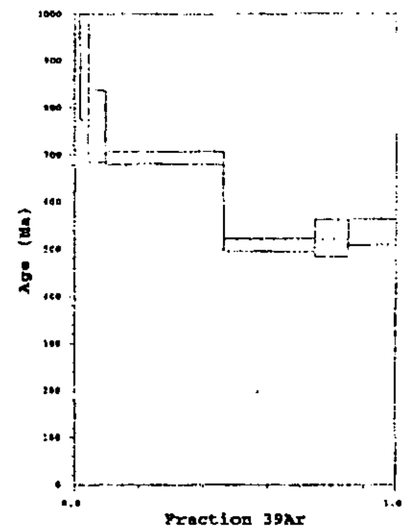

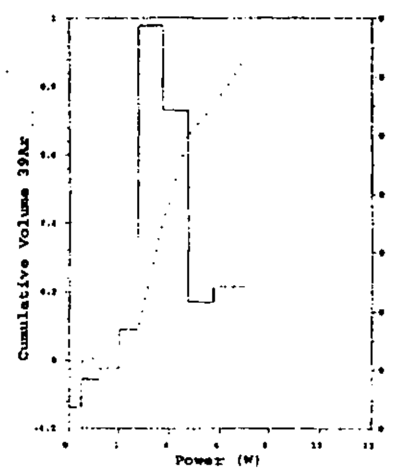

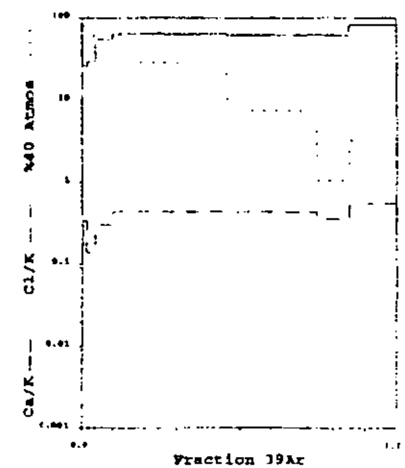

Measured volumes are x 1E-10 cm3 NTP. All errors are 2 x standard error. Intrim11 10-Jul-01

TU-321: AC-VL-B2 Bt 40-60

Run date: 2002/09/29 Can/Pos: 174/5 J Value: 0.007177
Printed: 2003/09/30 Mass: 1.0 mg ± 0.000108

Volume 39K: 2.72 x 1E-10 cm3 NTP Approx. % K
Integrated Age: 447.34 ± 7.25 Ma % Ca

Initial 40/36: 632.69 ± 265.51 (MSWD = 2.50, isochron between -0.41 and 3.83)
Correlation Age: 518.10 ± 61.66 Ma (26.2% of 39Ar, steps marked by >)

Power	36Ar/40Ar	39Ar/40Ar	r	Ca/K	%40Atm	%39Ar	40Ar*/39K	Age
0.50	0.003080±0.000165	0.005095±0.000235	0.049	1.369	90.99	1.40	17.656±9.537	215.24±109.60
1.25	0.002133 0.000095	0.030554 0.000255	0.034	4.180	62.91	15.29	12.118 0.926	150.46 11.03
2.00	0.001857 0.000052	0.020615 0.000130	0.040	3.073	54.79	23.81	21.913 0.766	263.51 8.58
2.75	0.000311 0.000069	0.022086 0.000171	0.008	0.305	9.13	15.95	41.138 0.985	465.73 9.85
3.50	0.000218 0.000064	0.015213 0.000153	0.086	0.394	6.40	10.61	61.522 1.309	659.78 12.40
4.25	0.000111 0.000106	0.015058 0.000212	0.003	0.299	3.26	8.70	64.245 2.275	684.07 20.16
5.25>	0.000622 0.000052	0.013332 0.000108	0.014	0.892	18.35	12.86	61.239 1.263	657.24 11.36
6.25>	0.000215 0.000131	0.017660 0.000242	0.005	1.347	6.34	6.75	53.034 2.307	581.89 21.63
7.00>	0.000139 0.000150	0.020789 0.000254	0.004	0.708	4.08	5.55	46.139 2.210	516.04 21.49

Power	40Ar	39Ar	38Ar	37Ar	36Ar	Blank 40Ar	Atmos 40/36
0.50	8.024±0.030	0.051±0.003	0.037±0.003	0.012±0.001	0.038±0.000	0.146	288.024
1.25	13.740 0.044	0.429 0.003	0.235 0.005	0.303 0.003	0.033 0.000	0.147	288.024
2.00	33.547 0.074	0.663 0.004	0.399 0.006	0.347 0.003	0.063 0.000	0.152	288.024
2.75	19.799 0.066	0.447 0.003	0.267 0.006	0.026 0.001	0.005 0.000	0.153	288.024
3.50	19.112 0.046	0.301 0.003	0.171 0.005	0.023 0.001	0.007 0.000	0.149	288.024
4.25	12.256 0.029	0.194 0.003	0.099 0.003	0.012 0.002	0.004 0.000	0.148	288.024
5.25>	26.376 0.058	0.362 0.003	0.195 0.005	0.056 0.002	0.019 0.000	0.147	288.024
6.25>	10.534 0.031	0.195 0.002	0.071 0.003	0.046 0.002	0.005 0.000	0.147	288.024
7.00>	8.719 0.040	0.189 0.002	0.046 0.003	0.025 0.001	0.004 0.000	0.146	288.024

TU-321: AC-VL-B2 Bt 40-60

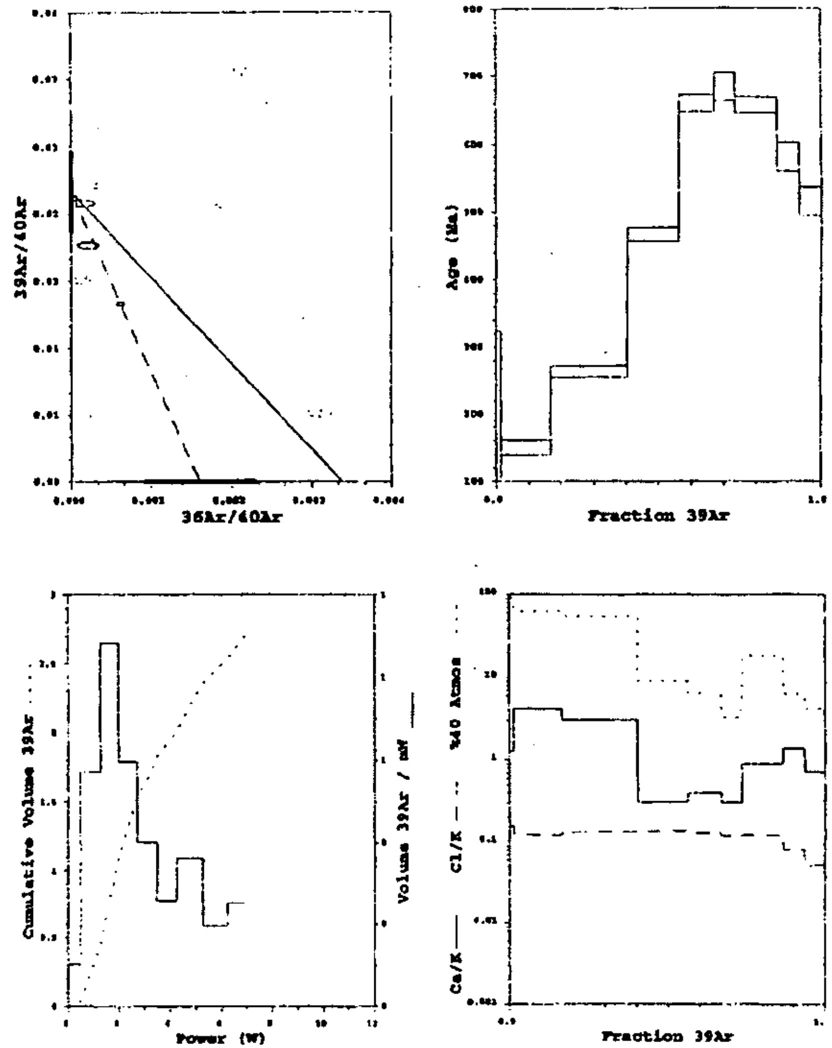

TU-323: AC-VL-B3 Bt 40-60

Run date: 2001/10/01 Can/Pos: 174/4 J Value: 0.007169
Printed: 2001/10/01 Mass: 1.0 mg ± 0.000146

Volume 39K: 44.18 x 1E-10 cm3 NTP Approx. % K
Integrated Age: 430.89 ± 5.96 Ma 3.02% Ca

Initial 40/36: Linear regression has positive slope.
Correlation Age:

Plateau Age: 448.90 ± 6.20 Ma (45.0% of 39Ar, steps marked by <)

Power	36Ar/40Ar	39Ar/40Ar	r	Ca/K	%40Atm	%39Ar	40Ar*/39K	Age
0.75	0.002813±0.000130	0.025277±0.008715	0.007	0.317	83.03	0.76	5.770±2.257	73.13±28.03
1.50	0.001498 0.000051	0.022298 0.000140	0.043	0.071	44.23	1.55	25.008 0.710	297.51 7.79
2.00	0.001093 0.000112	0.027458 0.000432	0.118	0.043	32.25	1.09	24.663 1.310	293.72 14.40
2.50	0.000387 0.000068	0.032618 0.000434	0.063	0.012	11.41	2.04	27.151 0.733	320.86 7.93
3.00	0.000073 0.000047	0.029323 0.000203	0.003	0.012	2.15	2.17	33.370 0.531	386.96 5.54
3.50	0.000024 0.000023	0.025674 0.000153	0.003	0.010	0.69	6.67	38.679 0.355	441.54 3.40
4.00	0.000021 0.000019	0.025540 0.000146	0.002	0.013	0.60	7.80	38.917 0.318	443.96 3.22
4.50	0.000019 0.000023	0.025113 0.000165	0.004	0.013	0.56	9.49	39.598 0.377	450.82 3.80
5.00	0.000010 0.000019	0.025121 0.000139	0.002	0.011	0.28	13.19	39.695 0.313	451.80 3.15
5.50	0.000008 0.000019	0.024956 0.000153	0.001	0.007	0.22	10.27	39.984 0.335	454.70 3.36
< 6.00	0.000007 0.000023	0.025308 0.000160	0.001	0.007	0.20	6.79	39.436 0.373	449.18 3.76
< 6.50	0.000008 0.000023	0.025178 0.000172	0.001	0.004	0.23	5.90	39.628 0.385	451.12 3.88
< 7.00	0.000005 0.000024	0.025367 0.000175	0.001	0.004	0.15	6.25	39.362 0.390	448.43 3.93
< 7.75	0.000003 0.000029	0.025170 0.000161	0.001	0.005	0.08	6.10	39.698 0.426	451.82 4.29
< 8.00	0.000009 0.000024	0.025392 0.000137	0.001	0.007	0.27	19.93	39.276 0.356	447.57 3.59

Power	40Ar	39Ar	38Ar	37Ar	36Ar	Blank 40Ar	Atmos 40/36
0.75	11.661±0.052	0.346±0.100	0.070±0.021	0.020±0.001	0.035±0.000	0.121	298.024
1.50	30.941 0.092	0.699 0.004	0.046 0.003	0.011 0.001	0.050 0.000	0.130	298.024
2.00	17.667 0.241	0.494 0.004	0.036 0.004	0.006 0.001	0.022 0.000	0.178	298.024
2.50	27.849 0.334	0.918 0.005	0.060 0.004	0.005 0.001	0.016 0.000	0.190	298.024
3.00	33.926 0.106	0.975 0.006	0.046 0.005	0.004 0.001	0.005 0.000	0.153	298.024
3.50	115.255 0.414	2.983 0.014	0.202 0.010	0.008 0.004	0.085 0.000	0.466	298.024
4.00	135.483 0.450	3.487 0.016	0.246 0.011	0.009 0.003	0.046 0.000	0.461	298.024
4.50	167.601 0.840	4.239 0.018	0.306 0.015	0.011 0.004	0.006 0.000	0.432	298.024
5.00	231.639 0.750	5.883 0.026	0.416 0.019	0.014 0.005	0.005 0.000	0.419	298.024
5.50	183.317 0.636	4.582 0.023	0.331 0.014	0.009 0.004	0.004 0.000	0.427	298.024
< 6.00	119.170 0.484	3.041 0.015	0.210 0.013	0.006 0.003	0.003 0.000	0.477	298.024
< 6.50	104.129 0.454	2.645 0.014	0.183 0.008	0.005 0.002	0.003 0.000	0.553	298.024
< 7.00	109.800 0.465	2.798 0.013	0.195 0.009	0.005 0.003	0.003 0.000	0.470	298.024
< 7.75	107.686 0.436	2.733 0.013	0.197 0.008	0.005 0.003	0.003 0.000	0.498	298.024
< 8.00	347.432 1.194	8.876 0.038	0.599 0.026	0.013 0.007	0.006 0.000	0.393	298.024

TU-323: AC-VL-B3 Bt 40-60

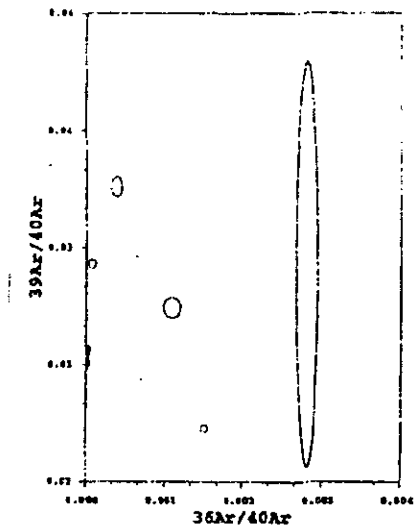

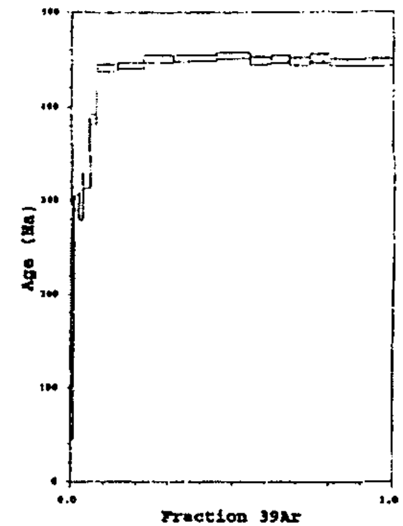

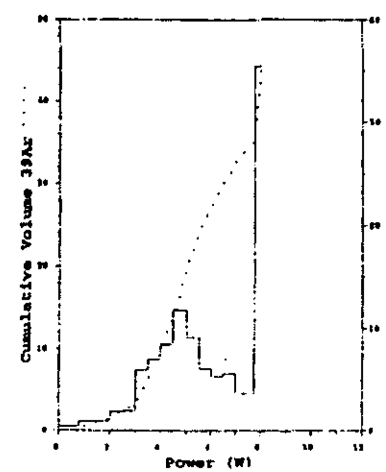

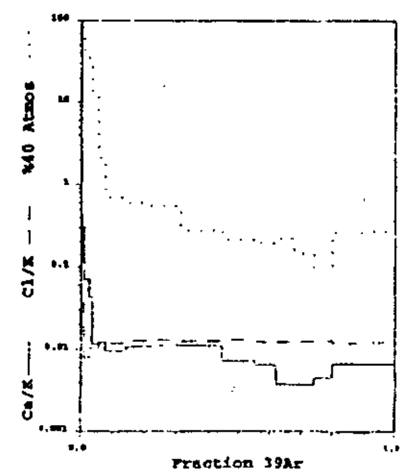

TU-322: AC-VL-B4 Bt 40-60

Run date:	2001/09/30	Can/Pos:	174/7	J Value:	0.007194
Printed:	2001/09/30	Mass:	1.0 mg		± 0.000098

Volume 39K: 49.60 x 1E-10 cm3 NTP   Approx. % K
Integrated Age: 437.02 ± 5.02 Ma   % Ca

Initial 40/36: 2224.22 ±1584.73 (MSWD = 0.79, isochron between 0.97 and 1.65)
Correlation Age: 431.88 ± 16.63 Ma (93.4% of 39Ar, steps marked by >)

Plateau Age: 438.96 ± 5.20 Ma (55.7% of 39Ar, steps marked by <)

Power	36Ar/40Ar	39Ar/40Ar	r	Ca/K	%40Atm	%39Ar	40Ar*/39K	Age
0.75	0.003212±0.000102	0.009132±0.000182	0.273	1.902	94.90	0.38	5.561±3.127	78.76±41.52
1.50	0.001169 0.000063	0.022398 0.000490	0.347	0.795	34.52	1.22	29.224 1.217	344.25 13.05
2.00	0.000257 0.000034	0.025765 0.000175	0.023	0.299	7.59	5.03	35.863 0.464	414.08 4.78
2.50>	0.000058 0.000025	0.025726 0.000146	0.004	0.216	1.69	9.05	38.214 0.366	438.17 3.73
2.75>	0.000023 0.000029	0.025834 0.000141	0.002	0.200	0.67	6.97	38.448 0.394	440.55 4.01
3.00>	0.000026 0.000027	0.025422 0.000135	0.003	0.339	0.76	7.04	39.035 0.381	446.51 3.86
3.25>	0.000023 0.000031	0.025546 0.000142	0.003	0.426	0.68	4.76	38.879 0.418	444.93 4.24
3.75>	0.000024 0.000028	0.025134 0.000141	0.003	0.717	0.70	4.57	39.507 0.403	451.29 4.07
4.25>	0.000034 0.000024	0.025521 0.000141	0.007	1.011	1.00	5.62	38.792 0.349	444.05 3.51
< 4.75>	0.000030 0.000035	0.025802 0.000146	0.003	0.550	0.87	3.06	38.421 0.455	440.27 4.63
< 5.25>	0.000023 0.000029	0.025895 0.000161	0.003	0.622	0.68	6.25	38.355 0.409	439.60 4.16
< 5.75>	0.000020 0.000024	0.025934 0.000150	0.003	0.392	0.58	5.99	38.300 0.356	439.06 3.62
< 6.25>	0.000023 0.000025	0.026098 0.000163	0.004	0.419	0.66	7.45	38.064 0.370	436.64 3.77
< 6.75>	0.000014 0.000032	0.026067 0.000163	0.001	0.119	0.40	2.74	38.240 0.416	438.43 4.24
< 7.50>	0.000008 0.000030	0.026139 0.000132	0.001	0.101	0.22	5.58	38.174 0.388	437.77 3.95
< 8.00>	0.000013 0.000025	0.025985 0.000118	0.001	0.105	0.37	24.67	38.340 0.339	439.45 3.45

Power	40Ar	39Ar	38Ar	37Ar	36Ar	Blank 40Ar	Atmos 40/36
0.75	20.693±0.263	0.201±0.003	0.039±0.003	0.065±0.002	0.071±0.000	0.202	288.024
1.50	27.317 0.562	0.624 0.004	0.076 0.003	0.087 0.002	0.036 0.000	0.179	288.024
2.00	97.144 0.420	2.525 0.013	0.265 0.011	0.133 0.004	0.029 0.000	0.188	288.024
2.50>	174.707 0.493	4.527 0.022	0.511 0.018	0.171 0.006	0.014 0.000	0.170	288.024
2.75>	126.488 0.351	3.293 0.025	0.380 0.023	0.116 0.005	0.006 0.000	0.177	288.024
3.00>	137.633 0.292	3.526 0.017	0.409 0.016	0.207 0.007	0.007 0.000	0.176	288.024
3.25>	92.767 0.247	2.391 0.011	0.282 0.010	0.177 0.004	0.005 0.000	0.155	288.024
3.75>	90.434 0.140	2.294 0.012	0.270 0.010	0.284 0.005	0.006 0.000	0.201	288.024
4.25>	109.531 0.360	2.819 0.012	0.333 0.012	0.490 0.007	0.007 0.000	0.183	288.024
< 4.75>	59.033 0.155	1.540 0.008	0.185 0.007	0.167 0.003	0.005 0.000	0.203	288.024
< 5.25>	120.086 0.405	3.141 0.016	0.390 0.014	0.338 0.006	0.008 0.000	0.228	288.024
< 5.75>	114.922 0.332	3.003 0.015	0.370 0.013	0.205 0.006	0.006 0.000	0.191	288.024
< 6.25>	141.023 0.586	3.730 0.017	0.452 0.016	0.270 0.006	0.007 0.000	0.176	288.024
< 6.75>	52.384 0.134	1.381 0.007	0.166 0.005	0.032 0.002	0.004 0.000	0.161	288.024
< 7.50>	106.223 0.226	2.800 0.013	0.341 0.014	0.052 0.004	0.005 0.000	0.190	288.024
< 8.00>	471.498 0.655	12.325 0.053	1.474 0.038	0.225 0.015	0.010 0.000	0.155	288.024

Measured volumes are x 1E-10 cm3 NTP.   All errors are 2 x standard error.   Intrial1 10-Jul-01

TU-322: AC-VL-B4 Bt 40-60

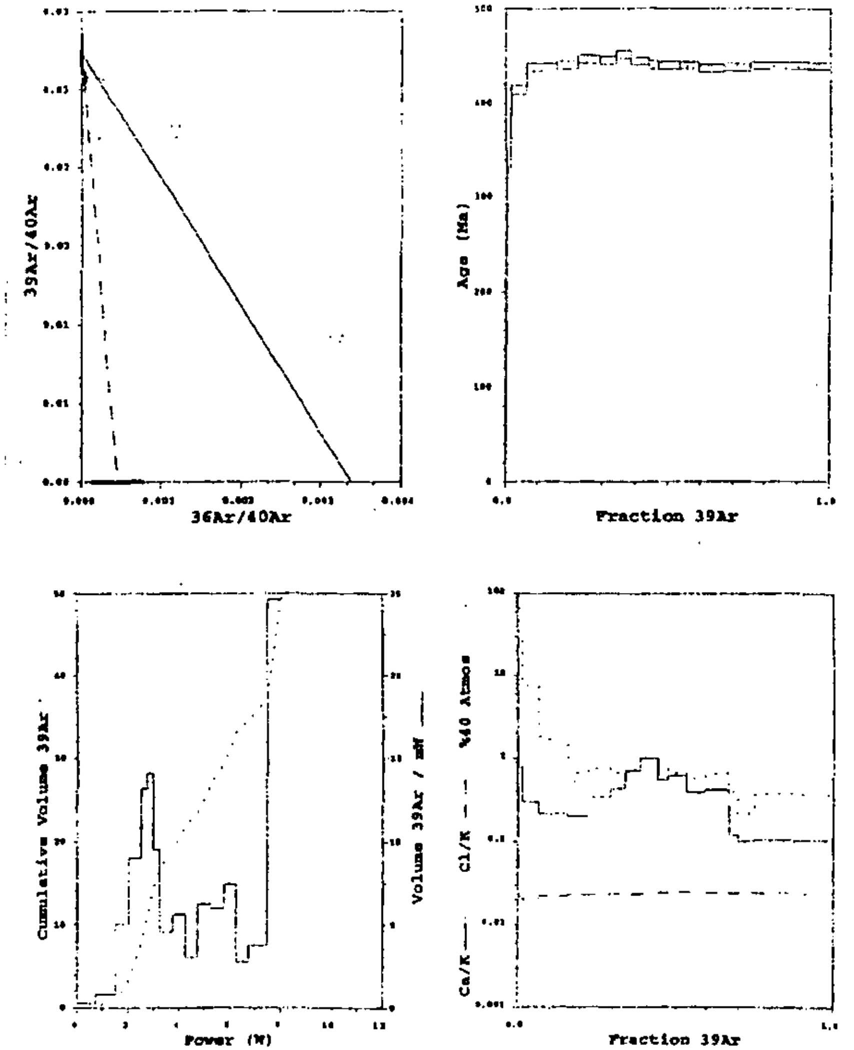

Measured volumes are x 1E-10 cm3 NTP.   All errors are 2 x standard error.   Intrial1 10-Jul-01

<u>TU-326: AC-VL-B6 Bt 40-60</u>

Run date:	2002/10/02	Can/Pos:	174/2	J Value:	0.007151
Printed:	2001/10/02	Mass:	1.0 mg		± 0.000116

Volume 39K: 6.43 x 1E-10 cm3 NTP   Approx. % K
Integrated Age: 460.53 ± 6.99 Ma   % Ca
Initial 40/36: Linear regression has positive slope.
Correlation Age:

Power	36Ar/40Ar	39Ar/40Ar	r	Ca/K	%40Atm	%39Ar	40Ar*/39K	Age
0.75	0.001003±0.000151	0.027644±0.008718	0.003	3.172	29.61	3.53	25.454±1.750	301.69±19.10
1.50	0.000279 0.000065	0.029329 0.000345	0.006	3.670	8.23	8.50	31.289 0.753	364.29 7.34
2.25	0.000006 0.000067	0.025282 0.000465	0.001	0.021	0.18	8.61	39.483 1.075	448.66 10.81
3.00	-0.000000 0.000048	0.024323 0.000365	0.000	0.004	-0.01	12.96	41.117 0.851	465.02 8.48
3.75	-0.000000 0.000062	0.023931 0.000412	0.000	0.002	-0.01	9.46	41.789 1.050	471.71 10.42
4.50	-0.000000 0.000041	0.024328 0.000201	0.000	0.009	-0.01	12.78	41.109 0.605	464.94 6.03
5.25	0.000002 0.000032	0.024325 0.000173	0.000	0.031	0.06	15.18	41.086 0.489	464.71 4.88
6.00	0.000001 0.000050	0.024497 0.000240	0.000	0.084	0.02	9.41	40.815 0.746	462.01 7.45
7.00	-0.000001 0.000083	0.024018 0.000416	0.000	0.174	-0.03	5.43	41.647 1.253	470.29 12.45
7.50	-0.000001 0.000045	0.025089 0.000343	0.000	0.246	-0.04	14.14	39.872 0.763	452.57 7.66

Power	40Ar	39Ar	38Ar	37Ar	36Ar	Blank 40Ar	Atmos 40/36
0.75	8.306±0.020	0.252±0.006	0.022±0.002	0.121±0.002	0.011±0.000	0.139	298.024
1.50	18.732 0.041	0.573 0.006	0.043 0.002	0.337 0.004	0.008 0.000	0.140	298.024
2.25	22.022 0.231	0.588 0.008	0.055 0.003	0.006 0.001	0.003 0.000	0.195	298.024
3.00	34.388 0.303	0.874 0.010	0.084 0.004	0.005 0.002	0.007 0.000	0.230	298.024
3.75	25.542 0.234	0.645 0.009	0.062 0.003	0.006 0.001	0.002 0.000	0.304	298.024
4.50	33.823 0.032	0.849 0.007	0.079 0.003	0.005 0.001	0.002 0.000	0.243	298.024
5.25	40.177 0.038	1.003 0.007	0.095 0.004	0.008 0.001	0.002 0.000	0.139	298.024
6.00	24.760 0.042	0.631 0.006	0.057 0.003	0.012 0.001	0.002 0.000	0.141	298.024
7.00	14.680 0.026	0.375 0.006	0.037 0.003	0.014 0.001	0.002 0.000	0.144	298.024
7.50	36.348 0.284	0.949 0.010	0.090 0.005	0.042 0.002	0.002 0.000	0.220	298.024

Measured volumes are x 1E-10 cm3 NTP. All errors are 2 x standard error. Intrinsic 10-Jul-01

TU-326: AC-VL-B6 Bt 40-60

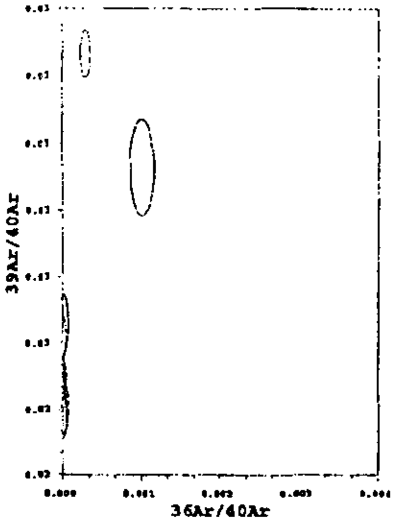

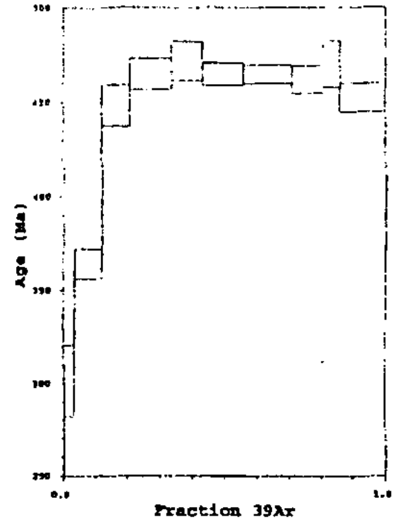

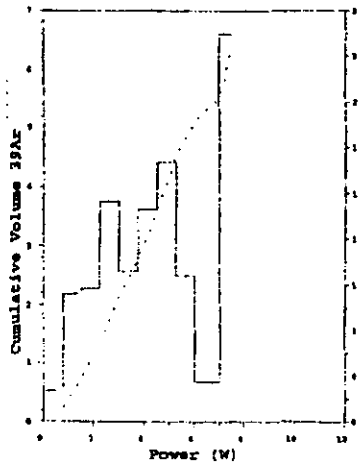

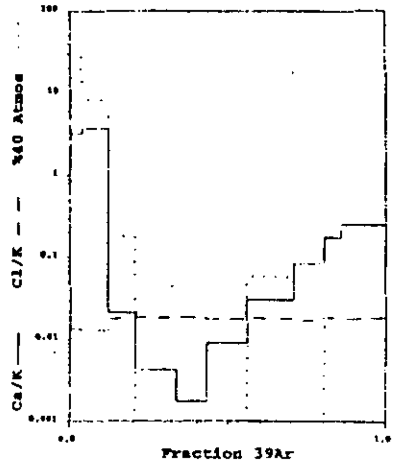

Measured volumes are x 1E-10 cm3 NTP. All errors are 2 x standard error. Intrinsic 10-Jul-01